STUDIES ON SEISMIC ENERGY OF GROUND VIBRATIONS DUE TO BLASTING BASED ON SIGNAL PROCESSING AND ELECTRICAL ENERGY GENERATION

Thesis

Submitted in partial fulfillment of the requirements for the degree of

DOCTOR OF PHILOSOPHY

by

RAGHU CHANDRA GARIMELLA

145004 MN 14 F 02

DEPARTMENT OF MINING ENGINEERING

NATIONAL INSTITUTE OF TECHNOLOGY KARNATAKA

SURATHKAL, MANGALORE – 575 025

DECEMBER, 2018

NATIONAL INSTITUE OF TECHNOLOGY KARNATAKA, SURATHKAL

D E C L A R A T I O N

by the Ph.D. Research Scholar

I hereby *declare* that the Research Thesis entitled **"Studies on seismic energy of ground vibrations due to blasting based on signal processing and electrical energy generation"** which is being submitted to the **National Institute of Technology Karnataka, Surathkal,** in partial fulfillment of the requirements for the award of the Degree of **Doctor of Philosophy** in **Mining Engineering,** is a *bonafide report of the research work carried out by me*. The material contained in this Research Thesis has not been submitted to any University or Institution for the award of any degree.

145004 MN 14 F 02, RAGHU CHANDRA GARIMELLA
Department of Mining Engineering

Place: NITK, Surathkal
Date:

NATIONAL INSTITUE OF TECHNOLOGY KARNATAKA, SURATHKAL

C E R T I F I C A T E

This is to certify that the Research Thesis entitled **"Studies on seismic energy of ground vibrations due to blasting based on signal processing and electrical energy generation"** Submitted by **Mr. Raghu Chandra Garimella**, (Register Number: **145004 MN 14 F 02**) as the record of the Research work carried out by him, is accepted as the Research Thesis submission in partial fulfillment of the requirements for the award of degree of **Doctor of Philosophy**.

Prof. V.R. Sastry
Research Guide

Chairman - DRPC
(Signature with Date and Seal)

ACKNOWLEDGEMENTS

The most pleasant point of presenting a thesis is the opportunity to thank those who have contributed to it. Unfortunately, the list of expressions of thank no matter how extensive is always incomplete and inadequate. Indeed these pages of acknowledgment shall never be able to touch the horizon of generosity of those who tendered their help to me.

First and foremost, I would like to thank my loving Creator, the almighty, for making me a curious being who loves to explore his creation and for giving me the opportunity to write this thesis. Without Him, I can do nothing. I also wish to thank the Almighty for inspiring and giving me the guidance, discipline, strength, patience, perseverance and endurance until the end of my studies in the form of my research supervisor, Professor Vedala Rama Sastry.

This Ph.D. research would not have been possible without the support from National Institute of Technology Karnataka, Surathkal. Many thanks also go to Professor Vedala Rama Sastry for extending financial support in many ways during the period of my research.

It cannot be argued with that, the most influential person in my research career has been my advisor, Professor Vedala Rama Sastry. His passion, guidance, and discipline have been indispensable to my growth as a scientist and as a person over these past three years. I am especially grateful to Sastry Sir for devotion towards his students' education and success. He is one of the rarest Professors who go so far out of his way to make sure students are prepared for whatever the next step in their journeys may be. He introduced me to the new era of research world. I sincerely thank my supervisor for seeing the potential in me and for his valuable and excellent motivation, guidance and constructive input throughout this project. Always, he is in touch with me and made sure that I finish the project on time.

I am especially indebted to my progress assessment members (RPAC) and thesis assessment committee members (DTAC), who have been simply unreal with their supreme level of blessings. Professor M. Govinda Raj, my committee chair and

former Head of the Department, Mining Engineering, has done a surprising job of keeping me in line of research, not to mention the insights he has provided in discussing my ideas and the depth to which he forces me to think. Professor A. Vittal Hegde, Department of Applied Mechanics and Hydraulics, have been a constant source of support that has proven to be truly invaluable over the past three years, when life has seemed so overwhelming. He has been asking me regularly how my research is going for years. In all seriousness, all of my committee members have been very gracious and generous with their time, ideas, and recommendation letters. Thank you so much to all of them.

I thank Dr. Karra Ram Chandar for his constant encouragement and precise advice all the way through. He helped me a lot to clarify the research issues, especially during the crucial phase of my work. His professional working attitudes have also influenced me, from which I will gain benefits for my future career.

I have the great pleasure of working on my research with the help of Mr. Raghavendra M.A.N.S., Department of Electronics and Communications and Mr. Palakolanu Ramana Reddy, Department of Physics, my seniors, who are the most influential scholars to me for doing research works with more effectiveness. I am grateful to Mr. Raghavendra M.A.N.S., for making me to develop the Piezo-Gen circuit with microcontroller interface on my own. Also, it is my gratitude to mention his name for helping me to learn that there is more than one way to approach a problem. He is a brilliant scientist, and I am very sure that he will be an amazing professor. Mr. Palakolanu Ramana Reddy taught me everything from what a worthy publication means, to how to publish an article with clear research impact. Their hard work and friendship over the past years have been very critical.

Amazingly, I come across some people in my department and outside of the department who became close friends to me, and it turns out that many of them have become my critical and constant supporters. I would not be the same person without the friendships of them. Thanks to my Mining team – Balla Kalyan, Sandi Kumar Reddy, K.V. Nagesha, Sripad, Sreekanth R. Lamani, V.S.S. Ramalingeshwaradu, D. Kumar, Abhisek Kumar Tripati, Harish Kumar N.S., Harish H., S. Vijay Kumar,

Ch. Vijay Kumar, G.N.V. Sarath Babu, J. Balaraj, Ch. Laxminarayana, Ravindra, K. Sandeep Reddy, B.C. Gayana, Tejaswarn, team Electrical – Srikakulapu Ramu, M. Vijay, Nagraj bhayya, Gururaj, Sai Krishna, Deshpande Abhilash Krishna, team Computers – Y.V.S. Murthy (Vishnu sir), Siva, team Mathematics – G. Ramu, Balakrishna, Ahmed, Pavan, Suresh Dara, Srinivas (Seenu anna), team Electronics – K. Shareef Babu, S. Gnaneswar nadh (Gnani), Jayaram Reddy, Parasuram, one man army of Management department – Anil Kumar, team Physics – M. Raveendra Kiran, I. Ramesh Reddy, P. Kiran, B. Naveen Kumar Reddy, Applied Mechanics – Jagalingam Pusparaj (Jaggu sir), Mechanical – B. Abdulrajak, Metallurgy – Sangamesh Rajole, Chemistry – Naik, and obviously, Mr. P. Ramana Reddy, for the many lunches, cups of coffee/tea and nostalgic memories that brought me out of depression and made me optimistic for so many times. You guys have all been truly amazing friends, and I am so thankful for all the times you've scraped me off the ground and reassembled me into a human again.

The various members of our *Sastry Sir Team* (E. Muralidhar, N. Adithya, Mohammed Shoeb Mohiuddin, Swetha Sahu, Vaishnavi, Sahana Poornima, Sharika, C. Karthik, Hari Prasad, B. Rajasekhar, Parvathy, T.G. Sruthi, M. Raghu Ram, Saikat Kuili, T. Murali, J. Prudhvi and many more graduates) have provided a diverse, tumultuous environment that has not only shaped me as a valued researcher, but also as a person. Through all the ups and downs of the 72+ hours/week that we spend together, it is impossible to replace any individual person that I had an opportunity to work with. The early lab members were instrumental to me in learning techniques and in how to think about research. My departmental scholars are an awesome crew. I really enjoyed their friendship.

I am ever grateful to my baymate, Darshan G.C., for teaching me technical skills like CAD Designs, computer skills and so many things as the list will be endless. Enough cannot be said about him who was there for me always and who liked all the same music as me.

Most people are lucky to have one friend as a constant supporter and close to their heart as Smt. Bharathi Ma'm is to mine. I have a great fortune during my research

career of meeting such a person. She has become a critical appendage over the years. To lose her would be like losing an arm. She has become like an own sister to me, which is exciting because I never had a sister! I will just say to her that You are irreplaceable Ma'm.

I also sincerely thank the supporting staff (non-teaching) of our department, Sri D. Chandrahasa Rai, Sri Bhaskar D., Sri Mahabala Poojary, Sri Surendra, Smt. Chandrakshi, Sri Santosh, Smt. Gayatri, for their continuous support, guidance, cooperation, encouragement and for facilitating all the requirements, going out of their way. They taught me another aspect of life, that, "*goodness can never be defied and good human beings can never be denied*". I owe a lot of gratitude to them for always being there for me and I feel privileged to be associated with such people in my life.

Amma and Nanna, I love you both and I wish you all the happiness and adventure that you have ensured. There are no enough words to describe how thankful I am to the both of you. You both have taught me so much, and going away to college and being apart from you has made me realize how much you both mean to me. Also, my dear brother (Atchyut) without your support and guidance I would have not done anything perfectly and properly. You have all contributed irreversibly to the person I have become. Thank you for always being there for me. Without you, I don't know where I would be. If I have learned anything while being away from you, it is that you are the most important people in my life, and I love you all more than anything. I cannot thank you enough, EVER.

Raghu Chandra Garimella

This thesis is dedicated to my devotional parents

Smt. Satya Sita Maha Lakshmi and Sri Umamaheswara Sada Siva Sastry

for showing me the value of education, the importance of perseverance and for the suffering they went through to make me what I am today !!

I also dedicate this thesis to my beloved brother **Sri Atchyut Narayan** (My Bestie), his virtuous wife **Smt. Srivani Deepthi** (Motherly friend of mine) and their children (My Cutie Pie), **Gynana Asritha Sai Venkata Adi Sadasiva Ikshwak** and **Phani Kausthubha Sri Virat**, who always supported me in every way I travelled...

Finally, a small dedication with huge amount of love to my dear soul mate

Venkata Lakshmi Surya Gayathri

- This is for you -

ABSTRACT

Blasting may be considered as the most crucial process in opencast mines. It is, therefore, important for mining engineers to understand the effect of blast design parameters on the results of blasting. Blasting operations in mines and quarries always result in ground vibrations, which are of major environmental concern. In general, a meager percentage of total explosive energy is utilized in rock fragmentation process, while the rest is wasted. Wasted explosive energy manifests in the form of various environmental effects such as ground vibrations, air over pressure and fly rock (Dowding, 1985). Ground vibrations caused by blasting cannot be totally eliminated, yet they can be minimized through a suitable blasting methodology. Substantial amount of research associated with identification of ground vibrations and assessing the blast performance in terms of intensity of ground vibrations has been carried out, so far. Nonetheless, very little research has gone into seismic energy and utilizing this energy in understanding the performance of blasts. Modern tools like high speed videography and seismic energy analysis reveal many aspects of fragmentation process, which otherwise are difficult to visualize and understand (Sastry, 2015).

In the current research study, an attempt was made for the assessment and estimation of seismic energy dissipated into the ground due to blast induced ground vibrations at different distances from blast site. Studies were carried out in three mines having hard limestone formation, one soft limestone mine formation, one underground coal mine formation, two sandstone formations, and five quarries of hard granite rock formation. Initial studies were carried out by determining the geotechnical parameters influencing the propagation of ground vibrations in the laboratory, using the samples collected from mines and quarries of respective formations. Later, altogether 116 ground vibration events in hard limestone formation, 37 ground vibration events in soft limestone formation, 86 ground vibration events in an underground coal formation, 43 ground vibration events in sandstone formation, and 94 vibration events in granite formation were recorded resulting from various blast rounds using ground vibration monitors. Further, digital signal processing computation was done using Advanced Blastware and DADiSP software for all ground vibration waveforms. Most

of the blasts studied were recorded using High Speed Video Camera of 1000fps capacity for analyzing the blast dynamics. Multiple regression analysis was carried out for assessing the influence of Maximum Charge/Delay, Scaled Distance, Distance, and PPV on seismic energy. Also, ANOVA analysis was carried out for estimation of seismic energy with given blast design parameters using MATLAB.

An attempt was made to tap electrical energy from blast induced ground vibrations using the Piezo-Generator (Piezo-Gen) circuit. Validation of Piezo-Gen circuit was done by comparing its output (generated voltage) with the vibration data obtained from geophones. It was evident from the results that the working of developed Piezo-Gen circuit is appropriate and analogous with vibration monitors. The developed Piezo-Gen circuits were placed adjacent to the seismographs at different short to long range distances to tap electrical energy from ground vibrations. In total, electrical energy was tapped from 66 blast induced ground vibrations in limestone formation, 36 in coal formation, 41 in sandstone formation and 94 in granite formation. Electrical voltage tapped from the blast induced ground vibrations during studies was used for running low powered VLSI systems as ambient power source. The tapped electrical energy was correlated with the PPV and seismic energy.

Additionally, numerical modelling was carried out as a parametric study for predicting the seismic energy component resulting from a given blast. Altogether, 98 models were developed using SIMULIA Abaqus / CAE interface. Among them, 28 models are in limestone formation, 14 models are in coal formation, 15 models are in sandstone formation and 41 models are in granitic rock formation. Typical size of each developed model after running the job was upto 3.71GB in limestone formation, 461MB in underground coal formation, 6.02GB in sandstone formation and 5.47GB in granite formation. Each model job run took upto 8-27hrs for completion, in different rock formations. SIMULIA Abaqus based Finite Element Analysis (FEA), with both Python Scripting and Graphic User Interface (GUI) was used to estimate the magnitude of ground vibration intensity (PPV) resulting from a given blast. Additional parameter observed during a blast in the simulated models of four formations was stress components at integral points. Validation of results obtained

from developed models was done by comparing with the field results by carrying out three dimensional regression analysis.

A proper correlation (>75%) between seismic energy and scaled distance was observed in all four rock formations. Also, from the regression analysis made, an excellent correlation (>90%) between seismic energy and electrical energy was observed in all formations. It indicated the possibility of assessing seismic energy dissipated by ground vibrations with the electrical energy generated by the developed Piezo-Gen circuit. From the numerical modelling analysis, higher stress values were observed at lower distances from blast location indicating dissipation of greater seismic energy. Also, PPV was found to increase in proportional to the distance in all four formations. From the three dimensional curve fitting analysis made among PPVs resulting from modelling study, PPVs obtained in field investigations, and electrical voltages obtained from Piezo-Gen circuit, a very good correlation between the modelling results and seismic data generated from vibration monitoring and electrical data generated from piezo electric generator was observed. Study indicated that the working of Piezo-Gen circuit in tapping ground vibrations is as accurate as traditional ground vibration monitors.

TABLE OF CONTENTS

Contents	Page No.
TABLE OF CONTENTS	i
LIST OF FIGURES	vi
LIST OF TABLES	xii
CHAPTER 1 INTRODUCTION	01
1.1 Piezo-Gen Concept	07
1.2 Seismographs	11
1.3 Statement of Problem	13
1.4 Organization of the Thesis	14
CHAPTER 2 LITERATURE REVIEW	16
2.1 Blast Performance	18
2.2 Fragmentation	18
2.3 Fragmentation Analysis	19
2.3.1 Screening / Sieving	20
2.3.2 Observational method	20
2.3.3 Boulder count method	20
2.3.4 Explosive consumption in secondary blasting	20
2.3.5 Digital image processing	21
2.3.6 WipFrag	21
2.4 Ground Vibrations	23
2.4.1 Prediction of ground vibrations	24
2.5 Explosive Energy	26
2.5.1 Fragmentation energy	27
2.5.2 Seismic energy	27
2.6 High Speed Videography	28
2.7 Delay Timing	29
2.8 PIEZOGEN – Tapping Electricity from Vibrations	32

2.8.1 Construction of the piezo generator (Piezo-Gen) 35
2.8.2 Working principle of piezo sensor 37
2.8.3 Types of piezo sensors 37
2.8.4 Applications 38
2.9 Regression Analysis 42
2.9.1 Recognition of control variables 42
2.9.2 ANOVA 43
2.9.2.1 Implementation of ANOVA 43
2.9.3 Approximation of regression coefficients 44
2.9.4 Standard table (F-Ratio) 45
2.9.4.1 Construction of F-table 45
2.9.5 Development of statistical model 46
2.10 Numerical Modelling 46
2.10.1 Methods of analysis in Abaqus 46
2.10.2 Units 47
CHAPTER 3 INVESTIGATIONS 48
3.1 Field Investigations related to Seismic Energy 49
3.1.1 Seismic energy 49
3.1.2 Ground vibration monitoring 50
3.1.3 Vibration monitoring equipment 50
3.1.3.1 Geophone unit 51
3.1.3.2 Event monitoring 51
3.1.4 Signal processing analysis 52
3.1.4.1 Collection 53
3.1.4.2 Extraction 53
3.1.4.3 Importation 53
3.1.4.4 Reconstruction 53
3.1.5 Estimation of seismic energy 54
3.1.6 Field investigations in limestone formation 57

3.1.7 Field investigations in coal formation 59
3.1.8 Field investigations in sandstone bench formation 61
3.1.9 Field investigations in granite formation 62
3.2 Piezo Generator (Piezo-Gen) Circuit 64
3.2.1 Development of piezo generator circuit 66
3.2.2 Modified piezo generator circuit 67
3.2.3 Validation of piezo generator circuit 73
3.3 Field Investigations with Piezo Generator Circuit 77
3.3.1 Electrical energy analysis in limestone formation 78
3.3.2 Electrical energy analysis in coal formation 80
3.3.3 Electrical energy analysis in sandstone formation 81
3.3.4 Electrical energy analysis in granite formation 82
3.4 Geotechnical Parameters 83
3.4.1 Compression testing of rock samples 83
3.4.2 Data collection 86
3.4.3 Young's modulus 86
3.4.4 Poisson's ratio 86
3.4.5 Bulk modulus 87
3.4.6 Shear modulus 87
3.5 Numerical Modelling 88
3.5.1 Calibration of developed models 88
3.5.2 Development of models in all four formations 89
CHAPTER 4 RESULTS AND DISCUSSION 91
4.1 Seismic Energy Analysis 92
4.1.1 Limestone formation 92
4.1.2 Comparison of hard limestone formation and soft limestone formation 98
4.1.3 Coal formation 101
4.1.4 Sandstone formation 104

4.1.5 Granite formation 109

4.2 Piezo Generator (Piezo-Gen) 112

4.2.1 Validation results 112

4.2.2 Limestone formation 114

4.2.3 Comparison of hard limestone formation and soft limestone formation 115

4.2.4 Coal formation 118

4.2.5 Sandstone formation 118

4.2.6 Granite formation 119

4.3 Comparison of Seismic Energy with Electrical Energy 120

4.3.1 Limestone formation 120

4.3.2 Coal formation 124

4.3.3 Sandstone formation 126

4.3.4 Granitic formation 129

4.4 Numerical Modelling Analysis 131

4.4.1 Model validation 131

4.4.1.1 Limestone formation 131

4.4.1.2 Coal formation 133

4.4.1.3 Sandstone formation 134

4.4.1.4 Granite formation 135

4.4.2 Numerical modelling results in limestone formation 138

4.4.3 Comparison of model results with field results in limestone formation 140

4.4.4 Numerical modelling results in underground coal formation 141

4.4.5 Comparison of model results with field results in coal formation 142

4.4.6 Numerical modelling results in sandstone formation 143

4.4.7 Comparison of model results with field results in sandstone formation 145

4.4.8 Numerical modelling results in granite formation 146

4.4.9 Comparison of model results with field results in granite formation 148

CHAPTER 5 CONCLUSIONS AND SCOPE FOR FURTHER WORK 151

5.1 Conclusions 151

5.2 Scope for Further Work 153

REFERENCES 154

APPENDIX-I **LIMESTONE FORMATION (High Speed Camera Sequence Photos)** A1

APPENDIX-II **SANDSTONE FORMATION (High Speed Camera Sequence Photos)** A2

APPENDIX-III **LIMESTONE FORMATION (Wipfrag Analysis)** A3

APPENDIX-IV **SUMMARY TABLES** A9

APPENDIX-V **MATLAB CODES** A54

APPENDIX-VI **SANDSTONE FORMATION (Wipfrag Analysis)** A81

APPENDIX-VII **LIMESTONE FORMATION (Input Parameters used for Numerical Modelling)** A84

APPENDIX-VIII **NUMERICAL MODELLING ANALYSIS OF LIMESTONE FORMATION** A85

APPENDIX-IX **COAL FORMATION (Input Parameters used for Numerical Modelling)** A99

APPENDIX-X **NUMERICAL MODELLING ANALYSIS OF COAL FORMATION** A100

APPENDIX-XI **SANDSTONE FORMATION (Input Parameters used for Numerical Modelling)** A110

APPENDIX-XII **NUMERICAL MODELLING ANALYSIS OF SANDSTONE FORMATION** A111

APPENDIX-XIII **GRANITE FORMATION (Input Parameters used for Numerical Modelling)** A119

APPENDIX-XIV **NUMERICAL MODELLING ANALYSIS OF GRANITE FORMATION** A120

LIST OF FIGURES

Figure No.	Title	Page No.
1.1	Need for mining due to development of mineral usage	02
1.2	Zones of rock deformation around a blasthole	05
1.3	Body waves and surface waves	06
1.4	Piezo electric and converse piezo mechanisms	08
1.5	Working mechanism of simple piezo transducer	10
1.6	A seismograph record	12
2.1	Effect of fragmentation on downstream operations	19
2.2	Fragmented muck pile captured with 0.5m x 0.5m calibrator	21
2.3	Fragmentation analysis of a muckpile using Wipfrag software	22
2.4	Body waves	24
2.5	Surface waves	24
2.6	Required burden movement before blasting of next row	30
2.7	Equivalent circuit of a piezo generator	37
2.8	Types of piezo transducer systems	38
2.9	Connection setup of piezo-transducer system	38
2.10	A piezoelectric motor	40
2.11	A common piezoelectric sensor	41
2.12	Power generating mats in a JR east railway station	42
3.1	Geophone sensor operation	51
3.2	Event monitoring in Minimate Plus, Instantel, Canada	52
3.3	Typical ground vibration event	52
3.4	Quantized discrete signal	53
3.5	Signal with discrete sample magnitudes	54
3.6	Reconstruction of a signal with discrete samples (phase-1)	54
3.7	Reconstruction of a signal with discrete samples (phase-2)	54
3.8	Reconstructed quantized signal	54

Figure No.	Title	Page No.
3.9	Reconstructed discrete signal	54
3.10	Typical reconstructed vibration wave aligned in all three mutually orthogonal directions	55
3.11	Computation of DFT to random vibration signal aligned in all three mutually orthogonal directions	55
3.12	Computation of power spectrum density to the random vibration signal aligned in three mutually orthogonal directions after DFT operation	56
3.13	Seismic energy of the blast induced ground vibration wave	57
3.14	General view of limestone mines	58
3.15	Monitoring of ground vibrations in limestone mines at different locations during research field studies	59
3.16	General view of SRP-3&3A underground coal mine	60
3.17	Monitoring of ground vibrations in an underground coal mine at different seams and partings	61
3.18	General view of sandstone bench formations	61
3.19	Monitoring of ground vibrations in sandstone bench formations at different locations during research field studies	62
3.20	Locations of blasts carried out during research studies	63
3.21	Monitoring of ground vibrations in granite stone formations at different locations during research field studies	64
3.22	Electrical energy tapping from blast induced ground vibrations using piezo generator circuit	65
3.23	Schematic of basic piezo generator circuit developed	67
3.24	Schematic of LM-358 differential OP-AMP	68
3.25	Pin configuration of LM-358	69
3.26	Pin diagram of ATMega328P-PU microcontroller	69
3.27	Schematic of improved piezo generator circuit	70
3.28	Schematic of final piezo generator circuit	71
3.29	Validation of piezo generator circuit	74
3.30	Validation of piezo generator circuit (outside)	75

Figure No.	Title	Page No.
3.31	Tapping of electrical voltage from ground vibrations in limestone mines using basic circuit model	79
3.32	Tapping of electrical voltage from ground vibrations in limestone mines using microcontroller based piezo generator circuit	80
3.33	Tapping of electrical voltage from ground vibrations in coal formation using microcontroller based piezo generator circuit	81
3.34	Tapping of electrical voltage from ground vibrations in sandstone bench formations using microcontroller based piezo generator circuit	82
3.35	Tapping of electrical voltage from ground vibrations in granitic formations using microcontroller based piezo generator circuit	83
3.36	Placement of rock samples into compression testing machine	84
3.37	PC based DAQ system integrated with compression testing machine	85
4.1	Locations of blasts in limestone mines	93
4.2	Relationship between seismic energy and fragmentation in limestone formation	96
4.3	Results obtained from vibration studies in limestone formation	97
4.4	Comparison of seismic energy in harder and softer limestone formations at similar scaled distances	99
4.5	Comparison of seismic energy in harder and softer limestone formations at similar distances	100
4.6	Comparison of seismic energy in harder and softer limestone formations at similar maximum explosive charge per delays	101
4.7	Locations of blasts in underground coal mine	102
4.8	Locations of blasts carried out during research studies in sandstone formation	105
4.9	Relationship between seismic energy and fragmentation in sandstone formation	107
4.10	Results obtained from vibration studies in sandstone formation	108
4.11	Locations of blasts carried out during research studies in granite formation	110
4.12	Validation results of piezo generator circuit in the laboratory	113
4.13	Validation results of piezo generator circuit outside the laboratory	113

Figure No.	Title	Page No.
4.14	Tapped electrical voltage and electrical energy in limestone formation with basic piezo circuit	114
4.15	Tapped electrical voltage and electrical energy in limestone formation with piezo generator circuit	115
4.16	Comparison of electrical energy generation in harder and softer limestone formations at similar scaled distances	116
4.17	Comparison of electrical energy generation in harder and softer limestone formations at similar distances	116
4.18	Comparison of electrical energy generation in harder and softer limestone formations at similar maximum explosive charge per delays	117
4.19	Tapped electrical voltage and electrical energy in coal formation with piezo generator circuit	118
4.20	Summary of tapped electrical voltage and electrical energy in sandstone formation with piezo generator circuit	119
4.21	Tapped electrical voltage and electrical energy in granitic rock formation with piezo generator circuit	120
4.22	Vibration capturing with vibration monitor and developed piezo generator circuit in limestone formation	121
4.23	Seismic energy versus electrical energy with basic circuit in limestone formation	121
4.24	Correlation between seismic energy and electrical energy with basic circuit in hard limestone formation	122
4.25	Seismic energy versus electrical energy with improved piezo circuit in hard limestone formation	123
4.26	Correlation between seismic energy and electrical energy with improved piezo circuit in hard limestone formation	123
4.27	Seismic energy versus electrical energy with piezo circuit in soft limestone formation	124
4.28	Correlation between seismic energy and electrical energy with piezo circuit in soft limestone formation	124
4.29	Vibration capturing with vibration monitor and developed piezo generator circuit in underground coal formation	125
4.30	Seismic energy versus electrical energy in coal formation	126
4.31	Correlation between seismic energy and electrical energy in coal formation	126

Figure No.	Title	Page No.
4.32	Vibration capturing with vibration monitor and developed piezo generator circuit in sandstone formation	127
4.33	Seismic energy versus electrical energy in sandstone formation	128
4.34	Correlation between seismic energy and electrical energy in sandstone formation	128
4.35	Vibration capturing with vibration monitor and developed piezo generator circuit in granite formation	129
4.36	Seismic energy versus electrical energy in granite formation	130
4.37	Correlation between seismic energy and electrical energy in granite formation	130
4.38	Model for validation in limestone formation	132
4.39	Spatial velocity contours observed at nodes	132
4.40	Un-deformed (left) and deformed (right) shape of validation model	132
4.41	Model for validation in coal formation	133
4.42	Spatial velocity contours observed at nodes	133
4.43	Un-deformed (left) and deformed (right) shape of validation model	133
4.44	Model for validation in sandstone formation	134
4.45	Spatial velocity contours observed at nodes	134
4.46	Un-deformed (left) and deformed (right) shape of validation model	135
4.47	Model for validation in granite formation	135
4.48	Spatial velocity contours observed at nodes	135
4.49	Un-deformed (left) and deformed (right) shape of validation model	136
4.50	Correlation between model PPV and field PPV values in four rock formations	137
4.51	Comparison of model results with field results in limestone formation	140
4.52	Comparison of model results with field results in coal formation	143
4.53	Comparison of model results with field results in sandstone formation	145
4.54	Comparison of model results with field results in granite formation	149
A8.1	Stress components at integral points in a model of limestone formation	288

Figure No.	Title	Page No.
A8.2	Spatial velocity contours observed at nodes in a model of limestone formation	292
A8.3	Un-deformed and deformed shapes of blast models in limestone formation	297
A10.1	Stress components at integral points in the model of coal formation	302
A10.2	Spatial velocity contours observed at nodes in coal formation	305
A10.3	Un-deformed and deformed shapes of blast models in coal formation	308
A12.1	Stress components at integral points in a sandstone model	312
A12.2	Spatial velocity contours observed at nodes in a sandstone model	314
A12.3	Un-deformed and deformed shapes of blast models in sandstone formation	317
A14.1	Stress components at integral points in a typical granite model	324
A14.2	Spatial velocity contours observed at nodes in a granite model	329
A14.3	Un-deformed and deformed shapes of blast models in granite formation	337

LIST OF TABLES

Table No.	Title	Page No.
2.1	Delay time required between rows based on high speed videography	30
2.2	Recommended delay intervals by different researchers	32
2.3	Values of F- ratio at 5% significance level	45
2.4	Typical units to be used in the Abaqus / CAE	47
3.1	Summary of weight drop for validation of piezo generator circuit in the laboratory	76
3.2	Summary of weight drop for validation of piezo generator circuit outside the laboratory	77
3.3	Details of rock samples used	83
3.4	Summary of geotechnical parameters	88
3.5	Parameters used in numerical modelling	89
3.6	Details of explosives employed in the numerical modelling	90
4.1	Summary of fragmentation analysis carried out in limestone formation hard limestone formation	94
4.2	Summary of fragmentation analysis carried out in soft limestone formation	96
4.3	Regression analysis for limestone formation	98
4.4	ANOVA (Analysis of Variance) for limestone formation	98
4.5	Relationship between critical blast parameters and seismic energy in limestone formation	98
4.6	Summary of seismic energy in harder and softer limestone formations at similar scaled distances	99
4.7	Summary of seismic energy in harder and softer limestone formations at similar distances	99
4.8	Summary of seismic energy in harder and softer limestone formations at similar maximum explosive charge per delays	100
4.9	Regression analysis for coal formation	103
4.10	ANOVA (Analysis of Variance) for coal formation	104
4.11	Relationship between critical blast parameters and seismic energy in coal formation	104

Table No.	Title	Page No.
4.12	Summary of fragmentation analysis in sandstone formation	106
4.13	Regression analysis for sandstone formation	109
4.14	ANOVA (Analysis of Variance) for sandstone formation	109
4.15	Relationship between critical blast parameters and seismic energy in sandstone formation	109
4.16	Regression analysis for granite formation	111
4.17	ANOVA (Analysis of Variance) for granite formation	112
4.18	Relationship between critical blast parameters and seismic energy in granite formation	112
4.19	Summary of electrical energy generation in harder and softer limestone formations at similar scaled distances	115
4.20	Summary of electrical energy generation in harder and softer limestone formations at similar distances	116
4.21	Summary of electrical energy generation in harder and softer limestone formations at similar maximum explosive charge per delays	117
4.22	Input parameters considered for calibration of numerical modelling	131
4.23	Summary of validation results of numerical modelling	136
4.24	Input parameters considered for numerical modelling in limestone formation	138
4.25	Input parameters considered for numerical modelling in coal formation	141
4.26	Input parameters considered for numerical modelling in sandstone formation	144
4.27	Input parameters considered for numerical modelling in granite formation	146
A4.1	Summary of ground vibration monitoring in limestone formation (Harder formation)	208
A4.2	Summary of ground vibration monitoring in limestone (Softer formation)	211
A4.3	Summary of longitudinal wave and transverse wave velocities in limestone (Harder formation)	212
A4.4	Summary of longitudinal wave and transverse wave velocities in limestone (Softer formation)	216

Table No.	Title	Page No.
A4.5	Summary of ground vibration monitoring in coal formation	217
A4.6	Summary of longitudinal wave and transverse wave velocities in coal formation	219
A4.7	Summary of ground vibration monitoring in sandstone formation	222
A4.8	Summary of longitudinal wave and transverse wave velocities in sandstone formation	223
A4.9	Summary of ground vibration monitoring in granite formation	224
A4.10	Summary of longitudinal wave and transverse wave velocities in granite formation	227
A4.11	Summary of tapped electrical voltage and electrical energy from blast induced ground vibrations in limestone mines with basic piezo-gen circuit	228
A4.12	Summary of tapped electrical voltage and electrical energy from blast vibrations in limestone mines with piezo generator circuit	229
A4.13	Summary of tapped electrical voltage and electrical energy from blast induced ground vibrations in coal formation with piezo generator circuit	230
A4.14	Summary of tapped electrical voltage and electrical energy from blast vibrations in sandstone formation with piezo generator circuit	231
A4.15	Summary of tapped electrical voltage and electrical energy from blast vibrations in granitic rock formation with piezo generator circuit	232
A4.16	Summary of seismic energy and electrical energy obtained in hard limestone formation with basic piezo circuit model	235
A4.17	Summary of seismic energy and electrical energy obtained in hard limestone formation with piezo generator circuit	235
A4.18	Summary of seismic energy and electrical energy obtained in soft limestone formation with piezo generator circuit	237
A4.19	Summary of seismic energy and electrical energy obtained in coal formation with piezo generator circuit	238
A4.20	Summary of seismic energy and electrical energy obtained in sandstone formation with piezo generator circuit	240
A4.21	Summary of seismic energy and electrical energy obtained in granite formation with piezo generator circuit	241
A4.22	Comparison of field and modelling results in limestone formation	244
A4.23	Comparison of field and modelling results in coal formation	247

Table No.	Title	Page No.
A4.24	Comparison of field and modelling results in sandstone formation	248
A4.25	Comparison of field and modelling results in granite formation	250

CHAPTER – 1

INTRODUCTION

Coal plays a pivotal role in sustainable development. It is the most widely used energy source for electricity generation and is an essential input for steel production. India has long history of commercial coal mining since 1774 and nationalization of coal mines, w.e.f. 01.05.1973. As per Integrated Energy Policy Committee of Planning Commission, coal will remain India's most important energy source till 2031-32 and possibly beyond. In India, about 80% coal output is consumed in power sector. In addition, other industries like steel, cement, fertilizer, chemical, paper and a score of medium and small-scale industries are dependent on coal for their process and energy requirements. India ranks 3rd in world coal production (Anon, 2017). The production of coal was 565.8 Mt in 2014-15, which increased by 7.7% to 609.2 Mt in 2015-16. Drebenstedt (2014) explained the need for mining and blasting in his survey conducted for past 70 years of human life. He concluded that the need for mining is rapidly growing with increase in the demand for minerals. Fig. 1.1a depicts the need for mining in world community. Achzet (2012) conducted a survey on mineral use development from several centuries considering stone age and concluded that usage of minerals increases according to the needs of human life. Fig. 1.1b depicts the development of mineral use in the world.

Mining industry in India is a major economic activity which contributes significantly to the economy of India. The GDP contribution of mining industry varies from 2.2% to 2.5% only, but going by the GDP of the total industrial sector, it contributes around 10% to 11%. Mining is also done on small scale, and it contributes 6% to the entire mineral production. Indian mining industry provides job opportunities to around 7,00,000 individuals (Anon, 2016a).

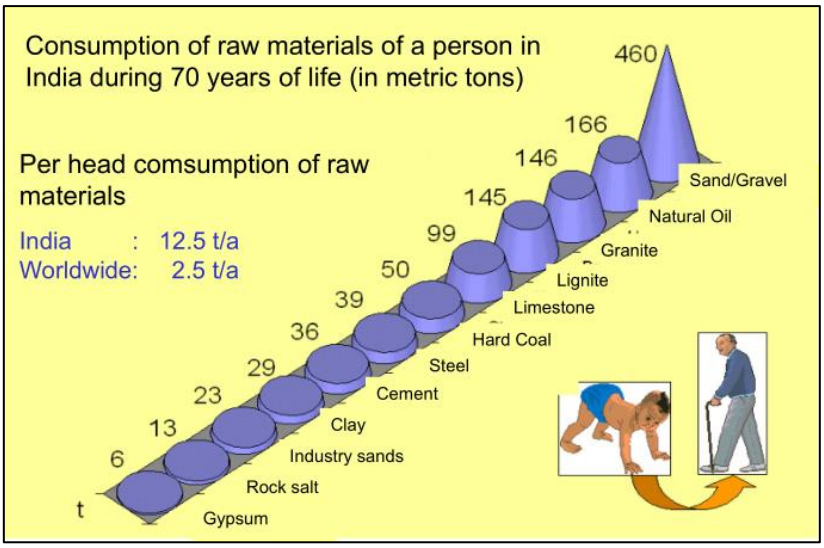

(a)

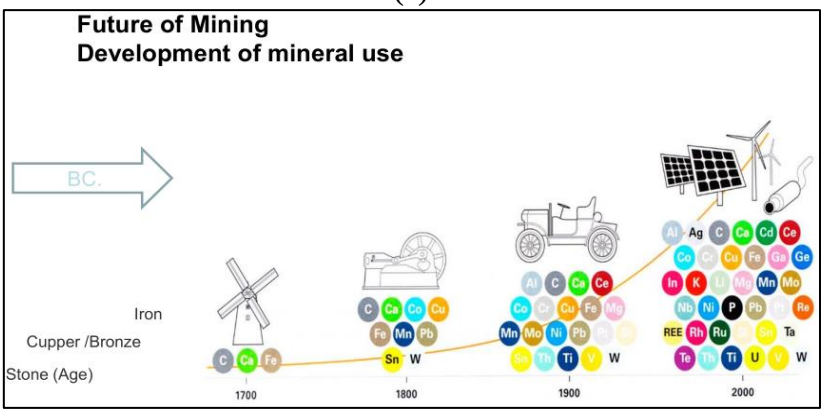

(b)

(a) Need for mining in world community (Drebenstedt, 2014) **(b)** Development of mineral use (Achzet, 2012)

Fig. 1.1 Need for mining due to the development of mineral usage

Enhanced demand for coal and minerals in the country has developed an interest on the environmental problems, which may have potential harm and cause disturbance. Blasting is an essential operation, in every civil and mining project, whether underground or surface, as a major proportion of rock or ore is still excavated by drilling and blasting. No other source of concentrated energy is found till date that can replace the explosives usage as far as economy, safety, and case of operation are concerned. Drilling and blasting operations which were considered to be an art till recent, require sound scientific background, due to changing scenario of Indian Mineral Industry and demands from other allied sectors. The increased production targets, leading to the deployment of huge earth moving equipment in the mines, like

40-50cu.m. capacity walking draglines, 20cu.m. capacity shovels, 170t dumpers are forcing the technocrats to adopt improved and effective drilling and blasting techniques.

Developments in explosives are in tune with the requirements of mineral industry. This may be judged by the range of explosives we have today, from gun powder to the modern bulk explosive systems like HANFO, SMS, Emulsion, etc. and accessories, ranging from ordinary detonator to Raydets, Hercudets, Electronic Detonators, etc. However, the effective utilization of explosive energy still remains a problem area.

Ground vibrations generated due to blasting operations in mines and quarries are very important environmental aspect to be looked into by the researchers. It is established that a meager amount of total explosive energy is being utilized in blasting for breakage of rock mass while the rest is being wasted. The amount of wasted energy causes various environmental issues such as ground vibrations, air over pressure and fly rock. Ground vibrations caused by blasting cannot be totally eliminated, yet they can be minimized as far as possible, through a suitable blasting methodology. Explosive weight per delay and distance of blast site are the two critical parameters which control the intensity of ground vibrations (Dowding, 1985). The nature of shock waves generated by the detonation of explosives is predominantly influenced by rock mass characteristics. Extensive research is going on to measure the amount of shock energy being utilized for rock breaking and furthermore to comprehend the propagation of vibration and its decaying characteristics. Advancement in the development of vibration monitoring instruments resulted in assessing the intensity of ground vibrations and further calculation of seismic energy associated (Sastry, 2015).

Explosive energy can be characterized by two types of pressures: *detonation pressure*, dynamic pressure associated with detonation wave, and *explosion pressure*, pressure developed when explosive reacts to resulting in gaseous products. Further, the detonation of explosive in a confined hole creates two types of energy: *strain energy*, carried by the shock waves in the rock and *gas energy*, remaining in the blasthole

(Sadwin and Junk, 1965). Explosive energy in blastholes is transferred into rock mass as shock energy for fragmenting the surrounding rock mass medium. Such a mechanism of fast energy delivery for getting the desired fragmentation and throw also results in undesirable results, such as the seismic waves in the rock (Sanchidrián et al., 2007).

As a matter of fact, Berta (1985), Spathis (1999) and Ouchterlony et al. (2003) tried to calculate the amount of explosive energy transformed in the form of kinetic energy, shock energy for fracture generation and seismic wave representing as vibrations. Seismic energy has received special attention since earlier times. Spathis (1999) proposed, the functional utilization of energy balance to empower blast designs, which coordinate accessible energy into fragmenting work and henceforth control energy split between fracture energy, kinetic energy and radiated seismic energy, bringing out more proficient utilization of the explosive energy.

In rock blasting, energy in general goes into:

- Extending old fractures
- Creating new fractures
- Displacing parts of rock mass relative to others (loosening)
- Moving the center of gravity forward (heave)
- Undesirable effects: ground vibrations, air blast, fly rock

How the energy is partitioned into these different categories depends upon:

- Explosive parameters
- Rock/rock mass parameters
- Blast geometry parameters

When the explosive charge detonates in a blasthole under confinement, the chemical energy of the explosive is converted into gases and works towards the surroundings with an enormous pressure according to the first principle of thermodynamics (Johansson and Persson, 1970). Explosion of a spherical charge in an infinite rock medium results in three major zones: (1) Explosion cavity - where explosion energy is liberated and the process is hydrodynamic; (2) Transition zone - where plastic flow, crushing and cracking occur; and (3) Seismic zone - where strain waves travel as seismic waves (Atchison et al., 1963; Nicholls, 1962; Sastry, 1989).

Ground vibration is generally a wave motion diffusing outwards from the blast, beyond fragmentation zone (Fig. 1.2), just like an eddy wave distributed in a pool of water due to stone dropping. When a certain quantity of explosive detonates at a certain depth below the earth's surface, approximately 20% to 30% of its energy is utilized in fragmenting the rock mass or other materials around. However, as explosion is an imperfect use of energy, there is loss of energy transmitted through the earth in the form of waves or vibrations.

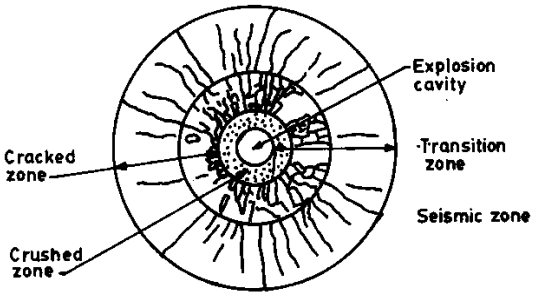

Fig. 1.2 Zones of rock deformation around a blasthole (Atchison, 1968)

Explosion generated ground vibration seismic waves are of two types, namely, body and surface waves, travelling at different velocities (Singh et al., 1993). Body waves travel through medium and surface waves travel along surfaces or discontinuities. Body waves may be reflected or refracted to the surface to become surface waves (Fig. 1.3). Body waves are of two types, Primary (P-wave) and Secondary (S-wave). Surface waves generate when the radiating body waves impinge on a stress free plane, like surface or any discontinuity. These waves travel along the surface and discontinuities. Rayleigh waves are the best known surface waves and include both dilation and distortion of medium. Surface waves carry maximum percentage of radiated energy and are predominant at longer distances from the blast source, since their attenuation rate is slower than body waves. In addition, frequency of surface waves is lower than body waves and frequently found to be in the range most favourable for structural response (Holloway et al., 1983). All these waves are characterized by exponential decrease in particle oscillation amplitude as distance from energy source increases (Taqieddin, 1982).

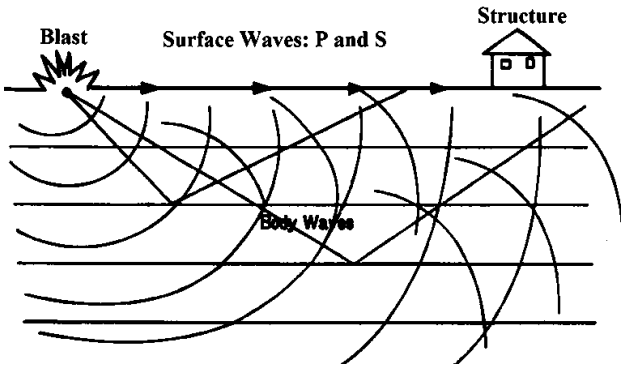

Fig. 1.3 Body waves and surface waves

In general, the intensity of ground vibration is identified by displacement or velocity or acceleration (Rosenthal et al., 1987). Displacement is the phenomenon of movement of ground particles from their equilibrium position due to the passage of seismic waves. Velocity is the rate of change of movement with respect to time, also can be understood as speed at which the rock particle moves when it leaves its rest position. Force exerted by vibrating particle is proportional to the rate of change of its velocity, called as acceleration (Konya and Walter, 1990; Sedlák, 1997).

There are several variables affecting the intensity of ground vibrations and the seismic effects. Some of the major variables are: total explosive charge per blast (kg), maximum explosive charge per delay (kg), distance between blast location and monitoring point (m), number of holes per blast round, delay-time interval (ms) and geological conditions of the blast location (Sanchidrián et al., 2007; Zhang and Zhong, 2011).

There are many methods available for the assessment of blast performance. Blast results like degree of fragmentation, diggability of muck pile, profile of muck pile and back break as well as side effects like fly rock, *ground vibrations* and stemming ejection are generally considered for assessment of blast performance. Seismographs, high-speed video camera and fragmentation monitoring systems are being used to measure different parameters like seismic waves (ground vibrations), initial velocity of blasted rock mass and fragment size distribution in muck pile generated, respectively, from which various energy terms were calculated. Considerable amount of work has been done to identify ground vibrations and minimize the impact of

ground vibrations. However, not much research has gone into the energy and the possible electric current associated with ground vibrations generated from the production blasts in mines, and utilizing this energy in understanding the performance of blast rounds.

Current research studies carried out have indicated that in opencast mines there is a potential of seismic energy generation based on piezo electricity from a given blast, which may be significant from power utilization point of view. Also studies have indicated possible correlation between maximum charge per delay and the seismic energy. Therefore, a study leading to the possible estimation of energy dissipated at different distances from the blast site may be of industrial utility.

1.1 Piezo-Gen Concept

Piezoelectricity is defined as a change in electric polarization with a change in applied stress (direct piezoelectric effect) as shown in Fig. 1.4(a). Piezoelectricity is a phenomenon of electricity accumulated in some solid materials (such as crystalline particles, certain ceramic substances, and biological composition for example bone, DNA and various proteins) due to applied mechanical stress. Therefore, electricity resulting from applied pressure is known as piezoelectricity. Piezo was derived from the Greek word “piezein”, means to squeeze or press, and “electric” or “electron”, derived from “amber”, which is an ancient source of electric charge. Piezoelectricity was discovered in 1880 by French physicists Jacques Curie and Pierre Curie (Anon, 2015a; Curie and Curie, 1880; Tingley, 2013).

Piezoelectricity is the ability of some materials such as crystals and certain ceramics, to generate an electric potential in response to applied mechanical stress (Curie and Curie, 1881; Pramethesth and Ankur, 2013). When the Piezo crystals are not short-circuited, the applied pressure induces a voltage across the material. Another interesting property of piezoelectric material is the change in their dimensions (contract or expand) when an electric field is applied to them, known to be converse piezoelectric effect. Converse piezoelectric effect is the change of strain or stress in a material due to an applied electric field as shown in Fig. 1.4(b).

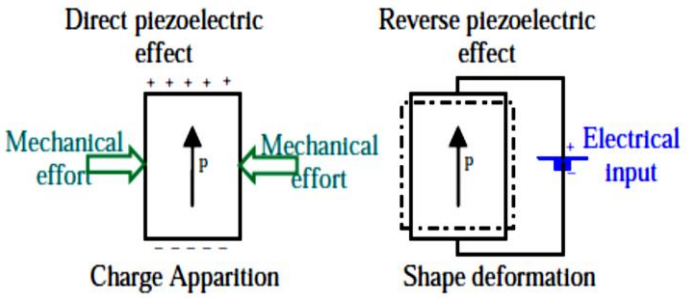

Fig. 1.4 Piezo electric and converse piezo mechanisms (Henderson, 2002)

Major concept of piezo effect is the disturbance of ionic charges in a crystalline material. When there is no external stress on a crystalline structure, then the charge distribution will be symmetric and net electric dipole moment will be zero inducing no electricity. However, when there is a change in strain on the body, the charge will be displaced randomly and charge becomes asymmetrical causing net polarization. In some cases, a crystal possesses unique polar axis even in unstrained condition. This can result in alteration of electric charge due to uniform change of temperature, called pyroelectric effect. Most of the force, pressure, vibration and acceleration sensors work on direct piezoelectric effect, and actuator and displacement devices on the converse effect (Curie and Curie, 1880).

Some important piezo materials are barium titanate, lithium niobate, polyvinyledene difluoride (PVDF), and lead zirconate titanate (PZT). There are several formulations of the PZT compound, each with different electro-mechanical properties. $Pb(Zr,Ti)O_3$ (PZT) ceramics, the most common piezoelectric ceramics, show a high piezoelectric 'd' coefficient with a negligible contribution of electrostriction. Piezoelectric 'd' coefficient or Piezoelectric Modulus, aka d, quantifies the volume change when a piezoelectric material is subject to an electric field, or the polarization on application of a stress:

$$d = \frac{P}{\sigma} \qquad \textbf{(1.1)}$$

where,

P = Polarization

σ = Stress

On the other hand, relaxer $Pb(Mg,Nb)O_3$ (PMN) and $Pb(Zn,Nb)O_3$ (PZN) ceramics are well known as typical electrostrictive materials. Commercially available PZT-based soft piezoelectric ceramics (Cat. No. N10, NEC-Tokin Inc., Sendai, Japan) and laboratory-made PMN and $0.8Pb(Mg_{1/3}Nb_{2/3})O_3–0.2PbTiO_3$ (PMN–PT) ceramics are also being used for various applications (Hayakawa, 1991; Izumi et al., 2012; Tashiro et al., 2003; Tingley, 2013; Tressler et al., 1998).

Nature of the piezoelectric effect is closely related to the occurrence of electric dipole moments in solids. Latter, may either be induced for ions on crystal lattice sites with asymmetric charge surroundings (as in $BaTiO_3$ and PZTs) or may directly be carried by molecular groups (as in cane sugar). Dipole density or polarization (dimensionality - Cm/m^3) may easily be calculated for crystals by summing up the dipole moments per volume of crystallographic unit cell. As every dipole is a vector, the dipole density 'P' is a vector field. Dipoles near each other tend to be aligned in regions called Weiss domains. These domains are usually randomly oriented, but can be aligned using the process of poling (not the same as magnetic poling), a process by which a strong electric field is applied across the material, usually at elevated temperatures. Not all piezoelectric materials can be poled of decisive importance, for the piezoelectric effect is the change of polarization 'P', when applying a mechanical stress. This might either be caused by a re-configuration of the dipole-inducing surroundings or by re-orientation of molecular dipole moments under the influence of external stress. Piezoelectricity may then manifest into a variation of the polarization strength, its direction or both, with the details depending on:

1. The orientation of 'P' within the crystal
2. Crystal symmetry
3. Applied mechanical stress

Alteration in 'P' appears as a variation of surface charge density upon the crystal faces, i.e. variation of electrical field extending between faces, since units of surface charge density and polarization are same:

$$[C/m^2] = [Cm/m^3] \text{ ----------} \quad \textbf{(1.2)}$$

where,

C = Coulomb
m = meter

Cm = Coulomb meter

However, piezoelectricity is not caused by a change in charge density on the surface, but by dipole density in the bulk. For example, a $1cm^3$ cube of quartz with 2kN of applied force can produce a voltage of 12,500 V (Curie and Curie, 1881).

Mechanical compression or tension in a poled piezoelectric ceramic element changes the dipole moment, creating a voltage. Compression along the direction of polarization, or tension perpendicular to the direction of polarization, generates voltage of the same polarity as the poling voltage (Fig. 1.5).

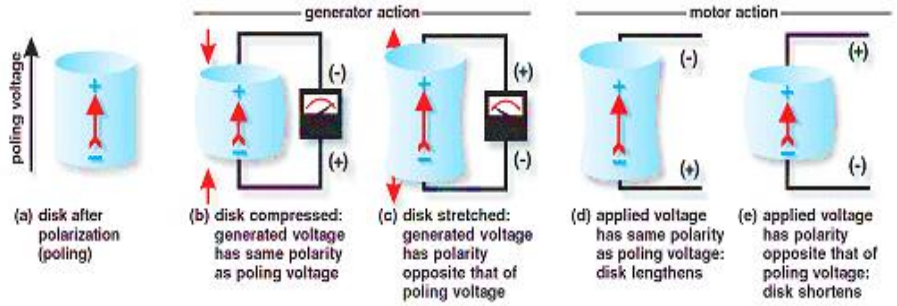

Fig. 1.5 Working mechanism of simple piezo transducer (Henderson, 2002)

Piezoelectric effect is a reversible process, in that materials exhibit the internal generation of electrical charge resulting from an applied mechanical force (Drobny, 2012). Energy generated from piezo transducer can be stored using a DC capacitor with the help of rectifier circuitry. Modern VLSI design towards the application of ambient-powered DSP and remote sensing devices creates an opportunity for the utilization of novel energy sources. Self-powered systems using ambient energy become practical alternatives, replacing the need for batteries (Amirtharajah and Chandrakasan, 1998). Several ambient sources have already been exploited in the ongoing generation. These include solar, electromagnetic, RF powered ID tags, inductively powered smart cards, or non-invasive pacemaker battery recharging, thermal gradients, fluid flow, energy produced by human body, action of gravitational fields and electric power generation from cactus and opentia plants (Bouvier et al., 1997; Damjanovic and Newnham, 1992; Friedman et al., 1997; Geddes, 1990; Hayakawa, 1991; Ikeda, 1996; Meninger et al., 2001; Starner, 1996; Williams and Yates, 1996).

In recent years, the demand for long battery life in portable systems and heat removal in non-portable ones has been increased in low power VLSI systems. Ambient energy is energy that is available in environment of the system and is not stored explicitly, for example, in a battery. Battery operated portable systems have a limited operating life, while a system operated by ambient source has an infinite life time. Power from ambient sources becomes advantageous for the long-lived systems, since the replacement of battery is uncertain. Numerous methodologies were proposed to abolish the need of battery in portable systems (Amirtharajah and Chandrakasan, 1998; Meninger et al., 2001; Newnham et al., 1997). The proposed research, therefore, is relevant in this context.

1.2 Seismographs

Many types of seismographs are available today. Each performs the basic function of measuring ground motion, but supplies much additional information. Most seismographs are equipped with meters that register and hold the maximum value of vibration components and sound level. Other seismographs are equipped to produce a printout which gives variety of information such as maximum value for each component, frequency of vibration for the maximum value, maximum displacement, maximum acceleration, vector sum, and sound level. Blast information such as date, blast number, time, location, job designation, and other pertinent information can also be added to the printout (Konya and Walter, 1990).

Normally, a seismograph record shows the following information (Fig. 1.6):

- Three lines or traces, one for each vibration component. A fourth line or trace for the acoustic or sound level.
- A calibration signal for each trace.
- Timing lines which appear as vertical lines running across all or part of the record.

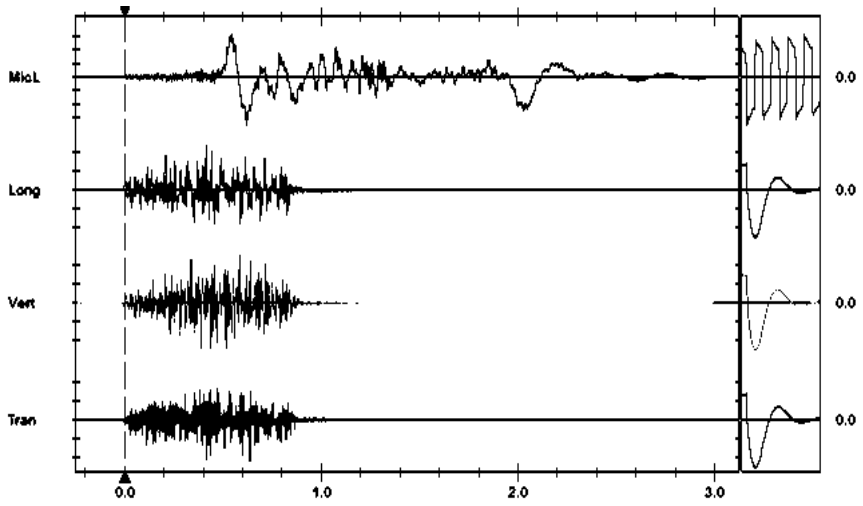

Fig. 1.6 A seismograph record

Application of piezo generator in blast field in the place of seismograph enables to generate electrical energy which is proportional to the seismic energy induced from a blast at given point. Electrical energy generated, if sufficient, can be used for running low powered VLSI systems as ambient power source. It is expected that obtained electrical energy will be in direct proportion to input ground vibration intensity. Hence, the amount of voltage which is acquired by piezo generator may be calibrated in such a way to obtain intensity of blast vibration with the developed piezo generator model.

An attempt has been made in the present research work to assess the seismic energy dissipated at different distances from the blast site and tap the electrical energy from blast induced ground vibrations. Major objectives of proposed research work are as follows:

1. To assess and analyse the seismic energy dissipated by ground vibrations at specified distances as captured by blast vibration monitors using signal processing software in different formations and to assess the relationship between seismic energy and fragmentation.
2. To develop a Piezo generator circuit that converts undesirable ground vibrations into useful electrical energy, as an innovative renewable energy generation technique by utilizing the wasted blast energy.

3. To compare the electrical output generated from the piezo generator with the seismic data generated from blast vibration monitors and assess the relationship between these two.
4. To carry out numerical modelling by simulating the blast conditions for assessing the seismic energy component resulting from a given blast as a parametric study, and correlate the results with the data generated from vibration monitoring and piezo electric generator.
5. To assess the potential of generating electrical energy from ground vibrations resulting from blasting operations, which may be used for running low powered VLSI based circuits or ambient power based loads and in particular, for finding intensity of ground vibrations on par with traditional vibration monitors.

1.3 Statement of Problem

Major aim of a mine blast is to get maximum fragmentation of rock mass with minimum effect on surroundings. Also, it is expected to get lesser ground vibrations and noise. Proper adjustment of blast variables creates the most favorable conditions for efficient utilization of explosive energy. In addition, the efficient management of explosive energy and on-site conditions have a direct influence on the economics of blasting, the rate of productivity through better fragmentation, and the reduction of ground vibrations, air blast and fly rock. During the blast, some of the explosive energy is being utilized for extraction of rock mass and much of energy is being wasted in the form of ground vibrations, which cannot be retractable for any other use.

Proposed research work focuses on the assessment and estimation of seismic energy as monitored by seismographs and analyzed with signal processing software for assessing blast performance, in particular, in four different rock formations – Limestone, Coal, Sandstone and Granite. Also, generation of electrical energy using undesirable ground vibrations, with developed piezo generator model was accomplished, in all four formations. Further, comparison of the obtained electrical energy (output) with the seismic energy (input) of ground vibrations was carried out. Various blasts were carried out in different geo-mining conditions for finding the

efficiency of piezo generator developed. Parametric studies were carried out using FEM based numerical modelling technique for the assessment of seismic energy component resulting from a given blast. Also, correlation of model results with the data generated from vibration monitors and piezo electric generator was accomplished.

1.4 Organization of the Thesis

The thesis is divided into five major chapters for disseminating the significant information.

Chapter – 1 gives a brief introduction to the research topic giving the background information. Introduction includes various types of blast induced ground vibrations, seismic energy, piezo-gen based electrical energy, seismographs and objectives of the research study. Further the statement of the problem is also defined.

Chapter – 2 provides a comprehensive review of literature. In the light of literature review, the need and scope of the present research study has been highlighted. It includes review of related works and developments carried out by various researchers in this area of research. Literature related to studies describing the ground vibrations, seismic energy, fragmentation analysis, high speed videography, piezo-gen technique, regression analysis and numerical modelling are presented in this chapter.

Chapter – 3 deals with the methodology adopted for the research study and field investigations. Field instrumentation adopted and details of the field investigations carried out in four different rock formations are described. MATLAB based regression analysis carried out in all four formations is discussed in the chapter. Also, numerical modelling study using Python script based Simulia Abaqus/CAE FEM software for simulation and analysis of different blasts as a parametric study is discussed in this chapter.

Chapter – 4 describes the results obtained from various field investigations and MATLAB based regression analysis. The analysis of results is also presented in this

Chapter. Further, numerical modelling results and comparison with field results is presented.

Chapter – 5 presents significant conclusions drawn from the research study and recommendations for future work.

A novel approach directing to the generation of electrical energy using piezo sensors by tapping electrical voltage from undesirable ground vibrations generated from blasts in mines, as an innovation is presented in the thesis.

CHAPTER 2

LITERATURE REVIEW

Main objectives of rock blasting are to fragment the strata for achieving required yield with desirable fragmentation and minimum side effects. Though the side effects like ground vibrations, noise, fly rock, etc. cannot be avoided completely, these can be minimized by selecting suitable explosives, initiating devices and using proper blast design in given geo-mining conditions. Higher intensity of unwanted results indicates improper utilization of explosive energy in fragmenting the rock mass, as the total amount of energy released by unit quantity of explosive is constant. Earlier research findings established that in a properly designed blast, around 15 to 20 per cent of the energy is found to do useful work and the remaining is wasted in generating side detrimental effects. Ineffective utilization of energy not only results in improper fragmentation, but also generates side effects like venting out of explosive energy from stemming zone, more generation of ground vibrations and more seismic energy, etc.

Energy released by an explosive, can be grouped into gaseous energy and shock energy, working on the surrounding strata resulting in fragmenting the medium through various rock breakage mechanisms. Some of these mechanisms are responsible for - (a) fracturing energy, that ultimately is responsible for creating new surfaces in the rock fragments, (b) energy transferred in the form of shock waves into the rock mass propagating as seismic waves or ground vibrations beyond the fragmentation zone, and (c) energy to displace the fragmented material and form the muck pile, that appears as kinetic energy. This energy partitioning is related to the characteristics of explosives and the strata, and to some extent to the blast geometry.

Normal approach to the assessment of blast results or explosives selection by the mining industry has been the conventional powder factor or percentage of secondary blasting. In some cases, where ground vibrations are of concern, the intensity in terms of PPV is measured additionally, and the concerned blast is rated as good or bad. Not

much attention has been paid to analyze blast results based on the energy, in terms of its utilization or wastage.

In general, in a properly designed blast, around a meager 15 per cent of the energy is doing useful work and the remaining is wasted in generating side detrimental effects (Hagan, 1973). Berta (1985) approximately estimated the distribution of utilization of total explosive energy into following categories:

Fracture in-situ	: <1 %
Breakage	: 15%
Displacement	: 4%
Crushing in the vicinity of the hole	: 1.5 to 2%
Fly-rock	: <1%
Deformation of solid rock behind the shot	: <1%
Ground vibrations	: 40%
Air blast/noise	: 38 to 39 %

From the above, it is very clear that even one percentage of additional positive utilization of explosive energy is a big contribution to the industry.

Selection of explosives purely based on powder factor is not technically fully justifiable, as it takes into consideration only the quantity of muck pile generated, but not the quality of fragmentation (fragmentation size) and new surface area created, which are indicative of breakage effected by explosive energy in given geological conditions and for a given blast design.

It is aimed through this research to analyze the blast performance in terms of ground vibrations and seismic energy using field instrumentation, indicating effectiveness of explosive energy and to tap the electrical energy from blast induced ground vibrations. Later, it is intended to compare the seismic data with electrical data. Finally, FEA based numerical modelling is planned to carry out based on field studies, to predict the ground vibration intensity, if possible.

2.1 Blast Performance

Blasting is carried out to excavate hard rock / mineral deposit / waste overburden in mining projects. Every blast yields some unwanted results along with the required fragmentation. Therefore, blast results need to be assessed for both positive and negative effects.

A good blast could be defined as a blast that results in optimum fragmentation with minimum side effects like ground vibrations, without any toe and backbreaks. Normally, following aspects should be looked into for assessing blast results:

- Fragmentation
- Muck pile profile and displacement
- Hard toe and un-diggable areas
- Backbreak and overbreak
- Ground vibrations and air blast
- Fly rock

2.2 Fragmentation

The term fragmentation refers to post blast size distribution of rock mass. In other way, fragmentation means economically significant size range of a definable volume. Optimum blasting has been suggested as obtaining proper degree of fragmentation to achieve the lowest combined cost of drilling, blasting, loading, hauling and crushing (MacKenzie, 1966). Da Gama and Jimeno (1993) indicated that at optimum fragmentation, environmental impacts are also minimum.

Fragmentation obtained in the blasting process influences the downstream costs like loading, transportation, processing, etc. (Fig. 2.1). Fragment size should be suitable for further handling and processing equipment in order to reduce the total production cost. Various parameters influencing the fragmentation are rock properties, explosive properties, which include initiating devices and blast geometry parameters.

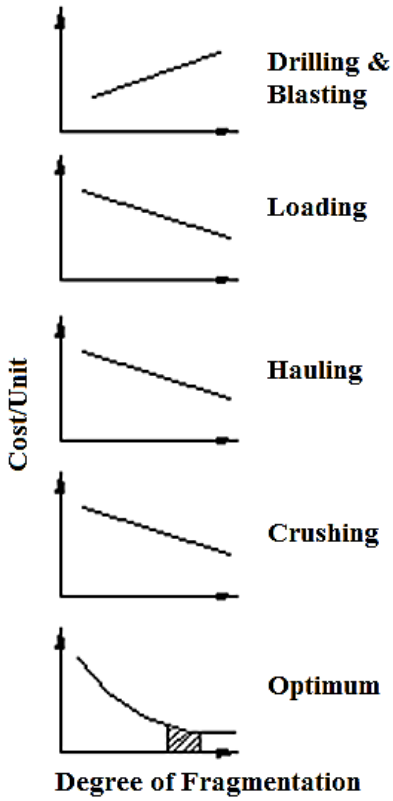

Fig. 2.1 Effect of fragmentation on downstream operations (MacKenzie, 1966)

There is considerable evidence that blasting does affect crushing and grinding results (Eloranta, 1995; Paley and Kojovic, 2001). The use of greater energy input in blasting unit operations will often be less costly than expanding the energy into downstream operations (Workman and Eloranta, 2003). Improved fragmentation accomplished in blasting not only reduces the work load in crushing and grinding, but also improves loading rates and reduces maintenance in the mine (Eloranta, 1995).

2.3 Fragmentation Analysis

Fragmentation analysis methods to quantify the size distribution of muck pile are grouped as direct and indirect methods. There is no universally accepted method of fragmentation analysis till now. Various fragmentation analysis methods are:

Direct methods

- Screening / Sieving

Indirect methods

- Observational methods /physical inspection
- Boulder count method
- Explosive consumption in secondary blasting

- Shovel cycle time
- Power consumption of excavator
- Power consumption of crusher
- Bridging delay at crusher
- Digital image processing of muck pile

2.3.1 Screening / Sieving

Among the above, the direct method, i.e. sieving / screening is a reliable, accurate and unbiased method of evaluating fragmentation quantitatively. A complete sieve analysis requires that the entire muck pile be screened. This technique is frequently adopted in laboratory and reduced scale studies, but in production blasts, sieving is not practicable.

2.3.2 Observational method

It depends on experience and common sense of the expert, and is a widely used technique to assess the blast performance for approximation. Blasting engineer assesses the fragmentation and other blasting results like toe formation and backbreak subjectively. This method is not a scientific method as it does not give any information about size distribution (Kemeny et al., 1993; Wu and Kemeny, 1992).

2.3.3 Boulder count method

In this method, after the muck pile removal by shovel–dumper combination, boulders which were left by shovel (which cannot be handled by the shovel) are counted manually and an index is prepared for the number of boulders produced per 1000t of material (Sastry and Ram Chandar, 2004). A higher index denotes more boulders and poor fragmentation and vice versa.

2.3.4 Explosive consumption in secondary blasting

Boulders produced in primary blasting need to be further fragmented in secondary blasting to suit the loading operations. In general, the quantity of explosive used in secondary blasting gives an indication of effectiveness of primary blasting. Consumption of higher quantity of explosive in secondary blasting is due to improper (more boulders) fragmentation in primary blasting and vice versa.

2.3.5 Digital image processing

Generally, the most popular method to quantify the fragmentation is determination of size distribution using digital image processing technique. This is cheaper, consumes less time, and does not interrupt production process at the site. This is a more reliable method after sieve analysis. This technique involves the usage of reliable software to quantify the geometric aspects of images in two dimensions like area, diameter, perimeter of fragments, number of fragments, etc. It involves the capturing of images of muck pile in the field, keeping a calibrator on the muck pile (Fig. 2.2). Images are subsequently imported to the software either by photographic / video-graphic pictures. Later, the images are enhanced / reduced, contrasted depending upon facilities available in the software, to finally give the size distribution of fragments (Higgins et al., 1999; Kemeny et al., 1999). Output could be in the form of Rossin-Rammler distribution curve or data in a tabular form, which varies from software to software. Some of the commercial software packages developed based on image processing technique are TUCIPS, FRAGSCAN, WIPFRAG, FRAGALYST, SPLIT, etc. WipFrag is used for the research work and is described below.

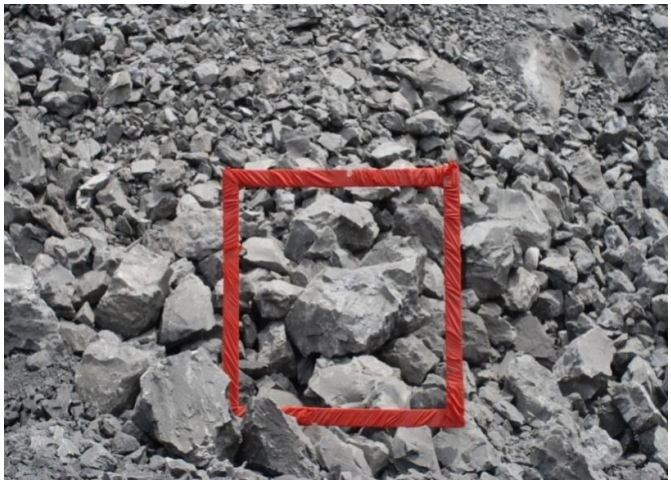

Fig. 2.2 Fragmented muck pile captured with 0.5m x 0.5m calibrator

2.3.6 WipFrag

This was developed by John A. Franklin and Norbert H. Maerz, in collaboration with researchers from the University of Waterloo and with industrial groups, with an understanding of blasting, mining methods, geotechnical influences, and mineral processing requirements. Using digital image analysis of photographs of rock fragments and videotape images with granulometry system, grain size distribution

may be obtained by WipFrag. Photographic images are digitized using WipFrag from slides, prints or negatives, using a desktop copy stand. In order to overcome size limitations inherent with a single image, WipFrag has the function for zoom-merge analysis. Therefore, combined analysis of images taken at different scales of observation may be analyzed. In addition, using Edge Detection Variables (EDV), fragment boundaries are analyzed efficiently, and manual editing can improve edge detection process (Maerz et al., 1996). Fig. 2.3a shows fragmentation photos taken with known size calibrator. Fig. 2.3b shows the intermediate step in processing of fragmentation images, and typical fragmentation distribution curve obtained for each processed image.

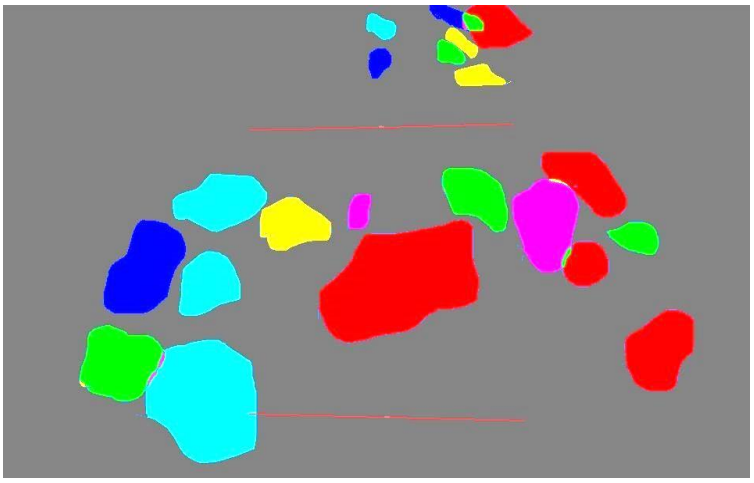

(a)

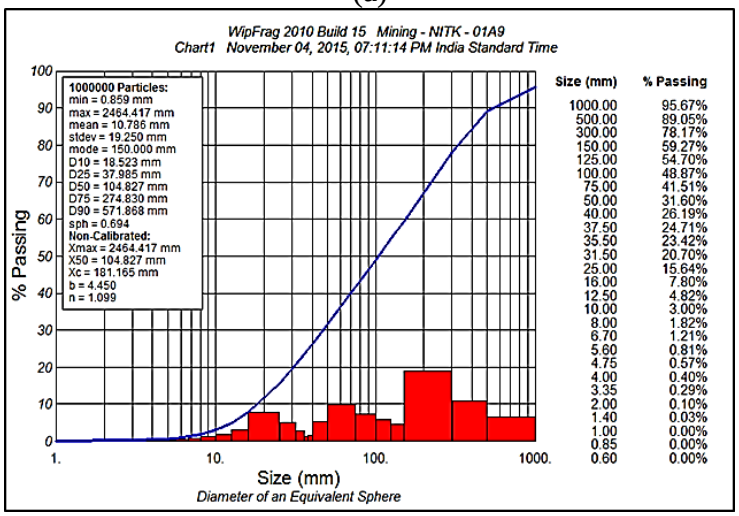

(b)

(a) Processing of the captured image **(b)** Fragmentation distribution curve obtained

Fig. 2.3 Fragmentation analysis of a muckpile using Wipfrag software

If fragment size uniformity is high and thickness of layer is low, image-processing program is useful and efficient. However, if the uniformity of fragment size is low and thickness of layer is significant, the user should be careful in accepting the results of image analysis (Cunningham, 1996). It is very difficult and hard to obtain accurate estimates of rock fragmentation after blasting. Following are the main reasons for error in using image analysis programs (Liu and Tran, 1996):

- Image analysis can only process what can be seen with the eye.
- Image analysis programs cannot take into account the internal rock mass. So the sampling strategies should be carefully considered.
- Analyzed particle size can be over-divided or combined, i.e. larger particles can be divided into smaller particles and smaller particles can be grouped into larger particles. This is a common problem in all image-processing programs.
- Fine particles can be underestimated especially.

In order to reduce these errors, image-sampling strategy should be effective and for each image analysis, manual editing needs to be carried out.

2.4 Ground Vibrations

Gaseous pressure generated by explosive in blastholes upon initiation of explosive charges produces shock waves in the surrounding strata. Rock fragmentation takes place in the zone, where shock energy is effective and intensity of which is sufficient to cause breakage of rock mass due to various rock breakage mechanisms. However, beyond the fragmentation zone, shock waves travel further into rock mass carrying certain amount of energy. This energy is insufficient to cause any permanent deformation in rock mass and is sufficient to oscillate the ground particles. These waves in the seismic zone are denoted as seismic waves or ground vibrations. Energy carried by these waves is known as seismic energy. Two basic types of waves are generated (Anon, 2007). First ones are body waves, which travel through the interior of the ground, and represented by Longitudinal and Transverse waves (Fig. 2.4).

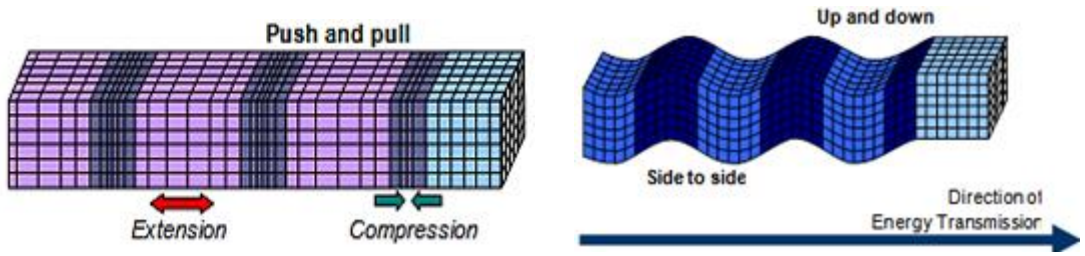

(a) (b)

(a) Longitudinal waves **(b)** Transverse waves

Fig. 2.4 Body waves

Second ones are surface waves, produced when body waves impinge upon a free surface or the latter's equilibrium is suddenly disturbed and are represented by vertical and horizontal shear waves – with back and forth motion, identified by Love waves or Rayleigh waves (Fig. 2.5).

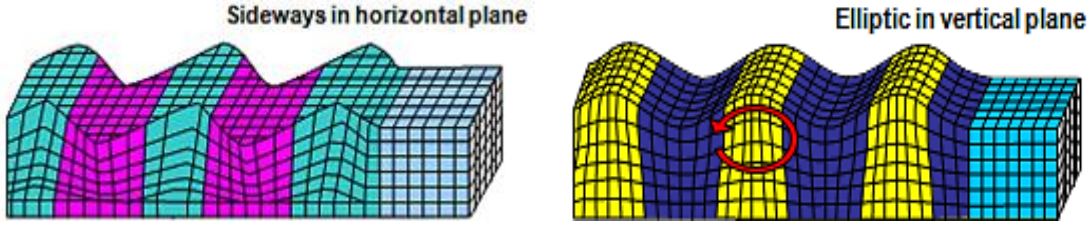

(a) (b)

(a) Love waves **(b)** Rayleigh waves

Fig. 2.5 Surface waves

All these waves are characterized by an exponential decrease in particle oscillation amplitude as distance from the energy source increases. Principle concerns of the most ground vibration studies are quantity of explosive and distance from the source of a blast to the measuring device (Duvall et al., 1963; Nicholls et al., 1971). Ground vibrations are generally quantified as displacements that vary with time, accelerations, or particle velocities at particular ground locations (Duvall and Fogelson, 1962). Currently, the most widely accepted measurement of ground vibration is the Peak Particle Velocity (PPV), defined as the speed at which earth particle moves (Anon, 2016b). Based on the field studies, many researchers have proposed various empirical formulae to predict the intensity of ground vibrations.

2.4.1 Prediction of ground vibrations

The propagation equation suggested by Morris (1950) is as follows:

$$A = K (Q^{0.5}/ D) \quad \text{----------} \quad \textbf{(2.1)}$$

where,

A = Maximum particle amplitude, mm
Q = Explosive charge weight, kg
K = Characteristic constant of the site which varies from 0.57 to 3.4
D = Distance from the blast to recording station, m

Habberjam and Whetton (1952) suggested a higher power for the charge weight in the above formula as $Q^{0.85}$. Assuming cylindrical explosive geometry for long cylindrical charges, Duvall and Fogelson (1962), Duvall et al. (1963), Daemen (1983), have concluded that any linear dimension should scale with the square root of charge weight. Blasts should be scaled to equivalent distance or scaled distance, which is defined as the actual distance (D) divided by square root of charge weight (Q). Corresponding relationship assumes the following form:

$$V = K (D/Q^{0.5})^{-B} \quad \text{----------} \quad \textbf{(2.2)}$$

where,

B = Slope of the best-fit straight line of V (peak particle velocity) versus $(D/Q^{0.5})$ plot on log-log scale
K = Intercept on Y-axis when $(D/Q^{0.5}) = 1$

Devine and Duvall (1963) from USBM suggested the following equation to predict ground vibration velocity:

$$V = K (DS/Q^{0.5})^{-n} \quad \text{----------} \quad \textbf{(2.3)}$$

where,

K and n are constants

Langefors et al. (1958) suggested the following relationship for various charge levels to estimate the peak particle velocity as:

$$V = K [(D/Q^{3/2})]^{B/2} \quad \text{----------} \quad \textbf{(2.4)}$$

Attewell (1964), Davies et al. (1964), Birch and Chaffer (1983), Daemen (1983) considered no particular charge symmetry and used a general equation as follows:

$$V = K D^{-B} Q^{A} \quad \text{----------} \quad \textbf{(2.5)}$$

where,

K, A, B are empirical constants

Holmberg and Persson (1978) suggested a general equation to predict the intensity of ground vibrations as:

$$V = K Q^a \times DS^b \quad \text{----------} \quad \textbf{(2.6)}$$

where,

K, a, b are empirical constants to be estimated for a site

2.5 Explosive Energy

Explosive energy is rated in a number of ways, obtained either from theoretical calculations or from experimental tests. However, it is very difficult to determine the amount of explosive energy transferred to the rock mass and converted into efficient work in the application of rock blasting. Although, measurement of some of the effects of explosive energy in rock is customary (vibration, fragmentation and to some extent rock movement), they are usually conducted for blast control purpose, and the results are rarely cast in terms of their energy content. Reason for this may be that, it is not the energy consumption in this or that phenomenon that matters, but rather the end results, i.e. degree of fragmentation, throw and ground vibration levels. Data and estimations on energy components in rock blasting are thus limited to a few researchers. Berta (1985), Spathis (1999) and Ouchterlony et al. (2003) estimated the amount of energy transformed into kinetic energy of the rock, fracture generation and seismic waves.

Energy released by an explosive, can be grouped into gaseous energy and shock energy, working on the surrounding strata resulting in fragmenting the medium through various breakage mechanisms. Some of these mechanisms are responsible for - (a) fracturing energy, that ultimately is responsible for creating new surfaces in the rock fragments, (b) energy transferred as shock waves into the rock mass propagating as seismic waves or ground vibrations beyond the fragmentation zone, and (c) energy to displace the fragmented material and form the muck pile, that appears as kinetic energy. This energy partitioning is related to the characteristics of explosives and the strata, and to some extent to the blast geometry. Energy balance of the blast can thus be expressed as (Spathis, 1999):

$$EE = EF + ES + EK + ENM \quad \text{----------} \quad \textbf{(2.7)}$$

where,

EE = Explosive energy
EF = Fragmentation energy
ES = Seismic energy
EK = Kinetic energy
ENM = Energy forms not measured

2.5.1 Fragmentation energy

This is a specific amount of energy that is required to create a new fracture surface. If GF is energy per unit surface, the fragmentation energy can thus be calculated using the following equation (Grady, 1982):

EF = AF*GF ---------- **(2.8)**

where,

AF = Surface area of the fragments generated by the blast
GF = Specific fracture energy

Specific fracture energy (GF) can be calculated from experimental fragmentation tests under a controlled energy input by means of mechanical combination, leading to the Rittinger coefficient (crushing efficiency, the surface area created per unit energy input), or derived from material properties of the rock - the fracture toughness and the elastic modulus. For estimation of the fragmentation efficiency by blasting, where a great amount of fines are produced, the inverse of Rittinger coefficient is used as specific fracture energy. Crushing efficiency concept assumes that such efficiency is constant for all fragment sizes.

2.5.2 Seismic energy

Energy transferred into the strata in the form of seismic waves is calculated as integral of energy flow past a control surface at a given distance from the blast. Energy flux (power or rate of energy dissipated per unit area) is the scalar product of stress at the surface and particle velocity (Achenbach, 2012). Calculations of seismic energy and its comparison with explosive energy have been reported by Howell and Budenstein (1955), Fogelson et al. (1959), Berg and Cook (1961), Nicholls (1962), Atchison (1968), and more recently by Hinzen (1998). Berta (1985) attempted to use some of the energy concepts in his principles of blast design, though this is seldom used in practice.

The seismic energy dissipated by a ground vibration event at a given distance from blast site could be a critical component in assessing performance of blasts, and it could be correlated with the fragmentation achieved in a given blast.

2.6 High Speed Videography

During the blast, events occur so rapidly that human eye cannot judge the performance of individual elements of blast progress and elements involved like venting out of gaseous energy, performance of delays / initiation, burden rock movement, etc. This requires blasting engineer to redesign the blast without a complete understanding of the dynamics involved. High speed videography can provide an extended time base to study these elements. Major use of high speed motion picture studies of individual events of a blasting process have been well documented (Blair, 1960; Chiappetta and Mammele, 1988; Winzer et al., 1979). Information derived from videos can help the blast designer to understand explosive and geological dynamics involved while reducing number of costly field trials necessary to optimize the design and selection of explosives. The process of evaluating a given blast with fixed parameters of high speed motion picture photography includes precise surveying, accurate analysis of video output, and careful cost accounting to determine the most efficient plan for specific location. Following are the information that can be generated by high speed video camera for optimizing the use of explosives for overburden or waste excavation incorporating motion picture photography and computer-assisted analysis:

- Initial face movement
- Differential face velocity
- Face trajectory
- Range of material cast
- Performance of various explosives types
- Benefit of different primer / booster combinations
- Effects of the delay timing configuration
- Performance of various blast designs
- Gas venting occurrence

High speed motion picture videography coupled with computer-assisted motion picture analysis software is a cost effective tool to fine-tune blast designs and

explosive selection. Response of rock mass to a given blast design and explosive components can be quantified. Once the dynamics of a blast are understood, then appropriate steps can be taken to maximize utilization of explosive energy for a given blast. This process can eliminate many of costly field trials necessary to optimize a blast design. Improvement in blast performance provided by refinement of design using high-speed videography can make the difference between a profitable and non-profitable mine operation.

2.7 Delay Timing

Properly designed delays minimize the superimposition of vibration waveforms generated from successive charges, in turn reducing the severity of ground vibration and also the air blast. Detonating cord is a major source of high frequency pressure pulse. Application of shocktube initiation system for down the hole initiation and also for trunkline or surface initiation has been found to be an effective tool in providing effective delay timing in blast rounds.

According to Hagan and Kennedy (1978), bottom initiation usually results in less noise but slightly higher ground vibration levels. Studies carried out by Sastry and Ram Chandar (2015) revealed that ground vibrations could be better controlled with primer located above grade level. Gupta and Misra (1998) and Spathis (1999) have observed that down the hole shocktube initiation system resulted in lower vibration levels than multi point initiation systems.

Delay intervals between rows may vary from 10ms/m of burden for hard rock to 30ms/m of burden for soft rock (Olofsson, 1990). Initiation sequence in a blast is very important, and is a vital factor to be considered in blast design, since several initiation sequences radically alter effective burden and spacing during the blasting process. It also affects rock movement with respect to face and thereby influences the amount of rock shearing and design boundaries of blast pattern. A systematic release of explosive energy from one hole/row to the other is crucial in maintaining a continuous momentum required for inter-hole/row delay displacements. It has been suggested by earlier researchers that the burden from first row of blastholes should be displaced by

at least one third of the burden distance (1/3 B) before next row of blastholes is fired, for an efficient blast (Fig. 2.6).

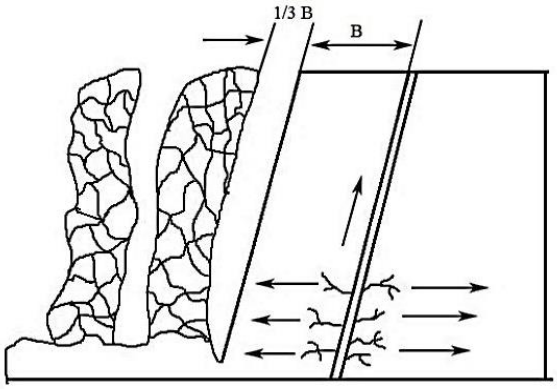

Fig. 2.6 Required burden movement before blasting of next row

Burden rock velocity was calculated for different conditions by tracking down the movement of burden rock mass (Sastry et al., 2015). ProAnalyst software was used for tracking down the burden rock movement, for determining the velocity of rock mass. Based on the burden movement velocity, the minimum delay timing required between rows was analyzed (Table-2.1). Study has shown that as BH/B, Bench height to burden ratio, increasing, the required delay time per metre distance throw of burden rock mass is decreasing. For a BH/B ratio condition of two, the delay time required was determined as 12.5ms per metre, whereas with BH/B value of 3.75 the required delay reduced to 8ms per metre distance. This is because as BH/B is increasing, the bench is becoming less stiff and more flexible resulting in faster movement of burden rock mass.

Table – 2.1 Delay time required between rows based on high speed videography (Sastry et al., 2015)

BH/B* Ratio	**Avg. Burden Velocity (m/s)**	**Delay Time Required (ms/m)**
2.0	79.8	12.5
2.5	95.6	10.5
3.2	100.7	10.0
3.75	127.9	8.0

*BH/B = Bench height to burden ratio

An optimum inter-row delay gives good fragmentation and displacement without cut-offs. Improper delay gives rise to problems of fly rock, ground vibrations, toe and backbreak. For large diameter blastholes, optimum inter-row delay usually varies from about 5ms/m of effective burden for strong massive rocks to about 10ms/m for weak and highly fissured strata (Hagan, 1983). In addition to burden and rock type, Konya and Walter (1990) have suggested delay timing depending on the desired end results based on their priority. The best possible fragmentation can be achieved with delay timing of 10 to 20ms/m of burden. Douglas and James (2000) found that an optimum delay of 2ms/0.6m between holes in a row for massive rock gave improved fragmentation. Optimum fragmentation is achieved at a critical delay. According to Anderson et al. (1985) and Winzer et al. (1983) very short delays (1ms/0.3m) give the poorest fragmentation, but a higher delay in spacing degrades the fragmentation.

Usually, rock or burden response of the blast and the post blast muck pile are also dependent on timing sequence of the blast. Too little time between holes or rows results in a stacked muck pile that is very difficult for the excavator to efficiently excavate. Excessive delay between holes or rows can result in unsafe blasts creating excessive air blast levels and fly rock.

In the selection of initiators, precise number of milliseconds of time between initiator periods is important in rock breakage. Poor timing is a common occurrence, which causes blastholes to malfunction. Initiation timing is one of the most easily corrected causes of malfunctioning of blastholes. Minimum time for design is controlled by the stress wave travel distance in order for radial cracking to begin to develop, contributing to the detachment of rock mass in the vicinity of hole. This detachment forms an internal free face, to which successive detonation will interact with the reflection of stress waves. The minimum timing is therefore,

$$T = 2B_e/C \qquad \text{----------} \qquad \textbf{(2.9)}$$

where,

T = Stress wave travel time, ms
Be = Effective burden, m
C = Sound wave velocity in rock, m/s

Generally, it is assumed that the poor fragmentation is observed at opening and final blastholes in a blast. Work on the delay effect on fragmentation assumes that there is some interaction between the actions of individual boreholes in a multi-hole blast, which improves fragmentation, though basic mechanisms for this interaction remain uncertain. It appears that a single hole shot has an unfavourable partition between the energy used for fragmentation and that wasted in ground vibrations. Blasthole detonated subsequent to the first hole should then generate a ground vibration with lower amplitude than the single hole shot (Douglas and James, 2000). Generally, recommended delay intervals proposed by different researchers are given in Table-2.2.

Table – 2.2 Recommended delay intervals by different researchers
(Bhandari, 1997)

Sl. No.	Researcher	Delay Interval
1	Lang and Favreau, 1972	5 to 8.3ms/m of burden
2	Langefors and Kihlstrom, 1973	2 to 5ms/m of burden
3	Bergmann et al., 1974	3.3 to 6.6ms/m of burden
4	Hagan, 1977	8ms/m of burden for long collars, soft rock and 4ms/m of burden for short collars, massive rock
5	Winzer, 1978	11ms/m of relief between holes and about 28.7ms/m diagonal
6	Anderson et al., 1981	8.4ms/0.3m of effective burden
7	Andrews, 1981	3.3 to 17ms/m of spacing between adjacent holes in a row and 6.6 to 50ms/m between rows

2.8 PIEZOGEN – Tapping Electricity from Vibrations

Piezo-Generation is a new approach to generate electrical energy from the sensing cum converting equipment called piezo sensor / piezo buzzer. It mainly works on a principle of Piezo electric effect, which is creating pressure energy on a crystalline material viz., quartz crystal to generate electricity. Jacques and Pierre Curie discover Piezo electric effect in 1880 during studies into the effect of pressure on the generation of electrical charge by crystals (such as quartz).

Piezo was derived from the Greek “Piezein”, which means to squeeze or press. Piezo material exhibits both “Direct piezo electric effect” as well as ‘Converse piezo electric effect”. Direct piezo electric effect is the production of electricity when crystals are mechanically stressed and converse piezo electric effect is the stress or strain in crystals when an electric potential is applied. Lead zirconate titanate (PZT) crystals are the most common crystals being used.

Piezo effect finds many applications such as production and detection of sound, generation of high voltages, electronic frequency generation, microbalances, and ultra-fine focusing of optical assemblies. It is also the basis of a number of scientific instrumental techniques with atomic resolution, scanning probe microscopes and everyday uses such as push-start propane starter for barbecues.

Piezoelectric materials, (PZT), can be utilized as instruments to convert surrounding vibrations into electricity into that can be preserved and used to control different gadgets. With the modern surge of miniaturized scale gadgets, PZT became a renewable alternative to conventional power sources used to run various types of sensors/actuators, telemetry, and MEMS gadgets.

Piezoelectric materials kind transducers can exchange electrical energy and mechanical movement or force. These materials, in this way, can be utilized as instruments to exchange encompassing movement (typically vibration) into electrical energy. By integrating power-harvesting mechanism, portable systems can be developed that do not require additional power, like battery, which has a restricted working life. Recent findings show the practicality of utilizing PZT gadgets as power sources. Umeda et al. (1996) utilizes a free-falling ball to influence a plate with a piezo-ceramic wafer appended to its underside, and built up an electrical proportional model of the PZT changing mechanical effect to electrical power. Umeda et al. (1997) explored the energy storage characteristics of the PZT with a diode bridge rectifier and a capacitor. Starner (1996) analyzed the energy obtainable from leg movement of a person and reviewed other human movement sources of mechanical energy including circulatory system of blood.

Kymissis et al. (1998) examined application of piezo-film in accession to the ceramic accommodate ability to lighten a bulb with a shoe, exclusively from walking motion. Kimura's US Patent centers acclimatized electrical energy in the form of rectified voltage signal by vibrating a small plate (Kimura, 1998). This accomplishment seems to be motivated by offering abundant energy to run a small transmitter anchored to wandering birds for transmitting their identification cipher and location.

Goldfarb and Jones (1999) presented a linearized paradigm of a PZT assemblage and analyzed the ability of it. It was evident that the best ability of the device occurs in a low frequency range considerably lower than the structural resonance of the PZT stack. Furthermore, Clark and Ramsay (2000) suggested and compared the force attained in the poling direction (d33 mode) with the transverse force (d31 mode) in a PZT generator. Their plan showed that the d31 approach has an advantage by converting applied stress into electricity. They determined that a $1cm^2$ piezo-ceramic powered a MEMS gadget in microwatt range. Elvin et al. (2001) apparently and experimentally investigated the function of self-powered strain sensors with PVDF (Polyvinylidene fluoride). Their half-bridge diode rectifier circuit was integrated with wireless sensor for human bone strain monitoring. Kasyap et al. (2002) devised a new model to characterize the performance of PZT in assorted domains. Their paradigm was absolute experimentally through 1-d anatomy with maximum energy efficiencies of about 20%. Gonzalez et al. (2001) analyzed the anticipation of piezo electric energy conversion, and recommended various mechanisms to increase the magnitude of resultant electrical energy.

According to Ramadass and Chandrakasan (2010), the Piezo effect is classified as follows:

- Direct Effect - Electric polarization produced by mechanical strain, changing its sign with reversal of the strain.
- Converse Effect - Mechanical stress produced by the application of an electric field, changing its sign with reversal of field. All piezo-electric crystals necessarily exhibit both direct and converse effect.

- Longitudinal Effect - Dilatation in a given direction is accompanied by an electric polarization in the same direction.
- Transverse Effect - Dilatation takes places at right angles to the associated electric field.

Types of vibrations

- Longitudinal Vibrations – Commonly occurring in rods or more extended masses in which the motion of the vibrating particles is parallel to the direction of propagation of the wave, which is normal to the wave front. Vibrations of this type are also called "compressional" and "extensional". Longitudinal vibrations may be produced in either fluids or solids (Cady, 1930).
- Transverse Vibrations - The vibrating particles move in a direction parallel to the wave front and normal to the direction of propagation. Familiar examples are electromagnetic radiations, vibrating strings, membranes, and thin plates. With Piezo-electric crystals, transverse (distortional) vibrations may occur when the direction of the electric field is such that the field produces a shearing stress about same axis.
- Flexural Vibrations - These usually occur in elongated plates or bars and are frequently called "transverse" or "lateral" vibrations. They are associated with a bending of the specimen in a certain plane; hence, it is best to refer, for example, to "flexural vibrations in the YZ plane".
- Torsional Vibrations – Vibrations take place in a cylinder or prism between adjacent cross-sections, in a relatively angular displacement (shearing strain) about the axis (Cady, 1930).

2.8.1 Construction of the piezo generator (Piezo-Gen)

Battery powered mobile devices have recently been rapidly gaining widespread popularity. However, they must always be charged before use. If they are equipped with a portable generator which transforms mechanical impact energy during travel to electric energy, batteries can be charged without any electrical power sources. Portable generator consists of a steel ball and a piezoelectric vibrator. Impact of ball against generator produces electrical energy via piezoelectric effect. By introducing a

diode bridge-rectifier and a capacitor, it is able to study the energy storage characteristics both theoretically and experimentally. Efficiency and the stored charge are discussed with respect to the initial voltage and the capacity of the capacitor.

Piezoelectric generators (PEGs) are ingenuous, low-cost, and extremely condensed gadgets. However, they are inherently low-energy accessories with greater energy density of about 1 J/cm^3, which restricted their functionality to particular specific applications. Primitive studies of piezo sensors had two fundamental themes, employing ferroelectric or piezoelectric substances as the functional device and using shock waves to depolarize these materials. Most of the aboriginal studies focused on either individual crystals or ferro-ceramic abstracts such as barium titanate, Tibalit, lithium niobate, and particularly, lead zirconate titanate (PZT).

One of the initial researches made by Besancon et al. (1966) advised the possibility of application of PEGs as pulsed energy sources. Subsequently, others recommended their usefulness as pulsed energy supplies including Ludu et al. (1987), Staines et al. (2003), Shkuratov et al. (2001), and Tkach et al. (2002).

Prishchepenko and his research group apparently hold a lot of acquaintance with PEGs with work commencing from 1983 and research works on going through late 1990s. They have handled their PEGs to power capacitive loads and in aggregation with ferromagnetic generators (Prishchepenko and Shchelkachev, 1996). Initially, it was perceived by Ludu et al. (1987) that these generators function more efficiently with damped shock pressures. They examined the effect of stress on PZT plate and discovered that, with pressure above 50 kbar, the electric current exponentially decreases. They hypothesized the phenomena as internal short-circuit between PZT terminals. Two types of attenuators were acclimated in their experiments: copper-Plexiglas and steel.

To simulate the generation and storage mechanism, we employ an electrical equivalent circuit model as shown in Fig. 2.7, which was established by previous research.

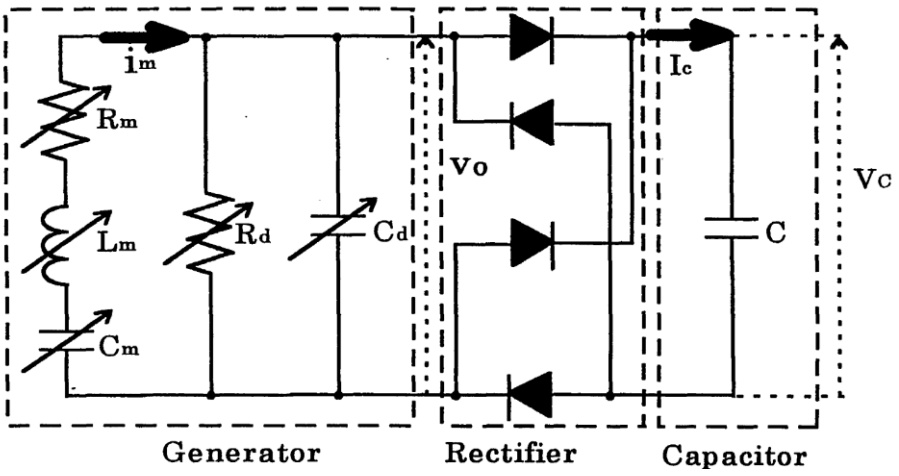

Fig. 2.7 Equivalent circuit of a piezo generator

2.8.2 Working principle of piezo sensor

In a piezoelectric crystal, positive and negative electrical charges are separated, but together symmetrically distributed. This makes the crystal electrically neutral. Each of these sides forms an electric dipole and dipoles near each other tend to be aligned in regions called "Weiss domains". Usually, these domains are randomly oriented, but can be aligned during poling, a process by which a strong electric field is applied across the material, usually at elevated temperatures. When a mechanical stress is applied, this symmetry is disturbed, and the charge asymmetry generates a voltage across the material. In Converse piezoelectric effect, application of an electrical field creates mechanical deformation in the crystal.

Flexible Piezoelectric Materials are attractive for power harvesting applications because of their ability to withstand large amounts of strain. Larger strains provide more mechanical energy available for conversion into electrical energy. A second method of increasing the amount of energy harvested from a piezoelectric sensor is to utilize a more efficient coupling mode.

2.8.3 Types of piezo sensors

Various models and types of piezo transducer systems are depicted in Fig. 2.8:

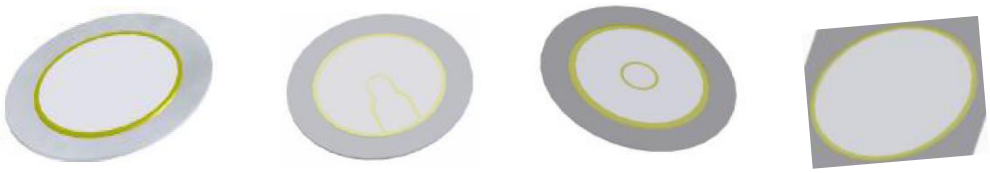

(a) (b) (c) (d)

(a) Two-terminal circle type with stainless steel, brass and nickel alloy metal
(b) Three-terminal circle with brim feedback, brass and stainless steel metal
(c) Three-terminal circle with center feedback, brass and stainless steel metal
(d) Two-terminal square type with nickel alloy metal

Fig. 2.8 Types of piezo transducer systems (Anon, 2016c)

Piezo transducer is to be connected to a connector with two or three wires, accordingly, to tap electrical energy from mechanical vibrations (Fig. 2.9).

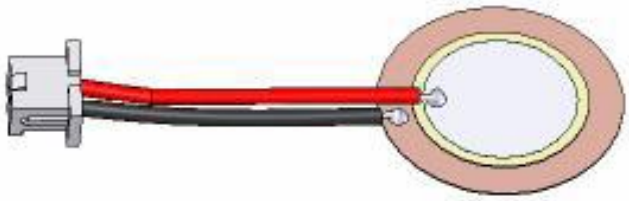

Fig. 2.9 Connection setup of piezo-transducer system (Anon, 2016c)

2.8.4 Applications

The best-known applications of piezo crystals are:

- Direct piezoelectricity of some substances like quartz, can generate potential differences of thousands of volts.
- As chemical and biological sensors, piezoelectric microbalances are used as very sensitive chemical and biological sensors. Piezos are also used as strain gauges (Janssen, 1951).
- Piezo-resistive effect of semiconductors has been used for sensor devices employing all kinds of semiconductor materials such as germanium, polycrystalline silicon, amorphous silicon, and single crystal silicon. Since, nowadays silicon is the material of choice for integrated digital and analog circuits, the use of piezo-resistive silicon devices has been of great interest. It enables the easy integration of stress sensors with Bipolar and CMOS circuits (Doppalapudi et al., 2001). Piezo-resistors made from a Piezo-resistive material are used for measurement of mechanical stress. They are the simplest form of Piezo-resistive devices (Wingrove, 1970).

- In musical instruments, piezoelectric transducers are used in electronic drum pads to detect the impact of the drummer's sticks. It works on Piezo-resistive effect. It is the changing electrical resistance of a material due to applied mechanical stress. Piezo-resistive effect differs from the piezoelectric effect. In contrast to the piezoelectric effect, the Piezo-resistive effect causes a change in resistance and does not produce an electric potential (Tanaka, 1977; Trimarchi, 2008).
- A similar idea is being researched by DARPA (Defense Advanced Research Projects Agency) in the United States in a project called Energy Harvesting (Huang et al., 2006). This includes an attempt to power battlefield equipment by piezoelectric generators embedded in soldiers' boots. However, these energy-harvesting sources by association have an impact on the body. DARPA's effort to harness 1–2 Watts from continuous shoe impact while walking were abandoned due to the impracticality and the discomfort from the additional energy expended by a person wearing the shoes (Ghandi, 2000).
- Automotive engine management systems use a piezoelectric transducer to detect detonation by sampling the vibrations of engine block. Ultrasonic Piezo sensors are used in the detection of acoustic emissions in acoustic emission testing (Carullo and Parvis, 2001).
- A piezoelectric transformer is a type of AC voltage multiplier. Unlike a conventional transformer, which uses magnetic coupling between input and output, the piezoelectric transformer uses acoustic coupling. An input voltage is applied across a short length of a bar of Piezo-ceramic material such as PZT, creating an alternating stress in the bar by the inverse piezoelectric effect and causing the whole bar to vibrate. The vibration frequency is chosen to be the resonant frequency of the block, typically in the 100 kHz to 1 MHz range. A higher output voltage is then generated across another section of the bar by the piezoelectric effect. An extra feature of this transformer is that, by operating it above its resonant frequency, it can be made to appear as an inductive load, which is useful in circuits that require a controlled soft start. These devices can be used in DC-AC inverters to drive cold cathode fluorescent lamps. Piezo transformers are some of the most compact high voltage sources (Flynn and Sanders, 2002).

- Piezoelectric elements are also being used in the detection and generation of sonar waves. Applications include power monitoring in high power applications such as medical treatment, sono-chemistry, industrial processing, etc. (Gautschi, 2002).
- Piezoelectric sensors are used with high frequency sound in ultrasonic transducers for medical ultra sound imaging. For many sensing techniques, the sensor can act as both a sensor and an actuator (Ritter et al., 2002). Ultrasonic transducers, for example, can inject ultrasound waves into the body, receive the returned wave, and convert it to an electrical signal (a voltage).
- This principle is adopted to piezoelectric motors, sound or ultrasound generating devices, and many other products, i.e. when a voltage is applied to the piezoelectric element, it expands some distance X, where motor consequently moves some object by a distance X (Fig. 2.10). Generator action is used in fuel-igniting devices, solid-state batteries, and other products. Motor action is adopted to piezoelectric motors, sound or ultrasound generating devices, and many other products (Arnone et al., 2003).

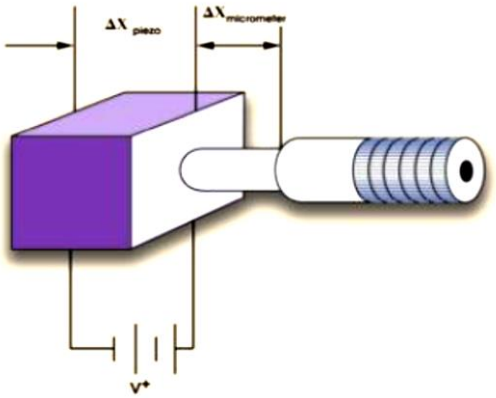

Fig. 2.10 A piezoelectric motor

- A new design, devised by Lucy (2010), a developer at the Technion-Israel Institute of Technology in Haifa, Israel, may hold the key to harnessing the power of moving vehicles to create electricity. Piezoelectric crystals could be used to absorb heavy traffic and convert a 1km stretch of highway into a 400kW power plant, much like Japan's railway project. Innowattech, Abramovich's Haifa-based spin-off company, already announced its intentions of testing the new system as early as January 2009, on a short stretch of highway, about 100m long, in Northern Israel. Critics to the Israeli system say that inserting this type of materials in the surface of

the road would increase the traction force cars would have to exert on the road, as the surface of the street would resemble that of a mud-covered area. This would mean that fuel consumption would increase, though even opponents admit that powering roadside structures would be very beneficial to everyone (Anon, 2008a; Brian, 2011; Valone, 2009).

- Like sensing elements, detection of pressure variations in the form of sound is the most common sensor application, e.g. piezoelectric microphones (Fig. 2.11). Sound waves bend the piezoelectric material, creating a change in voltage.

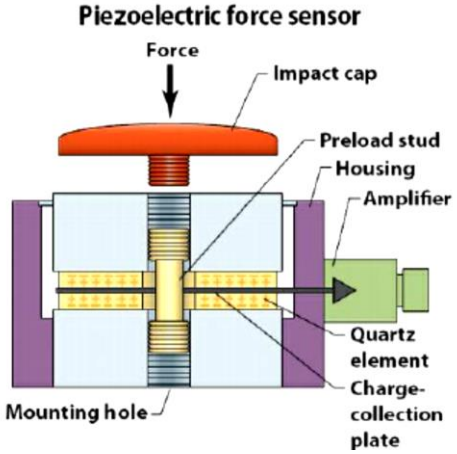

Fig. 2.11 A common piezoelectric sensor (Tingley, 2013)

- The East Japan Railway Company (JR East) has announced that it will outfit the floor of its Tokyo railway station with piezoelectric devices that have the capacity to draw electricity from the steps of those passing in front of ticket booths. For now, the experiment will be fairly limited, covering a small area, but, if successful, the system will be implemented at a large scale, probably in all railway or subway stations in Japan, or even worldwide. The JR East Railway Station had tested piezoelectric energy harvesting in 2008 (Fig. 2.12). A floor mat was made with an array of piezoelectric disks, and roughly, the same product was used in piezoelectric energy harvester. These mats were placed in the automatic ticket readers so that passengers would walk on them when they scan their train tickets. Roughly 10,000 watt-seconds were produced per day from the installation of these piezoelectric floor mats in only six ticket gates. This is not a huge amount of electricity, but if the mats were placed in all ticket gates, could be enough to contribute to the power requirements of the train station such as lighting and power for ticket gates (Tingley, 2013).

Fig. 2.12 Power generating mats in a JR east railway station (Anon, 2008b)

- Other energy harvesting ideas include harvesting the energy from human movements in railway stations or other public places and converting a dance floor to generate electricity. Vibrations from industrial machinery can also be harvested by piezoelectric materials to charge batteries for backup supplies or to power low-power microprocessors and wireless radios (Ambudkar et al., 2014).

2.9 Regression Analysis

In regression analysis, the system fits a straight line to a set of data points for estimation of the correlation between the parameters studied. It may use a series of mathematical equations to find the best possible fitting line to the data points (Anon, 2009). Following power regression equation may be used to calculate the coefficient of correlation and coefficient of determination between two different parameters.

$$Y = K\,(X^{-a/b}) \qquad \text{----------} \qquad \textbf{(2.10)}$$

where,

Y = Output variable
K = Site constant
X = Input variable
a = Geology
b = Critical blast design parameters

2.9.1 Recognition of control variables

Identification of appropriate factors is very important in regression analysis to get a good and accurate fit model. Therefore, ANOVA has become a part of regression

analysis for improving the goodness of fit (gof) between two or more variables (Anon, 2009).

2.9.2 ANOVA

ANOVA is an acronym of Analysis of Variance. A statistical approach estimates control variables influencing the output based on various tests. Fisher originated ANOVA in the year 1918 as the extension of *t* test and *z* test (Fisher, 1930). ANOVA is so-called to be Fisher analysis of variance, which was being used to perform the analysis of variance for different variables between groups (regression parameters) and within the groups (residual parameters), whenever the groups are greater than two. Earlier, the t-test and z-test were commonly used for fit analysis. T-test has a constraint in functionality, i.e. it cannot be applied for more than two groups. Further, ANOVA creates a way to test several null hypotheses at a time (Anon, 2013).

2.9.2.1 Implementation of ANOVA

ANOVA is very commonly used in all goodness of fit (gof) based regression analysis. To compare the influence of different variables on each other, ANOVA may be performed. ANOVA can be implemented in three different ways, viz. one-way ANOVA, two-way ANOVA, and N-way or Multivariate ANOVA, as explained below:

- One-Way: Comparing more than two groups, based on one parameter, i.e. independent variable.
- Two-Way: Comparing more than two groups based on two parameters, i.e. two independent variables. Two-way ANOVA's are useful to understand the influence of one variable / factor on the other, or it will be employed to observe the interaction between two variables / factors. Two-way ANOVA might be useful in both balanced and unbalanced conditions. Sometimes, to solve an unbalanced problem, there will be various methodologies in ANOVA. Such methodologies are: hierarchical approach or type-1 analysis (data may not intend to be unbalanced but there may be some type of hierarchy between the factors), classical experimental design or type-2 analysis (data may not intend to be unbalanced and may not find any hierarchy), and full regression approach or type-3 analysis (data

may be unbalanced because this may be a reflection of population and it may be intended).

- N-Way: Whenever there is a factor comparison, then it is said to be n-way ANOVA, i.e. comparing more than two groups based on 'n' independent parameters / variables.

2.9.3 Approximation of regression coefficients

In view of the orthogonal property, approximated coefficients are not associated with the other, since, least squares method was used to evaluate the minimum variance. In general, regression coefficients of model are processed using a formula, based on least squares, as given below:

$$B_j = X_{ji} Y_i N \quad \text{----------} \quad \textbf{(2.11)}$$

where,

j = 0, 1, 2,…, k
N = Number of trails made
X = Size of the matrix
X_i= Value of a factor
Y_i= Average

Coefficients estimated by using above equation were employed to build models and those models were utilized to develop models for the output variable. Models were determined by applying analysis of variance (ANOVA). Later, F-ratio (Fisher Ratio) was determined and is assessed with the standard calibration values for 95% confidence of the model developed. When the measured values are lesser than values available in F-table, then the model is considered as adequate. F-ratio may be determined by using following equation:

$$F_{ratio} = 2 \text{ x } (S_{ad}^2 / S_y^2) \quad \text{----------} \quad \textbf{(2.12)}$$

where,

S_{ad}^2 = Variance of adequacy or residual variance
S_y^2 = Variance of optimization parameter of reproducibility variance

Variance of adequacy was estimated by the following equation:

$$S_{ad}^2 = \frac{2\,(y_{avg} - y_{pre})^2}{DOF} \quad \text{----------} \quad \textbf{(2.13)}$$

where,

y_{avg} = Value of response predicted
DOF = Degree of freedom and is equal to (n-(K+1))

N = No. of field experimental trials
K = No. of independent variables

Further, Variance of optimization parameter of reproducibility variance was estimated by the following equation:

$$S_y^2 = \frac{2\,(y_1 - y_{avg})^2}{DOF} \quad \text{----------} \quad \textbf{(2.14)}$$

where,

y_{avg} = Average of response observed
y_1 = Other of the values of response parameter
DOF= Degree of freedom is equal to the number of experimental runs

2.9.4 Standard table (F-Ratio)

A ratio was developed in statistical analysis that is very appropriate for testing a hypothesis on adequacy of a model. There is flexibility with F-Ratio in effectively reducing the testing hypothesis to compare N tabulated value.

2.9.4.1 Construction of F-table

Generally, columns are related to a definite number of degrees of freedom, DOF_1, and rows for the denominator, DOF_2. Critical values of F-ratio are found at corresponding rows and columns. A significance level of 5% (confidence level of 95%) is used in all general technical problems. Standard F-table with values of the F-ratio at significance level of 5% is shown in Table-2.3.

Table – 2.3 Values of F- ratio at 5% significance level

	1	**2**	**3**	**4**	**5**	**6**	**12**	**24**
1	164.4	199.5	215.7	224.6	230.2	234.0	244.9	249.0
2	18.5	19.2	19.3	19.3	19.3	19.4	19.4	19.4
3	10.1	9.6	9.3	9.1	9.0	8.9	8.7	8.7
4	7.7	6.9	6.6	6.4	6.3	6.2	5.9	5.8
5	6.6	5.8	5.4	5.2	5.1	5.0	4.7	4.5
6	6.0	5.1	4.8	4.5	4.4	4.3	4.0	3.8
7	5.5	4.7	4.4	4.1	4.0	3.9	3.6	3.4
8	5.3	4.5	4.1	3.8	3.7	3.6	3.3	3.1
9	5.1	4.3	3.9	3.6	3.5	3.2	2.9	2.7
10	5.0	4.1	3.7	3.5	3.3	3.2	2.9	2.7
11	4.8	4.0	3.6	3.4	3.2	3.0	2.9	2.5
12	4.8	3.9	3.5	3.3	3.1	3.0	2.7	2.5
13	4.7	3.8	3.4	3.2	3.0	2.9	2.6	2.4
14	4.6	3.7	3.3	3.1	3.0	2.9	2.5	2.3
15	4.5	3.7	3.3	3.1	2.0	2.8	2.5	2.3
16	4.5	3.6	3.2	3.0	2.9	2.7	2.4	2.2
17	4.5	3.6	3.2	2.9	2.8	2.7	2.4	2.2

	1	2	3	4	5	6	12	24
18	4.4	3.6	3.2	2.9	2.8	2.7	2.3	2.1
19	4.4	3.5	3.1	2.9	2.7	2.6	2.3	2.1
20	4.4	3.5	3.1	2.9	2.7	2.6	2.3	2.1
22	4.3	3.4	3.1	2.8	2.7	2.6	2.2	2.0
24	4.3	3.4	3.0	2.8	2.6	2.5	2.2	2.0
26	4.2	3.4	3.0	2.7	2.6	2.5	2.2	2.0
28	4.2	3.3	3.0	2.7	2.6	2.4	2.1	1.0
30	4.2	3.3	2.9	2.7	2.5	2.4	2.1	1.9
40	4.1	3.2	2.9	2.6	2.5	2.3	2.0	1.8
60	4.0	3.2	2.8	2.5	2.4	2.3	1.9	1.7
120	3.9	3.1	2.7	2.5	2.3	2.2	1.8	1.6

2.9.5 Development of statistical model

Final statistical model is established by considering significant coefficients from ANOVA statistical analysis. Values predicted by a model are to be verified by field investigation results to obtain satisfactory results. Then the models may be used for drawing graphs and analyzing results with predicted values.

2.10 Numerical Modelling

Pre-processing of ABAQUS / CAE (Computer-Aided Engineering) in python script and GUI (Graphical User Interface) may be used for carrying out of numerical modelling as a parametric study of field investigations (Anon, 2012a; b, 2015; Khennane, 2013; McMillan, 2013; Puri, 2011; Wierszycki and Sielicki, 2012; Xiaoguang, 2011; Yang and Turcotte, 1994; Yang, 1997).

2.10.1 Methods of analysis in Abaqus

- Interactive mode
  - To create an FE model and analysis using GUI
  - Advantage: Automatic discretization and no need to remember commands
  - Disadvantage: No automatic procedures for changing model or parameters
- Python script
  - All GUI user actions will be saved as Python script
  - Advantage: Users can repeat the same command procedure
  - Disadvantage: Need to learn Python script language

2.10.2 Units

Abaqus does not have built-in units. It is required to use consistent units throughout the model. Table-2.4 depicts typical units to be used in the modelling to maintain consistency during the analysis (Barbero, 2013; Hibbett et al., 1998; Khennane, 2013).

Table – 2.4 Typical units to be used in the Abaqus / CAE

Quantity	**SI**	**SI (mm)**	**US Unit (ft)**	**US Unit (in)**
Length	m	mm	ft	in
Force	N	N	lbf	lbf
Mass	kg	tonne (10^3 kg)	slug	lbf s^2/in
Time	s	s	s	s
Stress	Pa (N/m^2)	MPa (N/mm^2)	lbf/ft^2	psi (lbf/in^2)
Energy	J	mJ (10^{-3} J)	ft lbf	in lbf
Density	kg/m^3	$tonne/mm^3$	$slug/ft^3$	lbf s^2/in^4

CHAPTER 3

INVESTIGATIONS

Initially, research studies were aimed to study the geotechnical parameters influencing the propagation of ground vibrations, particularly, P-wave and S-wave velocities. Further, assessment and estimation of the seismic energy dissipated by ground vibrations at specified distances as captured by blast vibration monitors using signal processing approach was carried out in four different formations – Limestone, Coal, Sandstone and Granite. Also, relationship between critical parameters in blast design (maximum charge per delay, distance, geology) and seismic energy was made in all rock formations using regression based ANOVA statistical analysis. Similarly, relationship between seismic energy and fragmentation was assessed.

Later, a piezo generator circuit that converts undesirable ground vibrations into useful electrical energy, as an innovative renewable energy generation technique by utilizing the wasted blast energy was developed. Furthermore, comparison of the electrical output generated from piezo generator with the seismic data generated from blast vibration monitors was made in all four formations and the relationship was assessed. Finally, the potential of generated electrical energy from ground vibrations resulting from blasting operations was used for running low powered LED based VLSI circuit (ambient power based load).

Besides, numerical modelling was carried out using Simulia Abaqus / CAE based on python script by simulating the blast conditions for assessing the seismic energy component resulting from a given blast as a parametric study, and correlated the results with data generated from vibration monitoring and piezo electric generator using regression analysis.

Investigations were carried out in three stages as mentioned below:

- Stage-1: This stage of study involved field investigations carried out on blasting related ground vibrations for assessing and analysing the seismic energy dissipated at specified distances in four different formations – Limestone, Coal, Sandstone and Granite. Also, correlation and relationship between seismic energy with other blast parameters was determined.
- Stage-2: During this stage, a piezo generator circuit was developed to convert undesirable ground vibrations into useful electrical energy, by utilizing the wasted blast energy in the form of seismic energy. Validation of electrical output generated from the piezo generator was done with the seismic data generated from blast vibration monitors. Finally, generated electrical energy from ground vibrations was used to run a low powered LED based VLSI circuit as ambient power based load.
- Stage-3: Three dimensional (3D) numerical modelling was carried out as a parametric study using Simulia Abaqus / CAE based on python script by simulating the blast conditions for assessing the seismic energy component (PPV) resulting from a given blast during this stage of study. Later, correlation of modelling results with data generated from vibration monitoring and piezo electric generator was performed using regression analysis.

3.1 Field Investigations related to Seismic Energy

3.1.1 Seismic energy

Earlier, substantial amount of work related to identification of ground vibrations and assessing the blast performance in terms of intensity of ground vibrations has been carried out (Sastry, 2001). Nonetheless, very little research has gone into the seismic energy and utilizing this energy in understanding the performance of blast rounds (Sastry and Chandar, 2008). In current research investigations, it is proposed to attempt for the assessment and estimation of seismic energy dissipated at different distances from blast site using signal processing approach with the help of Advanced

Blastware and DADiSP software in four different formations, viz. Limestone, Coal, Sandstone and Granite.

In total, 116 blast vibration events from three limestone mines of harder formation, 37 blast vibration events from a limestone mine of softer formation, 86 blast vibration events from an underground coal mine, 43 blast vibration events from sandstone bench formations in two opencast coal mines and 94 blast vibration events from five granitic rock formations were collected using ground vibration monitors for signal processing analysis of seismic energy. Blast induced ground vibrations were recorded in three orthogonal directions, collecting 2000-2500 particle motion samples for each vibration event. Also, the muckpile in blast rounds was observed to assess the relationship between seismic energy and fragmentation in limestone and sandstone bench formations.

3.1.2 Ground vibration monitoring

Ground vibrations induced from blasting operations were monitored at different distances using Microprocessor based Blast Vibration Monitors of Instantel, Canada. Monitoring instruments were placed at minimum to maximum possible distances from the blast field, depending upon the type of formation and blast design parameters, i.e., from 30m to 485m in the case of hard limestone formation, from 100m to 560m in the case of soft limestone formation, from 15m to 125m in the case of underground coal formation, 100m to 2000m in the case of sandstone formation, and 20m to 300m in the case of granitic rock formation.

3.1.3 Vibration monitoring equipment

Minimate Plus, Instantel, Canada, offers an advanced monitoring technology, with versatility and flexibility to meet current needs and future requirements. It operates as a basic compliance monitor with intuitive functions and records an event quickly. This instrument also offers advanced functions for specific applications requiring more information to be collected and analysed (Anon, 2015c).

3.1.3.1 Geophone unit

Functionally a geophone sensor is a coil of wire suspended around a magnet. The magnet is free to move in a field of magnetic flux lines. By Lenz's Law, induced voltage is proportional to the speed at which flux lines are traversed. Induced coil voltage is, therefore, proportional to the relative velocity of the coil to the magnet. In practice, it does not matter whether the coil or the magnet moves. Only the motion and speed relative to each other are important. Hence, geophone is a transducer which converts the ground vibration signals into electrical signals, according to the principle of Faraday's Laws of Electromagnetic Induction (Fig. 3.1). Further, the electrical signals obtained are used and the intensity of ground vibration is measured by choosing a calibrated value programmed in the recording unit.

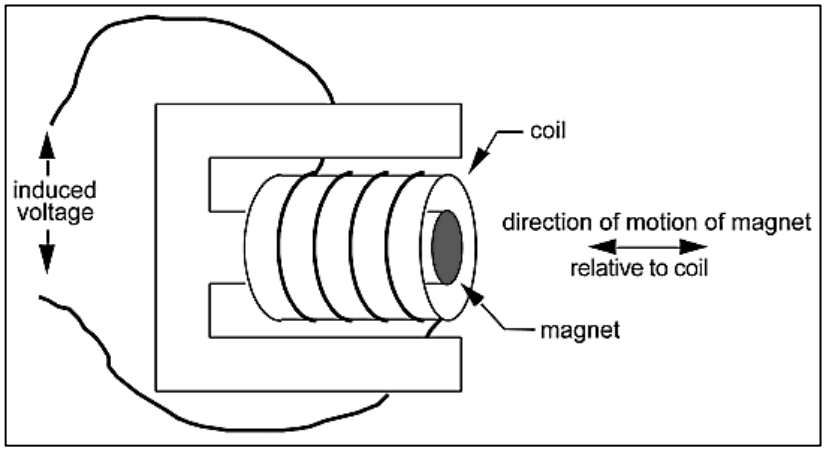

Fig. 3.1 Geophone sensor operation (Anon, 2015c)

3.1.3.2 Event monitoring

Event monitoring measures both ground vibrations and air overpressure. The monitor measures transverse, vertical, and longitudinal components of ground vibrations. Transverse ground vibrations agitate particles in a side to side motion. Vertical ground vibrations agitate particles in an up and down motion. Longitudinal ground vibrations agitate particles in a forward and backward motion progressing outward from the event site (Fig. 3.2).

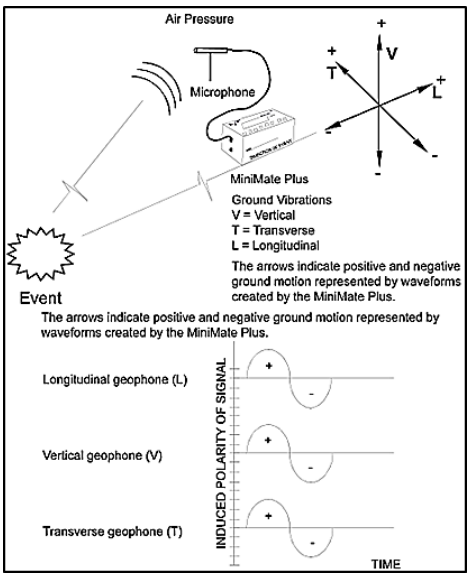

Fig. 3.2 Event monitoring in Minimate Plus, Instantel, Canada (Anon, 2015c)

3.1.4 Signal processing analysis

Ground vibrations were analysed using signal processing approaches with the help of Advanced Blastware and DADiSP software. Each ground vibration event in one direction comprised of 2,000-2,500 particle motion discrete samples. A typical wave form obtained is shown in Fig. 3.3. Initially, the vibration samples of ground vibration events were converted into ASCII file using Advanced Blastware.

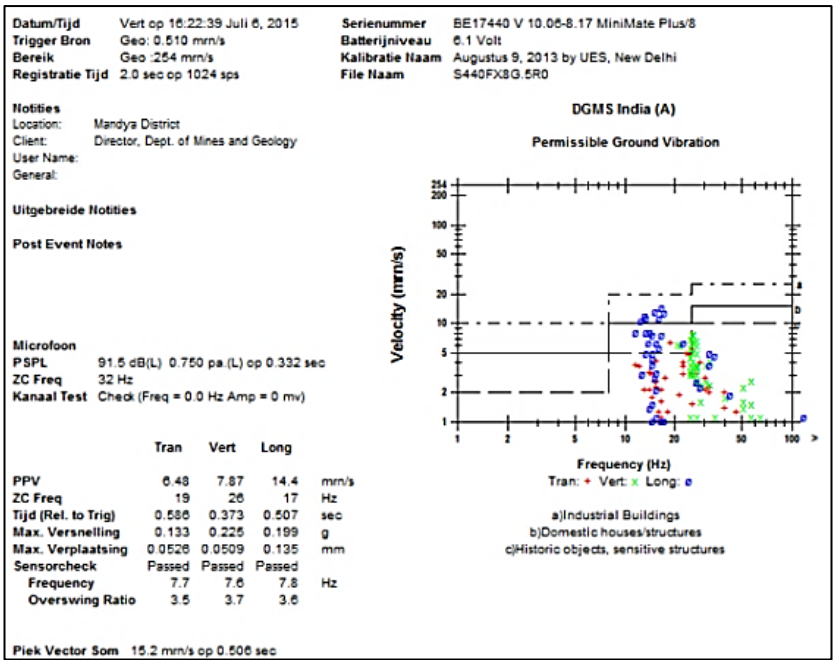

Datum/Tijd	Vert op 16:22:39 Juli 6, 2015			**Serienummer**	BE17440 V 10.06-8.17 MiniMate Plus/8	
Trigger Bron	Geo: 0.510 mm/s			**Batterijniveau**	6.1 Volt	
Bereik	Geo :254 mm/s			**Kalibratie Naam**	Augustus 9, 2013 by UES, New Delhi	
Registratie Tijd	2.0 sec op 1024 sps			**File Naam**	S440FX8G.5R0	
Notities						
Location:	Mandya District					
Client:	Director, Dept. of Mines and Geology					
User Name:						
General:						
Uitgebreide Notities						
Post Event Notes						
Microfoon						
PSPL	91.5 dB(L) 0.750 pa.(L) op 0.332 sec					
ZC Freq	32 Hz					
Kanaal Test	Check (Freq = 0.0 Hz Amp = 0 mv)					
	Tran	**Vert**	**Long**			
PPV	6.48	7.87	14.4	mm/s		
ZC Freq	19	26	17	Hz		
Tijd (Rel. to Trig)	0.586	0.373	0.507	sec		
Max. Versnelling	0.133	0.225	0.199	g		
Max. Verplaatsing	0.0526	0.0509	0.135	mm		
Sensorcheck	Passed	Passed	Passed			
Frequency	7.7	7.6	7.8	Hz		
Overswing Ratio	3.5	3.7	3.6			
Piek Vector Som	15.2 mm/s op 0.506 sec					

Fig. 3.3 Typical ground vibration event

Signal processing computation has been done in four stages as follows:

3.1.4.1 Collection

Each ground vibration event in one direction comprised of 2000-2500 particle motion discrete samples and collectively in all three mutually orthogonal directions 6000-7500 vibration samples were collected at respective distances using ground vibration monitor.

3.1.4.2 Extraction

In this stage, discrete vibration sample magnitudes of ground vibration events were extracted into an ASCII file using Advanced Blastware Software by removing the noise carefully (Fig. 3.4).

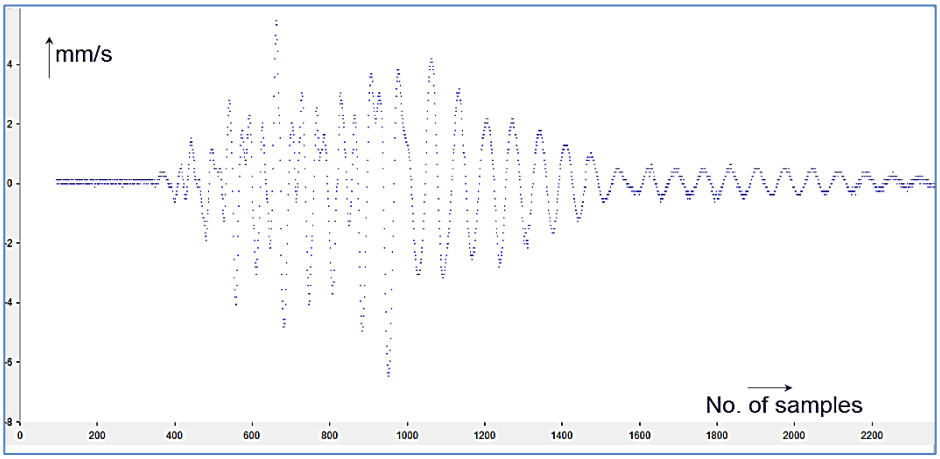

Fig. 3.4 Quantized discrete signal

3.1.4.3 Importation

ASCII values obtained were imported into DADiSP for further signal processing analysis. Further, obtained values from ASCII file were imported into DADiSP for signal processing analysis.

3.1.4.4 Reconstruction

Vibration samples collected were having discrete magnitudes, henceforth those sample magnitudes were further processed to obtain a reconstructed vibration wave using 'Reconstruction Signal Analysis' available in DADiSP software which is illustrated in steps below (Figs. 3.5 to 3.9). The reconstructed signal was processed further to obtain the seismic energy of the vibration event.

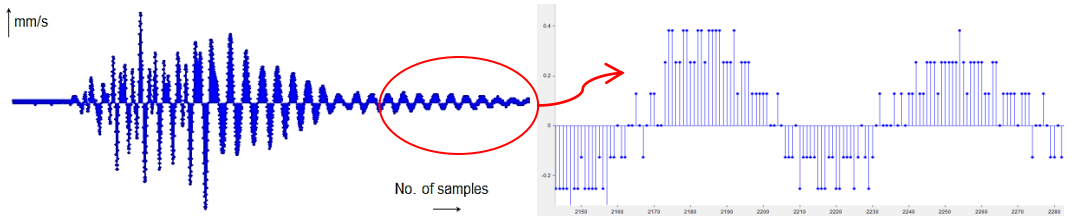

Fig. 3.5 Signal with discrete sample magnitudes

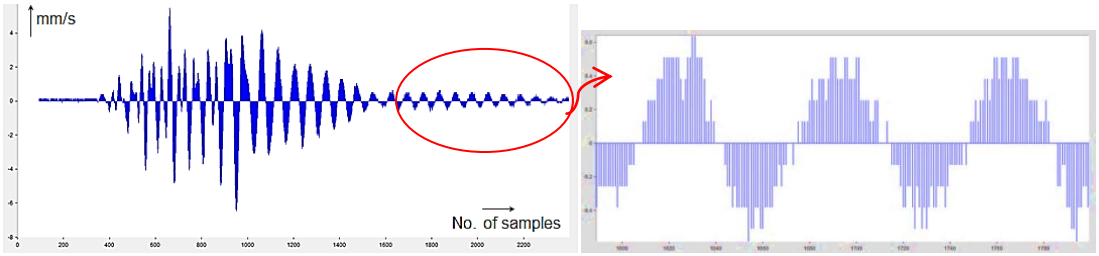

Fig. 3.6 Reconstruction of a signal with discrete samples (phase-1)

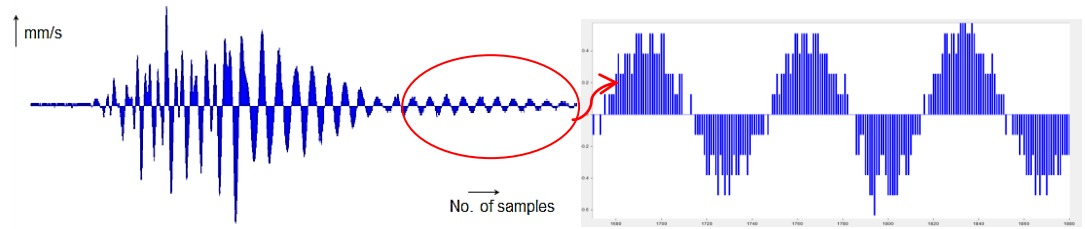

Fig. 3.7 Reconstruction of a signal with discrete samples (phase-2)

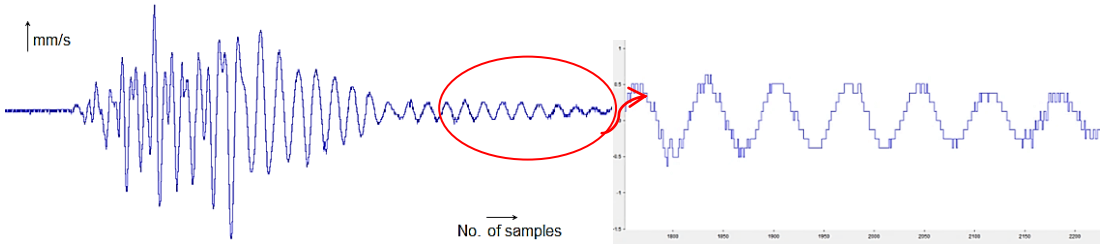

Fig. 3.8 Reconstructed quantized signal

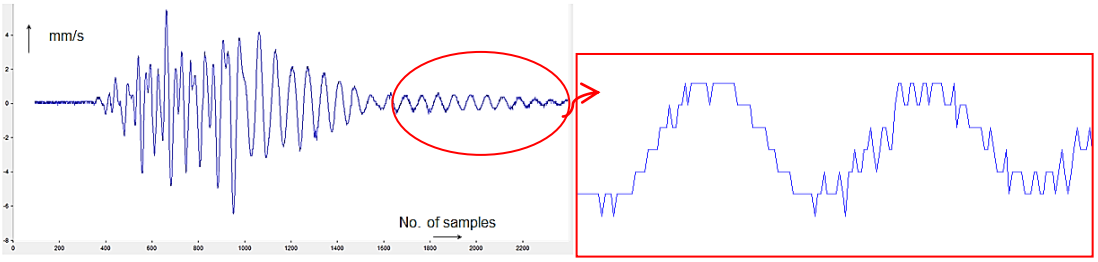

Fig. 3.9 Reconstructed discrete signal

3.1.5 Estimation of seismic energy

After the reconstruction process, the reconstructed blast induced vibration waves were considered in all three orthogonal directions together (Fig. 3.10).

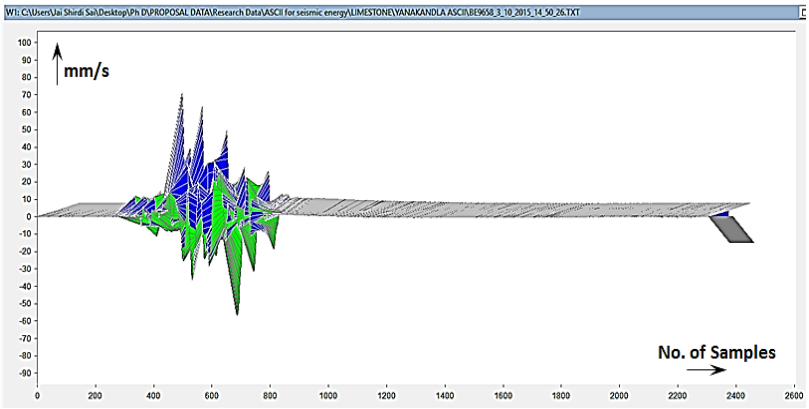

Fig. 3.10 Typical reconstructed vibration wave aligned in all three mutually orthogonal directions

The waveforms which are in time domain were converted to frequency domain by applying Discrete Fourier Transformation (DFT). Since, the reconstructed blast wave is a non-periodic discrete wave, application of direct Fourier Transformations for finding the frequency is not possible. Application of Discrete Fourier Transformation remains the system magnitude with same units but in frequency domain (Fig. 3.11).

- Input (before DFT) – Vibration velocity in time domain (mm/s)
- Output (after DFT) – Vibration velocity in frequency domain (mm/s)

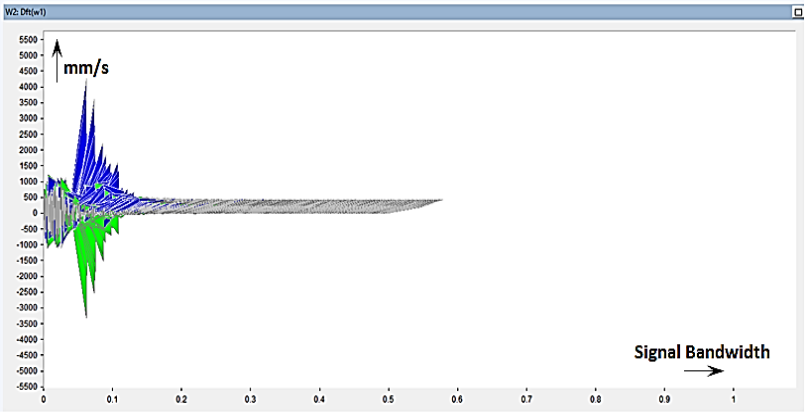

Fig. 3.11 Computation of DFT to random vibration signal aligned in all three mutually orthogonal directions

This indicates no change in the state of signal. After DFT using DADiSP package, signals were further processed to find Power Spectrum Density (PSD), which is a measure of intensity of signal's power in the frequency domain. PSD provides a useful way to characterize the amplitude versus frequency content of a random signal (Brüel and Kjær, 2015).

When the input random vibration signal in frequency domain is having units as 'G', the amplitude values of a PSD are normally expressed in 'G^2/Hz', where the term 'G' indicates units of the random vibration signal, mm/s, in frequency domain. Typical computed power spectrum density after DFT operation is shown in Fig. 3.12.

- Input (before PSD) – Vibration Velocity in frequency domain (mm/s)
- Output (after PSD) – $(mm/s)^2$/Hz → $(\mu m^2/s^2)$/Hz → $\mu.(m^2/s)$

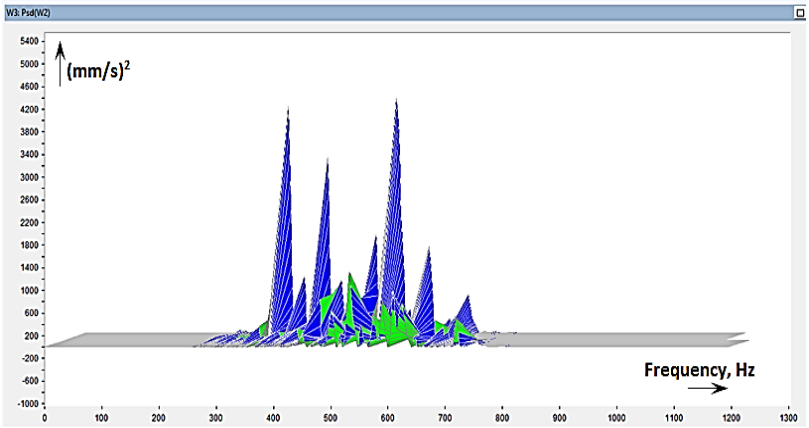

Fig. 3.12 Computation of power spectrum density to the random vibration signal aligned in three mutually orthogonal directions after DFT operation

It is assumed that the vibration wave has a unit mass, M in kg. Therefore, the output after PSD operation is changed as μ ($kg.m^2/s$). Output is in the form of angular momentum (L). The angular momentum, *L*, of a rigid body with moment of inertia, *I*, rotating with angular velocity ω, is given by:

$$L = I.\omega \quad \text{----------} \quad \textbf{(3.1)}$$

where,

L = Angular momentum, kg-m^2/s
I = Moment of inertia, kg-m^2
ω = Angular velocity, rad/s

Rotational kinetic energy for a mechanical system considering the total mechanical energy of a rigid body is defined as,

$$KE_r = \int_0^{\omega} L\, d\omega = \int_0^{\omega} (I.\omega)\, d\omega = \frac{1}{2} I.\omega^2 \quad \text{----------} \quad \textbf{(3.2)}$$

where,

KE_r = Rotational kinetic energy, μJ

Hence, from the above analysis, it is needed to apply integration to the output of vibration data after PSD operation. Integration is applied only for continuous signals and for discrete signals, it is not possible. Hence, "Partial Sum" operation was computed for finding the Rotational Kinetic Energy available in the waveform (Anon, 1997). Therefore,

$$KE_r = \sum_0^{\omega} L = \sum_0^{\omega} I.\,\omega \qquad \text{----------} \qquad \textbf{(3.3)}$$

Areas under a vibration signal were calculated for each sample and summed up using "*Partial Sum*" technique by the command `area(abs(w4))`, which gives the *Seismic Energy* of blast induced vibration wave, where term `w4` indicates label of the specific window, where Partial Sum operation is processed (Fig. 3.13).

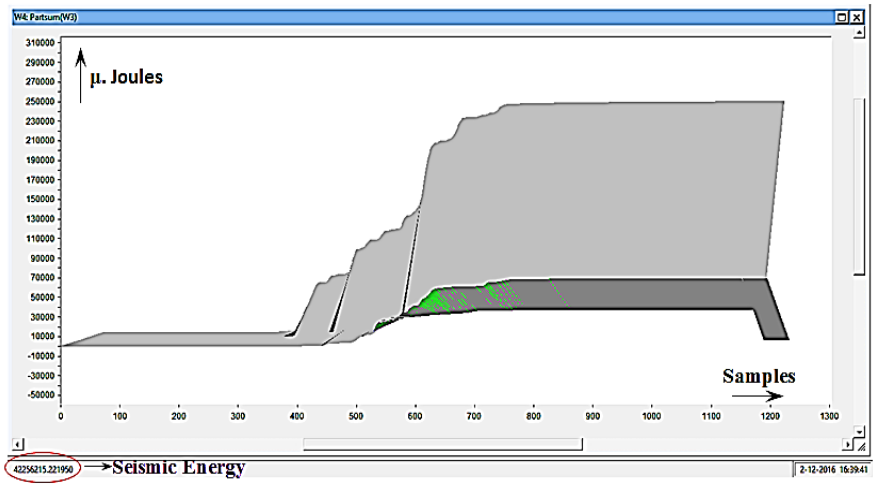

Fig. 3.13 Seismic energy of the blast induced ground vibration wave

3.1.6 Field investigations in limestone formation

Studies related to blast induced ground vibrations were carried out in three different limestone mines of harder formation and one limestone mine of softer formation. Among three different limestone mines of harder formation, two mines belong to M/S My Home Industries Private Limited, viz. Choutapalli Limestone Mine and Yepalamadhavaram Limestone Mine, Mellacheruvu Mandal, Nalgonda District, Telangana State and the third one belongs to M/S Sree Jayajothi Cements Limited (A 100% subsidiary of My Home Industries Private Limited), viz. Yanakandla Limestone Mine, Yanakandla Area, Kurnool District, Andhra Pradesh State. For softer

formation, research studies were carried out in a limestone belonging to M/S The Ramco Cements Limited, i.e. Periyanagalur Limestone Mine, in Periyanagalur Village of Ariyalur Mandal in Ariyalur District, Tamilnadu.

Fig. 3.14 shows general view of these mines.

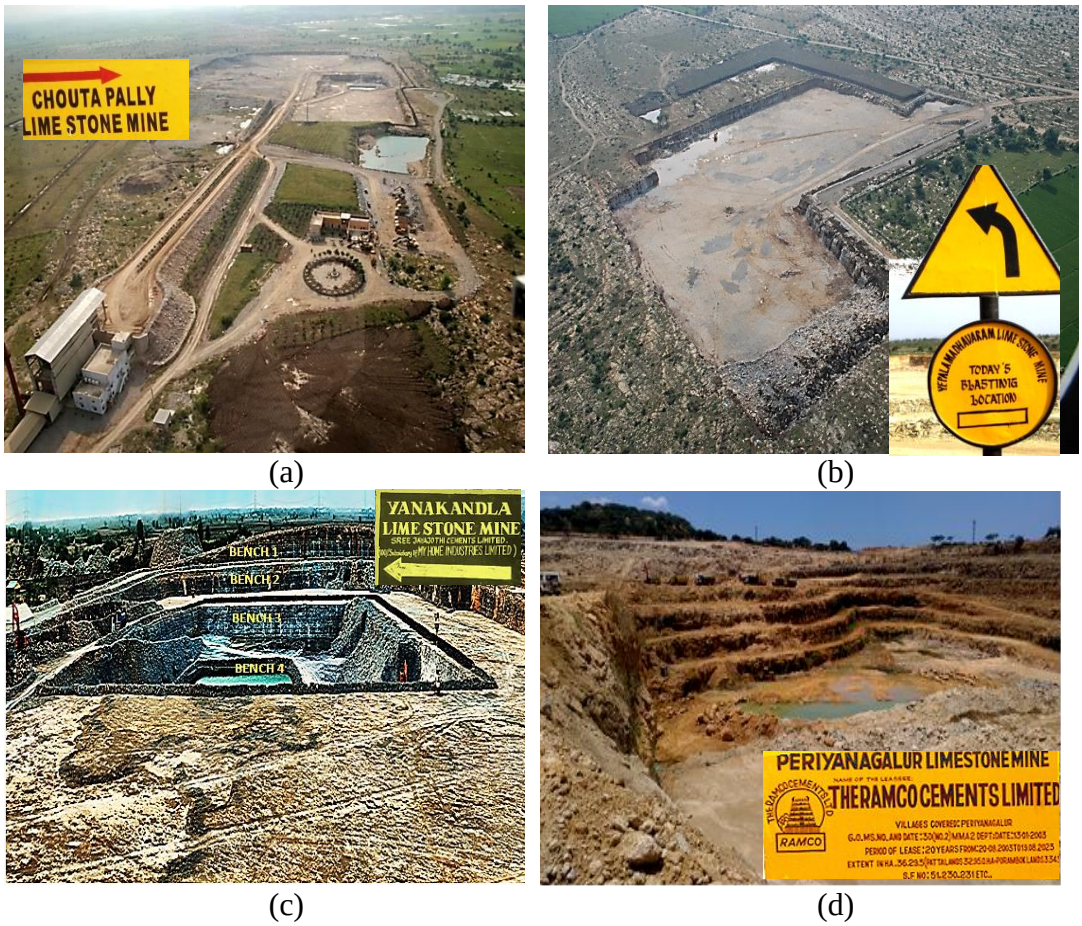

(a) (b)

(c) (d)

(a) Choutapally mine **(c)** Yanakandla mine
(b) Yepalamadhavaram mine **(d)** Periyanagalur mine

Fig. 3.14 General view of limestone mines

Ground vibrations were monitored in different locations at various distances. Entirely, 116 blast vibrations were collected in harder formation and 37 blast vibrations were collected in softer formation from various blast rounds. Typical monitoring of ground vibrations is shown in Fig. 3.15.

Blasts were conducted by varying blast design parameters to observe the change in vibration propagation, which in turn the seismic energy to find out the relationship

between seismic energy and critical blast parameters. Distance between monitoring point and blast location was varied from 30m to 485m in harder formation and 100m to 560m in softer formation, covering short range and long range monitoring. Most of the blasts were recorded and progress of blasts was analysed using High Speed Video Camera having the capability of 1,000 frames per second and the ProAnalyst software. Typical screenshots of blast progress in different blast rounds as recorded with the High Speed Video camera are shown in Appendix-I.

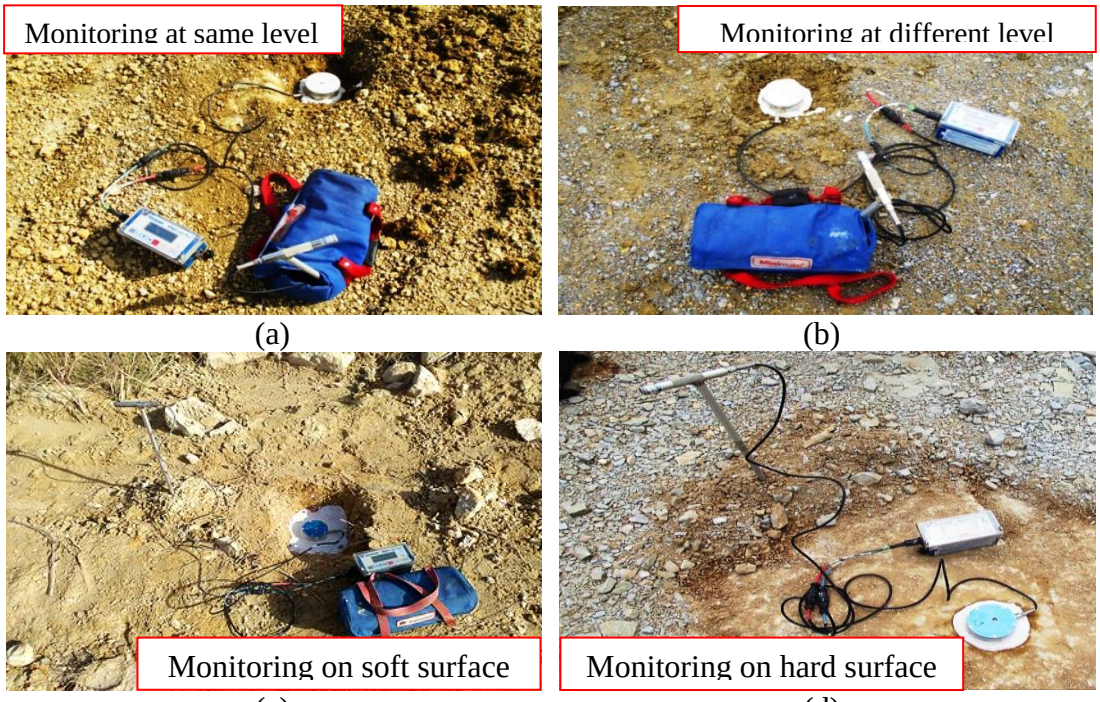

Fig. 3.15 Monitoring of ground vibrations in limestone mines at different locations during research field studies

3.1.7 Field investigations in coal formation

Ground vibrations associated with blasting operations were studied in an underground coal mine belonging to The Singareni Collieries Company Limited. The Singareni Collieries Company Limited (SCCL) is operating SRP-3 & 3A Incline Mine in Srirampur Area, Adilabad District, Telangana State. This mine was under development during studies.

Fig. 3.16 shows general view of the underground coal mine.

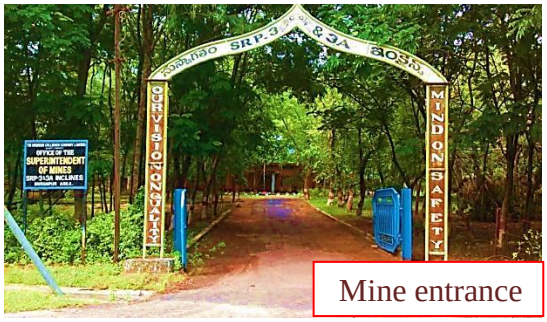

Mine entrance

(a)

Way to surface (740m to surface)

(b)

Junction to reach different seams

(c)

Rope ladder for safe walking

(d)

Fig. 3.16 General view of SRP-3&3A underground coal mine

Conventional drilling and blasting method is used for dislodging coal from the faces for further loading and transporting. Ground vibrations were monitored in different locations covering different seams and partings. Studies in the mine were carried out with 34 blasts. In total, 86 blast vibration events were recorded from various blast rounds. Typical locations of ground vibration monitoring at various seams and partings are shown in Fig. 3.17. Likewise, distance between monitoring point and blast location was varied from 15m to 125m.

Monitoring in the same seam

(a)

Monitoring in a different seam with more vertical parting

(b)

(c) (d)

Fig. 3.17 Monitoring of ground vibrations in an underground coal mine at different seams and partings

3.1.8 Field investigations in sandstone formation

Studies were carried out in two different sandstone bench formations. Among them, one mine belongs to The Singareni Collieries Company Limited. The Singareni Collieries Company Limited is operating the RG OC-I and RG OC-III opencast mines, major mechanized opencast mines of SCCL in Godavarikhani Area, Karimnagar District, Telangana. Explosive energy is used for fragmenting and displacing the overburden and coal from in-situ. The other location is Singareni Thermal Power Project (STPP), Mancherial Area, Jaipur Mandal, Adilabad District, Telangana State. Fig. 3.18 shows general view of the sandstone bench formations considered for research studies.

(a) (b)

Fig. 3.18 General view of sandstone bench formations

Ground vibrations were monitored at different locations. In total, 43 blast vibration events were collected from various blast rounds. Typical monitoring of ground vibrations in these projects is shown in Fig. 3.19. Most of the blasts were recorded and progress of blasts was analysed using High Speed Video Camera. Typical screenshots of blast progress in different blasts rounds as recorded with the high speed video camera are shown in Appendix-II.

Fig. 3.19 Monitoring of ground vibrations in sandstone bench formations at different locations during research field studies

Blasts were carried out in two sandstone bench formations by varying blast design parameters in different blasts to observe the changes in vibration propagation, which in turn influence the seismic energy distribution and to find out the relationship between seismic energy and critical blast parameters. Distance between monitoring point and blast location was varied from 100m to 2,033m.

3.1.9 Field investigations in granite formation

Research studies related to blast induced ground vibrations were carried out in five different granite quarries (Fig. 3.20):

1. A stone quarry operating in Shivapura Village, Karkala Taluk, Udupi District, Karnataka.

2. A stone quarry operating in Doddamavathuru Village, Kunigal Taluk, Tumkur District, Karnataka.
3. A stone quarry operating in Nitte Village, Karkala Taluk, Udupi District, Karnataka.
4. A Stone quarry existing in Hosuru Village, Udupi Taluk, Udupi District, Karnataka.
5. Stone quarries belonging to M/S Bhairava Stone Crushers Private Limited adjoining two villages, Ajjappanahalli Village and Amalapura Village, Tumkur Taluk, Tumkur District, Karnataka.

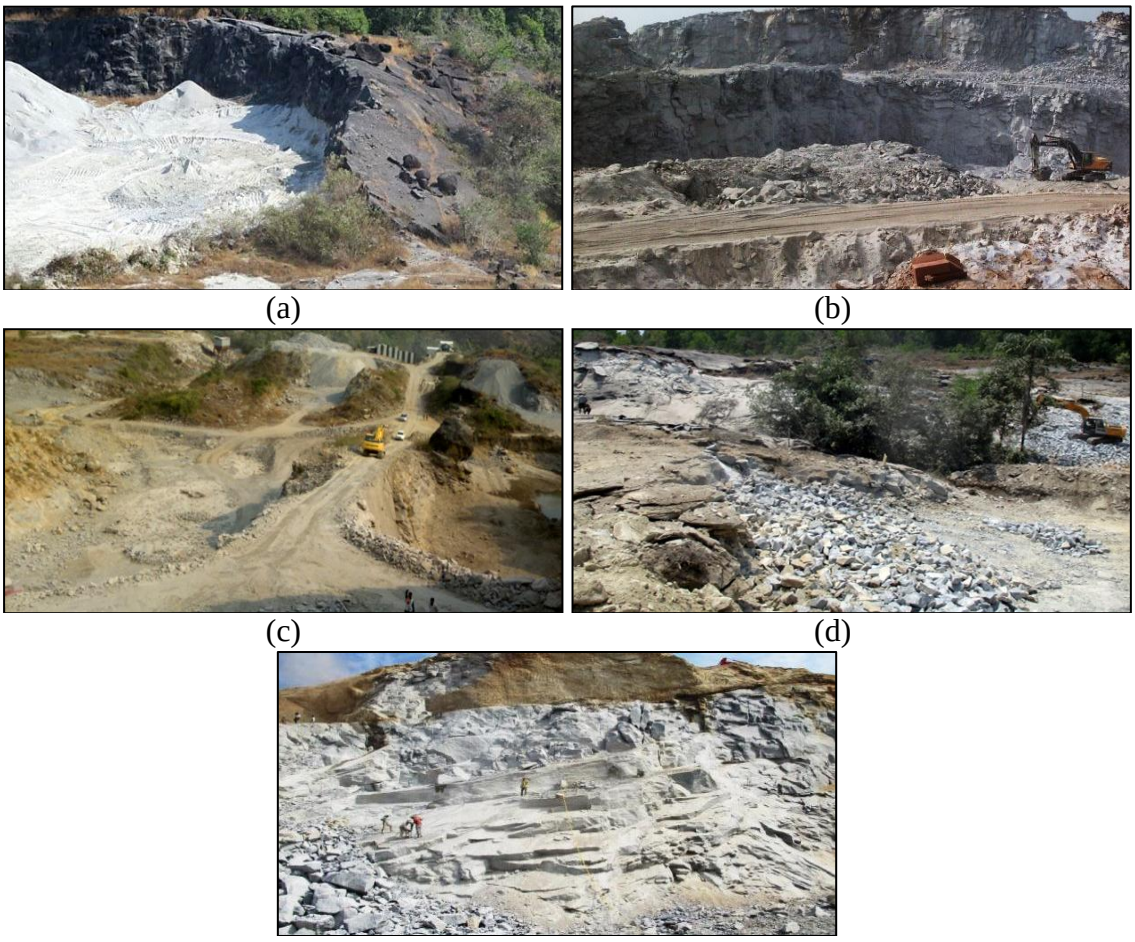

(a) (b)

(c) (d)

(e)

(a) Granite stone formation-1
(b) Granite stone formation-2
(c) Granite stone formation-3
(d) Granite stone formation-4
(e) Granite stone formation-5

Fig. 3.20 Locations of blasts carried out during research studies

Hard granitic rock formations were proposed to be excavated in these stone quarries using drilling and blasting methodology. Ground vibrations were monitored in different locations covering different parts of five quarries. Altogether, 94 ground

vibration events were collected from various blast rounds. Typical monitoring of ground vibrations in granitic formation is shown in Fig. 3.21. Distance between monitoring point and blast location was varied from 20m to 300m.

Fig. 3.21 Monitoring of ground vibrations in granite stone formations at different locations during research field studies

3.2 Piezo Generator (Piezo-Gen) Circuit

Blasting is an important activity in all the mines and quarries, carried out regularly, for fragmenting and displacing rock mass for further loading and transporting. Ground vibrations of different intensities are generated from each blast carried out in mines and quarries. Ground vibrations carry seismic energy, a part of the wasted explosive energy in the blasting process. Intensity of ground vibrations varies from few hundreds of mm/s at closed distances from the blast site to a few mm/s at longer distances. There is a potential for tapping of electrical energy from the ground vibrations generated due to blasts carried out in mines and quarries using piezo sensors.

Proposed research work focuses on tapping of electrical energy using undesirable ground vibrations caused due to blasting operations, with developed piezo sensor based circuit model. Basic principle of the circuit is piezo based electricity generation. Whenever there is a compression of the ceramic PZT (lead ziconate titanate) sensor,

then a positive pulse of electricity is produced whereas tension on the sensor unit gives rise to negative pulse. In such a way, the generation of electrical energy was accomplished through the ground vibrations using piezo based ceramic sensor. The circuit was placed at a distance, d, (in m) from the blasting location. On the occurrence of blast, shock waves resulting from ground vibrations were tapped using piezo sensor and an electrical potential (voltage) was generated. Fig. 3.22 shows the outline of electrical energy tapping from blast induced ground vibrations using piezo generator circuit.

Sensor unit was placed towards blast field in such a way that the ground vibrations may create the tension and compression in the circuit, which will deliberately cause disturbance of electrical polarization in sensor unit, thereby generating electrical potential across the sensor unit. Generated potential may be used by placing a proper electrical load across the sensor. In the present basic circuit scenario, capacitor with parallel connected Power LED (5V capacity) was used as a load and the voltage generated was perceived using Multimeter (Fig. 3.22). Later, the basic circuit model was modified by integrating a microcontroller and other circuitry for getting optimized output.

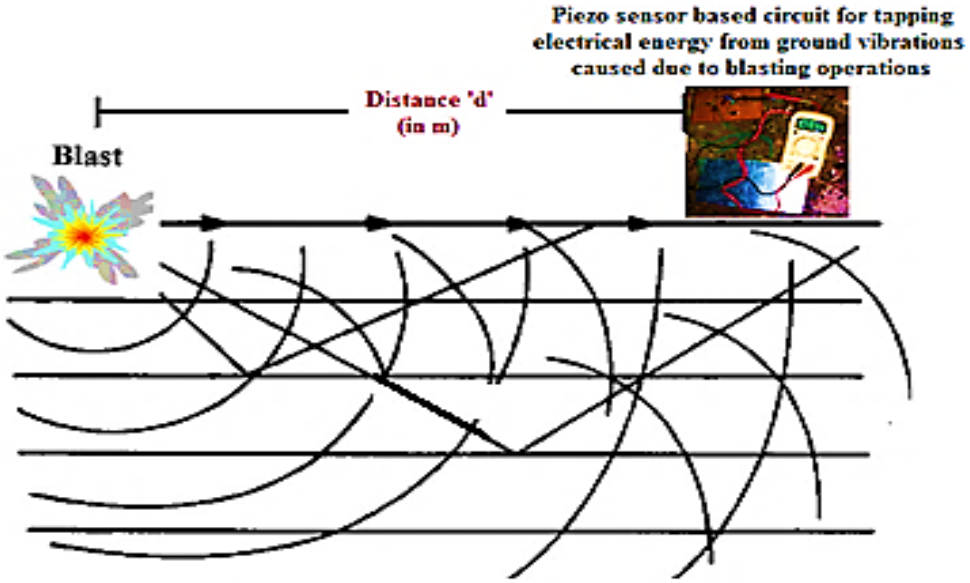

Fig. 3.22 Electrical energy tapping from blast induced ground vibrations using piezo generator circuit

3.2.1 Development of piezo generator circuit

Experiments were carried out rigorously during development and improvement process of piezo generator circuits to achieve the devised output. Initially, circuits were developed on an electronic bread board and required modifications in the circuit layout were made. After getting satisfactory results, the final circuits were developed by incorporating all the required modifications on Printed Circuit Boards (PCBs).

Initially, a basic circuit model was developed with simple piezo ceramic sensor, available as a piezo buzzer or piezo disc. Generated electrical potential was having improper frequency with more unwanted ripples (harmonics). Hence, the generated AC voltage was converted back to DC voltage using four germanium based diodes, forming a simple bridge rectifier circuit. Germanium based diodes were used which may further reduce losses in the output (in the form of voltage drop) compared to silicon based diodes. Thereafter, the obtained electrical voltage was stored in a DC Capacitor having 2,200μf, 25V capacity for utilization purpose. Besides, a Power LED having 5V capacity with a switch was connected across the capacitor to discharge higher voltages, if any, in case the capacitor gets fully charged, as a preventive measure of capacitor from damage. A switch control was employed in the circuit, to enable the LED to ON/OFF. The magnitude of obtained voltage due to blast induced ground vibrations was assessed using multimeter by connecting the instrument terminals across the capacitor (Fig. 3.23).

Following components were used during the development of basic circuit for tapping electrical energy from blast induced ground vibrations:

- Piezo Ceramic Disc (PZT) – 4 Nos.
- Germanium diodes (1n34) – 4 Nos.
- Push-to-On switch – 1 No.
- Power LED (5V) – 1 No.
- Capacitor (2,200μf) – 1 No.
- Connecting wires – As required

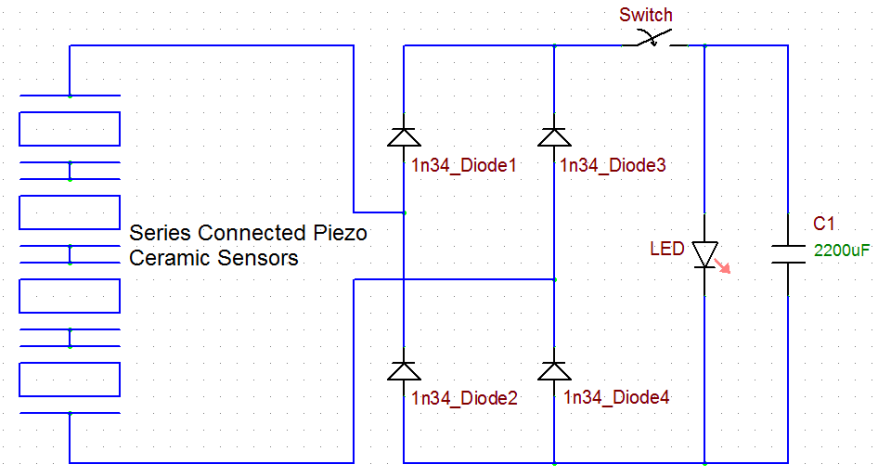

Fig. 3.23 Schematic of basic piezo generator circuit developed

Later, to determine the exact magnitude of generated voltage tapped from blast induced ground vibrations, the circuit was modified by integrating a microcontroller to piezo sensor along with microSD card (to store generated voltage magnitude values), which is discussed in the following section.

3.2.2 Modified piezo generator circuit

Following components were used in the second version of the circuit:

- Microcontroller (ATMega328P-PU) – 1 No.
- Operational-AMPlifier (LM-358) – 1 No.
- MicroSD Module with card (32GB) – 1No.
- 7805 voltage regulator (0-5V) – 1 No.
- Capacitor (22pF) – 2 Nos.
- Capacitor (10^1 x 104 pF) – 1 No.
- Resistor (330ohms) – 3 Nos.
- LEDs (3.5-5V) – 2 Nos.
- Crystal Oscillator (10MHz) – 1 No.
- Push-to-On-Push-to-Off Switch – 1 No.
- 9V battery with connector clip – 1 No.
- Connector for PC communication – 1 No.
- Piezo ceramic sensor (PZT) – 1 No.
- Connecting wires – As required

Blast induced ground vibrations were tapped using piezo sensor, analogous to basic circuit model. In the improved version of basic circuit model, piezo sensor was connected to LM-358 (Op-Amp) differential amplifier to convert the input analog

data (voltage magnitude value) into digital data (machine language, for storage purpose). The LM-358 is having a resolution of 1024 size (digital), which means 5V of analog voltage generated due to piezo sensor can be replicated in digital form of up to a maximum value of 1024. Since, the input generated voltage (tapped from ground vibrations) is restricted to 5V using voltage regulator, to prevent the microcontroller (having a maximum capacity of 5V) from damage. Therefore, output of the Op-Amp represents 1 (Digital) = 4.89mV (Analog). Similarly, all digital values (values stored in microSD card) need to be multiplied by the factor (4.89×10^{-3}) to obtain the actual magnitude of voltage generated from blast vibrations. An LED was also connected in the circuit, for which LED be glowing whenever the blast vibration gets tapped and voltage is generated. Figs. 3.24 and 3.25 show the schematic and pin configuration of OP-AMP (LM-358) adopted in the modified circuit model.

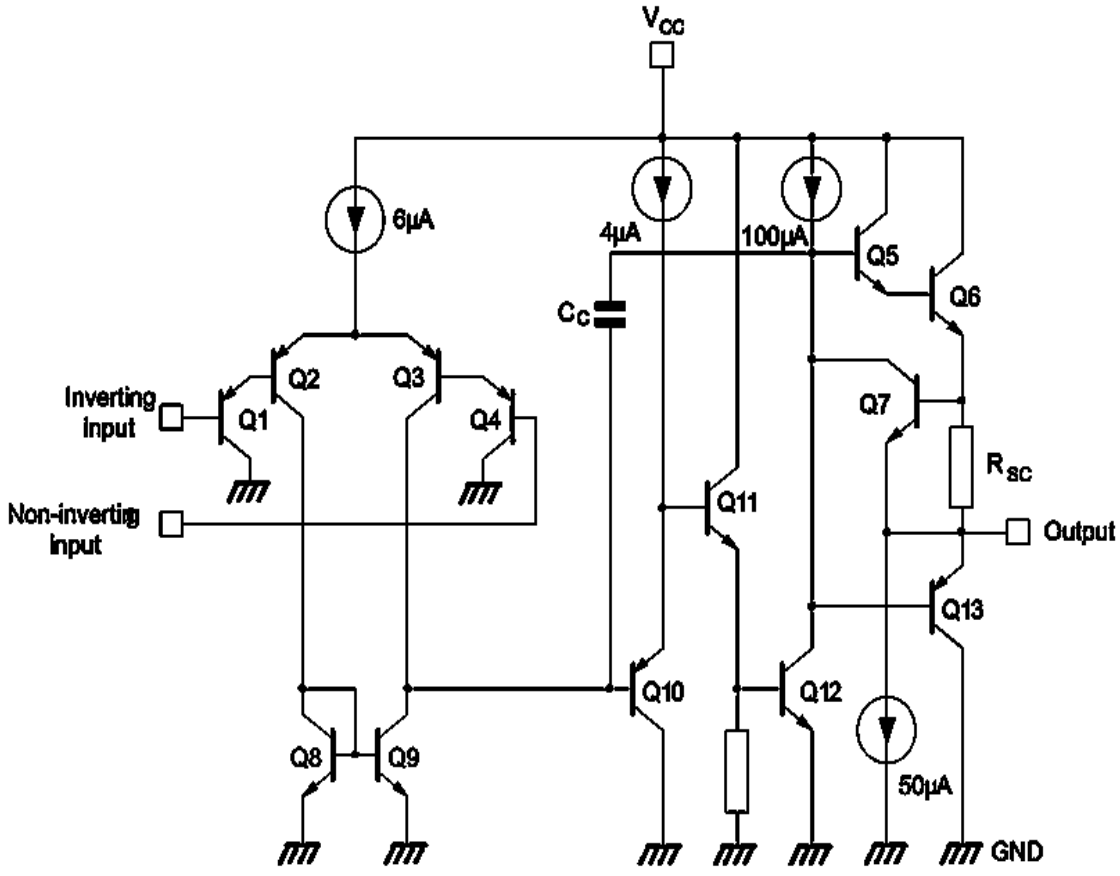

Fig. 3.24 Schematic of LM-358 differential OP-AMP (Anon, 2000)

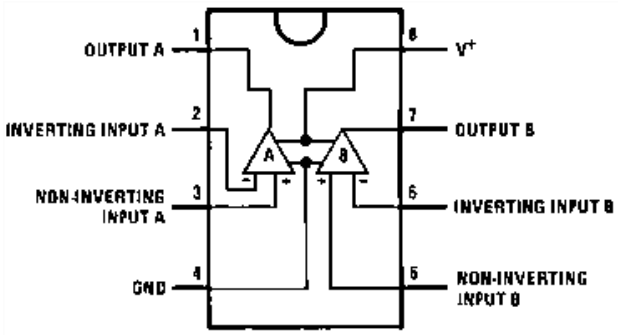

Fig. 3.25 Pin configuration of LM-358 (Anon, 2000)

All the above processes of tapping ground vibrations, indication of vibration tapping and voltage generation, storing the value of voltage magnitude into microSD card, were controlled by a microcontroller (ATMega328P-PU). Power was supplied to the circuit through 9V battery for running Microcontroller, Op-Amp and Memory Module. Oscillator circuit to generate clock pulses for finding the next vibration was connected to the microcontroller. Fig. 3.26 shows the pin diagram of ATMega328P-PU microcontroller used in the circuit model.

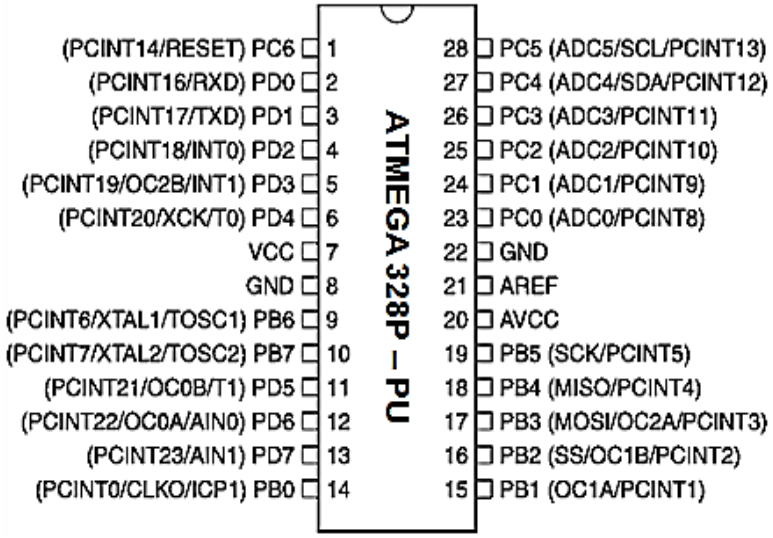

Fig. 3.26 Pin diagram of ATMega328P-PU microcontroller (Anon, 2005)

Final circuit to find out the exact magnitude of electrical voltage generated (tapped from blast induced ground vibrations) was developed by assembling all the components and integrating ATMega328P-PU microcontroller to the piezo sensor

along with microSD card (to store output magnitude values). Fig. 3.27 shows the improved version of basic piezo generator circuit.

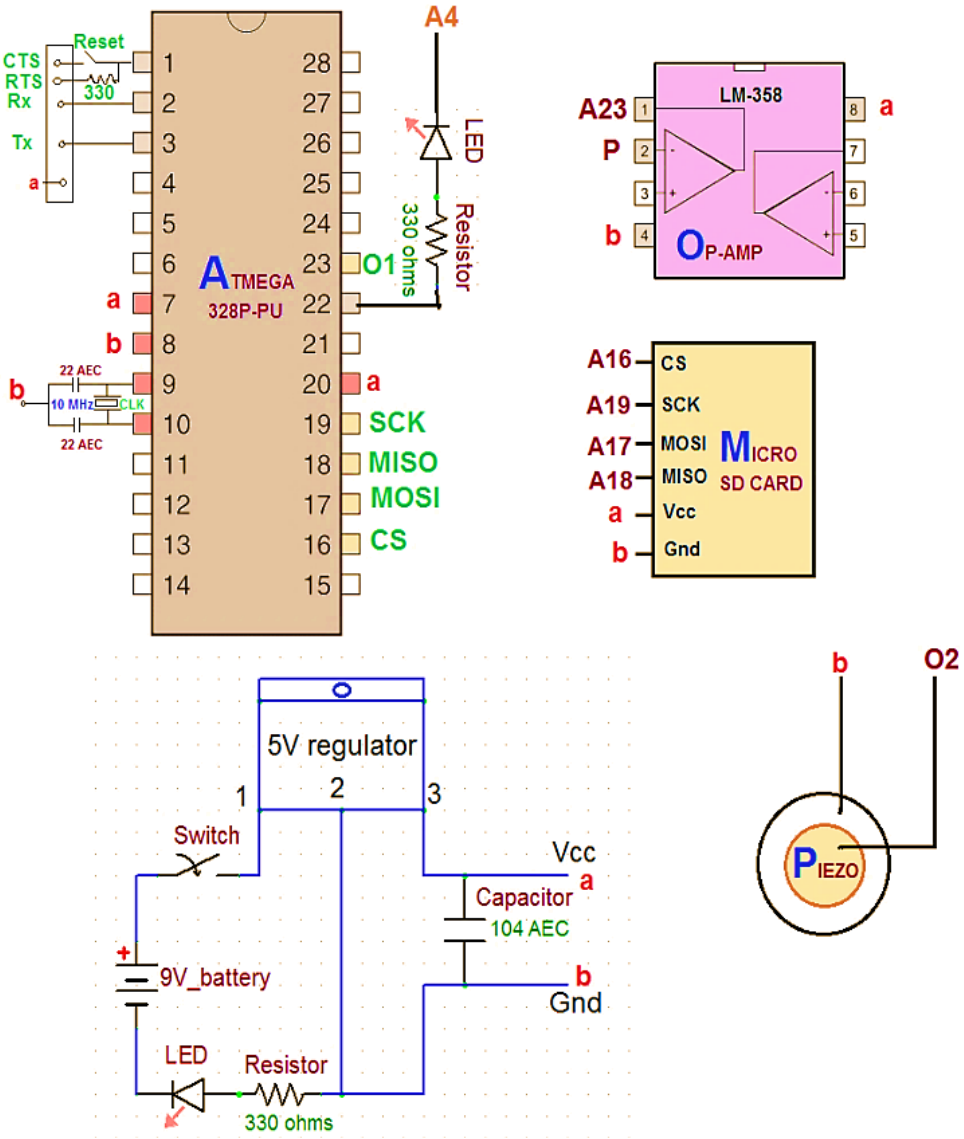

Fig. 3.27 Schematic of improved piezo generator circuit

Yet again, it was noticed that with mere modification in improved circuit version, output may be much enhanced, i.e. from mV to V. Hence, the following final circuit model was adopted for tapping electrical voltage from blast induced ground vibrations (Fig. 3.28).

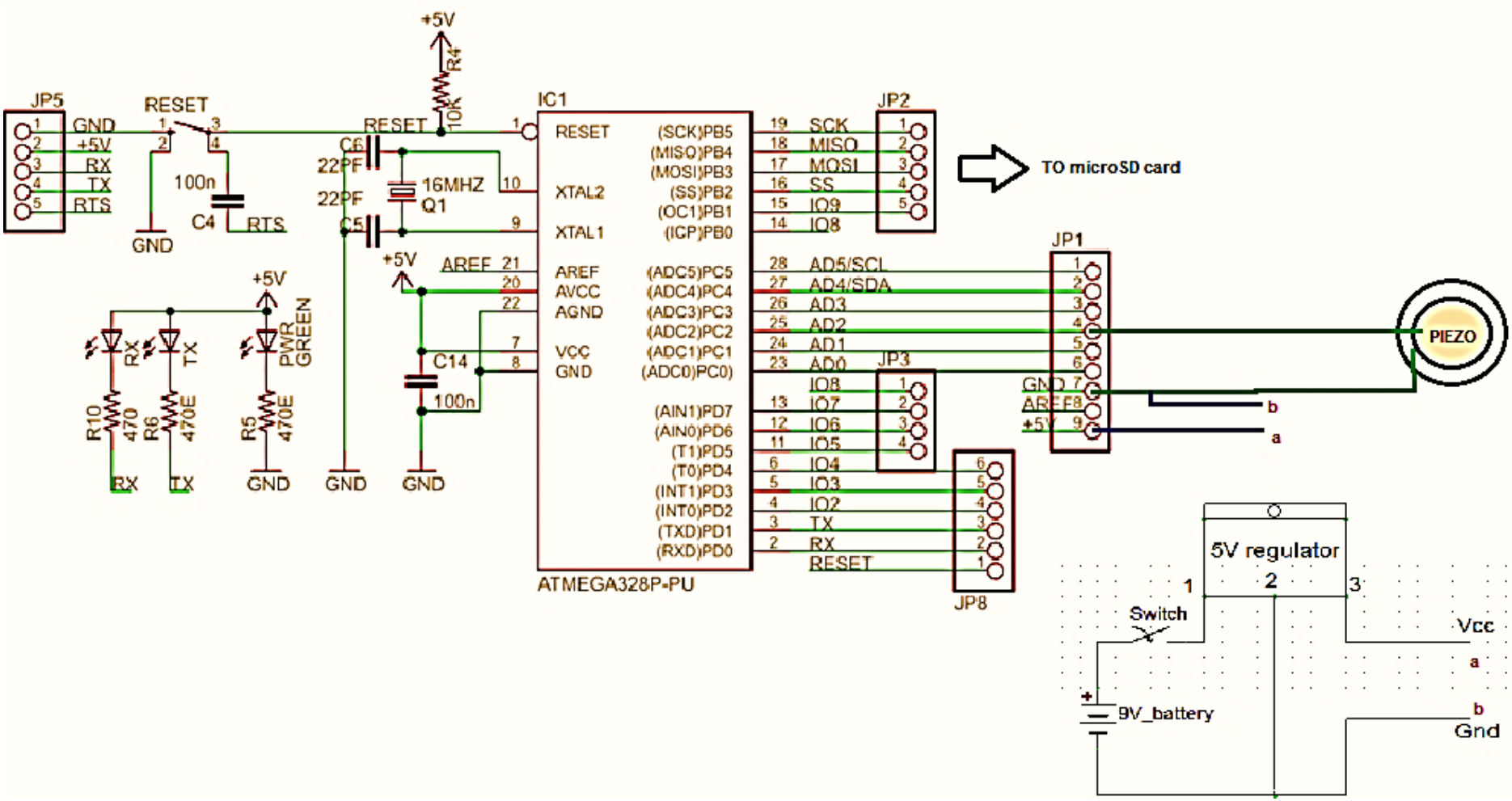

Fig. 3.28 Schematic of final piezo generator circuit

Microcontroller (ATMega328P-PU) was operated with set of commands programmed in it, for obtaining the magnitude of tapped electrical potential (generated electrical voltage) from blast induced ground vibrations.

Code (.ino or .odt) programmed in the microcontroller for achieving the entire process of tapping electrical energy from ground vibrations is illustrated below:

```
%% MICROCONTROLLER CODE for tapping electrical energy from
    ground vibrations

#include <SD.h>
#include <Time.h>
#include <Wire.h>
#include <DS1307RTC.h>
File myFile;
const int analogInPin = A2;  // Analog input pin that the Piezo is attached to
const int analogOutPin = 9; // Analog output pin that the LED is attached to
int sensorValue = 0;        // value read from the Piezo sensor
int outputValue = 0;
int outputVal=0;
void setup()
{
  Serial.begin(9600);
  while (!Serial) {
}
Serial.print("Initializing SD card...");
pinMode(10,OUTPUT);
//void loop() {
if (!SD.begin(4)) {
Serial.println("initialization failed!");
return;
}
Serial.print("Initialization done...");
//}
}
void loop() {
myFile = SD.open("test.txt",FILE_WRITE);
if (myFile){
sensorValue = analogRead(analogInPin);
// map it to the range of the analog out:
outputValue = map(sensorValue, 0, 1023, 0, 2047);
Serial.print(outputValue);
 if (outputValue<1)
    {outputVal=0;}
else
    {outputVal=outputValue;
}
analogWrite(analogOutPin, outputVal);
Serial.println();
Serial.print("Writing to test.txt");
//myFile.println("Writing to test3...");
myFile.print(hour());
myFile.print(":");
myFile.print(minute());
myFile.print(":");
myFile.print(second());
myFile.print(" ");
myFile.print(outputVal);
myFile.println();
myFile.close();
}
else {
Serial.print("Error writing to test.txt...");
}
delay(1000);
}
```

3.2.3 Validation of piezo generator circuit

Validation of piezo generator circuit was done by comparing its output (generated voltage) with the vibration data obtained from geophones of Minimate Plus, Instantel, Canada.

Initially, piezo sensor and geophone were completely glued to the ground surface with double gum sticker, in the laboratory. Vibrations were monitored by dropping a standard weight from specified height of 1m, thereby identifying intensity of ground vibrations using both the instruments. Experiments were carried out as shown in Fig. 3.29.

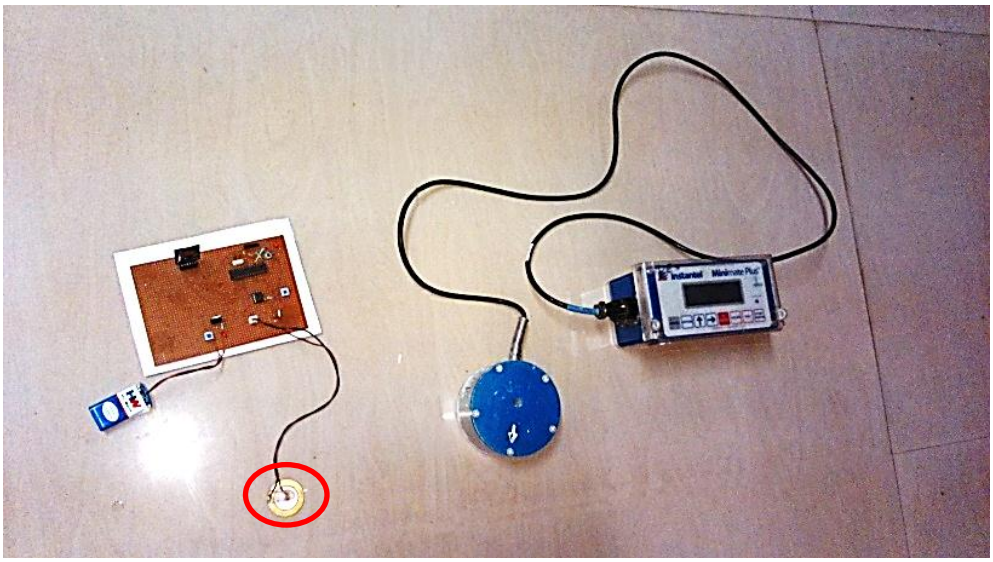

(a)

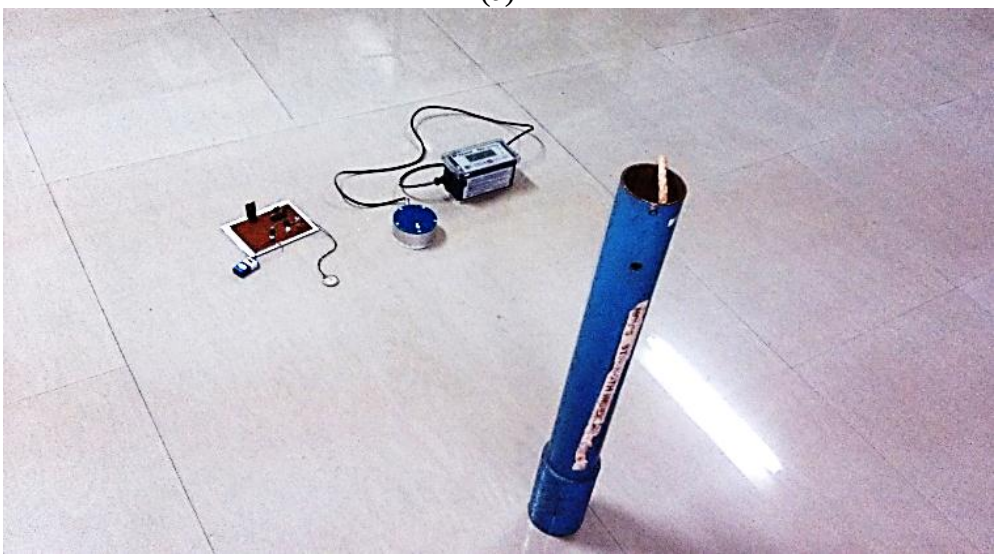

(b)

(c)

(a) Piezo sensor and geophone attached to the ground

(b) Drop weight setup

(c) Dropping a weight from 1m specified height

Fig. 3.29 Validation of piezo generator circuit

In total, 34 readings were collected by dropping a weight of 2.5kg, from specified height of 1m and instruments were placed at 1m distance from the vibration source to verify and validate the functionality of developed piezo generator circuit. Piezo generator circuit and vibration monitor were placed at same distance from the drop weightage. Readings were taken 34 times to find out the precision and accuracy of the piezo device developed.

Similarly, ground vibrations were recorded by dropping a weight from specified height of 1.5m, thereby identifying the PPV of ground vibrations using both instruments, outside the laboratory. Experiments were carried out as shown in Fig. 3.30.

(a)

(b)

(a) Piezo generator circuit and Minimate Plus, Instantel, Canada **(b)** Piezo sensor sandwiched to the ground

Fig. 3.30 Validation of piezo generator circuit (outside)

In total, 30 readings were collected by dropping a weight of 2.5kg, from specified height of 1.5m. Readings were taken 30 times to find out the precision and accuracy of the piezo generator circuit developed. Summary of results obtained from standard weight drop are given in Tables-3.1 and 3.2.

Table – 3.1 Summary of weight drop for validation of piezo generator circuit in the laboratory

Sl. No.	Minimate Values *(mm/s)*	Piezo Values *(digital)*	DC Voltage generated {1 (digital) = 4.883mV} *(mV)*
1	7.24	615.40	3,004.998
2	6.48	550.80	2,689.556
3	6.09	517.65	2,527.685
4	6.35	539.75	2,635.599
5	6.85	582.25	2,843.127
6	5.84	496.40	2,423.921
7	5.21	442.85	2,162.437
8	6.73	572.05	2,793.320
9	5.58	474.30	2,316.007
10	8.00	680.00	3,320.440
11	6.22	528.70	2,581.642
12	6.85	582.25	2,843.127
13	6.73	572.05	2,793.320
14	6.09	517.65	2,527.685
15	5.82	494.70	2,415.620
16	8.00	680.00	3,320.440
17	8.25	701.25	3,424.204
18	7.49	636.65	3,108.762
19	7.87	668.95	3,266.483
20	7.36	625.60	3,054.805
21	9.14	776.90	3,793.603
22	8.51	723.35	3,532.118
23	9.78	831.30	4,059.238
24	9.01	765.85	3,739.646
25	8.64	734.40	3,586.075
26	10.03	852.55	4,163.002
27	8.00	680.00	3,320.440
28	7.62	647.70	3,162.719
29	7.24	615.40	3,004.998
30	11.43	971.55	4,744.079
31	13.84	1,176.40	5,744.361
32	15.62	1,327.70	6,483.159
33	14.48	1,230.80	6,009.996
34	11.30	960.50	4,690.122

Table – 3.2 Summary of weight drop for validation of piezo generator circuit outside the laboratory

Sl. No.	Minimate Values *(mm/s)*	Piezo Values *(digital)*	Dc voltage generated {1 (digital) = 4.883mV} *(mV)*
1	14.35	287	1,401.42
2	33.02	660	3,224.73
3	25.27	505	2,467.87
4	27.69	554	2,704.21
5	27.43	549	2,678.81
6	28.19	564	2,753.04
7	23.37	467	2,282.31
8	0.89	18	86.82
9	27.05	541	2,641.70
10	21.34	427	2,084.06
11	26.29	526	2,567.48
12	22.61	452	2,208.09
13	19.43	389	1,897.53
14	29.59	592	2,889.76
15	24.00	480	2,343.84
16	27.05	541	2,641.70
17	27.05	541	2,641.70
18	27.69	554	2,704.21
19	26.42	528	2,580.18
20	27.05	541	2,641.70
21	1.40	28	136.43
22	27.94	559	2,728.62
23	25.91	518	2,530.37
24	27.81	556	2,715.92
25	28.83	577	2,815.54
26	25.53	511	2,493.26
27	27.81	556	2,715.92
28	28.96	579	2,828.23
29	16.38	328	1,599.67
30	29.72	594	2,902.46

3.3 Field Investigations with Piezo Generator Circuit

Studies for generation of electrical voltage from blast induced ground vibrations were carried out in four different formations. Studies were carried out in two phases in

limestone formation. In the initial phase of studies, basic piezo generator circuit model was employed in field investigations. Later on, improved piezo generator circuit model (with microcontroller and memory module to store voltage magnitude values) was adopted in the studies. Readings were collected using final improved version of the piezo generator circuit model in all other three formations.

3.3.1 Electrical energy analysis in limestone formation

Piezo generator circuit model and vibration monitor (Minimate Plus, Instantel, Canada) were positioned at identical distance from the blast location. Immediately after the blast, the magnitude of obtained voltage (resulting from ground vibrations) was noticed using multimeter, Mastech. During the initial phase of studies, Electrical energy was tapped from nine (9) blast induced ground vibrations (Fig. 3.31).

Electrical Energy, was calculated from the obtained voltage:

$$E = \frac{1}{2} CV^2 \quad \text{----------} \quad \textbf{(3.4)}$$

where,

E = Electrical energy (J or µJ)
C = Capacitance of the capacitor connected across the load, 2200µF
V = Electrical voltage tapped from ground vibrations (V or mV)

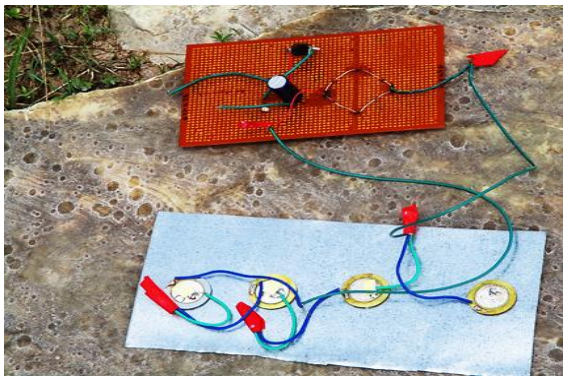

(a)

(b)

(c)

(a) Basic piezo generator model **(b)** Minimate with piezo circuit
(c) Observing the tapped voltage

Fig. 3.31 Tapping of electrical voltage from ground vibrations in limestone mines using basic circuit model

Later on, improved model of piezo generation circuit was used in the studies along with vibration monitor (Minimate Plus, Instantel, Canada) in which both were placed at same location. During this phase of studies, electrical energy was tapped from 57 blast induced ground vibrations, in hard limestone formation, and 37 blast induced ground vibrations, in soft limestone formation (Fig. 3.32). During studies, the piezo circuit model with microcontroller and memory module was used in the field to tap electrical voltage from blast induced ground vibrations, and thereby electrical energy.

Electrical Energy, was calculated from the obtained voltage using the formula:

$$E = \frac{V^2}{R} t \qquad \text{----------} \qquad \textbf{(3.5)}$$

where,

E = Electrical energy (J or µJ)
V = Electrical voltage tapped from ground vibrations (V or mV)
R = Resistance of the circuit, 1Ω
t = Time period of tapped vibration(s)

(a) (b)

(a) Fixing piezo generator **(b)** Minimate with piezo circuit

Fig. 3.32 Tapping of electrical voltage from ground vibrations in limestone mines using microcontroller based piezo generator circuit

3.3.2 Electrical energy analysis in coal formation

Studies related to electrical energy tapped from ground vibrations were carried out in SRP-3 & 3A underground coal mine belonging to The Singareni Collieries Company Limited, Srirampur Area, Adilabad District, Telangana State. Piezo generator circuit model and vibration monitor were placed at identical distance from the blast location. Electrical energy was tapped from 36 blast induced ground vibrations (Fig. 3.33).

(a) (b)

(c) (d)

(a) Minimate with piezo circuit **(c)** During blasting operation
(b) Piezo circuit output **(d)** Vibration detection

Fig. 3.33 Tapping of electrical voltage from ground vibrations in coal formation using microcontroller based piezo generator circuit

3.3.3 Electrical energy analysis in sandstone formation

At this stage, studies were carried out in two different sandstone bench formations of a coal mines. One mine belongs to The Singareni Collieries Company Limited. The Singareni Collieries Company Limited is operating the RG OC-I and RG OC-III opencast mines, major mechanized opencast mines of SCCL in Godavarikhani Area, Karimnagar District, Telangana. The other location is Singareni Thermal Power Project (STPP), Mancherial Area, Jaipur Mandal, Adilabad District, Telangana State.

During field studies, Microcontroller based piezo generator circuit stored magnitudes of tapped electrical potential (voltage) in the microSD card using memory module. Electrical energy was tapped from 41 blast induced ground vibrations (Fig. 3.34).

(a) (b)

(c)

(a) Piezo generator circuit **(b)** Fixing microSd card
(c) During blasting operation

Fig. 3.34 Tapping of electrical voltage from ground vibrations in sandstone bench formations using microcontroller based piezo generator circuit

3.3.4 Electrical energy analysis in granite formation

Studies related to electrical energy tapping from ground vibrations were carried out in five granite formations. During research studies, the piezo generator circuit model was employed to tap electrical voltage from blast induced ground vibrations along with vibration monitor (Minimate Plus, Instantel, Canada). Electrical energy was tapped from 94 blast induced ground vibrations (Fig. 3.35).

Fig. 3.35 Tapping of electrical voltage from ground vibrations in granitic formations using microcontroller based piezo generator circuit

3.4 Geotechnical Parameters

3.4.1 Compression testing of rock samples

Calculation of geotechnical parameters was carried out for four different formations, viz. Limestone, Coal, Sandstone and Granite, by taking samples of the respective rock formations as explained below:

Initially, samples belonging to four different formations were prepared into cylindrical shape in 2.5:1 or above ratio, as per the ISRM standards, using rock cutting machine (Anon, 2008c; Dudley et al., 2016). In each formation, 3 samples were taken and the obtained results were averaged. The length to diameter ratio of test specimens was taken as 2.5-3.0 (Lama and Vutukuri, 1978). Average dimensions of the rock samples (in four different formations viz. Limestone, Coal, Sandstone and Granite) used for compression testing are listed in Table-3.3.

Table – 3.3 Details of rock samples used

Type of formation	Length, L (mm)	Diameter, D (mm)	Volume, V* (cc)	Mass, M (g)
Limestone	135	54	309.180	779
Coal	118	42	163.482	208
Sandstone	151	54	345.823	571
Granite	140	54	320.631	923

*$Volume = \frac{\pi}{4}.D^2.L$

After finding the dimension of samples, individual sample was taken and placed into compression testing machine for measuring the stress and strain to calculate Young's Modulus (E) and Poisson's Ratio (μ), thereby finding Bulk Modulus (k) and Shear Modulus (G), for carrying out parametric study using numerical modelling. Placement of rock samples belonging to four different formations (Limestone, Coal, Sandstone and Granite) with LVDT's (Linear Variable Differential Transformers) into compressive testing machine for finding Young's Modulus (E) and Poisson's Ratio (μ) is depicted in Fig. 3.36.

(a)

(b)

(c)

Fig. 3.36 Placement of rock samples into compression testing machine

Testing process was started by surrounding the rock sample with three LVDT's which were placed horizontally, in which each LVDT was separated by 120^0 angle to another LVDT, for measuring strain of the rock sample accurately. In addition, one more LVDT was placed in vertical direction during compression testing to measure the vertical strain. LVDT unit was in connection to the PC based data acquisition system (DAQ), KAPTL Instrumentation (Model KI_L_4100_4_S).

PC based data acquisition (DAQ) system when integrated with compression testing machine computes horizontal deformation of rock sample, vertical deformation of rock sample, applied load, horizontal strain, vertical strain, stress acting on the rock sample, Young's Modulus and Poisson's ratio values with a rate up to 200 data values per second (Fig. 3.37). Measurement of those parameters for four formations with different rock samples was performed in steps by increasing the load on rock sample till occurrence of failure. Similar, methodology was followed to successive rock samples.

Fig. 3.37 PC based DAQ system integrated with compression testing machine

Values corresponding to respective rock formations were saved in the PC using DAQ (Data Acquisition System) for further analysis after the occurrence of sample failure. After failure of rock sample due to applied load, the rock sample was removed safely by resetting the pressure load acting on that and next sample was placed for testing. Furthermore, the *load at failure* was noted for the failed rock sample for further analysis.

3.4.2 Data collection

For limestone formation, 5,141 data values were collected till the occurrence of rock sample failure using PC based DAQ system for finding various parameters which include horizontal deformation of rock sample, vertical deformation of rock sample, applied load, horizontal strain, vertical strain, stress acting on the rock sample, Young's Modulus and Poisson's ratio by averaging the obtained data values for three rock samples. Similarly, for coal formation 5,391 data values, for sandstone bench formation 1,283 data values and for granite formation 4,989 data values were collected till the occurrence of failure of respective rock samples.

3.4.3 Young's modulus

It is defined as the ratio of stress (force per unit area, also applied pressure) to the strain (proportional deformation) developed in a rock sample. Whenever load is applied to the rock sample, it will get deformed and elastic material body will come back to its original shape once the load is removed. Further, the information related to solid material stiffness can be obtained by Young's Modulus (Anon, 2016d). The formula for the Young's Modulus is given by,

$$E = \frac{Stress}{Strain} \qquad \text{----------} \qquad \textbf{(3.6)}$$

where,

E = Young's Modulus, Pa or N/m^2

Stress = $\frac{Load\ in\ kN}{Area\ in\ m^2}$

Strain = $\frac{Deformation}{Original\ dimension} = \frac{\Delta l}{l} = \left|\frac{l_1 - l_2}{l}\right|$

3.4.4 Poisson's ratio

When load is applied on a material in one direction, it typically has a tendency to grow in the other two directions opposite to the heading of pressure. This mechanism is known as Poisson effect. On the other hand, if the material is extended, in one direction, then it normally tends to contract in the directions transverse to the heading of expansion. That is a typical perception when an elastic band is extended, it turns out to be discernibly more slender (Anon, 2016e).

It is the ratio of Lateral Strain to the Longitudinal Strain and is given by,

$$\mu = \frac{(\Delta r/r)}{(\Delta l/l)} = \frac{(|r_1 - r_2|/r)}{|l_1 - l_2|/l)} \quad \text{----------} \quad \textbf{(3.7)}$$

where,

μ = Poisson's ratio
$\Delta r/r$ = Lateral strain
$\Delta l/l$ = Longitudinal strain
r_1 = Initial radius of the sample
r_2 = Final radius of the sample
r = Actual radius of the sample
l_1 = Initial length of the sample
l_2 = Final length of the sample
l = Actual length of the sample

3.4.5 Bulk modulus

Bulk Modulus of a rock sample is defined as the change in stress (pressure) to the change in volumetric strain, which expresses the stress built for change in 1% of volumetric strain, i.e.,

$$\text{Volumetric Strain} = \frac{Change\ in\ Volume}{Actual\ Volume} = \frac{\Delta V}{V} = \left|\frac{V_1 - V_2}{V}\right| \quad \text{----------} \quad \textbf{(3.8)}$$

where,

V_1 = Initial volume of the material
V_2 = Final volume of the material

The formula for the Bulk Modulus is given by,

$$B = \frac{E}{3(1-2\mu)} \quad \text{----------} \quad \textbf{(3.9)}$$

where,

B = Bulk Modulus, Pa
E = Young's Modulus, Pa
μ = Poisson's ratio

3.4.6 Shear modulus

Reaction of the material to applied stress can be described by Shear Modulus or Rigidity Modulus, G. Also, called as Modulus of Rigidity, it is the coefficient of flexibility for a shearing force.

The formula for the Shear Modulus is given by,

$$G = \frac{E}{2(1+\mu)} \quad \text{----------} \quad \textbf{(3.10)}$$

where,

G = Shear Modulus, Pa
E = Young's Modulus, Pa
μ = Poisson's ratio

Summary of geotechnical parameters obtained for four different rock formations are listed in Table-3.4. It was observed from the results obtained that granitic formation is having the highest compressive strength whereas the coal formation is having the lowest strength (Table-3.4).

Table – 3.4 Summary of geotechnical parameters

Type of formation	**ρ (g/cc)**	**UCS (MPa)**	**E (GPa)**	**μ**	**B (GPa)**	**G (GPa)**
Limestone	2.52	68.84	11.15	0.20	6.19	4.65
Coal	1.27	17.78	1.46	0.39	2.21	0.53
Sandstone	2.23	56.30	3.36	0.32	3.11	1.27
Granite	2.88	151.10	20.79	0.19	11.18	8.74

ρ - Average Density, UCS – Unconfined Compression Strength, E - Young's Modulus, μ - Poisson's Ratio, B - Bulk Modulus, G - Shear Modulus

3.5 Numerical Modelling

Numerical modelling methods can be extensively used to simulate the blast conditions as a parametric study. SIMULIA Abaqus / CAE based Finite element method with both *Python Scripting and GUI* was used to estimate the ground vibration velocity (PPV) resulted from a given blast. Parameters observed during a blast in the simulated model are stress components at integral points and spatial velocities at nodes (PPVs). Initially, calibration was done by developing models with field conditions in each formation. Later, validation of results obtained from developed models was done by comparing with the field results.

3.5.1 Calibration of developed models

Calibration of numerical modelling was carried out for assessing the reliability of models. Initially, four models were developed in four different rock formations by considering actual field conditions. Later, models were developed with variation in the field conditions in all four formations as a parametric study.

3.5.2 Development of models in all four formations

After calibration of developed models, numerical modelling for all four formations was carried out to simulate the blast conditions for assessing the seismic energy component (PPV) resulting from a given blast as a parametric study, and correlate the results with data generated in earlier field investigations from vibration monitoring and piezo electric generator. Models were developed in all four formations (viz. Limestone, Coal, Sandstone and Granite) with parameters similar to field values, to maintain the analogous between simulation results and field results. Altogether, 98 blast models were created using SIMULIA Abaqus / CAE interface, among them, 28 models in limestone formation, 14 models in coal formation, 15 models in sandstone, and 41 models in granitic rock formation. Typical size of each developed model after running the job was up to 3.71GB in limestone formation, 461MB in coal formation, 6.02GB in sandstone formation and 5.47GB in granite formation. Each model job run took up to 8-27hrs for completion, in different rock formations.

Different parameters like elastic properties, explosive properties were used during the development of models (Table-3.5).

Table – 3.5 Parameters used in numerical modelling

Rock formation / Parameter	Limestone	Coal	Sandstone	Granite
i. Elastic properties of rock formations				
Young's Modulus (GPa)	14.86	0.46	15.15	32.79
Poisson's Ratio	0.20	0.39	0.32	0.19
Density (g/cc)	2.52	1.27	2.23	2.88
ii. Explosives used				
Type of explosive used	ANFO	Slurry	Slurry	Emulsion
iii. *Dimensions of face*				
Area of the blast location (m^2)	21 to 1,512	5 to 8	396 to 3,630	3 to 200
Height / Depth of the face (m)	6 to 10	1.80	4.5 to 20.7	1.2 to 6

During numerical modelling, both total explosive charge per blast and detonation pressure of the explosive were chosen as loading parameters. Total explosive charge per blast was obtained from field investigations. Detonation pressure of an explosive was determined from velocity of detonation and density (properties of respective

explosives provided by those manufacturers) of an explosive using the following equation (Anon, 2015d):

$$P_d = \frac{2.5 \times V_d \times \rho}{0.0000001} \quad \text{----------} \quad \textbf{(3.13)}$$

where,

P_d = Detonation pressure, Pa
V_d = Velocity of detonation of an explosive, m/s
ρ = Density of an explosive, g/cc

Details of various explosives with their respective density and VOD (velocity of detonation) values given in Table-3.6 below were used during the development of models. All the explosive details are obtained from corresponding explosive manufacturers' data sheets (Anon, 2016f; g).

Table – 3.6 Details of explosives employed in the numerical modelling

Type of Explosive / Description	ANFO	Slurry	Emulsion
Density (g/cc)	0.85	1.20	1.33
Velocity of detonation, VOD (m/s)	3,900-4,200	4,200-4,400	4,800

CHAPTER 4

RESULTS AND DISCUSSION

Results obtained from field investigations, finite element modelling studies and statistical analysis are presented and discussed below:

1. Case Studies: Assessment and estimation of seismic energy dissipated by ground vibrations at specified distances in four different formations – Limestone, Coal, Sandstone and Granite, using signal processing approach.
2. Correlation of seismic energy with critical blast parameters using MATLAB based multiple regression analysis was carried out. Also, development of a statistical model for seismic energy was done, based on critical blast parameters using ANOVA analysis.
3. Assessment of relationship between seismic energy and average fragmentation was carried out.
4. Comparison of electrical output generated from the piezo generator with the seismic data generated from blast vibration monitors was performed, and also the relationship between them was assessed.
5. Parametric study was carried out with a blast load by simulating blast conditions for assessing the seismic energy component (PPV) resulting from a given blast and following responses of the bench (blast location) to dynamic load were observed in four different formations:
   a. Stress components at integral points, S
   b. Spatial velocities at nodes (PPVs), V
6. MATLAB based three-dimensional (3D) regression analysis was subsequently carried out for the results of dynamic analysis, to find the correlation of model results with data generated from vibration monitoring and piezo electric generator.

4.1 Seismic Energy Analysis

4.1.1 Limestone formation

Seismic energy analysis of ground vibrations based on the results of field investigations carried out in three different opencast limestone mines of harder formation and one opencast limestone mine of softer formation, are discussed in this section. In total, 116 blast vibration events from harder limestone formation and 37 blast vibration events from softer limestone formation were collected using ground vibration monitors for signal processing analysis of seismic energy. Locations of blasts conducted in four limestone mines of both harder and softer formations are depicted in Fig. 4.1.

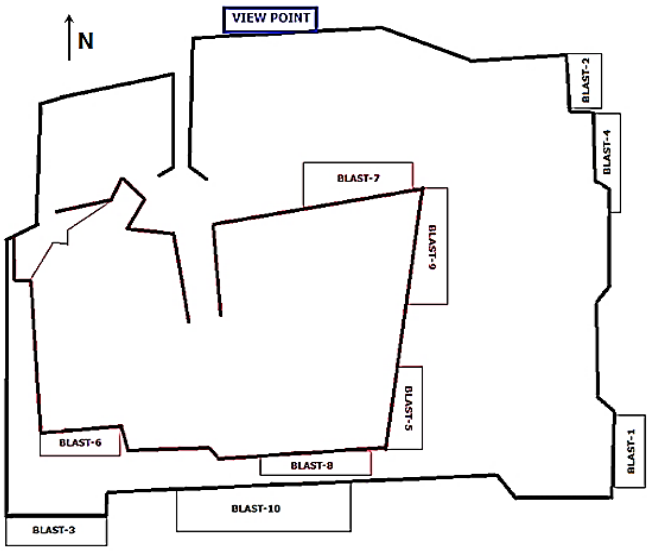

(a)

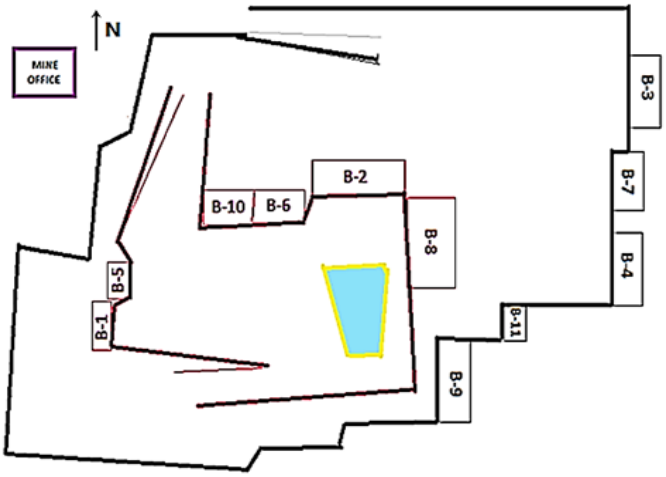

B-1,2,3,…. indicates respective blast locations

(b)

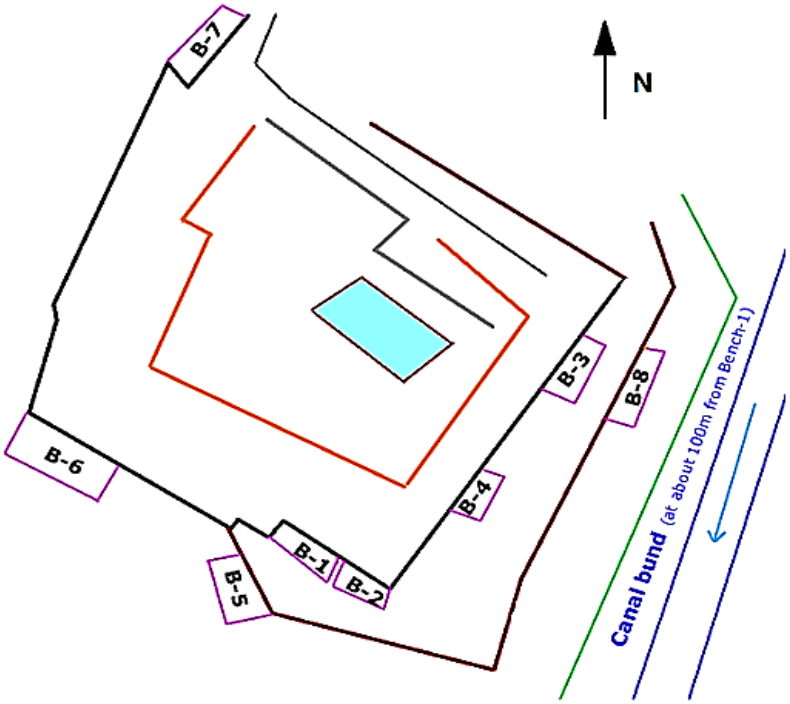

B-1,2,3,…. indicates respective blast locations

(c)

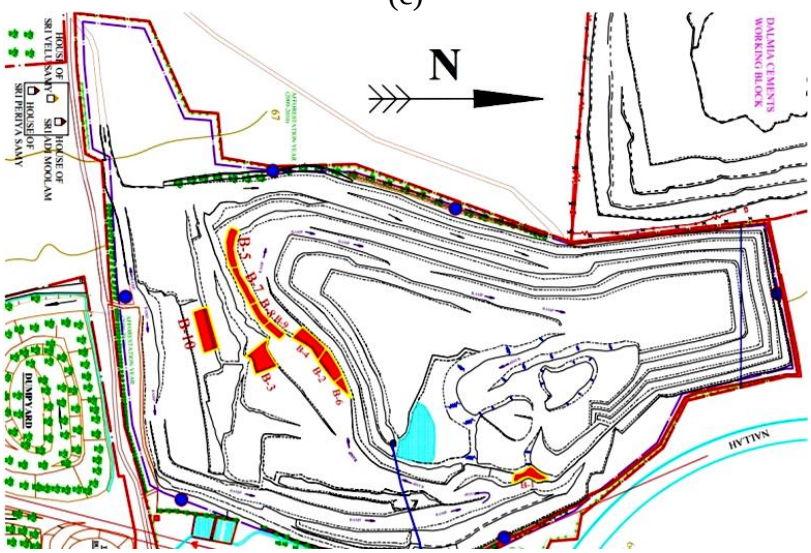

(d)

(a) Limestone Mine-1 (harder formation)
(b) Limestone Mine-2 (harder formation)
(c) Limestone Mine-3 (harder formation)
(d) Limestone Mine-4 (softer formation)

Fig. 4.1 Locations of blasts in limestone mines

Maximum charge per delay (MCD), was varied as 14.35kg, 24.58kg, 28.33kg, 30.17kg, 30.36kg, 30.79kg, 34.04kg, 34.65kg, 34.49kg, 36.57kg, 36.67kg, 37.5kg, 38.33kg, 39.06kg, 39.28kg, 41.67kg, 43.92kg, 45.65kg, 46.15kg, 47.32kg, 48.32kg,

48.53kg, 49.24kg, 50.42kg, 51.25kg, 51.40kg, 54.77kg, 61.76kg, 70.14kg, 81.72kg, 91.18kg and 94.26kg, in harder formation and 19.46kg, 25.02kg, 30.58kg, 36.14kg, 44.48kg and 66.72kg, in softer formation, for different blast rounds. Minimum and maximum values of seismic energy component obtained from blast induced ground vibration events are 26,762μJ and 11,12,59,278μJ, respectively in harder formation and 6,715μJ and 5,46,976μJ, respectively in softer formation. From the analysis of field data, it was noticed that L-wave velocity for limestone mines is in the range of 120m/s to 5,275m/s, in harder formation, 444m/s to 3,50,000m/s, in softer formation, and T-wave velocity for limestone mines is in the range of 92m/s to 4289m/s, in harder formation and 246m/s to 25,385m/s, in softer formation. Furthermore, it was observed that the propagation of ground vibrations (Longitudinal wave and Transverse wave) is influenced by MCD, distance and geology.

Blast locations were surveyed twice, i.e. before and after blasting operations and respective muckpiles were examined thoroughly to acquire the fragmentation and a relationship between seismic energy and fragmentation was identified. Muck pile images of different blasts were processed using Wipfrag software (Appendix-III). Average fragmentation size (K_{50}) was considered for analysis from fragmentation distribution curves of different blasts. It was tried to correlate the average fragmentation size with seismic energy from all the blasts. Summary of fragmentation analysis carried out in limestone formation using Wipfrag software is given in Tables-4.1 and 4.2.

Table – 4.1 Summary of fragmentation analysis carried out in hard limestone formation

No. of Holes	Percentage Passing						50% Passing	Seismic Energy (μJ)
	-1000 (mm)	-500 (mm)	-300 (mm)	-150 (mm)	-125 (mm)	-100 (mm)	(mm)	
40	79.35	64.54	55.01	41.73	38.41	34.38	243.46	30,47,499
33	97.67	85.49	73.97	58.62	54.82	50.28	98.87	92,902
29	84.94	66.18	52.45	38.02	34.91	31.25	274.50	51,39,689
84	63.11	46.84	35.62	23.28	20.82	17.91	350.00	1,11,47,879
53	97.40	85.10	70.37	54.39	50.64	46.37	121.24	4,42,636
46	92.12	80.85	68.26	52.07	48.55	44.27	135.31	7,61,090
59	79.10	61.41	49.79	36.06	33.24	30.14	303.55	51,62,528

No. of Holes	Percentage Passing						50% Passing	Seismic Energy (µJ)
	-1000 (mm)	-500 (mm)	-300 (mm)	-150 (mm)	-125 (mm)	-100 (mm)	(mm)	
61	89.42	78.22	68.14	52.43	48.18	42.94	135.73	7,90,078
68	86.99	75.33	65.02	50.46	46.30	41.05	147.23	13,32,951
28	88.74	74.20	61.56	44.66	40.19	34.91	197.40	18,68,921
27	96.77	90.49	81.82	66.70	62.32	57.68	68.77	31,994
34	92.05	81.90	72.36	58.25	53.96	48.40	107.21	1,53,858
30	94.44	81.84	72.71	59.48	55.17	49.54	102.05	1,13,669
34	85.58	73.46	64.84	51.54	48.19	43.71	138.53	9,15,484
26	80.40	70.27	63.10	51.56	47.79	42.27	139.66	12,42,062
34	90.55	82.63	74.79	62.48	59.02	54.57	81.94	59,698
26	90.35	78.46	71.15	59.76	55.73	50.51	98.45	87,351
53	92.79	77.31	65.94	54.94	51.60	47.60	115.01	2,68,663
63	93.50	83.17	75.27	60.42	55.38	48.79	104.60	1,14,899
22	99.30	89.24	78.06	62.90	59.43	55.50	72.36	55,412
41	83.99	69.51	57.34	41.61	37.90	33.34	230.03	22,55,137
30	95.67	89.05	78.17	59.27	54.70	48.87	104.83	1,35,798
30	95.24	85.26	74.26	55.88	51.17	45.42	119.90	4,07,380
24	94.08	82.58	72.39	56.45	52.00	46.16	116.43	3,33,637
18	93.99	83.80	71.62	56.02	51.53	46.09	117.96	3,34,437
16	95.23	84.23	75.04	57.93	52.99	46.73	113.05	2,24,877
21	97.54	87.77	75.25	56.67	52.18	47.11	114.27	2,67,454
18	95.41	82.40	69.44	49.05	43.96	38.58	156.95	18,32,992
20	90.74	74.16	57.34	36.63	31.75	25.97	246.84	40,10,754
18	98.09	94.63	82.36	59.76	54.78	48.75	105.17	1,44,073
14	93.22	76.82	60.80	38.21	32.27	25.32	228.28	21,37,921
10	100.00	97.44	90.18	67.10	61.09	52.06	94.95	81,447
20	93.22	76.82	60.80	38.21	32.27	25.32	228.28	20,77,140
17	95.23	84.23	75.04	57.93	52.99	46.73	113.05	1,93,712
14	100.00	97.44	90.18	67.10	61.09	52.06	94.95	79,350
12	95.24	85.26	74.26	55.88	51.17	45.42	119.90	3,89,359
17	84.61	65.33	52.54	38.10	34.19	29.03	273.61	49,71,507
20	95.97	89.48	78.24	62.70	58.40	51.16	98.89	1,00,293
22	92.49	78.76	66.75	49.61	45.30	39.61	153.40	15,24,805
15	95.34	81.51	70.22	53.91	48.74	42.54	131.11	5,34,415
10	100.00	84.75	77.85	61.18	57.19	52.51	91.28	70,570
13	95.41	82.40	69.44	49.05	43.96	38.58	156.95	15,39,811
27	90.74	74.16	57.34	36.63	31.75	25.97	246.84	37,55,633

Table – 4.2 Summary of fragmentation analysis carried out in soft limestone formation

No. of Holes	Percentage Passing						50% Passing	Seismic Energy (µJ)
	-1000 (mm)	-500 (mm)	-300 (mm)	-150 (mm)	-125 (mm)	-100 (mm)	(mm)	
20	97.77	87.78	74.71	55.09	49.05	42.19	128.91	5,07,013
21	100.00	91.49	79.93	62.17	58.46	52.63	91.03	61,670
23	97.21	83.41	73.72	55.35	50.36	43.88	123.60	4,62,495
20	100.00	90.42	83.62	68.83	64.65	60.28	67.31	26,792
18	92.35	79.18	68.90	56.00	52.62	52.62	109.12	1,92,021
13	89.87	73.76	58.59	36.12	31.15	25.83	242.66	26,36,438
24	96.22	82.69	70.37	53.20	48.28	42.24	133.73	5,57,814
16	97.36	81.67	67.52	49.77	45.30	40.85	151.98	13,96,885
10	97.14	78.22	66.56	50.53	46.73	41.62	146.50	13,25,460
25	100.00	94.56	85.55	70.44	66.33	61.30	68.95	36,152

A very good correlation between seismic energy and K_{50} (average fragment size) was observed from the Wipfrag analysis in both harder and softer formations (Fig. 4.2).

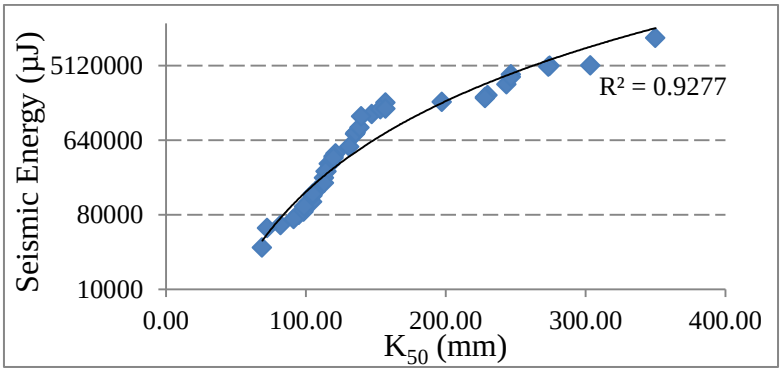

(a)

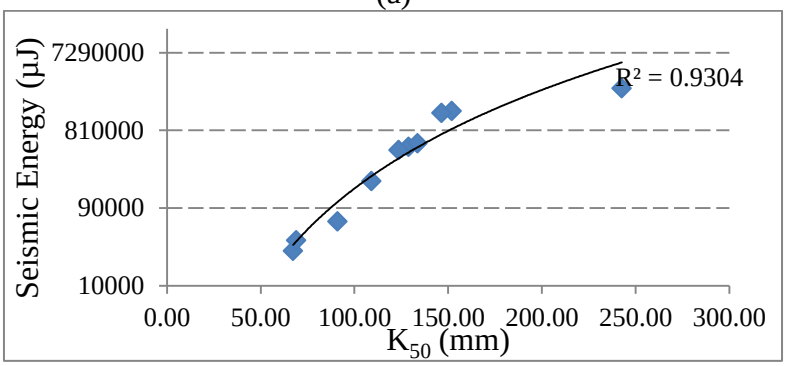

(b)

(a) Seismic Energy Vs. K_{50} (Average fragment size) of harder formation
(b) Seismic Energy Vs. K_{50} (Average fragment size) of softer formation

Fig. 4.2 Relationship between seismic energy and fragmentation in limestone formation

Summary of ground vibrations, seismic energy and fragmentation results obtained for both harder and softer limestone formations are given in Tables-A4.1 and A4.2 (Appendix-IV). Values of Longitudinal wave and Transverse wave velocities influencing ground vibration propagation in both harder and softer limestone formations are given in Tables-A4.3 and A4.4 (Appendix-IV). MATLAB based regression and ANOVA analysis was carried out and results obtained from different limestone mines of harder and softer formations are depicted with corresponding code (Appendix-V).

Further, a proper correlation with R squared value of >70% was observed for L-wave and T-wave velocities with scaled distance in limestone formation. Results obtained from vibration studies in different limestone mines corresponding to L-wave and T-wave velocities are shown in Fig. 4.3.

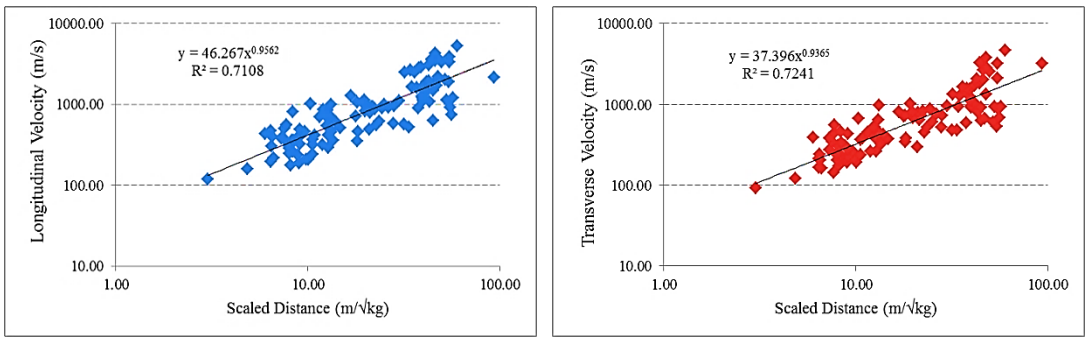

(a) (b)

(a) L-wave Velocity Vs. SD **(b)** T-wave Velocity Vs. SD

Fig. 4.3 Results obtained from vibration studies in limestone formation

From the regression analysis made, relationship between critical parameters (maximum charge per delay, distance, geology) and seismic energy was established for limestone formation using MATLAB (Wiss and Linehan, 1979). It may be stated that from R^2 and adjusted R^2 values, estimation of seismic energy gives more than 82 per cent satisfactory results with a standard error of 6 per cent. Similarly, F-test and P-test carried out using ANOVA analysis also resulted in better validation of results (Tables-4.3 to 4.5). MATLAB code used for ANOVA analysis in limestone formation is given in Appendix-V.

Table – 4.3 Regression analysis for limestone formation

Multiple R	0.906
R Square	0.821
Adjusted R Square	0.815
Standard Error	0.058
Observations	116

Table – 4.4 ANOVA (Analysis of Variance) for limestone formation

	df	*SS*	*MS*	*F*	*Significance F*
Regression	4	1.769E+16	4.423E+15	127.550	1.442E-40
Residual	111	4.849E+15	4.467E+13	-	-
Total	115	3.154E+16	-	-	-

** df – Degree of freedom, SS – Sum of Squares, MS – Mean Square, F – F-test value, Significance F – P-value*

Table – 4.5 Relationship between critical blast parameters and seismic energy in limestone formation

	Coefficients	*Standard Error*	*t-Stat*	*P-value*
Intercept	-74,34,261.85	0.031	-3.36	0.02
MCD (kg)	68,509.68	0.069	-0.99	0.32
Distance (m)	-36,504.07	0.032	1.13	0.26
Scaled Distance (m/√kg)	-55,515.62	0.021	-0.26	0.79
PPV (mm/s)	7,14,390.21	0.036	19.79	4.28E-38

* MCD – Maximum Charge per Delay, PPV – Peak Particle Velocity

From the obtained results, Equation 4.1 was developed to estimate the seismic energy from critical blast parameters based on the field results of Limestone formation:

$$SE = (-74,34,261.86) + (68,509.68).MCD - (36,504.07).D - (55,515.62).SD + (7,14,390.21).PPV \quad \textbf{(4.1)}$$

where,

SE = Seismic energy (μJ)
MCD = Maximum charge per delay (kg)
D = Distance between blast location and monitoring point (m)
SD = Scaled distance (m/√kg)
PPV = Peak particle velocity (mm/s)

4.1.2 Comparison of hard limestone formation and soft limestone formation

An attempt was made to compare the results obtained in four different limestone mines for harder and softer formations. It was observed from the results that softer formation resulted in more seismic energy loss compared to harder formations.

Comparisons were performed considering similar critical blast parameters for both formations, i.e. distance, scaled distance and maximum charge per delay.

Table-4.6 shows the summary of seismic energy in harder and softer limestone formations at similar scaled distances using *staked line with markers* approach. Results obtained are depicted in Fig. 4.4.

Table – 4.6 Summary of seismic energy in harder and softer limestone formations at similar scaled distances

Sl. No.	SD (m/√kg)	Seismic Energy (µJ)	
		Hard Limestone	Soft Limestone
1	10	92,64,400	2,95,524
2	12	20,40,307	5,46,976
3	14	33,66,361	2,42,413
4	18	33,31,585	95,328
5	22	4,46,799	2,53,022

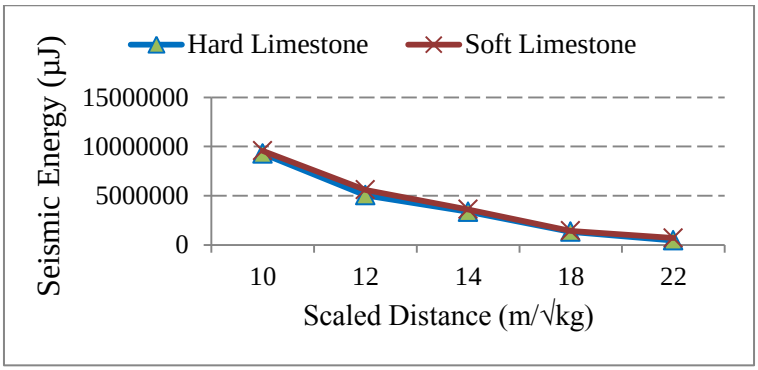

Fig. 4.4 Comparison of seismic energy in harder and softer limestone formations at similar scaled distances

Table-4.7 gives the summary of seismic energy in harder and softer limestone formations at similar distances using *staked line with markers* approach. Results obtained are depicted in Fig. 4.5 below.

Table – 4.7 Summary of seismic energy in harder and softer limestone formations at similar distances

Sl. No.	Distance (m)	Seismic Energy (µJ)	
		Hard Limestone	Soft Limestone
1	56	2,70,09,086	2,95,524
2	80	2,89,70,681	546976

Sl. No.	Distance (m)	Seismic Energy (µJ)	
		Hard Limestone	Soft Limestone
3	94	2,46,91,269	2,42,413
4	133	3,59,719	1,89,693

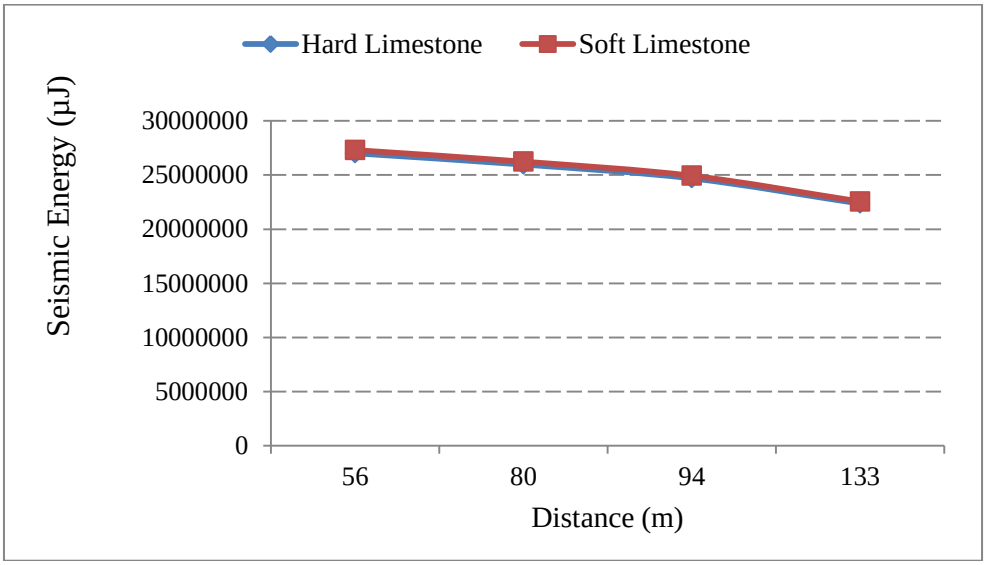

Fig. 4.5 Comparison of seismic energy in harder and softer limestone formations at similar distances

Table-4.8 shows the summary of seismic energy in harder and softer limestone formations at similar MCDs using *staked line with markers* approach. Results obtained are depicted in Fig. 4.6 below.

Table – 4.8 Summary of seismic energy in harder and softer limestone formations at similar maximum explosive charge per delays

Sl. No.	MCD (kg)	Seismic Energy (µJ)	
		Hard Limestone	Soft Limestone
1	25	46,54,975	4,51,380
2	25	34,82,80	3,91,806
3	25	1,10,253	1,16,544
4	25	88,722	81,229
5	30	11,22,775	2,95,524
6	30	5,50,885	2,53,022
7	30	1,68,241	1,90,186
8	30	24,416	81,506
9	37	2,83,287	37,645
10	37	1,23,606	6,715

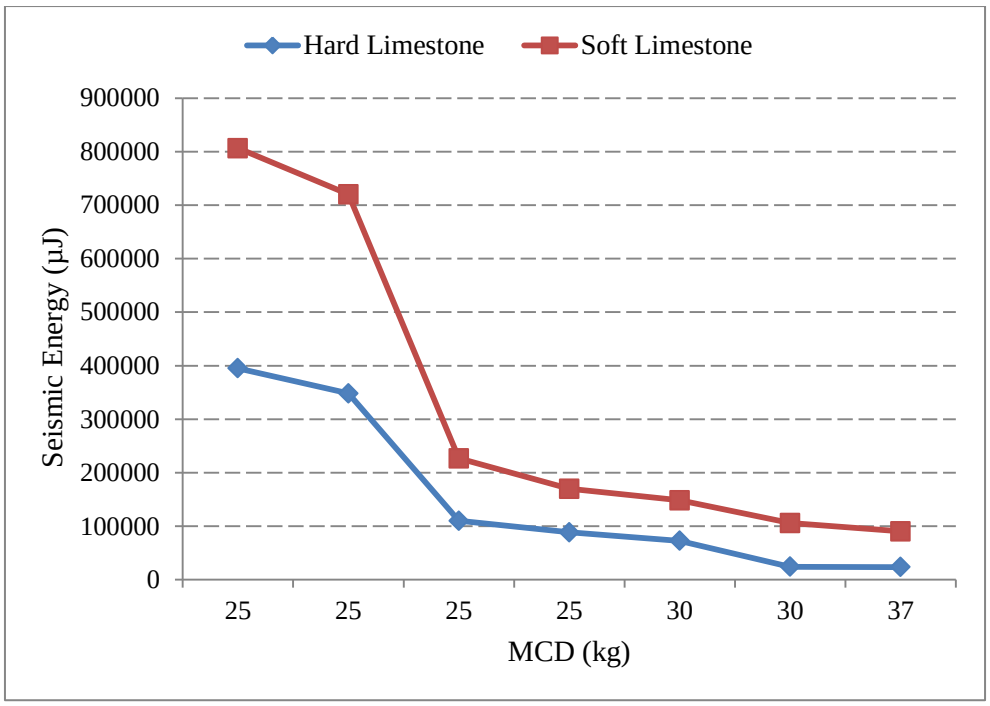

Fig. 4.6 Comparison of seismic energy in harder and softer limestone formations at similar maximum explosive charge per delays

The above analysis also reiterated earlier results that the softer formation results in greater seismic energy loss, through ground vibrations. This point may be of significance while choosing an appropriate type of explosive in given formation

4.1.3 Coal formation

Ground vibrations based seismic energy analysis on the results of field investigations carried out in an underground coal mine are discussed in this section. In total, 86 blast vibration events from underground coal mine were collected using ground vibration monitors for signal processing analysis. Blasts were conducted in two different seams (Seam-5&6) and monitoring was done in seven different seams (Seams – A, 1, 2, 3, 4, 5 and 6). Locations of blasts conducted in the underground coal mine are depicted in Fig. 4.7.

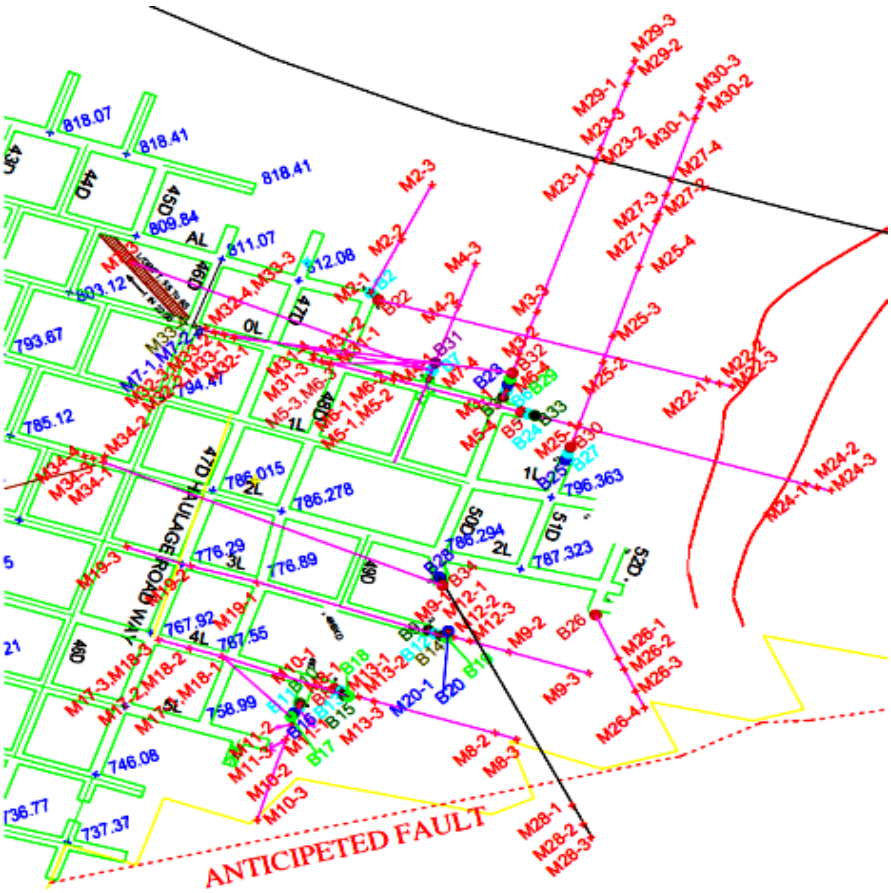

(a)

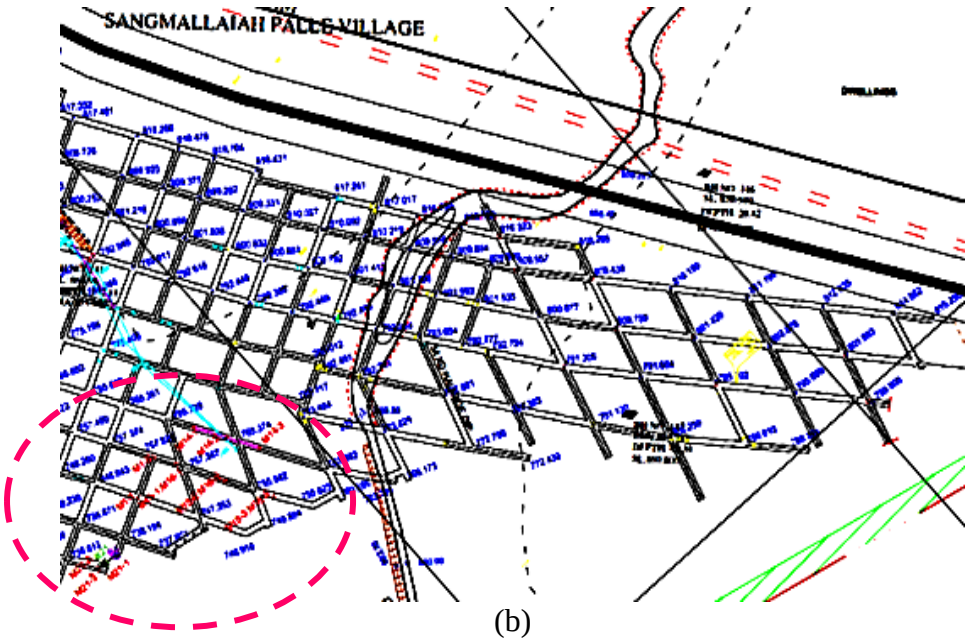

(b)

(a) Underground Coal Mine (Seam-5) **(b)** Underground Coal Mine (Seam-6)

Fig. 4.7 Locations of blasts in underground coal mine

During field studies, MCD was varied as 3.22kg, 3.59kg, 3.77kg, 3.96kg, 4.33kg, 4.70kg, 4.88kg, 4.07kg, 4.81kg and 5.18kg in different blast rounds. Seismic energy component caused due to blast induced ground vibrations was found to vary from 4,250μJ to 19,04,089μJ.

A relationship between seismic energy and fragmentation was noticed. Finer coal was obtained till the seismic energy is 10,000μJ, which has become coarser with further increase in seismic energy. In four blasts, there was no proper sized coal produced and for those the seismic energy values obtained were 13,98,101μJ, 16,54,101μJ, 17,87,182μJ and 19,04,089μJ from signal processing analysis, which are greater to all other values. This clearly indicates that higher is the seismic energy dissipation, coarser is the fragmentation.

Detailed ground vibration monitoring values, seismic energy calculated and fragmentation results obtained are given in the Table-A4.5 (Appendix-IV). Values of Longitudinal wave and Transverse wave velocities influencing ground vibration propagation are given in the Table-A4.6 (Appendix-IV). MATLAB based regression and ANOVA analysis was carried out and results obtained from different seams of underground coal mine are depicted with corresponding code (Appendix-V).

Using regression analysis, the estimation of seismic energy components was done (Wiss and Linehan, 1979). It can be quantified from the coefficient of determination that the estimation of seismic energy gives satisfactory results (more than 86 per cent) with a standard error of 18 per cent. Similarly, F-test and P-test were carried out using ANOVA analysis, which resulted in better validation of results (Tables – 4.9 to 4.11). MATLAB code used for ANOVA analysis in coal formation is given Appendix-V.

Table – 4.9 Regression analysis for coal formation

Multiple R	0.931
R Square	0.867
Adjusted R Square	0.854
Standard Error	0.18
Observations	86

Table – 4.10 ANOVA (Analysis of Variance) for coal formation

	df	*SS*	*MS*	*F*	*Significance F*
Regression	4	9.004E+12	3.251E+12	65.325	5.305E-17
Residual	40	1.378E+12	34,45,99,96,751	-	-
Total	44	1.038E+13	-	-	-

** df – Degree of freedom, SS – Sum of Squares, MS – Mean Square, F – F-test value, Significance F – P-value*

Table – 4.11 Relationship between critical blast parameters and seismic energy in coal formation

	Coefficients	*Standard Error*	*t Stat*	*P-value*
Intercept	-74,34,261.85	0.031	-3.35	0.02
MCD (kg)	4,25,725.40	0.016	-3.58	0.01
Distance (m)	-58,478.38	0.021	3.70	0.01
PPV (mm/s)	87,188.94	0.074	11.65	1.95E-14
Scaled Distance (m/$\sqrt[3]{}$kg)	-83,565.44	0.031	-3.62	0.01

* MCD – Maximum Charge per delay, PPV – Peak Particle Velocity

Equation 4.2 was developed to estimate the seismic energy from critical blast parameters based on the field results of underground coal mine formation:

SE = (–74,34,261.85) + (4,25,725.40).MCD – (58,478.38).D + (8,87,188.94).PPV – (83,565.44).SD ---------- **(4.2)**

where,

SE = Seismic energy (μJ)
MCD = Maximum charge per delay (kg)
D = Distance between blast location and monitoring point (m)
PPV = Peak particle velocity (mm/s)
SD = Scaled distance (m/$\sqrt[3]{}$kg)

4.1.4 Sandstone formation

Seismic energy analysis of ground vibrations carried out in two different sandstone formations is discussed in this section. In total, 43 blast vibration events from sandstone bench formation were collected using ground vibration monitors for signal processing analysis of seismic energy. Locations of blasts conducted in two different sandstone bench formations are depicted in Fig. 4.8.

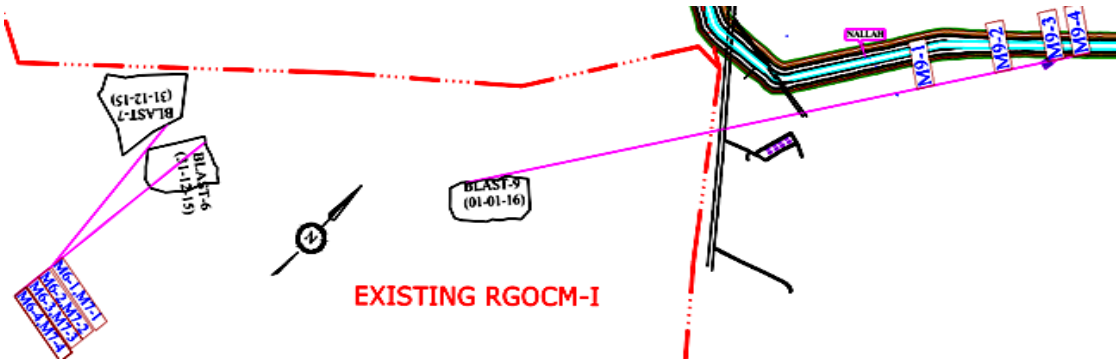

(a)

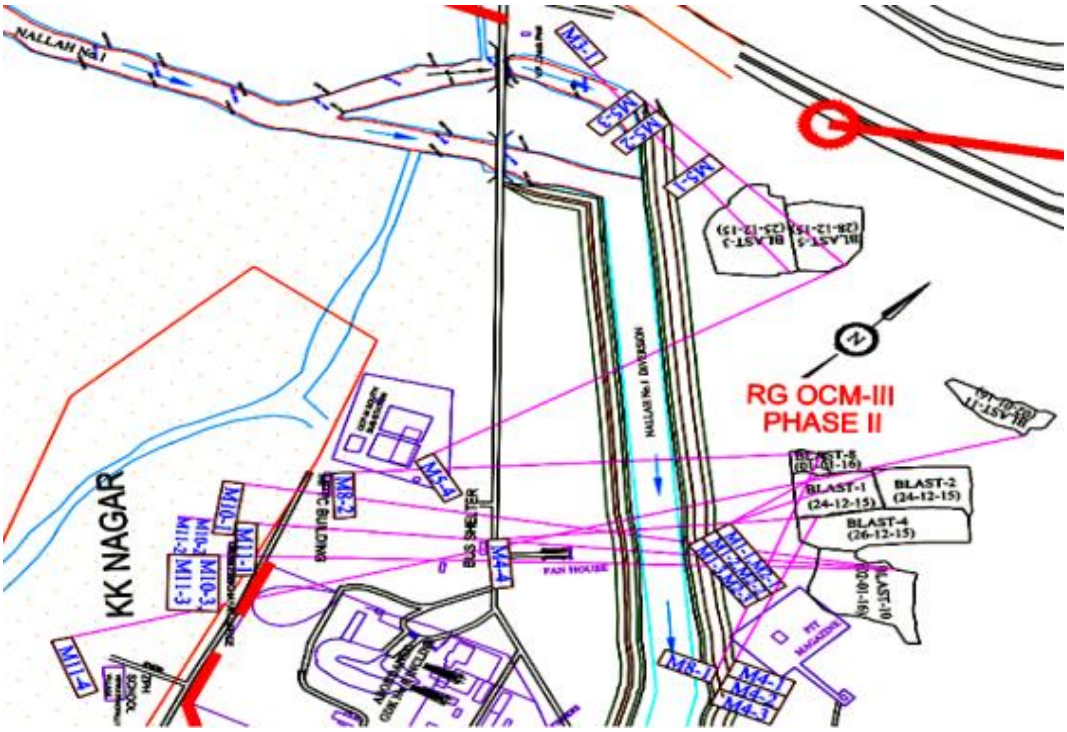

(b)

(a) Sandstone Bench-1 **(b)** Sandstone Bench-2

Fig. 4.8 Locations of blasts carried out during research studies in sandstone formation

In various blast rounds, the MCD was varied as 11.12kg, 20.85kg, 23.24kg, 27.61kg, 34.75kg, 50kg, 66kg, 85kg, 88kg, 90kg, 100kg, 450kg, 460kg and 1,953kg to acquire the relation between the ground vibration propagation and explosive energy. From the results, seismic energy component was found to be ranging from 10,311μJ to 2,73,88,321μJ. Blast locations and the muckpile were inspected before blast and after blast, and the correlation between seismic energy and fragmentation was assessed. Average fragmentation size (K_{50}) was considered for analysis from fragmentation

distribution curves of different blasts. An attempt was made to correlate the average fragmentation size with seismic energy from all the blasts.

It was observed that whenever the seismic energy was greater than 70,000μJ, the corresponding muckpile of the blast was coarser. Moreover, in some blasts very large boulders resulted. The intensity of seismic energy resulting for those blasts was as high as 1,05,44,797.69μJ, 1,47,09,468.86μJ, 1,51,16,635.32μJ, 2,73,88,321.38μJ. This indicates that increase in seismic energy results in lesser utilization of explosive energy, in turn leading to coarser fragmentation. Muck pile images of different blasts were processed using Wipfrag software (Appendix-VI). Summary of fragmentation analysis carried out in sandstone formation from different blasts using Wipfrag software is given in Table-4.12.

Table – 4.12 Summary of fragmentation analysis in sandstone formation

No. of Holes	Percentage Passing						Seismic Energy (μJ)
	-1000 (mm)	-500 (mm)	-300 (mm)	-150 (mm)	-100 (mm)	50% Passing (mm)	
26	86.92	65.20	50.22	31.06	21.07	298.36	2,73,88,321.38
45	89.24	72.81	57.17	38.80	28.18	241.46	84,61,652.43
25	98.96	85.90	68.88	43.48	30.97	188.49	15,62,458.55
30	96.41	80.83	64.08	39.98	28.92	212.36	22,80,225.67
23	96.28	77.59	60.99	40.51	30.88	219.50	36,65,445.40
80	100.00	100.00	92.38	73.30	57.11	74.10	1,34,876.62
29	93.49	77.90	57.99	32.06	21.58	253.77	1,05,44,797.69
29	96.91	80.02	61.33	35.31	23.94	234.68	52,45,447.10
41	86.92	65.20	50.22	30.50	21.07	298.36	1,51,16,635.32
40	89.24	72.81	57.17	38.80	28.18	241.46	69,16,156.65
44	98.69	83.57	61.22	30.70	17.30	266.89	1,47,09,468.86
48	95.82	77.04	55.60	30.24	20.59	244.85	92,77,651.80
20	98.69	83.57	61.22	30.70	17.30	189.06	19,80,472.55
19	100.00	80.14	60.15	38.55	29.33	229.53	47,47,405.68
28	100.00	89.25	78.14	60.40	49.79	101.00	3,76,992.65
42	97.89	93.25	80.90	62.43	53.20	92.51	1,71,645.30
70	92.39	78.64	66.32	48.42	38.14	163.22	10,55,142.78
54	100.00	92.76	84.41	67.67	57.48	87.55	1,36,859.22

No. of Holes	Percentage Passing						Seismic Energy (µJ)
	-1000 (mm)	-500 (mm)	-300 (mm)	-150 (mm)	-100 (mm)	50% Passing (mm)	
64	96.63	91.35	82.19	65.39	54.37	91.32	1,60,142.93
40	100.00	93.59	81.69	64.33	52.98	123.97	5,13,484.49

A very good correlation was observed between seismic energy and K_{50} (average fragment size) from the Wipfrag analysis in sandstone bench formations (Fig. 4.9).

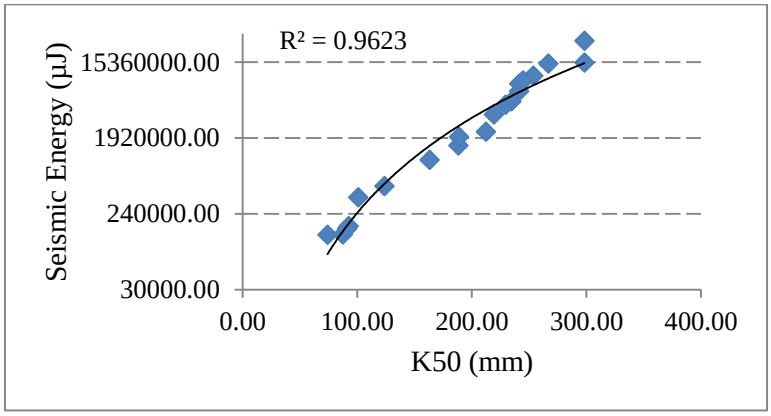

Fig. 4.9 Relationship between seismic energy and fragmentation in sandstone formation

Summary of ground vibrations, seismic energy and fragmentation results obtained for sandstone formations are given in Table-A4.7 (Appendix-IV). Values of Longitudinal wave and Transverse wave velocities influencing ground vibration propagation in sandstone formation are given in Tables-A4.8 (Appendix-IV). MATLAB based regression and ANOVA analysis was carried out and results obtained from different sandstone benches of coal mines are depicted with corresponding code (Appendix-V).

Analysis of field data revealed that the L-wave velocity and T-wave velocity for sandstone bench formation are in the range of 109.05m/s to 75,000m/s and 108.70m/s to 20,000m/s, respectively. Further, a proper correlation was observed for L-wave and T-wave velocity components of ground vibrations with scaled distance in sandstone bench formation. Results obtained from vibration studies in sandstone bench formations corresponding to L-wave and T-wave velocities are shown in Fig. 4.10.

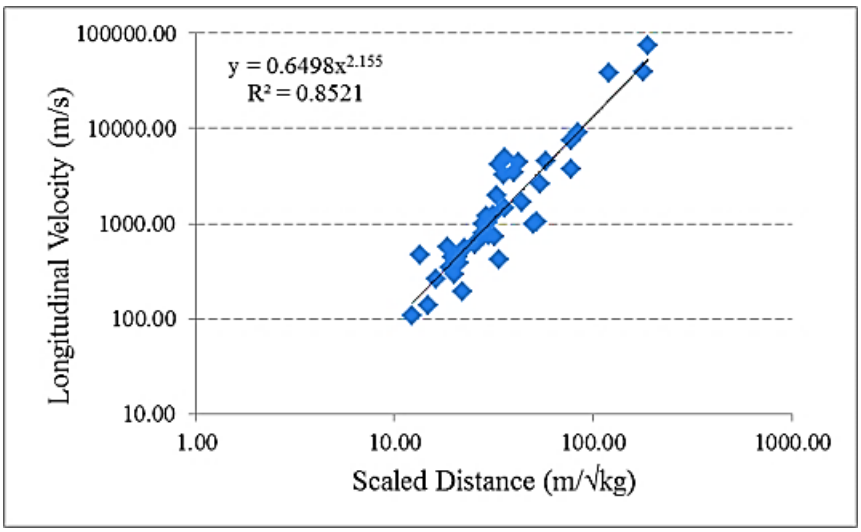

(a)

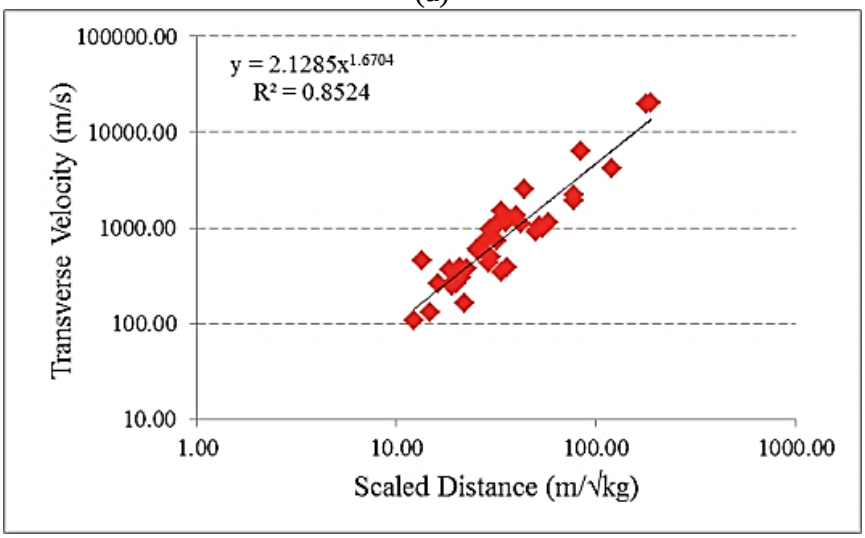

(b)

(a) L-wave Velocity Vs. SD **(b)** T-wave Velocity Vs. SD

Fig. 4.10 Results obtained from vibration studies in sandstone formation

From the regression analysis made, relationship between critical parameters in blast design and seismic energy was established for sandstone bench formation using MATLAB (Wiss and Linehan, 1979). It may be stated that from R^2 and adjusted R^2 values, estimation of seismic energy gives more than 95 per cent satisfactory results with a standard error of 12 per cent. Similarly, F-test and P-test carried out using ANOVA analysis also resulted in better validation of results (Tables – 4.13 to 4.15). MATLAB code used for ANOVA analysis in sandstone formation is given in Appendix-V.

Table – 4.13 Regression analysis for sandstone formation

Multiple R	0.97
R Square	0.95
Adjusted R Square	0.95
Standard Error	0.12
Observations	43

Table – 4.14 ANOVA (Analysis of Variance) for sandstone formation

	df	*SS*	*MS*	*F*	*Significance F*
Regression	4	1.20E+15	4.01E+14	200.62	5.39E-25
Residual	38	5.70E+13	1.50E+12	-	-
Total	42	1.26E+15	-	-	-

** df – Degree of freedom, SS – Sum of Squares, MS – Mean Square, F – F-test value, Significance F – P-value*

Table – 4.15 Relationship between critical blast parameters and seismic energy in sandstone formation

	Coefficients	*Standard Error*	*t-Stat*	*P-value*
Intercept	-33,79,407.00	0.076	-4.42	8.05E-05
MCD (kg)	1,733.23	0.021	-0.82	0.42
Distance (m)	-2,799.90	0.025	1.11	0.27
Scaled Distance (m/√kg)	5,33,836.40	0.024	21.96	4.42E-23
PPV (mm/s)	-32,269.67	0.015	3.04	0.05

* MCD – Maximum Charge per Delay, PPV – Peak Particle Velocity

From the obtained results, an equation was developed to estimate the seismic energy from critical blast parameters based on the field results of sandstone bench formation:

$$SE = (-33,79,407) + (1,733.23).MCD - (2,799.90).D + (5,33,836.40).PPV - (32,269.67).SD \quad \textbf{(4.3)}$$

where,

SE = Seismic energy (μJ)
MCD = Maximum charge per delay (kg)
D = Distance between blast location and monitoring point (m)
SD = Scaled distance (m/√kg)
PPV = Peak particle velocity (mm/s)

4.1.5 Granite formation

Seismic energy analysis of ground vibrations based on the results of field investigations carried out in five different granite quarries, are discussed in this section. Altogether, 94 blast vibration events in granite formation were collected from

various blasts using ground vibration monitors for signal processing analysis of seismic energy. Locations of blasts conducted in five different granite quarries are depicted in Fig. 4.11.

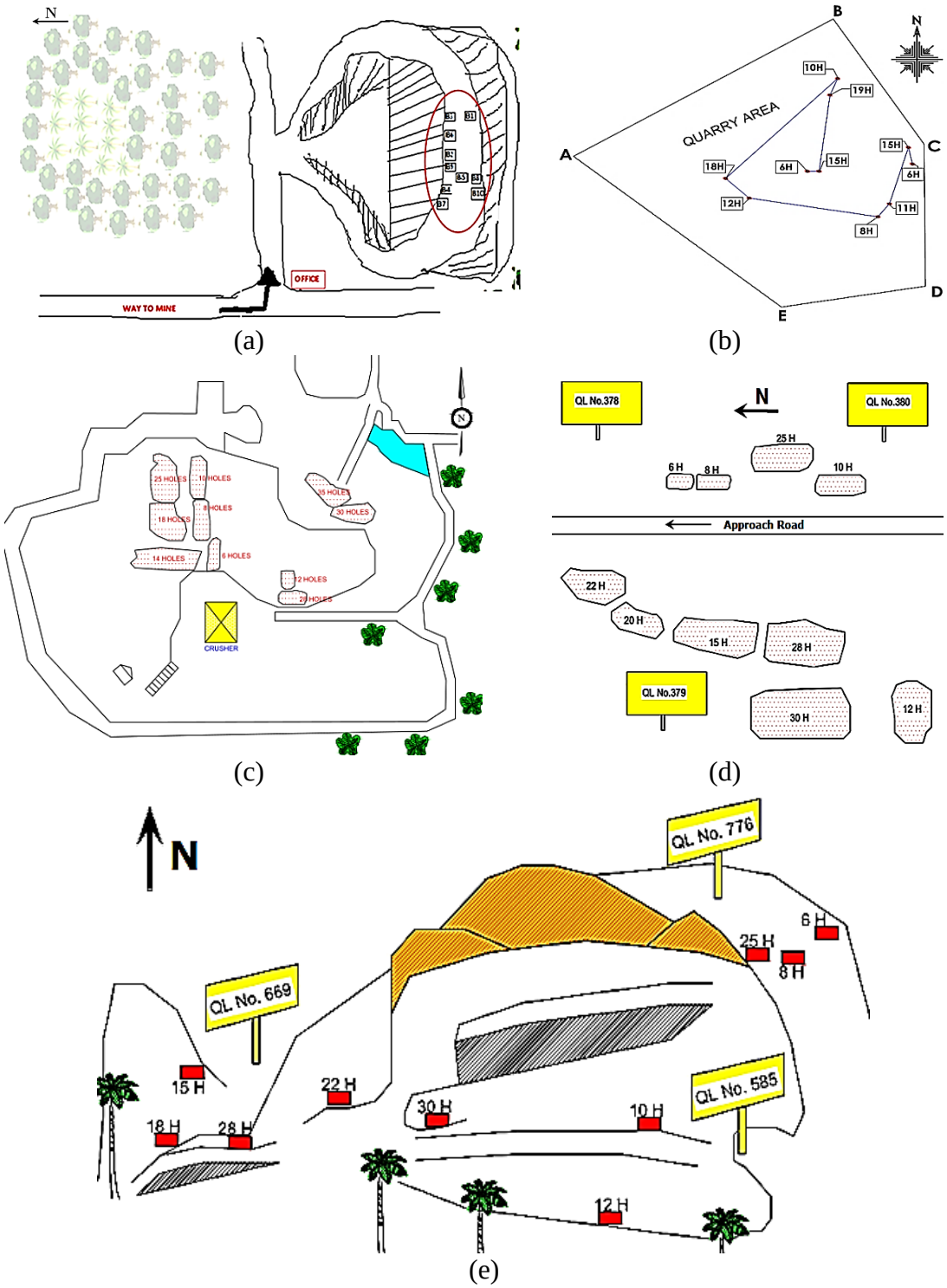

Fig. 4.11 Locations of blasts carried out during research studies in granite formation

One of the critical parameters in blast design, Maximum Charge per Delay (MCD), was varied as 0.125kg, 0.25kg, 0.5kg, 0.75kg, 1kg, 1.25kg, 1.5kg, 16.68kg, 18.63kg, 19.46kg, 22.22kg, 36.14kg and 44.48kg, in different blast rounds. Seismic energy component caused due to blast induced ground vibrations was varying from 7,972μJ and 4,39,693μJ. Blast locations were surveyed twice, i.e. before and after blasting operations and respective muckpiles were examined thoroughly to acquire the information of fragmentation and a relationship between seismic energy and fragmentation was identified. From the results, it was observed that higher seismic energy distribution is giving rise to coarser fragmentation, due to more loss of explosive energy as strain waves. Blast locations and the muckpile were inspected before blast and after blast, and the correlation between seismic energy and fragmentation was assessed. Summary of fragmentation analysis carried out in granite formation from different blasts using Wipfrag software is given in Table-A4.9 (Appendix-IV). Values of Longitudinal wave and Transverse wave velocities of ground vibration propagation are given in the Table-A4.10 (Appendix-IV). MATLAB based regression and ANOVA analysis was carried out and results obtained from different granite quarries are depicted with corresponding code (Appendix-V).

From the regression analysis made, relationship between critical parameters in blast design and seismic energy was established for granite formation using MATLAB (Wiss and Linehan, 1979). It may be stated that from R^2 and adjusted R^2 values, estimation of seismic energy gives more than 92 per cent satisfactory results with a standard error of 14 per cent. Similarly, F-test and P-test carried out using ANOVA analysis also resulted in better validation of results (Tables – 4.16 to 4.18). MATLAB code used for ANOVA analysis in granite formation is given in Appendix-V.

Table – 4.16 Regression analysis for granite formation

Multiple R	0.95
R Square	0.92
Adjusted R Square	0.91
Standard Error	0.14
Observations	94

Table – 4.17 ANOVA (Analysis of Variance) for granite formation

	df	*SS*	*MS*	*F*	*Significance F*
Regression	5	5.32E+11	1.33E+11	237.07	1.45E-46
Residual	89	4.99E+10	5.61E+08	-	-
Total	94	5.82E+11	-	-	-

** df – Degree of freedom, SS – Sum of Squares, MS – Mean Square, F – F-test value, Significance F – P-value*

Table – 4.18 Relationship between critical blast parameters and seismic energy in granite formation

	Coefficients	*Standard Error*	*t-Stat*	*P-value*
Intercept	53,021.82	6,563.23	8.08	3E-12
MCD (kg)	2,341.33	468.70	4.99	2.91E-06
Distance (m)	-324.42	65.74	-4.93	3.71E-06
Scaled Distance (m/√kg)	-36.96	49.16	-0.75	0.45
PPV (mm/s)	33,974.46	2,294.08	14.81	9.66E-26

* MCD – Maximum Charge per Delay, PPV – Peak Particle Velocity

From the obtained results, Equation 4.4 was developed to estimate the seismic energy from critical blast parameters based on the field results in granite formation:

$$SE = (53{,}021.82) + (2{,}341.33).MCD - (324.42).D - (36.96).SD + (33{,}974.46).PPV \quad \textbf{(4.4)}$$

where,

SE = Seismic energy (μJ)
MCD = Maximum charge per delay (kg)
D = Distance between blast location and monitoring point (m)
SD = Scaled distance (m/√kg)
PPV = Peak particle velocity (mm/s)

4.2 Piezo Generator (Piezo-Gen)

4.2.1 Validation results

Validation of piezo generator developed was carried out in two stages:

- Dropping a weight of 2.5kg, from specified height of 1m and instruments were placed at 1m distance from the vibration source, in the laboratory.
- Dropping a weight of 2.5kg, from specified height of 1.5m and instruments were placed at 1m distance from the vibration source, outside the laboratory.

In the laboratory, 34 readings were taken by dropping same weight (2.5kg) from same height (1m) while the recording instruments are placed at same distance (1m) from

vibration source to find the precision and accuracy of the Piezo-Gen circuit. It was evident from the results that the working of developed piezo generator is appropriate in analogous with vibration monitor. Therefore, assessment of seismic energy can be done using the output (electrical energy) of piezo generator circuit (Fig. 4.12). Similarly, outside the laboratory, 30 readings were collected by dropping a weight of 2.5kg, from specified height of 1.5m. Laboratory scale studies have revealed that there was a resemblance between the results obtained with developed piezo generator circuit model and conventional vibration monitor (Fig. 4.13).

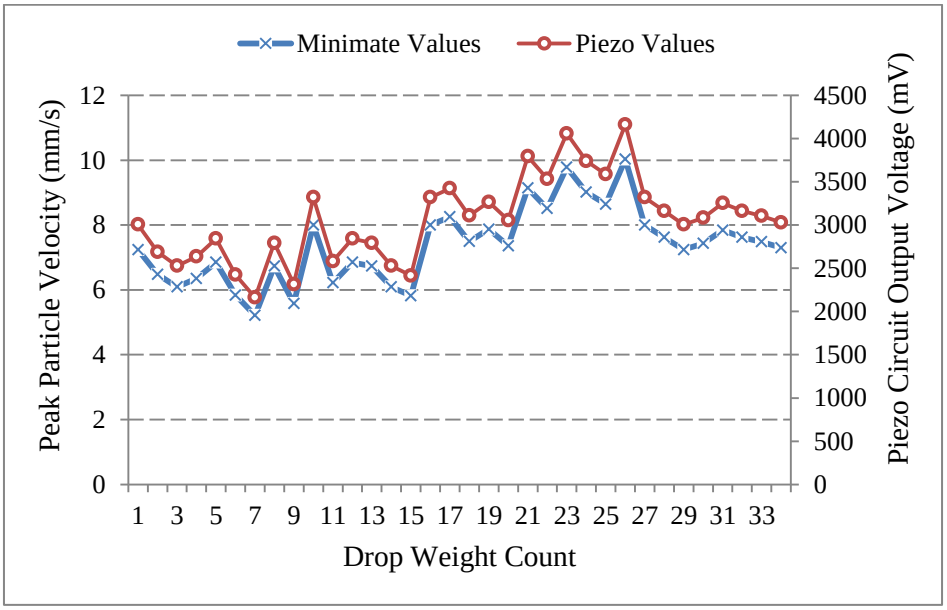

Fig. 4.12 Validation results of piezo generator circuit in the laboratory

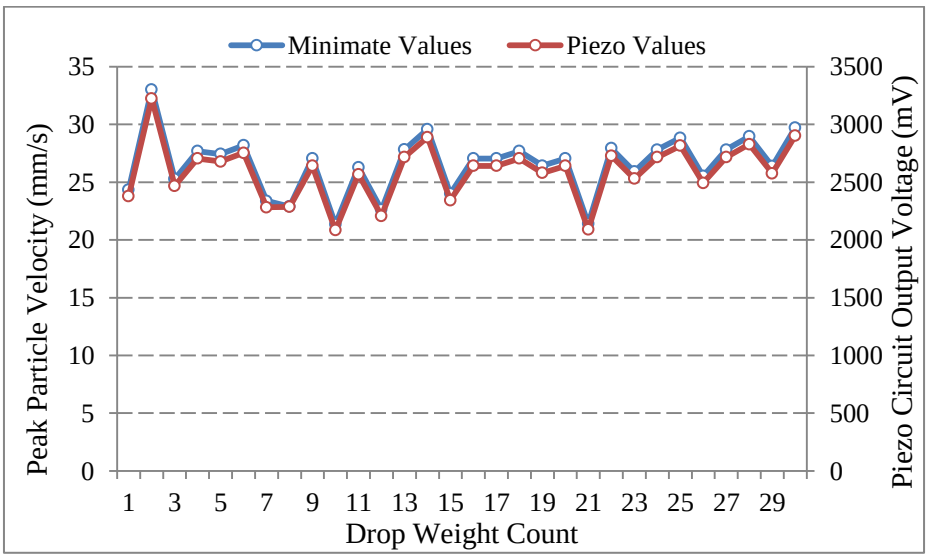

Fig. 4.13 Validation results of piezo generator circuit outside the laboratory

4.2.2 Limestone formation

During initial stage, basic circuit model with multimeter (i.e. without microcontroller) was used in field investigations to tap electrical voltage from blast induced ground vibrations, and thereby electrical energy. Table-A4.11 provides the summary of tapped electrical voltage and electrical energy resulting from blast induced ground vibrations with basic circuit model in limestone formation (Appendix-IV). Fig. 4.14 shows tapped electrical voltage and electrical energy resulting from blast induced ground vibrations with basic circuit model in limestone formation.

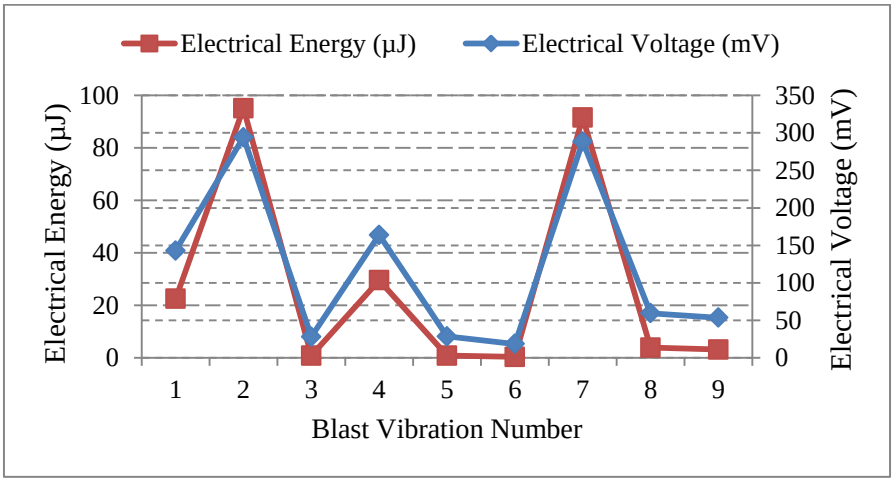

Fig. 4.14 Tapped electrical voltage and electrical energy in limestone formation with basic piezo circuit

Later on, improved model of piezo generation circuit was used in the studies along with vibration monitor (Minimate Plus, Instantel, Canada) in which both were placed at same location. Table-A4.12 gives the summary of tapped electrical voltage and electrical energy resulting from blast induced ground vibrations with piezo generator circuit model in limestone formation (Appendix-IV). Fig. 4.15 shows tapped electrical voltage and electrical energy resulting from blast induced ground vibrations with microcontroller based piezo generator circuit model in limestone formation.

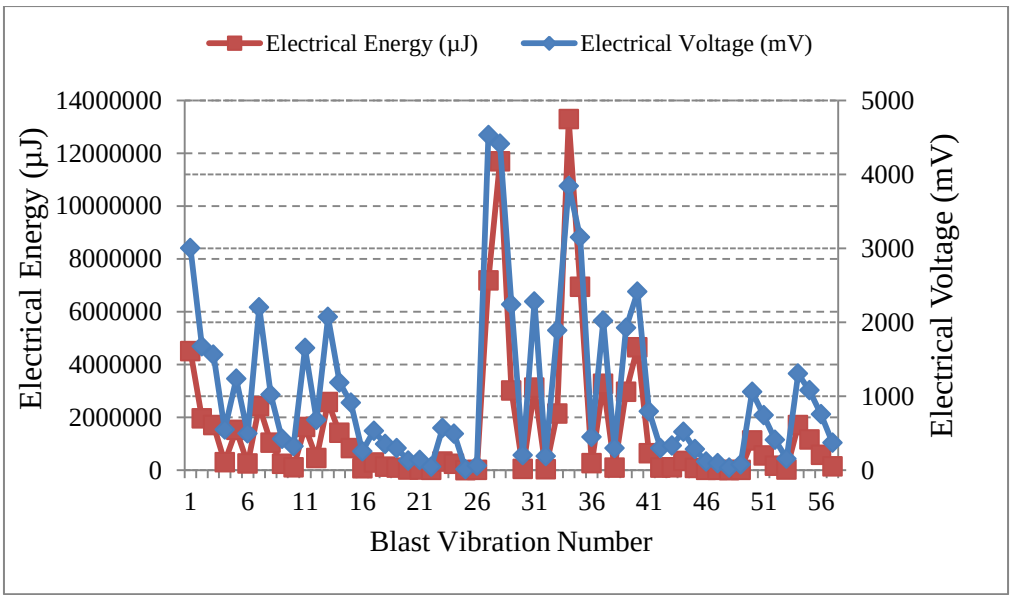

Fig. 4.15 Tapped electrical voltage and electrical energy in limestone formation with piezo generator circuit

4.2.3 Comparison of hard limestone formation and soft limestone formation

An attempt was made to compare the results obtained in four different limestone mines for harder and softer formations related to electrical energy generation. It was observed from the results that softer formation resulted in more electrical energy generation compared to harder formations. Comparisons were performed considering similar critical blast parameters for both formations, i.e. Distance, Scaled distance and Maximum charge per delay.

Table-4.19 shows the summary of electrical energy generation in harder and softer limestone formations at similar scaled distances using *staked line with markers* approach. Results obtained are depicted in Fig. 4.16 below.

Table – 4.19 Summary of electrical energy generation in harder and softer limestone formations at similar scaled distances

Sl. No.	SD (m/√kg)	Electrical Energy (µJ)	
		Hard Limestone	Soft Limestone
1	10	6,33,503	3,10,935
2	12	40,081	5,47,409
3	14	88,722	2,44,205
4	18	88,722	95,566
5	22	6,104	2,57,100

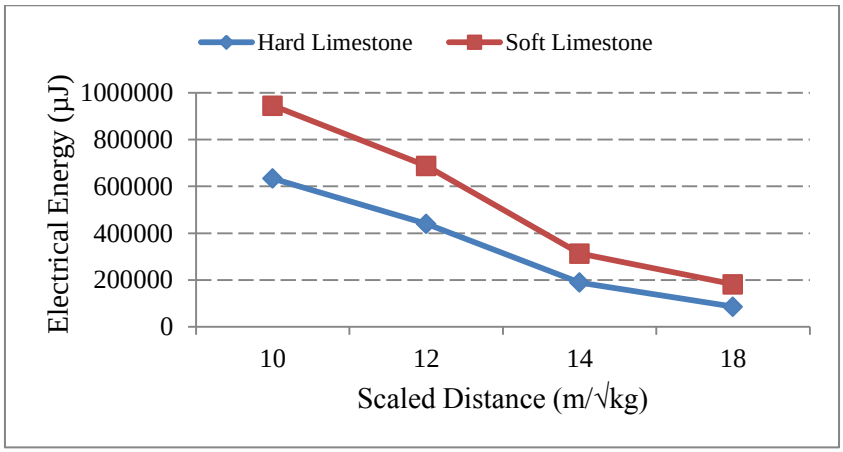

Fig. 4.16 Comparison of electrical energy generation in harder and softer limestone formations at similar scaled distances

Table-4.20 shows the summary of electrical energy generation in harder and softer limestone formations at similar distances using *staked line with markers* approach and the results are shown in Fig. 4.17.

Table – 4.20 Summary of electrical energy generation in harder and softer limestone formations at similar distances

Sl. No.	Distance (m)	Electrical Energy (µJ)	
		Hard Limestone	Soft Limestone
1	55	30,14,047	3,10,935
2	80	31,20,028	5,47,409
3	95	32,69,370	2,44,205
4	134	3,433	1,90,693

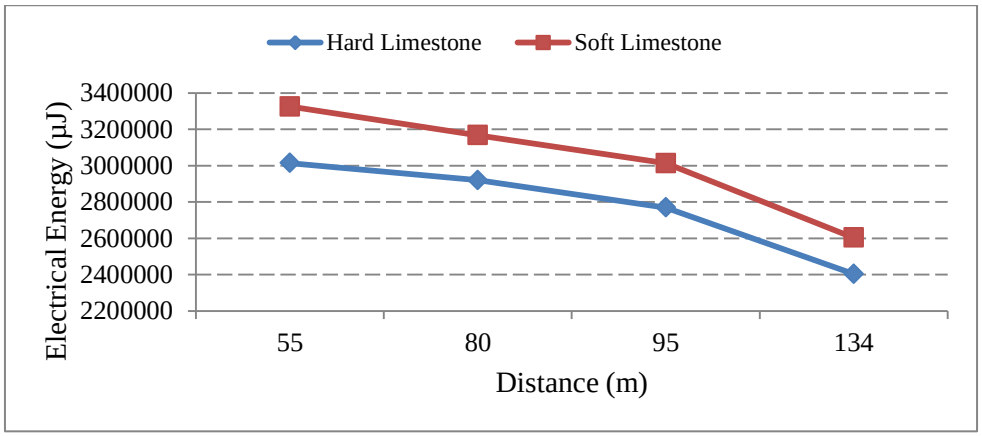

Fig. 4.17 Comparison of electrical energy generation in harder and softer limestone formations at similar distances

Table-4.21 shows the summary of electrical energy generation in harder and softer limestone formations at similar MCDs. Results obtained are depicted in Fig. 4.18 below.

Table – 4.21 Summary of electrical energy generation in harder and softer limestone formations at similar maximum explosive charge per delays

Sl. No.	MCD (kg)	Electrical Energy (µJ)	
		Hard Limestone	Soft Limestone
1	25	4,57,539	3,81,33,182
2	25	3,93,371	64,92,304
3	25	1,16,781	40,60,162
4	25	81,739	33,31,585
5	30	3,10,935	1,24,51,737
6	30	2,57,100	85,52,912
7	30	1,94,937	53,50,973
8	30	82,447	12,41,977
9	37	37,750	65,48,821
10	37	6,838	44,53,486

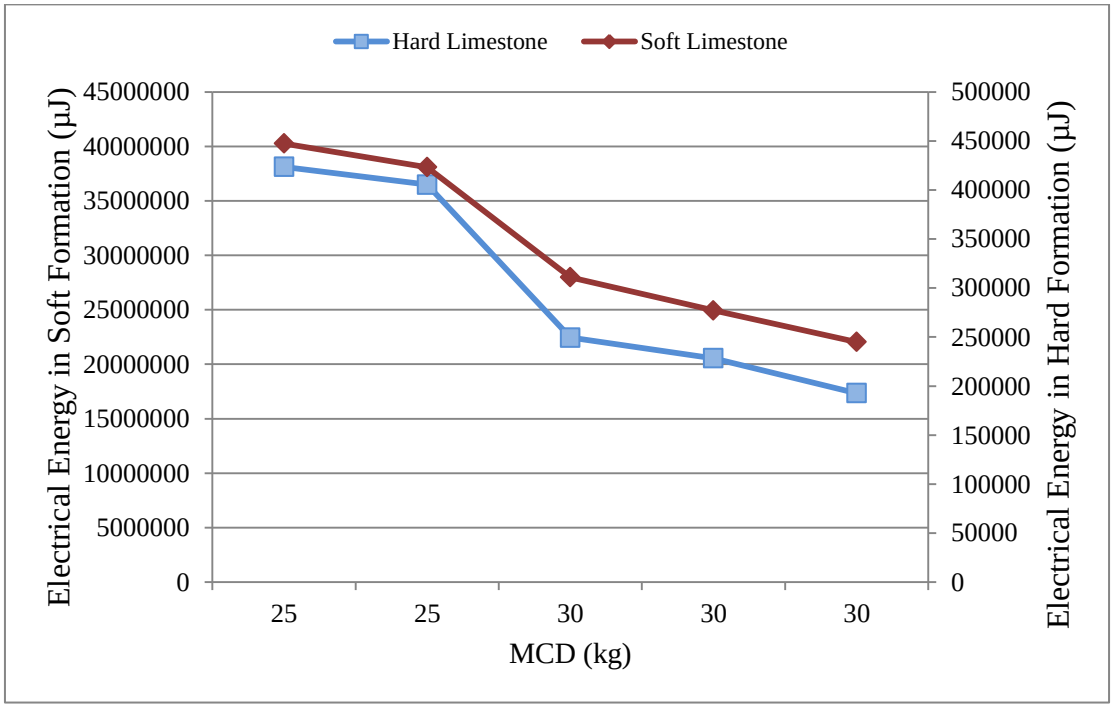

Fig. 4.18 Comparison of electrical energy generation in harder and softer limestone formations at similar maximum explosive charge per delays

Research results clearly indicated higher electrical energy at similar MCDs in the case of softer formation, reiterating results of seismic energy investigations.

4.2.4 Coal formation

Piezo generator circuit model (microcontroller based) and vibration monitors were placed at identical distance from the blast location. Table-A4.13 gives the summary of tapped electrical voltage and electrical energy resulting from blast induced ground vibrations with microcontroller based piezo generator circuit (Appendix-IV). Fig. 4.19 shows tapped electrical voltage and electrical energy resulting from blast induced ground vibrations with microcontroller based piezo generator circuit model in underground coal formation. Research results clearly indicated that higher amounts of electrical energy and electrical voltage generation were occurred at smaller scaled distances. Further, it was also noticed that the amount of generation of electrical voltage varied in proportion with the value of scaled distance.

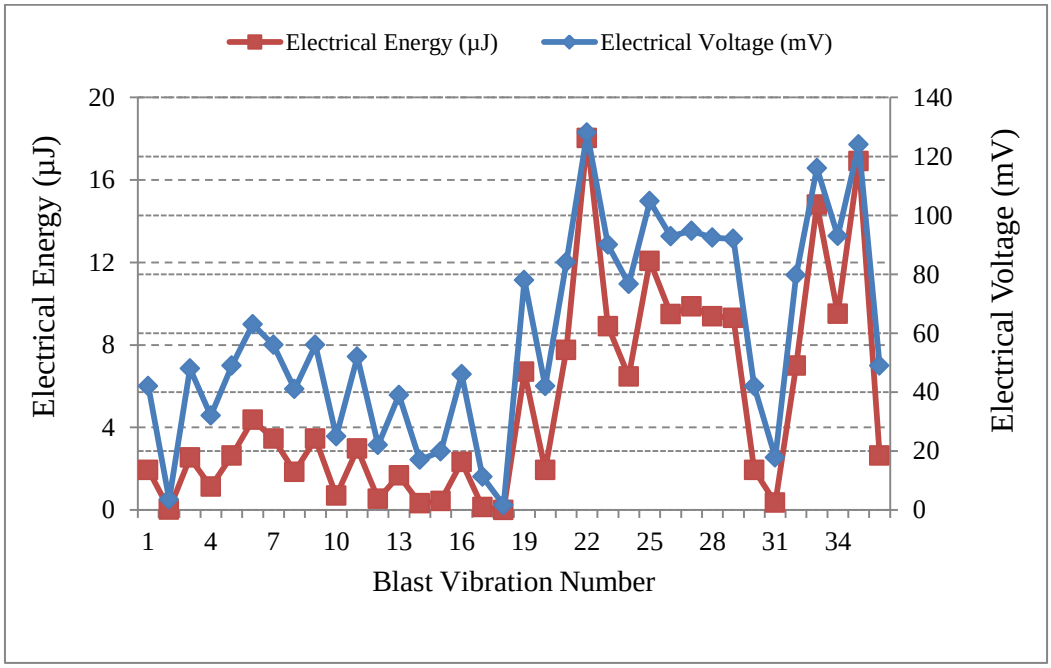

Fig. 4.19 Tapped electrical voltage and electrical energy in coal formation with piezo generator circuit

4.2.5 Sandstone formation

Table-A4.14 gives the summary of tapped electrical voltage and electrical energy resulting from blast induced ground vibrations with microcontroller based piezo

generator circuit in sandstone formation (Appendix-IV). Fig. 4.20 shows tapped electrical voltage and electrical energy resulting from blast induced ground vibrations with microcontroller based piezo generator circuit model in sandstone formation. Research studies clearly indicated that the amount of electrical voltage generation was in proportion with the value of respective scaled distance.

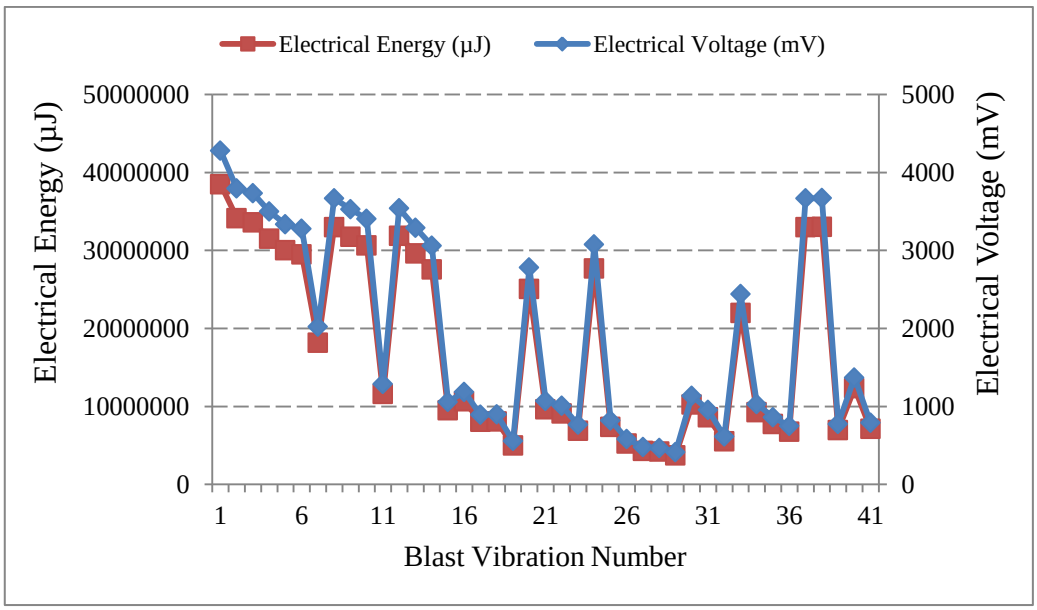

Fig. 4.20 Summary of tapped electrical voltage and electrical energy in sandstone formation with piezo generator circuit

4.2.6 Granite formation

During research studies, the piezo generator circuit model was employed to tap electrical voltage from blast induced ground vibrations along with vibration monitor (Minimate Plus, Instantel, Canada). Table-A4.15 gives the summary of tapped electrical voltage and electrical energy resulted from blast induced ground vibrations with microcontroller based piezo generator circuit in granitic rock formation (Appendix-IV). Fig. 4.21 shows tapped electrical voltage and electrical energy resulting from blast induced ground vibrations with microcontroller based piezo generator circuit model in granite formation.

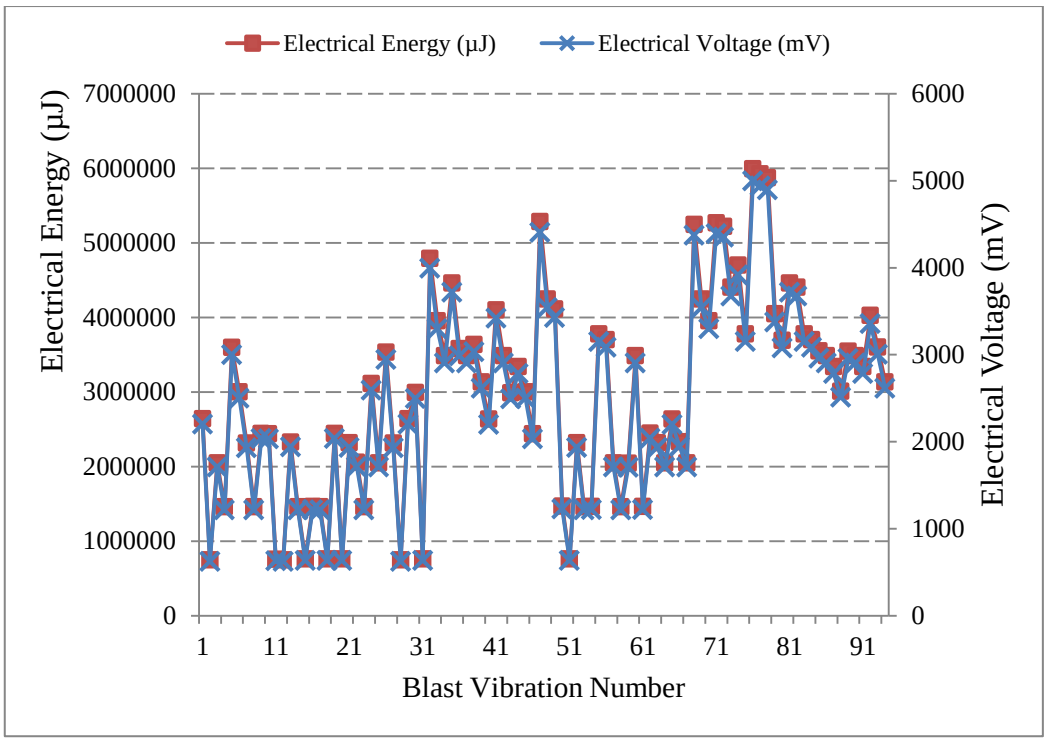

Fig. 4.21 Tapped electrical voltage and electrical energy in granitic rock formation with piezo generator circuit

4.3 Comparison of Seismic Energy with Electrical Energy

An attempt was made to assess Seismic Energy (SE) with Electrical Energy (EE), by comparing these two. A proper correlation between them was found in all four rock formations. MATLAB based comparison was made to assess the relationship between seismic energy and electrical energy for all four different rock formations of limestone, coal, sandstone and granite.

4.3.1 Limestone formation

Research studies were carried out in three different limestone mines of harder formation and one limestone mine of softer formation for the extraction of electrical energy resulting from blast induced ground vibrations. Ground vibrations resulting from blasting operation were captured using Minimate Plus, Instantel, Canada and Piezo generator circuit, by placing both the instruments at a specified and similar distance from blast location (Fig. 4.22). Distance between monitoring point and blast location was varied from 30m to 485m covering short range and long range monitoring.

(a) (b)

Fig. 4.22 Vibration capturing with vibration monitor and developed piezo generator circuit in limestone formation

Comparison of seismic energy with electrical energy was done to find the amount of strain energy extracted from piezo generator circuit model. Table-A4.16 gives the summary of seismic energy and electrical energy obtained in hard limestone formation with basic piezo circuit model (Appendix-IV). From the field data obtained with basic piezo generator circuit, MATLAB based comparison was made for finding relationship between seismic energy and electrical energy (Appendix-V). Fig. 4.23 shows the MATLAB based comparison of seismic energy and electrical energy with basic circuit in limestone mine of harder formation. Regression analysis was carried out to assess the seismic energy from electrical energy with basic piezo-gen circuit in limestone formation. Fig. 4.24 shows the correlation of seismic energy with electrical energy based on the obtained field results with basic piezo-gen circuit in limestone formation.

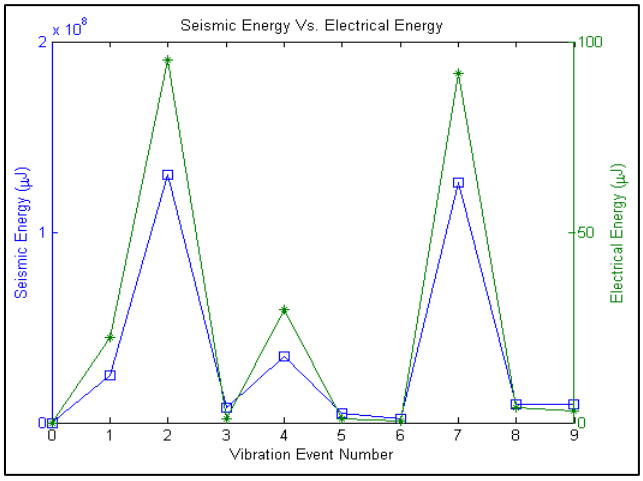

Fig. 4.23 Seismic energy versus electrical energy with basic circuit in limestone formation

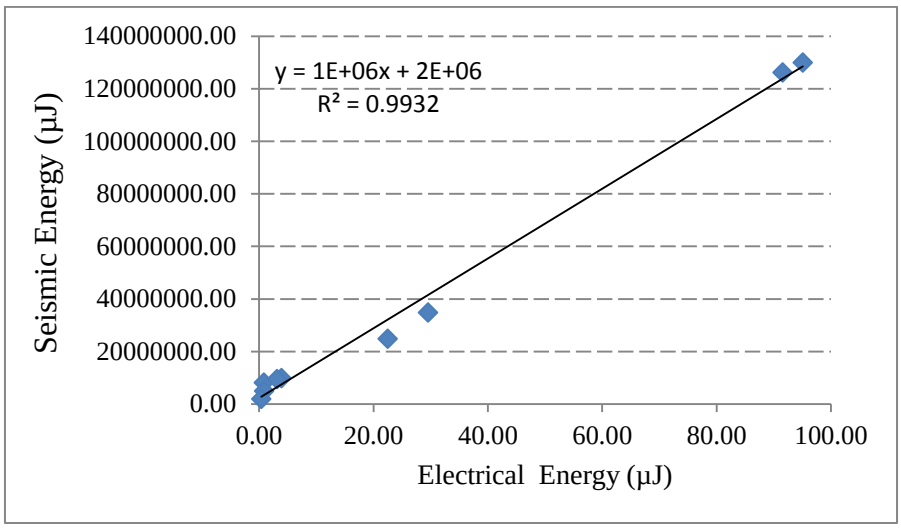

Fig. 4.24 Correlation between seismic energy and electrical energy with basic circuit in hard limestone formation

Table-A4.17 gives the summary of seismic energy and electrical energy obtained in hard limestone formation with microcontroller based piezo generator circuit (Appendix-IV). From the field data obtained with piezo generator circuit, MATLAB based comparison for finding relationship between seismic energy and electrical energy was carried out (Appendix-V). Fig. 4.25 shows the MATLAB based comparison of seismic energy and electrical energy with microcontroller based piezo generator circuit in limestone mine of harder formation. Regression analysis was carried out to assess the seismic energy from the obtained electrical energy with microcontroller based piezo generator circuit in harder limestone formation. Fig. 4.26 shows the correlation of seismic energy with electrical energy based on the obtained field results with microcontroller based piezo generator circuit in harder limestone formation.

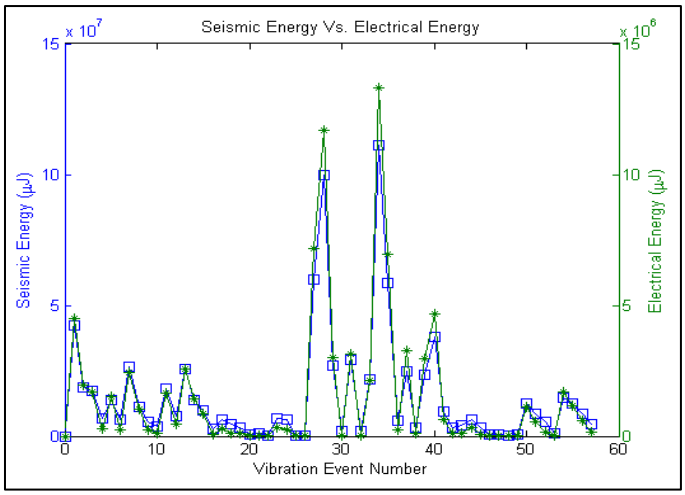

Fig. 4.25 Seismic energy versus electrical energy with improved piezo circuit in hard limestone formation

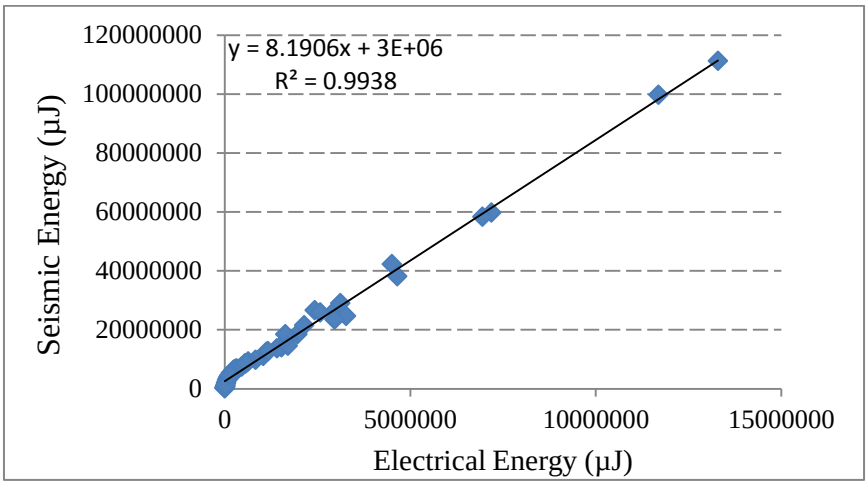

Fig. 4.26 Correlation between seismic energy and electrical energy with improved piezo circuit in hard limestone formation

Table-A4.18 gives the summary of seismic energy and electrical energy obtained in soft limestone formation with microcontroller based piezo generator circuit (Appendix-IV). From the field data obtained with microcontroller piezo generator circuit, MATLAB based comparison for finding relationship between seismic energy and electrical energy was carried out (Appendix-V). Fig. 4.27 shows the MATLAB based comparison of seismic energy and electrical energy with microcontroller based piezo generator circuit in limestone mine of softer formation. Regression analysis was carried out to assess the seismic energy from the obtained electrical energy with microcontroller based piezo generator circuit in limestone mine of softer formation. Fig. 4.28 shows the correlation of seismic energy with electrical energy based on the

obtained field results with microcontroller based piezo generator circuit in limestone mine of softer formation.

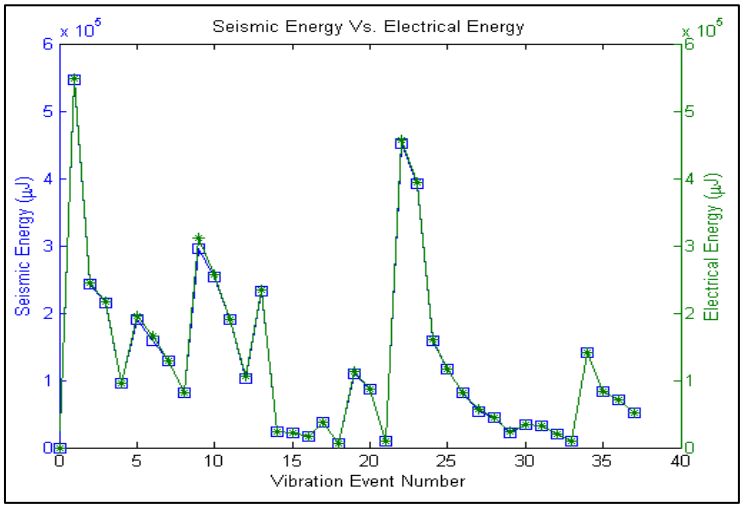

Fig. 4.27 Seismic energy versus electrical energy with piezo circuit in soft limestone formation

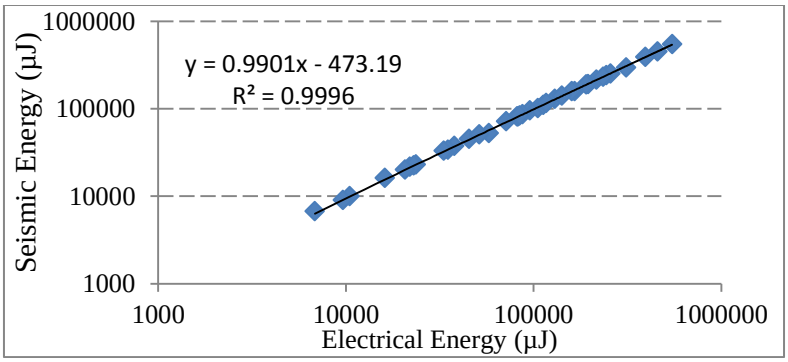

Fig. 4.28 Correlation between seismic energy and electrical energy with piezo circuit in soft limestone formation

From the obtained results, an excellent correlation between seismic energy and electrical energy was observed. Research results also revealed that the assessment of seismic energy with electrical energy is possible.

4.3.2 Coal formation

Research studies were carried out in underground coal mine formation for the extraction of electrical energy resulting from blast induced ground vibrations. Ground vibrations resulting from blasting operation were captured using Minimate Plus, Instantel, Canada and Piezo generator circuit, by placing both the instruments at a specified and similar distance from blast location (Fig. 4.29). Distance between

monitoring point and blast location was varied from 15m to 125m covering various partings and levels. Parting between monitoring point and blast location was varied from 0m to 65m in the studies.

(a) (b)

Fig. 4.29 Vibration capturing with vibration monitor and developed piezo generator circuit in underground coal formation

Comparison of seismic energy with electrical energy was made to assess the strain energy extracted from piezo generator circuit. Table-A4.19 gives the summary of seismic energy and electrical energy obtained in coal formation with microcontroller based piezo generator circuit (Appendix-IV). From the field data obtained with basic piezo generator circuit, MATLAB based comparison was made for finding relationship between seismic energy and electrical energy (Appendix-V). From the field data obtained, MATLAB based comparison for finding relationship between seismic energy and electrical energy was made and the corresponding code is given below (Fig. 4.30). Regression analysis was carried out to assess the seismic energy from the obtained electrical energy with basic circuit in coal formation. Fig. 4.31 shows the correlation of seismic energy with electrical energy based on the obtained field results with developed circuit in coal formation.

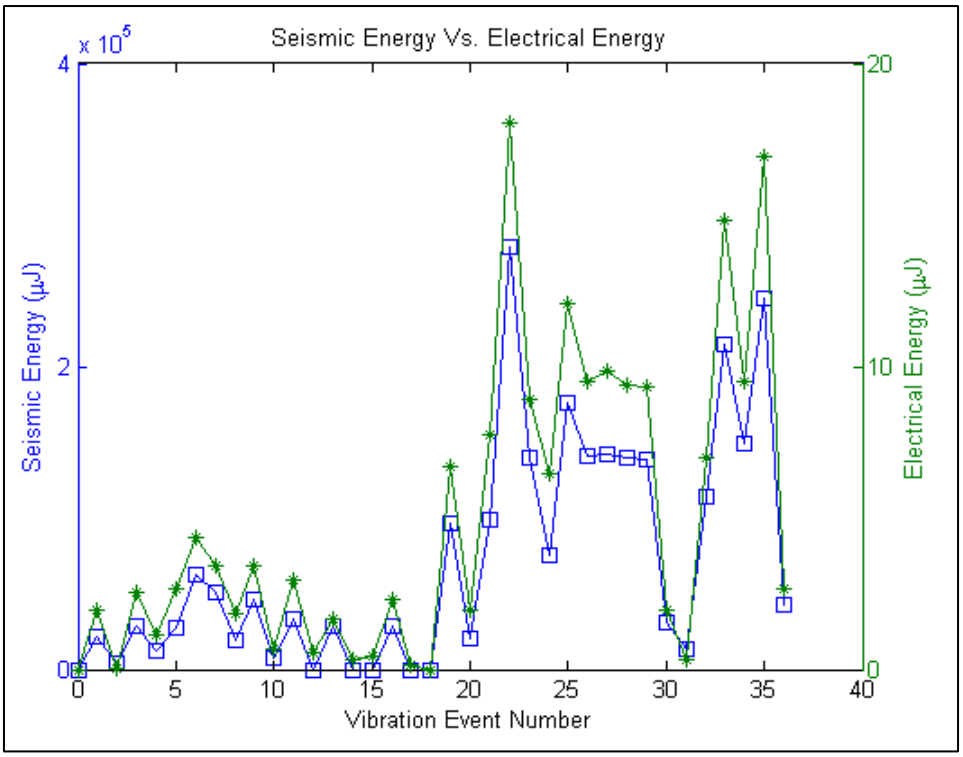

Fig. 4.30 Seismic energy versus electrical energy in coal formation

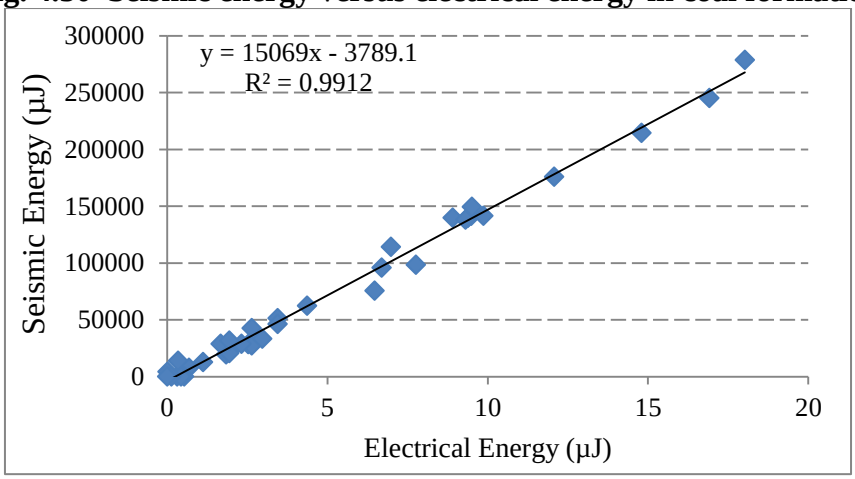

Fig. 4.31 Correlation between seismic energy and electrical energy in coal formation

Research results indicated an excellent correlation between seismic energy and electrical energy. Studies also revealed that assessment of seismic energy through electrical energy is possible.

4.3.3 Sandstone formation

Research studies were carried out in two sandstone bench formations for the extraction of electrical energy resulting from blast induced ground vibrations. Ground

vibrations resulting from blasting operation were captured using Minimate Plus, Instantel, Canada and Piezo generator circuit, by placing both the instruments at a specified and similar distance from blast location (Fig. 4.32). Distance between monitoring point and blast location was varied from 100m to 2033m covering various locations.

(a) (b)

Fig. 4.32 Vibration capturing with vibration monitor and developed piezo generator circuit in sandstone formation

Strain energy extracted from piezo generator circuit was assessed by comparing the seismic energy with electrical energy. Table-A4.20 gives the summary of seismic energy and electrical energy obtained in sandstone formation with microcontroller based piezo generator circuit (Appendix-IV). MATLAB based comparison for finding relationship between seismic energy and electrical energy was carried out (Appendix-V). From the field data obtained, MATLAB based comparison for finding relationship between seismic energy and electrical energy was made and its corresponding code is given below (Fig. 4.33). Regression analysis was carried out to assess the seismic energy from the obtained electrical energy in sandstone bench formation. Fig. 4.34 shows the correlation of seismic energy with electrical energy based on the obtained field results sandstone formation.

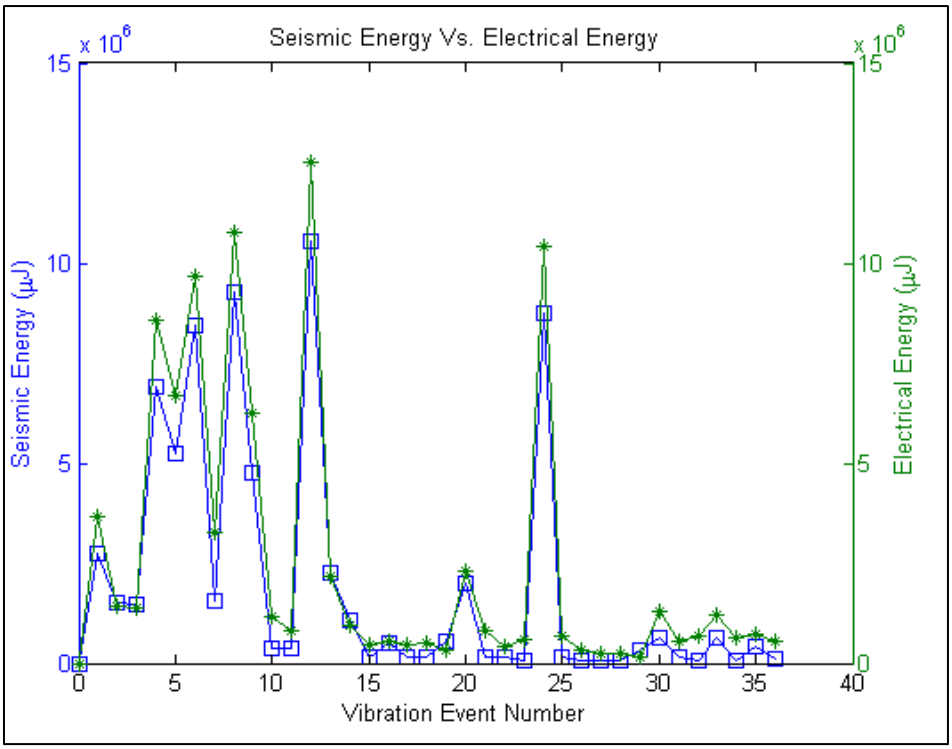

Fig. 4.33 Seismic energy versus electrical energy in sandstone formation

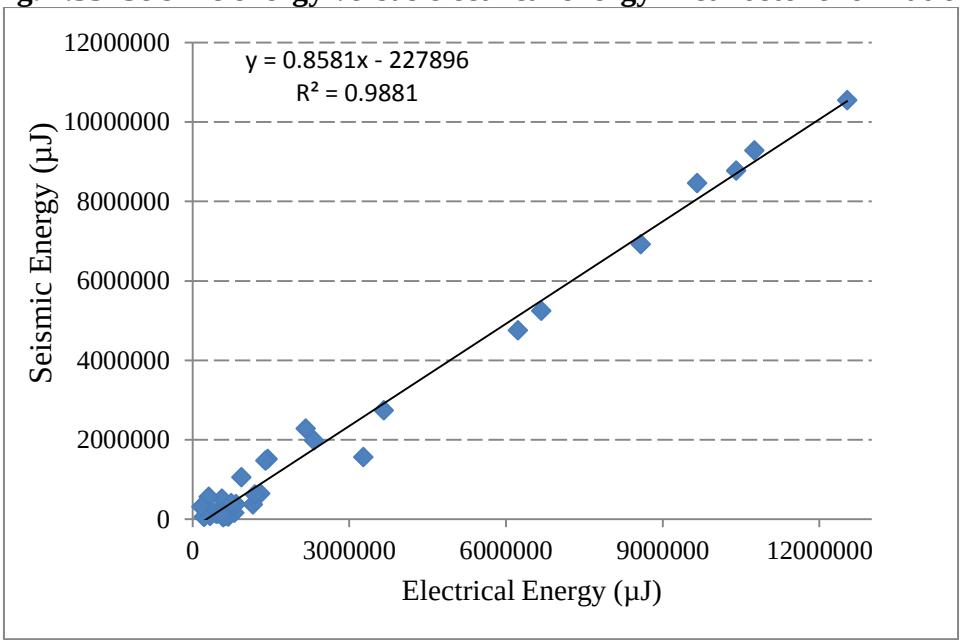

Fig. 4.34 Correlation between seismic energy and electrical energy in sandstone formation

Research studies indicated an excellent correlation between seismic energy and electrical energy. From the obtained results, further, it was clearly understood that assessment of seismic energy through electrical energy is possible.

4.3.4 Granite formation

Research studies were carried out in five granitic rock formations for the extraction of electrical energy resulting from blast induced ground vibrations. Ground vibrations resulting from blasting operation were captured using Minimate Plus, Instantel, Canada and Piezo generator circuit, by placing both the instruments at a specified and same distance from blast location (Fig. 4.35). Distance between monitoring point and blast location was varied from 20m to 300m covering various locations.

(a) (b)

Fig. 4.35 Vibration capturing with vibration monitor and developed piezo generator circuit in granite formation

Strain energy extracted from piezo generator circuit was assessed by comparing the seismic energy with electrical energy. Table-A4.21 gives the summary of seismic energy and electrical energy obtained in granite formation with microcontroller based piezo generator circuit (Appendix-IV). MATLAB based comparison for finding relationship between seismic energy and electrical energy was carried out (Appendix-V). From the field data obtained, MATLAB based comparison for finding relationship between seismic energy and electrical energy was made and its corresponding code is given below (Fig. 4.36). Regression analysis was carried out to assess the seismic energy from the obtained electrical energy granite formation. Fig. 4.37 shows the correlation of seismic energy with electrical energy based on the obtained field results in granite formation.

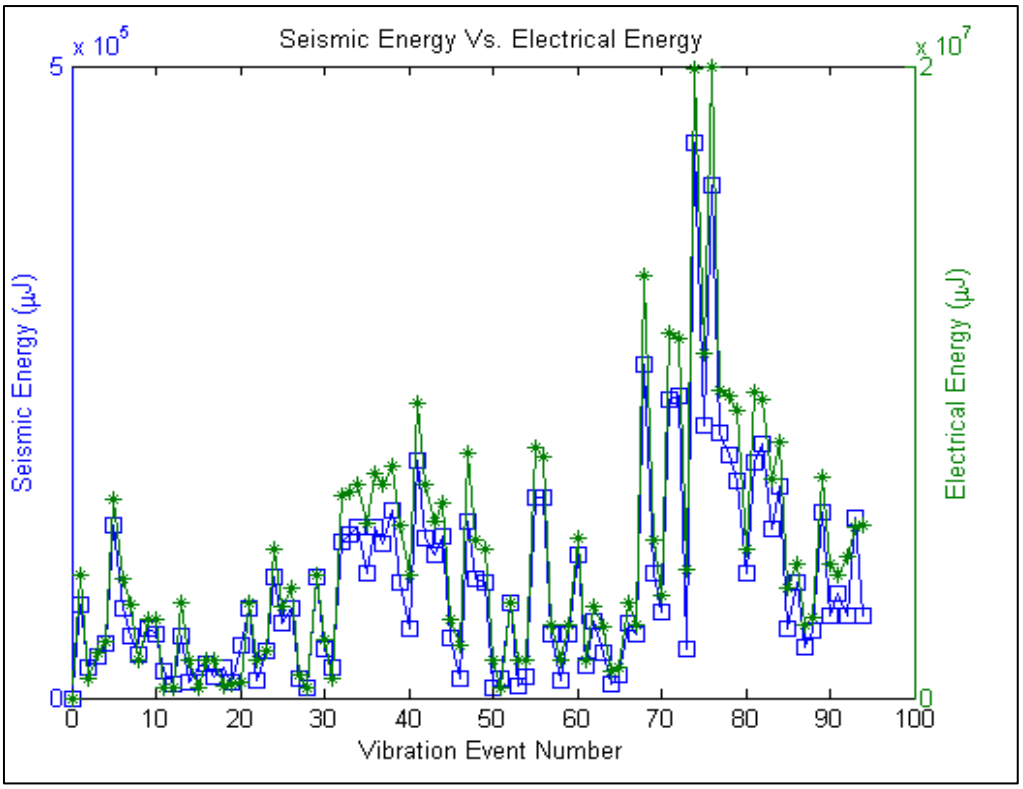

Fig. 4.36 Seismic energy versus electrical energy in granite formation

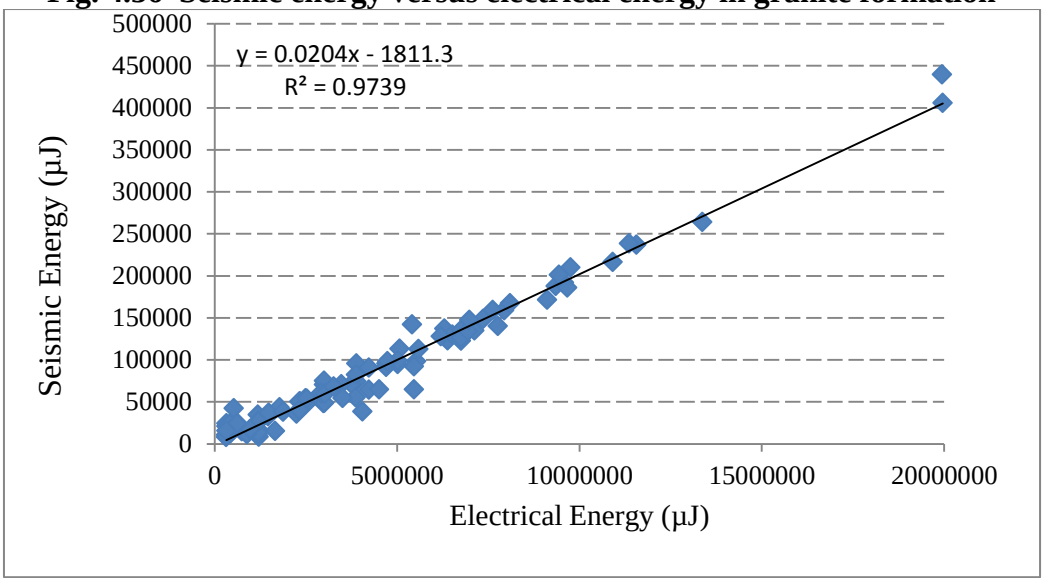

Fig. 4.37 Correlation between seismic energy and electrical energy in granite formation

An excellent correlation was observed between seismic energy and electrical energy. From the obtained results, it is very clear that the assessment of seismic energy is possible from the electrical energy generated.

4.4 Numerical Modelling Analysis

Numerical modelling analysis was carried out developing 98 models in four different rock formations. Particularly, analysis was carried out to predict the ground vibrations in terms of particle velocities for given blast configuration. Initially, validity of numerical modelling was assessed by comparing results from four models considering input parameters similar to real time field studies. Initially, four models were developed in four different rock formations by considering field conditions. Furthermore, analysis was made to assess the tapped electrical potential of Piezo-Gen circuit, in all four rock formations.

4.4.1 Model validation

Input parameters considered for calibration were similar to real time blasts studied earlier, during field investigations. For assessing validity of numerical modelling, one blast in each rock formation was considered replicating field conditions. Table-4.22 gives details of input parameters considered for modelling in all four rock formations.

Table – 4.22 Input parameters considered for calibration of numerical modelling

Parameters / ***Formation***	**B or W (m)**	**S or H (m)**	**D (m)**	**N**	**E/h (kg)**	**MCD (kg)**	**TC (kg)**	**TD (ms)**
Limestone	3.5	6.0	7.0	2	28.33	28.33	56.66	25
Coal	3.0	1.3	1.8	6	0.65	3.88	3.88	25
Sandstone	4.0	5.0	5.5	6	25.00	25.00	150.00	125
Granite	0.6	0.9	1.2	6	0.25	0.25	1.50	150

B – Burden, W – Width of the face, S – Spacing, H – Height of the face, D – Depth of the blasthole, N – No. of blastholes, E/h – Explosive charge per hole, MCD – Maximum charge per delay, TC – Total explosive charge per blast, TD – Total duration of blast

4.4.1.1 Limestone formation

In limestone formation, a model was developed similar to field conditions (Fig. 4.38). Execution of a model in limestone formation was carried out with 2 steps of simulation and total simulation time of 25ms.

(a)

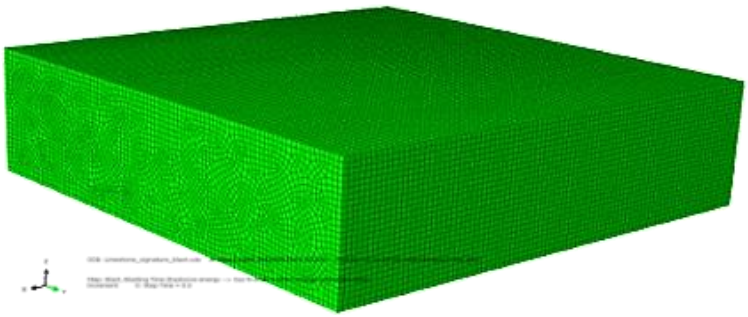

(b)

(a) Field blast layout **(b)** Developed model in limestone

Fig. 4.38 Model for validation in limestone formation

In the output field, spatial velocities at nodes (PPVs) were observed at particular distances similar to field studies. Fig. 4.39 shows spatial velocity (PPV) contours observed at nodes in the model at each step of simulation.

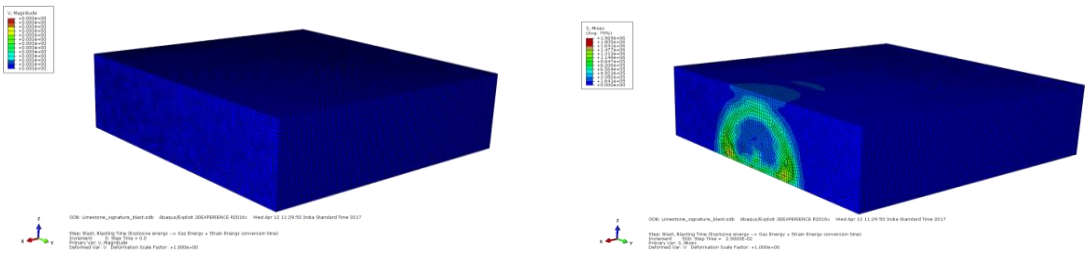

0ms 25ms

Fig. 4.39 Spatial velocity contours observed at nodes

Calibration model of the limestone formation was analysed with *Iso-surface cut visualization* (indicating overall stress acting on the bench during the blast), to obtain a blasted region on the bench. Fig. 4.40 shows the un-deformed and deformed shapes of blast model in limestone formation.

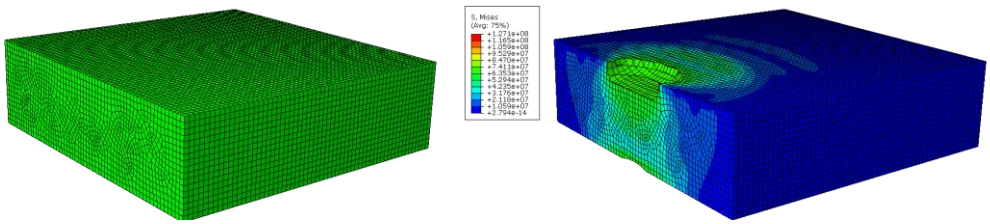

Fig. 4.40 Un-deformed (left) and deformed (right) shape of validation model

4.4.1.2 Coal formation

The model developed in coal formation was similar to actual field conditions (Fig. 4.41). Execution of a model for validation in coal formation was carried out considering total simulation time of 25ms.

(a) (b)

(a) Actual blast layout **(b)** Developed model

Fig. 4.41 Model for validation in coal formation

In the output field, spatial velocities at nodes (PPVs) were observed at particular distances similar to field studies. Fig. 4.42 shows observed spatial velocities (PPV) contours at nodes in the model at each step during simulation.

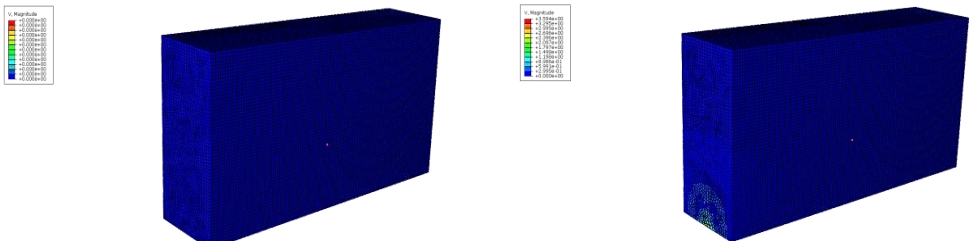

0ms 25ms

Fig. 4.42 Spatial velocity contours observed at nodes

Model of the coal formation was analysed with *Iso-surface cut visualization* (indicating overall stress acting on the bench during the blast) and blasted region on the bench was observed. Fig. 4.43 shows the un-deformed and deformed shapes of calibrated blast model in coal formation.

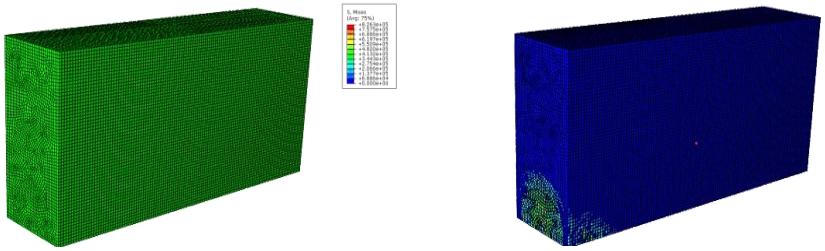

Fig. 4.43 Un-deformed (left) and deformed (right) shape of validation model

4.4.1.3 Sandstone formation

Fig. 4.44 shows the model developed in sandstone formation. Execution of a calibrated model in sandstone formation was carried out with 6 steps of simulation and total simulation time of 125ms, similar to field condition.

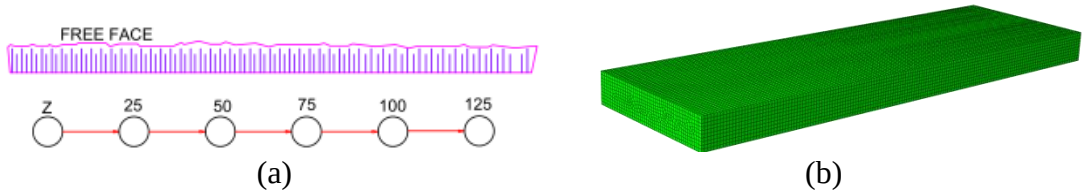

(a) (b)

(a) Field blast layout **(b)** Developed model

Fig. 4.44 Model for validation in sandstone formation

In the output field, spatial velocities at nodes (PPVs) were observed at particular distances similar to field investigations of the blast. Fig. 4.45 shows PPV contours observed at nodes in the model at each step of simulation.

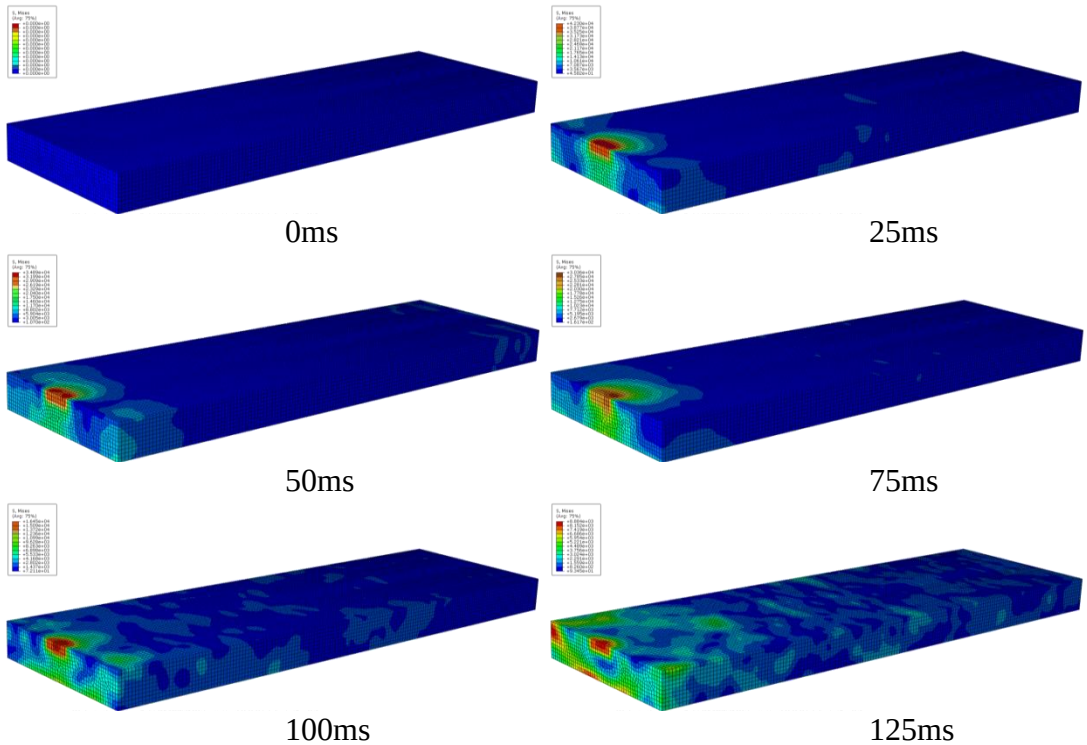

Fig. 4.45 Spatial velocity contours observed at nodes

Validity model in sandstone formation was assessed with *Iso-surface cut visualization* (indicating overall stress acting on the bench during the blast) and blasted region on

the bench was obtained. Fig. 4.46 shows the un-deformed and deformed shapes of blast model in sandstone formation.

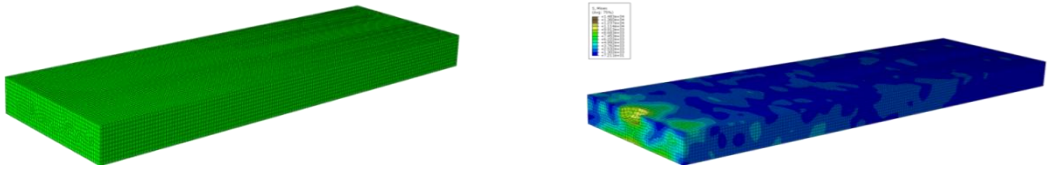

Fig. 4.46 Un-deformed (left) and deformed (right) shape of validation model

4.4.1.4 Granite formation

In granite formation, execution of a calibrated model was carried out with 6 steps of simulation and total simulation time of 150ms, equivalent to field studies (Fig. 4.47).

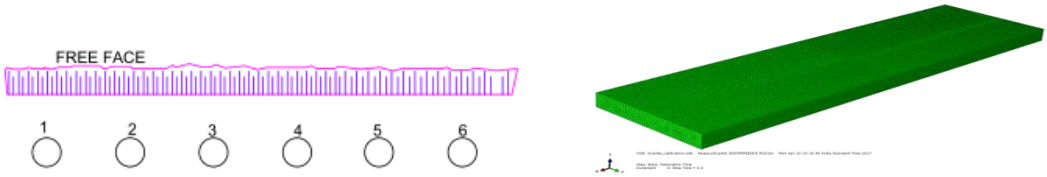

(a) (b)

(a) Field blast layout **(b)** Developed model

Fig. 4.47 Model for validation in granite formation

In the output field, spatial velocities at nodes (PPVs) were observed at particular distances similar to field investigations of the blast. Fig. 4.48 shows spatial velocity (PPV) contours observed at nodes in the model at each step of simulation.

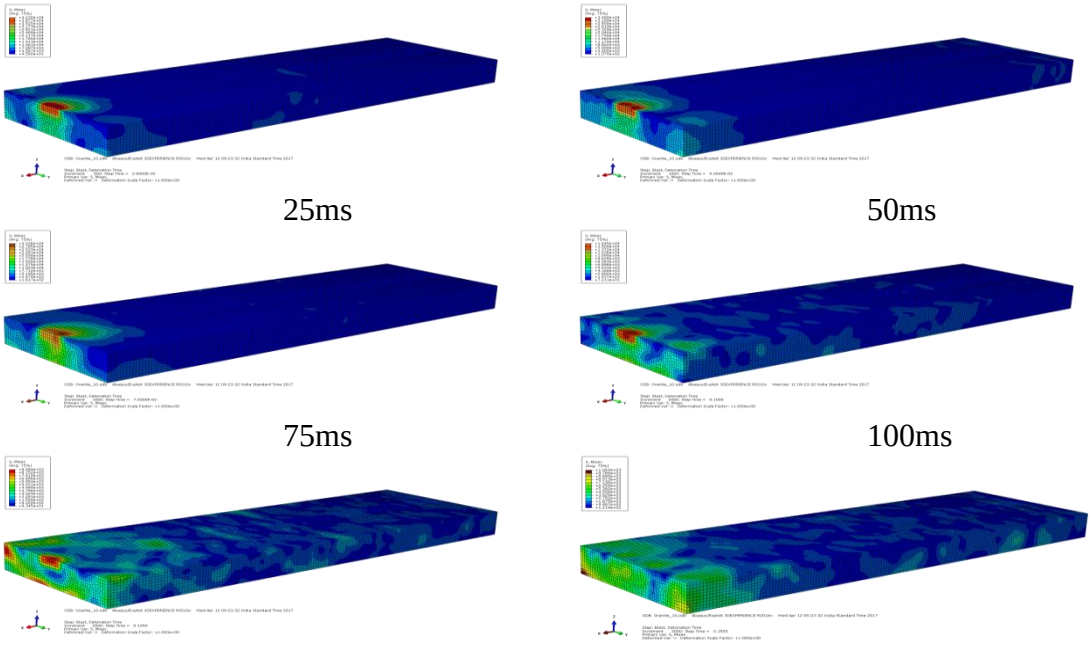

25ms 50ms

75ms 100ms

125ms 150ms

Fig. 4.48 Spatial velocity contours observed at nodes

Calibration model of the granite formation was analysed with *Iso-surface cut visualization* (indicating overall stress acting on the bench during the blast) and blasted region on the bench was obtained. Fig. 4.49 shows the un-deformed and deformed shapes of the developed blast model in granite formation.

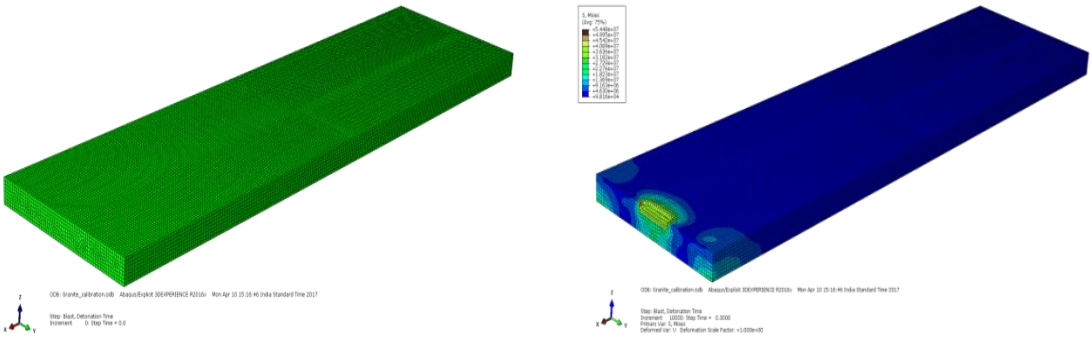

Fig. 4.49 Un-deformed (left) and deformed (right) shape of validation model

Percentage error was calculated between PPVs obtained in the field and model using the following equation.

% Error = (|Exact Value-Approximate Value|)/Exact Value] x 100% ---------- **(4.5)**

Percentage of error was about <20% in most of the cases indicating consistency of modelling results on par with field results. Table-4.23 gives the summary of model validation results in four different rock formations.

Table – 4.23 Summary of validation results of numerical modelling

Formation	Distance (m)	Model PPV (mm/s)	Field PPV (mm/s)	Error (%)
Limestone	15	25.36	26.8	5.68
	20	23.86	23.6	1.09
	30	20.82	20.7	0.58
	40	14.21	12.2	14.14
	50	9.81	9.65	1.63
Coal	55	4.33	4.19	3.23
	58	2.69	2.67	0.74
	68	1.16	1.02	12.06
Sandstone	45	1.04	0.889	14.51
	150	0.86	0.64	11.58

Formation	Distance (m)	Model PPV (mm/s)	Field PPV (mm/s)	Error (%)
	200	0.70	0.64	8.96
	250	0.62	0.51	17.74
Granite	20	3.31	3.68	11.17
	25	2.61	2.03	22.22
	30	1.78	1.65	7.30
	35	1.46	1.51	3.42

Later, an attempt was made to determine the correlation between model results of PPV and field generated PPV using regression analysis. R^2 of about 94.47% was obtained between model PPV and field PPV values, indicating validity of the modelling (Fig. 4.50).

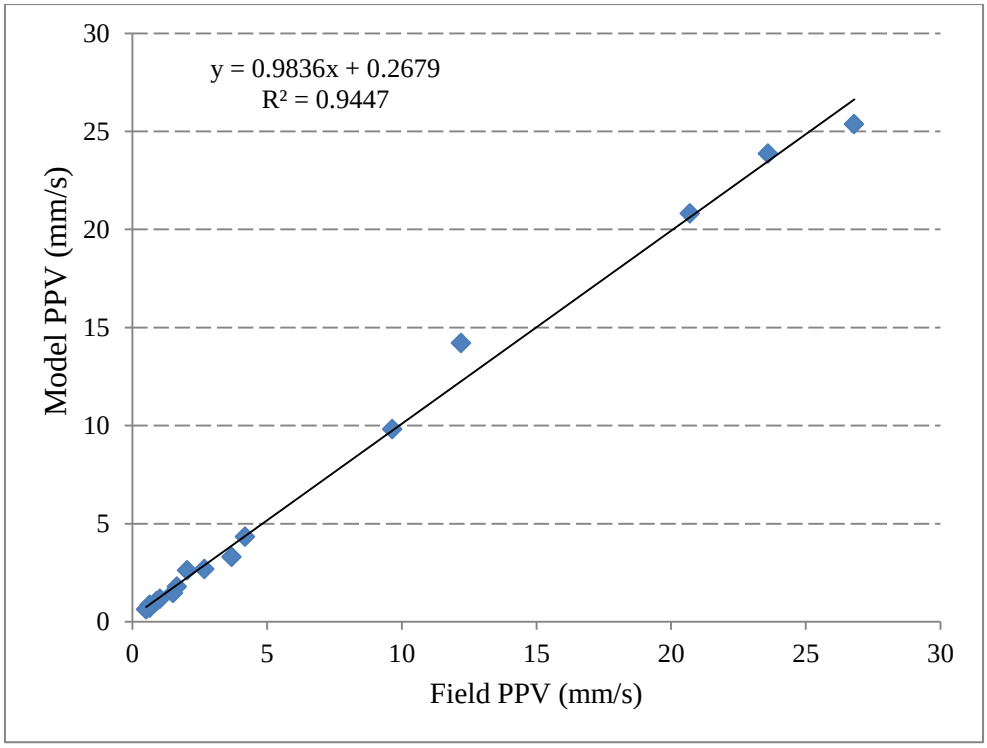

Fig. 4.50 Correlation between model PPV and field PPV values in four rock formations

Subsequently, a parametric study was carried out in all four rock formations. Further, an attempt was made to compare the modelling results with data generated from field investigations.

4.4.2 Numerical modelling results in limestone formation

In limestone formation, totally 28 models were developed using SIMULIA Abaqus/CAE interface. Further, python script for development of the models in limestone formation was coded. In particular, models were developed similar to field conditions based on the burden and spacing of the blast location, height of the bench, type of explosive used, and total explosive charge used per blast. Typical size of each model in limestone formation was 500mx500m with a depth 5 times the bench height. Similar to field investigations carried out earlier, ANFO and Slurry type of explosives were used in the modelling. Table-4.24 shows major input parameters considered for numerical modelling in limestone formation. All the necessary parameters considered in limestone formation for numerical modelling studies are tabulated in Appendix-VII.

Table – 4.24 Input parameters considered for numerical modelling in limestone formation

Sl. No.	Burden (m)	Spacing (m)	Bench height (m)	Area of the blast location (m^2)	Total charge per blast (kg)
1	3.50	6.00	7.0	210.0	**283.3**
2	3.50	6.00	7.0	294.0	**425.0**
3	3.50	6.00	6.0	420.0	**491.6**
4	3.00	5.50	7.0	336.0	**625.0**
5	3.50	6.00	7.0	378.0	**658.3**
6	3.00	6.00	8.5	396.0	**758.8**
7	3.50	6.00	7.8	441.0	**824.9**
8	3.50	6.00	7.0	504.0	**841.7**
9	3.00	5.50	7.0	429.0	**874.9**
10	3.00	6.00	6.5	478.5	**874.9**
11	3.00	6.00	10.0	462.0	**925.1**
12	3.50	6.00	9.3	378.0	**925.2**
13	3.00	5.50	7.0	561.0	**1,049.9**
14	3.00	5.50	8.0	495.0	**1,100.1**
15	3.50	6.00	8.5	486.0	**1,125.1**
16	3.50	6.00	7.0	630.0	**1,149.9**
17	3.00	5.50	8.5	468.0	**1,199.9**

Sl. No.	Burden (m)	Spacing (m)	Bench height (m)	Area of the blast location (m^2)	Total charge per blast (kg)
18	3.00	3.50	7.5	430.5	**1,262.4**
19	3.00	6.00	9.0	612.0	**1,550.1**
20	3.00	6.00	9.0	594.0	**1,624.9**
21	3.00	6.00	10.0	720.0	**2,050.0**
22	3.00	6.20	9.0	848.7	**2,099.9**
23	3.00	5.30	8.5	992.3	**2,574.2**
24	3.00	6.00	10.0	954.0	**2,849.8**
25	3.00	6.00	10.0	1,098.0	**2,874.9**
26	3.00	6.30	10.0	1,106.3	**2,974.8**
27	3.00	6.30	10.0	1,275.0	**3,285.8**
28	3.00	6.00	9.0	1,512.0	**3,974.9**

Execution of a model in limestone formation was carried out in steps with simulation time equal to total blast time. Each job run took about 16-20hrs for completion. Depending on the input parameters, typical size of models developed varied from 380MB to 3.71GB. In the output field, stress components at integral points and spatial velocities at nodes (PPVs) were observed. Fig. A8.1 shows stress contours observed at integral points in the output field for a typical model in limestone formation. Fig. A8.2 shows observed spatial velocity contours at nodes in the output field for a typical model in limestone formation. Each model in limestone formation was analysed with *Iso-surface cut visualization* (indicating overall stress acting on the bench during the blast), to obtain a blasted region on the bench. Fig. A8.3 shows the un-deformed and deformed shapes of designed blast models in limestone formation (Appendix-VIII).

PPVs resulting from typical blasts were also calculated in each model at various distances. Distance of monitoring was varied from 30m to 485m in field investigations. From the numerical modelling, particle velocities were obtained in all three directions (Longitudinal, Transverse, and Vertical) at a specified distance and the greatest vibration magnitude among them was considered as PPV. A percentage error of about <15% was observed in all developed models. This indicates a proper correlation between field results and modelling results. Table-A4.22 shows

comparison between field investigation results and modelling results in limestone formation (Appendix-IV).

4.4.3 Comparison of model results with field results in limestone formation

An attempt was made to compare the model PPVs obtained at particular distances in parametric study with the results of data generated from vibration monitoring and piezo electric generator at similar distances in limestone formation (Fig. 4.51). Also, MATLAB based regression analysis was carried out to evaluate the correlation between model PPVs, field PPVs and electrical voltage.

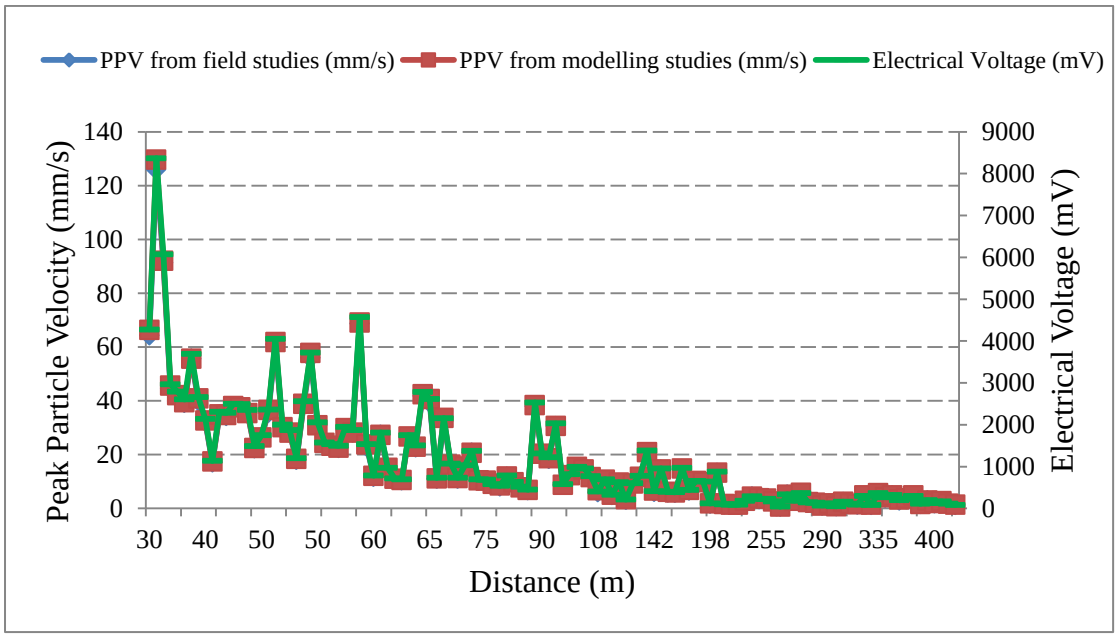

Fig. 4.51 Comparison of model results with field results in limestone formation

Initially, curve fitting analysis was made between PPVs from the models and field. MATLAB based analysis for curve fitting and regression analysis code between model PPVs and field PPVs in limestone formation are given in Appendix-V. Further, MATLAB based three dimensional curve fitting analysis was carried out for model PPV with field PPV and electrical voltage. 'R' squared value of 86% with model PPV, field PPV and electrical voltage, all three together, was obtained indicating an excellent correlation between these parameters. Results obtained from MATLAB based analysis for curve fitting and regression analysis code between model PPV,

field PPV and electrical voltage, altogether, in limestone formation are depicted in Appendix-V.

4.4.4 Numerical modelling results in underground coal formation

In coal formation, entirely 14 models were developed using SIMULIA Abaqus/CAE interface. Further, python script was coded for development of the models in coal formation. In particular, various models were developed similar to field conditions based on width of the face, height of the face, type of explosive used, and total explosive charge used per blast. Typical length and height of each model in coal formation was taken as 180mx60m with a width of 30m. It was considered an infinite region at the bottom of the face in each model. Similar to field investigations carried out earlier, slurry type of explosive was used in the modelling. Table-4.25 shows major input parameters considered for numerical modelling in coal formation. All the necessary parameters considered in coal formation for numerical modelling studies are tabulated in Appendix-IX.

Table – 4.25 Input parameters considered for numerical modelling in coal formation

Model No.	Width (m)	Height of the face (m)	Area of the blast location (m^2)	Total charge per blast (kg)
1	3.6	1.9	6.84	**5.74**
2	3.5	1.2	4.20	**6.48**
3	3.4	1.6	5.44	**6.66**
4	3.5	1.7	5.95	**6.66**
5	3.4	1.6	5.44	**6.85**
6	3.4	1.6	5.44	**6.85**
7	3.5	1.5	5.25	**6.85**
8	3.4	1.5	5.10	**7.03**
9	3.4	1.6	5.44	**7.59**
10	3.5	1.7	5.95	**7.59**
11	3.5	1.8	6.30	**8.14**
12	3.7	1.7	6.29	**8.14**
13	3.5	1.7	5.95	**8.88**
14	3.6	2.4	8.64	**8.88**

Execution of a model in coal formation was carried out in steps with total simulation time equal to total duration of blast. Each job run took about 8-10hrs for completion. Typical size of models developed varied from 174MB to 461MB. In the output field, stress components at integral points and spatial velocities at nodes (PPVs) were observed. Fig. A10.1 shows stress contours observed at integral points in the output field for a typical model in coal formation. Fig. A10.2 shows observed spatial velocity contours at nodes in the output field for a typical model in coal formation. Each model in coal formation was analyzed with Iso-surface cut visualization (indicating overall stress acting on the bench during the blast), to obtain a blasted region in the bench. Fig. A10.3 shows the un-deformed and deformed shapes of blast models in underground coal formation (Appendix-X).

PPVs resulting from typical blasts were also calculated in each model at various distances considering field studies. Distance of monitoring varied from 35m to 114m. From the numerical modelling, particle velocities were obtained in all three mutually orthogonal directions at a specified distance and the greatest vibration magnitude among them was considered as a PPV of the blast. It was observed that percentage error between field results and modelling results has exceeded >20% in some cases. This may be due to variation in geology of coal strata with more parting of about 65m between blast location and monitoring point. Table-A4.23 shows comparative results of field investigation and modelling results in coal formation.

4.4.5 Comparison of model results with field results in coal formation

Resemblance between model PPVs obtained at particular distances in parametric study and the results of data generated from vibration monitoring and piezo electric generator at similar distances was observed in coal formation (Fig. 4.52). Also, MATLAB based regression analysis was carried out to evaluate the correlation between model PPVs, field PPVs and electrical voltage.

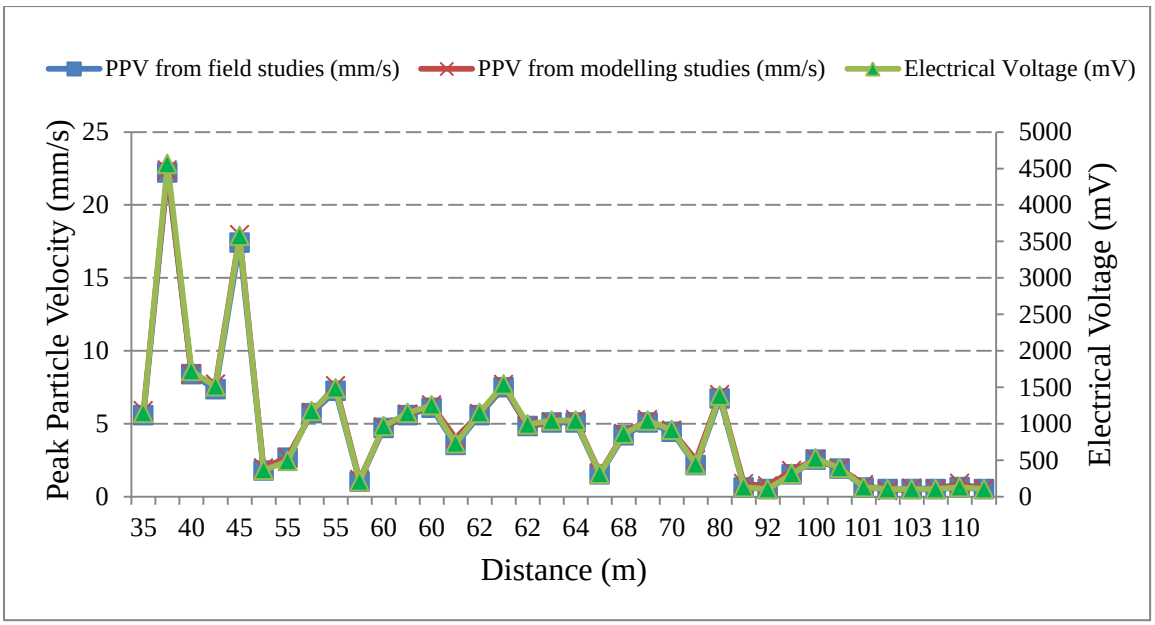

Fig. 4.52 Comparison of model results with field results in coal formation

Initially, curve fitting analysis was carried out between model PPVs and field generated PPVs. MATLAB based analysis for curve fitting and regression analysis code between model PPV and field PPV in coal formation are given in Appendix-V. Further, MATLAB based three dimensional curve fitting analysis was carried out for model PPV with field PPV and electrical voltage. 'R' squared value of 82% was obtained. Results obtained from MATLAB based analysis for curve fitting and regression analysis code between model PPV, field PPV and electrical voltage, altogether, in coal formation (Appendix-V).

4.4.6 Numerical modelling results in sandstone formation

In sandstone bench formation, 15 models were developed using SIMULIA Abaqus/CAE interface. Further, python script was developed for numerical modelling analysis in sandstone bench formation. Various models were developed similar to field conditions based on the burden and spacing of the blast location, height of the bench, type of explosive used, and total explosive charge used per blast. Models were developed based on field investigations carried out earlier. Typical size was chosen as 400mx400m for 12 different models and 750mx750m for 2 different models (model nos. 9 and 13) with a depth 10 times the bench height in sandstone bench formation. One model (model no. 11) was developed with a length to width ratio of

2050mx500m and a depth of 3 times the bench height, similar to field studies. Table-4.26 shows major input parameters considered for numerical modelling in sandstone bench formation. All the necessary parameters considered in sandstone formation for numerical modelling studies are tabulated in Appendix-XI. Similar to field investigations carried out earlier, ANFO and Slurry type of explosives were used in the modelling.

Table – 4.26 Input parameters considered for numerical modelling in sandstone formation

Model No.	Burden (m)	Spacing (m)	Bench height (m)	Area of the blast location (m^2)	Total charge per blast (kg)
1	3	3	5.0	495	**308.0**
2	3	3	5.0	360	**402.8**
3	3	3	5.0	396	**457.2**
4	3	3	5.0	441	**489.0**
5	3	4	5.0	696	**730.8**
6	5	6	4.5	900	**1,500.0**
7	5	6	14.0	1,320	**1,980.0**
8	5	6	20.7	1,290	**2,150.0**
9	4	5	5.5	2,100	**2,625.0**
10	5	5	5.5	2,025	**2,673.0**
11	5	6	5.5	2,100	**2,772.0**
12	5	6	5.8	3,630	**5,324.0**
13	7	9	5.0	2,205	**16,100.0**
14	7	9	5.0	2,394	**17,100.0**
15	5	7	14.0	1,645	**42,948.6**

Execution of a model in sandstone bench formation was carried out in steps with total simulation time equal to respective blast time for different models. Each job run took about 24-27hrs for completion. Based on the input parameters, typical size of models developed varied from 466MB to 6.02GB. In the output field, stress components at integral points, logarithmic strain components, spatial displacement at nodes, spatial velocity at nodes and spatial acceleration at nodes were observed. Fig. A12.1 shows stress contours observed at integral points in the output field for a typical model in sandstone bench formation. Fig. A12.2 shows observed spatial velocity contours at nodes in the output field for a typical model in sandstone bench formation. Each model in sandstone bench formation was analysed with *Iso-surface cut Visualization*

(indicating overall stress acting on the bench during the blast), to obtain a blasted region on the bench. Fig. A12.3 shows the un-deformed and deformed shapes of blast models in sandstone bench formation (Appendix-XII).

Peak Particle Velocities resulting from typical blasts were calculated in each model at various distances. Distance of monitoring was varied from 100m to 2033m field investigations. From the numerical modelling, particle velocities were obtained in all three directions (Longitudinal, Transverse, and Vertical) at specified distances.

In some cases, a percentage error of about >20% was observed from the results. This may be due to variation in some parameters like geology with developed models. Table-A4.24 shows comparative results of field investigation and modelling results in sandstone bench formation (Appendix-IV).

4.4.7 Comparison of model results with field results in sandstone formation

Based on parametric study, an attempt was made to compare the model PPVs obtained at particular distances with the results of data generated from vibration monitoring and piezo electric generator at similar distances in sandstone bench formation (Fig. 4.53). Also, MATLAB based regression analysis was carried out to evaluate the correlation between model PPV, field PPV and electrical voltage.

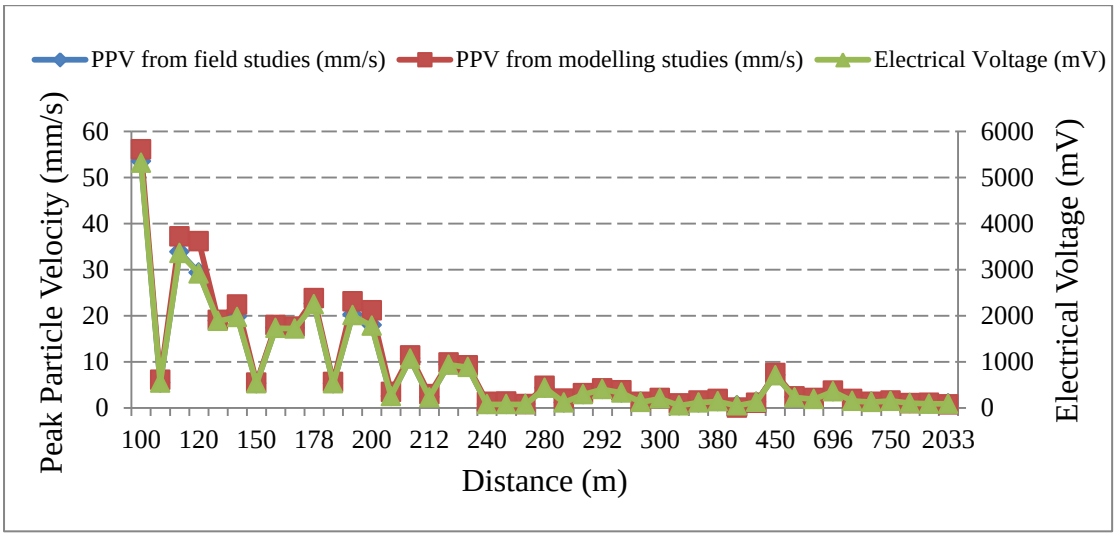

Fig. 4.53 Comparison of model results with field results in sandstone formation

Initially, curve fitting analysis was made between model PPV obtained from parametric study and field PPV obtained from field investigations carried out earlier. MATLAB based analysis for curve fitting and regression analysis code between model PPV and field PPV in sandstone bench formation are given in Appendix-V. Further, MATLAB based three dimensional curve fitting analysis was carried out for model PPVs with field PPVs and electrical voltage. Analysis resulted in 'R' squared value of 85% with model PPV, field PPV and electrical voltage, all three together, in sandstone bench formation. Results obtained from MATLAB based analysis for curve fitting and regression analysis code between model PPV, field PPV and electrical voltage, altogether, in sandstone bench formation are depicted in Appendix-V.

4.4.8 Numerical modelling results in granite formation

In granitic rock formation, 41 models were developed using SIMULIA Abaqus/CAE interface. Further, python script for numerical modelling analysis in granite formation was developed. In particular, various models were developed similar to field conditions based on the burden and spacing of the blast location, height of the bench, type of explosive used, and total explosive charge used per blast. Models were developed based on field investigations carried out earlier. Typical size of model was chosen with a length to width ratio as 400mx50m with a depth 5 times the bench height in granite formation. Since, the faces modelled in granitic rock formation are having a maximum width of 10m. Hence, width of the model was chosen as 5 times the width of the face. Similar to field investigations carried out earlier, Slurry and Emulsion type of explosives were used in the modelling. Table-4.27 shows major input parameters considered for numerical modelling in sandstone bench formation. All the necessary parameters considered in granite formation for numerical modelling studies are tabulated in Appendix-XIII.

Table – 4.27 Input parameters considered for numerical modelling in granite formation

Model No.	Burden (m)	Spacing (m)	Bench height (m)	Area of the blast location (m^2)	Total charge per blast (kg)
1	2.0	2.5	1.2	25.00	**0.63**
2	0.6	0.9	1.2	3.24	**1.50**
3	0.6	0.9	1.5	3.24	**1.50**

Model No.	Burden (m)	Spacing (m)	Bench height (m)	Area of the blast location (m^2)	Total charge per blast (kg)
4	2.0	3.0	1.2	36.00	**1.50**
5	0.6	0.9	1.2	4.32	**2.00**
6	0.6	0.9	1.5	4.32	**2.00**
7	2.0	2.5	1.2	40.00	**2.00**
8	2.0	3.0	1.5	48.00	**2.00**
9	0.6	0.9	1.2	5.40	**2.50**
10	0.6	0.9	1.5	5.40	**2.50**
11	2.0	2.5	1.2	50.00	**2.50**
12	2.0	3.0	1.2	60.00	**2.50**
13	0.6	0.9	1.2	6.48	**3.00**
14	0.6	0.9	1.5	6.48	**3.00**
15	2.0	2.5	1.2	60.00	**3.00**
16	2.0	3.0	1.5	72.00	**3.00**
17	0.6	0.9	1.2	8.10	**3.75**
18	0.6	0.9	1.5	8.10	**3.75**
19	2.0	2.5	1.2	75.00	**3.75**
20	0.6	0.9	1.5	9.72	**4.50**
21	0.6	0.9	1.5	10.80	**5.00**
22	2.0	2.5	1.2	100.00	**5.00**
23	0.6	0.9	1.5	11.88	**5.50**
24	2.0	2.5	1.2	110.00	**5.50**
25	0.6	0.9	1.5	12.96	**6.00**
26	0.6	0.9	1.5	13.50	**6.25**
27	0.6	0.9	1.5	15.12	**7.00**
28	1.2	1.2	1.5	40.32	**7.00**
29	0.6	0.9	1.5	16.20	**7.50**
30	1.2	1.2	1.5	43.20	**7.50**
31	2.0	3.0	1.2	180.00	**7.50**
32	3.0	3.0	6.0	54.00	**119.40**
33	2.0	2.5	5.0	30.00	**119.52**
34	3.0	3.0	5.0	72.00	**141.76**
35	2.9	3.0	5.5	87.00	**186.30**
36	2.5	3.0	5.0	82.50	**194.59**
37	2.0	3.0	5.0	72.00	**200.16**
38	2.0	3.0	5.0	90.00	**205.65**
39	2.9	3.0	6.0	130.50	**294.45**
40	2.0	3.0	5.0	108.00	**325.26**
41	3.0	3.5	6.0	199.50	**394.63**

Execution of a model in granite formation was carried out with 50 steps of simulation and total simulation time of 2000ms for different models. Each job run took about 18-

20hrs for completion. Depending on the input parameters, typical size of models developed varied from 119MB to 5.47GB. In the output field, stress components at integral points and spatial velocities at nodes (PPVs) were observed. It was observed that after 1720ms, stress components at integral points were redistributed in all models. Fig. A14.1 shows stress contours observed at integral points in the output field for a typical model in granite formation. Fig. A14.2 shows observed spatial velocity (PPV) contours at nodes in the output field for a typical model in granite formation. Each model in granite formation was analyzed with Iso-surface cut visualization (indicating overall stress acting on the bench during the blast), to obtain a blasted region on the bench. Fig. A14.3 shows the un-deformed and deformed shapes of blast models in granite formation (Appendix-XIV).

Peak Particle Velocities resulting from typical blasts were also calculated in each model at various distances. Distance of monitoring was varied from 20m to 300m considering field investigations carried out earlier. From the numerical modelling, particle velocities were obtained in all three directions (Longitudinal, Transverse, and Vertical) at a specified distance and the greatest vibration magnitude among them was considered as a PPV of the blast. A percentage error of about <15% was obtained between field results and model results in all developed models. This indicates a proper consistency of developed models on par with field studies. Table-A4.25 shows comparative table between field investigation and modelling results in granite formation (Appendix-IV).

4.4.9 Comparison of model results with field results in granite formation

Model PPVs obtained at particular distances from parametric study were compared with the results of data generated from vibration monitoring and piezo electric generator at similar distances in granite formation (Fig. 4.54).

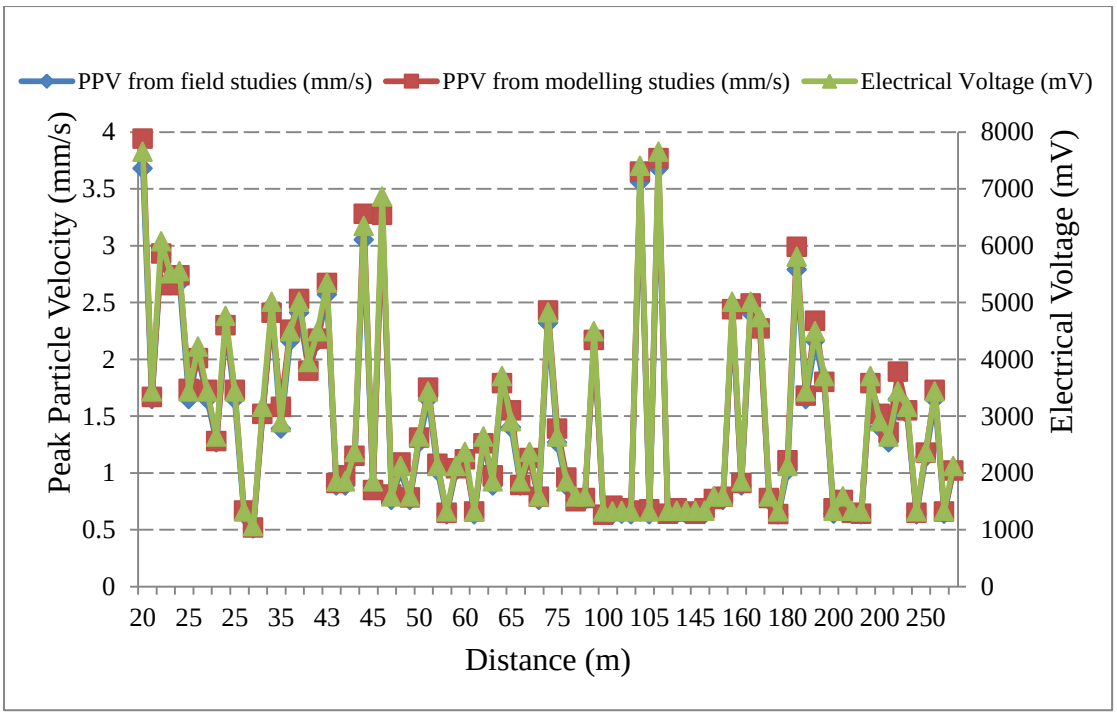

Fig. 4.54 Comparison of model results with field results in granite formation

Also, MATLAB based regression analysis was carried out to evaluate the correlation between model PPV, field PPV and electrical voltage. Initially, curve fitting analysis was made between model PPV and field PPV. MATLAB based analysis for curve fitting and regression analysis code between model PPV and field PPV in granite formation are given in Appendix-V. Further, MATLAB based three-dimensional curve fitting analysis was carried out for model PPV with field PPV and electrical voltage. It resulted in a 'R' squared value of 87% for model PPV, field PPV and electrical voltage, with all three together. Results obtained from MATLAB based analysis for curve fitting and regression analysis code between model PPV, field PPV and electrical voltage, altogether, in granite formation are depicted in Appendix-V.

Data obtained from numerical modelling studies was analysed using regression analysis with MATLAB in all four formations. Regression analysis was carried out in two stages:

1. Regression analysis was performed to obtain the relationship of the independent variables with dependent variables. Using regression analysis, gof (goodness of fit) was determined to find R^2 and adjusted R^2, standard error of the estimate.

These parameters measure how well the regression model describes the data. Initial regression analysis was carried out with PPV obtained from numerical modelling studies and PPV obtained from field investigations carried out.

2. Later, three-dimensional analysis was carried out with PPV obtained from numerical modelling studies, PPV obtained from field investigations carried out and electrical voltage obtained from piezo electric generator circuit developed.

Modelling study has clearly established the reliability of monitoring of electrical energy by a Piezo-Gen circuit, in assessing the wastage of seismic energy through ground vibrations caused by blasting.

CHAPTER 5

CONCLUSIONS AND SCOPE FOR FURTHER WORK

5.1 Conclusions

In the present research study, detailed field investigations were carried out to estimate the seismic energy dissipated by ground vibrations caused due to blasting operations, using signal processing approach and to tap electricity from blast induced ground vibrations by piezo generator. Studies were carried out in four different formations viz., Limestone, Coal, Sandstone, and Granite. Following are the main conclusions drawn from the research study:

- The minimum and maximum values of seismic energy dissipated by ground vibrations at different distances in four formations are - 26,792μJ and 11,12,59,278μJ in hard limestone, 46,715μJ and 5,46,976μJ in soft limestone, 4,250μJ and 19,04,089μJ in coal, 10,311μJ and 2,73,88,321μJ in sandstone, and 7,972μJ and 4,39,693μJ in granitic rock formations.
- There exists a proper correlation between seismic energy dissipated through ground vibrations and scaled distance in all four formations. In hard limestone formation it is about 80.26%, in soft limestone formation it is about 75.56%, in coal formation it is about 86.83%, in sandstone formation it is about 94.79%, and in granitic rock formation it is about 84.85%.
- MATLAB based analysis done in four different rock formations indicated a direct relationship between seismic energy and ground vibrations intensity. Higher is the vibration intensity, more will be the seismic energy value.
- The working of Piezo-Gen circuit in tapping ground vibrations was found to be as accurate as traditional ground vibration monitors.

- Electrical energy generated from the ground vibration waves was used to run a LED connected across capacitor and a PCB based circuit (low powered VLSI based circuit or ambient power based load), for finding out vibration intensities.
- The range of voltage tapped from ground vibrations is varying from 9.77mV to 4531.42mV in hard limestone, 89.65mV to 4552.91mV in soft limestone, 1.60mV to 128mV in coal, 415.06mV to 4277.51mV in sandstone, and 625.02mV to 4995.31mV in granite formations.
- Values of electrical energy tapped from ground vibrations in four different rock formations are upto 1,32,91,238μJ in hard limestone, 5,47,409μJ in soft limestone, 18μJ in underground coal, 3,84,97,572μJ in sandstone and 59,94,37,080μJ in granite formations, indicating harder formation to yield good amount of electrical energy.
- Based on research study carried out in medium strata limestone, coal mines, and small stone quarries, it could be concluded that there is much greater potential to tap electrical energy from ground vibrations caused by blasting in large opencast mining projects.
- Numerical modelling analysis results indicated, higher stress values at lower distances from blast location, indicating greater dissipation of seismic energy, which decreased with increase in distance in all four formations.
- MATLAB based regression analysis established a very good coefficient of determination between seismic energy and electrical energy, with values >90% in all four formations. It reveals that the assessment of seismic energy dissipated by ground vibrations is possible with the electrical energy generated by the developed Piezo-Gen circuit.
- Three dimensional curve fitting analysis made among PPVs resulting from modelling study, PPVs obtained in field investigations, and electrical voltages obtained from Piezo-Gen circuit, resulted in a coefficient of determination of 86% with sum of squares error of 0.308×10^{-7} in limestone formation, 82% with sum of squares error of 0.0013 in coal formation, 85% with sum of squares error of 6.513×10^{-29} in sandstone formation, and 87% with sum of squares error of 2.465×10^{-31} in

granite formation. Research study revealed a very good correlation between the modelling results and the seismic data generated from vibration monitoring and electrical data from piezo electric generator.

5.2 Scope for Further Work

Proposed research work focuses on the estimation of seismic energy dissipated by ground vibrations and tapping of electricity from blast induced ground vibrations using piezo generator. Also, finite element modelling studies and three dimensional regression analysis were carried out for all four formations. The following suggestions are made for future research on the subject.

1. In the present investigations, Limestone, Coal, Sandstone, and Granite formations were considered for assessing the seismic energy, and tapping of electrical energy from ground vibrations. In future work, more number of rock formations may be considered for a better assessment.
2. Similarly, studies may be extended to large scale blasts to assess the potential of utilizing non-conventional electrical energy generated by blast induced ground vibrations by tapping with appropriate Piezo-Gen circuit.
3. At present, the developed Piezo-Gen circuit is suited for ambient power based loads. Hence, further research studies may be taken up to enhance the obtained voltage of developed piezo-gen circuit from blast induced ground vibrations and also to harvest the electrical energy in larger scales.
4. Piezo-Gen circuit may be developed further to signal a prescribed ground vibration level, for the benefit of mines, quarries, and construction industry.

REFERENCES

Achenbach, J. (2012). *Wave propagation in elastic solids*. Elsevier.

Achzet, B. (2012). *Empirische Analyse von preis- und verf gbarkeitsbeeinflussenden Indikatoren unter Ber cksichtigung der Kritikalitt von Rohstoffen*. disserta Verlag.

Ambudkar, P.B., Rajule, M.N., Gowhar, S., Pawar, S., and Raut, A. (2014). "Use of Human Voice for Mobile Battery Charging." *Int. J. Res. Comput. Eng. Electron.*, 3(5).

Amirtharajah, R., and Chandrakasan, A.P. (1998). "Self-powered signal processing using vibration-based power generation." *IEEE J. Solid-State Circuits*, 33(5), 687–695.

Anderson, D.A., Riter, A.P., Winzer, S.R., and Reil, J.W. (1985). "A method for site specific prediction and control of ground vibration from blasting." *Proc 1 St Mini Symp. Explos. Blasting Res.*, San Diego, CA, 28–43.

Anon. (1997). "Rotational Kinetic Energy." <http://theory.uwinnipeg.ca/physics/rot/node6.html> (Jan. 12, 2017).

Anon. (2000). "LM158/LM258/LM358/LM2904 Low Power Dual Operational Amplifiers (Rev. I) - lm2904-n.pdf." *Tex. Instrum.*, <http://www.ti.com/lit/ds/symlink/lm2904-n.pdf> (Jan. 13, 2017).

Anon. (2005). "ATmega48PA/88PA/168PA/328P - Gravitech_ATMEGA328_data sheet.pdf." <http://www.mouser.com/pdfdocs/Gravitech_ATMEGA328_data sheet.pdf> (Jan. 13, 2017).

Anon. (2007). "Introduction to seismic processing and imaging. Copyright Leiv-J. Gelius/GeoCLASS." *INF-GEO 3310*, <http://docplayer.net/21060040-Inf-geo-3310-introduction-to-seismic-processing-and-imaging-copyright-leiv-j-gelius-geoclass-2007.html> (Oct. 12, 2018).

Anon. (2008a). "Piezoelectric Crystals Turn Roads into Power Plants." <http://news.softpedia.com/news/Piezoelectric-Crystals-Turn-Roads-into-Power-Plants-99776.shtml> (Jan. 12, 2017).

Anon. (2008b). “Demonstration Experiment of the ‘Power-Generating Floor’ at Tokyo Station.” <http://www.jreast.co.jp/e/development/press/20080111.pdf> (Jan. 12, 2017).

Anon. (2008c). *Standard practices for preparing rock core as cylindrical test specimens and verifying conformance to dimensional and shape tolerances*. (ASTM D4543-08), West Conshohocken, PA: American Society for Testing and Materials.

Anon. (2009). “Multiple Regression – Inference for Multiple Regression and A Case Study.” *WH Freeman Co.*, <http://www.stat.wmich.edu/~hzz3534/stat2600/ppt/ch11.pdf> (Jan. 12, 2017).

Anon. (2012a). “Student_Guide_Abaqus.” *altairuniversity*, <http://www.altairuniversity.com/wp-content/uploads/2012/04/Student_Guide_161-192.pdf> (Jan. 13, 2017).

Anon. (2012b). “CUED - ABAQUS.” <http://www-h.eng.cam.ac.uk/help/programs/fe/abaqus/faq68/abaqusf7.html> (Jan. 13, 2017).

Anon. (2013). “ANOVA - Statistics Solutions.” <http://www.statisticssolutions.com/manova-analysis-anova/> (Jan. 12, 2017).

Anon. (2015a). “All About Heaven - Some science behind the scenes - Piezoelectricity.” <http://www.allaboutheaven.org/science/149/121/piezoelectricity> (Jan. 12, 2017).

Anon. (2015b). “SIMULIA -Dassault Systèmes.” <http://www.simulia.com/services/training/V67%C2%ADIntroduction%C2%ADDEMO/movies/> (May 30, 2016).

Anon. (2015c). “Minimate Plus Operator Manual - 716U0101.” <http://www.instantel.com/pdf/manuals/716U0101-Rev-15-Minimate-Plus-Operator-Manual.pdf> (Jan. 12, 2017).

Anon. (2015d). *Formulae for ammunition management*. International Ammunition Technical Guideline (IATG) 01.80:2015[E], 8.

Anon. (2016a). “Mineral and Mining Industry in India.” *Min. India*, <http://www.cci.in/pdf/surveys_reports/mineral-mining-industry.pdf>.

Anon. (2016b). “Wave Velocity through Solids and Liquids.” <http://webcache.googleusercontent.com/search?q=cache:gBcXyM3ZT7QJ:schools.matter.org.uk/Content/Seismology/solidsandliquidsexplained.html+&cd=1&hl=en&ct=clnk&gl=in&client=firefox-b-ab> (Apr. 24, 2016).

Anon. (2016c). “BeStar Piezoelctric acoustic generator.” <http://www.bestartech.com/wp-content/uploads/2016/08/BeStar_Piezo_Technology_Manual.pdf> (Jan. 12, 2017).

Anon. (2016d). “Young’s modulus - Wikipedia.” <https://en.wikipedia.org/wiki/Young%27s_modulus> (Jan. 12, 2017).

Anon. (2016e). “Poisson’s ratio - Wikipedia.” <https://en.wikipedia.org/wiki/Poisson%27s_ratio> (Jan. 12, 2017).

Anon. (2016f). “IDL Explosives - Explosives.” <http://idlexplosives.com/explosives.php> (Apr. 10, 2017).

Anon. (2016g). “Slurry Explosives - IDEAL Industrial Explosives Ltd.” <http://www.idealexplosives.com/slurry%C2%ADexplosives.html> (Sep. 11, 2016).

Anon. (2017). “Indian Minerals Yearbook 2015 (Part- III : Mineral Reviews), 54 th Edition, Coal & Lignite (Advance Release).” Nagpur, India: Indian Bureau of Mines, Ministry of Mines, Government of India, 24.

Arnone, D., Pelt, A.V., and Dessau, K.L. (2003). “Piezoelectric Motors Control Set-and-Hold Semiconductor Applications-With the shift to tighter integrated circuit manufacturing specs and 157-nm lithography, motion control increasingly demands.” *Photonics Spectra*, 37(2), 70–75.

Atchison, T.C. (1968). “Fragmentation principles.” *Surf. Min.*, 355–372.

Atchison, T.C., Duvall, W.I., and Pugliese, J.M. (1963). *Effect of decoupling on explosion-generated strain pulses in rock*. Bureau of Mines, College Park, MD (USA).

Attewell, P.B. (1964). *Recording and Interpretation of Shock Effects in Rocks*. Toothill Press.

Barbero, E.J. (2013). *Finite element analysis of composite materials using AbaqusTM*. CRC press.

Berg, J.W., and Cook, K.L. (1961). “Energies, magnitudes, and amplitudes of seismic waves from quarry blasts at Promontory and Lakeside, Utah.” *Bull. Seismol. Soc. Am.*, 51(3), 389–399.

Berta, G. (1985). *L’esplosivo strumento di lavoro*. Italesplosivi.

Besancon, J.E., David, J., and Vedel, J. (1966). “Ferroelectric transducers.” *Proc. Conf. Megagauss Magn. Field Gener. Explos. Relat. Exp. Eds H Knoepfel F Herlach EUR.*

Bhandari, S. (1997). “Engineering rock blasting operations.” *Balkema 388*, 388.

Birch, W.J., and Chaffer, R. (1983). “Prediction of ground vibrations from blasting on opencast sites.” *Inst. Min. Metall. Trans.*, 92.

Blair, B.E. (1960). *Use of high-speed camera in blasting studies*. US Dept. of the Interior, Bureau of Mines.

Bouvier, J., Thorigne, Y., Hassan, S.A., Revillet, M.J., and Senn, P. (1997). “A smart card CMOS circuit with magnetic power and communication interface.” *Solid-State Circuits Conf. 1997 Dig. Tech. Pap. 43rd ISSCC 1997 IEEE Int.*, IEEE, 296–297.

Brian, B. (2011). “Harnessing the power on the highways.” <http://webcache.googleusercontent.com/search?q=cache:itV2Y9qxqzoJ:mfa.gov.il/MFA/InnovativeIsrael/Pages/Harnessing_power_on_highways-Feb_2011.aspx+&cd=1&hl=en&ct=clnk&gl=in> (Sep. 26, 2015).

Brüel, and Kjær. (2015). “PSD (Power spectral density).” <https://www.bksv.com/ServiceCalibration/> (Jun. 6, 2015).

Cady, W.G. (1930). “Piezo-Electric Terminology.” *Proc. Inst. Radio Eng.*, 18(12), 2136–2142.

Carullo, A., and Parvis, M. (2001). “An ultrasonic sensor for distance measurement in automotive applications.” *IEEE Sens. J.*, 1(2), 143–147.

Chiappetta, R.F., and Mammele, M.E. (1988). “Use Of High-Speed Motion Picture Photography In Blast Evaluation And Design.” *31st Annu. Tech. Symp.*, International Society for Optics and Photonics, 319–336.

Clark, W.W., and Ramsay, M.J. (2000). “Smart material transducers as power sources for MEMS devices.” *Int. Symp. Smart Struct. Microsyst. Hong Kong Oct*, 19–21.

Cunningham, C.V.B. (1996). “Keynote address—optical fragmentation assessment, a technical challenge.” *Meas. Blast Fragm. Proc. FRAGBLAST*, 13–19.

Curie, J., and Curie, P. (1880). “Development by pressure of polar electricity in hemihedral crystals with inclined faces.” *Bull Soc Min Fr.*, 3, 90–93.

Curie, J., and Curie, P. (1881). “Contractions et dilatations produites par des tensions électriques dans les cristaux hémièdres à faces inclinées.” *Comptes-Rendus L’Académie Sci.*, 93, 1137–1140.

Da Gama, C.D., and Jimeno, C.L. (1993). “Rock fragmentation control for blasting cost minimisation and environmental impact abatement.” *Int. Symp. ROCK Fragm. BLASTING*, 5–8.

Daemen, J.J.. (1983). *Ground and air vibrations caused by surface blasting*. USA.

Damjanovic, D., and Newnham, R.E. (1992). “Electrostrictive and piezoelectric materials for actuator applications.” *J. Intell. Mater. Syst. Struct.*, 3(2), 190–208.

Davies, B., Farmer, I.W., and Attewell, P.B. (1964). “Ground vibration from shallow sub-surface blasts.” *Engineer*, 217(5644).

Devine, J.P., and Duvall, W.I. (1963). “Effect of charge weight on vibration levels for millisecond delayed quarry blasts.” *Seismol. Res. Lett.*, 34(2), 16–24.

Doppalapudi, D., Moustakas, T.D., Mlcak, R., and Tuller, H.L. (2001). *Semiconductor piezoresistor*. Google Patents.

Douglas, A.A., and James, W.R. (2000). “Measuring fragmentation efficiency of a blast using ground vibrations.” *Proc Annu. Conf. Int. Soc. Explos. Eng.*

Dowding, C.H. (1985). *Blast vibration monitoring and control*. Prentice-Hall Englewood Cliffs.

Drebenstedt, C. (2014). “The Responsible Mining Concept – Contributions on the Interface between Science and Practical Needs.” *Mine Plan. Equip. Sel. Proc. 22nd MPES Conf. Dresd. Ger. 14th – 19th Oct. 2013*, C. Drebenstedt and R. Singhal, eds., Cham: Springer International Publishing, 3–24.

Drobny, J.G. (2012). *Polymers for electricity and electronics: materials, properties, and applications*. John Wiley & Sons.

Dudley, J.W., Brignoli, M., Crawford, B.R., Ewy, R.T., Love, D.K., McLennan, J.D., Ramos, G.G., Shafer, J.L., Sharf-Aldin, M.H., Siebrits, E., and others. (2016). "ISRM Suggested Method for Uniaxial-Strain Compressibility Testing for Reservoir Geomechanics." *Rock Mech. Rock Eng.*, 49(10), 4153–4178.

Duvall, W.I., and Fogelson, D.E. (1962). *Review of criteria for estimating damage to residences from blasting vibrations*. US Department of the Interior, Bureau of Mines.

Duvall, W.I., Johnson, C.F., and Meyer, A.V.C. (1963). *Vibrations from blasting at Iowa limestone quarries*. US Dept. of the Interior. Bureau of Mines.

Eloranta, J. (1995). *Selection of powder factor in large diameter blastholes*. International Society of Explosives Engineers, Cleveland, OH (United States).

Elvin, N.G., Elvin, A.A., and Spector, M. (2001). "A self-powered mechanical strain energy sensor." *Smart Mater. Struct.*, 10(2), 293.

Fisher, R.A. (1930). *The genetical theory of natural selection: a complete variorum edition*. Oxford University Press.

Flynn, A.M., and Sanders, S.R. (2002). "Fundamental limits on energy transfer and circuit considerations for piezoelectric transformers." *IEEE Trans. Power Electron.*, 17(1), 8–14.

Fogelson, D.E., Atchison, T.C., Duvall, W.I., and others. (1959). "Propagation of peak strain and strain energy for explosion-generated strain pulses in rock." *3rd US Symp. Rock Mech. USRMS*, American Rock Mechanics Association.

Friedman, D., Heinrich, H., and Duan, D.-W. (1997). "A low-power CMOS integrated circuit for field-powered radio frequency identification tags." *Solid-State Circuits Conf. 1997 Dig. Tech. Pap. 43rd ISSCC 1997 IEEE Int.*, IEEE, 294–295.

Gautschi, G. (2002). *Piezoelectric sensorics: force, stain, pressure, acceleration and acoustic emission sensors, materials and amplifiers*. Springer.

Geddes, L.A. (1990). "Historical highlights in cardiac pacing." *IEEE Eng. Med. Biol. Mag.*, 9(2), 12–18.

Ghandi, K. (2000). "Compact piezoelectric based power generation." *Contin. Controls Inc DARPA Energy Harvest. Program Rev.*

Goldfarb, M., and Jones, L.D. (1999). “On the efficiency of electric power generation with piezoelectric ceramic.” *J. Dyn. Syst. Meas. Control*, 121(3), 566–571.

Gonzalez, J.L., Rubio, A., and Moll, F. (2001). “A prospect on the use of piezoelectric effect to supply power to wearable electronic devices.” *Proc. Int. Conf. Mater. Eng. Resour. ICMR*, 202–206.

Grady, D.E. (1982). “Local inertial effects in dynamic fragmentation.” *Journal of Applied Physics*, 53(1), 322–325.

Gupta, R.N., and Misra, A.K. (1998). “An investigation of shocktube down the hole initiation system for reduction of ground vibration and air overpressure.” *Proc Visfotak98*, DOE, Govt. of India, Nagpur, 147–154.

Habberjam, G.M., and Whetton, J.T. (1952). “On the relationship between seismic amplitude and charge of explosive fired in routine blasting operations.” *Geophysics*, 17(1), 116–128.

Hagan, T.N. (1973). “Rock Breakage by Explosives Nat.” *Symp Rock Fragm.*

Hagan, T.N. (1983). “The influence of controllable blast parameters on fragmentation and mining costs.” *Proc. 1st Int. Symp. Rock Fragm. Blasting*, 31–32.

Hagan, T.N., and Kennedy, B.J. (1978). “Practical approach to the reduction of blasting nuisances from surface operations: Aust Min, V69, N11, Nov 1977, P36–46.” *Int. J. Rock Mech. Min. Sci. Geomech. Abstr.*, Pergamon, 65.

Hayakawa, M. (1991). *Electronic wristwatch with generator*. Google Patents.

Henderson, I.R. (2002). “Piezoelectric Ceramics: Principles and Applications.” *APC Int. Pa. USA*.

Hibbett, Karlsson, and Sorensen. (1998). *ABAQUS/standard: User’s Manual*. Hibbitt, Karlsson & Sorensen.

Higgins, M.R.T., BoBo, T., Girdner, K., Kemeny, J., and Seppala, V. (1999). “Integrated software tools and methodology for optimisation of blast fragmentation.” *25th Annu. Conf. Explos. Blasting Tech.*, International Society of Explosives Engineer, 355–368.

Hinzen, K.G. (1998). “Comparison of seismic and explosive energy in five smooth blasting test rounds.” *Int. J. Rock Mech. Min. Sci.*, 35(7), 957–967.

Holloway, R., Lundborg, N., and Runquist, G. (1983). *Ground vibrations and damage criteria*. SWEDEFO Report R85:1981.

Holmberg, R., and Persson, P.A. (1978). *The Swedish approach to contour blasting*. SveDeFo.

Howell, B.F., and Budenstein, D. (1955). "Energy distribution in explosion-generated seismic pulses." *Geophysics*, 20(1), 33–52.

Huang, J., O'handley, R.C., and Bono, D. (2006). *High efficiency vibration energy harvester*. Google Patents.

Ikeda, T. (1996). *Fundamentals of piezoelectricity*. Oxford university press.

Izumi, T., Hagiwara, M., Hoshina, T., Takeda, H., and Tsurumi, T. (2012). "Analysis of vibration waveforms of electromechanical response to determine piezoelectric and electrostrictive coefficients." *IEEE Trans. Ultrason. Ferroelectr. Freq. Control*, 59(8), 1632–1638.

Janssen, W.H. (1951). *Piezoelectric strain gauge*. Google Patents.

Johansson, C.H., and Persson, P.-A. (1970). "Detonics of high explosives."

Kasyap, A., Lim, J., Johnson, D., Horowitz, S., Nishida, T., Ngo, K., Sheplak, M., and Cattafesta, L. (2002). "Energy reclamation from a vibrating piezoceramic composite beam." *Proc. 9th Int. Congr. Sound Vib.*, 36–43.

Kemeny, J., Girdner, K., Bobo, T., and Norton, B. (1999). "Improvements for fragmentation measurement by digital imaging: accurate estimation of fines." *Sixth Int. Symp. Rock Fragm. Blasting SAIMM*, 103–110.

Kemeny, J.M., Devgan, A., Hagaman, R.M., and Wu, X. (1993). "Analysis of rock fragmentation using digital image processing." *J. Geotech. Eng.*, 119(7), 1144–1160.

Khennane, A. (2013). *Introduction to finite element analysis using MATLAB® and Abaqus*. CRC Press.

Kimura, M. (1998). *Piezo-electricity generation device*. Google Patents.

Konya, C.J., and Walter, E.J. (1990). *Surface blast design*. Prentice-Hall.

Kymissis, J., Kendall, C., Paradiso, J., and Gershenfeld, N. (1998). "Parasitic power harvesting in shoes." *Wearable Comput. 1998 Dig. Pap. Second Int. Symp. On*, IEEE, 132–139.

Lama, R.D., and Vutukuri, V.S. (1978). *Handbook on mechanical properties of rocks-testing techniques and results-volume iii*.

Langefors, U.L.F., Kihlstrom, B., and Westerberg, H. (1958). *Ground vibrations in blasting*. Nitrogglycerin Aktiebolaget.

Liu, Q., and Tran, H. (1996). "Comparing systems-validation of fragscan, wipfrag and split." *Meas. Blast Fragm. Frankl. Katsabanis Eds*, 151–155.

Lucy, E.A. (2010). "Innowattech: Harvesting Energy and Data - A stand alone technology." *First Int. Symp. Highw. Innov.*, Tel Aviv, Israrel: Israel National Roads Company Limited.

Ludu, A., Nicolau, P., and Novac, B.M. (1987). "Shock Wave-Explosive Energy Generator of PZT Ferroelectric Ceramics." *Megagauss Technol. Pulsed Power Appl.*, 369–375.

MacKenzie, A.S. (1966). "Cost of explosives—do you evaluate it properly." *Min. Congr. J.*, 32–41.

Maerz, N.H., Palangio, T.C., and Franklin, J.A. (1996). "WipFrag image based granulometry system." *Proc. FRAGBLAST 5 Workshop Meas. Blast Fragm. Montr. Quebec Can.*, AA Balkema, 91–99.

McMillan, A.J. (2013). "Computational modeling of ultrasound propagation using Abaqus explicit." *SIMULIA UK RUM Crewe UK*.

Meninger, S., Mur-Miranda, J.O., Amirtharajah, R., Chandrakasan, A., and Lang, J.H. (2001). "Vibration-to-electric energy conversion." *IEEE Trans. Very Large Scale Integr. VLSI Syst.*, 9(1), 64–76.

Morris, G. (1950). "Vibrations due to Blasting and their Effects on Building Structure." *The Engineer*, 190, 394.

Newnham, R.E., Sundar, V., Yimnirun, R., Su, J., and Zhang, Q.M. (1997). "Electrostriction: nonlinear electromechanical coupling in solid dielectrics." *J. Phys. Chem. B*, 101(48), 10141–10150.

Nicholls, H.R. (1962). "Coupling explosive energy to rock." *Geophysics*, 27(3), 305–316.

Nicholls, H.R., Johnson, C.F., and Duvall, W.I. (1971). *Blasting vibrations and their effects on structures*. US Government Printers.

Olofsson, S.O. (1990). *Applied explosives technology for construction and mining*. Applex.

Ouchterlony, F., Nyberg, U., Olsson, M., Bergquist, I., Granlund, L., and Grind, H. (2003). "The energy balance of production blasts at Nordkalk's Klinthagen quarry." *EFEE World Conf. Explos. Blasting Tech. 10092003-12092003*, Balkema Publishers, AA/Taylor & Francis The Netherlands, 193–203.

Paley, N., and Kojovic, T. (2001). "Adjusting blasting to increase SAG mill throughput at the Red Dog mine." *Proc. Annu. Conf. Explos. BLASTING Tech.*, ISEE; 1999, 65–82.

Pramethesth, T., and Ankur, S. (2013). "Future Source Of Electricity." *Int. J. Sci. Eng. Technol.*, 2(4).

Prishchepenko, A.B., and Shchelkachev, M.V. (1996). "The work of the explosive type generator with capacitive load." *Proc. Megagauss VII Magn. Field Gener. Pulsed Power Appl.*, 304–307.

Puri, G. (2011). *Python scripts for Abaqus: learn by example*. Gautam Puri.

Ramadass, Y.K., and Chandrakasan, A.P. (2010). "An efficient piezoelectric energy harvesting interface circuit using a bias-flip rectifier and shared inductor." *IEEE J. Solid-State Circuits*, 45(1), 189–204.

Ritter, T.A., Shrout, T.R., Tutwiler, R., and Shung, K.K. (2002). "A 30-MHz piezo-composite ultrasound array for medical imaging applications." *IEEE Trans. Ultrason. Ferroelectr. Freq. Control*, 49(2), 217–230.

Rosenthal, M.F., Morlock, G.L., John, L.H.S., James, W.R., and Foster, G.A. (1987). "Blasting guidance manual."

Sadwin, L.D., and Junk, N.M. (1965). *Measurement of lateral pressure generated from cylindrical explosive charges*. US Dept. of the Interior, Bureau of Mines.

Sanchidrián, J.A., Segarra, P., and López, L.M. (2007). "Energy components in rock blasting." *Int. J. Rock Mech. Min. Sci.*, 44(1), 130–147.

Sastry, V. (2001). "Elimination of Ground Vibration and Fly Rock: A Case Study of an Open Cast Mine." *Proc. Annu. Conf. Explos. BLASTING Tech.*, ISEE; 1999, 301–312.

Sastry, V.R. (1989). "A Study into the effect of some parameters on rock fragmentation by blasting." BHU, India, Varanasi.

Sastry, V.R. (2015). *Assessment of Performance of Explosives / Blast Results based on Explosive Energy Utilization*. R&D Project Report, Submitted to CMPDI, Ranchi.

Sastry, V.R., and Chandar, K.R. (2008). "Assessment of Blast Performance Based on Energy Distribution." *42nd US Rock Mech. Symp. USRMS*, American Rock Mechanics Association.

Sastry, V.R., Chandra, G.R., Adithya, N., and Saiprasad, S.A. (2015). "Application of High-Speed Videography in Assessing the Performance of Blasts." *Int. J. Geol. Geotech. Eng.*, 1(1), 37–51.

Sastry, V.R., and Ram Chandar, K. (2004). "Shock tube initiation for better fragmentation: A case study." *Fragblast*, 8(4), 207–220.

Sastry, V.R., and Ram Chandar, K. (2015). *Unpublished report of Jayajothi Cements Limited*.

Sedlák, V. (1997). "Energy evaluation of de-stress blasting." *Acta Montan. Slovaca Roč.*, 2, 11–15.

Shkuratov, S.I., Kristiansen, M., Dickens, J., Neuber, A., Altgilbers, L.L., Tracy, P.T., and Tkach, Y. (2001). "Experimental study of compact explosive driven shock wave ferroelectric generators." *Pulsed Power Plasma Sci. 2001 PPPS-2001 Dig. Tech. Pap.*, IEEE, 959–962.

Singh, B., Roy, P.P., and Singh, R.B. (1993). *Blasting in ground excavations and mines*. AA Balkema.

Spathis, A.T. (1999). "Energy efficiency of blasting." *Proc. 6th Int. Symp. Rock Fragm. Blasting*.

Staines, G., Hofmann, H., Dommer, J., Altgilbers, L., and Tkach, Y. (2003). "Compact Piezo-Based High Voltage Generator-Part I: Quasi-Static Measurements." *Electromagn Phenom*, 3, 373–383.

Starner, T. (1996). "Human-powered wearable computing." *IBM Syst. J.*, 35(3.4), 618–629.

Tanaka, T. (1977). *Vibration detecting device having a piezoelectric ceramic plate and a method for adapting the same for use in musical instruments*. Google Patents.

Taqieddin, S. (1982). “The role of borehole pressure containment on surface ground vibration levels at close scaled distances (Missouri).”

Tashiro, S., Ishii, K., and Nagata, K. (2003). “Comparison of nonlinearity between lead magnesium niobate electrostrictive and lead zirconate titanate piezoelectric ceramics.” *Jpn. J. Appl. Phys.*, 42(9S), 6068.

Tingley, R. (2013). *Method and application of piezoelectric energy harvesting as a mobile power source*. New Hampshire.

Tkach, Y., Shkuratov, S.I., Talantsev, E.F., Dickens, J.C., Kristiansen, M., Altgilbers, L.L., and Tracy, P.T. (2002). “Theoretical treatment of explosive-driven ferroelectric generators.” *IEEE Trans. Plasma Sci.*, 30(5), 1665–1673.

Tressler, J.F., Alkoy, S., and Newnham, R.E. (1998). “Piezoelectric sensors and sensor materials.” *J. Electroceramics*, 2(4), 257–272.

Trimarchi, M. (2008). “Can house music solve the energy crisis?” *HowStuffWorks Com*.

Umeda, M., Nakamura, K., and Ueha, S. (1996). “Analysis of the transformation of mechanical impact energy to electric energy using piezoelectric vibrator.” *Jpn. J. Appl. Phys.*, 35(5S), 3267.

Umeda, M., Nakamura, K., and Ueha, S. (1997). “Energy storage characteristics of a piezo-generator using impact induced vibration.” *Jpn. J. Appl. Phys.*, 36(5S), 3146.

Valone, T. (2009). *The Future of Energy: An Emerging Science*. Integrity Research Institute.

Wierszycki, M., and Sielicki, P. (2012). “Blast wave propagation in the air and action on rigid obstacles.”

Williams, C.B., and Yates, R.B. (1996). “Analysis of a micro-electric generator for microsystems.” *Sens. Actuators Phys.*, 52(1), 8–11.

Wingrove, G.A. (1970). *Mesa t-bar piezoresistor*. Google Patents.

Winzer, S.R., Anderson, D.A., and Riter, A.P. (1983). “Rock Fragmentation by Explosives.” *Proc. 1st Int. Symp. Rock Fragm. Blasting*, Lulea, Sweden, 225–251.

Winzer, S.R., Montenyohl, V.I., and Ritter, A. (1979). “High-speed cinematography of production blasting operations.” *Min. Congr. J.*, J Allen Overton Jr 1920 N St Nw, Washington, DC 20036, 46.

Wiss, J.F., and Linehan, P. (1979). *Control of vibration and blast noise from surface coal mining*. Bureau of Mines.

Workman, L., and Eloranta, J. (2003). “The effects of blasting on crushing and grinding efficiency and energy consumption.” *Proc 29th Con Explos. Blasting Tech. Int Soc. Explos. Eng. Clevel. OH*, 1–5.

Wu, X., and Kemeny, J.M. (1992). “A segmentation method for multi-connected particle delineation.” *Appl. Comput. Vis. Proc. 1992 IEEE Workshop On*, IEEE, 240–247.

Xiaoguang, Y. (2011). “3.Preprocessing of Abaqus CAE _Jan 2011 Draft - abaqus3tutorial.pdf.” <https://intranet.birmingham.ac.uk/as/libraryservices/library/skills/digitaltechnologyskills/documents/public/abaqus3tutorial.pdf> (Jan. 13, 2017).

Yang, R., and Turcotte, R. (1994). “Blast damage modelling using ABAQUS/ Explicit.” *Users Conf. Proc. Newport R. I. USA*.

Yang, Z. (1997). “Finite element simulation of response of buried shelters to blast loadings.” *Finite Elem. Anal. Des.*, 24(3), 113–132.

Zhang, C., and Zhong, G. (2011). “Influence of explosion parameters on energy distribution of blast vibration signals with wavelet packet analysis.” *Mech. Autom. Control Eng. MACE 2011 Second Int. Conf. On*, IEEE, 2234–2237.

APPENDIX – I

LIMESTONE FORMATION
(High Speed Camera Sequence Photos)

CHOUTAPALLI LIMETSONE MINE (HARDER FORMATION)
M/S MY HOME INDUSTRIES PRIVATE LIMITED
NALGONDA DISTRICT, TELANGANA

0ms

200ms

400ms

600ms

800ms

1000ms

PROGRESS OF A TYPICAL BLAST

APPENDIX – II

SANDSTONE FORMATION
(High Speed Camera Sequence Photos)

RAMAGUNDAM OPENCAST MINE-I
THE SINGARENI COLLIERIES COMPANY LIMITED
KARIMNAGAR DISTRICT, TELANGANA

0ms

200ms

400ms

600ms

800ms

1000ms

PROGRESS OF A TYPICAL BLAST

APPENDIX – III

LIMESTONE FORMATION
(Wipfrag Analysis)

CHOUTAPALLI LIMETSONE MINE (HARDER FORMATION)
M/S MY HOME INDUSTRIES PRIVATE LIMITED
NALGONDA DISTRICT, TELANGANA

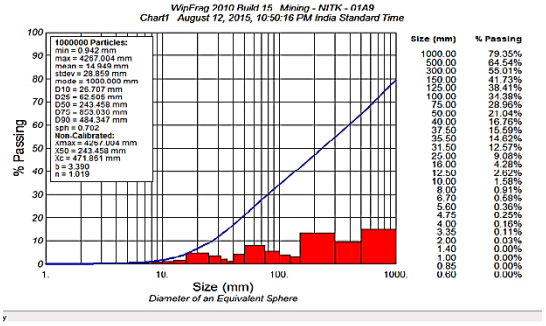

BLAST-1

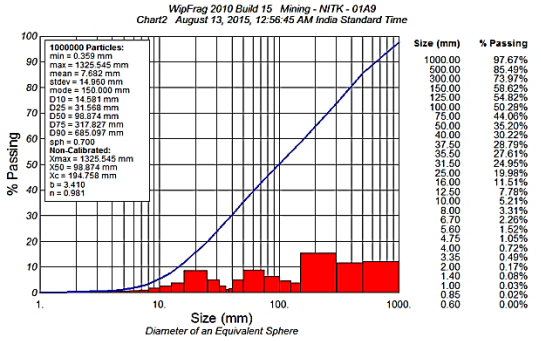

BLAST-2

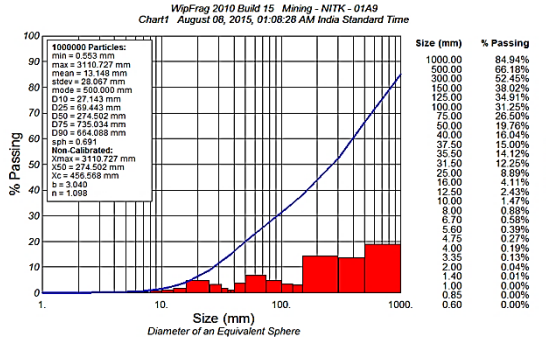

BLAST-3

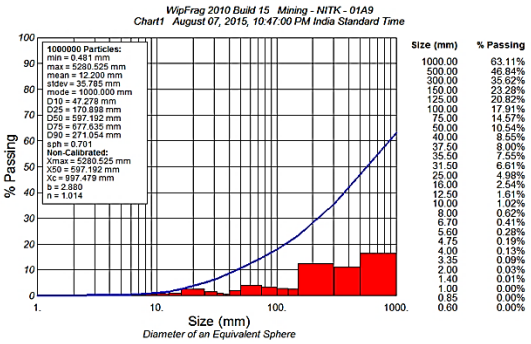

BLAST-4

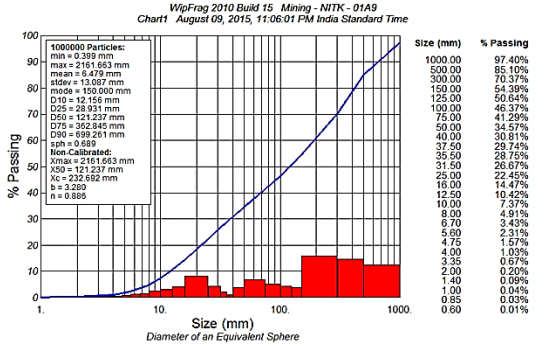

BLAST-5

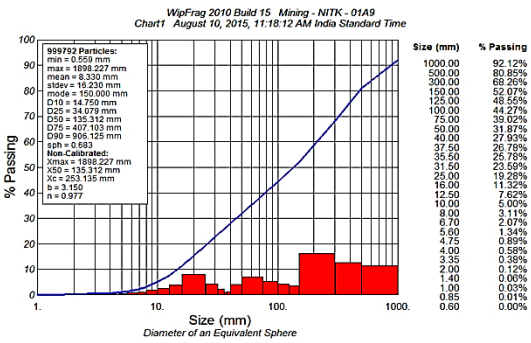

BLAST-6

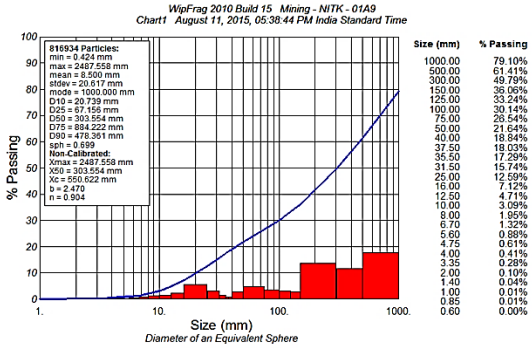

BLAST-7

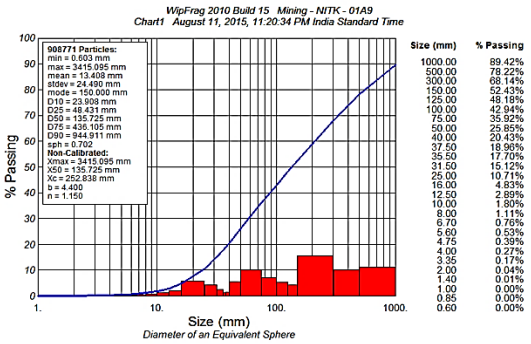

BLAST-8

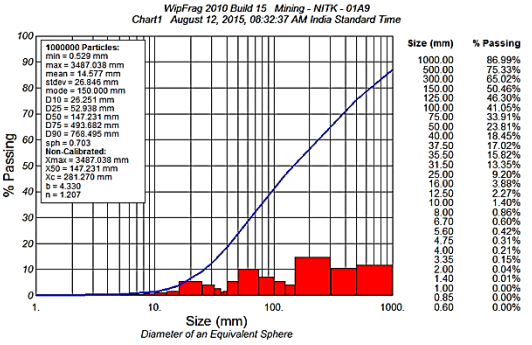

BLAST-9

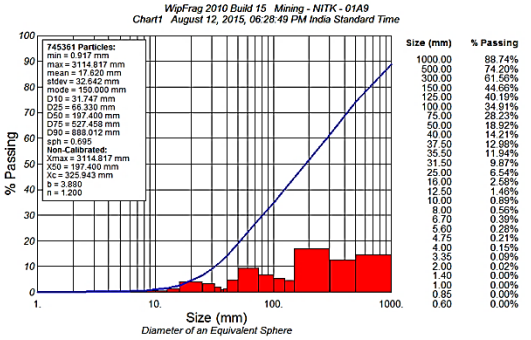

BLAST-10

YEPALAMADHAVARAM LIMETSONE MINE (HARDER FORMATION)
M/S MY HOME INDUSTRIES PRIVATE LIMITED
NALGONDA DISTRICT, TELANGANA

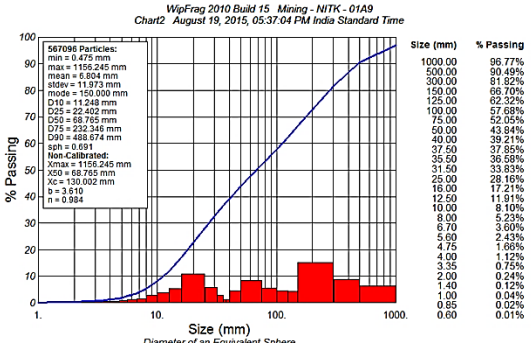

BLAST-1

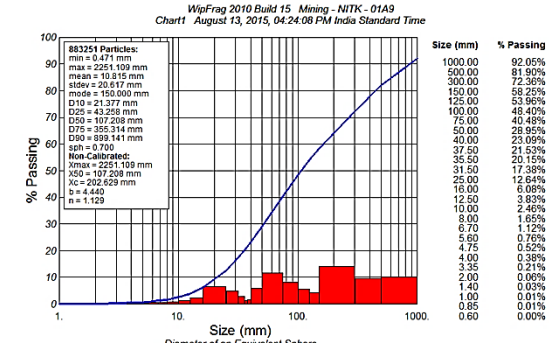

BLAST-2

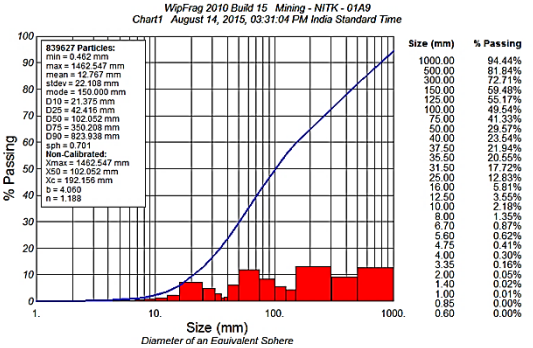

BLAST-3

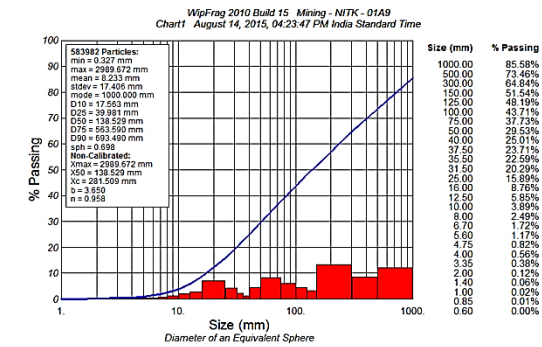

BLAST-4

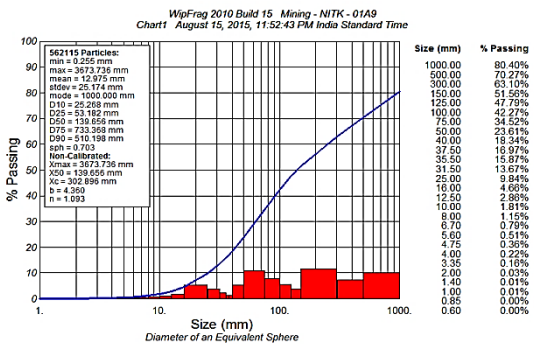

BLAST-5

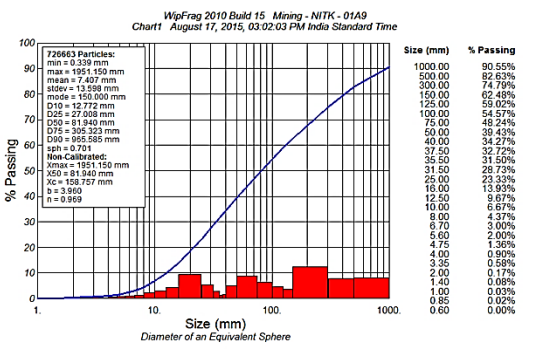

BLAST-6

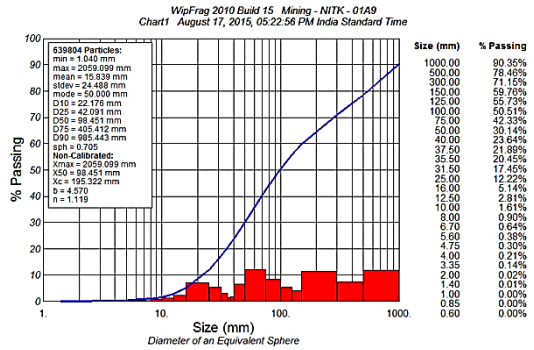

BLAST-7

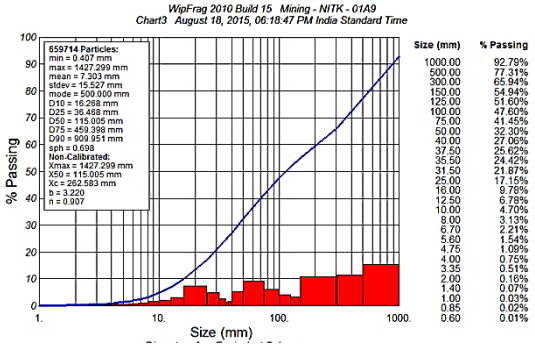

BLAST-8

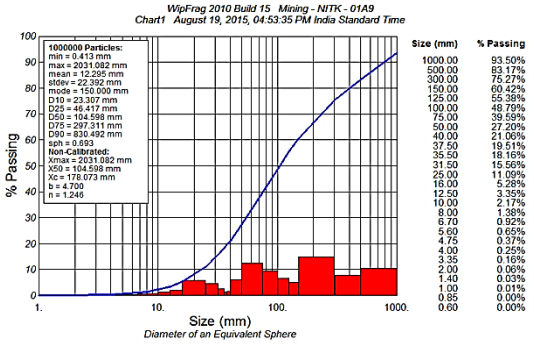

BLAST-9

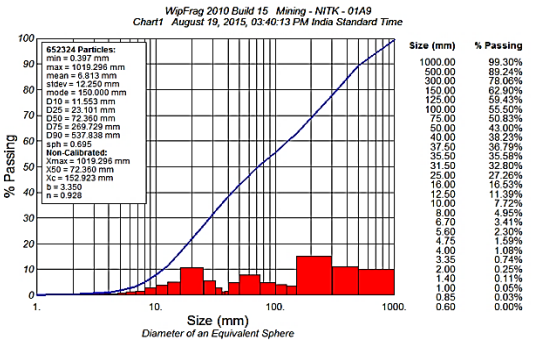

BLAST-10

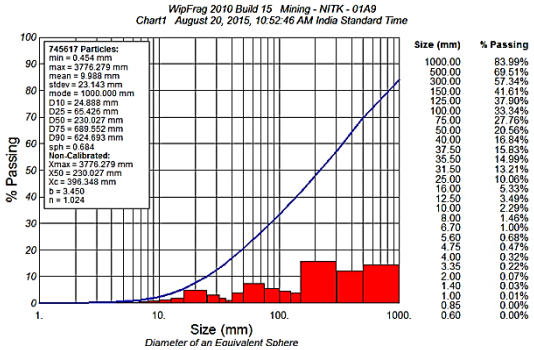

BLAST-11

YANAKANDLA LIMETSONE MINE (HARDER FORMATION)
M/S SREE JAYAJOTHI CEMENTS PRIVATE LIMITED
KURNOOL DISTRICT, ANDHRA PRADESH

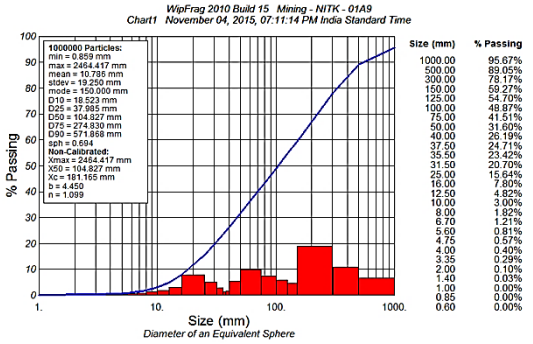

BLAST-1

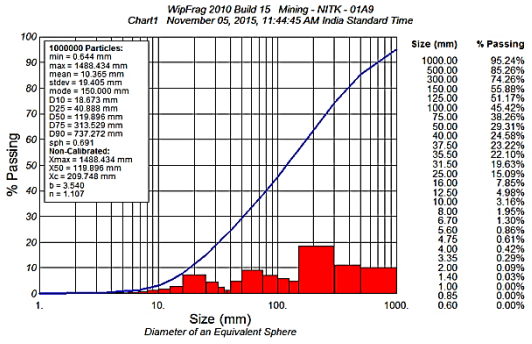

BLAST-2

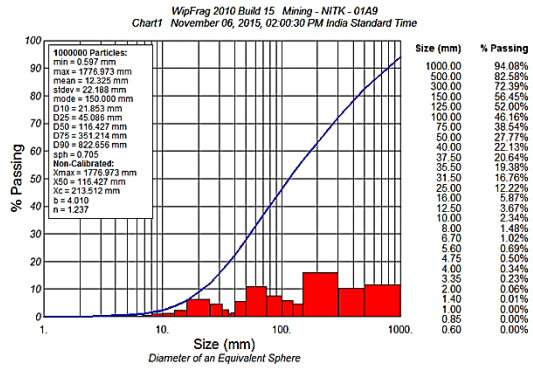

BLAST-3

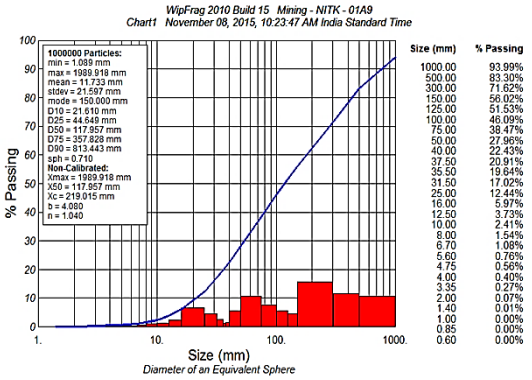

BLAST-4

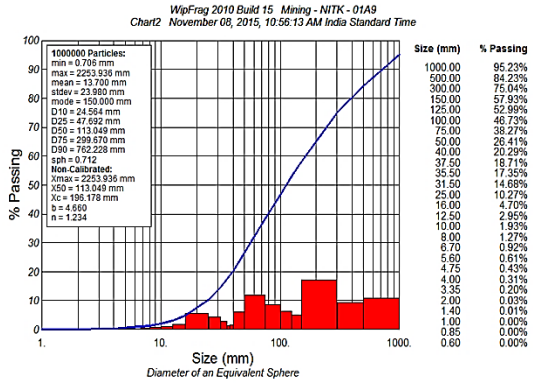

BLAST-5

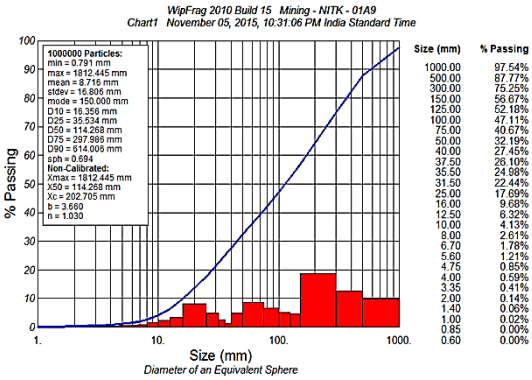

BLAST-6

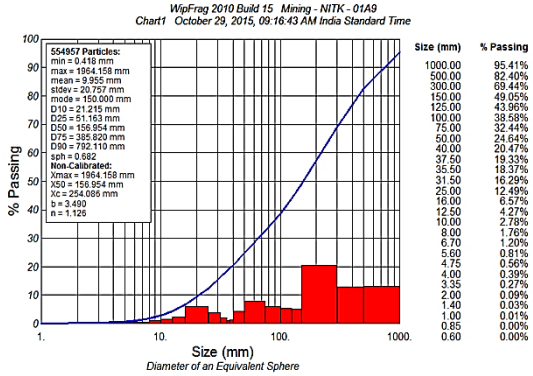

BLAST-7

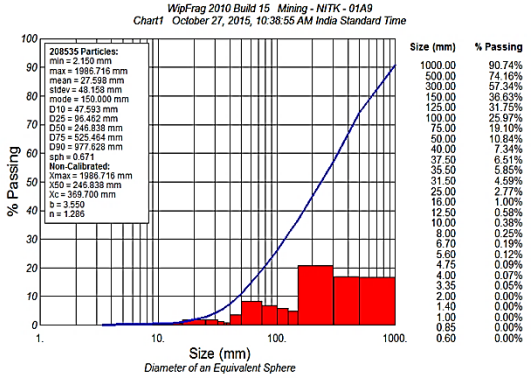

BLAST-8

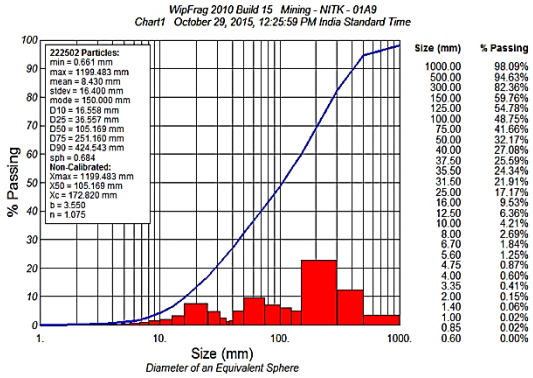

BLAST-9

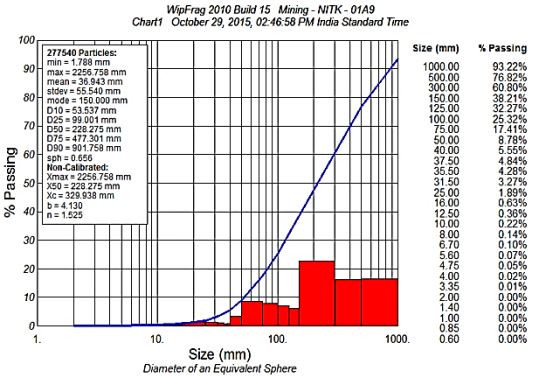

BLAST-10

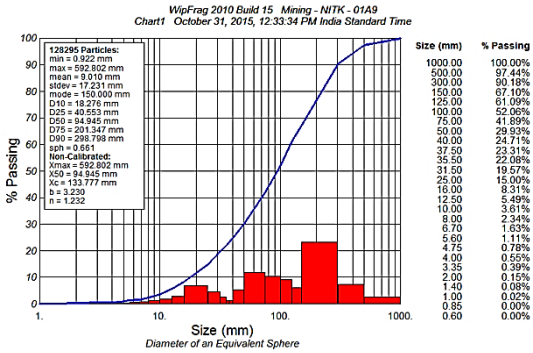

BLAST-11

PERIYANAGALUR LIMETSONE MINE (SOFTER FORMATION)
M/S THE RAMCO CEMENTS LIMITED
ARIYALUR DISTRICT, TAMILNADU

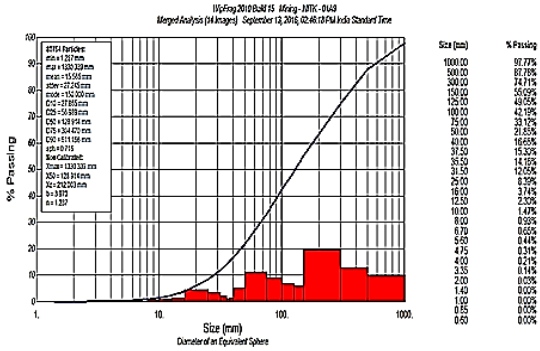

BLAST-1

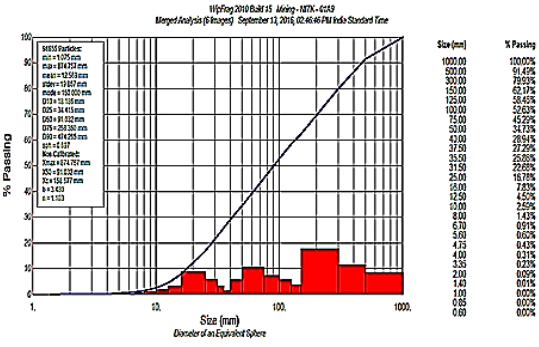

BLAST-2

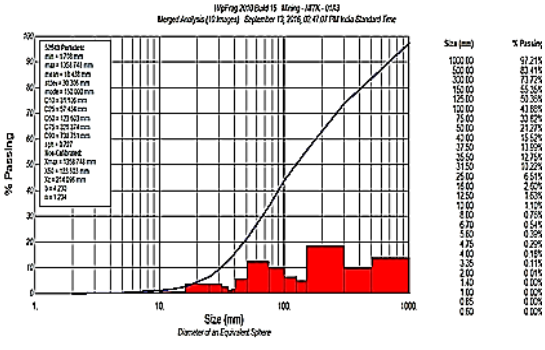

BLAST-3

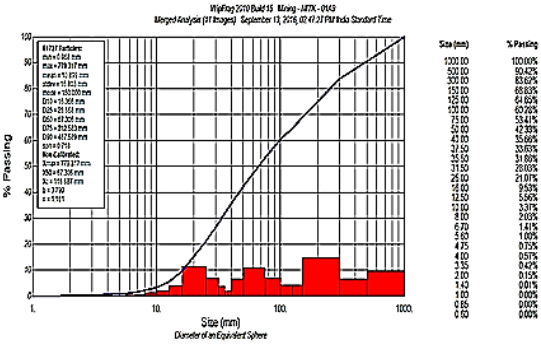

BLAST-4

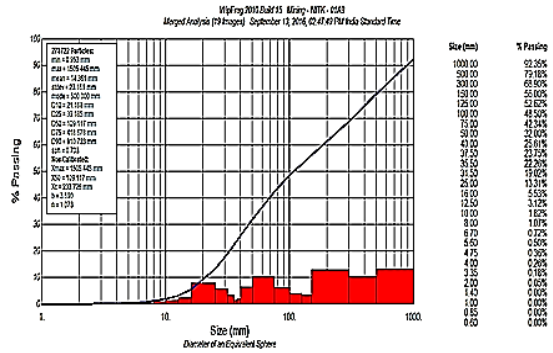

BLAST-5

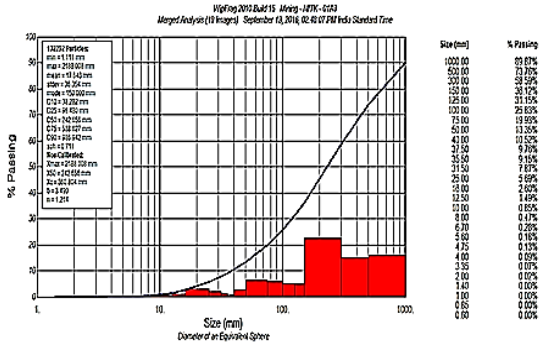

BLAST-6

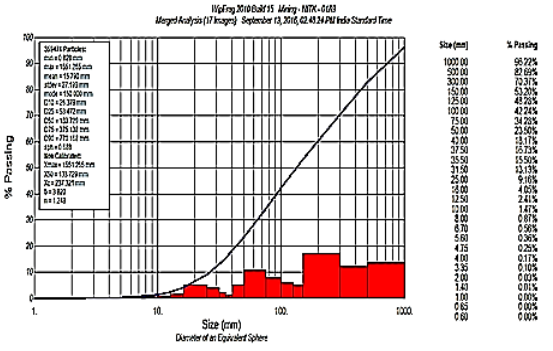

BLAST-7

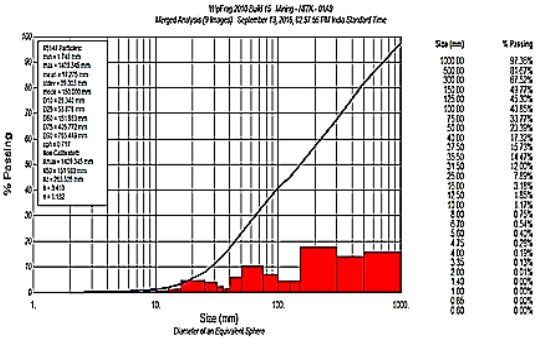

BLAST-8

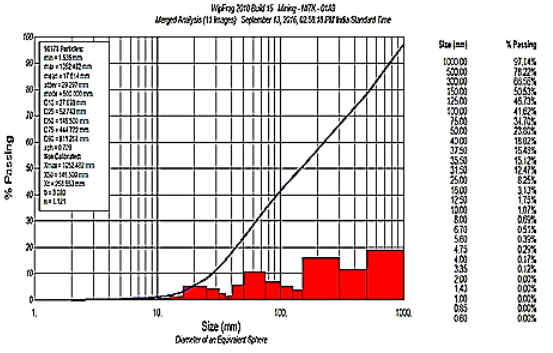

BLAST-9

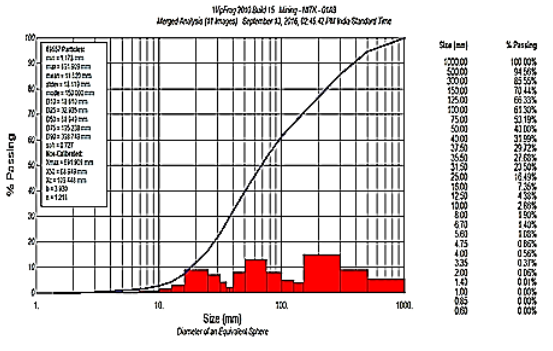

BLAST-10

APPENDIX – IV (SUMMARY TABLES)

Table – A4.1 Summary of ground vibration monitoring in limestone (Harder formation)

Sl. No.	Maximum Charge per Delay	Distance	Scaled Distance	Peak Particle Velocity	Seismic Energy	Fragmentation
	MCD (kg)	D (m)	SD (m/√kg)	PPV (mm/s)	SE (µJ)	Status
1	49.24	300	43.75	0.76	26,792	*Finer*
2	46.15	290	43.69	1.02	31,994	*Finer*
3	94.26	380	39.14	1.65	36,152	*Finer*
4	43.92	302	46.10	1.65	55,412	*Finer*
5	46.15	204	30.03	1.52	59,698	*Finer*
6	34.04	450	78.29	3.54	61,670	*Finer*
7	30.79	306	55.15	1.40	65,098	*Finer*
8	54.77	270	36.82	0.64	70,570	*Finer*
9	46.15	218	33.09	1.40	79,350	*Finer*
10	94.26	485	49.95	1.27	81,447	*Finer*
11	47.32	400	58.15	1.91	87,351	*Finer*
12	30.79	294	53.98	1.78	92,672	*Finer*
13	91.18	454	47.55	1.65	92,902	*Finer*
14	45.65	282	41.74	3.16	1,00,293	*Finer*
15	30.79	316	56.95	1.27	1,12,923	*Finer*
16	34.65	198	34.13	1.78	1,13,669	*Finer*
17	43.92	289	44.11	3.03	1,14,899	*Finer*
18	34.65	209	36.03	1.40	1,35,798	*Finer*
19	34.04	315	54.80	4.44	1,44,073	*Finer*
20	47.32	372	54.08	3.92	1,53,858	*Finer*
21	39.06	300	48.00	3.41	1,56,568	*Finer*
22	36.67	132	21.80	4.17	1,92,021	*Finer*
23	45.65	255	37.74	4.43	1,93,712	*Finer*
24	34.49	235	40.01	3.79	2,23,635	*Finer*
25	47.32	386	56.11	3.92	2,24,877	*Finer*
26	14.35	80	21.12	8.13	2,40,986	*Finer*
27	41.67	275	43.60	3.79	2,67,454	*Finer*
28	45.65	269	39.81	3.54	2,68,663	*Finer*
29	81.72	377	41.70	4.43	2,81,798	*Finer*
30	36.57	250	41.34	4.43	3,06,033	*Finer*
31	81.72	352	38.94	4.06	3,12,472	*Finer*
32	61.76	142	18.07	6.22	3,33,637	*Finer*

Sl. No.	Maximum Charge per Delay	Distance	Scaled Distance	Peak Particle Velocity	Seismic Energy	Fragmentation
	MCD (kg)	D (m)	SD (m/√kg)	PPV (mm/s)	SE (μJ)	Status
33	36.67	120	19.82	4.95	3,34,437	*Finer*
34	39.06	134	21.44	11.70	3,59,719	*Finer*
35	47.32	358	53.04	4.83	3,89,359	*Finer*
36	81.72	335	37.06	5.46	4,07,380	*Finer*
37	43.92	249	38.01	4.32	4,42,636	*Finer*
38	14.35	85	23.44	6.73	4,46,799	*Finer*
39	94.26	380	39.14	4.44	4,62,495	*Finer*
40	14.35	75	19.80	8.76	4,73,566	*Finer*
41	30.17	130	24.67	9.40	5,07,013	*Finer*
42	61.76	154	19.60	5.84	5,34,415	*Finer*
43	34.04	275	47.84	5.08	5,57,814	*Finer*
44	14.35	100	26.40	14.40	6,27,148	*Finer*
45	36.57	70	11.58	16.10	7,12,081	*Finer*
46	48.32	150	21.58	5.97	7,61,090	*Finer*
47	48.53	275	39.48	5.46	7,90,078	*Finer*
48	36.67	108	17.83	6.10	9,15,484	*Finer*
49	36.57	75	13.40	10.40	9,64,048	*Finer*
50	30.36	70	13.70	11.00	12,41,977	*Finer*
51	41.67	85	14.17	9.52	12,42,062	*Coarser*
52	49.24	104	14.82	11.60	13,25,460	*Coarser*
53	91.18	155	16.23	14.60	13,32,951	*Coarser*
54	51.25	150	20.95	14.40	13,96,885	*Coarser*
55	34.65	163	28.10	6.60	15,24,805	*Coarser*
56	50.42	120	16.90	10.50	15,39,811	*Coarser*
57	48.32	100	14.39	8.76	18,32,992	*Coarser*
58	61.76	132	16.80	9.02	18,68,921	*Coarser*
59	39.28	85	14.56	7.75	19,01,915	*Finer*
60	39.28	75	11.97	10.30	20,40,307	*Finer*
61	30.17	100	18.21	30.60	20,77,140	*Coarser*
62	48.53	170	24.40	9.91	21,37,921	*Coarser*
63	51.25	200	27.94	14.20	22,55,137	*Coarser*
64	48.53	184	26.41	9.65	26,36,438	*Coarser*
65	70.14	70	8.36	33.50	28,95,806	*Coarser*
66	91.18	135	14.14	20.80	30,47,499	*Coarser*
67	14.35	40	10.56	34.80	31,85,760	*Coarser*
68	36.57	55	9.09	28.20	32,32,849	*Coarser*

Sl. No.	Maximum Charge per Delay	Distance	Scaled Distance	Peak Particle Velocity	Seismic Energy	Fragmentation
	MCD (kg)	D (m)	SD (m/√kg)	PPV (mm/s)	SE (μJ)	Status
69	24.58	90	18.15	19.80	33,31,585	*Coarser*
70	51.40	100	14.95	13.30	33,66,361	*Coarser*
71	54.77	75	10.23	20.70	37,55,633	*Coarser*
72	37.50	60	9.80	27.30	39,03,284	*Coarser*
73	50.42	65	9.15	10.80	40,10,754	*Coarser*
74	24.58	95	19.16	18.40	40,60,162	*Coarser*
75	36.57	50	8.27	30.10	44,53,486	*Coarser*
76	28.33	70	14.15	15.50	45,02,870	*Coarser*
77	39.28	50	7.98	18.10	47,69,909	*Coarser*
78	50.42	70	9.86	11.00	49,71,507	*Coarser*
79	54.77	85	11.59	11.80	51,39,689	*Coarser*
80	48.32	65	9.35	10.50	51,62,528	*Coarser*
81	30.36	60	10.89	14.60	53,50,973	*Coarser*
82	37.50	55	8.98	29.30	541,9,536	*Coarser*
83	51.40	90	13.55	38.10	57,58,561	*Coarser*
84	39.28	40	6.38	17.10	59,72,767	*Coarser*
85	39.06	50	8.00	28.20	62,64,554	*Coarser*
86	38.33	60	9.69	11.80	63,77,533	*Coarser*
87	24.58	100	20.17	15.00	64,92,304	*Coarser*
88	36.57	40	6.61	40.00	65,48,821	*Coarser*
89	38.33	50	8.08	26.30	67,29,443	*Coarser*
90	39.06	40	6.40	33.20	68,93,020	*Coarser*
91	37.50	65	10.61	23.70	75,23,677	*Coarser*
92	30.36	50	9.07	24.10	85,52,912	*Coarser*
93	28.33	55	10.33	24.10	85,73,518	*Coarser*
94	24.58	50	10.09	24.70	92,64,400	*Coarser*
95	70.14	65	7.76	39.40	98,24,630	*Coarser*
96	37.50	50	8.16	35.60	1,11,03,330	*Coarser*
97	30.17	50	9.10	23.40	1,11,47,879	*Coarser*
98	30.36	40	7.26	34.40	1,24,51,737	*Coarser*
99	28.33	45	8.45	35.40	1,26,75,683	*Coarser*
100	70.14	65	7.76	41.90	1,36,66,773	*Coarser*
101	38.33	55	8.88	23.50	1,40,13,633	*Coarser*
102	28.33	40	7.52	37.60	1,45,65,085	*Coarser*
103	38.33	45	7.27	37.50	1,71,08,152	*Coarser*
104	37.50	65	10.61	26.40	1,84,19,851	*Coarser*

Sl. No.	Maximum Charge per Delay	Distance	Scaled Distance	Peak Particle Velocity	Seismic Energy	Fragmentation
	MCD (kg)	D (m)	SD (m/√kg)	PPV (mm/s)	SE (μJ)	Status
105	38.33	40	6.46	39.20	1,85,24,598	*Coarser*
106	51.40	50	6.97	56.00	2,15,03,717	*Coarser*
107	24.58	30	6.05	44.70	2,34,18,621	*Coarser*
108	51.40	50	6.97	30.90	2,46,91,269	*Coarser*
109	70.14	50	5.97	61.00	2,58,37,627	*Coarser*
110	37.50	40	6.53	55.60	2,66,56,654	*Coarser*
111	39.28	55	8.78	68.80	2,70,09,086	*Coarser*
112	39.28	50	7.98	38.60	2,89,70,681	*Coarser*
113	24.58	38	7.66	43.00	3,81,33,182	*Coarser*
114	38.33	30	4.85	64.40	4,22,56,215	*Coarser*
115	51.40	30	4.18	91.40	5,83,38,415	*Coarser*
116	51.40	30	4.18	126.00	11,12,59,278	*Coarser*

** Finer Fragmentation means ≤+300mm size,*
Coarser Fragmentation means ≥+300mm size

Table – A4.2 Summary of ground vibration monitoring in limestone (Softer formation)

Sl. No.	Maximum Charge per Delay	Distance	Scaled Distance	Peak Particle Velocity	Seismic Energy	Fragmentation
	MCD (kg)	D (m)	SD (m/√kg)	PPV (mm/s)	SE (μJ)	Status
1	36.14	360	59.88	0.889	6,715	*Finer*
2	25.02	330	65.97	0.51	9,063	*Finer*
3	19.46	285	64.61	1.27	9,983	*Finer*
4	66.72	350	42.85	0.762	16,127	*Finer*
5	25.02	260	51.98	0.762	20,155	*Finer*
6	66.72	335	41.01	0.762	21,708	*Finer*
7	25.02	306	61.18	0.762	22,529	*Finer*
8	66.72	325	39.79	1.52	23,113	*Finer*
9	25.02	254	50.78	0.889	32,984	*Finer*
10	25.02	216	43.18	1.27	34,059	*Finer*
11	36.14	350	58.22	1.14	37,645	*Finer*
12	25.02	235	46.98	1.14	45,142	*Finer*
13	19.46	310	70.27	1.52	50,941	*Finer*
14	25.02	230	45.98	1.52	52,724	*Finer*
15	19.46	304	68.91	1.65	71,853	*Finer*

Sl. No.	Maximum Charge per Delay	Distance	Scaled Distance	Peak Particle Velocity	Seismic Energy	Fragmentation
	MCD (kg)	D (m)	SD (m/√kg)	PPV (mm/s)	SE (μJ)	Status
16	25.02	193	38.58	2.54	81,229	*Finer*
17	30.58	188	34.00	1.65	81,506	*Finer*
18	19.46	253	57.35	2.16	83,893	*Finer*
19	19.46	275	62.34	1.78	86,357	*Finer*
20	44.48	120	17.99	9.4	95,328	*Finer*
21	30.58	144	26.04	7.24	1,01,851	*Coarser*
22	19.46	250	56.67	1.78	1,10,243	*Coarser*
23	25.02	175	34.99	2.16	1,16,544	*Coarser*
24	30.58	177	32.01	2.29	1,29,474	*Coarser*
25	19.46	250	56.67	1.52	1,40,554	*Coarser*
26	30.58	166	30.02	2.67	1,58,669	*Coarser*
27	25.02	160	31.99	3.43	1,58,876	*Coarser*
28	30.58	133	24.05	7.49	1,89,693	*Coarser*
29	30.58	155	28.03	4.44	1,90,186	*Coarser*
30	44.48	107	16.04	10	2,15,448	*Coarser*
31	66.72	300	36.73	2.29	2,31,644	*Coarser*
32	44.48	94	14.09	16.8	2,42,413	*Coarser*
33	30.58	122	22.06	8	2,53,022	*Coarser*
34	30.58	56	10.13	25.9	2,95,524	*Coarser*
35	25.02	150	29.99	3.68	3,91,806	*Coarser*
36	25.02	140	27.99	3.81	4,51,380	*Coarser*
37	44.48	80	12.00	24.3	5,46,976	*Coarser*

** Finer Fragmentation means ≤+300mm size,*
Coarser Fragmentation means ≥+300mm size

Table – A4.3 Summary of longitudinal wave and transverse wave velocities in limestone (Harder formation)

Sl. No.	Scaled Distance	Peak Particle Velocity	L-wave Velocity	T-wave Velocity
	SD (m/√kg)	PPV (mm/s)	(m/s)	(m/s)
1	4.00	44.70	120.00	93.02
2	4.85	64.40	161.29	120.48
3	7.66	43.00	361.90	143.32
4	6.61	40.00	216.22	161.94
5	6.40	33.20	198.02	165.98
6	8.16	35.60	175.44	174.61
7	10.09	24.70	208.33	189.39

Sl. No.	Scaled Distance	Peak Particle Velocity	L-wave Velocity	T-wave Velocity
	SD (m/√kg)	PPV (mm/s)	(m/s)	(m/s)
8	8.98	29.30	190.31	189.66
9	6.53	55.60	396.04	203.02
10	8.27	30.10	363.32	203.43
11	7.98	118.00	289.02	204.92
12	9.80	27.30	209.06	209.06
13	6.40	171.00	470.59	213.77
14	8.88	23.50	235.04	215.69
15	9.09	28.20	398.55	223.67
16	10.61	26.40	317.07	234.66
17	10.61	23.70	239.85	237.23
18	8.37	126.00	260.87	238.10
19	7.98	181.00	304.88	238.10
20	6.46	39.20	307.69	243.42
21	8.00	28.20	247.52	243.72
22	13.76	38.60	294.04	258.90
23	9.69	11.80	458.02	263.01
24	11.97	10.30	315.13	263.24
25	7.27	37.50	381.36	274.39
26	9.07	91.40	324.38	280.17
27	20.95	14.40	488.60	295.86
28	8.08	26.30	310.56	310.56
29	8.78	68.80	381.94	310.73
30	14.56	7.75	357.14	319.55
31	8.45	35.40	363.90	334.33
32	7.52	37.60	500.00	341.88
33	18.15	19.80	353.94	343.21
34	10.56	34.80	370.37	366.97
35	13.80	3.41	416.67	370.37
36	14.82	11.60	509.80	374.10
37	7.26	34.40	380.95	377.36
38	10.89	14.60	416.67	377.36
39	18.20	30.60	460.83	384.62
40	5.97	61.00	434.78	390.63
41	13.70	11.00	844.37	391.06
42	14.95	13.30	614.50	420.17
43	14.25	30.90	483.23	429.86
44	9.07	24.10	490.20	431.03
45	13.01	0.64	866.14	440.44

Sl. No.	Scaled Distance	Peak Particle Velocity	L-wave Velocity	T-wave Velocity
	SD (m/√kg)	PPV (mm/s)	(m/s)	(m/s)
46	7.76	41.90	560.34	445.21
47	14.20	14.40	454.55	446.43
48	23.75	23.40	560.54	449.64
49	11.58	16.10	700.00	451.61
50	14.23	4.43	707.96	451.98
51	8.36	33.50	804.60	464.58
52	34.82	11.80	523.11	475.10
53	31.77	20.70	564.16	479.42
54	13.55	38.10	548.78	517.24
55	27.93	14.20	579.71	519.48
56	24.66	9.40	619.05	520.00
57	13.40	10.40	735.29	524.48
58	54.07	3.92	1,907.69	534.48
59	7.76	39.40	560.34	555.56
60	37.74	4.43	907.47	591.65
61	53.04	4.83	2045.71	598.66
62	25.00	5.84	1000.00	601.56
63	45.08	8.76	635.08	633.53
64	21.44	11.70	930.56	647.34
65	14.15	15.50	707.07	648.15
66	47.08	5.97	1,731.58	670.06
67	10.33	24.10	1,018.52	670.73
68	56.11	3.92	744.74	678.38
69	19.82	4.95	821.92	685.71
70	17.83	6.10	715.23	705.88
71	18.07	6.22	1,059.70	724.49
72	20.17	15.00	990.10	724.64
73	21.80	4.17	929.58	734.33
74	28.10	6.60	964.50	734.23
75	26.41	9.65	915.42	751.02
76	21.12	8.13	793.08	793.08
77	19.80	8.76	1,136.36	806.45
78	44.07	10.50	1,090.58	814.51
79	16.80	9.02	1,269.23	814.81
80	23.44	6.73	876.29	817.31
81	55.15	1.40	916.17	874.29
82	24.40	9.91	904.26	880.83
83	40.01	3.79	1,114.74	917.97

Sl. No.	Scaled Distance	Peak Particle Velocity	L-wave Velocity	T-wave Velocity
	SD (m/√kg)	PPV (mm/s)	(m/s)	(m/s)
84	45.00	20.8	1,484.52	924.66
85	53.98	1.78	1,123.14	936.31
86	56.95	1.27	1,206.11	940.48
87	34.13	1.78	2,675.68	943.86
88	39.81	3.54	1,159.48	957.30
89	30.03	1.52	1,103.70	963.26
90	14.17	9.52	1,000.00	977.01
91	19.16	18.4	1,055.56	1,021.51
92	41.73	3.16	1,454.61	1,040.59
93	39.48	5.46	1,216.81	1,095.62
94	39.13	4.44	1,263.46	1,250.00
95	35.00	14.60	1,631.58	1,280.99
96	47.84	5.08	2,217.74	1,334.95
97	33.09	1.40	2,477.27	1,345.68
98	37.06	5.46	1,603.87	1,437.77
99	38.94	4.06	2,861.79	1,485.23
100	39.13	1.65	1,624.93	1,533.26
101	38.01	4.32	2,829.55	1,585.99
102	36.03	1.4	2,518.07	1,645.67
103	41.70	4.43	1,924.47	1,721.46
104	44.11	3.03	3,613.50	1,840.76
105	43.60	3.79	1,950.35	1,845.64
106	46.10	1.65	4,314.29	2,026.85
107	43.69	1.02	3,085.11	2,086.33
108	54.80	3.54	3,841.46	2,114.09
109	49.95	1.27	3,368.06	2,526.04
110	46.05	10.80	3,478.72	2,637.10
111	48.02	10.50	3,666.67	2,818.18
112	54.08	4.44	3,315.79	3,214.29
113	94.61	1.91	2,146.67	3,220.00
114	44.08	11.00	3,556.82	3,260.42
115	47.55	1.65	2,067.18	3,753.07
116	60.00	0.76	5,275.00	4,688.89

** L-wave and T-wave indicates Longitudinal and Transverse waves, respectively*

Table – A4.4 Summary of longitudinal wave and transverse wave velocities in limestone (Softer formation)

Sl. No.	Scaled Distance	Peak Particle Velocity	L-wave Velocity	T-wave Velocity
	SD (m/√kg)	PPV (mm/s)	(m/s)	(m/s)
1	59.88	0.889	2,553.19	1,434.26
2	65.97	0.51	3,30,000.00	25,384.62
3	64.61	1.27	1,096.15	855.86
4	42.85	0.762	3,50,000.00	3,723.40
5	51.98	0.762	1,843.97	893.47
6	41.01	0.762	3,284.31	2,218.54
7	61.18	0.762	4,636.36	2,615.38
8	39.79	1.52	2,443.61	2,110.39
9	50.78	0.889	1,739.73	1,938.93
10	43.18	1.27	2,16,000.00	1,459.46
11	58.22	1.14	13,461.54	2,777.78
12	46.98	1.14	1,053.81	1,004.27
13	70.27	1.52	1,169.81	1,095.41
14	45.98	1.52	1,040.72	982.91
15	68.91	1.65	1,151.52	1,055.56
16	38.58	2.54	1,678.26	1,269.74
17	34.00	1.65	1,790.48	1,579.83
18	57.35	2.16	1,345.74	1,134.53
19	62.34	1.78	3,021.98	1,141.08
20	17.99	9.4	5,714.29	3,333.33
21	26.04	7.24	1,358.49	1,333.33
22	56.67	1.78	5,555.56	2,272.73
23	34.99	2.16	925.93	469.17
24	32.01	2.29	4,022.73	1,923.91
25	56.67	1.52	1,773.05	1,207.73
26	30.02	2.67	1,824.18	1,611.65
27	31.99	3.43	634.92	531.56
28	24.05	7.49	1,254.72	796.41
29	28.03	4.44	5,535.71	1,534.65
30	16.04	10	4,863.64	2,675.00
31	36.73	2.29	2,054.79	721.15
32	14.09	16.8	2,350.00	1,402.99
33	22.06	8	1,129.63	532.75
34	10.13	25.9	444.44	245.61
35	29.99	3.68	496.69	387.60
36	27.99	3.81	891.72	760.87

Sl. No.	Scaled Distance	Peak Particle Velocity	L-wave Velocity	T-wave Velocity
	SD (m/√kg)	PPV (mm/s)	(m/s)	(m/s)
37	12.00	24.3	3,200.00	2,352.94

** L-wave and T-wave indicates Longitudinal and Transverse waves, respectively*

Table – A4.5 Summary of ground vibration monitoring in coal formation

Sl. No.	Maximum Charge per Delay	Distance	Scaled Distance	Peak Particle Velocity	Seismic Energy	Fragmentation
	MCD (kg)	D (m)	SD (m/$\sqrt[3]{kg}$)	PPV (mm/s)	SE (µJ)	Status
1	3.59	58.28	43.44	1.02	4,250	*Finer*
2	3.59	106.57	77.60	<0.51	5,203	*Finer*
3	4.81	118.20	70.02	<0.51	5,608	*Finer*
4	3.59	116.74	85.01	<0.51	6,498	*Finer*
5	3.96	89.27	63.17	0.51	6,902	*Finer*
6	3.59	99.91	73.75	<0.51	7,049	*Finer*
7	3.96	98.28	68.45	1.52	7,705	*Finer*
8	3.78	75.91	54.02	1.02	8,050	*Finer*
9	3.22	77.60	59.49	1.02	8,160	*Finer*
10	3.59	120.38	87.66	<0.51	9,164	*Finer*
11	3.96	125.17	87.18	0.76	9,777	*Finer*
12	3.59	104.22	75.16	0.76	10,711	*Finer*
13	4.33	61.85	41.42	7.49	12,605	*Finer*
14	4.07	89.00	55.74	1.02	12,704	*Finer*
15	4.81	123.13	73.35	<0.51	14,318	*Finer*
16	5.18	114.88	66.40	0.89	14,318	*Finer*
17	4.07	105.00	65.76	1.02	14,573	*Finer*
18	3.78	76.85	54.69	0.89	16,552	*Finer*
19	4.70	105.00	67.89	0.76	16,999	*Finer*
20	5.18	101.57	58.70	0.51	17,085	*Finer*
21	3.96	88.71	61.78	0.51	17,210	*Finer*
22	3.59	93.67	67.48	0.76	17,297	*Finer*
23	4.81	113.83	66.84	0.89	17,562	*Finer*
24	4.07	94.00	58.25	0.76	18,265	*Finer*
25	5.18	104.61	59.88	1.78	18,382	*Finer*
26	4.70	111.00	71.77	1.02	18,923	*Finer*
27	3.22	74.00	55.96	1.65	19,520	*Finer*
28	3.96	66.67	46.43	1.52	19,621	*Finer*
29	4.70	108.00	69.83	1.27	19,670	*Finer*

Sl. No.	Maximum Charge per Delay	Distance	Scaled Distance	Peak Particle Velocity	Seismic Energy	Fragmentation
	MCD (kg)	D (m)	SD ($m/\sqrt[3]{kg}$)	PPV (mm/s)	SE (µJ)	Status
30	3.78	79.31	56.44	0.64	19,915	*Finer*
31	3.96	61.85	44.08	4.83	20,739	*Finer*
32	4.70	105.00	67.89	1.14	20,846	*Finer*
33	3.59	54.75	39.87	3.67	21,978	*Finer*
34	4.07	103.00	64.89	1.14	23,140	*Finer*
35	3.59	96.66	70.39	0.64	24,005	*Finer*
36	3.59	100.00	73.82	1.78	24,135	*Finer*
37	3.96	100.00	69.65	1.27	24,272	*Finer*
38	4.07	99.00	63.01	1.52	26,150	*Finer*
39	3.22	94.07	71.34	1.02	26,750	*Finer*
40	5.18	110.78	64.03	1.27	27,265	*Finer*
41	4.33	64.64	43.62	5.08	27,482	*Finer*
42	4.07	86.00	54.86	1.40	28,190	*Finer*
43	5.18	105.18	60.79	1.27	28,258	*Finer*
44	3.59	67.80	49.37	4.19	28,468	*Finer*
45	3.96	101.08	70.40	0.64	28,828	*Finer*
46	3.59	88.71	64.60	0.64	28,829	*Finer*
47	3.96	110.26	76.79	0.64	33,174	*Finer*
48	3.59	114.12	83.37	0.76	37,937	*Finer*
49	4.07	96.00	60.13	1.52	40,237	*Finer*
50	3.96	100.00	69.65	1.91	42,657	*Finer*
51	3.96	74.62	51.27	3.15	46,189	*Finer*
52	4.07	84.00	51.99	1.52	46,318	*Finer*
53	3.96	61.81	44.05	4.55	51,304	*Finer*
54	3.96	100.00	69.65	3.54	51,496	*Finer*
55	4.33	68.74	46.03	5.08	62,190	*Finer*
56	3.96	65.20	45.41	4.43	81,452	*Finer*
57	3.96	43.58	29.66	5.08	94,630	*Finer*
58	4.89	35.00	23.26	5.84	95,738	*Finer*
59	4.33	63.09	41.58	5.08	95,980	*Finer*
60	3.96	48.49	34.77	4.05	97,770	*Finer*
61	3.96	61.81	44.05	5.59	98,277	*Finer*
62	3.96	35.88	24.99	7.75	1,09,777	*Coarser*
63	4.33	60.00	40.18	6.10	1,14,259	*Coarser*
64	3.96	70.00	48.75	4.43	1,26,305	*Coarser*
65	4.89	29.00	18.45	6.35	1,29,716	*Coarser*

Sl. No.	Maximum Charge per Delay	Distance	Scaled Distance	Peak Particle Velocity	Seismic Energy	Fragmentation
	MCD (kg)	D (m)	SD (m/$\sqrt[3]{}$kg)	PPV (mm/s)	SE (µJ)	Status
66	4.33	40.00	26.79	7.37	1,37,600	*Coarser*
67	3.96	60.00	41.79	6.73	1,38,105	*Coarser*
68	3.96	60.00	41.79	5.59	1,39,698	*Coarser*
69	3.59	60.00	44.69	4.70	1,41,563	*Coarser*
70	3.96	26.80	18.67	4.81	1,44,572	*Coarser*
71	3.96	55.00	38.31	5.72	1,49,313	*Coarser*
72	3.96	49.87	34.73	4.43	1,59,487	*Coarser*
73	3.22	65.70	50.36	4.56	1,98,666	*Coarser*
74	3.96	35.00	24.38	5.59	2,14,430	*Coarser*
75	3.96	40.00	27.86	4.45	2,45,240	*Coarser*
76	4.33	45.07	30.18	7.24	2,54,724	*Coarser*
77	4.89	33.00	20.36	6.10	2,90,980	*Coarser*
78	3.96	35.00	24.38	9.65	5,45,936	*Coarser*
79	3.59	40.00	29.13	8.38	5,85,798	*Coarser*
80	4.33	40.00	26.79	11.68	6,25,110	*Coarser*
81	3.96	30.22	21.05	13.80	7,15,224	*Coarser*
82	3.96	29.18	20.32	10.50	9,10,665	*Coarser*
83	4.33	20.00	14.39	17.40	13,98,101	*Coarser*
84	4.89	20.00	13.72	28.32	16,54,101	*Coarser*
85	4.33	15.11	10.12	23.22	17,87,182	*Coarser*
86	3.96	15.79	11.00	15.40	19,04,089	*Coarser*

** Finer Fragmentation means ≤+150mm size,*
Coarser Fragmentation means ≥+150mm size

Table – A4.6 Summary of longitudinal wave and transverse wave velocities in coal formation

Sl. No.	Scaled Distance	Peak Particle Velocity	L-wave Velocity	T-wave Velocity
	SD (m/$\sqrt[3]{}$kg)	PPV (mm/s)	(m/s)	(m/s)
1	18.67	4.81	26,800.00	8,934.33
2	21.73	4.43	1,200.00	1,155.56
3	26.79	7.37	20,000.00	20,000.00
4	26.79	11.68	13,334.33	10,000.00
5	40.18	6.10	4,285.71	2,857.14
6	24.38	5.59	2,693.31	2,500.00
7	24.38	9.65	11,666.67	1,843.11
8	38.31	5.72	9,166.67	5,000.00

Sl. No.	Scaled Distance	Peak Particle Velocity	L-wave Velocity	T-wave Velocity
	SD (m/$\sqrt[3]{kg}$)	PPV (mm/s)	(m/s)	(m/s)
9	48.75	4.45	1,029.41	945.95
10	48.75	4.43	2,800.00	1,094.75
11	20.75	15.4	4,255.71	4,255.71
12	24.99	7.75	2,760.00	1,708.57
13	34.73	4.43	2,266.82	2,168.26
14	21.05	13.8	3,777.50	2,324.62
15	29.66	5.08	2,241.05	1,704.20
16	46.79	1.27	3,733.22	1,101.31
17	20.32	10.50	2,918.00	2,653.73
18	34.77	4.05	865.89	655.27
19	53.35	0.76	2,277.88	1,566.04
20	24.51	23.22	3,511.00	215.40
21	30.19	17.4	5,635.00	2,049.09
22	36.88	7.24	6,118.89	316.49
23	29.13	8.38	6,666.67	430.11
24	36.41	1.78	7,143.86	4,545.45
25	44.69	4.70	383.17	383.17
26	41.79	5.59	2,857.14	2,857.14
27	55.72	6.73	266.67	266.67
28	69.65	3.54	8,334.33	2,857.14
29	18.45	6.35	3,625.00	3,223.22
30	20.36	6.10	3,555.56	1,883.35
31	23.26	5.84	11,666.67	7,000.00
32	23.27	28.32	5,003.04	3,890.48
33	51.99	1.52	6,916.67	5,187.50
34	54.86	1.40	3,185.19	1,564.64
35	55.74	1.02	7,416.67	2,283.05
36	60.13	1.52	6,400.00	2,461.54
37	63.01	1.52	12,375.00	2,750.00
38	64.89	1.14	9,273.73	5,666.67
39	65.76	1.02	2,234.04	2,100.00
40	67.89	1.14	8,076.92	3,500.00
41	67.89	0.76	3,724.14	3,176.47
42	39.87	3.67	1,659.09	1,074.53
43	43.44	1.02	58,280.00	1.19
44	49.37	4.19	11,300.00	2,825.00
45	41.42	7.49	4,417.86	4,124.33

Sl. No.	Scaled Distance	Peak Particle Velocity	L-wave Velocity	T-wave Velocity
	SD (m/$\sqrt[3]{kg}$)	PPV (mm/s)	(m/s)	(m/s)
46	43.62	5.08	2,194.48	1,224.85
47	46.03	5.08	2,545.93	1,636.67
48	44.05	4.55	6,867.78	4,120.67
49	46.43	1.52	2,223.33	2,150.65
50	51.27	3.15	12,270.00	2,300.63
51	41.58	5.08	5,174.17	3,880.63
52	44.08	4.83	5,623.73	1,030.83
53	68.45	1.52	49,140.00	49,140.00
54	76.79	0.64	79.44	79.44
55	64.60	0.64	88,710.00	17,743.00
56	70.40	0.64	10,10,800.00	1,01,080.00
57	83.37	0.76	56,560.00	12,568.89
58	67.48	0.76	9,26,700.00	2,808.18
59	75.16	0.76	25,805.00	3,686.43
60	50.36	4.56	3,650.00	2,986.36
61	55.96	1.65	4,866.67	4,055.56
62	59.49	1.02	4,311.11	2,586.67
63	71.34	1.02	46,535.00	3,003.26
64	54.69	0.89	7,685.00	1,921.25
65	56.44	0.64	7,93,100.00	11,330.00
66	58.08	<0.51	377.87	320.08
67	59.88	1.78	17,267.63	3,573.61
68	66.84	0.89	1,12,834.08	56,417.04
69	18.67	4.81	26,800.00	8,934.33
70	21.73	4.43	1,200.00	1,155.56
71	26.79	7.37	20,000.00	20,000.00
72	26.79	11.68	13,334.33	10,000.00
73	40.18	6.10	4,285.71	2,857.14
74	24.38	5.59	2,693.31	2,500.00
75	24.38	9.65	11,666.67	1,843.11
76	38.31	5.72	9,166.67	5,000.00
77	48.75	4.45	1,029.41	945.95
78	48.75	4.43	2,800.00	1,094.75
79	20.75	15.40	4,255.71	4,255.71
80	24.99	7.75	2,760.00	1,708.57
81	34.73	4.43	2,266.82	2,168.26
82	21.05	13.80	3,777.50	2,324.62

Sl. No.	Scaled Distance	Peak Particle Velocity	L-wave Velocity	T-wave Velocity
	SD (m/$\sqrt[3]{}$kg)	PPV (mm/s)	(m/s)	(m/s)
83	29.66	5.08	2,241.05	1,704.20
84	46.79	1.27	3,733.22	1,101.31
85	20.32	10.50	2,918.00	2,653.73
86	34.77	4.05	865.89	655.27

** L-wave and T-wave indicates Longitudinal and Transverse waves, respectively*

Table – A4.7 Summary of ground vibration monitoring in sandstone formation

Sl. No.	Maximum Charge per Delay	Distance	Scaled Distance	Peak Particle Velocity	Seismic Energy	Fragmentation
	MCD (kg)	D (m)	SD (m/√kg)	PPV (mm/s)	SE (µJ)	*Status*
1	20.85	355	77.75	0.64	10,311.23	*Finer*
2	23.24	397	84.18	0.64	21,005.32	*Finer*
3	34.75	295	50.04	1.27	37,393.55	*Finer*
4	460.00	721	34.62	1.27	45,698.08	*Finer*
5	11.12	260	77.97	0.76	46,266.25	*Finer*
6	20.85	240	53.56	0.76	48,574.58	*Finer*
7	1,953.00	2,033	46.00	0.89	49,481.50	*Finer*
8	27.61	284	54.05	1.14	61,901.33	*Finer*
9	90.00	379	39.95	1.14	61,901.33	*Finer*
10	23.24	275	58.31	0.76	63,601.77	*Finer*
11	1,953.00	1,856	43.00	0.89	71,031.38	*Finer*
12	100.00	290	29.00	3.92	73,406.11	*Finer*
13	1,953.00	1,591	36.00	1.02	79,584.75	*Finer*
14	100.00	440	44.00	1.27	1,08,396.33	*Finer*
15	34.75	200	34.93	3.54	1,29,891.09	*Finer*
16	85.00	295	33.00	4.30	1,34,876.62	*Finer*
17	450.00	719	34.89	1.52	1,36,859.22	*Finer*
18	34.75	212	35.96	3.29	1,42,154.54	*Finer*
19	460.00	636	29.65	3.29	1,60,143.93	*Finer*
20	460.00	678	31.61	1.90	1,66,647.59	*Finer*
21	450.00	750	35.36	1.52	1,71,645.30	*Finer*
22	100.00	380	38.00	1.40	1,72,599.58	*Finer*
23	100.00	300	30.00	3.03	1,72,677.92	*Finer*
24	88.00	292	31.13	4.06	3,76,993.65	*Finer*
25	11.12	100	29.99	5.46	4,01,518.22	*Finer*
26	450.00	696	33.81	4.56	5,13,484.49	*Finer*

Sl. No.	Maximum Charge per Delay	Distance	Scaled Distance	Peak Particle Velocity	Seismic Energy	Fragmentation
	MCD (kg)	D (m)	SD (m/√kg)	PPV (mm/s)	SE (µJ)	*Status*
27	100.00	280	28.00	4.32	6,15,874.46	*Finer*
28	23.24	150	31.81	5.33	6,61,024.88	*Finer*
29	85.00	234	25.38	8.89	10,55,143.78	*Coarser*
30	50.00	184	26.02	5.33	15,62,458.55	*Coarser*
31	100.00	220	23.00	9.40	17,69,781.29	*Coarser*
32	460.00	450	20.98	7.11	19,80,473.55	*Coarser*
33	85.00	209	23.67	10.70	22,80,225.67	*Coarser*
34	88.00	200	21.32	17.90	36,65,445.40	*Coarser*
35	88.00	188	20.04	20.20	47,47,405.68	*Coarser*
36	66.00	160	19.69	17.40	52,45,447.10	*Coarser*
37	66.00	150	18.46	18.92	69,16,156.65	*Coarser*
38	66.00	170	20.93	17.30	84,61,653.43	*Coarser*
39	88.00	178	18.97	23.61	92,77,651.80	*Coarser*
40	85.00	150	16.27	19.81	1,05,44,797.69	*Coarser*
41	66.00	120	14.77	29.30	1,47,09,468.86	*Coarser*
42	66.00	110	14.54	34.80	1,51,16,635.32	*Coarser*
43	66.00	100	13.31	54.50	2,73,88,321.38	*Coarser*

** Finer Fragmentation means ≤+300mm size,*
Coarser Fragmentation means ≥+300mm size

Table – A4.8 Summary of longitudinal wave and transverse wave velocities in sandstone formation

Sl. No.	Scaled Distance	Peak Particle Velocity	L-wave Velocity	T-wave Velocity
	SD (m/√kg)	PPV (mm/s)	(m/s)	(m/s)
1	13.31	54.50	109.05	108.70
2	14.54	34.80	473.10	448.98
3	14.77	29.30	136.36	131.43
4	18.46	18.92	574.71	361.45
5	19.69	17.40	437.16	276.34
6	20.93	17.30	444.86	387.24
7	26.02	5.33	630.14	574.21
8	18.97	23.61	349.02	248.60
9	20.04	20.20	289.23	264.04
10	21.32	17.90	384.62	298.51
11	16.27	19.81	260.42	258.18
12	23.67	10.70	547.12	371.23

Sl. No.	Scaled Distance	Peak Particle Velocity	L-wave Velocity	T-wave Velocity
	SD (m/√kg)	PPV (mm/s)	(m/s)	(m/s)
13	25.38	8.89	607.79	600.00
14	33.81	4.56	1,949.58	1,167.79
15	34.89	1.52	4,180.23	1,507.34
16	35.36	1.52	3,233.76	1,125.00
17	28.12	7.11	795.51	723.16
18	29.65	3.29	1,023.51	959.28
19	31.61	1.90	1,230.49	1,027.27
20	23.00	9.40	191.80	164.92
21	120.00	1.40	38,000.00	4,223.22
22	36.00	1.02	4,910.49	1,194.78
23	43.00	0.89	4,473.29	1,114.09
24	*180.00*	0.89	39,350.00	19,874.24
25	39.95	1.14	3,445.45	1,334.51
26	28.00	4.32	1,000.00	554.46
27	29.00	3.92	1,198.35	435.44
28	190.00	3.03	75,000.00	20,000.00
29	44.00	1.27	1,693.00	2,528.74
30	29.988	5.46	757.58	493.61
31	77.969	0.76	3,714.29	1,911.76
32	31.807	5.33	731.71	724.64
33	58.313	0.76	4,584.00	1,141.08
34	84.183	0.51	8,970.00	6,404.23
35	53.56	0.76	1,057.27	1,034.48
36	77.746	0.51	7,550.00	2,204.97
37	34.928	3.54	419.29	345.42
38	35.963	3.29	1,473.22	380.61
39	50.043	1.27	990.00	906.90
40	54.049	1.14	2,581.82	1,000.00

** L-wave and T-wave indicates Longitudinal and Transverse waves, respectively*

Table – A4.9 Summary of ground vibration monitoring in granite formation

Sl. No.	Maximum Charge per Delay	Distance	Scaled Distance	Peak Particle Velocity	Seismic Energy	Fragmentation
	MCD (kg)	D (m)	SD (m/√kg)	PPV (mm/s)	SE (µJ)	*Status*
1	0.75	300	346.41	0.64	7,972	*Finer*
2	0.25	200	400.00	0.64	8,374	*Finer*
3	0.50	200	282.84	0.64	10,153	*Finer*

Sl. No.	Maximum Charge per Delay	Distance	Scaled Distance	Peak Particle Velocity	Seismic Energy	Fragmentation
	MCD (kg)	**D (m)**	**SD (m/√kg)**	**PPV (mm/s)**	**SE (μJ)**	***Status***
4	0.50	200	282.84	0.64	10,604	*Finer*
5	0.50	170	240.42	0.76	11,524	*Finer*
6	0.25	180	360.00	0.64	11,998	*Finer*
7	0.50	180	254.56	0.64	12,931	*Finer*
8	1.25	220	196.77	0.64	13,197	*Finer*
9	0.50	150	212.13	0.76	14,387	*Finer*
10	0.75	160	184.75	0.89	14,880	*Finer*
11	0.50	200	282.84	0.76	15,313	*Finer*
12	0.25	100	200.00	0.64	15,488	*Finer*
13	0.25	100	200.00	0.64	16,777	*Finer*
14	1.00	175	175.00	0.64	16,817	*Finer*
15	0.50	150	212.13	0.76	17,696	*Finer*
16	0.50	150	212.13	0.64	20,765	*Finer*
17	1.00	135	135.00	0.64	24,093	*Finer*
18	1.00	130	130.00	0.64	24,358	*Finer*
19	0.50	145	205.06	0.64	24,382	*Finer*
20	0.25	55	110.00	0.64	26,275	*Finer*
21	1.00	100	100.00	0.64	26,911	*Finer*
22	1.00	110	110.00	0.64	29,567	*Finer*
23	0.125	50	141.42	0.76	32,698	*Finer*
24	0.75	100	115.47	0.64	34,750	*Finer*
25	0.50	60	84.85	0.89	35,675	*Finer*
26	0.25	60	120.00	0.64	36,995	*Finer*
27	1.00	60	60.00	1.27	38,202	*Finer*
28	22.22	300	63.64	1.02	38,312	*Finer*
29	19.46	250	56.67	1.14	40,566	*Finer*
30	0.125	30	84.85	0.64	43,456	*Finer*
31	0.50	50	70.71	1.27	47,157	*Finer*
32	0.75	75	86.60	0.89	48,441	*Finer*
33	0.50	45	63.64	0.89	48,822	*Finer*
34	1.25	85	76.03	0.76	49,900	*Finer*
35	0.50	80	113.14	0.76	50,109	*Finer*
36	1.50	70	57.15	0.76	50,318	*Finer*
37	0.75	55	63.51	1.02	51,161	*Finer*
38	19.46	203	46.02	1.27	53,540	*Finer*
39	0.75	50	57.74	1.02	54,229	*Finer*

Sl. No.	Maximum Charge per Delay	Distance	Scaled Distance	Peak Particle Velocity	Seismic Energy	Fragmentation
	MCD (kg)	**D (m)**	**SD (m/√kg)**	**PPV (mm/s)**	**SE (µJ)**	***Status***
40	19.46	200	45.34	1.78	54,435	*Finer*
41	1.00	70	70.00	1.14	55,113	*Finer*
42	0.50	45	63.64	0.89	59,637	*Finer*
43	0.50	50	70.71	0.76	59,777	*Finer*
44	0.50	55	77.78	1.02	60,635	*Finer*
45	16.68	204	49.95	1.65	64,459	*Finer*
46	19.46	250	56.67	1.65	64,681	*Finer*
47	19.46	200	45.34	1.4	64,718	*Finer*
48	0.50	50	70.71	1.65	68,162	*Finer*
49	0.25	30	60.00	0.64	70,328	*Finer*
50	0.50	45	63.64	0.89	70,592	*Finer*
51	0.75	65	75.06	1.78	70,841	*Finer*
52	1.50	75	61.24	1.27	71,058	*Finer*
53	1.00	60	60.00	1.14	74,150	*Finer*
54	1.00	65	65.00	0.89	75,183	*Finer*
55	16.68	212	51.91	1.52	82,448	*Finer*
56	19.46	185	41.94	1.65	90,651	*Finer*
57	0.50	45	63.64	3.05	91,460	*Finer*
58	1.00	65	65.00	1.4	92,078	*Finer*
59	0.50	40	56.57	2.16	94,768	*Finer*
60	0.75	45	51.96	1.14	95,497	*Finer*
61	0.50	35	49.50	1.39	95,550	*Finer*
62	0.25	20	40.00	2.04	98,287	*Finer*
63	36.14	192	31.94	2.16	98,416	*Finer*
64	0.50	45	63.64	3.30	99,035	*Finer*
65	0.50	25	35.36	1.27	1,12,925	*Coarser*
66	0.25	25	50.00	1.65	1,13,238	*Coarser*
67	0.25	20	40.00	1.65	1,22,602	*Coarser*
68	0.25	25	50.00	2.65	1,23,240	*Coarser*
69	0.50	25	35.36	1.65	1,26,449	*Coarser*
70	0.50	30	42.43	1.52	1,28,200	*Coarser*
71	0.25	25	50.00	2.67	1,29,988	*Coarser*
72	19.46	159	36.04	2.41	1,34,224	*Coarser*
73	0.25	25	50.00	2.03	1,34,997	*Coarser*
74	0.25	25	50.00	1.65	1,35,184	*Coarser*
75	1.50	40	32.66	1.90	1,37,313	*Coarser*

Sl. No.	Maximum Charge per Delay	Distance	Scaled Distance	Peak Particle Velocity	Seismic Energy	Fragmentation
	MCD (kg)	**D (m)**	**SD (m/√kg)**	**PPV (mm/s)**	**SE (μJ)**	***Status***
76	0.50	35	49.50	2.41	1,40,250	*Coarser*
77	19.46	88	19.95	2.16	1,41,979	*Coarser*
78	16.68	196	47.99	1.78	1,47,428	*Coarser*
79	1.00	35	35.00	2.16	1,48,757	*Coarser*
80	1.25	30	26.83	2.41	1,59,011	*Coarser*
81	1.25	25	22.36	2.29	1,59,079	*Coarser*
82	19.46	168	38.08	2.28	1,67,108	*Coarser*
83	36.14	180	29.94	2.79	1,71,487	*Coarser*
84	16.68	106	25.95	3.68	1,85,897	*Coarser*
85	0.50	20	28.28	2.92	1,87,859	*Coarser*
86	18.63	73	16.91	2.32	1,92,095	*Coarser*
87	16.68	100	24.49	3.56	2,01,246	*Coarser*
88	18.63	43	9.96	2.57	2,10,001	*Coarser*
89	44.48	160	23.99	2.41	2,16,314	*Coarser*
90	22.22	77	16.33	6.73	2,36,827	*Coarser*
91	22.22	67	14.21	4.95	2,38,353	*Coarser*
92	0.50	20	28.28	6.10	2,64,201	*Coarser*
93	18.63	35	8.11	9.14	4,05,780	*Coarser*
94	44.48	60	9.00	8.81	4,39,693	*Coarser*

** Finer Fragmentation means ≤+300mm size,*
Coarser Fragmentation means ≥+300mm size

Table – A4.10 Summary of longitudinal wave and transverse wave velocities in granite formation

Sl. No.	Scaled Distance	Peak Particle Velocity	L-wave Velocity	T-wave Velocity
	SD (m/√kg)	**PPV (mm/s)**	**(m/s)**	**(m/s)**
1	4.90	1.52	184	145
2	6.80	2.28	366	273
3	8.49	4.95	445	323
4	10.20	1.78	514	409
5	10.61	6.73	641	327
6	11.33	1.65	653	610
7	13.90	17.14	684	645
8	14.73	1.52	763	657
9	15.91	3.56	750	259
10	28.28	6.1	1,111	1,000

Sl. No.	Scaled Distance	Peak Particle Velocity	L-wave Velocity	T-wave Velocity
	SD (m/√kg)	PPV (mm/s)	(m/s)	(m/s)
11	28.58	1.27	1,458	875
12	35.36	3.3	1,250	893
13	46.19	1.02	1,905	506
14	84.85	0.762	3,000	1,224
15	98.99	2.67	4,118	854
16	101.61	0.51	8,800	1,100
17	192.00	0.635	19,200	2,462
18	200.00	0.51	20,000	1,333
19	200.00	1.4	22,222	3,226
20	212.13	1.02	37,500	3,000
21	247.49	0.51	1,75,000	2,035
22	282.84	0.51	2,00,000	3,333
23	282.84	3.3	2,00,000	2,105
24	288.50	0.762	2,04,000	5,100
25	353.55	0.762	2,00,000	3,125
26	400.00	0.635	2,50,000	3,175
27	424.00	0.64	1,06,000	5,556
28	424.26	1.27	3,00,000	6,839
29	622.25	0.762	4,10,000	1,10,000

** L-wave and T-wave indicates Longitudinal and Transverse waves, respectively*

Table – A4.11 Summary of tapped electrical voltage and electrical energy from blast induced ground vibrations in limestone mines with basic piezo-gen circuit

Sl. No.	Distance (m)	Scaled Distance (m/√kg)	Electrical Voltage (mV)	Electrical Energy (µJ)
1	100	18.21	143.00	22.49
2	125	22.76	294.00	95.08
3	130	23.67	28.30	0.88
4	108	17.83	164.00	29.59
5	120	19.82	28.70	0.91
6	132	21.80	18.70	0.38
7	132	16.80	288.50	91.56
8	142	18.07	59.60	3.91
9	154	19.60	53.70	3.17

Table – A4.12 Summary of tapped electrical voltage and electrical energy from blast vibrations in limestone mines with piezo generator circuit

Sl. No.	Distance (m)	Scaled Distance (m/√kg)	Electrical Voltage (mV)	Electrical Energy (µJ)
1	30	4.85	3,003.05	45,09,140
2	40	6.46	1,674.87	19,63,630
3	45	7.27	1,562.56	17,09,116
4	50	8.08	546.90	2,99,095
5	55	8.88	1,235.40	15,26,211
6	60	9.69	498.07	2,48,070
7	40	6.53	2,202.23	24,24,915
8	50	8.16	1,020.55	10,41,516
9	55	8.98	424.82	2,34,615
10	60	9.80	322.28	1,03,863
11	65	10.61	1,650.45	16,34,399
12	65	10.61	678.74	4,60,684
13	50	5.97	2,070.39	25,71,914
14	65	7.76	1,186.57	14,07,946
15	65	7.76	913.12	8,33,790
16	70	8.36	253.92	64,473
17	40	6.61	532.25	2,83,287
18	50	8.27	351.58	1,23,606
19	55	9.09	297.86	88,722
20	70	11.58	126.96	16,118
21	75	12.40	136.72	18,693
22	80	13.23	43.95	1,931
23	40	6.40	571.31	3,26,396
24	50	8.00	493.18	2,43,229
25	80	12.80	9.77	95
26	134	21.44	58.60	3,433
27	40	6.40	4,531.42	71,86,831
28	50	7.98	4,414.23	1,16,91,266
29	55	8.78	2,241.30	30,14,047
30	75	11.97	200.20	40,081
31	80	12.76	2,280.36	31,20,028
32	85	13.56	190.44	36,266
33	50	7.98	1,889.72	21,42,627
34	60	8.37	3,842.92	1,32,91,238
35	65	9.07	3,149.54	69,43,700
36	90	12.55	449.24	2,62,357
37	95	13.25	2,021.56	32,69,370

Sl. No.	Distance (m)	Scaled Distance (m/√kg)	Electrical Voltage (mV)	Electrical Energy (µJ)
38	100	13.95	297.86	88,722
39	30	6.05	1,923.90	29,61,119
40	38	7.66	2,412.20	46,54,975
41	50	10.09	795.93	6,33,503
42	90	18.15	297.86	88,722
43	95	19.16	332.04	1,10,253
44	100	20.17	517.60	3,48,280
45	40	10.56	283.21	80,210
46	50	13.20	117.19	13,734
47	75	19.80	92.78	8,608
48	80	21.12	34.18	1,168
49	85	22.44	78.13	6,104
50	40	7.26	1,059.61	11,22,775
51	50	9.07	742.22	5,50,885
52	60	10.89	410.17	1,68,241
53	70	12.70	156.26	24,416
54	40	7.52	1,303.76	16,99,793
55	45	8.45	1,079.14	11,64,550
56	55	10.33	756.87	5,72,845
57	70	13.15	371.11	1,37,721

Table – A4.13 Summary of tapped electrical voltage and electrical energy from blast induced ground vibrations in coal formation with piezo generator circuit

Sl. No.	Distance (m)	Scaled Distance (m/∛kg)	Electrical Voltage (mV)	Electrical Energy (µJ)
1	54.75	39.87	42.00	1.94
2	58.28	42.44	3.50	0.01
3	67.80	49.37	48.00	2.53
4	61.85	41.42	32.00	1.13
5	63.64	42.62	49.00	2.64
6	68.74	46.03	63.00	4.37
7	61.81	43.05	56.00	3.45
8	66.67	46.43	41.00	1.85
9	73.62	51.27	56.00	3.45
10	98.28	68.45	25.00	0.69
11	110.26	76.79	52.00	2.97
12	113.61	79.13	22.00	0.53
13	88.71	64.60	39.00	1.67
14	92.16	67.11	17.00	0.32

Sl. No.	Distance (m)	Scaled Distance (m/$\sqrt[3]{kg}$)	Electrical Voltage (mV)	Electrical Energy (μJ)
15	101.83	74.15	19.90	0.44
16	101.08	70.40	46.00	2.33
17	103.04	71.76	11.30	0.14
18	108.70	75.71	1.60	0.00
19	62.09	41.58	78.00	6.69
20	61.85	43.08	42.00	1.94
21	61.81	43.05	84.00	7.76
22	35.11	23.51	128.00	18.02
23	45.08	30.19	90.00	8.91
24	55.07	36.88	76.70	6.47
25	40.00	29.13	104.76	12.07
26	50.00	36.41	92.90	9.49
27	60.00	43.69	94.70	9.86
28	60.00	41.79	92.40	9.39
29	80.00	55.72	92.00	9.31
30	100.00	69.65	42.00	1.94
31	40.00	26.79	17.78	0.35
32	60.00	40.18	79.70	6.99
33	35.00	24.38	116.00	14.80
34	55.00	38.31	93.00	9.51
35	70.00	48.75	124.00	16.91
36	100.00	69.65	49.00	2.64

Table – A4.14 Summary of tapped electrical voltage and electrical energy from blast vibrations in sandstone formation with piezo generator circuit

Sl. No.	Distance (m)	Scaled Distance (m/√kg)	Electrical Voltage (mV)	Electrical Energy (μJ)
1	100	12.31	4,277.51	36,59,414.94
2	110	13.54	3,794.09	34,39,512.65
3	120	14.77	3,735.50	33,95,392.29
4	150	18.46	3,501.11	31,80,444.76
5	160	19.69	3,335.09	66,73,691.18
6	170	20.93	3,276.49	96,61,865.74
7	184	26.02	2,021.56	32,69,370.34
8	178	18.97	3,667.13	1,07,58,291.55
9	188	20.04	3,530.41	62,31,893.85
10	200	21.32	3,403.45	11,58,347.87
11	292	31.13	1,289.11	8,30,904.87
12	150	16.27	3,540.18	1,25,32,839.03

Sl. No.	Distance (m)	Scaled Distance (m/√kg)	Electrical Voltage (mV)	Electrical Energy (µJ)
13	209	22.67	3,291.14	21,66,323.13
14	234	25.38	3,061.64	9,37,364.56
15	295	32.00	1,059.61	4,49,110.19
16	696	32.81	1,186.57	5,63,178.40
17	719	33.89	893.59	4,79,100.78
18	750	35.36	898.47	4,84,351.16
19	800	37.71	556.66	3,09,872.58
20	603	28.12	2,783.31	23,24,044.37
21	636	29.65	1,069.38	8,00,497.02
22	678	31.61	1,010.78	4,08,671.29
23	721	33.62	766.63	5,87,723.09
24	220	22.00	3,076.29	1,04,09,916.18
25	380	38.00	820.34	6,72,964.28
26	1591	36.00	581.08	3,37,650.48
27	1856	42.00	478.53	2,28,994.79
28	2033	46.00	468.77	2,19,743.44
29	2121	47.99	415.06	1,72,270.65
30	304	32.04	1,137.74	12,94,450.03
31	332	35.00	957.07	5,49,587.49
32	379	39.95	615.26	6,81,376.33
33	280	28.00	2,441.50	11,92,184.45
34	290	29.00	1,030.31	6,36,926.93
35	300	30.00	859.41	7,38,582.11
36	440	44.00	751.98	5,65,476.93
37	100	29.99	3,667.13	53,79,145.78
38	150	31.81	3,672.02	80,90,220.90
39	115	25.19	776.40	6,02,792.30
40	200	33.93	1,372.12	18,82,721.53
41	284	54.05	791.05	6,25,753.77

Table – A4.15 Summary of tapped electrical voltage and electrical energy from blast vibrations in granitic rock formation with piezo generator circuit

Sl. No.	Distance (m)	Scaled Distance (m/√kg)	Electrical Voltage (mV)	Electrical Energy (µJ)
1	60	60.00	2,202.23	38,79,864.15
2	130	130.00	625.02	6,25,048.00
3	50	141.42	1,709.05	14,60,425.95
4	30	84.85	1,215.87	17,73,999.07
5	40	32.66	2,998.16	62,92,282.76

Sl. No.	Distance (m)	Scaled Distance (m/√kg)	Electrical Voltage (mV)	Electrical Energy (μJ)
6	75	61.24	2,500.10	37,50,288.01
7	75	86.60	1,928.79	29,76,169.26
8	100	115.47	1,215.87	11,82,666.05
9	50	57.74	2,036.21	24,87,693.14
10	55	63.51	2,031.33	24,75,776.07
11	150	212.13	629.91	3,17,426.26
12	200	282.84	625.02	3,12,524.00
13	45	63.64	1,938.55	30,06,383.98
14	180	254.56	1,215.87	11,82,666.05
15	145	205.06	634.79	3,22,366.68
16	100	100.00	1,220.75	11,92,184.45
17	175	175.00	1,215.87	11,82,666.05
18	110	110.00	634.79	4,02,958.34
19	180	360.00	2,036.21	4,14,615.52
20	30	60.00	634.79	5,23,845.85
21	45	63.64	1,933.67	29,91,257.55
22	150	212.13	1,713.93	11,75,026.53
23	60	120.00	1,215.87	14,78,332.56
24	35	49.50	2,592.87	47,06,093.28
25	50	70.71	1,709.05	29,20,851.90
26	65	75.06	2,944.45	34,67,911.97
27	160	184.75	1,928.79	7,44,042.32
28	300	346.41	625.02	3,12,524.00
29	45	51.96	2,202.23	38,79,864.15
30	60	60.00	2,495.21	18,67,826.37
31	135	135.00	634.79	6,04,437.52
32	25	50.00	3,994.29	63,81,753.82
33	25	50.00	3,296.03	65,18,268.48
34	25	50.00	2,905.39	67,53,009.60
35	20	40.00	3,715.96	55,23,352.41
36	25	50.00	2,983.51	71,21,079.86
37	20	40.00	2,905.39	67,53,009.60
38	35	35.00	3,032.34	73,56,083.26
39	65	65.00	2,612.41	54,59,727.91
40	70	70.00	2,197.35	38,62,677.62
41	20	28.28	3,418.10	93,46,726.09
42	25	35.36	2,905.39	67,53,009.60
43	25	35.36	2,490.33	55,81,569.16

Sl. No.	Distance (m)	Scaled Distance (m/√kg)	Electrical Voltage (mV)	Electrical Energy (μJ)
44	30	42.43	2,783.31	61,97,451.64
45	50	70.71	2,500.10	25,00,192.00
46	200	282.84	2,031.33	16,50,517.38
47	35	49.50	4,404.47	77,59,728.30
48	40	56.57	3,540.18	50,13,135.61
49	45	63.64	3,427.87	47,00,106.13
50	200	400.00	1,225.63	12,01,741.00
51	100	200.00	634.79	3,22,366.68
52	65	65.00	1,933.67	29,91,257.55
53	200	282.84	1,215.87	11,82,666.05
54	100	200.00	1,220.75	11,92,184.45
55	30	26.83	3,149.54	79,35,656.57
56	25	22.36	3,086.06	76,18,993.31
57	85	76.03	1,709.05	23,36,681.52
58	220	196.77	1,215.87	11,82,666.05
59	70	57.15	1,704.17	23,23,348.13
60	25	50.00	2,905.39	50,64,757.20
61	55	110.00	1,220.75	11,92,184.45
62	55	77.78	2,041.09	29,16,245.30
63	60	84.85	1,933.67	22,43,443.16
64	170	240.42	1,709.05	8,76,255.57
65	150	212.13	2,197.35	9,65,669.40
66	45	63.64	1,943.43	30,21,548.57
67	80	113.14	1,709.05	23,36,681.52
68	20	28.28	4,370.29	1,33,69,573.69
69	45	63.64	3,540.18	50,13,135.61
70	50	70.71	3,296.03	32,59,134.24
71	77	16.33	4,389.82	1,15,62,295.98
72	67	14.21	4,350.75	1,13,57,431.00
73	300	63.64	3,672.02	40,45,110.45
74	60	9.00	3,916.17	1,99,37,262.98
75	160	23.99	3,149.54	1,09,11,527.79
76	35	8.11	4,995.31	1,99,62,489.60
77	43	9.96	4,936.71	97,48,454.10
78	73	16.91	4,892.77	95,75,663.65
79	180	29.94	3,374.15	91,07,926.77
80	192	31.94	3,076.29	47,31,780.08
81	106	25.95	3,715.96	96,65,866.71

Sl. No.	Distance (m)	Scaled Distance (m/√kg)	Electrical Voltage (mV)	Electrical Energy (µJ)
82	100	24.49	3,672.02	94,38,591.05
83	159	36.04	3,149.54	69,43,699.50
84	168	38.08	3,086.06	80,95,180.39
85	200	45.34	2,959.10	35,02,504.39
86	185	41.94	2,905.39	42,20,631.00
87	250	56.67	2,783.31	23,24,044.37
88	203	46.02	2,509.86	25,19,762.90
89	196	47.99	2,954.22	69,81,909.01
90	204	49.95	2,905.39	42,20,631.00
91	212	51.91	2,783.31	38,73,407.28
92	250	56.67	3,354.62	45,01,392.82
93	88	19.95	3,003.05	54,10,967.56
94	200	45.34	2,612.41	54,59,727.91

Table – A4.16 Summary of seismic energy and electrical energy obtained in hard limestone formation with basic piezo circuit model

Sl. No.	Distance (m)	Scaled Distance (m/√kg)	Seismic Energy (µJ)	Electrical Energy (µJ)
1	100	18.21	2,48,25,450.94	22.49
2	125	22.76	12,99,39,768.98	95.08
3	130	23.67	80,99,368.41	0.88
4	108	17.83	3,47,91,952.21	29.59
5	120	19.82	49,50,200.13	0.91
6	132	21.80	19,05,659.25	0.38
7	132	16.80	12,61,05,017.12	91.56
8	142	18.07	98,32,891.89	3.91
9	154	19.60	93,87,707.90	3.17

Table – A4.17 Summary of seismic energy and electrical energy obtained in hard limestone formation with piezo generator circuit

Sl. No.	Distance (m)	Scaled Distance (m/√kg)	Seismic Energy (µJ)	Electrical Energy (µJ)
1	30	4.85	4,22,56,215	45,09,140
2	40	6.46	1,85,24,598	19,63,630
3	45	7.27	1,71,08,152	17,09,116
4	50	8.08	67,29,443	2,99,095
5	55	8.88	1,40,13,633	15,26,211
6	60	9.69	63,77,533	2,48,070

Sl. No.	Distance (m)	Scaled Distance (m/√kg)	Seismic Energy (µJ)	Electrical Energy (µJ)
7	40	6.53	2,66,56,654	24,24,915
8	50	8.16	1,11,03,330	10,41,516
9	55	8.98	54,19,536	2,34,615
10	60	9.80	39,03,284	1,03,863
11	65	10.61	1,84,19,851	16,34,399
12	65	10.61	75,23,677	4,60,684
13	50	5.97	2,58,37,627	25,71,914
14	65	7.76	1,36,66,773	14,07,946
15	65	7.76	98,24,630	8,33,790
16	70	8.36	28,95,806	64,473
17	40	6.61	65,48,821	2,83,287
18	50	8.27	44,53,486	1,23,606
19	55	9.09	32,32,849	88,722
20	70	11.58	7,12,081	16,118
21	75	12.40	9,64,048	18,693
22	80	13.23	3,06,033	1,931
23	40	6.40	68,93,020	3,26,396
24	50	8.00	62,64,554	2,43,229
25	80	12.80	1,56,568	95
26	134	21.44	3,59,719	3,433
27	40	6.40	5,97,27,766	71,86,831
28	50	7.98	9,96,99,604	1,16,91,266
29	55	8.78	2,70,09,086	30,14,047
30	75	11.97	20,40,307	40,081
31	80	12.76	2,89,70,681	31,20,028
32	85	13.56	19,01,915	36,266
33	50	7.98	2,15,03,717	21,42,627
34	60	8.37	11,12,59,278	1,32,91,238
35	65	9.07	5,83,38,415	69,43,700
36	90	12.55	57,58,561	2,62,357
37	95	13.25	2,46,91,269	32,69,370
38	100	13.95	33,66,361	88,722
39	30	6.05	2,34,18,621	29,61,119
40	38	7.66	3,81,33,182	46,54,975
41	50	10.09	92,64,400	6,33,503
42	90	18.15	33,31,585	88,722
43	95	19.16	40,60,162	1,10,253
44	100	20.17	64,92,304	3,48,280

Sl. No.	Distance (m)	Scaled Distance (m/√kg)	Seismic Energy (µJ)	Electrical Energy (µJ)
45	40	10.56	31,85,760	80,210
46	50	13.20	6,27,148	13,734
47	75	19.80	4,73,566	8,608
48	80	21.12	2,40,986	1,168
49	85	22.44	4,46,799	6,104
50	40	7.26	1,24,51,737	11,22,775
51	50	9.07	85,52,912	5,50,885
52	60	10.89	53,50,973	1,68,241
53	70	12.70	12,41,977	24,416
54	40	7.52	1,45,65,085	16,99,793
55	45	8.45	1,26,75,683	11,64,550
56	55	10.33	85,73,518	5,72,845
57	70	13.15	45,02,870	1,37,721

Table – A4.18 Summary of seismic energy and electrical energy obtained in soft limestone formation with piezo generator circuit

Sl. No.	Distance (m)	Scaled Distance (m/√kg)	Seismic Energy (µJ)	Electrical Energy (µJ)
1	80	12.00	5,46,976	5,47,409
2	94	14.09	2,42,413	2,44,205
3	107	16.04	2,15,448	2,16,261
4	120	17.99	95,328	95,566
5	155	28.03	1,90,186	1,94,937
6	166	30.02	1,58,669	1,65,220
7	177	32.01	1,29,474	1,29,640
8	188	34.00	81,506	82,447
9	56	10.13	2,95,524	3,10,935
10	122	22.06	2,53,022	2,57,100
11	133	24.05	1,89,693	1,90,693
12	144	26.04	1,01,851	1,05,286
13	300	36.73	2,31,644	2,34,973
14	325	39.79	23,113	23,560
15	335	41.01	21,708	21,890
16	350	42.85	16,127	16,148
17	350	58.22	37,645	37,750
18	360	59.88	6,715	6,838
19	250	56.67	1,10,243	1,12,594
20	275	62.34	86,357	87,138
21	285	64.61	9,983	10,467

Sl. No.	Distance (m)	Scaled Distance (m/√kg)	Seismic Energy (µJ)	Electrical Energy (µJ)
22	140	27.99	4,51,380	4,57,539
23	150	29.99	3,91,806	3,93,371
24	160	31.99	1,58,876	1,59,963
25	175	34.99	1,16,544	1,16,781
26	193	38.58	81,229	81,739
27	230	45.98	52,724	57,830
28	235	46.98	45,142	45,380
29	306	61.18	22,529	22,967
30	216	43.18	34,059	34,889
31	254	50.78	32,984	33,214
32	260	51.98	20,155	20,634
33	330	65.97	9,063	9,645
34	250	56.67	1,40,554	1,41,290
35	253	57.35	83,893	84,129
36	304	68.91	71,853	71,395
37	310	70.27	50,941	51,404

Table – A4.19 Summary of seismic energy and electrical energy obtained in coal formation with piezo generator circuit

Sl. No.	Distance (m)	Scaled Distance (m/∛kg)	Seismic Energy (µJ)	Electrical Energy (µJ)
1	54.75	39.87	21,978	1.94
2	58.28	42.44	4,250	0.01
3	67.80	49.37	28,468	2.53
4	61.85	41.42	12,605	1.13
5	63.64	42.62	27,482	2.64
6	68.74	46.03	62,190	4.37
7	61.81	43.05	51,304	3.45
8	66.67	46.43	19,621	1.85
9	73.62	51.27	46,189	3.45
10	98.28	68.45	7,705	0.69
11	110.26	76.79	33,174	2.97
12	113.61	79.13	0.001	0.53
13	88.71	64.60	28,829	1.67
14	92.16	67.11	0.001	0.32
15	101.83	74.15	0.001	0.44
16	101.08	70.40	28,828	2.33
17	103.04	71.76	0.001	0.14
18	108.70	75.71	0.001	0.00

Sl. No.	Distance (m)	Scaled Distance (m/$\sqrt[3]{kg}$)	Seismic Energy (µJ)	Electrical Energy (µJ)
19	62.09	41.58	95,980	6.69
20	61.85	43.08	20,739	1.94
21	61.81	43.05	98,277	7.76
22	35.11	23.51	2,78,718	18.02
23	45.08	30.19	1,39,810	8.91
24	55.07	36.88	75,472	6.47
25	40.00	29.13	1,75,798	12.07
26	50.00	36.41	1,41,350	9.49
27	60.00	43.69	1,41,563	9.86
28	60.00	41.79	1,39,698	9.39
29	80.00	55.72	1,38,105	9.31
30	100.00	69.65	31,496	1.94
31	40.00	26.79	13,760	0.35
32	60.00	40.18	1,14,259	6.99
33	35.00	24.38	2,14,430	14.80
34	55.00	38.31	1,49,313	9.51
35	70.00	48.75	2,45,240	16.91
36	100.00	69.65	42,657	2.64
2	54.75	39.87	21,978	1.94
3	58.28	42.44	4,250	0.01
4	67.80	49.37	28,468	2.53
5	61.85	41.42	12,605	1.13
6	63.64	42.62	27,482	2.64
7	68.74	46.03	62,190	4.37
8	61.81	43.05	51,304	3.45
9	66.67	46.43	19,621	1.85
10	73.62	51.27	46,189	3.45
11	98.28	68.45	7,705	0.69
12	110.26	76.79	33,174	2.97
13	113.61	79.13	0.001	0.53
14	88.71	64.60	28,829	1.67
15	92.16	67.11	0.001	0.32
16	101.83	74.15	0.001	0.44
17	101.08	70.40	28,828	2.33
18	103.04	71.76	0.001	0.14
19	108.70	75.71	0.001	0.00
20	62.09	41.58	95,980	6.69
21	61.85	43.08	20,739	1.94

Sl. No.	Distance (m)	Scaled Distance ($m/\sqrt[3]{kg}$)	Seismic Energy (µJ)	Electrical Energy (µJ)
22	61.81	43.05	98,277	7.76
23	35.11	23.51	2,78,718	18.02
24	45.08	30.19	1,39,810	8.91
25	55.07	36.88	75,472	6.47
26	40.00	29.13	1,75,798	12.07
27	50.00	36.41	1,41,350	9.49
28	60.00	43.69	1,41,563	9.86
29	60.00	41.79	1,39,698	9.39
30	80.00	55.72	1,38,105	9.31
31	100.00	69.65	31,496	1.94
32	40.00	26.79	13,760	0.35
33	60.00	40.18	1,14,259	6.99
34	35.00	24.38	2,14,430	14.80
35	55.00	38.31	1,49,313	9.51
36	70.00	48.75	2,45,240	16.91
37	100.00	69.65	42,657	2.64

Table – A4.20 Summary of seismic energy and electrical energy obtained in sandstone formation with piezo generator circuit

Sl. No.	Distance (m)	Scaled Distance ($m/\sqrt{kg}$)	Seismic Energy (µJ)	Electrical Energy (µJ)
1	100	12.31	27,38,832.38	36,59,414.94
2	110	13.54	15,11,665.32	34,39,512.65
3	120	14.77	14,70,468.86	33,95,392.29
4	150	18.46	69,16,156.65	31,80,444.76
5	160	19.69	52,45,447.10	66,73,691.18
6	170	20.93	84,61,652.43	96,61,865.74
7	184	26.02	15,62,458.55	32,69,370.34
8	178	18.97	92,77,651.80	107,58,291.55
9	188	20.04	47,47,405.68	62,31,893.85
10	200	21.32	3,66,544.54	11,58,347.87
11	292	31.13	3,76,992.65	8,30,904.87
12	150	16.27	105,44,797.69	125,32,839.03
13	209	22.67	22,80,225.67	21,66,323.13
14	234	25.38	10,55,142.78	9,37,364.56
15	295	32.00	1,34,876.62	4,49,110.19
16	696	32.81	5,13,484.49	5,63,178.40
17	719	33.89	1,36,859.22	4,79,100.78
18	750	35.36	1,71,645.30	4,84,351.16

Sl. No.	Distance (m)	Scaled Distance (m/√kg)	Seismic Energy (µJ)	Electrical Energy (µJ)
19	800	37.71	5,57,770.65	3,09,872.58
20	603	28.12	19,80,472.55	23,24,044.37
21	636	29.65	1,60,142.93	8,00,497.02
22	678	31.61	1,66,647.59	4,08,671.29
23	721	33.62	45,698.08	5,87,723.09
24	220	22.00	87,69,781.29	104,09,916.18
25	380	38.00	1,72,599.58	6,72,964.28
26	1591	36.00	79,583.75	3,37,650.48
27	1856	42.00	71,031.38	2,28,994.79
28	2033	46.00	49,481.50	2,19,743.44
29	2121	47.99	3,10,087.18	1,72,270.65
30	304	32.04	6,38,174.00	12,94,450.03
31	332	35.00	1,64,876.00	5,49,587.49
32	379	39.95	61,901.33	6,81,376.33
33	280	28.00	6,15,873.46	11,92,184.45
34	290	29.00	73,406.11	6,36,926.93
35	300	30.00	4,02,677.92	7,38,582.11
36	440	44.00	1,08,396.33	5,65,476.93
37	100	29.99	27,38,832.38	53,79,145.78
38	150	31.81	15,11,665.32	80,90,220.90
39	115	25.19	14,70,468.86	6,02,792.30
40	200	33.93	69,16,156.65	18,82,721.53
41	284	54.05	52,45,447.10	6,25,753.77

Table – A4.21 Summary of seismic energy and electrical energy obtained in granite formation with piezo generator circuit

Sl. No.	Distance (m)	Scaled Distance (m/√kg)	Seismic Energy (µJ)	Electrical Energy (µJ)
1	60	60.00	74,150	38,79,864.15
2	130	130.00	24,358	6,25,048.00
3	50	141.42	32,698	14,60,425.95
4	30	84.85	43,456	17,73,999.07
5	40	32.66	1,37,313	62,92,282.76
6	75	61.24	71,058	37,50,288.01
7	75	86.60	48,441	29,76,169.26
8	100	115.47	34,750	11,82,666.05
9	50	57.74	54,229	24,87,693.14
10	55	63.51	51,161	24,75,776.07

Sl. No.	Distance (m)	Scaled Distance (m/√kg)	Seismic Energy (µJ)	Electrical Energy (µJ)
11	150	212.13	20,765	3,17,426.26
12	200	282.84	10,604	3,12,524.00
13	45	63.64	48,822	30,06,383.98
14	180	254.56	12,931	11,82,666.05
15	145	205.06	24,382	3,22,366.68
16	100	100.00	26,911	11,92,184.45
17	175	175.00	16,817	11,82,666.05
18	110	110.00	23,653	4,02,958.34
19	180	360.00	11,998	4,14,615.52
20	30	60.00	42,196	5,23,845.85
21	45	63.64	70,592	29,91,257.55
22	150	212.13	14,387	11,75,026.53
23	60	120.00	36,995	14,78,332.56
24	35	49.50	95,550	47,06,093.28
25	50	70.71	59,777	29,20,851.90
26	65	75.06	70,841	34,67,911.97
27	160	184.75	14,880	7,44,042.32
28	300	346.41	7,972	3,12,524.00
29	45	51.96	95,497	38,79,864.15
30	60	60.00	38,202	18,67,826.37
31	135	135.00	24,093	6,04,437.52
32	25	50.00	1,23,240	63,81,753.82
33	25	50.00	1,29,988	65,18,268.48
34	25	50.00	1,35,184	67,53,009.60
35	20	40.00	98,287	55,23,352.41
36	25	50.00	1,34,997	71,21,079.86
37	20	40.00	1,22,602	67,53,009.60
38	35	35.00	1,48,757	73,56,083.26
39	65	65.00	92,078	54,59,727.91
40	70	70.00	55,113	38,62,677.62
41	20	28.28	1,87,859	93,46,726.09
42	25	35.36	1,26,449	67,53,009.60
43	25	35.36	1,12,925	55,81,569.16
44	30	42.43	1,28,200	61,97,451.64
45	50	70.71	47,157	25,00,192.00
46	200	282.84	15,313	16,50,517.38
47	35	49.50	1,40,250	77,59,728.30
48	40	56.57	94,768	50,13,135.61

Sl. No.	Distance (m)	Scaled Distance (m/√kg)	Seismic Energy (µJ)	Electrical Energy (µJ)
49	45	63.64	91,460	47,00,106.13
50	200	400.00	8,374	12,01,741.00
51	100	200.00	15,488	3,22,366.68
52	65	65.00	75,183	29,91,257.55
53	200	282.84	10,153	11,82,666.05
54	100	200.00	16,777	11,92,184.45
55	30	26.83	1,59,011	79,35,656.57
56	25	22.36	1,59,079	76,18,993.31
57	85	76.03	49,900	23,36,681.52
58	220	196.77	13,197	11,82,666.05
59	70	57.15	50,318	23,23,348.13
60	25	50.00	1,13,238	50,64,757.20
61	55	110.00	26,275	11,92,184.45
62	55	77.78	60,635	29,16,245.30
63	60	84.85	35,675	22,43,443.16
64	170	240.42	11,524	8,76,255.57
65	150	212.13	17,696	9,65,669.40
66	45	63.64	59,637	30,21,548.57
67	80	113.14	50,109	23,36,681.52
68	20	28.28	2,64,201	1,33,69,573.69
69	45	63.64	99,035	50,13,135.61
70	50	70.71	68,162	32,59,134.24
71	77	16.33	2,36,827	1,15,62,295.98
72	67	14.21	2,38,353	1,13,57,431.00
73	300	63.64	38,312	40,45,110.45
74	60	9.00	4,39,693	1,99,37,262.98
75	160	23.99	2,16,314	1,09,11,527.79
76	35	8.11	4,05,780	1,99,62,489.60
77	43	9.96	2,10,001	97,48,454.10
78	73	16.91	1,92,095	95,75,663.65
79	180	29.94	1,71,487	91,07,926.77
80	192	31.94	98,416	47,31,780.08
81	106	25.95	1,85,897	96,65,866.71
82	100	24.49	2,01,246	94,38,591.05
83	159	36.04	1,34,224	69,43,699.50
84	168	38.08	1,67,108	80,95,180.39
85	200	45.34	54,435	35,02,504.39
86	185	41.94	90,651	42,20,631.00

Sl. No.	Distance (m)	Scaled Distance (m/√kg)	Seismic Energy (μJ)	Electrical Energy (μJ)
87	250	56.67	40,566	23,24,044.37
88	203	46.02	53,540	25,19,762.90
89	196	47.99	1,47,428	69,81,909.01
90	204	49.95	64,459	42,20,631.00
91	212	51.91	82,448	38,73,407.28
92	250	56.67	64,681	45,01,392.82
93	88	19.95	1,41,979	54,10,967.56
94	200	45.34	64,718	54,59,727.91

Table – A4.22 Comparison of field and modelling results in limestone formation

Sl. No.	Input Parameters		Observations		% Error
	Total explosive charge per blast (kg)	Distance from blast location to monitoring point (m)	Field studies	Modelling studies	
			Peak Particle Velocity (mm/s)	Peak Particle Velocity (mm/s)	
1	258.30	40	34.80	34.95	0.43
2	258.30	100	14.40	14.46	0.42
3	258.30	75	8.76	9.13	4.22
4	258.30	80	8.13	8.59	5.66
5	258.30	85	6.73	6.89	2.38
6	283.30	40	37.60	38.08	1.28
7	283.30	45	35.40	35.47	0.20
8	283.30	55	23.10	23.79	2.99
9	283.30	70	15.50	15.58	0.52
10	425.04	40	34.40	34.75	1.02
11	425.04	50	23.10	23.35	1.08
12	425.04	60	14.60	15.09	3.36
13	425.04	70	11.00	11.22	2.00
14	491.60	30	44.70	45.72	2.28
15	491.60	38	42.00	42.05	0.12
16	491.60	50	23.70	24.31	2.57
17	491.60	90	19.80	20.27	2.37
18	491.60	95	18.40	18.70	1.63
19	491.60	100	15.00	15.44	2.93
20	624.96	40	32.20	32.67	1.46
21	624.96	50	28.20	28.22	0.07
22	624.96	300	2.41	2.49	3.32
23	624.96	134	11.70	11.71	0.09
24	658.26	40	40.00	40.95	2.38

Sl. No.	Input Parameters		Observations		% Error
	Total explosive charge per blast (kg)	Distance from blast location to monitoring point (m)	Field studies	Modelling studies	
			Peak Particle Velocity (mm/s)	Peak Particle Velocity (mm/s)	
25	658.26	50	30.10	30.21	0.37
26	658.26	55	28.20	28.21	0.04
27	658.26	70	16.10	16.25	0.93
28	658.26	75	10.40	10.47	0.67
29	658.26	250	3.43	3.74	9.04
30	758.78	235	2.79	2.85	2.15
31	824.88	40	17.10	17.42	1.87
32	824.88	50	18.10	18.39	1.60
33	824.88	55	68.80	69.10	0.44
34	824.88	75	10.30	10.34	0.39
35	824.88	50	38.60	38.84	0.62
36	824.88	85	7.75	7.78	0.39
37	841.68	50	61.00	61.79	1.30
38	841.68	65	41.90	42.45	1.31
39	841.68	65	39.40	40.61	3.07
40	841.68	70	32.50	33.61	3.42
41	874.90	163	6.60	6.84	3.64
42	874.90	198	1.78	1.84	3.37
43	874.90	209	1.40	1.44	2.86
44	874.93	100	30.60	30.62	0.07
45	874.93	50	22.40	22.45	0.22
46	874.93	130	9.40	9.59	2.02
47	925.12	275	5.08	5.08	0.00
48	925.12	315	4.44	4.83	8.78
49	925.12	450	2.54	2.75	8.27
50	925.20	50	56.00	57.84	3.29
51	925.20	30	126.00	129.63	2.88
52	925.20	30	91.40	92.03	0.69
53	925.20	90	38.10	38.38	0.73
54	925.20	50	30.90	30.93	0.10
55	925.20	100	12.30	12.31	0.08
56	1,049.92	132	9.02	9.22	2.22
57	1,049.92	142	6.22	6.69	7.56
58	1,049.92	154	5.84	5.96	2.05
59	1,100.10	108	6.10	6.75	10.66
60	1,100.10	120	4.95	5.14	3.84
61	1,100.10	132	3.17	3.45	8.83
62	1,125.00	40	55.60	55.67	0.13

Sl. No.	Input Parameters		Observations		% Error
	Total explosive charge per blast (kg)	Distance from blast location to monitoring point (m)	Field studies	Modelling studies	
			Peak Particle Velocity (mm/s)	Peak Particle Velocity (mm/s)	
63	1,125.00	50	35.60	36.67	3.01
64	1,125.00	55	29.30	29.79	1.67
65	1,125.00	60	27.30	27.32	0.07
66	1,125.00	65	26.40	26.73	1.25
67	1,125.00	65	22.70	22.98	1.23
68	1,125.09	85	9.52	9.70	1.89
69	1,125.09	275	2.79	2.79	0.00
70	1,149.90	30	64.40	66.38	3.07
71	1,149.90	40	39.20	39.48	0.71
72	1,149.90	45	37.50	37.54	0.11
73	1,149.90	50	26.30	26.37	0.27
74	1,149.90	55	22.50	22.54	0.18
75	1,149.90	60	11.80	12.15	2.97
76	1,199.90	204	1.52	1.66	9.21
77	1,199.90	218	1.40	1.46	4.29
78	1,199.90	290	1.02	1.04	1.96
79	1,262.39	294	1.78	1.85	3.93
80	1,262.39	306	1.40	1.49	6.43
81	1,262.39	316	1.27	1.41	11.02
82	1,550.06	135	20.80	20.94	0.67
83	1,550.06	155	14.60	14.87	1.85
84	1,550.06	454	1.65	1.80	9.09
85	1,624.92	104	11.60	11.63	0.26
86	1,624.92	300	0.76	0.79	3.95
87	1,650.02	170	9.91	10.16	2.52
88	1,650.02	184	9.65	9.68	0.31
89	1,650.02	275	5.46	5.83	6.78
90	2,050.00	150	14.40	14.45	0.35
91	2,050.00	200	13.20	13.34	1.06
92	2,099.90	255	3.43	3.68	7.29
93	2,099.90	269	2.54	2.65	4.33
94	2,099.90	282	2.16	2.36	9.26
95	2,274.76	249	4.32	4.33	0.23
96	2,274.76	289	2.03	2.13	4.93
97	2,274.76	302	1.65	1.76	6.67
98	2,574.18	335	5.46	5.68	4.03
99	2,574.18	352	4.06	4.09	0.74
100	2,574.18	377	3.43	3.82	11.37

Sl. No.	Input Parameters		Observations		% Error
	Total explosive charge per blast (kg)	Distance from blast location to monitoring point (m)	Field studies	Modelling studies	
			Peak Particle Velocity (mm/s)	Peak Particle Velocity (mm/s)	
101	2,849.81	75	20.70	20.72	0.10
102	2,849.81	85	11.80	11.89	0.76
103	2,849.81	270	0.64	0.69	7.81
104	2,874.93	380	4.44	4.84	9.01
105	2,874.93	380	1.65	1.66	0.61
106	2,874.93	485	1.27	1.36	7.09
107	2,974.78	70	11.00	11.20	1.82
108	2,974.78	65	10.80	10.99	1.76
109	2,974.78	120	10.50	10.72	2.10
110	3,285.76	65	10.50	10.58	0.76
111	3,285.76	100	8.76	8.83	0.80
112	3,285.76	150	5.97	6.19	3.69
113	3,974.88	358	4.83	4.86	0.62
114	3,974.88	372	2.92	3.30	13.01
115	3,974.88	386	2.92	2.96	1.37
116	3,974.88	400	1.91	1.99	4.19

Table – A4.23 Comparison of field and modelling results in coal formation

Sl. No.	Input Parameters		Observations		% Error
	Total explosive charge per blast (kg)	Distance from blast location to monitoring point (m)	Field studies	Modelling studies	
			Peak Particle Velocity (mm/s)	Peak Particle Velocity (mm/s)	
1	5.74	54.75	2.67	2.69	0.75
2	5.74	58.28	1.02	1.16	13.73
3	5.74	67.80	4.19	4.33	3.34
4	6.48	61.85	7.49	7.68	2.54
5	6.48	63.64	5.08	5.27	3.74
6	6.48	68.74	5.08	5.27	3.74
7	6.66	61.85	4.83	4.82	0.21
8	6.66	60.00	5.59	5.64	0.89
9	6.66	80.00	6.73	6.98	3.71
10	6.66	100.00	2.54	2.55	0.39
11	6.66	35.00	5.59	5.89	5.37
12	6.66	55.00	5.72	5.75	0.52
13	6.85	62.09	5.08	5.12	0.79
14	6.85	40.00	8.38	8.41	0.36

Sl. No.	Input Parameters		Observations		% Error
	Total explosive charge per blast (kg)	Distance from blast location to monitoring point (m)	Field studies	Modelling studies	
			Peak Particle Velocity (mm/s)	Peak Particle Velocity (mm/s)	
15	6.85	50.00	1.78	1.96	10.11
16	6.85	60.00	4.70	4.76	1.28
17	6.85	40.00	7.37	7.72	4.75
18	6.85	60.00	6.10	6.28	2.95
19	7.03	88.71	0.63	0.88	39.68
20	7.03	92.16	0.51	0.74	45.10
21	7.03	101.83	0.51	0.40	21.57
22	7.59	61.81	5.59	5.69	1.79
23	7.59	70.00	4.45	4.54	2.02
24	7.59	100.00	1.91	1.94	1.57
25	8.14	61.81	3.55	4.02	13.24
26	8.14	66.67	1.52	1.63	7.24
27	8.14	73.62	2.15	2.51	16.74
28	8.14	101.08	0.63	0.82	30.16
29	8.14	103.04	0.51	0.58	13.73
30	8.14	108.70	0.51	0.52	1.96
31	8.88	98.28	1.52	1.79	17.76
32	8.88	110.26	0.64	0.90	40.63
33	8.88	113.61	0.51	0.52	1.96
34	8.88	35.11	22.22	22.39	0.77
35	8.88	45.08	17.40	17.95	3.16
36	8.88	55.07	7.24	7.59	4.83

Table – A4.24 Comparison of field and modelling results in sandstone formation

Sl. No.	Input Parameters		Observations		% Error
	Total explosive charge per blast (kg)	Distance from blast location to monitoring point (m)	Field studies	Modelling studies	
			Peak Particle Velocity (mm/s)	Peak Particle Velocity (mm/s)	
1	308.0	100	5.46	6.05	9.75
2	308.0	260	0.762	1.33	42.71
3	402.8	240	0.76	1.29	41.09
4	402.8	355	0.51	0.89	42.70
5	457.2	200	2.54	3.45	26.38
6	457.2	212	2.29	2.93	21.84
7	457.2	295	1.27	1.27	0.00

Sl. No.	Input Parameters		Observations		% Error
	Total explosive charge per blast (kg)	Distance from blast location to monitoring point (m)	Field studies Peak Particle Velocity (mm/s)	Modelling studies Peak Particle Velocity (mm/s)	
8	489.0	150	5.33	5.45	2.20
9	489.0	275	0.76	0.8	5.00
10	489.0	397	0.51	0.47	7.84
11	730.8	284	1.14	1.94	41.24
12	1,500.0	220	9.4	9.79	3.98
13	1,500.0	380	1.4	1.91	26.70
14	1,980.0	379	1.14	1.57	27.39
15	2,150.0	280	4.32	4.76	9.24
16	2,150.0	290	2.92	3.17	7.89
17	2,150.0	300	2.03	2.12	4.25
18	2,150.0	440	1.27	1.08	17.59
19	2,625.0	184	5.33	5.56	4.14
20	2,673.0	100	53.5	56.04	4.53
21	2,673.0	110	33.8	37.17	9.07
22	2,673.0	120	29.3	36.09	18.81
23	2,772.0	150	18.92	19.07	0.79
24	2,772.0	160	17.4	17.91	2.85
25	2,772.0	170	17.3	17.59	1.65
26	3,270.0	150	19.81	22.38	11.48
27	3,270.0	209	10.7	11.36	5.81
28	3,270.0	234	8.89	9.21	3.47
29	3,270.0	295	3.3	3.79	12.93
30	5,324.0	178	22.61	23.75	4.80
31	5,324.0	188	20.2	23.04	12.33
32	5,324.0	200	17.9	21.13	15.29
33	5,324.0	292	4.06	4.22	3.79
34	16,100.0	450	7.11	7.49	5.07
35	16,100.0	636	2.29	2.48	7.66
36	16,100.0	678	1.9	2.13	10.80
37	16,100.0	721	1.27	1.28	0.78
38	17,100.0	696	3.56	3.69	3.52
39	17,100.0	719	1.52	1.91	20.42
40	17,100.0	750	1.52	1.55	1.94
41	42,949.0	1,591	1.02	0.99	3.03
42	42,949.0	1,856	0.89	1.04	14.42
43	42,949.0	2,033	0.89	0.7	27.14

Table – A4.25 Comparison of field and modelling results in granite formation

Sl. No.	Input Parameters		Observations		% Error
	Total explosive charge per blast (kg)	Distance from blast location to monitoring point (m)	Field studies	Modelling studies	
			Peak Particle Velocity (mm/s)	Peak Particle Velocity (mm/s)	
1	0.63	50	0.76	0.81	6.58
2	0.63	30	0.64	0.67	4.69
3	1.50	180	1.02	1.11	8.82
4	1.50	30	0.51	0.52	1.96
5	1.50	20	3.68	3.94	7.07
6	1.50	25	2.03	2.01	0.99
7	1.50	20	1.65	1.67	1.21
8	1.50	100	0.64	0.67	4.69
9	2.00	150	0.64	0.69	7.81
10	2.00	200	0.64	0.69	7.81
11	2.00	45	0.89	0.91	2.25
12	2.00	60	0.64	0.66	3.13
13	2.00	25	2.65	2.65	0.00
14	2.00	25	2.67	2.74	2.62
15	2.00	25	1.65	1.74	5.45
16	2.00	200	0.64	0.64	0.00
17	2.50	180	0.64	0.64	0.47
18	2.50	145	0.64	0.64	0.00
19	2.50	45	0.89	0.98	10.11
20	2.50	150	0.76	0.77	1.32
21	2.50	200	0.64	0.65	1.56
22	2.50	100	0.64	0.69	7.81
23	2.50	25	1.65	1.73	4.85
24	2.50	55	0.64	0.65	1.56
25	3.00	75	0.89	0.96	7.87
26	3.00	100	0.64	0.63	1.09
27	3.00	35	1.39	1.58	13.67
28	3.00	50	0.76	0.78	3.03
29	3.00	35	2.41	2.53	4.98
30	3.00	40	2.16	2.18	0.93
31	3.00	45	3.05	3.28	7.54
32	3.00	20	6.10	6.55	7.38
33	3.00	45	3.30	3.27	0.91
34	3.00	50	1.65	1.75	6.06

Sl. No.	Input Parameters		Observations		% Error
	Total explosive charge per blast (kg)	Distance from blast location to monitoring point (m)	Field studies	Modelling studies	
			Peak Particle Velocity (mm/s)	Peak Particle Velocity (mm/s)	
35	3.75	50	1.02	1.09	6.86
36	3.75	55	1.02	1.08	5.88
37	3.75	30	1.52	1.52	0.00
38	3.75	50	1.27	1.31	3.15
39	3.75	200	0.76	0.76	0.39
40	3.75	150	0.76	0.79	3.95
41	3.75	45	0.89	0.85	4.49
42	3.75	80	0.76	0.75	1.32
43	4.50	55	1.02	1.04	1.96
44	4.50	60	0.89	0.98	10.11
45	4.50	170	0.76	0.78	2.63
46	5.00	130	0.64	0.69	7.81
47	5.00	20	2.92	2.93	0.34
48	5.00	25	1.65	1.73	4.85
49	5.00	25	1.27	1.28	0.79
50	5.00	60	1.14	1.12	1.75
51	5.50	75	1.27	1.39	9.45
52	5.50	35	2.16	2.26	4.63
53	5.50	65	1.40	1.55	10.71
54	5.50	70	1.14	1.13	0.88
55	5.50	65	0.89	0.90	0.56
56	6.00	70	0.76	0.79	3.82
57	6.25	60	1.27	1.26	0.79
58	6.25	135	0.64	0.66	3.13
59	7.00	65	1.78	1.79	0.56
60	7.00	160	0.89	0.91	2.25
61	7.00	300	0.64	0.66	3.13
62	7.00	85	0.76	0.78	2.63
63	7.00	220	0.64	0.65	1.56
64	7.50	100	0.64	0.71	10.94
65	7.50	105	0.64	0.68	6.25
66	7.50	110	0.64	0.64	0.00
67	7.50	45	1.14	1.15	0.88
68	7.50	30	2.41	2.41	0.00
69	7.50	25	2.29	2.30	0.44
70	119.40	77	6.73	6.85	1.78
71	119.52	250	1.65	1.73	4.85

Sl. No.	Input Parameters		Observations		% Error
	Total explosive charge per blast (kg)	Distance from blast location to monitoring point (m)	Field studies	Modelling studies	
			Peak Particle Velocity (mm/s)	Peak Particle Velocity (mm/s)	
72	119.52	88	2.16	2.17	0.46
73	119.52	200	1.40	1.52	8.57
74	141.76	159	2.41	2.44	1.24
75	141.76	168	2.28	2.27	0.44
76	141.76	200	1.78	1.79	0.56
77	186.30	35	9.14	9.22	0.88
78	186.30	43	2.57	2.67	3.89
79	186.30	73	2.32	2.43	4.74
80	194.59	185	1.65	1.68	1.82
81	194.59	250	1.14	1.18	3.51
82	194.59	203	1.27	1.36	7.09
83	200.16	106	3.68	3.77	2.45
84	200.16	100	3.56	3.65	2.53
85	205.65	196	1.78	1.80	1.12
86	205.65	204	1.65	1.89	14.55
87	205.65	212	1.52	1.55	1.97
88	294.45	67	4.95	4.96	0.20
89	294.45	300	1.02	1.02	0.00
90	325.26	180	2.79	2.99	7.17
91	325.26	192	2.16	2.34	8.33
92	394.63	60	8.81	8.83	0.23
93	394.63	160	2.41	2.49	3.32

APPENDIX – V (MATLAB CODES)

%% CURVE FITTING ANALYSIS OF HARD LIMESTONE FORMATION

SEISMIC ENERGY Vs. DISTANCE

```
function [fitresult, gof] = createFit1(Distance, SeismicEnergy)
% SETTING MATLAB FOR FIT ANALYSIS
clc
clear
% INPUTTING LIMESTONE FORMATION DATA FOR ANALYSIS
load limestone_formation
% Fit: 'Limestone Formation'.
[xData, yData] = prepareCurveData( Distance, SeismicEnergy );
% Set up fittype and options.
ft = fittype( 'power1' );
opts = fitoptions( ft );
opts.Display = 'Off';
opts.Lower = [-Inf -Inf];
opts.StartPoint = [9165559707213.1 -3.17367429473067];
opts.Upper = [Inf Inf];
% Fit model to data.
[fitresult, gof] = fit( xData, yData, ft, opts )
% Plot fit with data.
Fig.( 'Name', 'Limestone Formation' );
h = plot( fitresult, xData, yData );
set(gca,'XScale','log')
set(gca,'YScale','log')
legend(h,'SeismicEnergy vs. Distance','Limestone
Formation','Location','NorthEast');
% Label axes
xlabel( 'Distance' );
ylabel( 'SeismicEnergy' );
grid on
% *RESULTS*
% ---------
```

```
fitresult =
     General model Power1:
     fitresult(x) = a*x^b
     Coefficients (with 95% confidence bounds):
     a =   3.907e+12  (-4.2e+12, 1.201e+13)
     b =  -3.281  (-3.867, -2.694)
gof =
     sse: 7.6082e-15
     rsquare: 0.8468
     dfe: 114
     adjrsquare: 0.8437
     rmse: 8.1694e-06
```

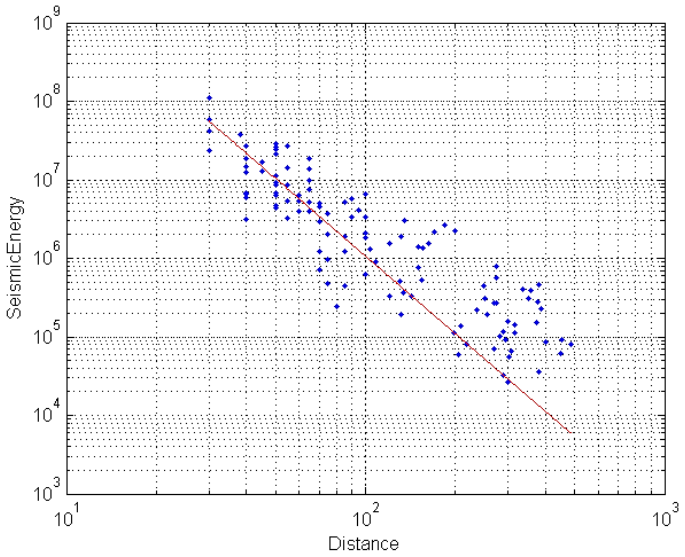

SEISMIC ENERGY Vs. PPV

```
% Fit: 'Limestone Formation'.
[xData, yData] = prepareCurveData( PPV, SeismicEnergy );
% Set up fittype and options.
ft = fittype( 'power1' );
opts = fitoptions( ft );
opts.Display = 'Off';
opts.Lower = [-Inf -Inf];
opts.StartPoint = [297163.873522685 0.904122305048337];
opts.Upper = [Inf Inf];
% Fit model to data.
[fitresult, gof] = fit( xData, yData, ft, opts )
% Plot fit with data.
Fig.( 'Name', 'Limestone Formation' );
h = plot( fitresult, xData, yData);
set(gca,'XScale','log')
set(gca,'YScale','log')
legend( h, 'SeismicEnergy vs. PPV', 'Limestone Formation',
'Location', 'NorthEast' );
% Label axes
xlabel( 'PPV' );
ylabel( 'SeismicEnergy' );
grid on
% *RESULTS*
% ---------
```

```
fitresult =
     General model Power1:
     fitresult(x) = a*x^b
     Coefficients (with 95% confidence bounds):
     a =   2.855e+04  (1.487e+04, 4.224e+04)
     b =   1.702  (1.594, 1.81)
gof =
     sse: 2.0735e-15
     rsquare: 0.9037
     dfe: 114
     adjrsquare: 0.9029
     rmse: 4.2648e-06
```

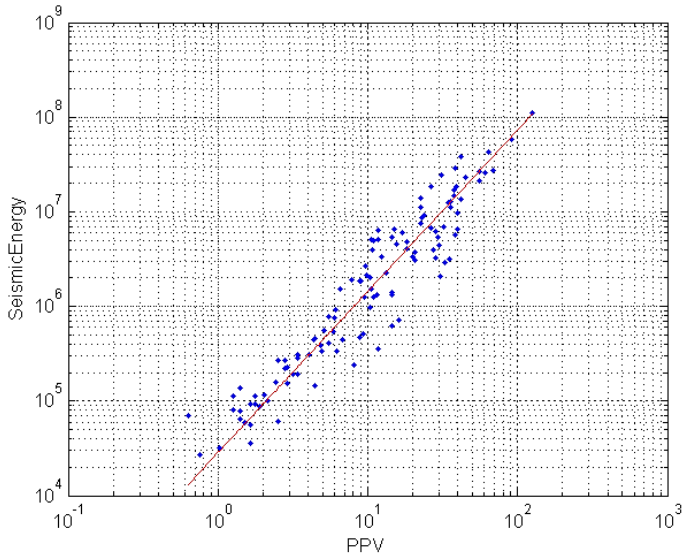

SEISMIC ENERGY Vs. SCALED DISTANCE

```
% Fit: 'Limestone Formation'.
[xData, yData] = prepareCurveData( SD, SeismicEnergy );
% Set up fittype and options.
ft = fittype( 'power1' );
opts = fitoptions( ft );
opts.Display = 'Off';
opts.Lower = [-Inf -Inf];
opts.StartPoint = [12969587721.1675 -3.03192412300106];
opts.Upper = [Inf Inf];
% Fit model to data.
[fitresult, gof] = fit( xData, yData, ft, opts )
% Plot fit with data.
Fig.( 'Name', 'Limestone Formation' );
h = plot( fitresult, xData, yData);
set(gca,'XScale','log')
set(gca,'YScale','log')
legend( h, 'SeismicEnergy vs. SD', 'Limestone Formation', 'Location',
'NorthEast' );
% Label axes
xlabel( 'SD' );
ylabel( 'SeismicEnergy' );
grid on
% *RESULTS*
% ---------
```

```
fitresult =
     General model Power1:
     fitresult(x) = a*x^b
     Coefficients (with 95% confidence bounds):
     a =   6.457e+09  (3.113e+09, 9.801e+09)
     b =  -3.064  (-3.381, -2.746)
gof =
     sse: 4.2531e-15
     rsquare: 0.8026
     dfe: 114
     adjrsquare: 0.8008
     rmse: 6.1080e-06
```

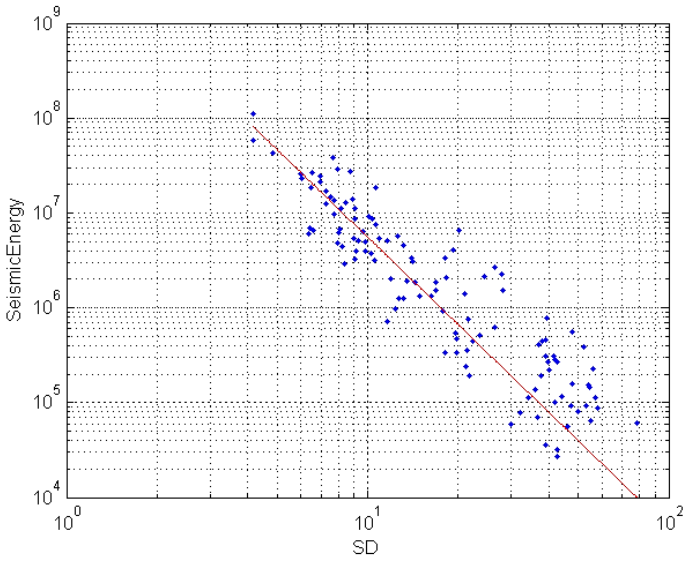


```
% END OF CURVE FITTING ANALYSIS OF HARD LIMESTONE FORMATION
```

%% CURVE FITTING ANALYSIS OF SOFT LIMESTONE FORMATION

SEISMIC ENERGY Vs. DISTANCE

```
function [fitresult, gof] = createFit1(Distance, SeismicEnergy)
% SETTING MATLAB FOR FIT ANALYSIS
clc
clear
% INPUTTING SOFT LIMESTONE FORMATION DATA FOR ANALYSIS
load SOFT_LIMESTONE_formation
% Fit: 'SOFT LIMESTONE Formation'.
[xData, yData] = prepareCurveData( Distance, SeismicEnergy );
% Set up fittype and options.
ft = fittype( 'power1' );
opts = fitoptions( ft );
opts.Display = 'Off';
opts.Lower = [-Inf -Inf];
opts.StartPoint = [9165559707213.1 -3.17367429473067];
opts.Upper = [Inf Inf];
% Fit model to data.
[fitresult, gof] = fit( xData, yData, ft, opts )
% Plot fit with data.
Fig.( 'Name', 'SOFT LIMESTONE Formation' );
h = plot( fitresult, xData, yData );
set(gca,'XScale','log')
set(gca,'YScale','log')
legend(h,'SeismicEnergy vs. Distance','SOFT LIMESTONE Formation',...
    'Location','NorthEast');
% Label axes
xlabel( 'Distance' );
ylabel( 'SeismicEnergy' );
grid on
% *RESULTS*
% ---------
           fitresult =
                General model Power1:
                fitresult(x) = a*x^b
```

```
        Coefficients (with 95% confidence bounds):
        a =   4.515e+09  (-7.979e+09, 1.701e+10)
        b =  -2.004  (-2.568, -1.439)
    gof =
        sse: 1.8982e+11
        rsquare: 0.7797
        dfe: 35
        adjrsquare: 0.7706
        rmse: 7.3644e+04
```

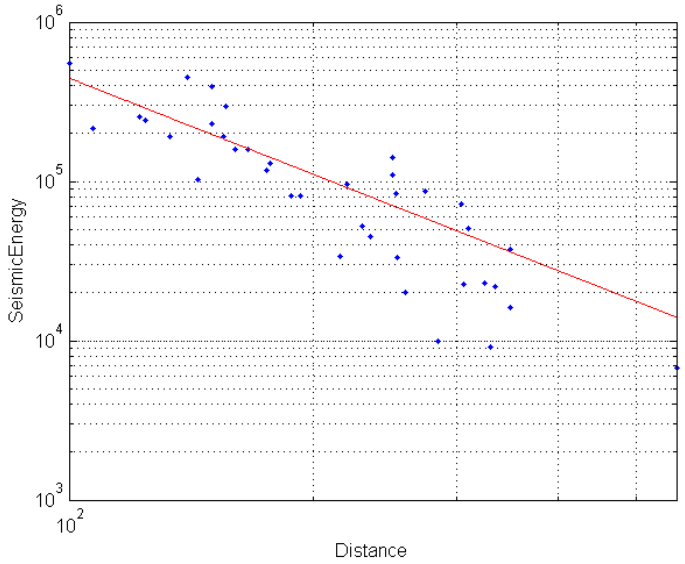

SEISMIC ENERGY Vs. PPV

```
% Fit: 'SOFT LIMESTONE Formation'.
[xData, yData] = prepareCurveData( PPV, SeismicEnergy );
% Set up fittype and options.
ft = fittype( 'power1' );
opts = fitoptions( ft );
opts.Display = 'Off';
opts.Lower = [-Inf -Inf];
opts.StartPoint = [297163.873522685 0.904122305048337];
opts.Upper = [Inf Inf];
% Fit model to data.
[fitresult, gof] = fit( xData, yData, ft, opts )
% Plot fit with data.
Fig.( 'Name', 'SOFT LIMESTONE Formation' );
h = plot( fitresult, xData, yData);
set(gca,'XScale','log')
set(gca,'YScale','log')
legend( h, 'SeismicEnergy vs. PPV', 'SOFT LIMESTONE Formation',...
    'Location', 'NorthWest' );
% Label axes
xlabel( 'PPV' );
ylabel( 'SeismicEnergy' );
grid on
% *RESULTS*
% ---------
          fitresult =
               General model Power1:
               fitresult(x) = a*x^b
               Coefficients (with 95% confidence bounds):
               a =   4.735e+04  (3.488e+04, 5.981e+04)
```

```
        b =   0.7555(0.6512, 0.8598)
gof =
        sse: 6.0169e+10
        rsquare: 0.8985
        dfe: 35
        adjrsquare: 0.8956
        rmse: 4.1462e+04
```

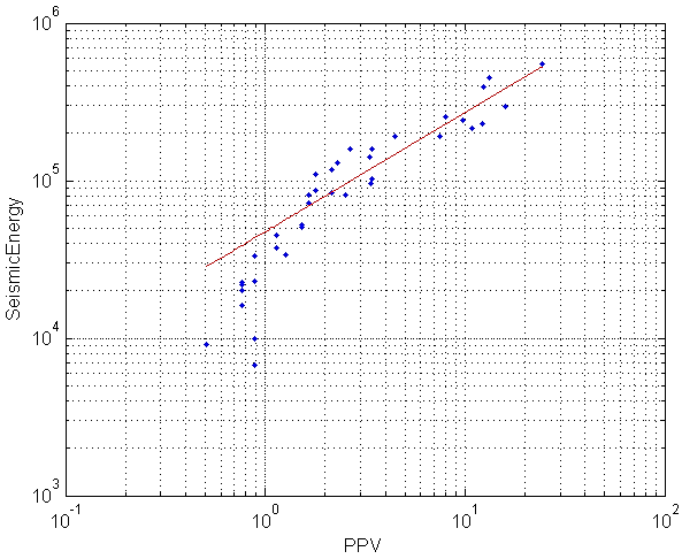

SEISMIC ENERGY Vs. SCALED DISTANCE

```
% Fit: 'SOFT LIMESTONE Formation'.
[xData, yData] = prepareCurveData( SD, SeismicEnergy );
% Set up fittype and options.
ft = fittype( 'power1' );
opts = fitoptions( ft );
opts.Display = 'Off';
opts.Lower = [-Inf -Inf];
opts.StartPoint = [12969587721.1675 -3.03192412300106];
opts.Upper = [Inf Inf];
% Fit model to data.
[fitresult, gof] = fit( xData, yData, ft, opts )
% Plot fit with data.
Fig.( 'Name', 'SOFT LIMESTONE Formation' );
h = plot( fitresult, xData, yData);
set(gca,'XScale','log')
set(gca,'YScale','log')
legend( h, 'SeismicEnergy vs. SD', 'SOFT LIMESTONE Formation',...
    'Location', 'NorthEast' );
% Label axes
xlabel( 'SD' );
ylabel( 'SeismicEnergy' );
grid on
% *RESULTS*
% ---------
          fitresult =
               General model Power1:
               fitresult(x) = a*x^b
               Coefficients (with 95% confidence bounds):
               a =   5.127e+08  (-4.749e+08, 1.5e+09)
               b =  -2.365  (-2.964, -1.766)
          gof =
```

```
sse: 1.4488e+11
rsquare: 0.7556
dfe: 35
adjrsquare: 0.7486
rmse: 6.4338e+04
```

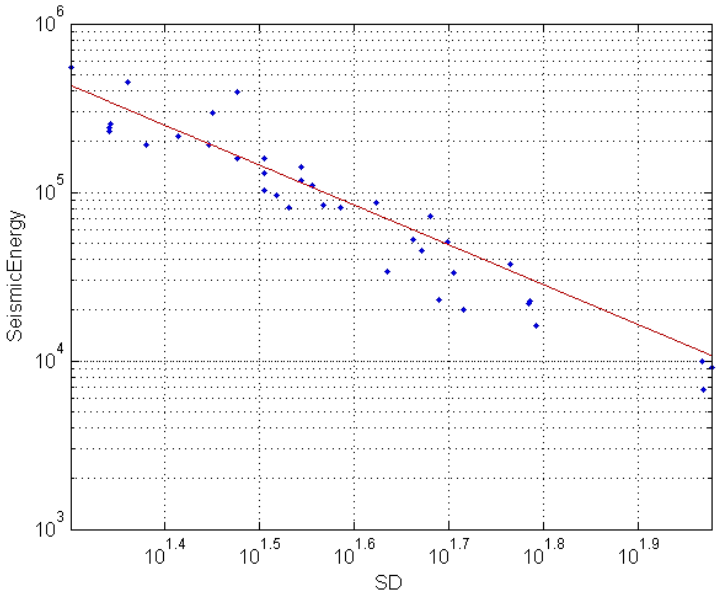


```
% END OF CURVE FITTING ANALYSIS OF SOFT LIMESTONE FORMATION
```

Published with MATLAB® R2013a

% ANOVA ANALYSIS OF LIMESTONE FORMATION

```
% function Limestone_anova
d = dataset(SeismicEnergy, Distance, SD, MCD, PPV);
lm = LinearModel.fit(d,'SeismicEnergy ~ Distance + SD + MCD + PPV')
anova(lm)
end
% One-way ANOVA analysis
% [SeismicEnergy,ANOVATAB,STATS] = anova1(MCD, SD, PPV, Distance);
```

%% CURVE FITTING ANALYSIS OF COAL FORMATION

SEISMIC ENERGY Vs. DISTANCE

```
function [fitresult, gof] = createFit(Distance, SeismicEnergy)
% SETTING MATLAB FOR FIT ANALYSIS
clc
clear
% INPUTTING COAL FORMATION DATA FOR ANALYSIS
load coal_formation
% Fit: 'Coal Formation'.
[xData1, yData1] = prepareCurveData( Distance, SeismicEnergy );
% Set up fittype and options.
ft = fittype( 'power1' );
opts = fitoptions( ft );
opts.Display = 'Off';
opts.Lower = [-Inf -Inf];
opts.StartPoint = [1211851681.04289 -2.35216753007063];
opts.Upper = [Inf Inf];
% Fit model to data.
```

```
[fitresult, gof] = fit( xData1, yData1, ft, opts )
% Plot fit with data.
Fig.( 'Name', 'Coal Formation' );
h = plot( fitresult, xData1, yData1 );
set(gca,'XScale','log')
set(gca,'YScale','log')
legend( h, 'SeismicEnergy vs. Distance', 'Coal Formation',
'Location', 'NorthEast' );
% Label axes
xlabel( 'Distance' );
ylabel( 'SeismicEnergy' );
grid on
% *RESULTS*
% ---------
```

fitresult =

General model Power1:
*fitresult(x) = a*x^b*
Coefficients (with 95% confidence bounds):
a = 6.924e+08 (2.361e+08, 1.149e+09)
b = -2.14 (-2.362, -1.917)

gof =

sse: 1.5636e-12
rsquare: 0.8696
dfe: 84
adjrsquare: 0.8681
rmse: 1.3643e-05

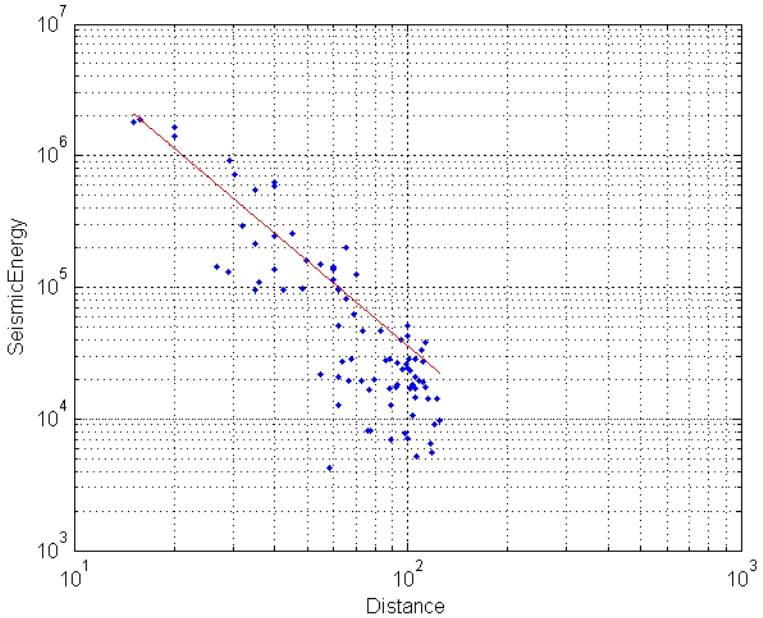

SEISMIC ENERGY Vs. PPV

```
%function [fitresult, gof] = createFit2(PPV, SeismicEnergy)
% Fit: 'Coal Formation'.
[xData2, yData2] = prepareCurveData( PPV, SeismicEnergy );
% Set up fittype and options.
ft = fittype( 'power1' );
opts = fitoptions( ft );
opts.Display = 'Off';
```

```
opts.Lower = [-Inf -Inf];
opts.StartPoint = [62685.8194292953 5.78626256721044];
opts.Upper = [Inf Inf];
% Fit model to data.
[fitresult, gof] = fit( xData2, yData2, ft, opts )
% Plot fit with data.
Fig.( 'Name', 'Coal Formation' );
h = plot( fitresult, xData2, yData2 );
set(gca,'XScale','log')
set(gca,'YScale','log')
legend( h, 'SeismicEnergy vs. PPV', 'Coal Formation', 'Location',
'NorthEast' );
% Label axes
xlabel( 'PPV' );
ylabel( 'SeismicEnergy' );
grid on

% *RESULTS*
% ---------
```

fitresult =

General model Power1:
*fitresult(x) = a*x^b*
Coefficients (with 95% confidence bounds):
a = 2.18e+04 (1.152e+04, 3.209e+04)
b = 1.377 (1.216, 1.537)

gof =

sse: 2.0052e-12
rsquare: 0.8328
dfe: 84
adjrsquare: 0.8308
rmse: 1.5450e-05

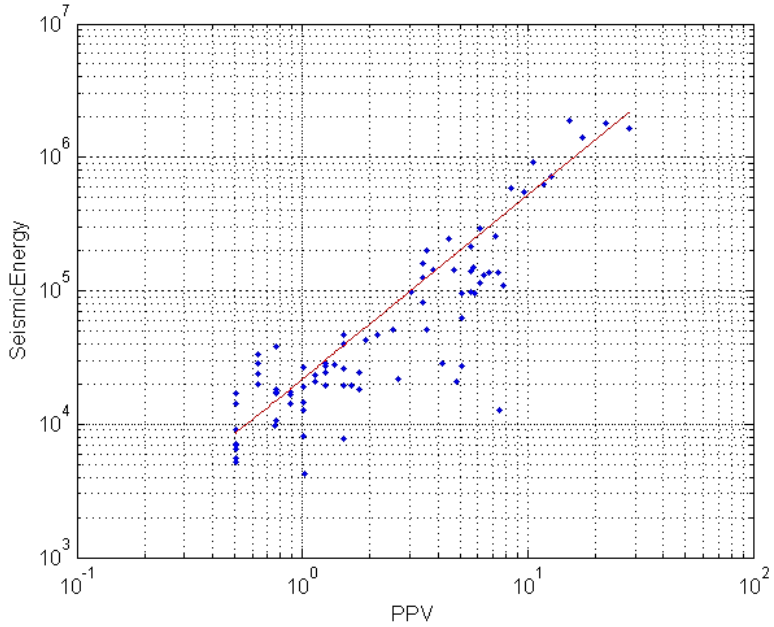

SEISMIC ENERGY Vs. SD

```
% function [fitresult, gof] = createFit1(SD, SeismicEnergy)
% Fit: 'Coal Formation'.
[xData, yData] = prepareCurveData( SD, SeismicEnergy );
% Set up fittype and options.
```

```
ft = fittype( 'power1' );
opts = fitoptions( ft );
opts.Display = 'Off';
opts.Lower = [-Inf -Inf];
opts.StartPoint = [467686629.285606 -2.33727623669886];
opts.Upper = [Inf Inf];
% Fit model to data.
[fitresult, gof] = fit( xData, yData, ft, opts )
% Plot fit with data.
Fig.( 'Name', 'Coal Formation' );
h = plot( fitresult, xData, yData );
set(gca,'XScale','log')
set(gca,'YScale','log')
legend( h, 'SeismicEnergy vs. SD', 'Coal Formation', 'Location',
'NorthEast' );
% Label axes
xlabel( 'SD' );
ylabel('SeismicEnergy');
grid on

% *RESULTS*
% ---------
```

```
fitresult =
     General model Power1:
     fitresult(x) = a*x^b
     Coefficients (with 95% confidence bounds):
     a =   3.066e+08  (1.249e+08, 4.884e+08)
     b =      -2.151  (-2.382, -1.921)
gof =
     sse: 1.5792e-12
     rsquare: 0.8683
     dfe: 84
     adjrsquare: 0.8668
     rmse: 1.3711e-05
```

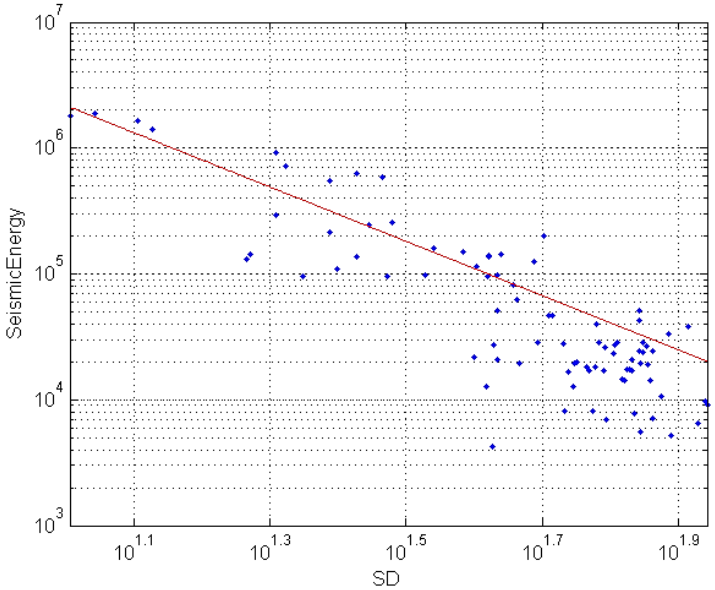


```
% END OF CURVE FITTING ANALYSIS
```

Published with MATLAB® R2013a

% ANOVA ANALYSIS OF COAL FORMATION

```
% function Coal_anova
d = dataset(SeismicEnergy, Distance, SD, MCD, PPV);
lm = LinearModel.fit(d,'SeismicEnergy ~ Distance + SD + MCD + PPV')
anova(lm)
end
% One-way ANOVA analysis
% [SeismicEnergy,ANOVATAB,STATS] = anova1(MCD, SD, PPV, Distance);
```

%% CURVE FITTING ANALYSIS OF SANDSTONE BENCH FORMATION

SEISMIC ENERGY Vs. SCALED DISTANCE

```
function [fitresult, gof] = createFit(SD, SeismicEnergy)
% SETTING MATLAB FOR FIT ANALYSIS
clc
clear
% INPUTTING SANDSTONE BENCH FORMATION DATA FOR ANALYSIS
load sandstone_formation
% Fit: 'Sandstone bench formation'.
[xData, yData] = prepareCurveData( SD, SeismicEnergy );
% Set up fittype and options.
ft = fittype( 'power1' );
opts = fitoptions( ft );
opts.Display = 'Off';
opts.Lower = [-Inf -Inf];
opts.StartPoint = [2989746742948.72 -4.5143316120027];
opts.Upper = [Inf Inf];
% Fit model to data.
[fitresult, gof] = fit( xData, yData, ft, opts )
% Plot fit with data.
Fig.( 'Name', 'Sandstone bench formation' );
h = plot( fitresult, xData, yData );
set(gca,'XScale','log')
set(gca,'YScale','log')
legend( h, 'SeismicEnergy vs. SD', 'Sandstone bench formation',
'Location', 'NorthEast' );
% Label axes
xlabel( 'SD' );
ylabel( 'SeismicEnergy' );
grid on
% *RESULTS*
% ---------
```

```
           fitresult =
                General model Power1:
                fitresult(x) = a*x^b
                Coefficients (with 95% confidence bounds):
                a =    2.068e+11  (8.388e+09, 4.052e+11)
                b =    -3.573  (-3.935, -3.21)
           gof =
                sse: 6.5660e+13
                rsquare: 0.9479
                dfe: 41
                adjrsquare: 0.9467
                rmse: 1.2655e+06
```

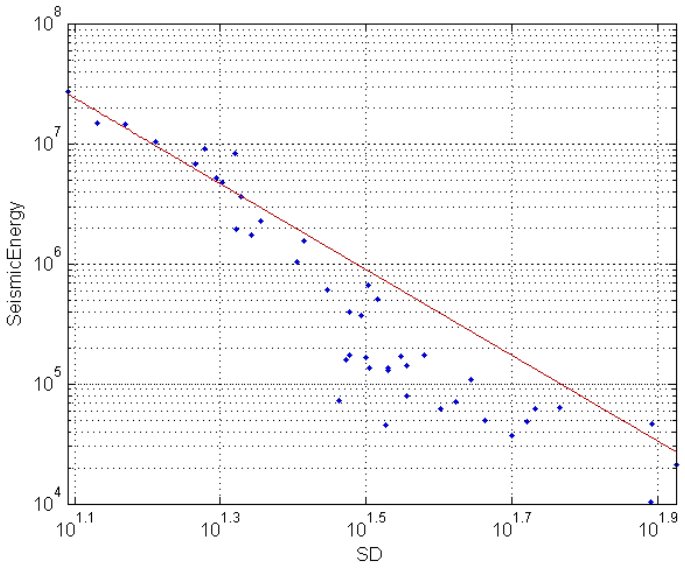

SEISMIC ENERGY Vs. PPV

```
%function [fitresult, gof] = createFit2(PPV, SeismicEnergy)
% Fit: 'Sandstone bench formation'.
[xData, yData] = prepareCurveData( PPV, SeismicEnergy );
% Set up fittype and options.
ft = fittype( 'power1' );
opts = fitoptions( ft );
opts.Display = 'Off';
opts.Lower = [-Inf -Inf];
opts.StartPoint = [30896.5304074331 2.41156124895953];
opts.Upper = [Inf Inf];
% Fit model to data.
[fitresult, gof] = fit( xData, yData, ft, opts )
% Plot fit with data.
Fig.( 'Name', 'Sandstone bench formation' );
h = plot( fitresult, xData, yData);
set(gca,'XScale','log')
set(gca,'YScale','log')
legend( h, 'SeismicEnergy vs. PPV', 'Sandstone bench formation',
'Location', 'NorthWest' );
% Label axes
xlabel( 'PPV' );
ylabel( 'SeismicEnergy' );
grid on

% *RESULTS*
% ---------
          fitresult =
               General model Power1:
               fitresult(x) = a*x^b
               Coefficients (with 95% confidence bounds):
               a =   1.208e+05  (7.176e+04, 1.698e+05)
               b =   1.37  (1.258, 1.482)
          gof =
               sse: 4.3761e+13
               rsquare: 0.9653
               dfe: 41
               adjrsquare: 0.9644
```

rmse: 1.0331e+06

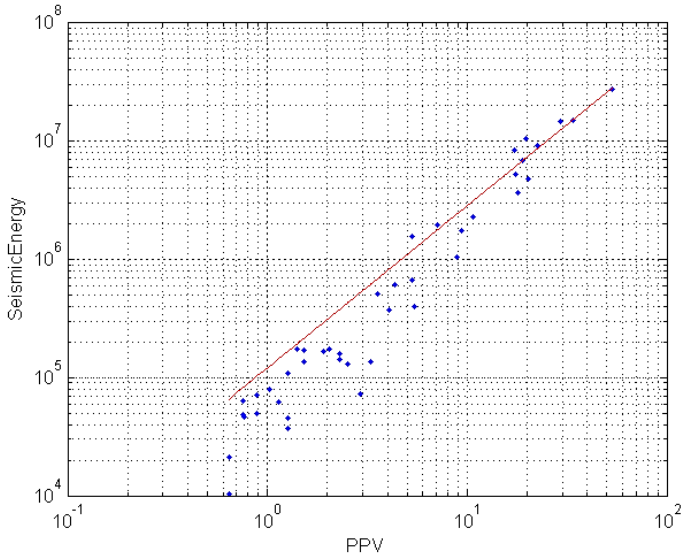


```
% END OF CURVE FITTING ANALYSIS
```

Published with MATLAB® R2013a

% ANOVA ANALYSIS OF SANDSTONE FORMATION

```
% function Limestone_anova
d = dataset(SeismicEnergy, Distance, SD, MCD, PPV);
lm = LinearModel.fit(d,'SeismicEnergy ~ Distance + SD + MCD + PPV')
anova(lm)
% One-way ANOVA analysis
end
```

%% CURVE FITTING ANALYSIS OF GRANITE FORMATION

SEISMIC ENERGY Vs. SCALED DISTANCE

```
function [fitresult, gof] = createFit(SD, SeismicEnergy)

% SETTING MATLAB FOR FIT ANALYSIS
clc
clear

% INPUTTING GRANITE FORMATION DATA FOR ANALYSIS
load granite_formation

% Fit: 'Granite Formation'.
[xData, yData] = prepareCurveData( SD, SeismicEnergy );

% Set up fittype and options.
ft = fittype( 'power1' );
opts = fitoptions( ft );
opts.Display = 'Off';
opts.Lower = [-Inf -Inf];
opts.StartPoint = [2646123.13859486 -0.889807383340468];
opts.Upper = [Inf Inf];

% Fit model to data.
```

```
[fitresult, gof] = fit( xData, yData, ft, opts )

% Plot fit with data.
Fig.( 'Name', 'Granite Formation' );
h = plot( fitresult, xData, yData, '*' );
set(gca,'XScale','log')
set(gca,'YScale','log')
legend( h, 'SeismicEnergy vs. SD', 'Granite Formation', 'Location',
'NorthEast' );

% Label axes
xlabel( 'SD' );
ylabel( 'SeismicEnergy' );
grid on

% *RESULTS*
% ---------
          fitresult =
               General model Power1:
               fitresult(x) = a*x^b
               Coefficients (with 95% confidence bounds):
               a =   2.267e+06  (1.763e+06, 2.77e+06)
               b =  -0.8236  (-0.8936, -0.7536)
          gof =
               sse: 8.8153e-10
               rsquare: 0.8485
               dfe: 92
               adjrsquare: 0.8469
               rmse: 3.0955e-04
```

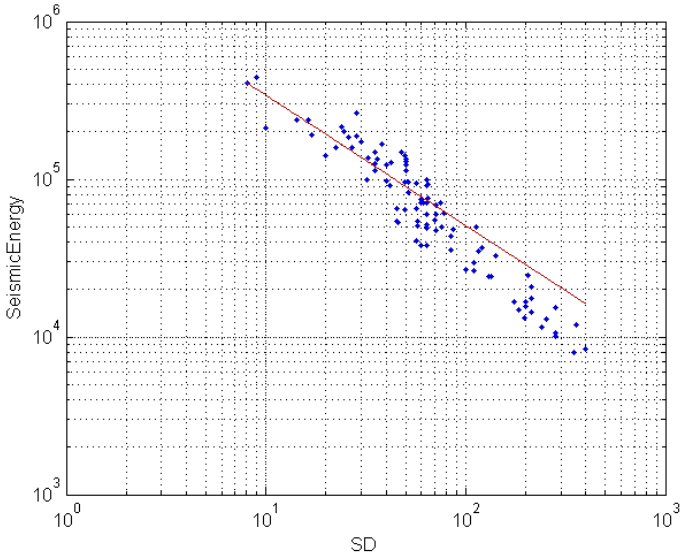

SEISMIC ENERGY Vs. PPV

```
%function [fitresult, gof] = createFit2(PPV, SeismicEnergy)
% Fit: 'Granite Formation'.
[xData, yData] = prepareCurveData( PPV, SeismicEnergy );
% Set up fittype and options.
ft = fittype( 'power1' );
opts = fitoptions( ft );
opts.Display = 'Off';
opts.Lower = [-Inf -Inf];
opts.StartPoint = [480238.42758864 -1.33327119384385];
```

```
opts.Upper = [Inf Inf];
% Fit model to data.
[fitresult, gof] = fit( xData, yData, ft, opts )
% Plot fit with data.
Fig.( 'Name', 'Granite Formation' );
h = plot( fitresult, xData, yData, '*' );
set(gca,'XScale','log')
set(gca,'YScale','log')
legend( h, 'SeismicEnergy vs. PPV', 'Granite Formation', 'Location',
'NorthWest' );
% Label axes
xlabel( 'PPV' );
ylabel( 'SeismicEnergy' );
grid on
% *RESULTS*
% ---------
```

```
fitresult =
     General model Power1:
     fitresult(x) = a*x^b
     Coefficients (with 95% confidence bounds):
     a =   5.878e+04  (5.258e+04, 6.499e+04)
     b =      0.8842  (0.8142, 0.9541)
gof =
     sse: 8.4863e-10 rsquare: 0.8542
     dfe: 92 adjrsquare: 0.8526
     rmse: 3.0371e-04
```

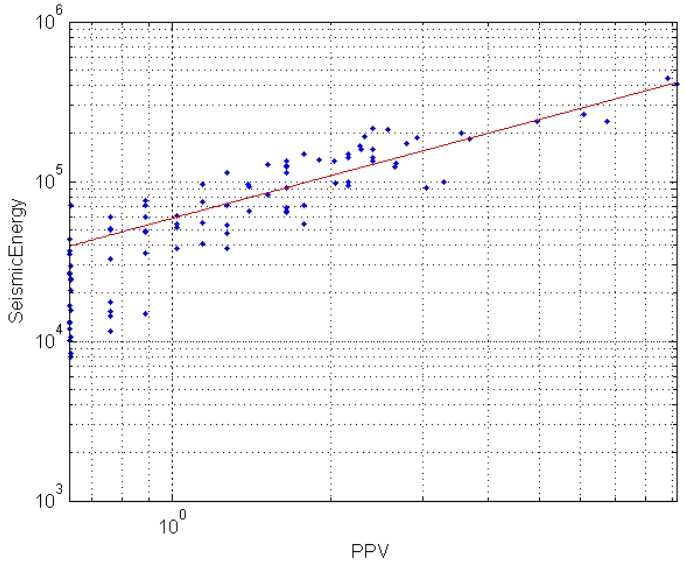


```
% END OF CURVE FITTING ANALYSIS
```

Published with MATLAB® R2013a

% ANOVA ANALYSIS OF GRANITE FORMATION

```
% function Limestone_anova
d = dataset(SeismicEnergy, Distance, SD, MCD, PPV);
lm = LinearModel.fit(d,'SeismicEnergy ~ Distance + SD + MCD + PPV')
anova(lm)
end
```

%% COMPARISON IN LIMESTONE FORMATION WITH BASIC CIRCUIT MODEL

```
function comparison_of_SE_and_EE

% MAKING MATLAB CODER READY FOR GIVING INPUTS
clear
clc

% LOADING INPUT DATA
load limestone_old_ckt

% EXTRACTING INPUT PARAMETERS FOR PLOTTING PURPOSE
x1=0:9;
x=transpose(x1);
y1=SE;
y2=EE;

% PLOTTING THE DATA FOR COMPARISON
Fig. % new Fig.
[hAx,hLine1,hLine2] = plotyy(x,y1,x,y2);
title('Seismic Energy Vs. Electrical Energy')
xlabel('Vibration Event Number')
ylabel(hAx(1),'Seismic Energy (\muJ)') % left y-axis
ylabel(hAx(2),'Electrical Energy (\muJ)') % right y-axis
%
```

Published with MATLAB® R2013a

%% COMPARISON IN LIMESTONE FORMATION WITH IMPROVED CIRCUIT MODEL IN HARD LIMESTONE FORMATION

```
% MAKING MATLAB CODER READY FOR GIVING INPUTS
clear
clc

% LOADING INPUT DATA
load limestone_new_ckt

% EXTRACTING INPUT PARAMETERS FOR PLOTTING PURPOSE
x1=0:57;
x=transpose(x1);
y1=SE;
y2=EE;

% PLOTTING THE DATA FOR COMPARISON
Fig. % new Fig.
[hAx,hLine1,hLine2] = plotyy(x,y1,x,y2);

title('Seismic Energy Vs. Electrical Energy')
xlabel('Vibration Event Number')

ylabel(hAx(1),'Seismic Energy (\muJ)') % left y-axis
ylabel(hAx(2),'Electrical Energy (\muJ)') % right y-axis
```

Published with MATLAB® R2013a

%% COMPARISON IN LIMESTONE FORMATION WITH IMPROVED CIRCUIT MODEL IN SOFT LIMESTONE FORMATION

```
% MAKING MATLAB CODER READY FOR GIVING INPUTS
clear
clc

% LOADING INPUT DATA
load soft_limestone

% EXTRACTING INPUT PARAMETERS FOR PLOTTING PURPOSE
x1=0:37;
x=transpose(x1);
y1=SE;
y2=EE;

% PLOTTING THE DATA FOR COMPARISON
Fig. % new Fig.
[hAx,hLine1,hLine2] = plotyy(x,y1,x,y2);

%set(hLine1,'marker','s')
set(hLine2,'marker','*')
hLine2.LineWidth = 3;
set(hLine1,'marker','s','color','blue')

%set(hLine2,'marker','x','color','blue')
title('Seismic Energy Vs. Electrical Energy')
xlabel('Vibration Event Number')
ylabel(hAx(1),'Seismic Energy (\muJ)') % left y-axis
ylabel(hAx(2),'Electrical Energy (\muJ)')% right y-axis

%ylabel(hAx(2),'Electrical Energy (\muJ)', 'color', 'red')
grid off

%
```

Published with MATLAB® R2013a

%% COMPARISON IN COAL FORMATION

```
function comparison_of_EE_and_SE
% MAKING MATLAB CODER READY FOR GIVING INPUTS
clear
clc

% LOADING INPUT DATA
load coal

% EXTRACTING INPUT PARAMETERS FOR PLOTTING PURPOSE
x1=0:36;
x=transpose(x1);
y1=SE;
y2=EE;

% PLOTTING THE DATA FOR COMPARISON
Fig. % new Fig.
[hAx,hLine1,hLine2] = plotyy(x,y1,x,y2);

title('Seismic Energy Vs. Electrical Energy')
```

```
xlabel('Vibration Event Number')

ylabel(hAx(1),'Seismic Energy (\muJ)') % left y-axis
ylabel(hAx(2),'Electrical Energy (\muJ)') % right y-axis
```

Published with MATLAB® R2013a

%% COMPARISON IN SANDSTONE FORMATION

```
function comparison_of_EE_and_SE

% MAKING MATLAB CODER READY FOR GIVING INPUTS
clear
clc

% LOADING INPUT DATA
load sandstone

% EXTRACTING INPUT PARAMETERS FOR PLOTTING PURPOSE
x1=0:36;
x=transpose(x1);
y1=SE;
y2=EE;

% PLOTTING THE DATA FOR COMPARISON
Fig. % new Fig.
[hAx,hLine1,hLine2] = plotyy(x,y1,x,y2);
title('Seismic Energy Vs. Electrical Energy')
xlabel('Vibration Event Number')
ylabel(hAx(1),'Seismic Energy (\muJ)') % left y-axis
ylabel(hAx(2),'Electrical Energy (\muJ)') % right y-axis
```

Published with MATLAB® R2013a

%% COMPARISON IN GRANITIC ROCK FORMATION

```
function comparison_of_EE_and_SE

% MAKING MATLAB CODER READY FOR GIVING INPUTS
clear
clc

% LOADING INPUT DATA
load granite

% EXTRACTING INPUT PARAMETERS FOR PLOTTING PURPOSE
x1=0:94;
x=transpose(x1);
y1=SE;
y2=EE;
```

```
% PLOTTING THE DATA FOR COMPARISON
Fig. % new Fig.
[hAx,hLine1,hLine2] = plotyy(x,y1,x,y2);

title('Seismic Energy Vs. Electrical Energy')
xlabel('Vibration Event Number')

ylabel(hAx(1),'Seismic Energy (\muJ)') % left y-axis
ylabel(hAx(2),'Electrical Energy (\muJ)') % right y-axis
```

Published with MATLAB® R2013a

%% CURVE FITTING ANALYSIS FOR MODELLING RESULTS OF LIMESTONE FORMATION

Model_PPV Vs. Field_PPV

```
function comparison_of_field_results_and_model_results
% MAKING MATLAB CODER READY FOR GIVING INPUTS
clear
clc
% LOADING INPUT DATA
load limestone_model
% Fit: 'Limestone Formation'.
[xData, yData] = prepareCurveData( Field_PPV, Model_PPV );
% Set up fittype and options.
ft = fittype( 'power1' );
opts = fitoptions( ft );
opts.Display = 'Off';
opts.Lower = [-Inf -Inf];
opts.StartPoint = [9165559707213.1 -3.17367429473067];
opts.Upper = [Inf Inf];
% Fit model to data.
[fitresult, gof] = fit( xData, yData, ft, opts )
% Plot fit with data.
Fig.( 'Name', 'Limestone Formation Modelling Results' );
h = plot( fitresult, xData, yData );
set(gca,'XScale','log')
set(gca,'YScale','log')
legend(h,'Model PPV Vs. Field PPV', 'Limestone Formation',...
 'Location', 'Northwest');
% Label axes
xlabel( 'Field PPV (mm/s)' );
ylabel( 'Model PPV (mm/s)' );
grid on
% *RESULTS*
% ---------
```

```
fitresult =
     General model Power1:
     fitresult(x) = a*x^b
     Coefficients (with 95% confidence bounds)
     a =    0.9977   (0.9846, 1.011)
     b =    1.005    (1.001, 1.008)
gof =
     sse: 12.0273e-10
     rsquare: 0.8597
     adjrsquare: 0.8597
```

```
rmse: 0.3248
dfe: 114
```

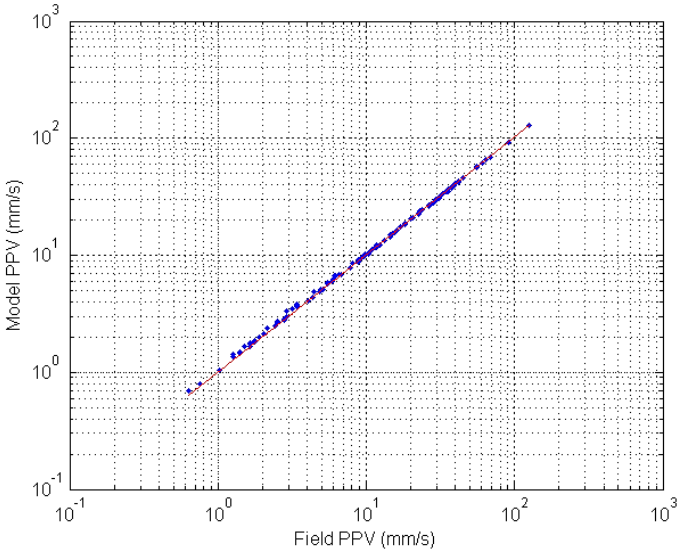

Published with MATLAB® R2013a

CREATEFIT(MODEL PPV, FIELD PPV, ELECTRICAL VOLTAGE)

```
function [fitresult, gof] = createFit(Model_PPV, Field_PPV,...
    Electrical_Voltage)
% SETTING MATLAB FOR FIT ANALYSIS
clc
clear
% LOADING INPUT DATA
load limestone_model
% Fit: 'Limestone'
[xData, yData, zData] = prepareSurfaceData( Electrical_Voltage, ...
    Field_PPV, Model_PPV );
% Set up fittype and options.
ft = fittype( 'biharmonicinterp' );
opts = fitoptions( ft );
opts.Normalize = 'on';
% Fit model to data.
[fitresult, gof] = fit( [xData, yData], zData, ft, opts )
% Plot fit with data.
Fig.( 'Name', 'Limestone' );
h = plot( fitresult, [xData, yData], zData );
legend( h, 'Limestone', 'Model PPV vs. Field PPV, Electrical
Voltage', 'Location', 'NorthWest' );
% Label axes
xlabel( 'Model PPV (mm/s)' );
ylabel( 'Field PPV (mm/s)' );
zlabel( 'Electrical Voltage (mV)' );
grid on
colorbar
view( -16.5, 26.0 );
          fitresult(x,y) =
               biharmonic surface computed from p
               where x is normalized by mean 1207 and std 1315
               and where y is normalized by mean 18.17 and std 19.79
               Coefficients: p = coefficient structure
```

```
gof =
      sse: 0.308e-7
      rsquare: 0.86000
      dfe: 0
      adjrsquare: 0.86000
      rmse: NaN
```

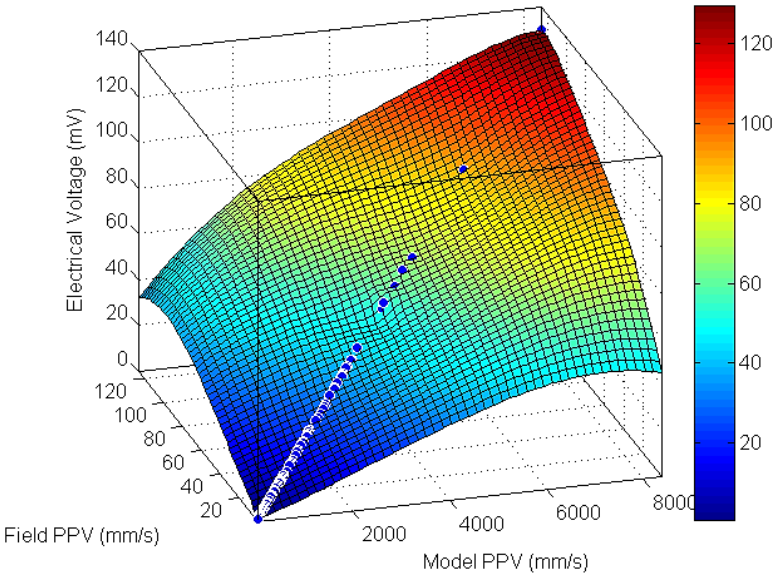

Published with MATLAB® R2013a

%% CURVE FITTING ANALYSIS FOR MODELLING RESULTS OF COAL FORMATION
Model_PPV Vs. Field_PPV

```
function comparison_of_field_results_and_model_results
clc
load Coal_model
 [xData, yData] = prepareCurveData( Field_PPV, Model_PPV );
ft = fittype( 'power1' );
opts = fitoptions( ft );
opts.Display = 'Off';
opts.Lower = [-Inf -Inf];
opts.StartPoint = [9165559707213.1 -3.17367429473067];
opts.Upper = [Inf Inf];
 [fitresult, gof] = fit( xData, yData, ft, opts )
Fig.( 'Name', 'Coal Formation Modelling Results' );
h = plot( fitresult, xData, yData );
set(gca,'XScale','log')
set(gca,'YScale','log')
legend(h,'Model PPV Vs. Field PPV',
'Coal Formation','Location','Northwest');
xlabel( 'Field PPV (mm/s)' );
ylabel( 'Model PPV (mm/s)' );
```

```
fitresult =
     General model Power1:
     fitresult(x) = a*x^b
     Coefficients (with 95% confidence bounds):
     a =  1.062  (1.032, 1.092)
     b =  0.9845  (0.9733, 0.9957)
gof =
```

```
    sse: 0.7186e-07
    rsquare: 0.8590
    dfe: 34
    adjrsquare: 0.8590
    rmse: 0.1454
```

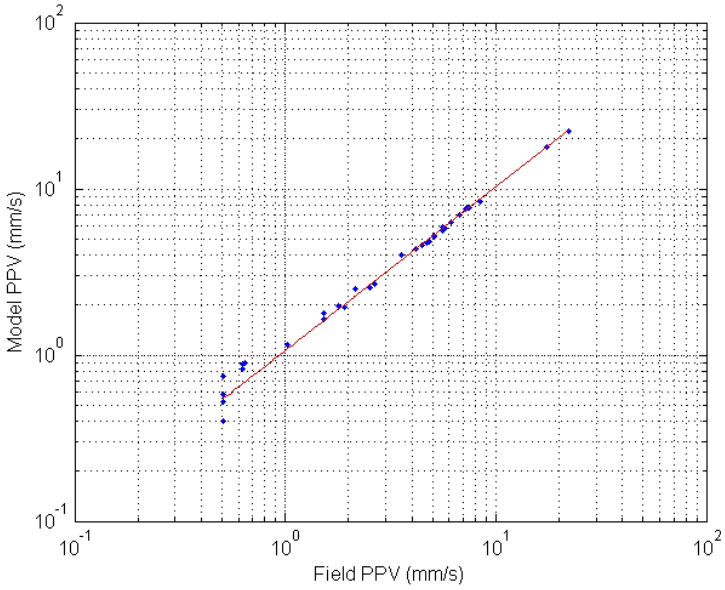

Published with MATLAB® R2013a

CREATEFIT(MODEL PPV, FIELD PPV, ELECTRICAL VOLTAGE)

```
function [fitresult, gof] = createFit(Electrical_Voltage, Field_PPV,
Model_PPV)
clc
clear
load coal_model
 [xData, yData, zData] = prepareSurfaceData( Electrical_Voltage,...
    Field_PPV, Model_PPV );
ft = 'linearinterp';
opts = fitoptions( ft );
opts.Normalize = 'on';
 [fitresult, gof] = fit( [xData, yData], zData, ft, opts )
Fig.( 'Name', 'Coal' );
h = plot( fitresult, [xData, yData], zData );
legend( h, 'Coal', 'Model PPV vs. Electrical Voltage, Field PPV',...
    'Location', 'NorthEast' );
xlabel( 'Electrical Voltage (mV)' );
ylabel( 'Field PPV (mm/s)' );
zlabel( 'Model PPV (mm/s)' );
grid on
colorbar
view( -17.5, 46.0 );
          gof =
               sse: 0.0013
               rsquare: 0.820000
               dfe: 0
               adjrsquare: 0.810000
               rmse: NaN
```

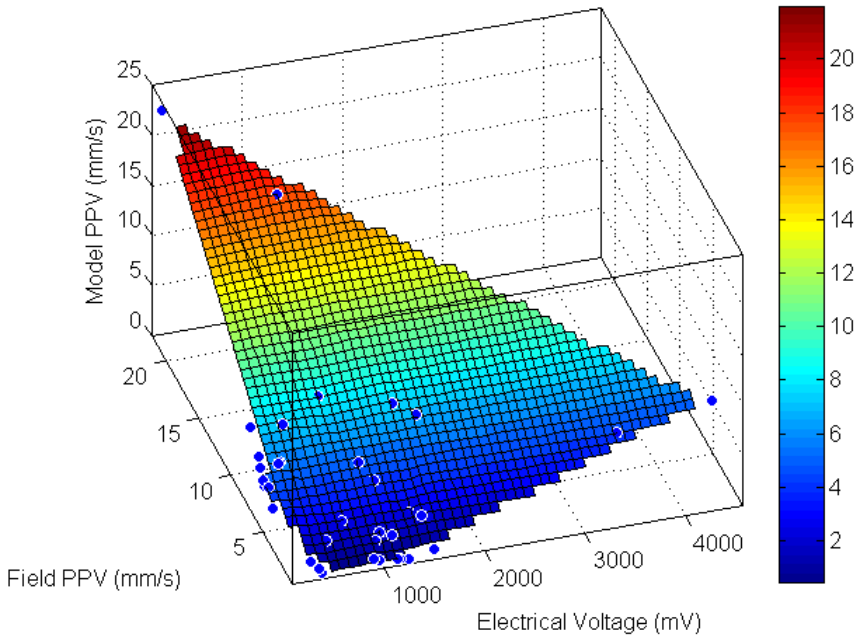

Published with MATLAB® R2013a

%% CURVE FITTING ANALYSIS FOR MODELLING RESULTS OF SANDSTONE BENCH FORMATION

Model_PPV Vs. Field_PPV

```
load Sandstone_model
 [xData, yData] = prepareCurveData( Field_PPV, Model_PPV );
ft = fittype( 'power1' );
opts = fitoptions( ft );
opts.Display = 'Off';
opts.Lower = [-Inf -Inf];
opts.StartPoint = [9165559707213.1 -3.17367429473067];
opts.Upper = [Inf Inf];
 [fitresult, gof] = fit( xData, yData, ft, opts )
Fig.( 'Name', 'Sandstone bench formation Modelling Results' );
h = plot( fitresult, xData, yData );
set(gca,'XScale','log')
set(gca,'YScale','log')
legend(h,'Model PPV Vs. Field PPV','Sandstone bench
formation','Location',...
    'Northwest');
xlabel( 'Field PPV (mm/s)' );
ylabel( 'Model PPV (mm/s)' );
```

```
           fitresult =
                General model Power1:
                fitresult(x) = a*x^b
                Coefficients (with 95% confidence bounds):
                a = 1.146  (1.021, 1.271)
                b = 0.9843  (0.9525, 1.016)
           gof =
                sse: 35.291e-7
                rsquare: 0.8542
                dfe: 41
                adjrsquare: 0.8541
```

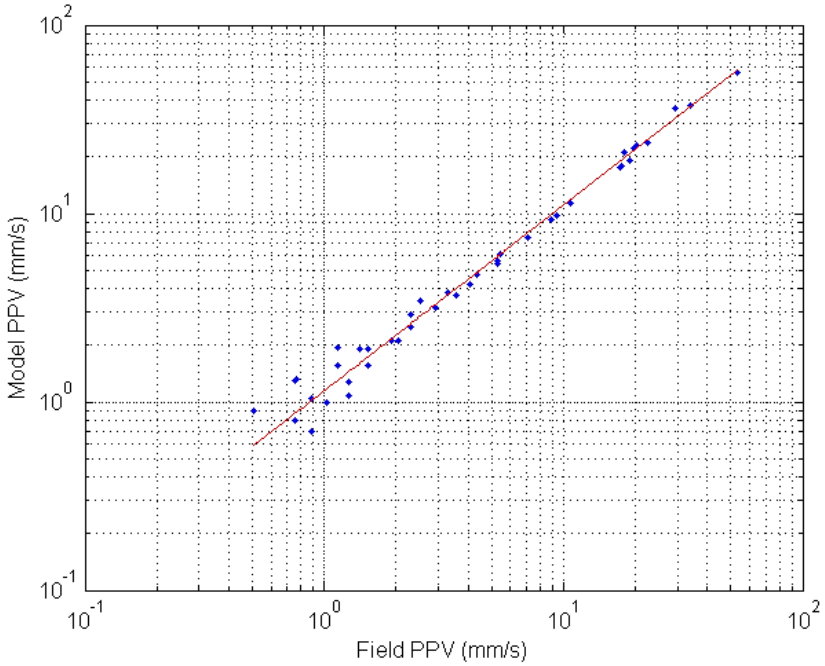

Published with MATLAB® R2013a

CREATEFIT(MODEL PPV, FIELD PPV, ELECTRICAL VOLTAGE)

```
function [fitresult, gof] = createFit(Model_PPV, Field_PPV, ...
    Electrical_Voltage)
load Sandstone_model
 [xData, yData, zData] = prepareSurfaceData( Electrical_Voltage, ...
    Model_PPV, Field_PPV );
ft = 'linearinterp';
opts = fitoptions( ft );
opts.Normalize = 'on';
 [fitresult, gof] = fit( [xData, yData], zData, ft, opts )
Fig.( 'Name', 'Sandstone' );
h = plot( fitresult, [xData, yData], zData );
legend( h, 'Sandstone', 'Field PPV vs. Electrical Voltage, Model
PPV',...
    'Location', 'NorthEast' );
xlabel( 'Electrical Voltage (mV)' );
ylabel( 'Model PPV (mm/s)' );
zlabel( 'Field PPV (mm/s)' );
colorbar
```

```
gof =
     sse: 6.5130e-29
     rsquare: 0.85000
     dfe: 0
     adjrsquare: 0.84000
     rmse: NaN
```

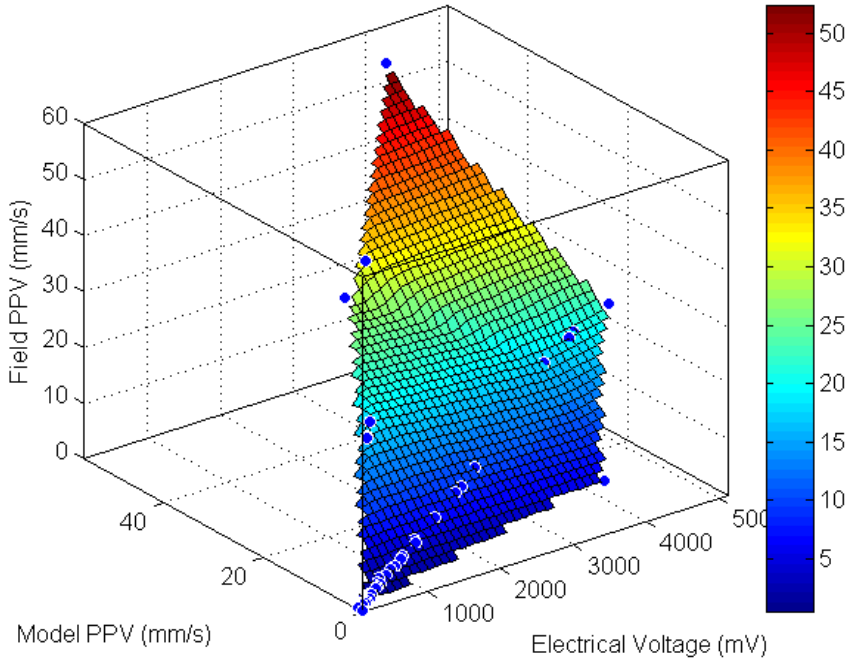

Published with MATLAB® R2013a

%% CURVE FITTING ANALYSIS FOR MODELLING RESULTS OF GRANITE FORMATION

Model_PPV Vs. Field_PPV

```
clc
clear

load Granite_model
 [xData, yData] = prepareCurveData( Field_PPV, Model_PPV );

ft = fittype( 'power1' );
opts = fitoptions( ft );
opts.Display = 'Off';
opts.Lower = [-Inf -Inf];
opts.StartPoint = [9165559707213.1 -3.17367429473067];
opts.Upper = [Inf Inf];
 [fitresult, gof] = fit( xData, yData, ft, opts )

Fig.( 'Name', 'Granite Formation Modelling Results' );
h = plot( fitresult, xData, yData );
set(gca,'XScale','log')
set(gca,'YScale','log')
legend(h,'Model PPV Vs. Field PPV',
'Granite Formation','Location','Northwest');
xlabel( 'Field PPV (mm/s)' );
ylabel( 'Model PPV (mm/s)' );

grid on
```

```
           fitresult =

                General model Power1:
```

```
fitresult(x) = a*x^b
Coefficients (with 95% confidence bounds):
a =  1.043  (1.029, 1.056)
b =  0.9876  (0.9798, 0.9955)

gof =

sse: 0.4140e-16
rsquare: 0.8582
dfe: 92
adjrsquare: 0.8582
rmse: 0.0671
```

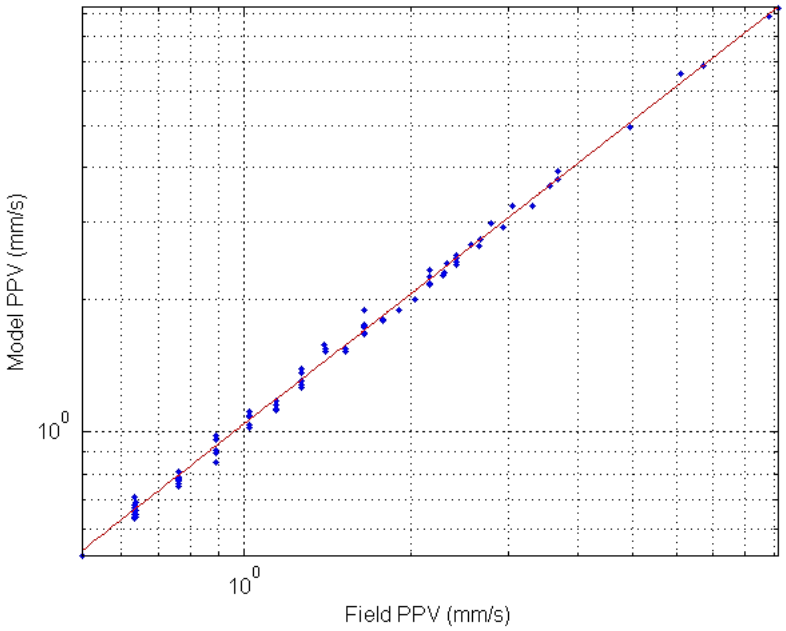

Published with MATLAB® R2013a

CREATEFIT(MODEL PPV, FIELD PPV, ELECTRICAL VOLTAGE)

```
function [fitresult, gof] = createFit(Electrical_Voltage, Model_PPV,
Field_PPV)

clc
clear

load Granite_model
 [xData, yData, zData] = prepareSurfaceData( Electrical_Voltage,...
    Model_PPV, Field_PPV );

ft = 'linearinterp';
opts = fitoptions( ft );
opts.Normalize = 'on';
 [fitresult, gof] = fit( [xData, yData], zData, ft, opts )

Fig.( 'Name', 'Granite' );
h = plot( fitresult, [xData, yData], zData );
legend( h, 'Granite', 'Field PPV vs. Electrical Voltage, Model PPV',
    'Location', 'NorthEast' );
xlabel( 'Electrical Voltage' );
```

```
ylabel( 'Model PPV' );
zlabel( 'Field PPV' );
colorbar
```

```
gof =
    sse: 2.4652e-31
    rsquare: 0.87000
    dfe: 0
    adjrsquare: 0.86000
    rmse: NaN
```

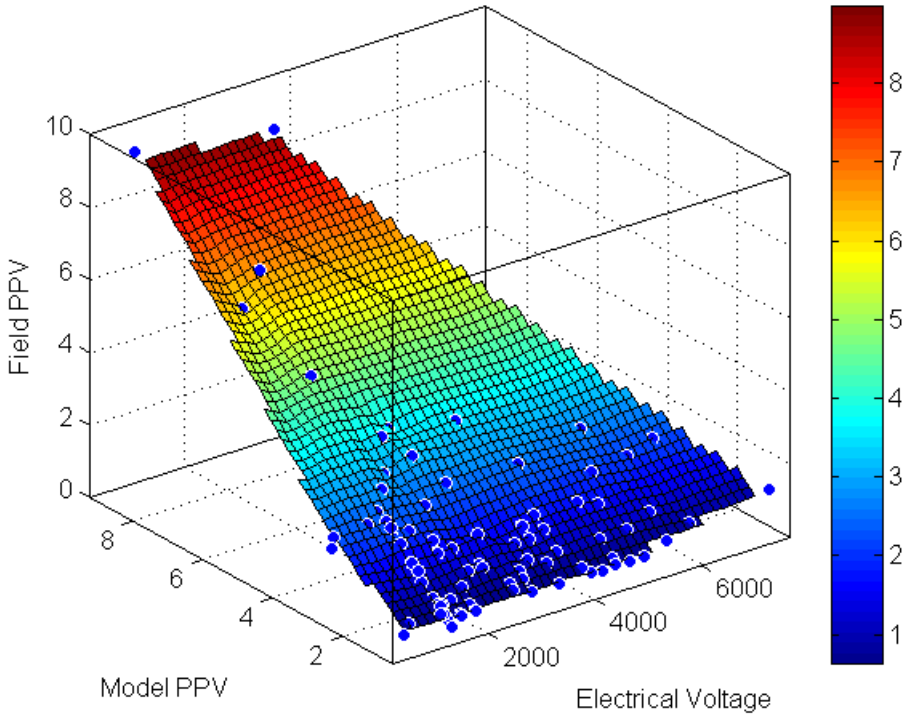

Published with MATLAB® R2013a

APPENDIX – VI

SANDSTONE FORMATION
(Wipfrag Analysis)

RAMAGUNDAM OPENCAST MINE-I
THE SINGARENI COLLIERIES COMPANY LIMITED
KARIMNAGAR DISTRICT, TELANGANA

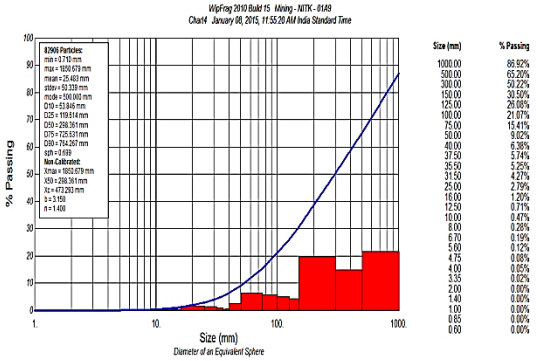

Size (mm)	% Passing
1000.00	86.92%
500.00	65.20%
300.00	50.22%
150.00	30.50%
125.00	26.08%
100.00	21.67%
75.00	15.41%
50.00	9.02%
40.00	6.38%
37.50	5.74%
35.50	5.25%
31.50	4.27%
25.00	2.79%
16.00	1.20%
12.50	0.71%
10.00	0.47%
8.00	0.28%
6.70	0.19%
5.60	0.12%
4.75	0.08%
4.00	0.05%
3.35	0.02%
2.00	0.00%
1.40	0.00%
1.00	0.00%
0.85	0.00%
0.60	0.00%

BLAST-1

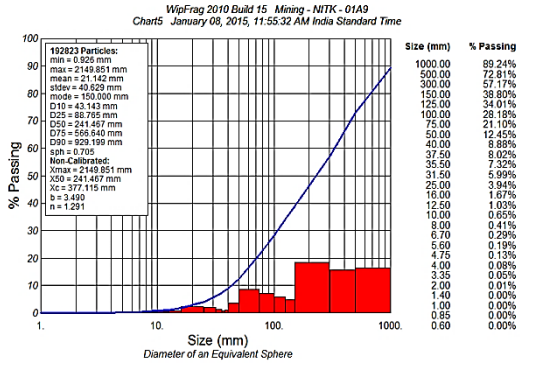

Size (mm)	% Passing
1000.00	89.24%
500.00	72.81%
300.00	57.17%
150.00	38.80%
125.00	34.01%
100.00	28.18%
75.00	21.10%
50.00	12.45%
40.00	8.88%
37.50	8.02%
35.50	7.32%
31.50	5.99%
25.00	3.94%
16.00	1.67%
12.50	1.03%
10.00	0.65%
8.00	0.41%
6.70	0.29%
5.60	0.19%
4.75	0.13%
4.00	0.08%
3.35	0.05%
2.00	0.01%
1.40	0.00%
1.00	0.00%
0.85	0.00%
0.60	0.00%

BLAST-2

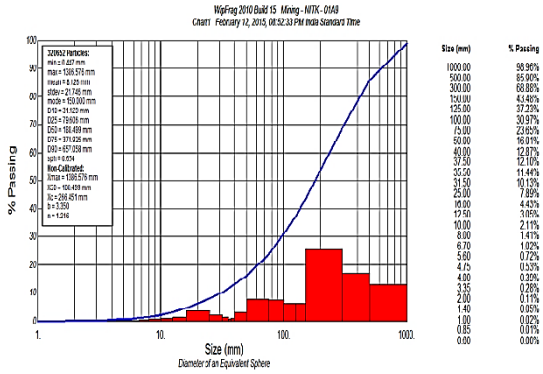

Size (mm)	% Passing
1000.00	98.96%
500.00	85.90%
300.00	68.88%
150.00	43.46%
125.00	37.23%
100.00	30.97%
75.00	23.65%
50.00	16.01%
40.00	12.27%
37.50	12.10%
35.50	11.44%
31.50	10.13%
25.00	7.89%
16.00	4.43%
12.50	3.05%
10.00	2.11%
8.00	1.41%
6.70	1.02%
5.60	0.72%
4.75	0.53%
4.00	0.39%
3.35	0.28%
2.00	0.11%
1.40	0.05%
1.00	0.02%
0.85	0.01%
0.60	0.00%

BLAST-3

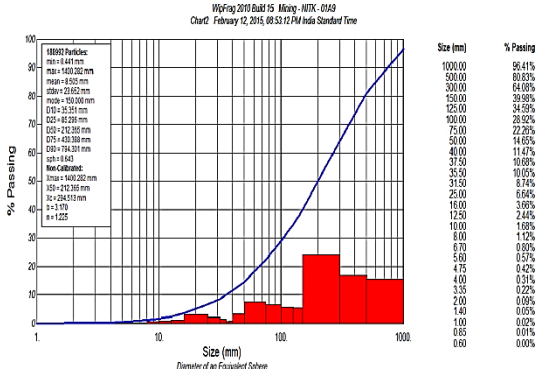

Size (mm)	% Passing
1000.00	96.41%
500.00	80.83%
300.00	64.08%
150.00	39.98%
125.00	34.89%
100.00	28.92%
75.00	22.26%
50.00	14.65%
40.00	11.47%
37.50	10.68%
35.50	10.05%
31.50	8.74%
25.00	6.64%
16.00	3.68%
12.50	2.44%
10.00	1.68%
8.00	1.12%
6.70	0.83%
5.60	0.57%
4.75	0.42%
4.00	0.31%
3.35	0.22%
2.00	0.09%
1.40	0.05%
1.00	0.02%
0.85	0.01%
0.60	0.00%

BLAST-4

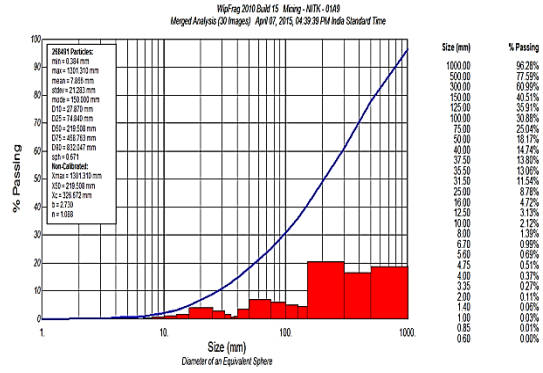

Size (mm)	% Passing
1000.00	96.28%
500.00	77.59%
300.00	60.99%
150.00	40.51%
125.00	35.91%
100.00	30.88%
75.00	25.04%
50.00	18.17%
40.00	14.74%
37.50	13.88%
35.50	13.06%
31.50	11.54%
25.00	8.78%
16.00	4.72%
12.50	3.13%
10.00	2.12%
8.00	1.39%
6.70	0.99%
5.60	0.69%
4.75	0.51%
4.00	0.37%
3.35	0.27%
2.00	0.11%
1.40	0.06%
1.00	0.03%
0.85	0.01%
0.60	0.00%

BLAST-5

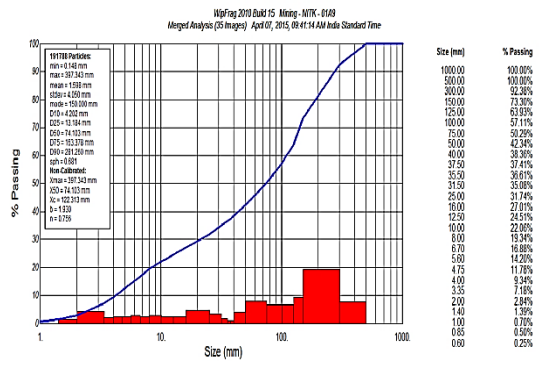

Size (mm)	% Passing
1000.00	100.00%
500.00	100.00%
300.00	92.38%
150.00	73.30%
125.00	63.93%
100.00	57.11%
75.00	50.29%
50.00	42.34%
40.00	38.36%
37.50	37.41%
35.50	36.61%
31.50	35.08%
25.00	31.74%
16.00	27.01%
12.50	24.51%
10.00	22.06%
8.00	19.34%
6.70	16.88%
5.60	14.20%
4.75	11.78%
4.00	9.34%
3.35	7.18%
2.00	2.84%
1.40	1.39%
1.00	0.70%
0.85	0.56%
0.60	0.25%

BLAST-6

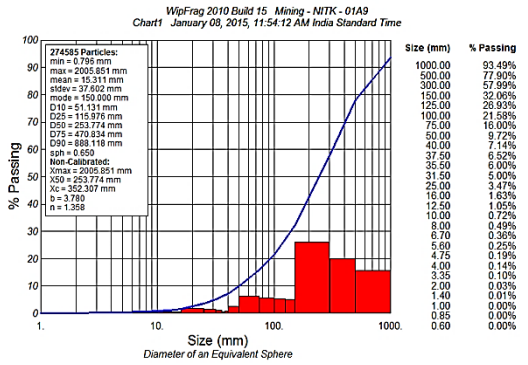

BLAST-7

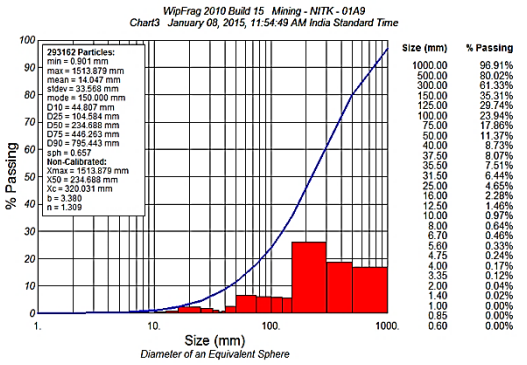

BLAST-8

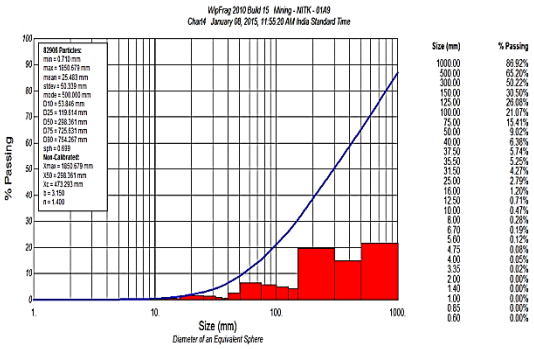

BLAST-9

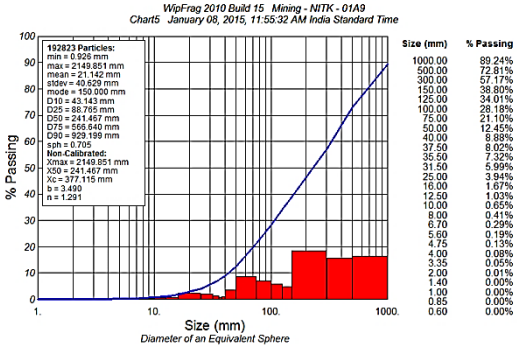

BLAST-10

RAMAGUNDAM OPENCAST MINE-III
THE SINGARENI COLLIERIES COMPANY LIMITED
KARIMNAGAR DISTRICT, TELANGANA

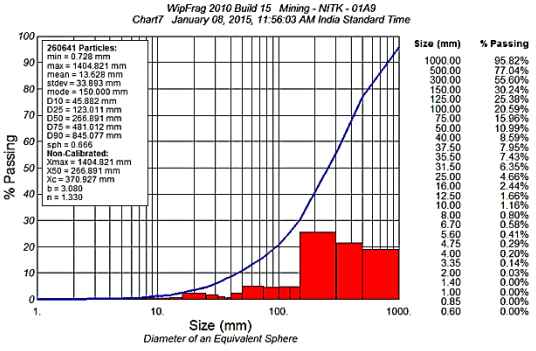

BLAST-1

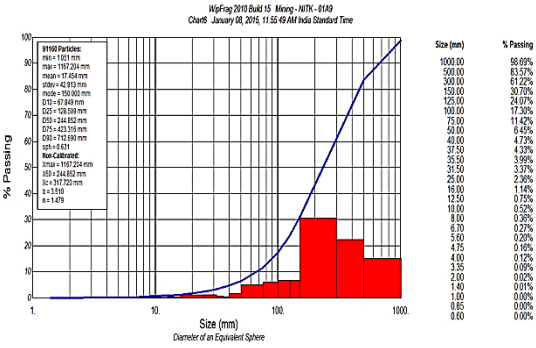

BLAST-2

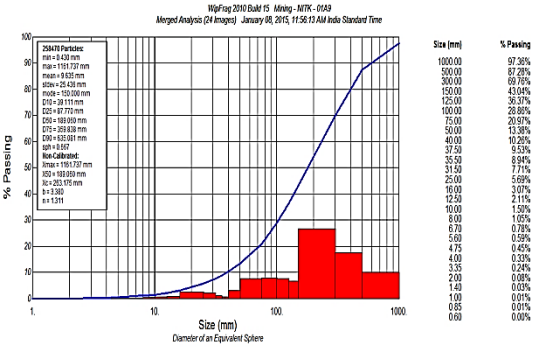

BLAST-3

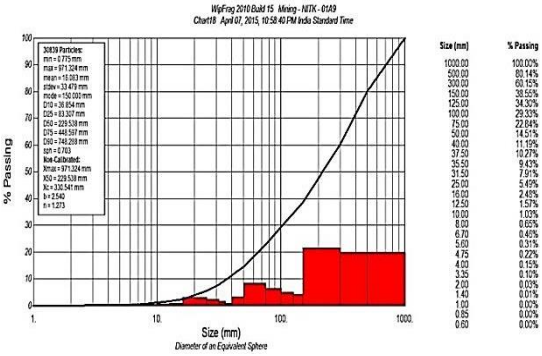

BLAST-4

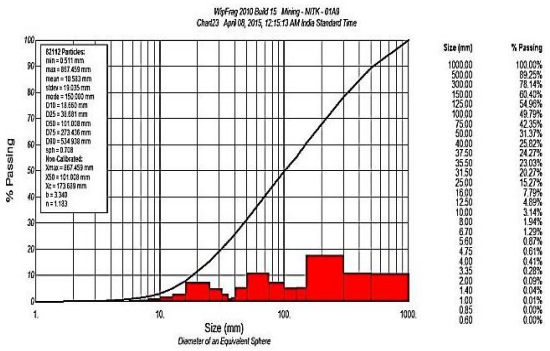

Size (mm)	% Passing
1000.00	100.00%
500.00	89.25%
300.00	78.14%
150.00	60.42%
125.00	54.96%
100.00	49.79%
75.00	42.35%
50.00	31.37%
40.00	25.82%
37.50	24.27%
35.50	23.03%
31.50	20.27%
25.00	15.27%
19.00	7.79%
12.50	4.89%
10.00	3.14%
8.00	1.94%
6.70	1.29%
5.60	0.87%
4.75	0.61%
4.00	0.41%
3.35	0.28%
2.00	0.09%
1.40	0.04%
1.00	0.01%
0.85	0.00%
0.60	0.00%

BLAST-5

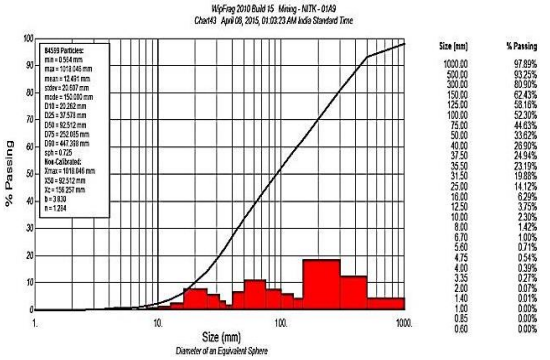

Size (mm)	% Passing
1000.00	97.89%
500.00	93.25%
300.00	80.90%
150.00	62.43%
125.00	58.16%
100.00	52.30%
75.00	44.63%
50.00	33.62%
40.00	28.90%
37.50	24.94%
35.50	23.19%
31.50	19.88%
25.00	14.12%
19.00	8.29%
12.50	3.75%
10.00	2.30%
8.00	1.42%
6.70	1.00%
5.60	0.71%
4.75	0.54%
4.00	0.39%
3.35	0.27%
2.00	0.07%
1.40	0.01%
1.00	0.00%
0.85	0.00%
0.60	0.00%

BLAST-6

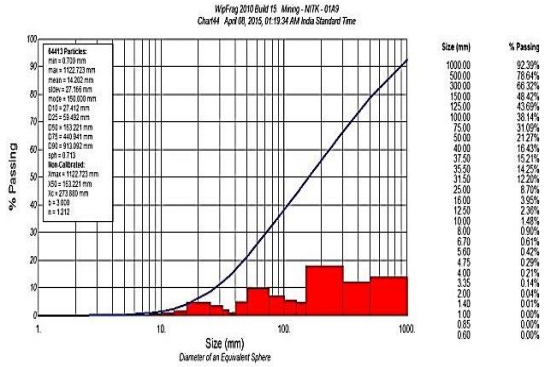

Size (mm)	% Passing
1000.00	92.39%
500.00	76.64%
300.00	66.32%
150.00	48.42%
125.00	43.69%
100.00	38.14%
75.00	31.09%
50.00	21.27%
40.00	16.43%
37.50	15.21%
35.50	14.25%
31.50	12.20%
25.00	8.70%
19.00	3.95%
12.50	2.36%
10.00	1.48%
8.00	0.90%
6.70	0.61%
5.60	0.42%
4.75	0.29%
4.00	0.21%
3.35	0.14%
2.00	0.04%
1.40	0.01%
1.00	0.00%
0.85	0.00%
0.60	0.00%

BLAST-7

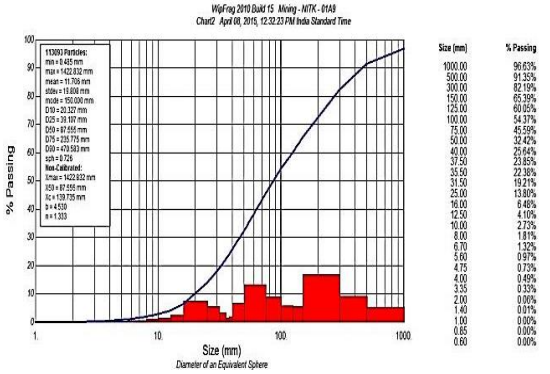

Size (mm)	% Passing
1000.00	96.63%
500.00	91.35%
300.00	82.19%
150.00	65.39%
125.00	60.05%
100.00	54.37%
75.00	45.59%
50.00	32.42%
40.00	25.64%
37.50	23.85%
35.50	22.38%
31.50	19.21%
25.00	13.80%
19.00	6.48%
12.50	4.10%
10.00	2.73%
8.00	1.81%
6.70	1.32%
5.60	0.97%
4.75	0.73%
4.00	0.49%
3.35	0.33%
2.00	0.06%
1.40	0.01%
1.00	0.00%
0.85	0.00%
0.60	0.00%

BLAST-8

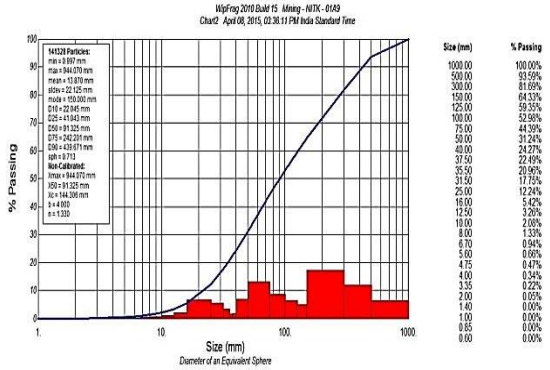

Size (mm)	% Passing
1000.00	100.00%
500.00	93.59%
300.00	81.69%
150.00	64.33%
125.00	59.35%
100.00	52.96%
75.00	44.39%
50.00	31.24%
40.00	24.27%
37.50	22.49%
35.50	20.96%
31.50	17.75%
25.00	12.24%
19.00	5.42%
12.50	3.26%
10.00	2.06%
8.00	1.33%
6.70	0.94%
5.60	0.66%
4.75	0.47%
4.00	0.34%
3.35	0.22%
2.00	0.05%
1.40	0.00%
1.00	0.00%
0.85	0.00%
0.60	0.00%

BLAST-9

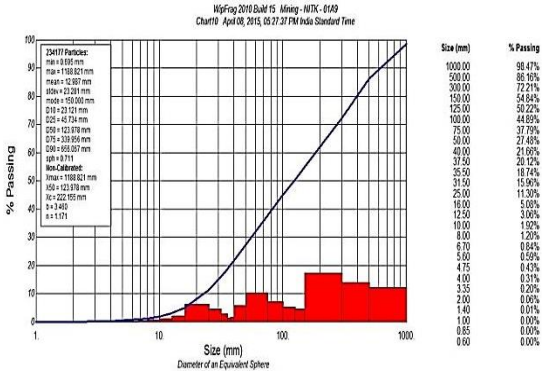

Size (mm)	% Passing
1000.00	98.47%
500.00	86.16%
300.00	72.21%
150.00	54.84%
125.00	50.22%
100.00	44.89%
75.00	37.79%
50.00	27.48%
40.00	21.66%
37.50	20.12%
35.50	18.74%
31.50	15.90%
25.00	11.30%
19.00	5.08%
12.50	3.06%
10.00	1.92%
8.00	1.20%
6.70	0.84%
5.60	0.59%
4.75	0.43%
4.00	0.31%
3.35	0.20%
2.00	0.06%
1.40	0.01%
1.00	0.00%
0.85	0.00%
0.60	0.00%

BLAST-10

APPENDIX – VII

LIMESTONE FORMATION
(Input Parameters used for Numerical Modelling)

Sl. No.	B (m)	S (m)	Blastholes	Length (m)	Width (m)	Depth (m)	E/h (kg)	MCD (kg)	TC (kg)
1	3.5	6	18	54	7	7	14.35	14.35	**258.30**
2	3.5	6	10	30	7	7	28.33	28.33	**283.30**
3	3.5	6	14	42	7	7	30.36	30.36	**425.04**
4	3.5	6	20	60	7	6	24.58	24.58	**491.60**
5	3.5	6	16	48	7	7	39.06	39.06	**624.96**
6	3.5	6	18	36	11	7	36.57	36.57	**658.26**
7	3	6	22	44	9	8.5	34.49	34.49	**758.78**
8	3.5	6	21	42	11	7.75	39.28	39.28	**824.88**
9	3.5	6	24	48	11	7	35.07	70.14	**841.68**
10	3	5.5	26	48	9	7	33.65	33.65	**874.90**
11	3	5.5	29	53	9	6.5	30.17	30.17	**874.93**
12	3	5.5	28	51	9	10	33.04	33.04	**925.12**
13	3.5	6	18	36	11	9.25	51.40	51.40	**925.20**
14	3	5.5	34	62	9	7	30.88	61.76	**1,049.92**
15	3	5.5	30	55	9	8	36.67	36.67	**1,100.10**
16	3.5	6	30	60	11	7	37.50	37.50	**1,125.00**
17	3	6	27	54	9	8.5	41.67	41.67	**1,125.09**
18	3.5	6	30	60	11	7	38.33	38.33	**1,149.90**
19	3	6	26	52	9	8.5	46.15	46.15	**1,199.90**
20	3	6	26	52	9	8.5	46.15	46.15	**1,199.90**
21	3	3.5	41	36	12	7.5	30.79	30.79	**1,262.39**
22	3	6	34	68	9	9	45.59	91.18	**1,550.06**
23	3	6	33	66	9	9	49.24	49.24	**1,624.92**
24	3	6	34	68	9	9	48.53	48.53	**1,650.02**
25	3	6	40	80	9	10	51.25	51.25	**2,050.00**
26	3	6.15	46	94	9	9	45.65	45.65	**2,099.90**
27	3	6	53	106	9	9	42.92	42.92	**2,274.76**
28	3	5.25	63	110	9	8.5	40.86	81.72	**2,574.18**
29	3	6	53	106	9	10	53.77	53.77	**2,849.81**
30	3	6	61	122	9	10	47.13	94.26	**2,874.93**
31	3	6.25	59	123	9	10	50.42	50.42	**2,974.78**
32	3	6.25	68	142	9	10	48.32	48.32	**3,285.76**
33	3	6	84	168	9	9	47.32	47.32	**3,974.88**

B – Burden, S – Spacing, E/h – Explosive charge per hole, MCD – Maximum charge per delay, TC – Total explosive charge per blast.

APPENDIX – VIII (NUMERICAL MODELLING ANALYSIS OF LIMESTONE FORMATION)

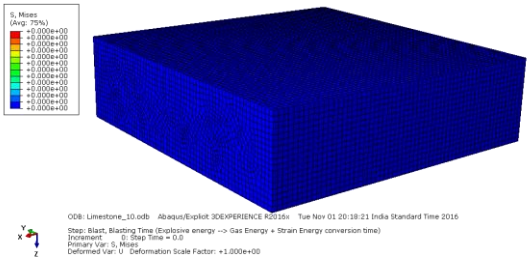

0ms

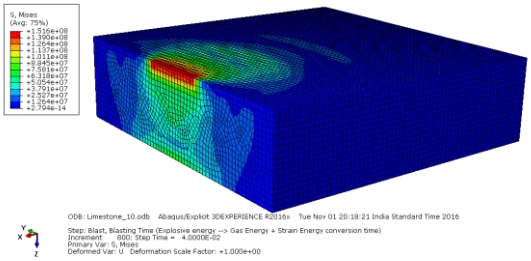

40ms

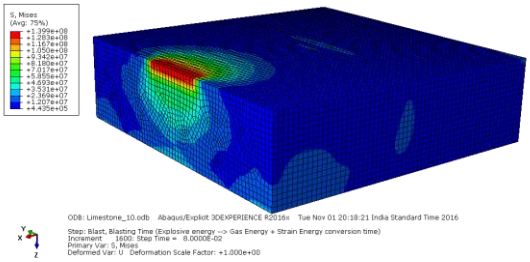

80ms

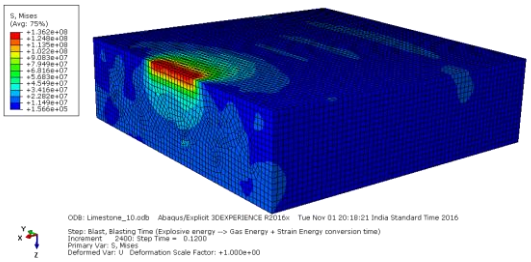

120ms

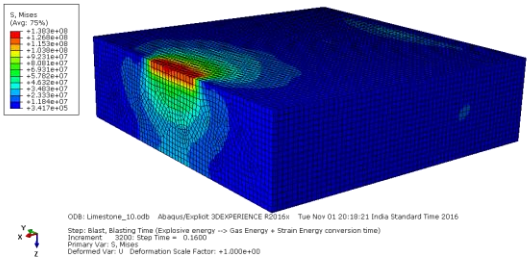

160ms

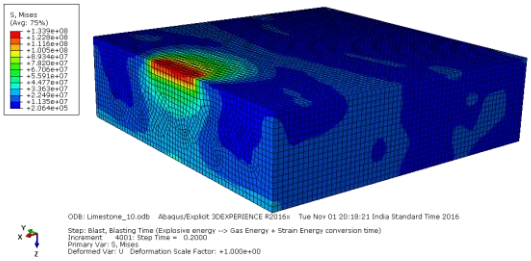

200ms

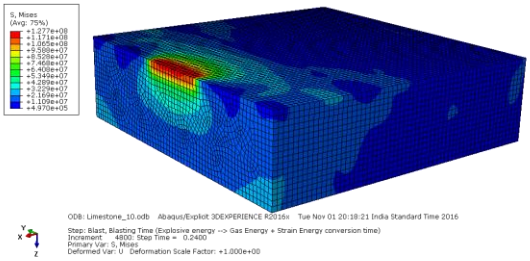

240ms

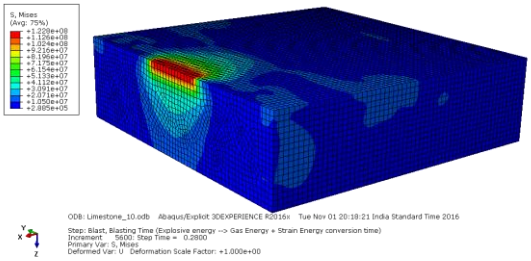

280ms

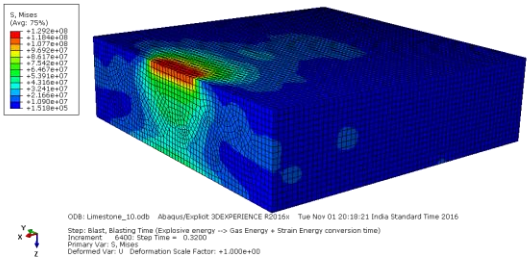

320ms

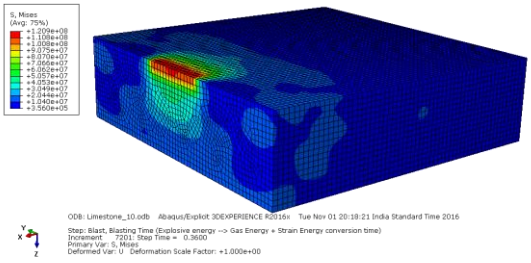

360ms

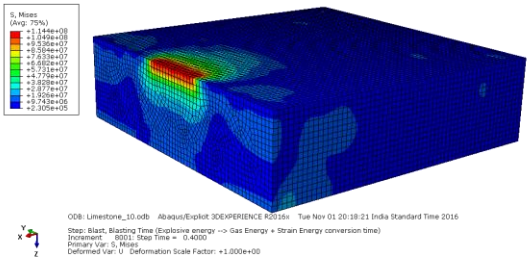

400ms

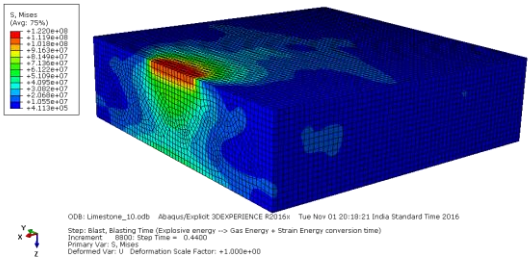

440ms

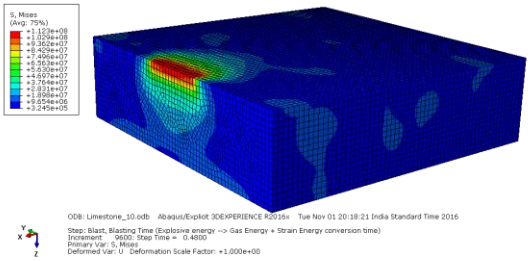

480ms

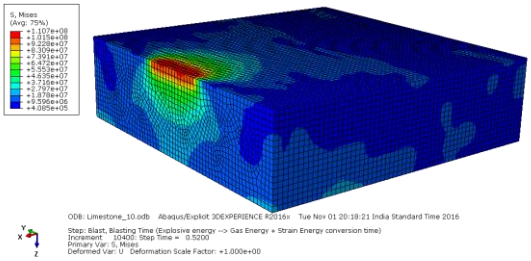

520ms

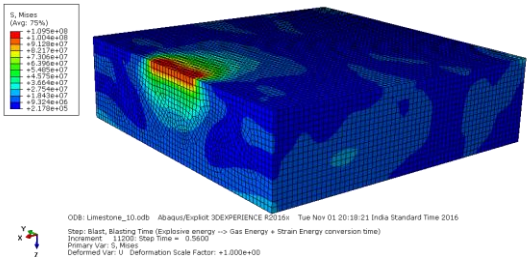

560ms

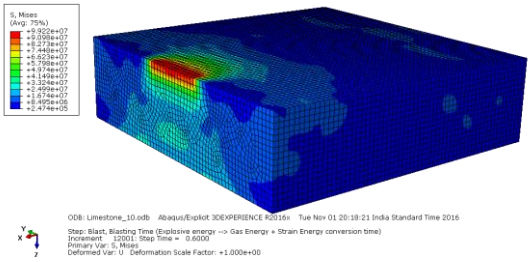

600ms

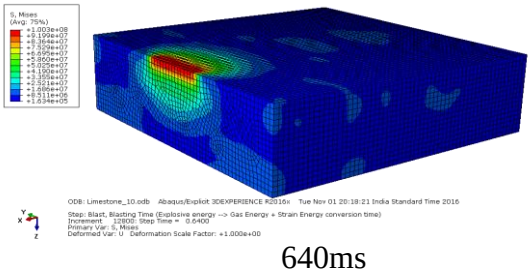

640ms

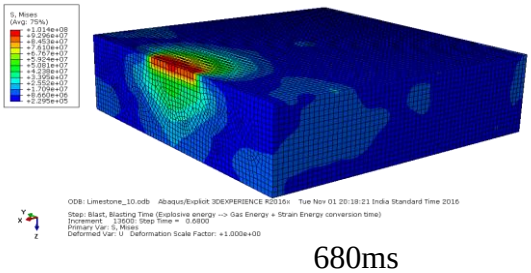

680ms

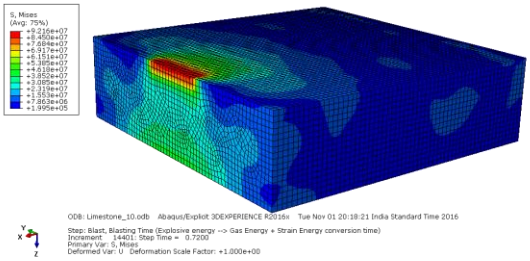

720ms

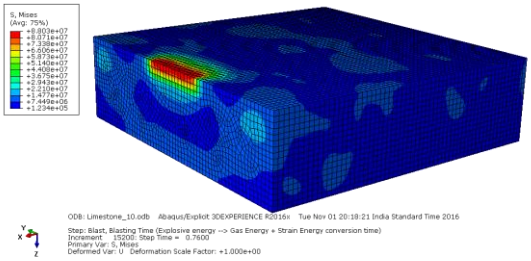

760ms

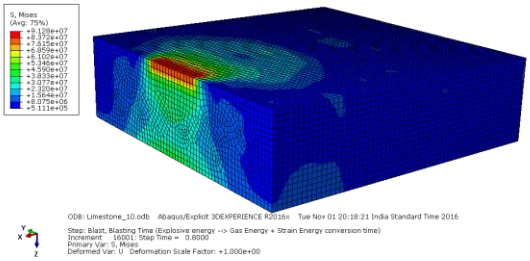

800ms

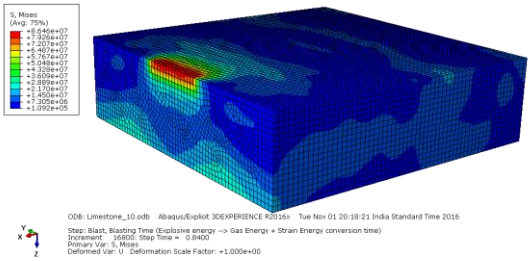

840ms

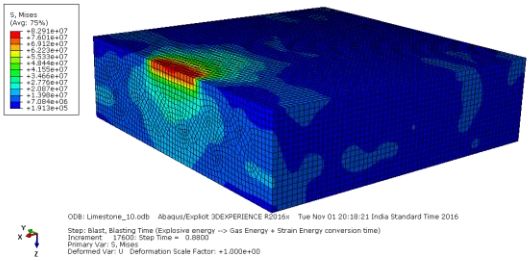

880ms

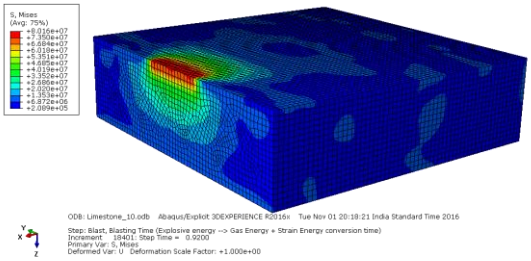

920ms

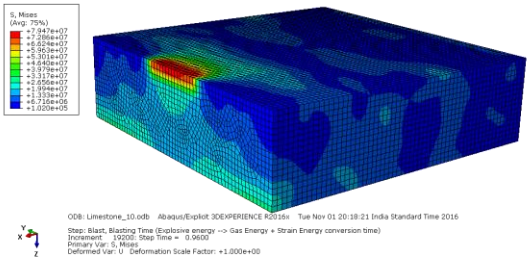

960ms

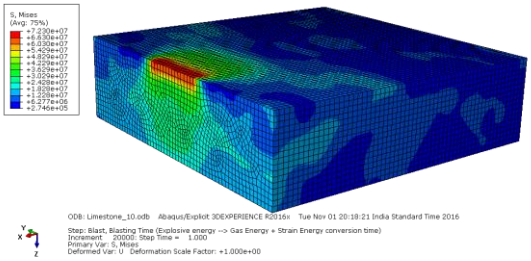

1000ms

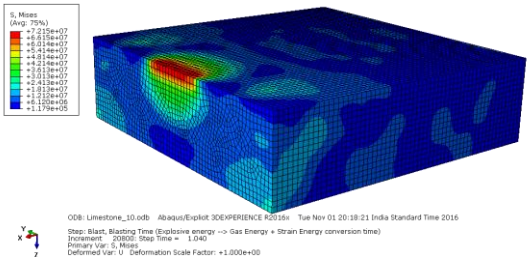

1040ms

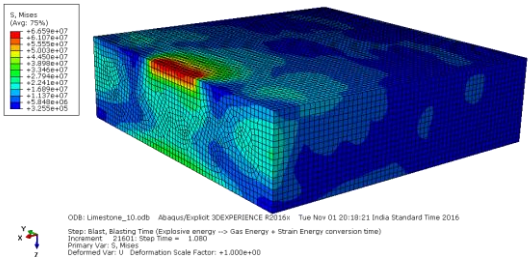

1080ms

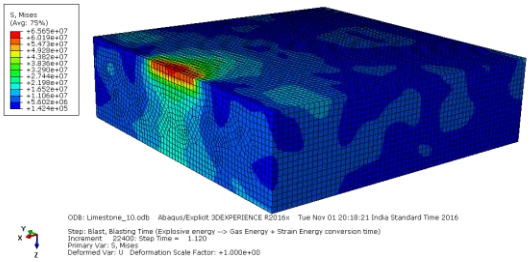

1120ms

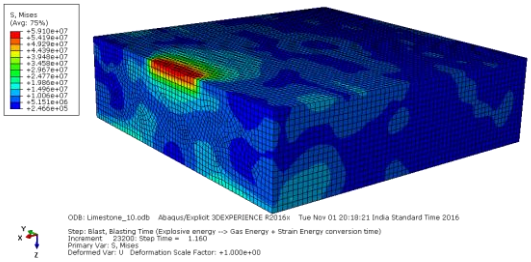

1160ms

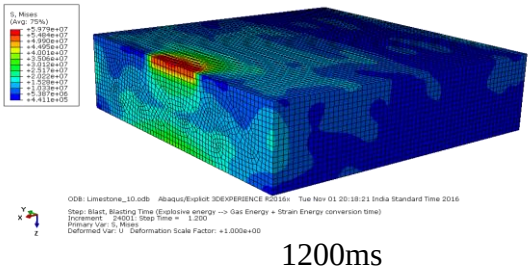

1200ms

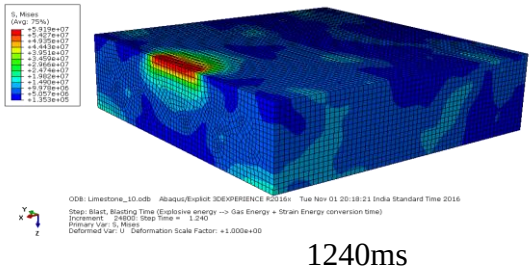

1240ms

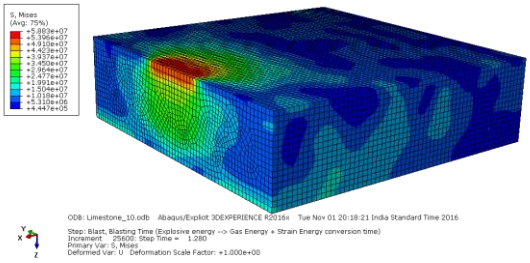

1280ms

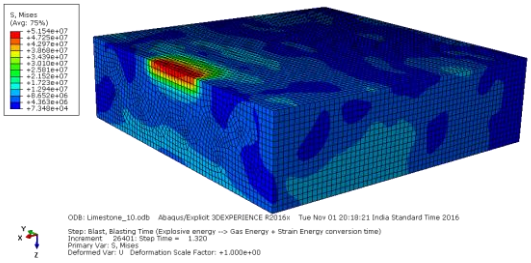

1320ms

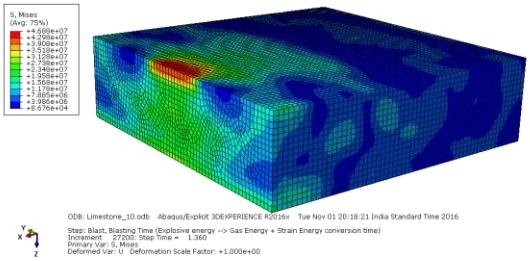

1360ms

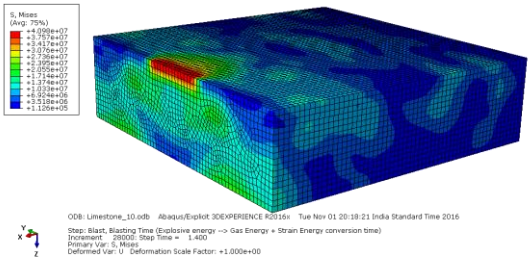

1400ms

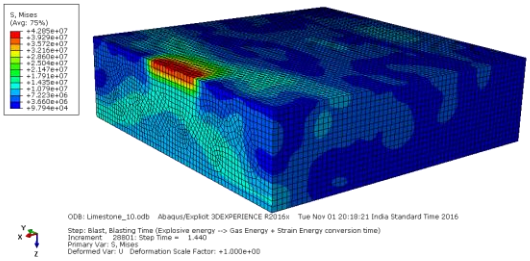

1440ms

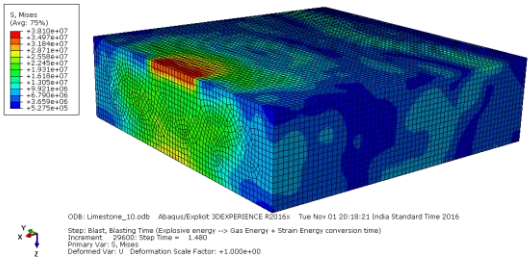

1480ms

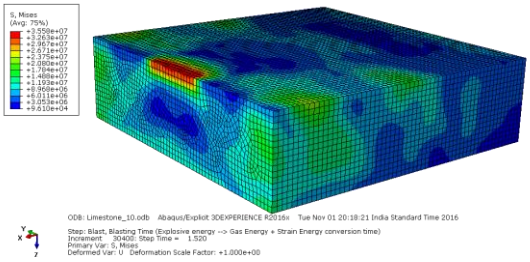

1520ms

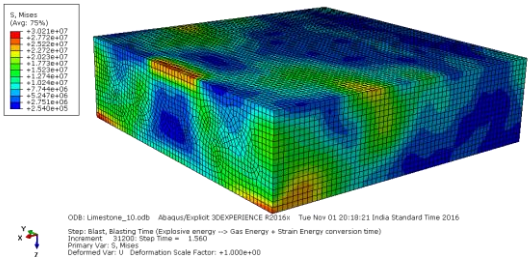

1560ms

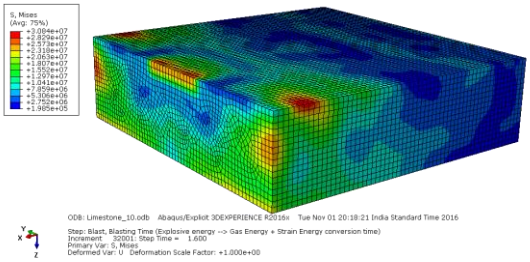

1600ms

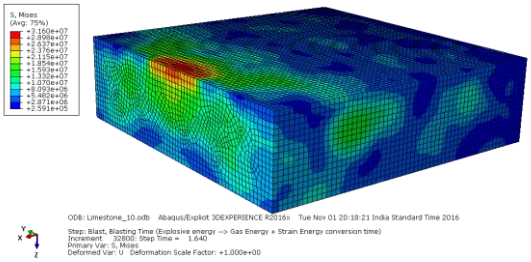

1640ms

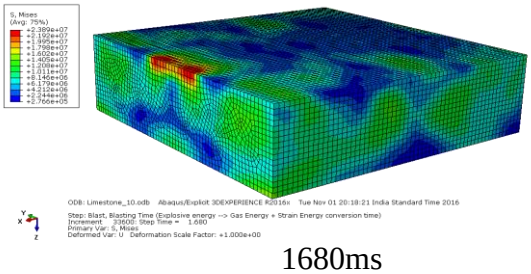

1680ms

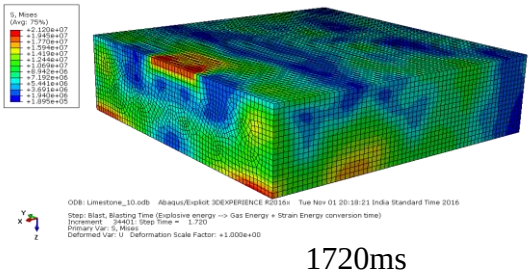

1720ms

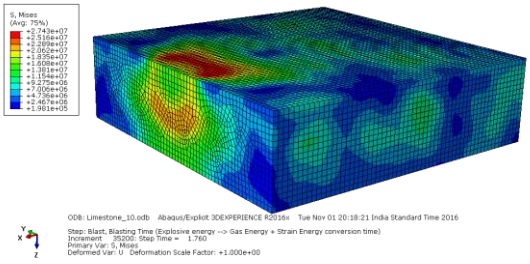

1760ms

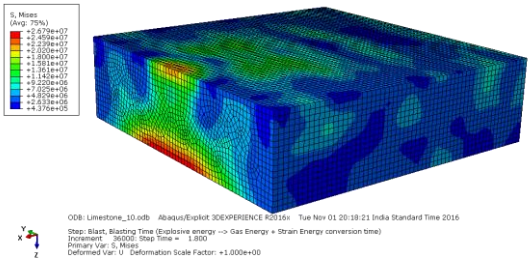

1800ms

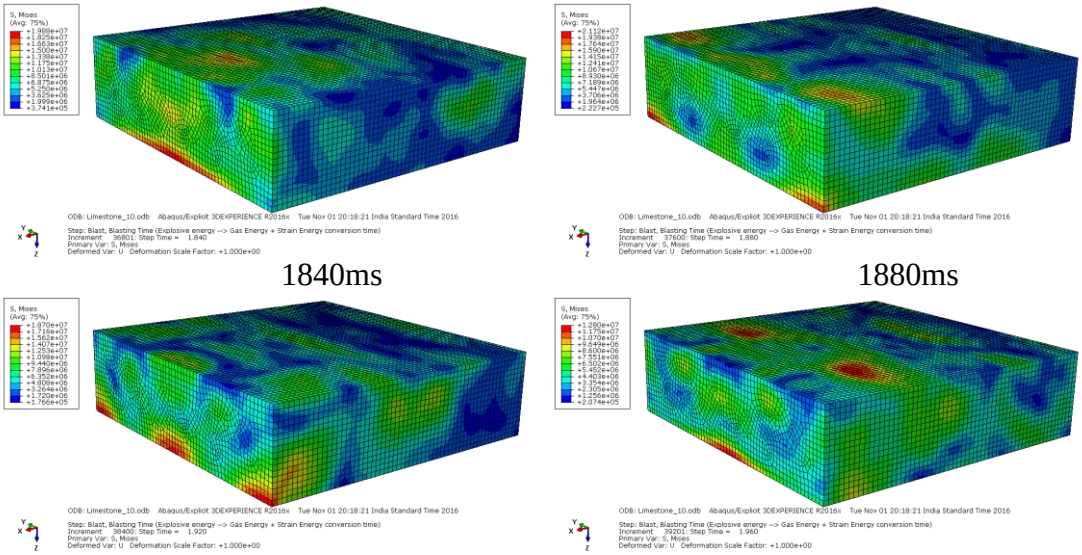

Fig. A8.1 Stress components at integral points in a model of limestone formation

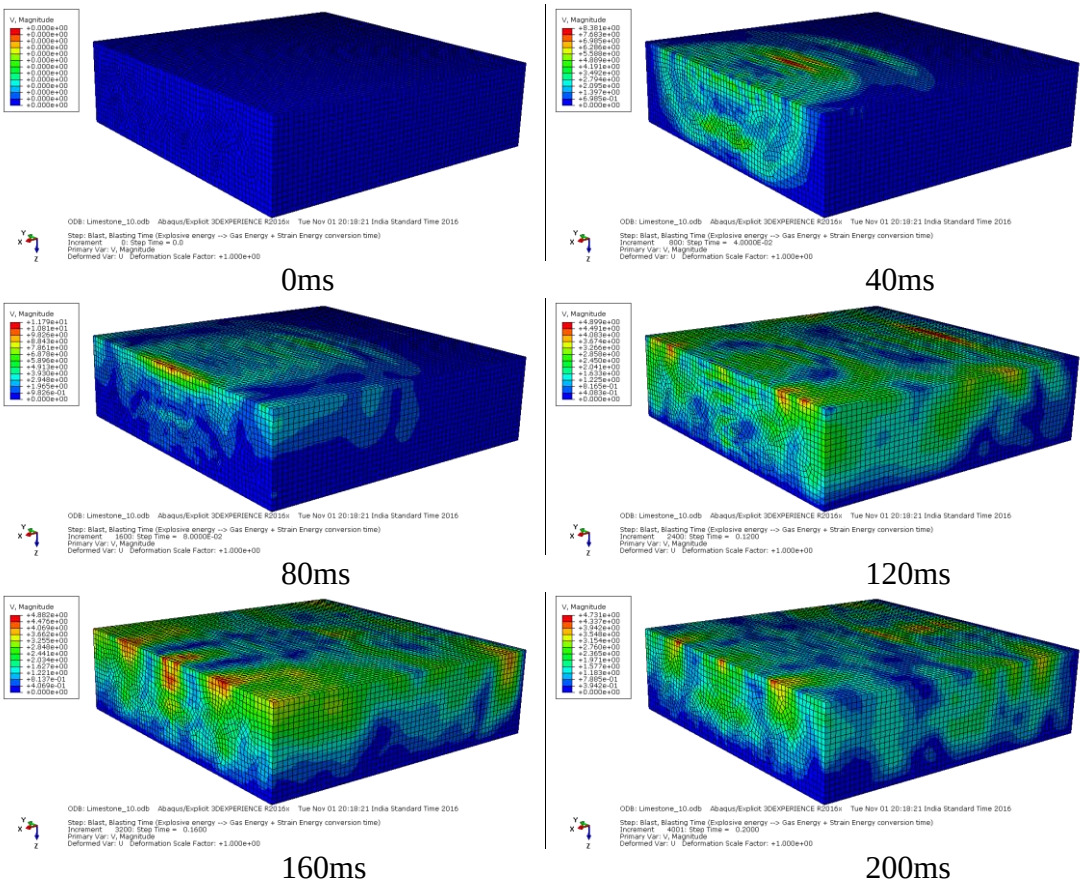

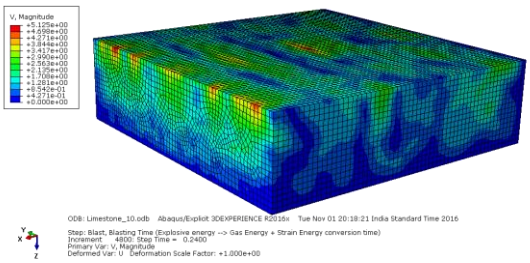

240ms

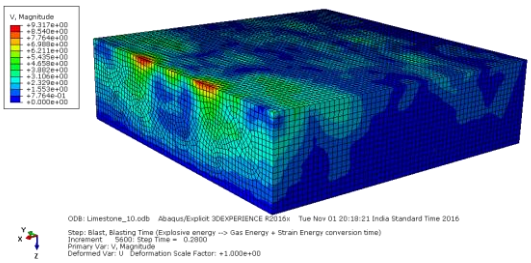

280ms

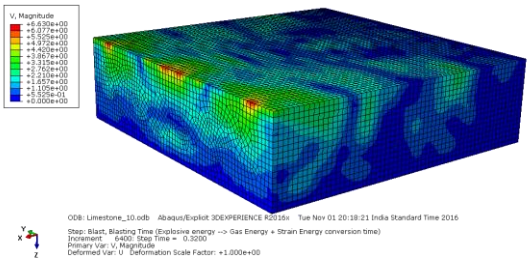

320ms

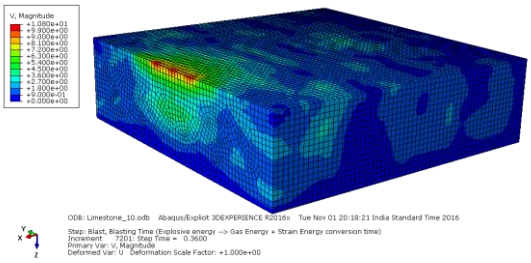

360ms

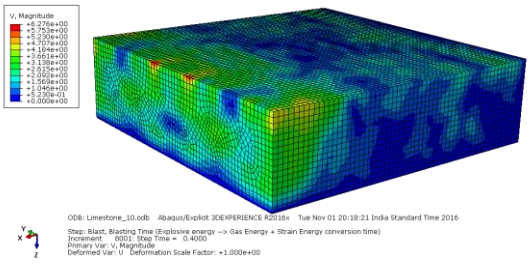

400ms

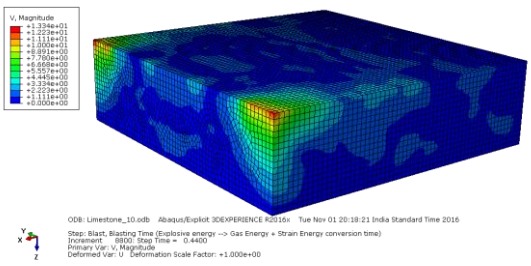

440ms

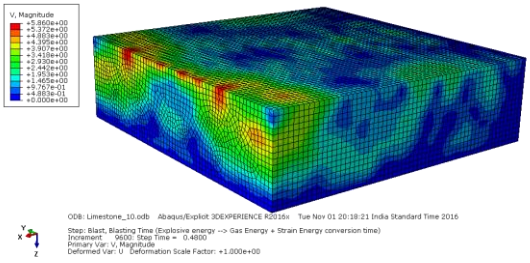

480ms

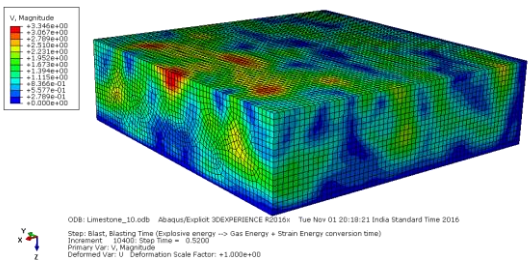

520ms

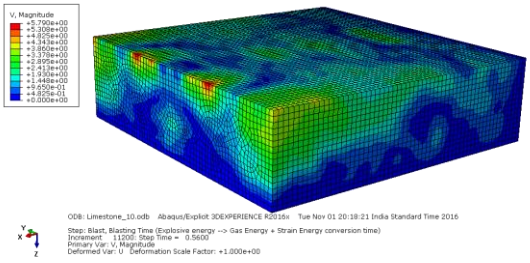

560ms

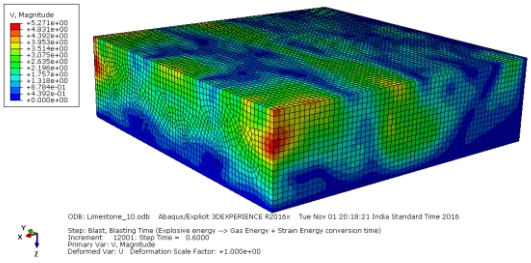

600ms

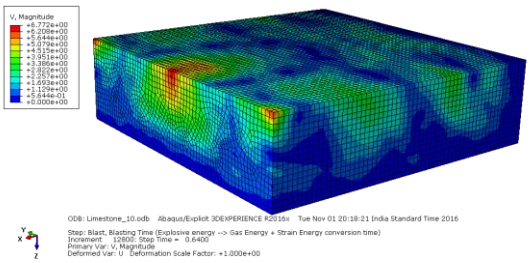

640ms

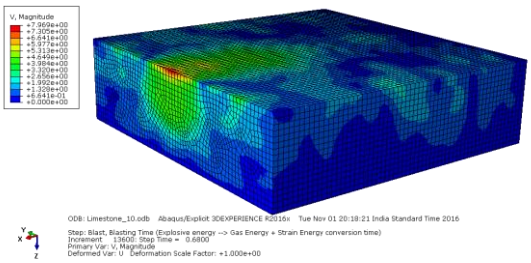

680ms

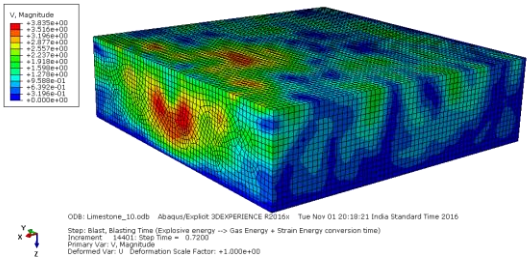

720ms

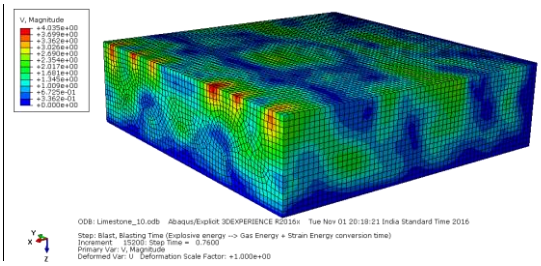

760ms

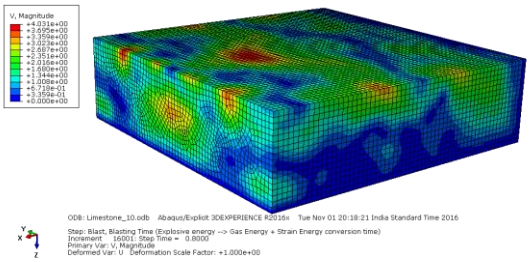

800ms

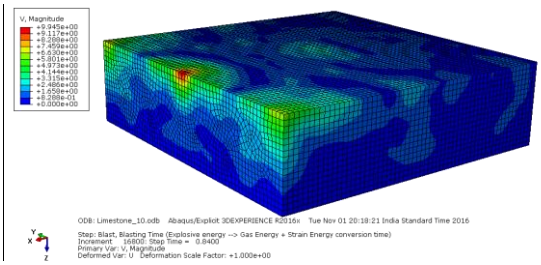

840ms

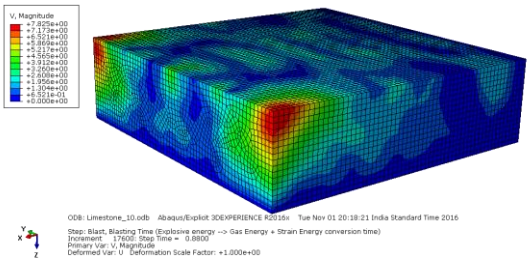

880ms

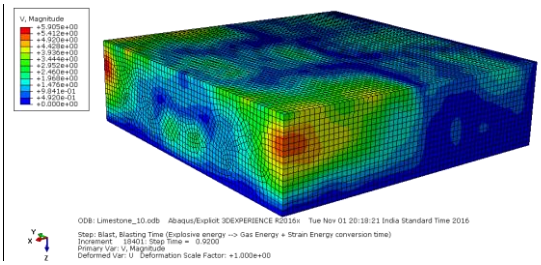

920ms

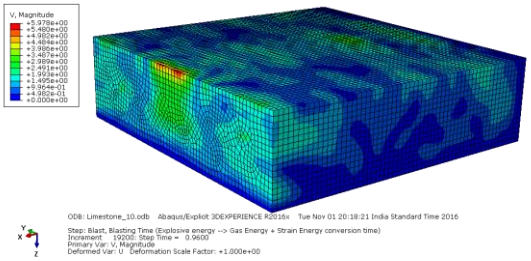

960ms

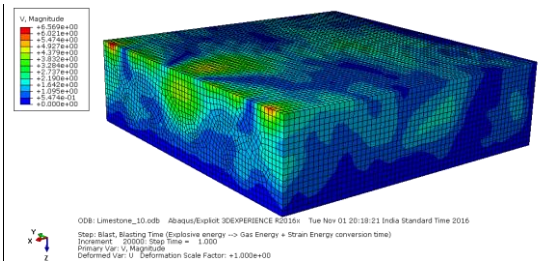

1000ms

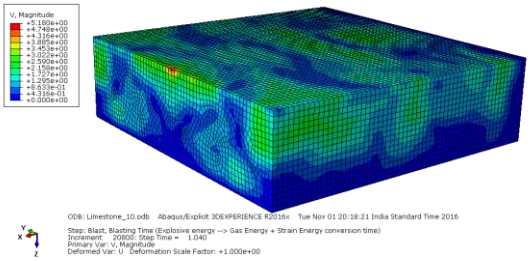

1040ms

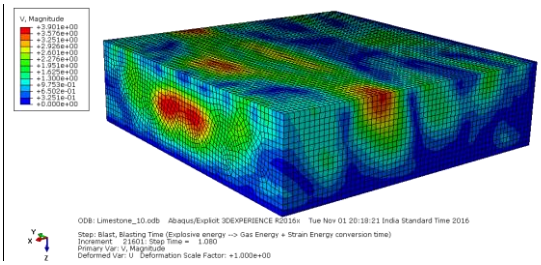

1080ms

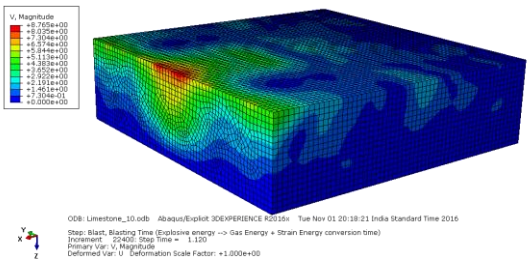

1120ms

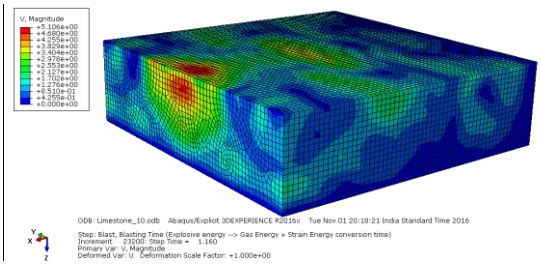

1160ms

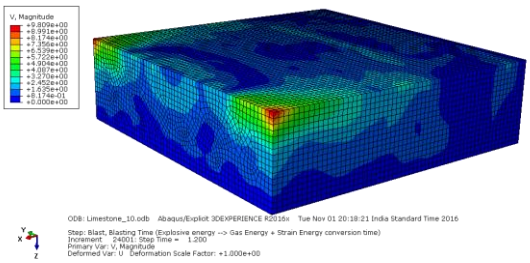

1200ms

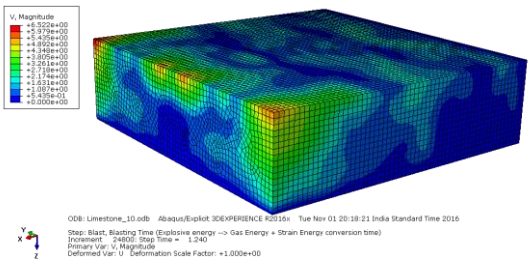

1240ms

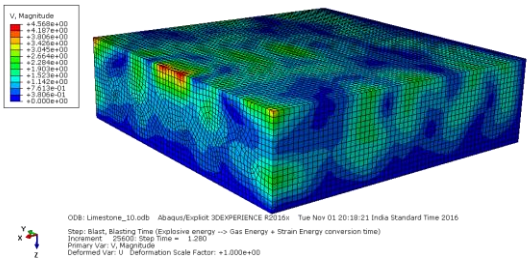

1280ms

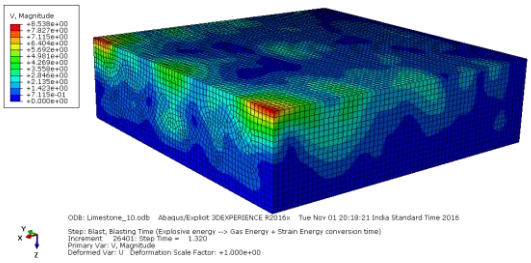

1320ms

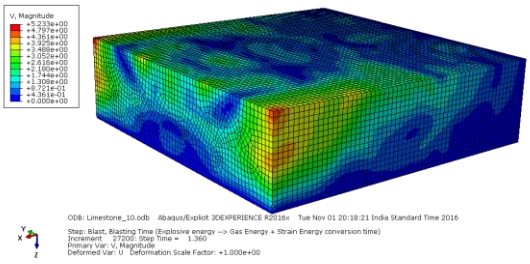

1360ms

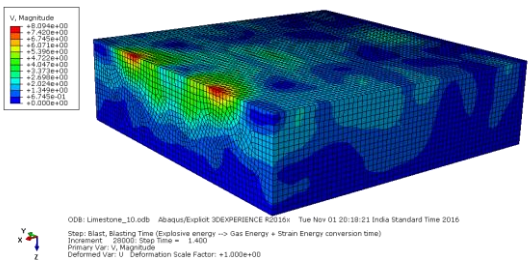

1400ms

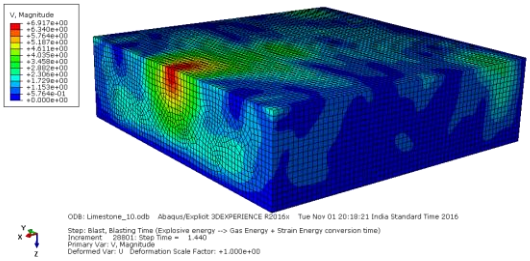

1440ms

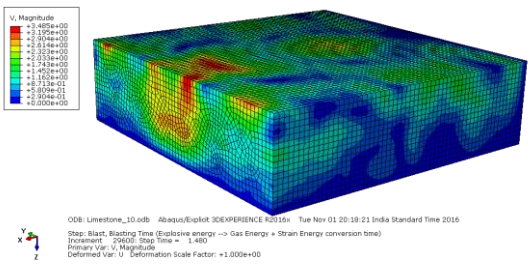

1480ms

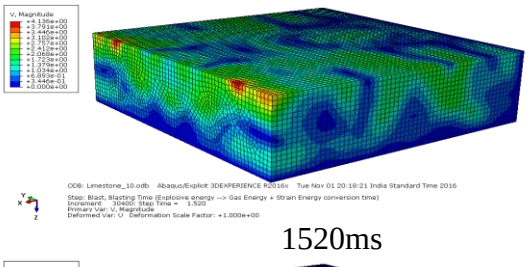

1520ms

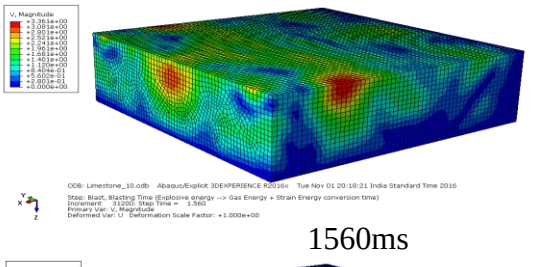

1560ms

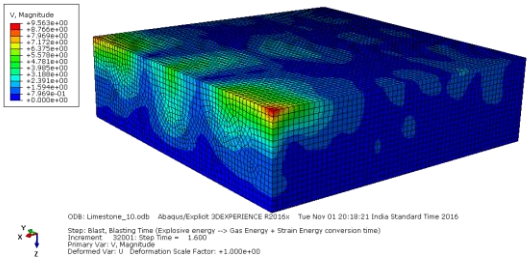

1600ms

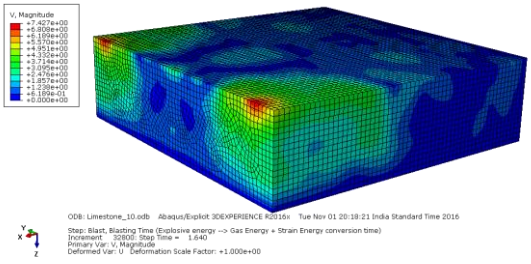

1640ms

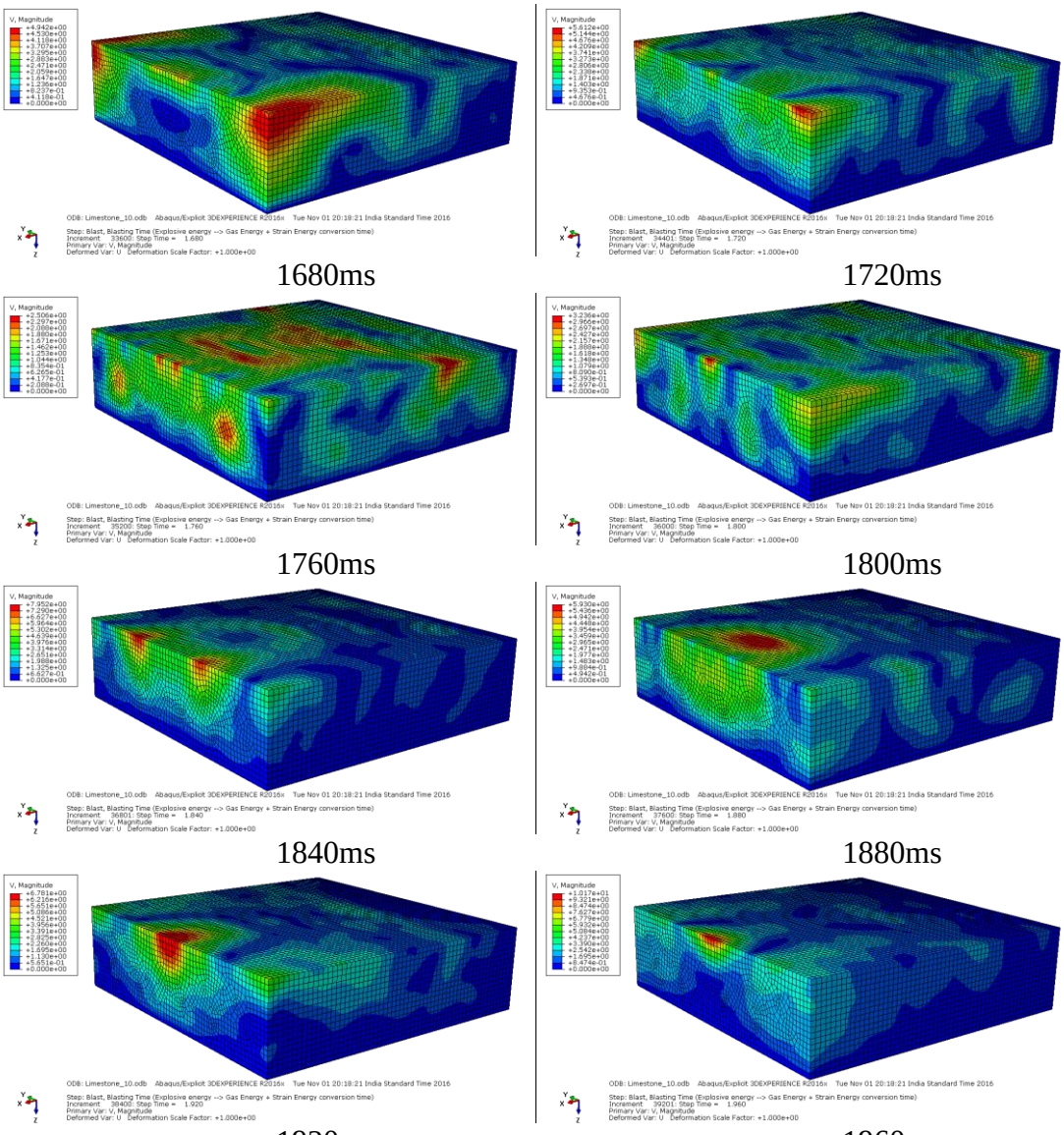

Fig. A8.2 Spatial velocity contours observed at nodes in a model of limestone formation

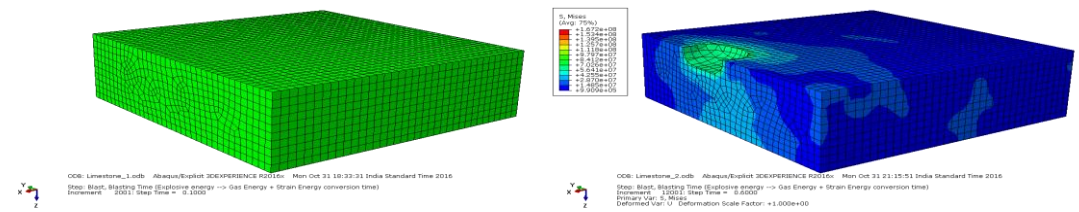

Limestone model no. 1 with un-deformed (left) and deformed (right) shapes

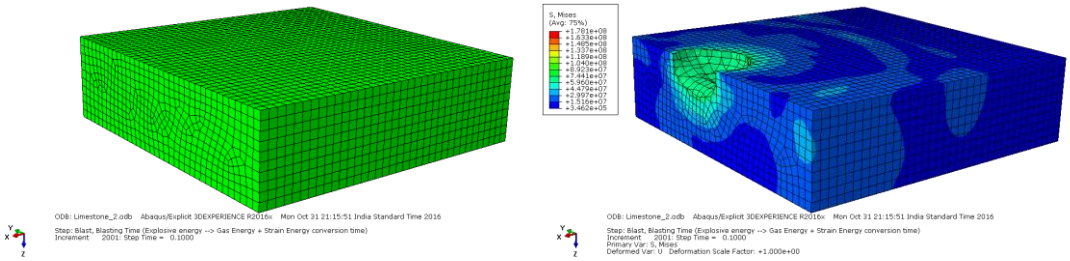

Limestone model no. 2 with un-deformed (left) and deformed (right) shapes

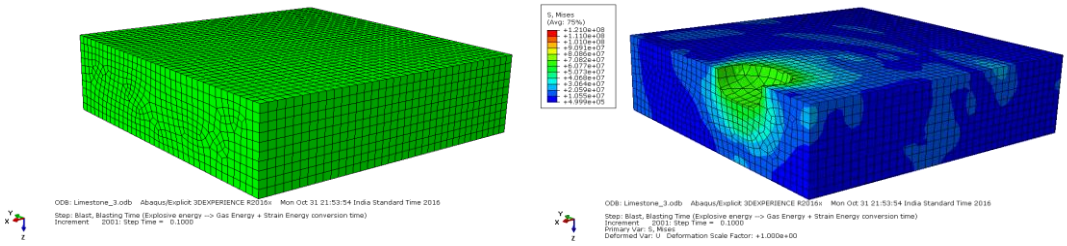

Limestone model no. 3 with un-deformed (left) and deformed (right) shapes

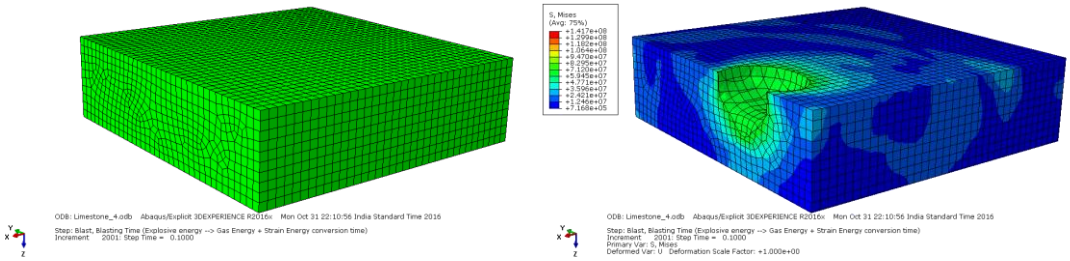

Limestone model no. 4 with un-deformed (left) and deformed (right) shapes

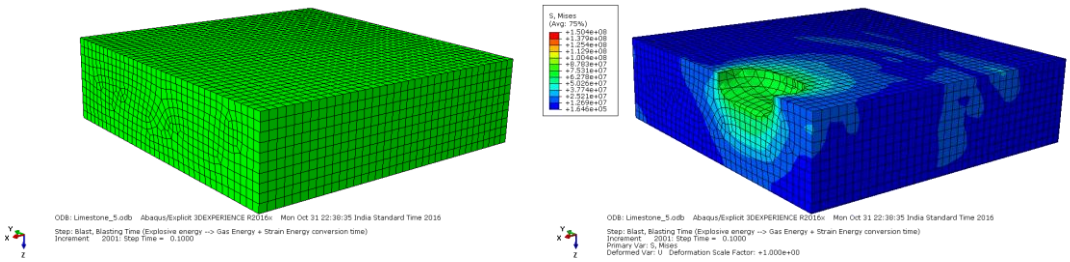

Limestone model no. 5 with un-deformed (left) and deformed (right) shapes

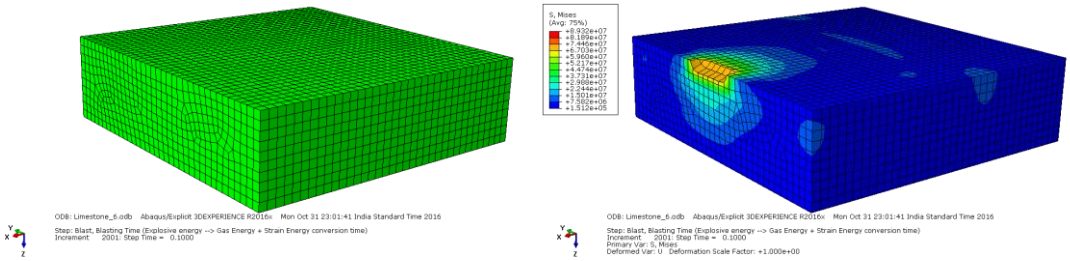

Limestone model no. 6 with un-deformed (left) and deformed (right) shapes

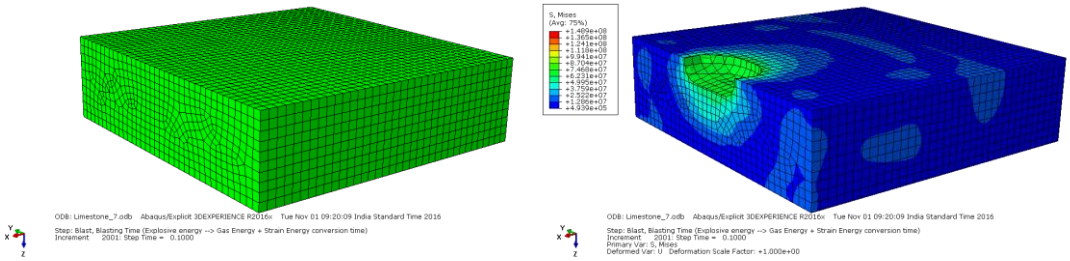

Limestone model no. 7 with un-deformed (left) and deformed (right) shapes

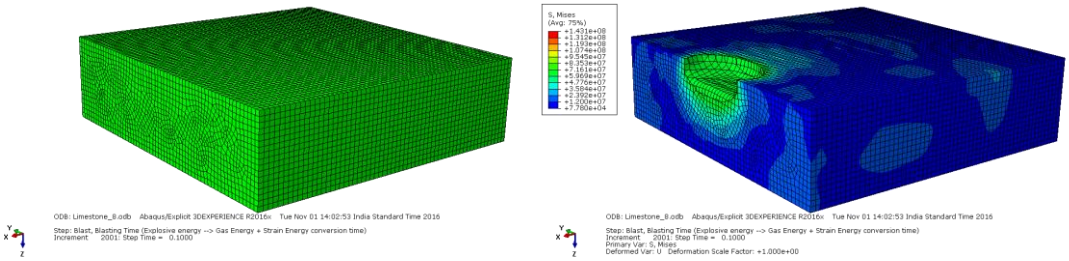

Limestone model no. 8 with un-deformed (left) and deformed (right) shapes

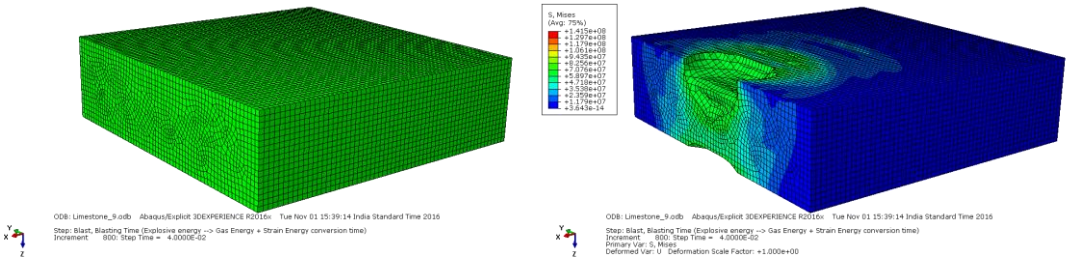

Limestone model no. 9 with un-deformed (left) and deformed (right) shapes

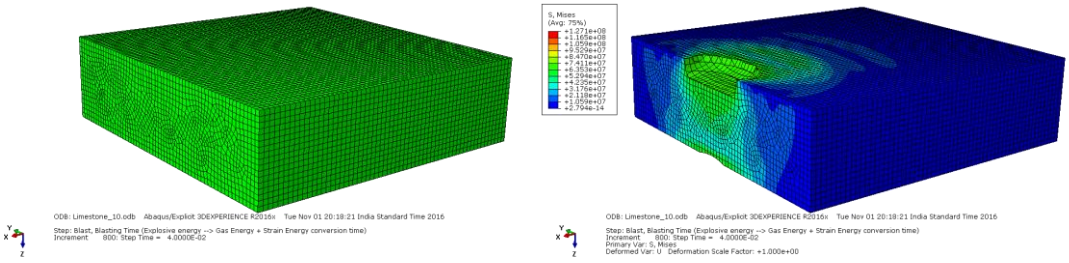

Limestone model no. 10 with un-deformed (left) and deformed (right) shapes

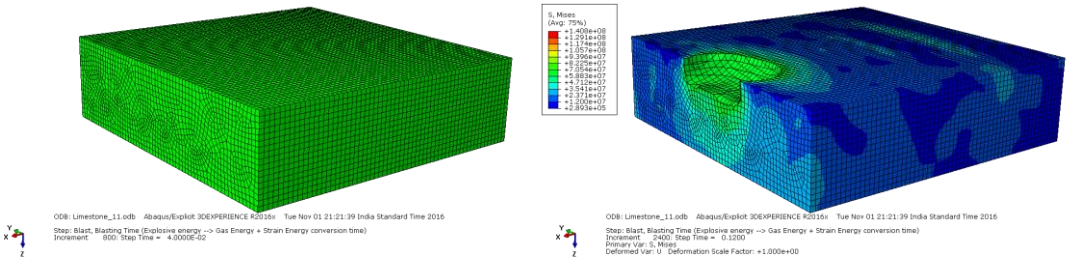

Limestone model no. 11 with un-deformed (left) and deformed (right) shapes

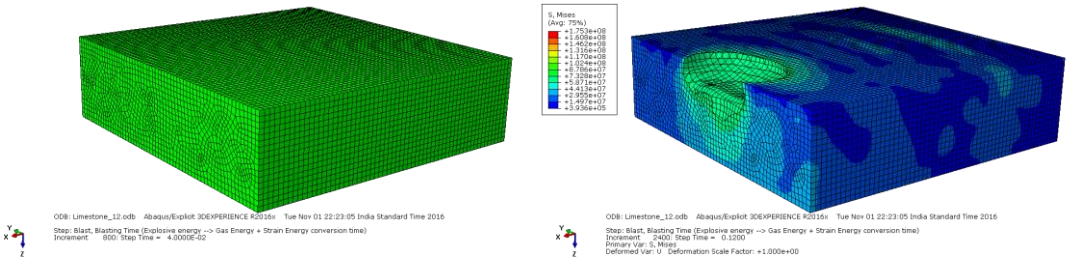

Limestone model no. 12 with un-deformed (left) and deformed (right) shapes

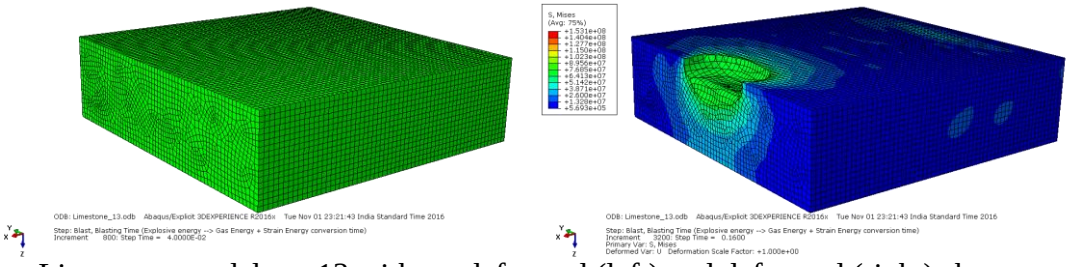

Limestone model no. 13 with un-deformed (left) and deformed (right) shapes

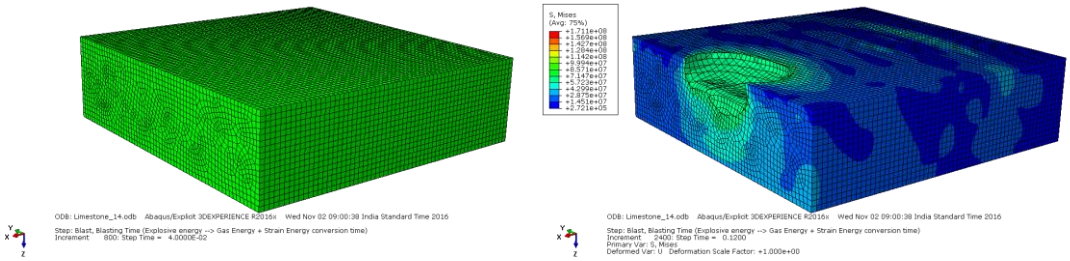

Limestone model no. 14 with un-deformed (left) and deformed (right) shapes

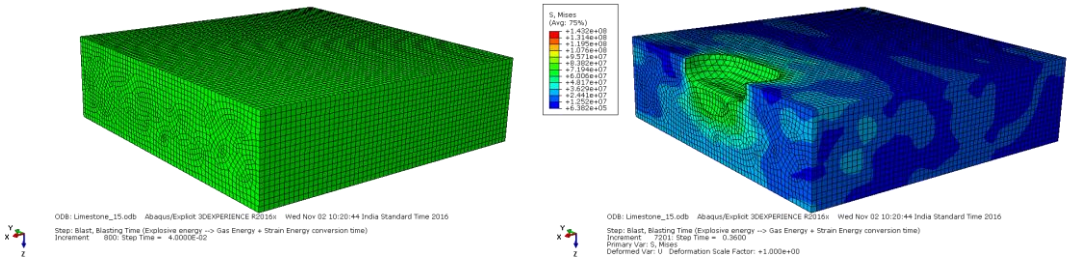

Limestone model no. 15 with un-deformed (left) and deformed (right) shapes

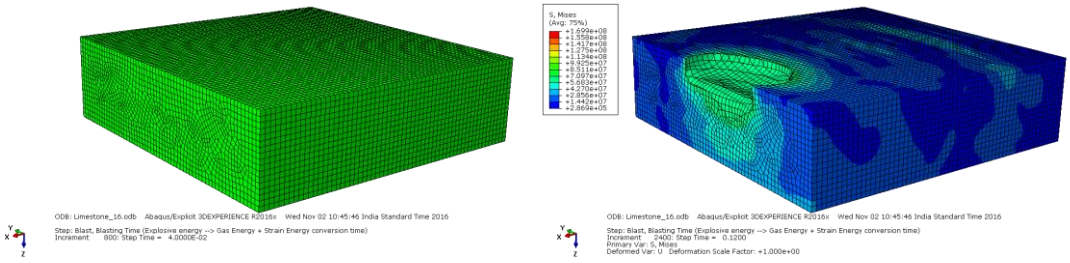

Limestone model no. 16 with un-deformed (left) and deformed (right) shapes

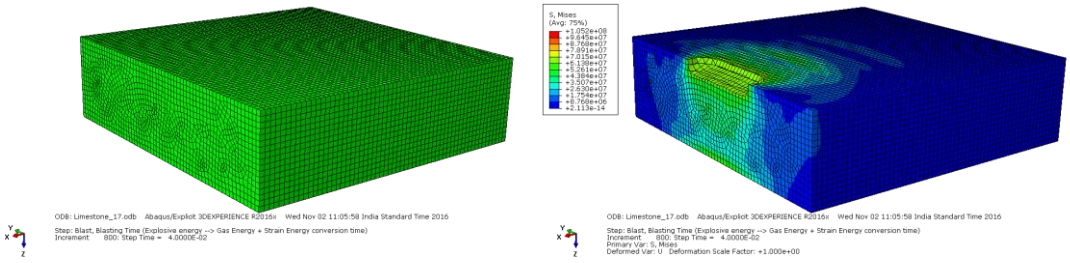

Limestone model no. 17 with un-deformed (left) and deformed (right) shapes

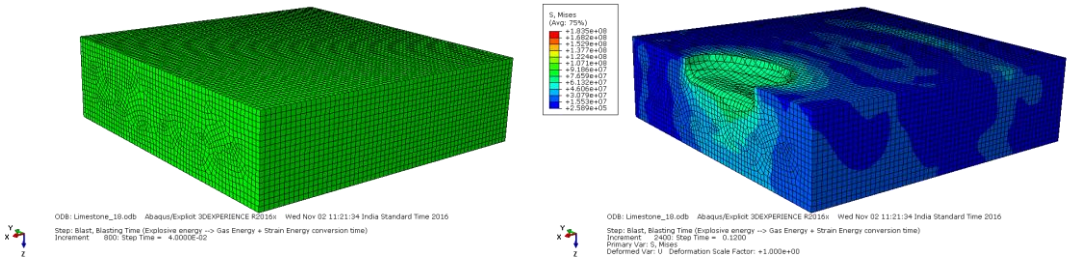

Limestone model no. 18 with un-deformed (left) and deformed (right) shapes

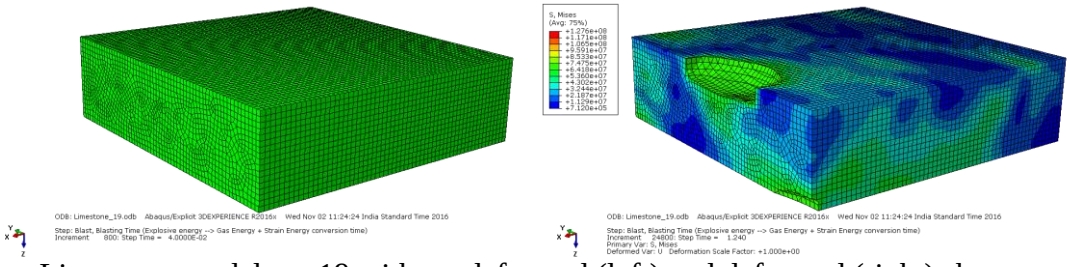

Limestone model no. 19 with un-deformed (left) and deformed (right) shapes

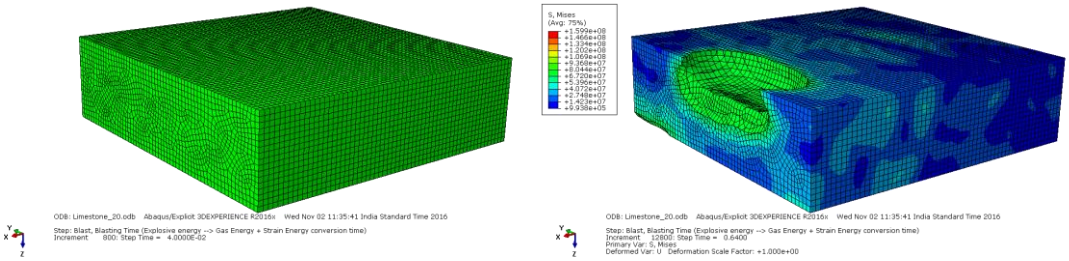

Limestone model no. 20 with un-deformed (left) and deformed (right) shapes

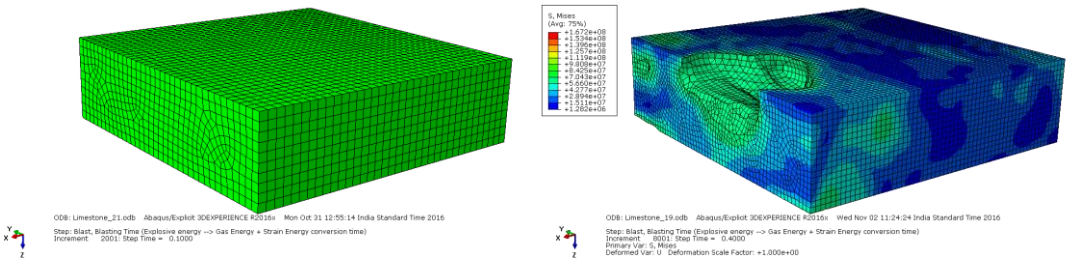

Limestone model no. 21 with un-deformed (left) and deformed (right) shapes

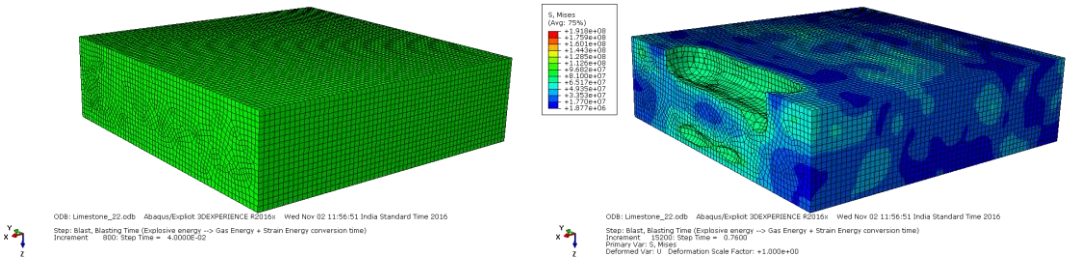

Limestone model no. 22 with un-deformed (left) and deformed (right) shapes

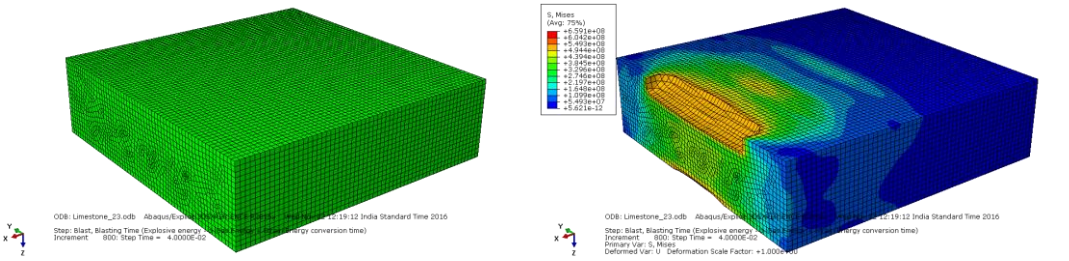

Limestone model no. 23 with un-deformed (left) and deformed (right) shapes

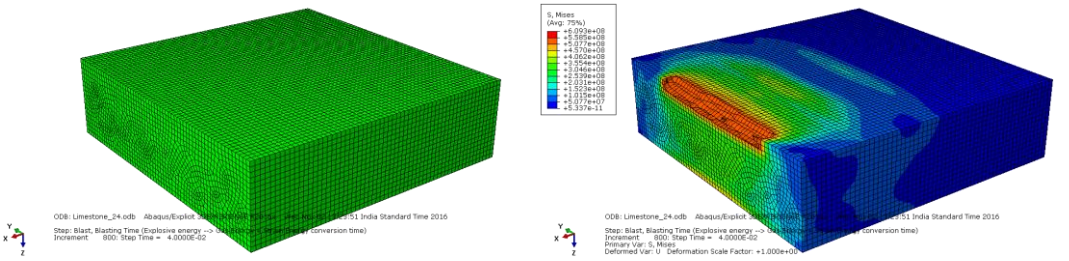

Limestone model no. 24 with un-deformed (left) and deformed (right) shapes

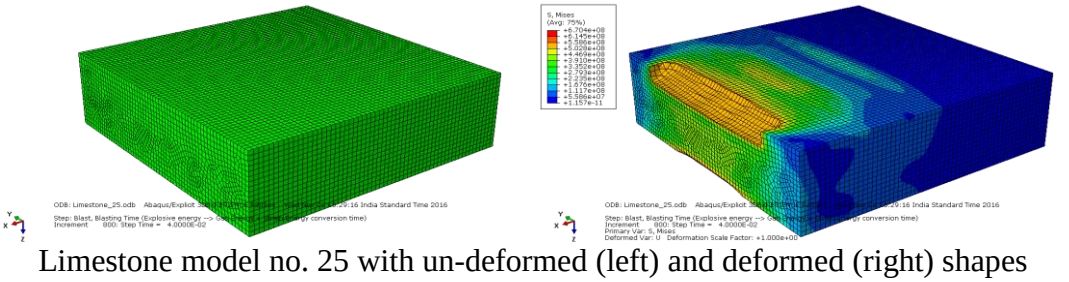

Limestone model no. 25 with un-deformed (left) and deformed (right) shapes

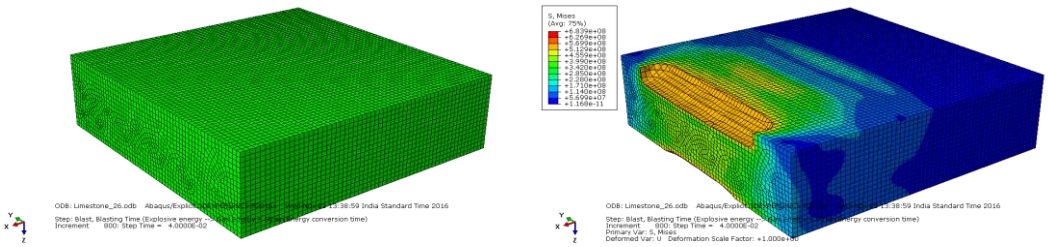

Limestone model no. 26 with un-deformed (left) and deformed (right) shapes

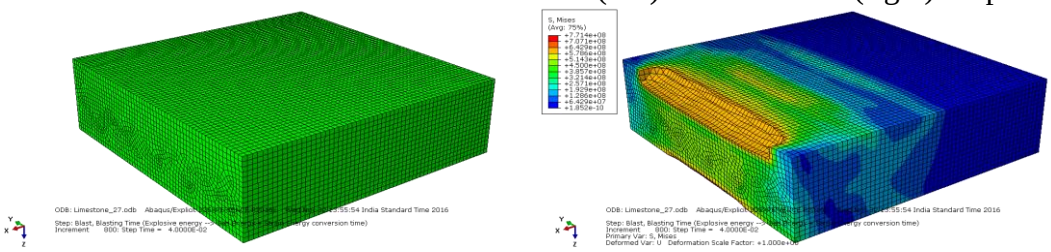

Limestone model no. 27 with un-deformed (left) and deformed (right) shapes

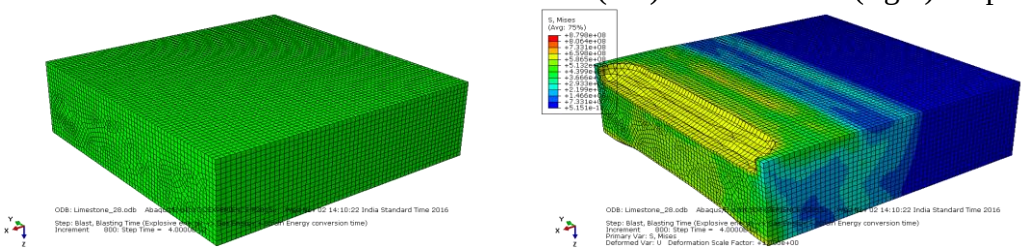

Limestone model no. 28 with un-deformed (left) and deformed (right) shapes

Fig. A8.3 Un-deformed and deformed shapes of blast models in limestone formation

APPENDIX – IX

COAL FORMATION
(Input Parameters used for Numerical Modelling)

Sl. No.	Blastholes	Width (m)	Height (m)	Depth (m)	E/h (kg)	MCD (kg)	TC (kg)
1	10	3.6	1.9	1.80	0.57	2.59	5.74
2	10	3.5	1.2	1.80	0.65	3.33	6.48
3	10	3.5	1.7	1.80	0.67	2.96	6.66
4	10	3.4	1.6	1.80	0.67	2.96	6.66
5	10	3.5	1.5	1.80	0.74	3.33	6.85
6	10	3.4	1.6	1.80	0.69	2.59	6.85
7	10	3.4	1.6	1.80	0.69	3.33	6.85
8	10	3.4	1.6	1.80	0.69	3.33	6.85
9	12	3.4	1.5	1.80	0.59	2.59	7.03
10	10	3.5	1.7	1.80	0.67	2.96	7.59
11	12	3.7	1.7	1.80	0.68	2.96	8.14
12	16	3.6	2.4	1.80	0.74	2.96	8.88
13	12	3.5	1.7	1.80	0.74	3.33	8.88
14	12	3.5	1.7	1.80	0.75	3.33	8.88

E/h – Explosive charge per hole, MCD – Maximum charge per delay, TC – Total explosive charge per blast.

APPENDIX – X (NUMERICAL MODELLING ANALYSIS OF COAL FORMATION)

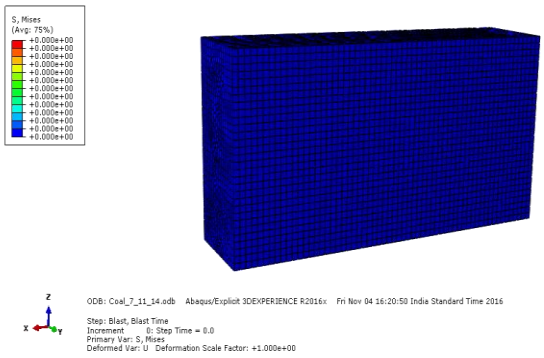

0ms

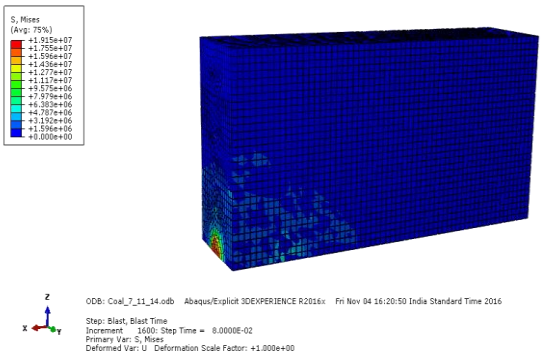

80ms

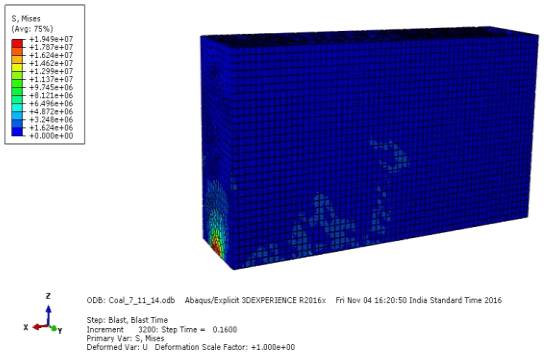

160ms

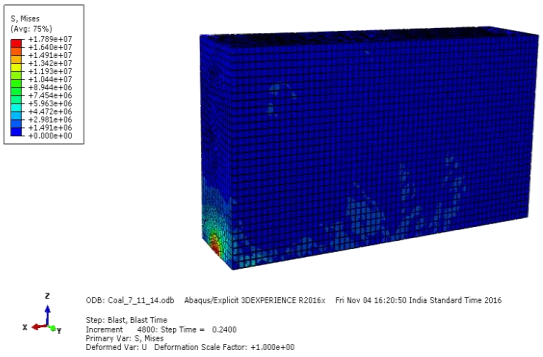

240ms

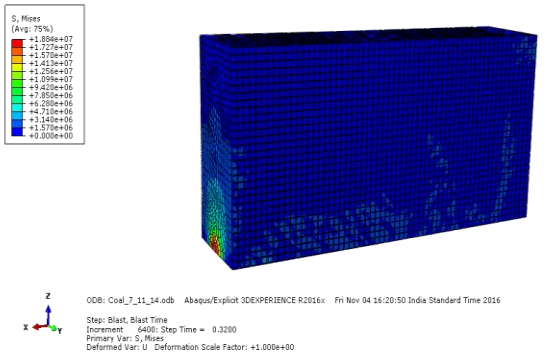

320ms

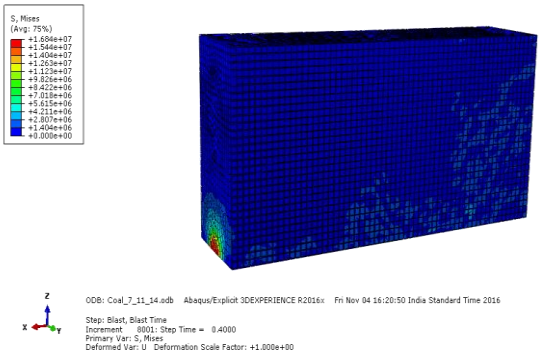

400ms

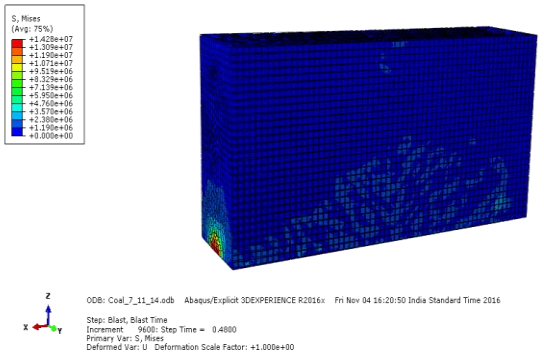

480ms

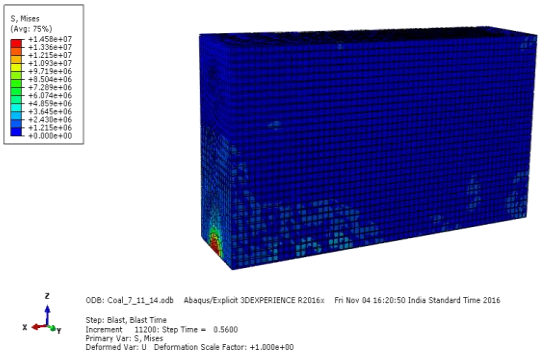

560ms

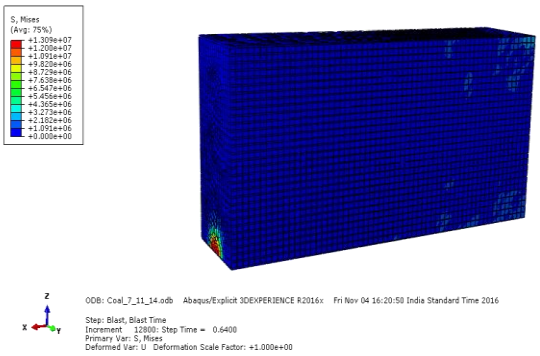

640ms

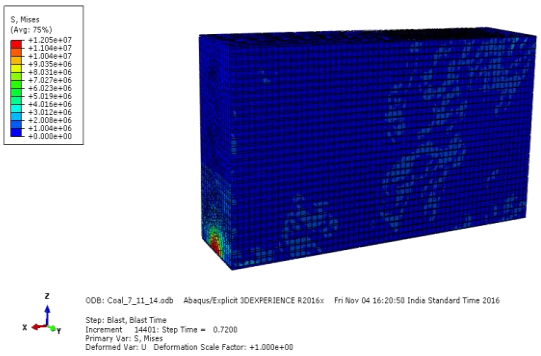

720ms

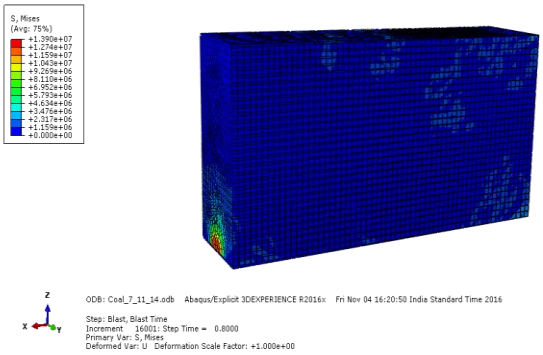

800ms

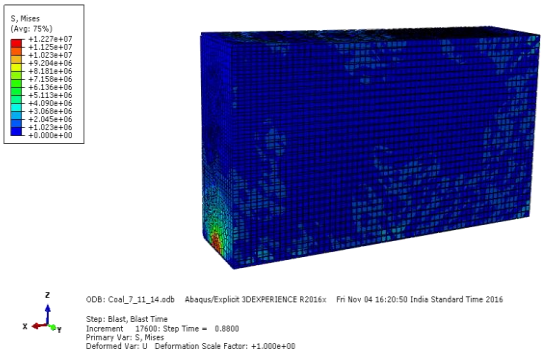

880ms

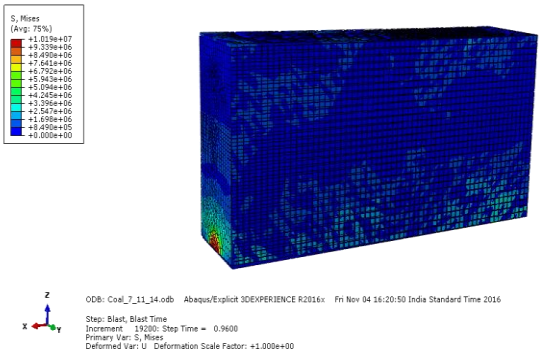

960ms

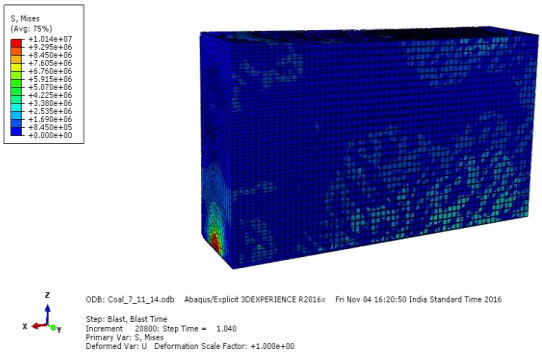

1040ms

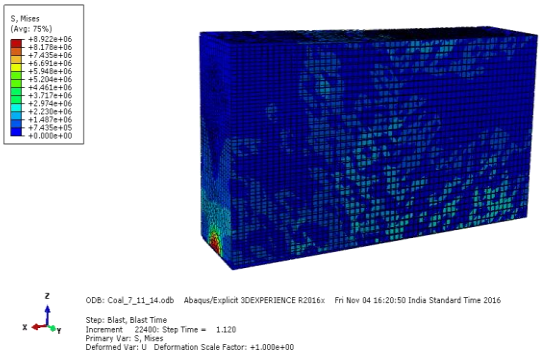

1120ms

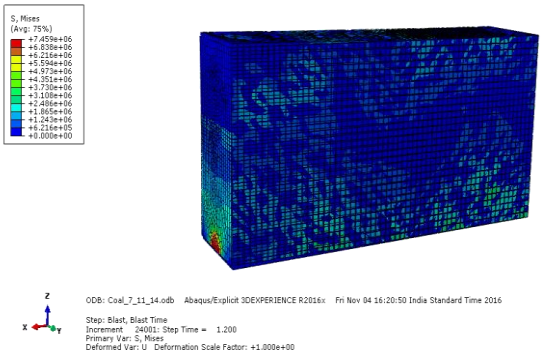

1200ms

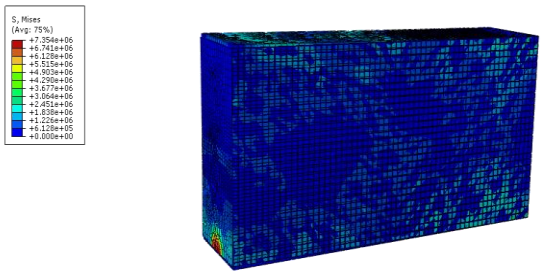

1280ms

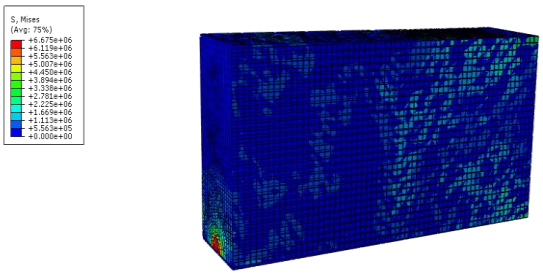

1360ms

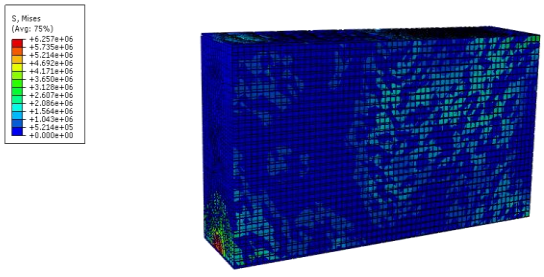

1440ms

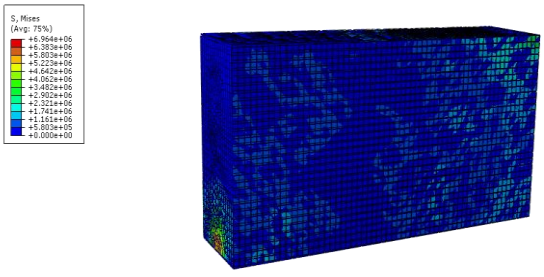

1520ms

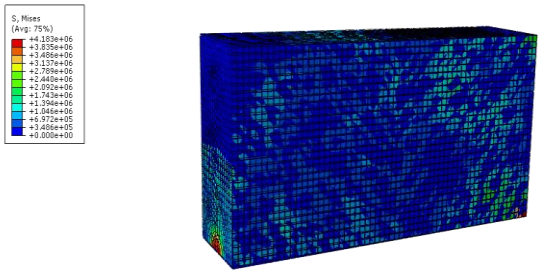

1600ms

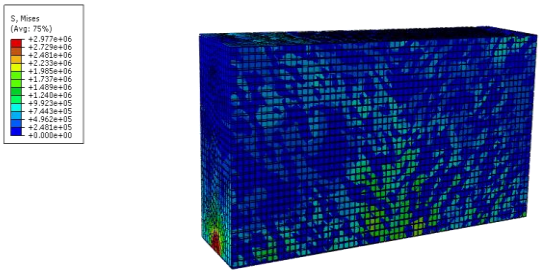

1680ms

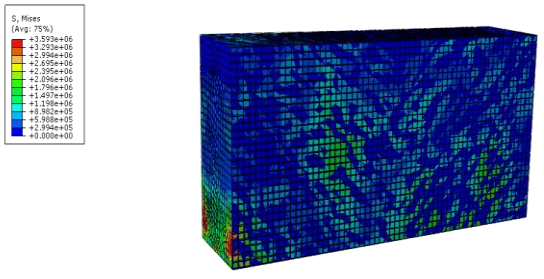

1760ms

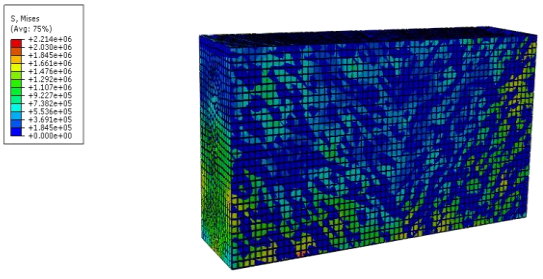

1840ms

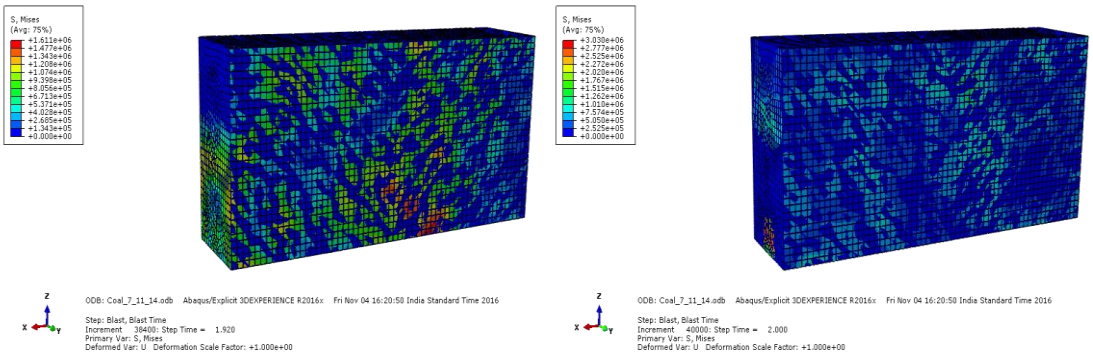

1920ms 2000ms

Fig. A10.1 Stress components at integral points in the model of coal formation

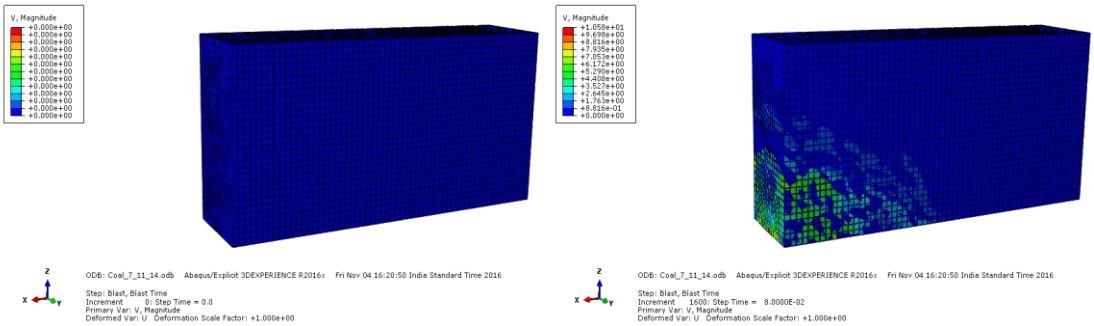

0ms 80ms

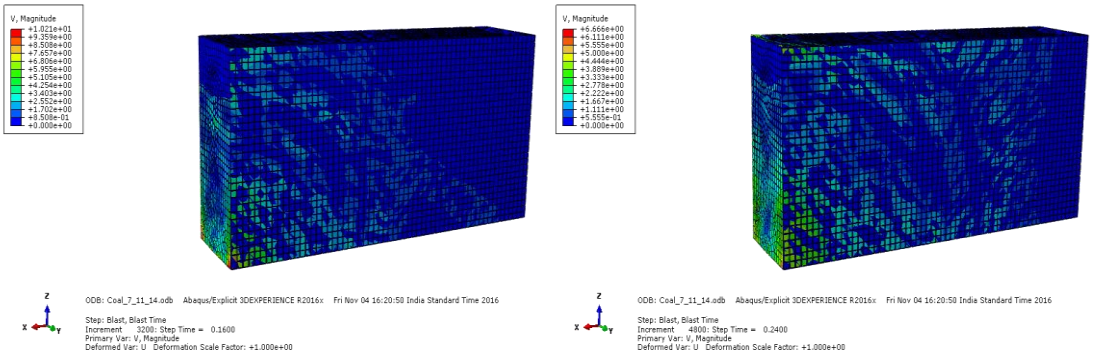

160ms 240ms

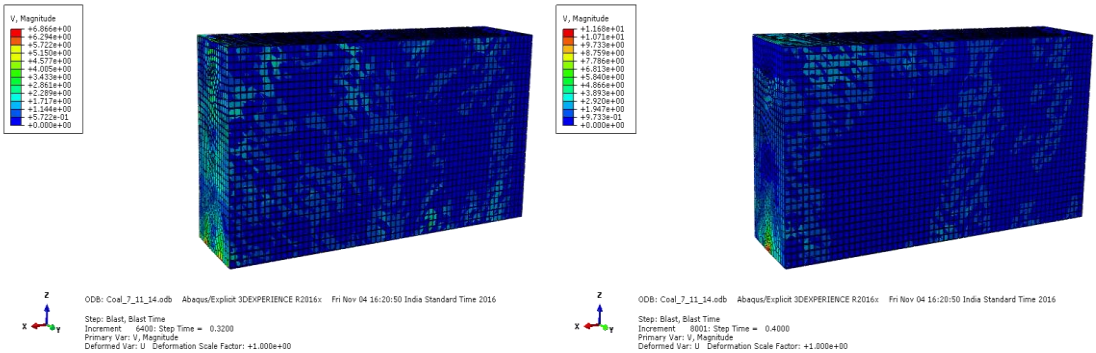

320ms 400ms

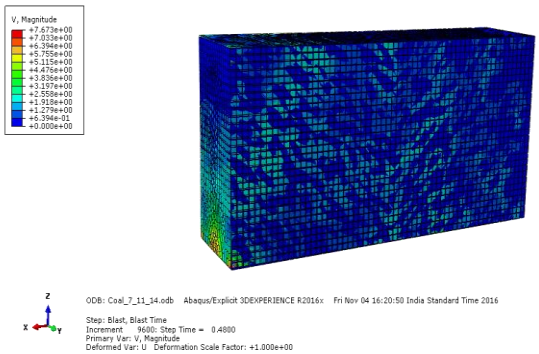

480ms

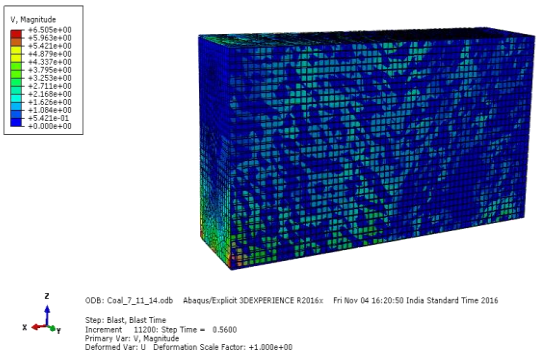

560ms

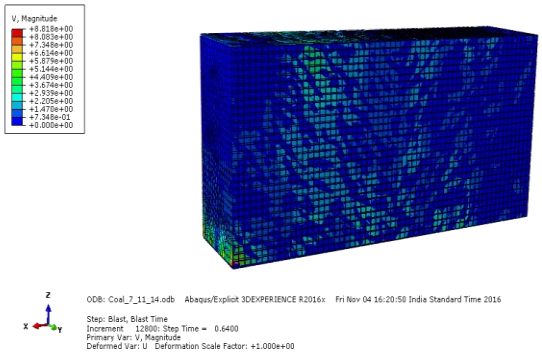

640ms

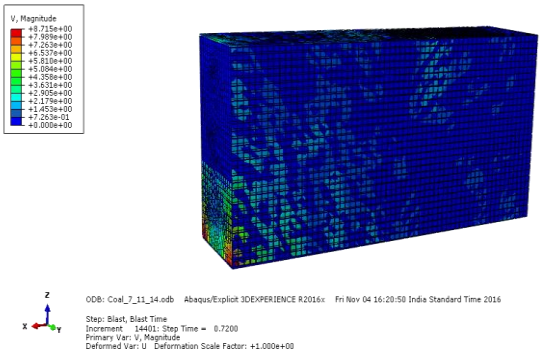

720ms

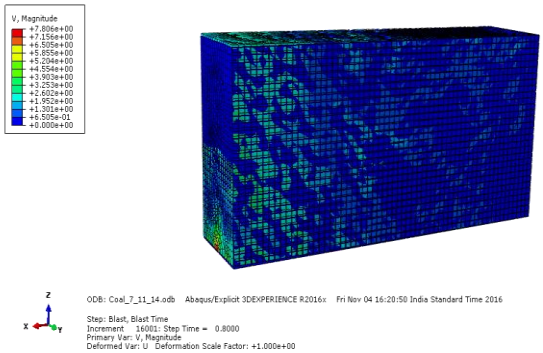

800ms

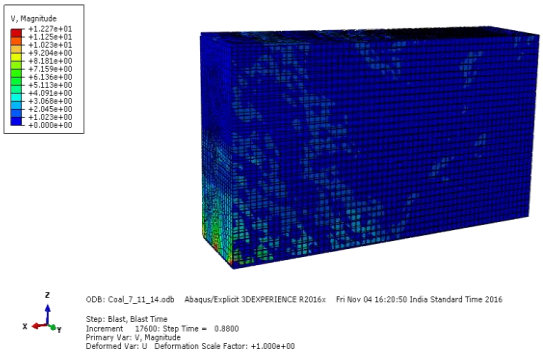

880ms

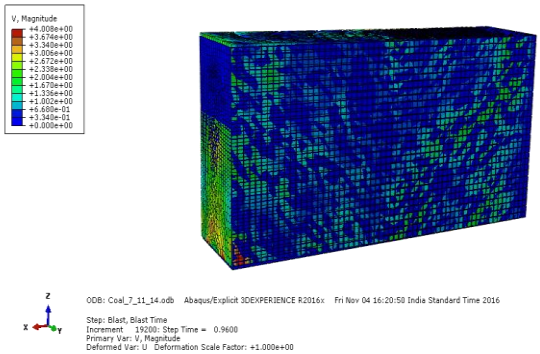

960ms

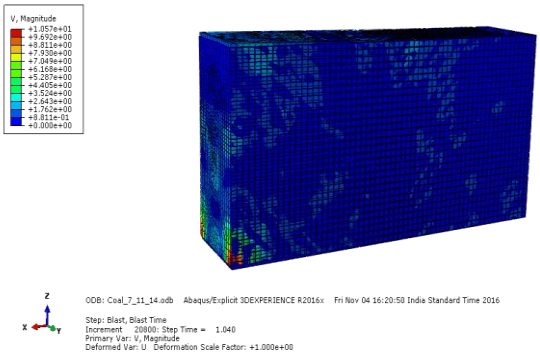

1040ms

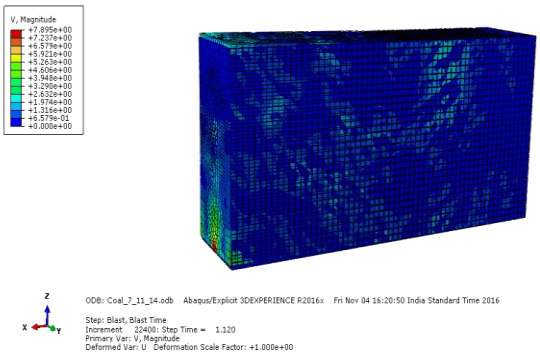

1120ms

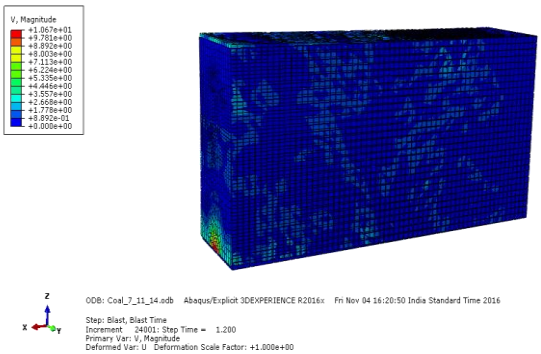

1200ms

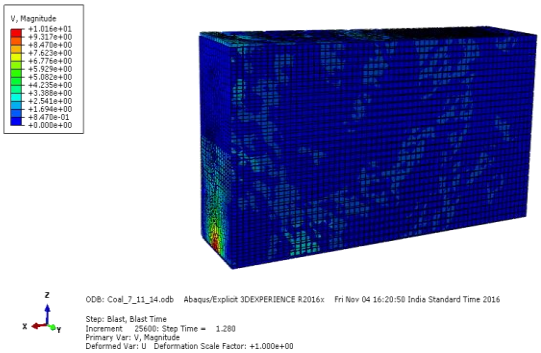

1280ms

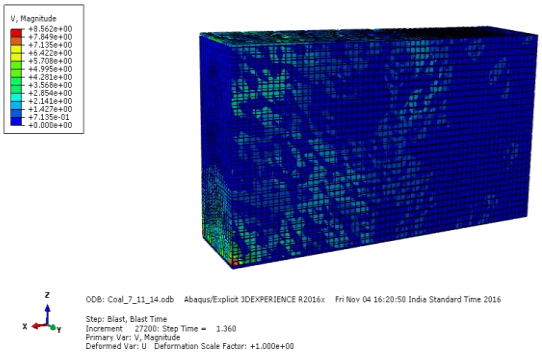

1360ms

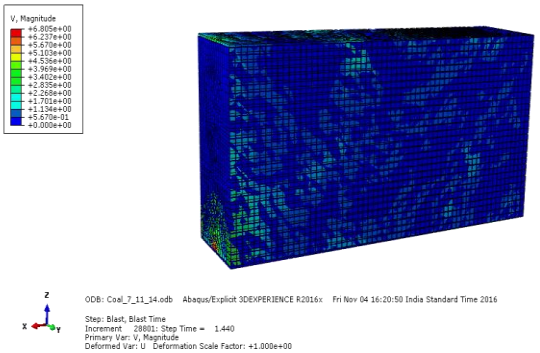

1440ms

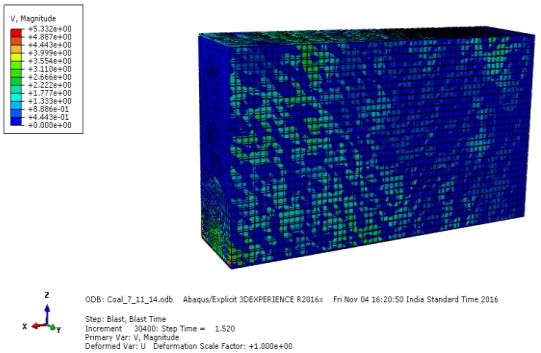

1520ms

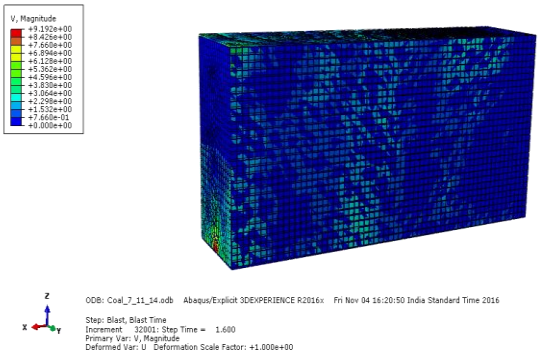

1600ms

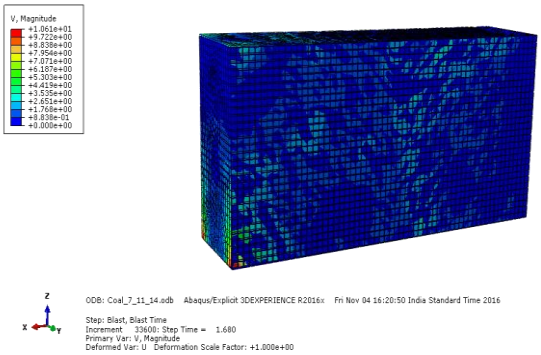

1680ms

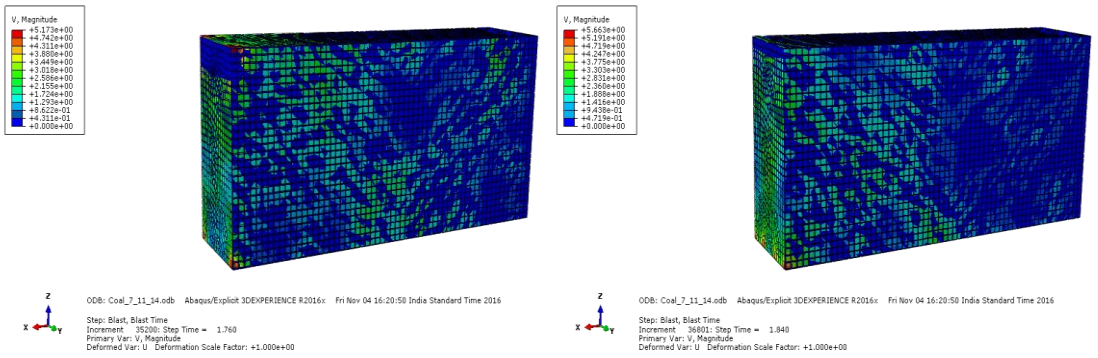

1760ms 1840ms

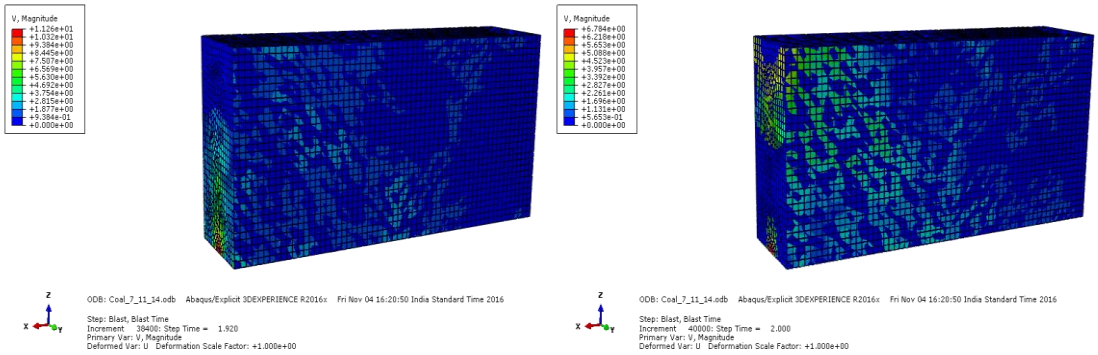

1920ms 2000ms

Fig. A10.2 Spatial velocity contours observed at nodes in coal formation

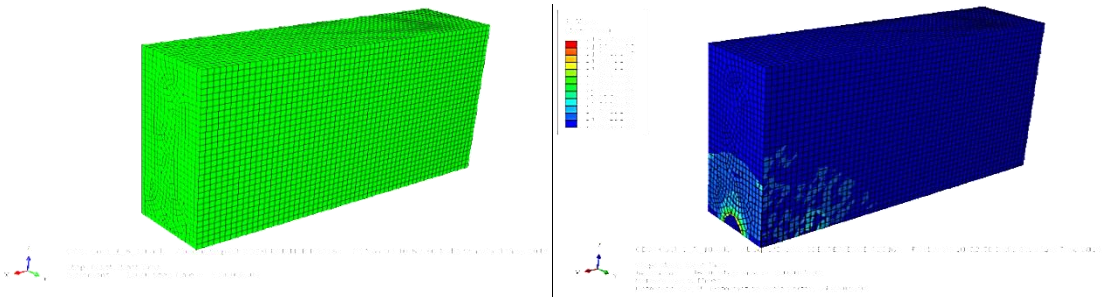

Coal model no. 1 with un-deformed (left) and deformed (right) shapes

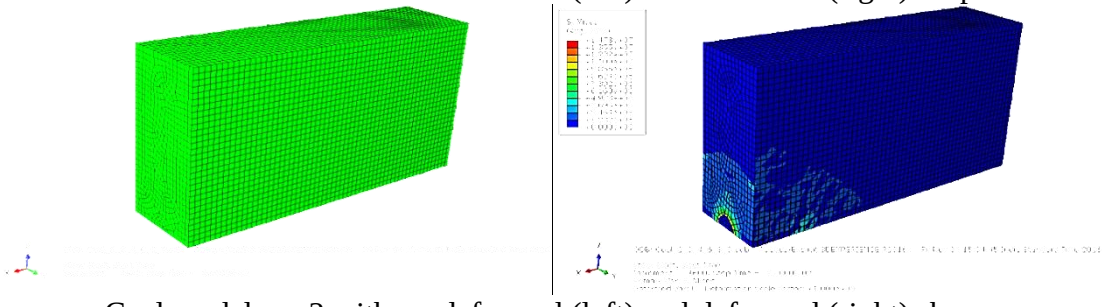

Coal model no. 2 with un-deformed (left) and deformed (right) shapes

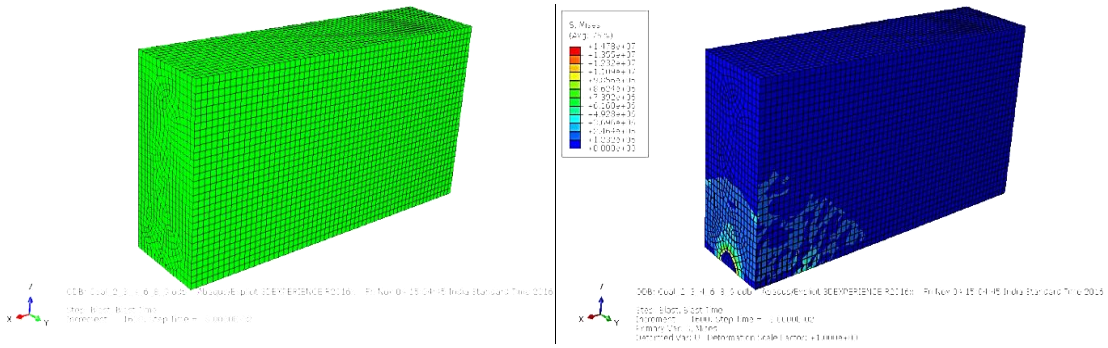

Coal model no. 3 with un-deformed (left) and deformed (right) shapes

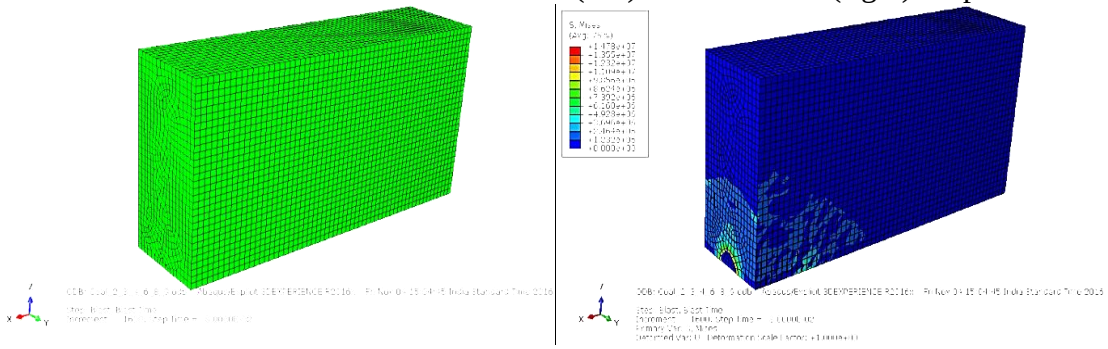

Coal model no. 4 with un-deformed (left) and deformed (right) shapes

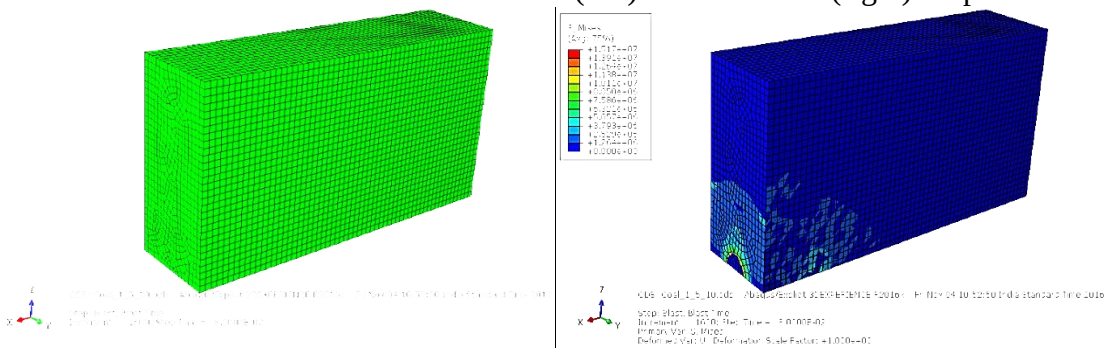

Coal model no. 5 with un-deformed (left) and deformed (right) shapes

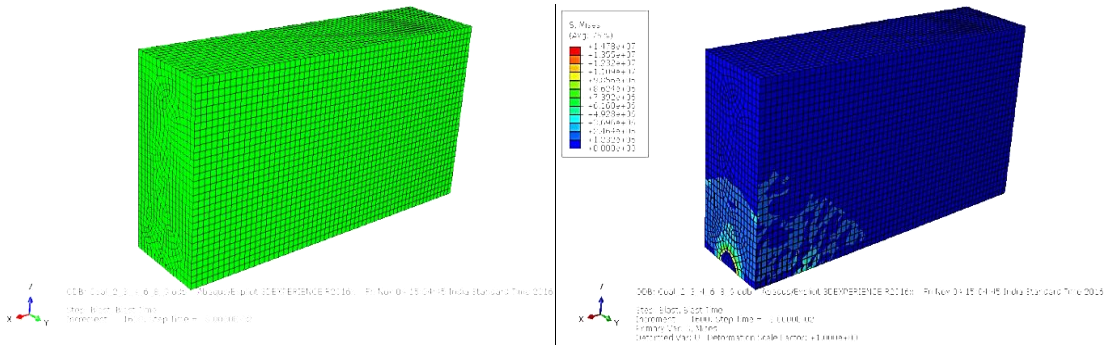

Coal model no. 6 with un-deformed (left) and deformed (right) shapes

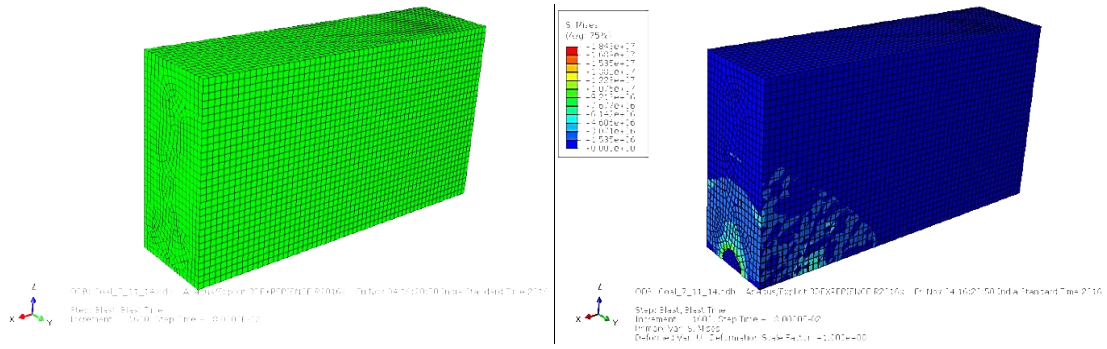

Coal model no. 7 with un-deformed (left) and deformed (right) shapes

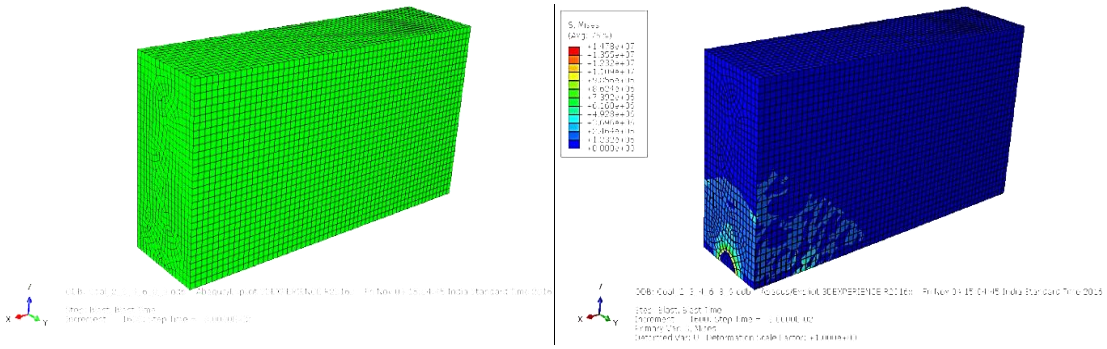

Coal model no. 8 with un-deformed (left) and deformed (right) shapes

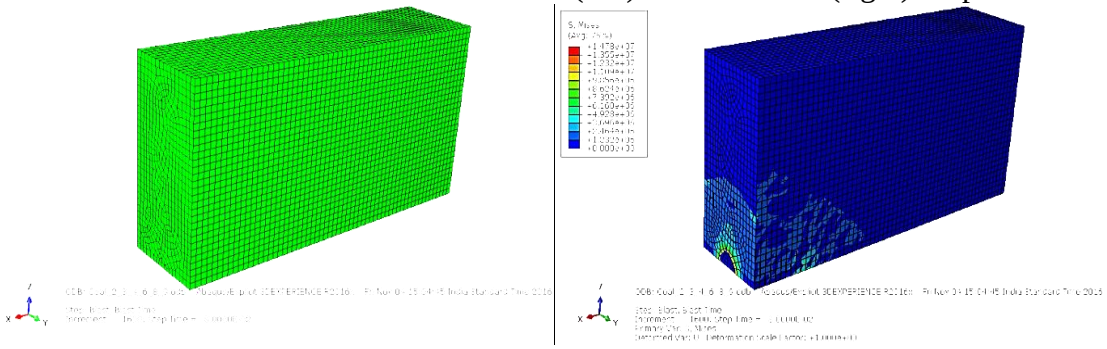

Coal model no. 9 with un-deformed (left) and deformed (right) shapes

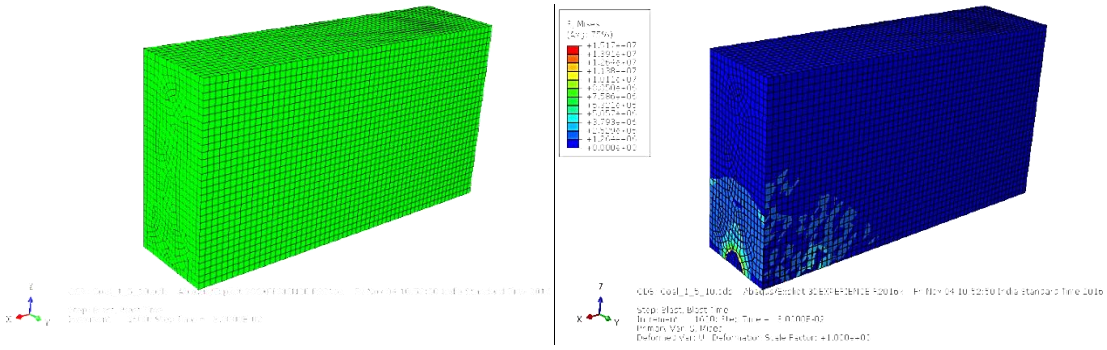

Coal model no. 10 with un-deformed (left) and deformed (right) shapes

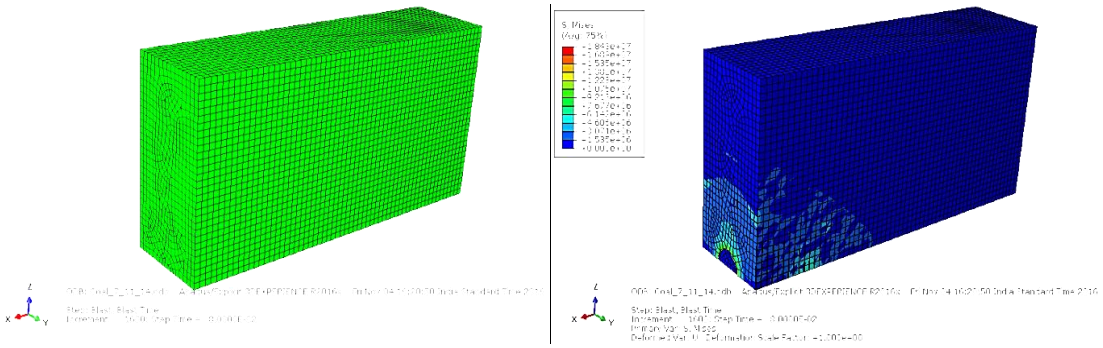

Coal model no. 11 with un-deformed (left) and deformed (right) shapes

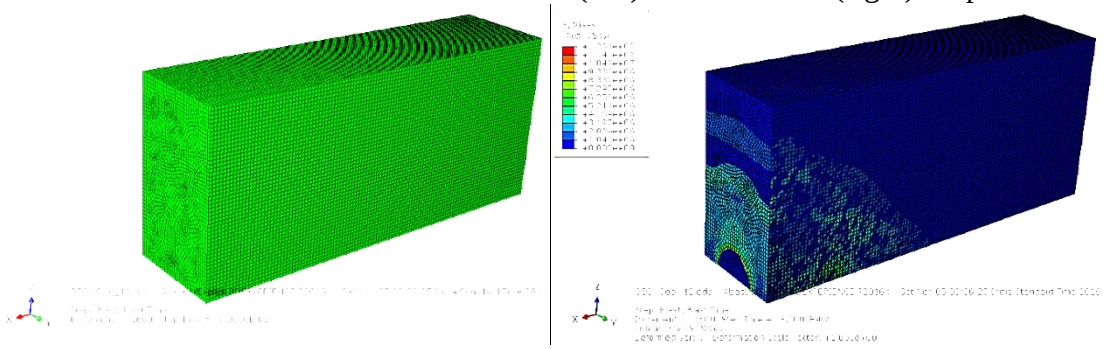

Coal model no. 12 with un-deformed (left) and deformed (right) shapes

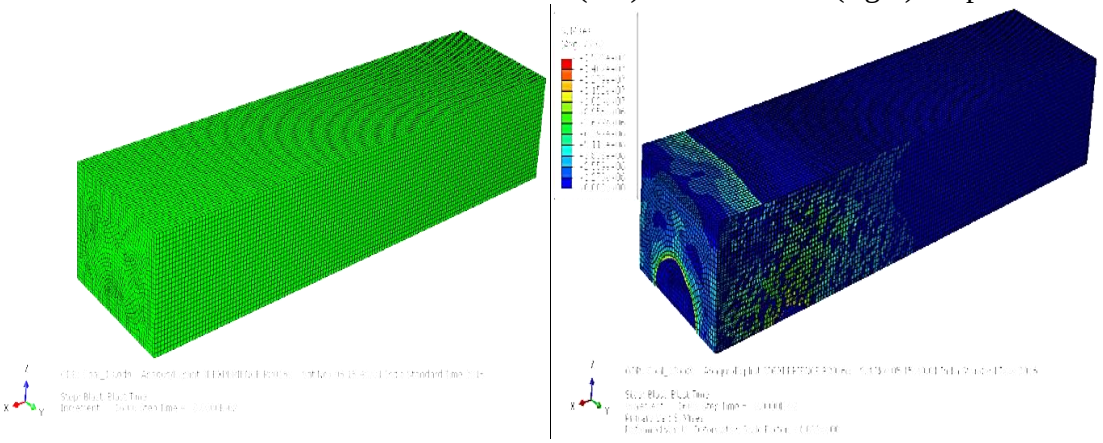

Coal model no. 13 with un-deformed (left) and deformed (right) shapes

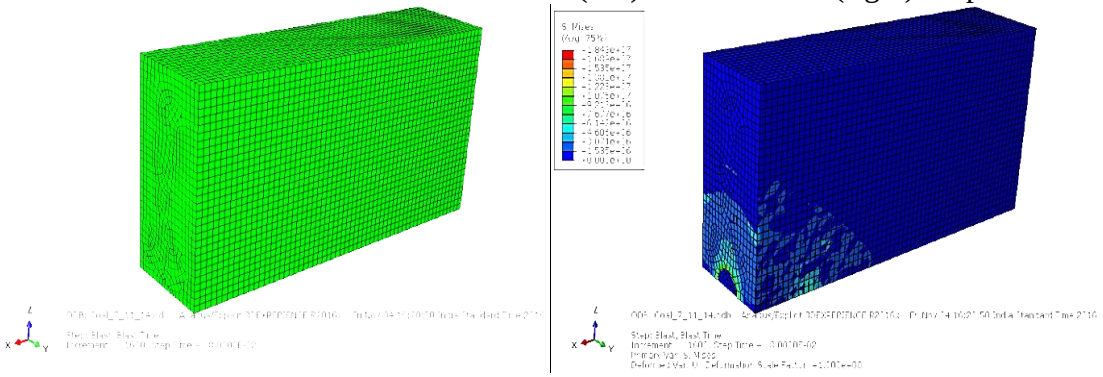

Coal model no. 14 with un-deformed (left) and deformed (right) shapes

Fig. A10.3 Un-deformed and deformed shapes of blast models in coal formation

APPENDIX – XI

SANDSTONE FORMATION
(Input Parameters used for Numerical Modelling)

Sl. No.	B	S	Blastholes	Length (m)	Width (m)	Depth (m)	E/h (kg)	MCD (kg)	TC (kg)
1	3	3	55	17	30	5.0	5.60	11.12	308.00
2	3	3	40	30	12	5.0	10.07	20.85	402.80
3	3	3	44	15	27	5.0	10.39	34.75	457.16
4	3	3	49	18	24	5.0	9.98	22.24	489.02
5	3	4	58	17	42	5.0	12.60	27.61	730.80
6	5	6	30	26	35	4.5	50.00	100.00	1,500.00
7	5	6	44	38	35	14.0	45.00	90.00	1,980.00
8	5	6	43	65	20	20.7	50.00	100.00	2,150.00
9	4	5	105	105	20	5.5	25.00	50.00	2,625.00
10	5	5	81	81	25	5.5	33.00	66.00	2,673.00
11	5	5	84	84	25	5.5	33.00	66.00	2,772.00
12	5	6	81	81	30	5.5	40.37	85.00	3,269.97
13	5	6	121	121	30	5.8	44.00	88.00	5,324.00
14	7	9	35	79	28	5.0	460.00	460.00	16,100.00
15	5	7	47	82	20	14.0	913.80	1,953.00	42,948.60

B – Burden, S – Spacing, E/h – Explosive charge per hole, MCD – Maximum charge per delay, TC – Total explosive charge per blast.

APPENDIX – XII (NUMERICAL MODELLING ANALYSIS OF SANDSTONE FORMATION)

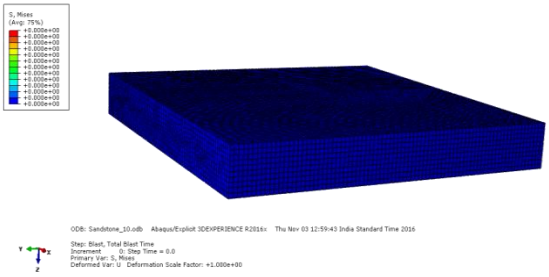

0ms

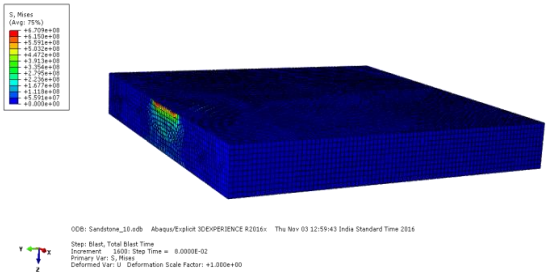

80ms

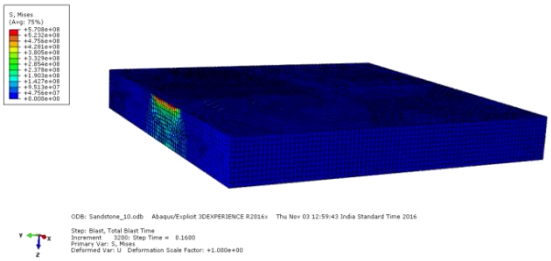

160ms

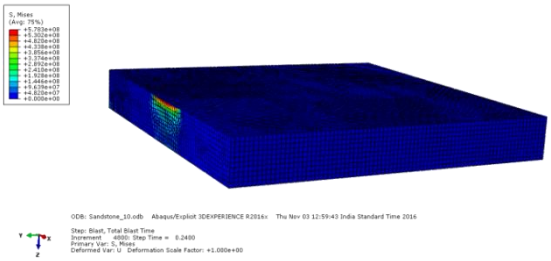

240ms

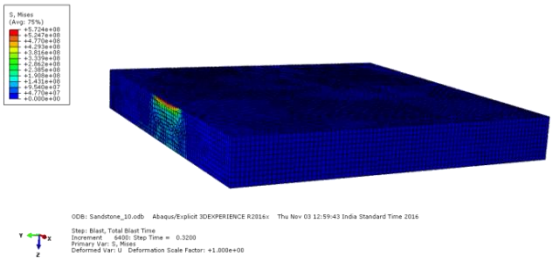

320ms

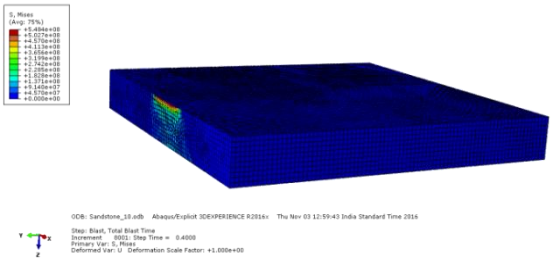

400ms

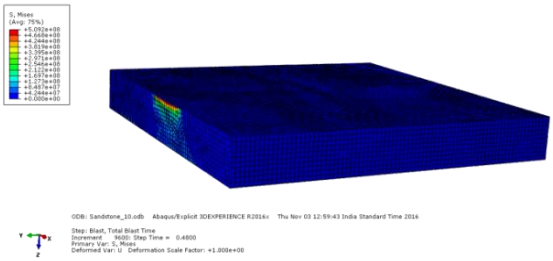

480ms

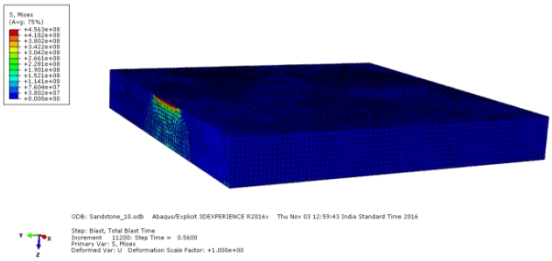

560ms

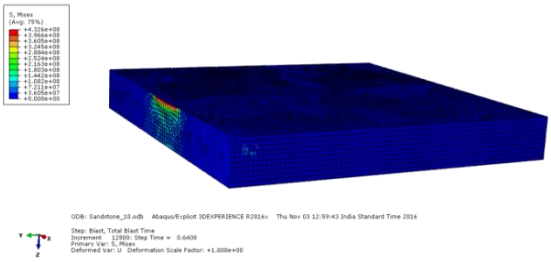

640ms

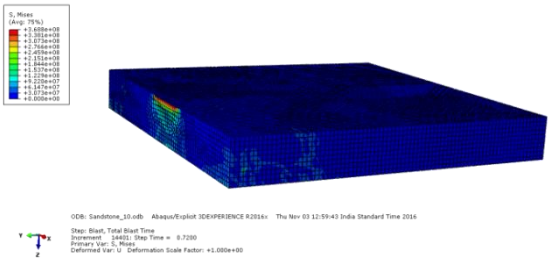

720ms

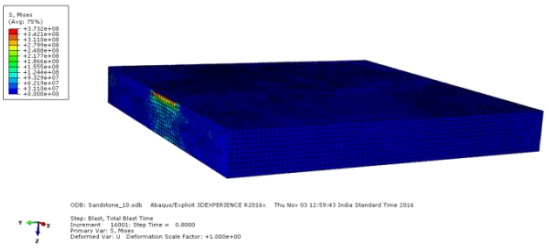

800ms

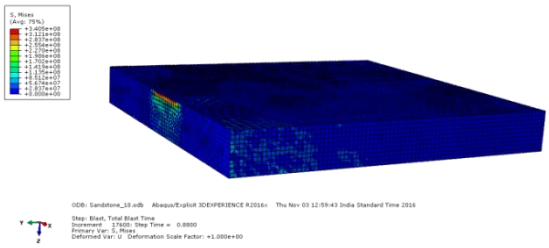

880ms

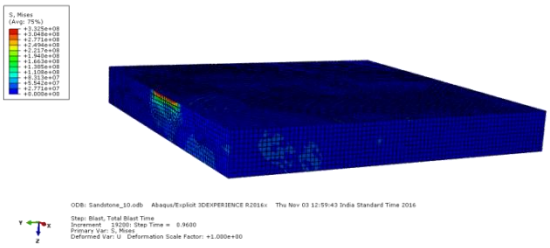

960ms

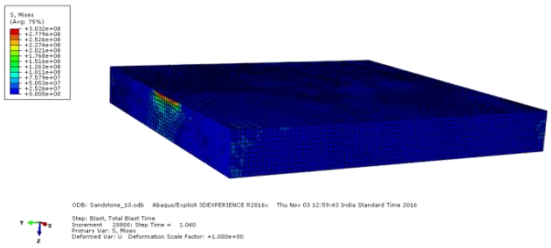

1040ms

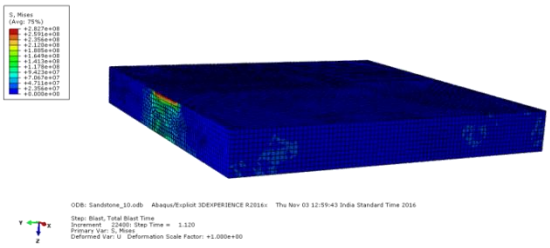

1120ms

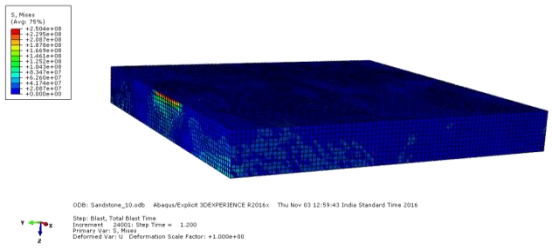

1200ms

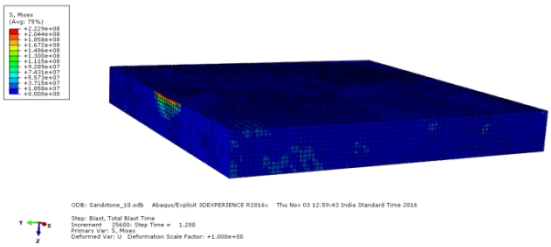

1280ms

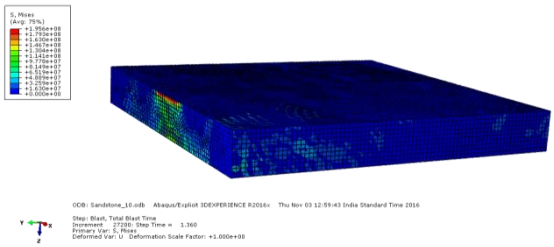

1360ms

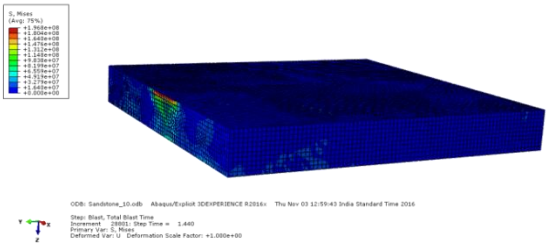

1440ms

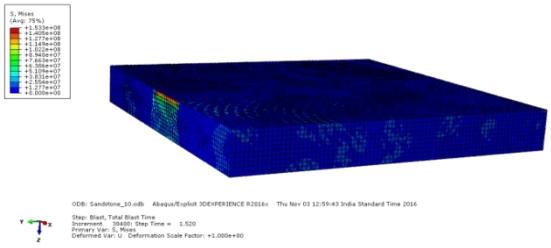

1520ms

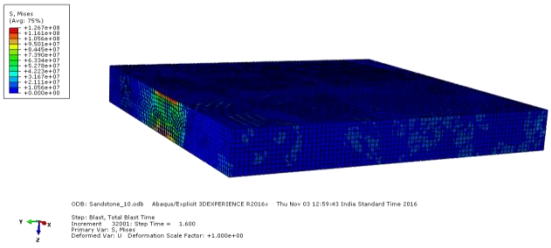

1600ms

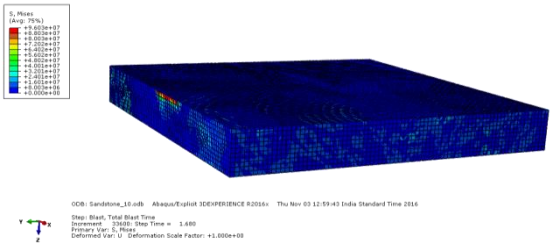

1680ms

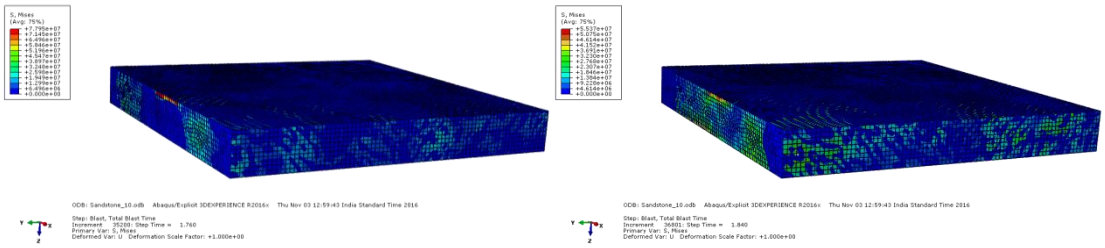

1760ms 1840ms

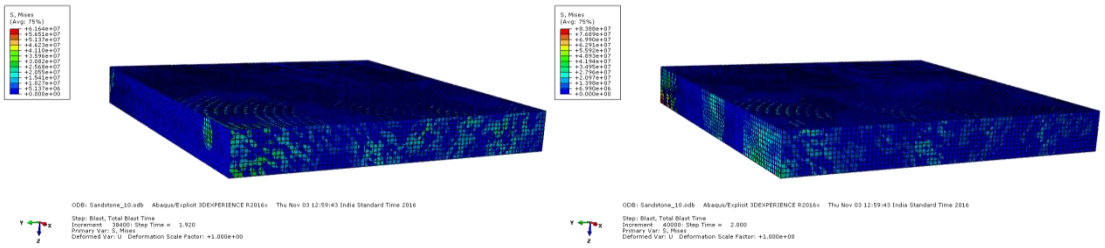

1920ms 2000ms

Fig. A12.1 Stress components at integral points in a sandstone model

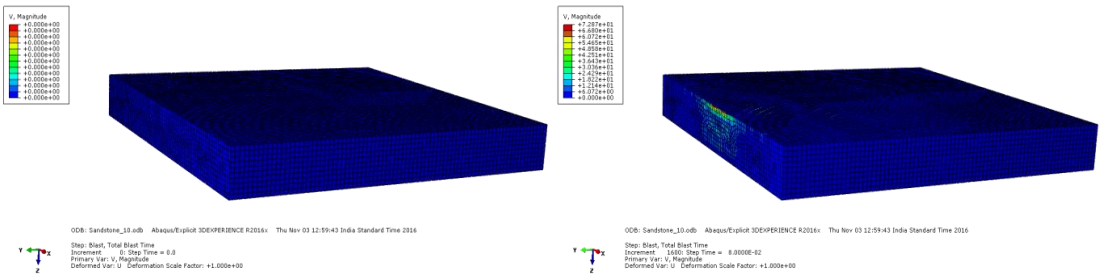

0ms 80ms

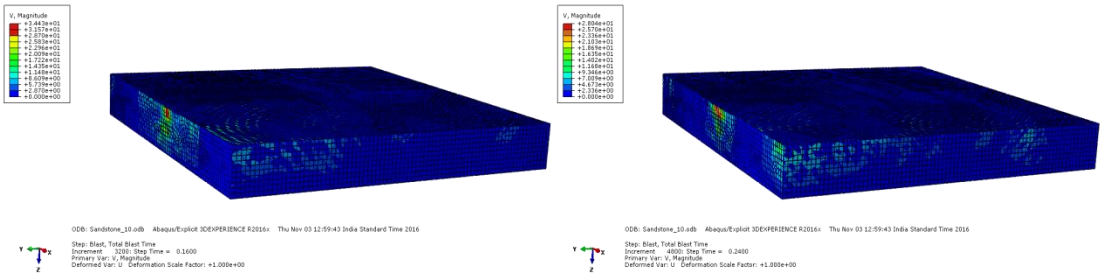

160ms 240ms

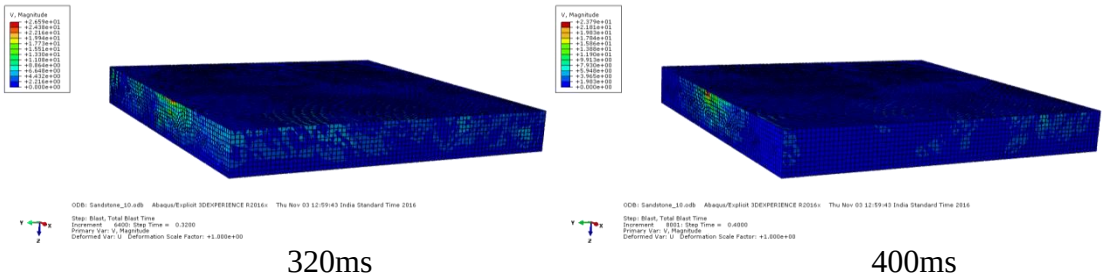

320ms 400ms

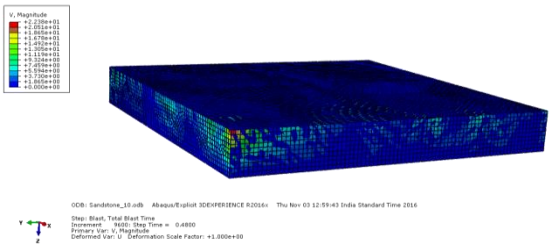

480ms

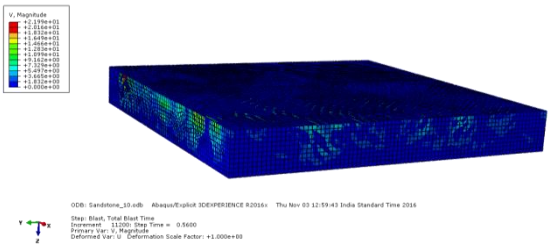

560ms

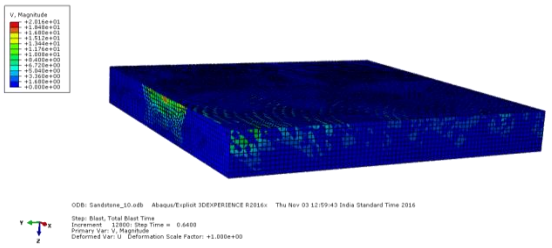

640ms

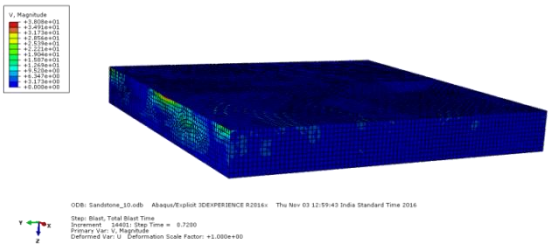

720ms

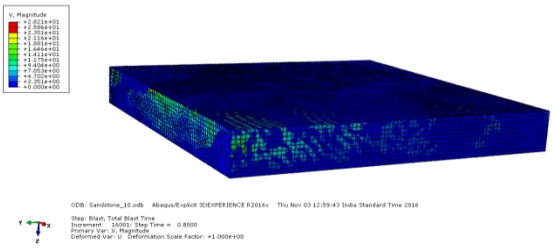

800ms

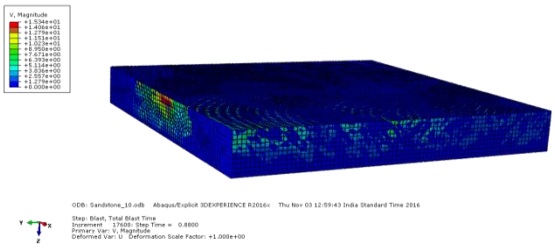

880ms

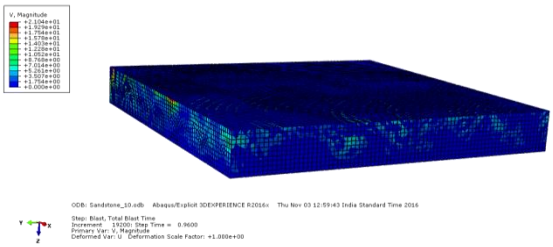

960ms

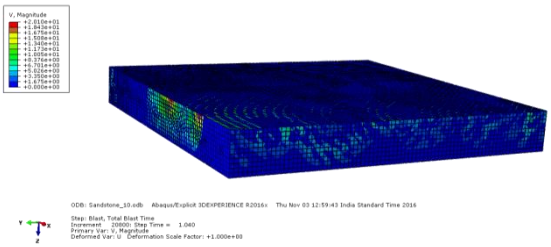

1040ms

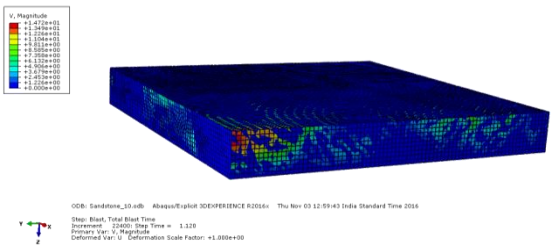

1120ms

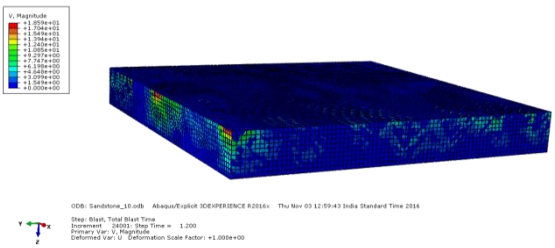

1200ms

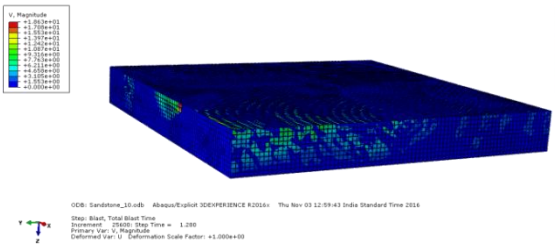

1280ms

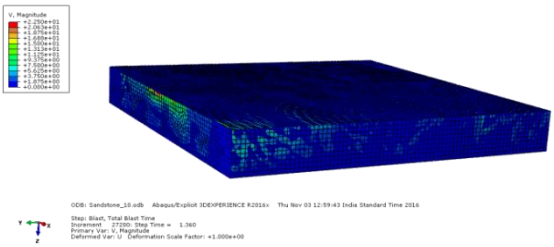

1360ms

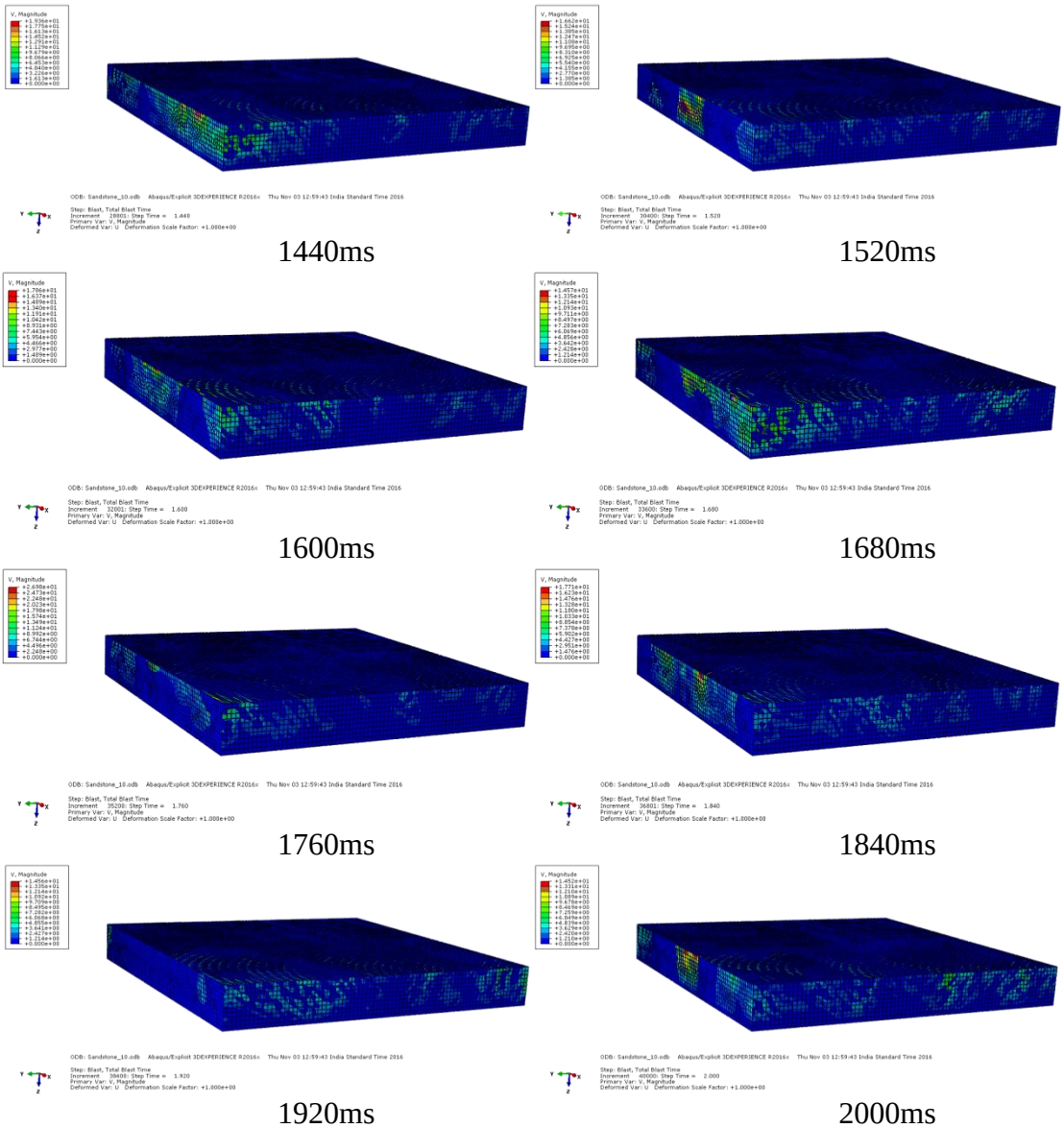

Fig. A12.2 Spatial velocity contours observed at nodes in a sandstone model

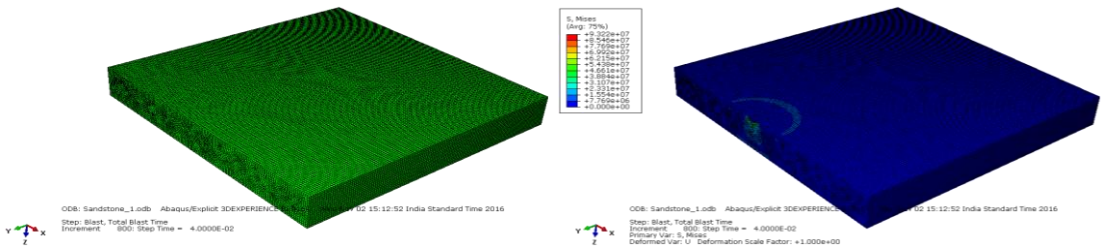

Sandstone model no. 1 with un-deformed (left) and deformed (right) shapes

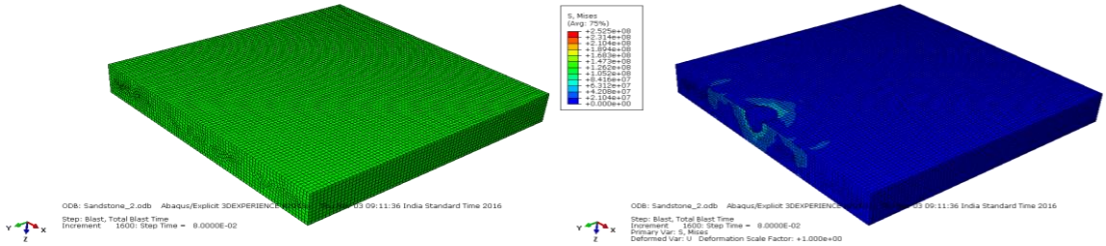

Sandstone model no. 2 with un-deformed (left) and deformed (right) shapes

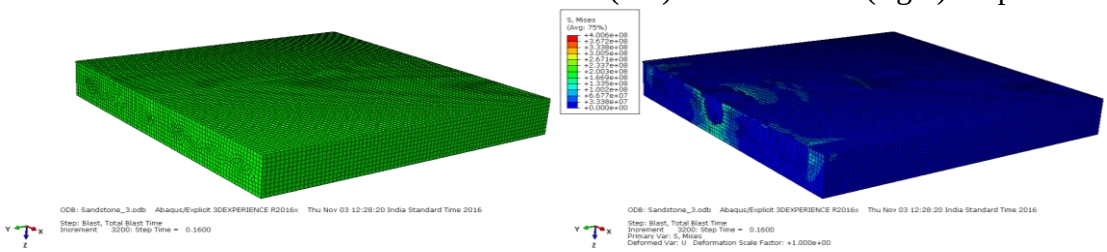

Sandstone model no. 3 with un-deformed (left) and deformed (right) shapes

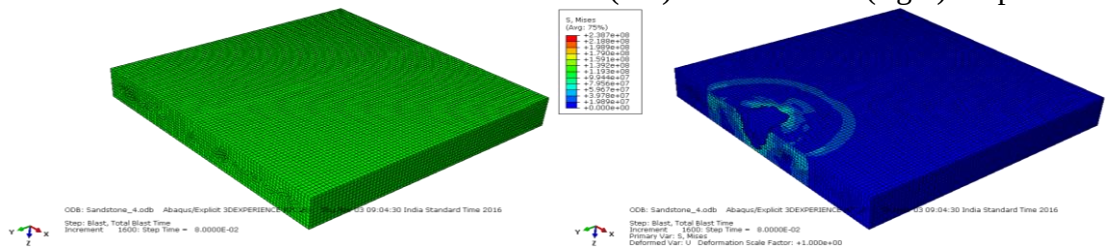

Sandstone model no. 4 with un-deformed (left) and deformed (right) shapes

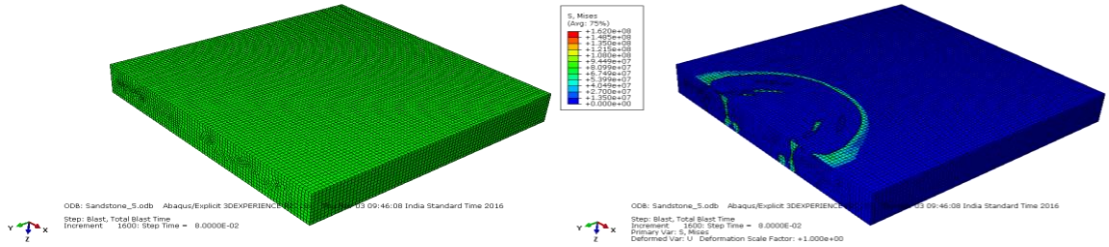

Sandstone model no. 5 with un-deformed (left) and deformed (right) shapes

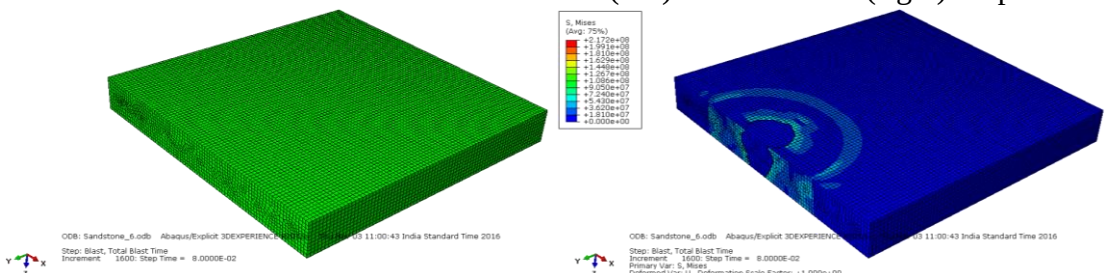

Sandstone model no. 6 with un-deformed (left) and deformed (right) shapes

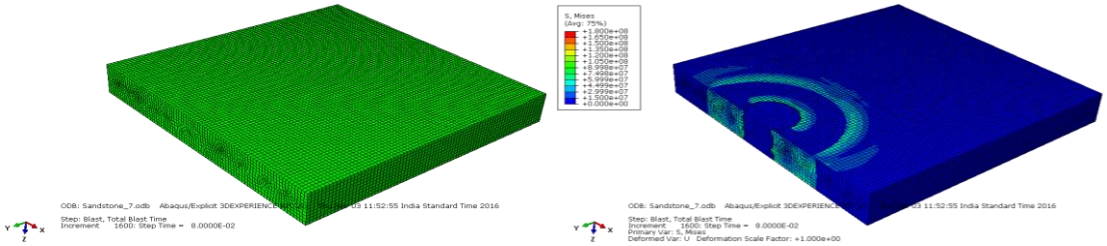

Sandstone model no. 7 with un-deformed (left) and deformed (right) shapes

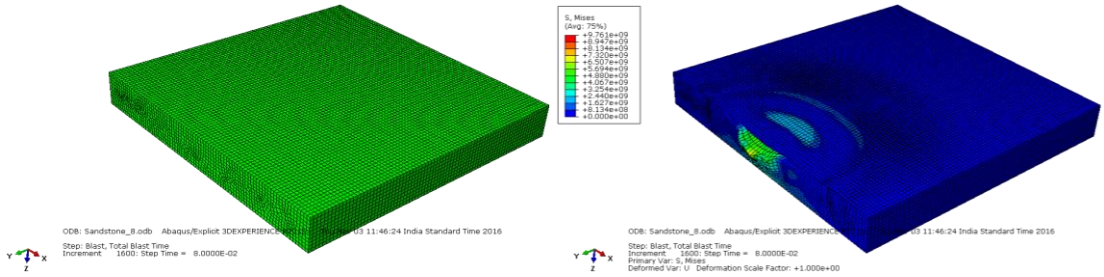

Sandstone model no. 8 with un-deformed (left) and deformed (right) shapes

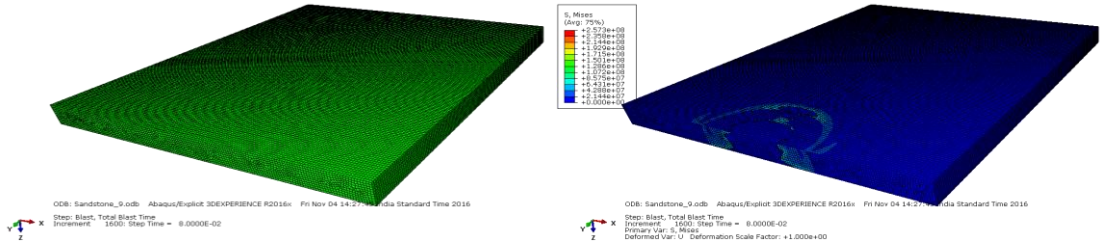

Sandstone model no. 9 with un-deformed (left) and deformed (right) shapes

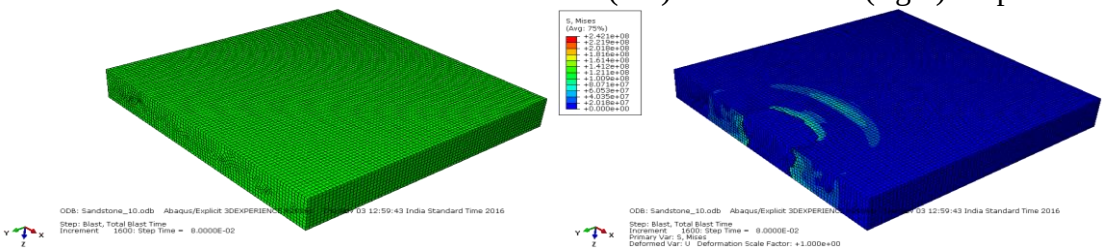

Sandstone model no. 10 with un-deformed (left) and deformed (right) shapes

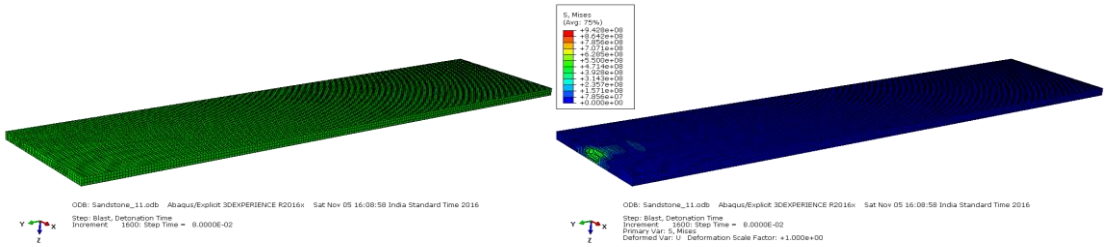

Sandstone model no. 11 with un-deformed (left) and deformed (right) shapes

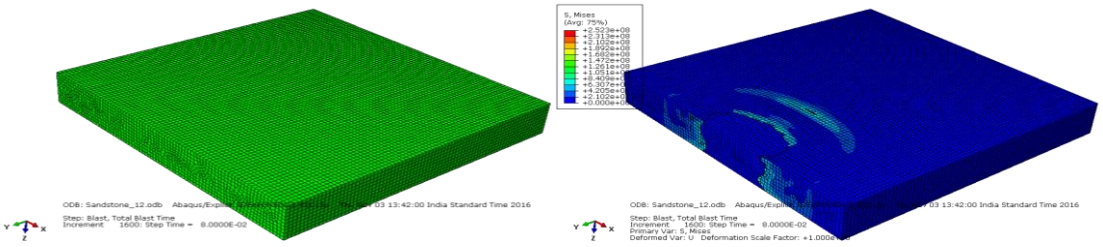

Sandstone model no. 12 with un-deformed (left) and deformed (right) shapes

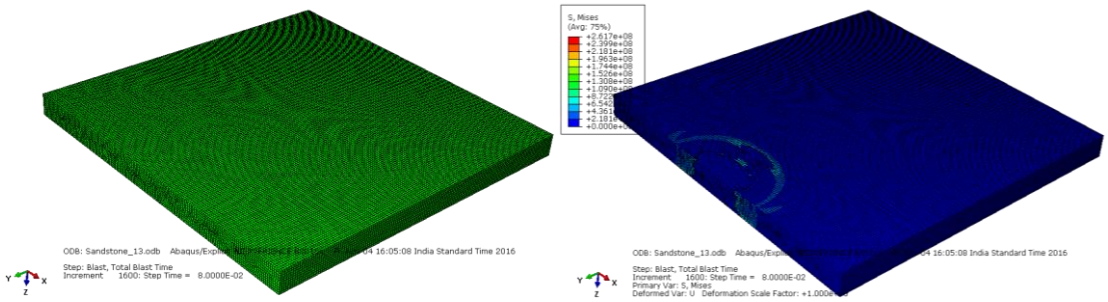

Sandstone model no. 13 with un-deformed (left) and deformed (right) shapes

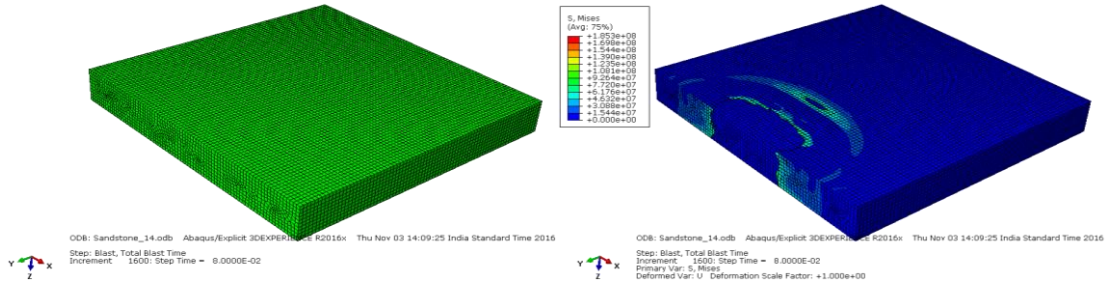

Sandstone model no. 14 with un-deformed (left) and deformed (right) shapes

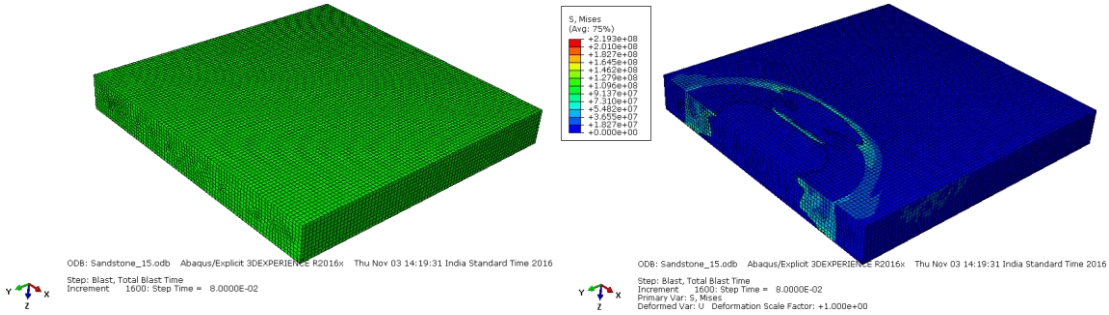

Sandstone model no. 15 with un-deformed (left) and deformed (right) shapes

Fig. A12.3 Un-deformed and deformed shapes of blast models in sandstone formation

APPENDIX – XIII

GRANITE FORMATION
(Input Parameters used for Numerical Modelling)

Sl. No.	B	S	Blastholes	Length (m)	Width (m)	Depth (m)	E/h (kg)	MCD (kg)	TC (kg)
1	2.0	2.5	5	6	4	1.2	0.125	0.125	0.625
2	2.0	3.0	6	9	4	1.2	0.25	0.25	1.50
3	0.6	0.9	6	3	1	1.5	0.25	0.25	1.50
4	2.0	2.5	8	10	4	1.2	0.25	0.50	2.00
5	0.6	0.9	8	4	1	1.5	0.25	0.25	2.00
6	0.6	0.9	8	2	2	1.5	0.25	0.50	2.00
7	2.0	3.0	10	15	4	1.2	0.25	0.50	2.50
8	2.0	2.5	12	8	8	1.2	0.25	0.75	3.00
9	2.0	3.0	12	18	4	1.5	0.25	0.50	3.00
10	0.6	0.9	15	5	2	1.5	0.25	0.50	3.75
11	2.0	2.5	20	10	10	1.2	0.25	1.00	5.00
12	0.6	0.9	20	6	2	1.5	0.25	0.50	5.00
13	2.0	2.5	22	14	8	1.2	0.25	1.50	5.50
14	0.6	0.9	22	7	2	1.5	0.25	1.00	5.50
15	0.6	0.9	24	7	2	1.5	0.25	1.50	6.00
16	0.6	0.9	25	5	3	1.5	0.25	1.00	6.25
17	1.2	1.2	28	11	4	1.5	0.25	0.75	7.00
18	0.6	0.9	28	8	2	1.5	0.25	1.25	7.00
19	2.0	3.0	30	15	12	1.2	0.25	1.00	7.50
20	1.2	1.2	30	12	4	1.5	0.25	0.75	7.50
21	0.6	0.9	30	9	2	1.5	0.25	1.25	7.50
22	3.0	3.0	6	9	6	6.0	19.90	22.22	119.40
23	2.0	2.5	6	8	4	5.0	19.92	19.46	119.52
24	3.0	3.0	8	12	6	5.0	17.72	19.46	141.76
25	2.9	3.0	10	15	6	5.5	18.63	18.63	186.30
26	2.5	3.0	11	17	5	5.0	17.69	19.46	194.59
27	2.0	3.0	12	18	4	5.0	16.68	16.68	200.16
28	2.0	3.0	15	23	4	5.0	13.71	16.68	205.65
29	2.9	3.0	15	15	9	6.0	19.63	22.22	294.45
30	2.0	3.0	18	18	6	5.0	18.07	36.14	325.26
31	3.0	3.5	19	33	6	6.0	20.77	44.48	394.63

B – Burden, S – Spacing, E/h – Explosive charge per hole, MCD – Maximum charge per delay, TC – Total explosive charge per blast.

APPENDIX – XIV (NUMERICAL MODELLING ANALYSIS OF GRANITE FORMATION)

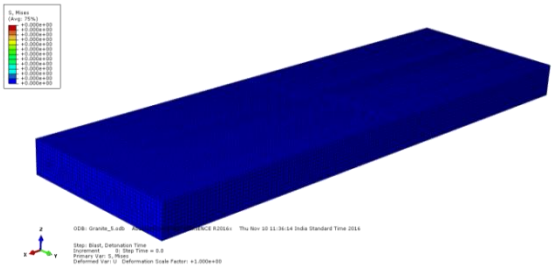

0ms

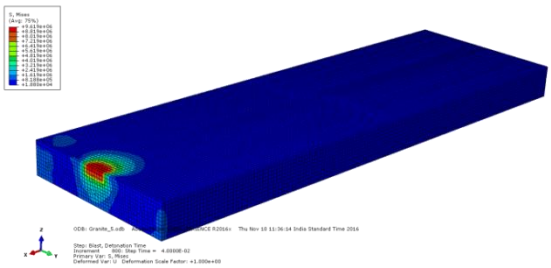

40ms

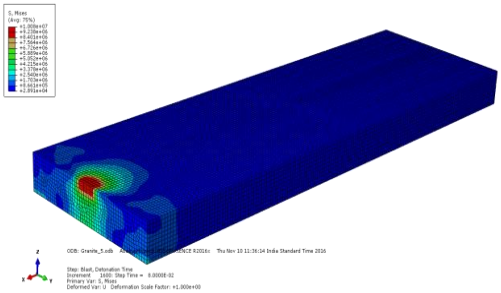

80ms

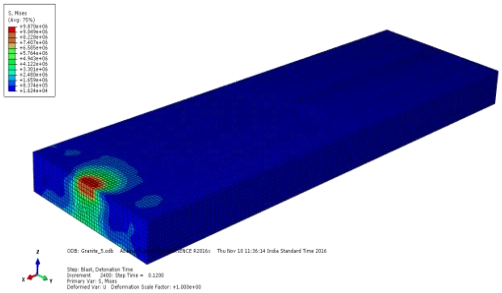

120ms

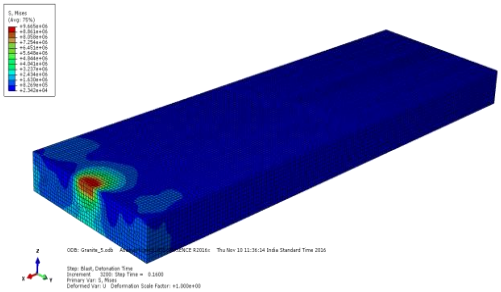

160ms

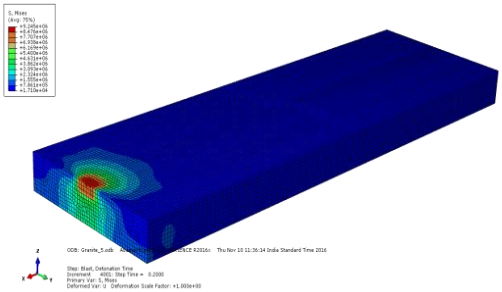

200ms

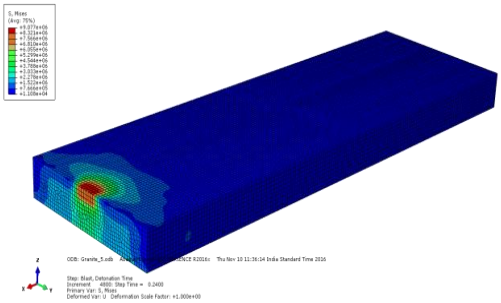

240ms

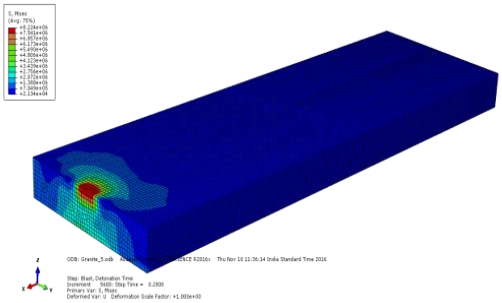

280ms

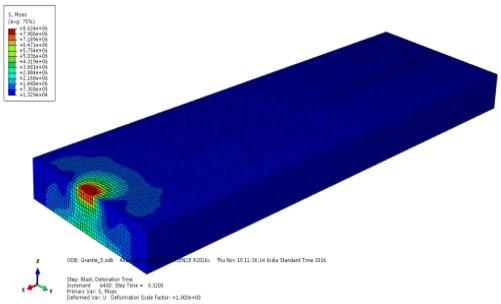

320ms

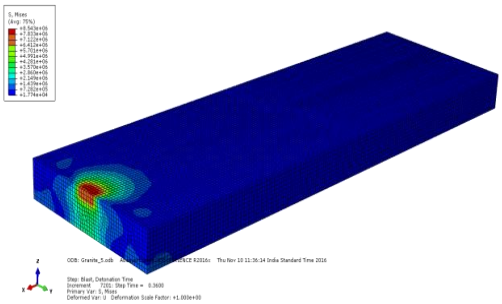

360ms

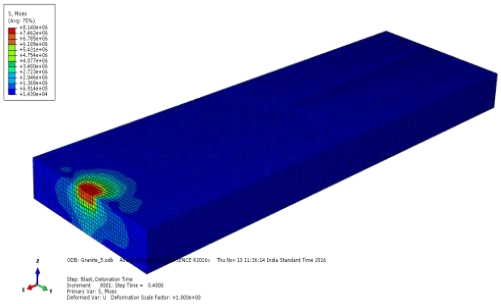

400ms

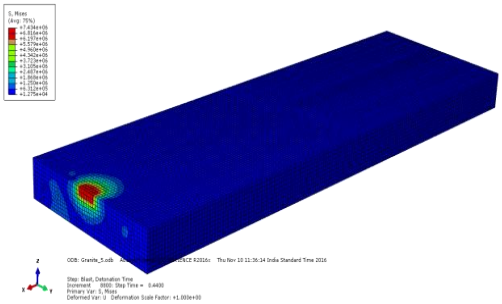

440ms

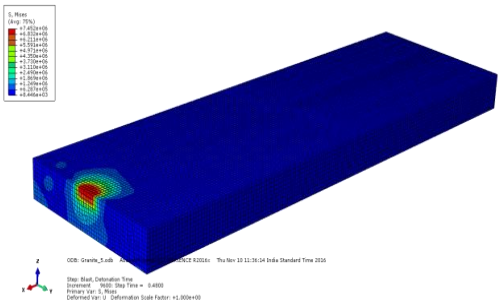

480ms

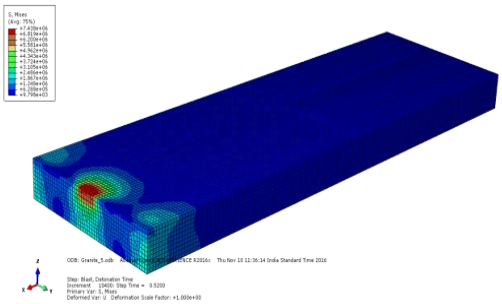

520ms

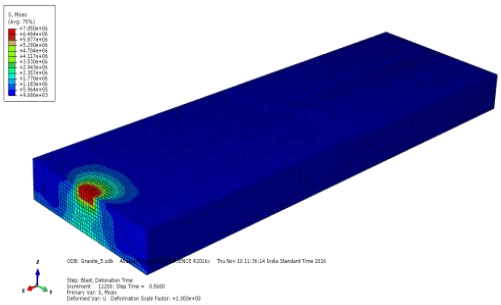

560ms

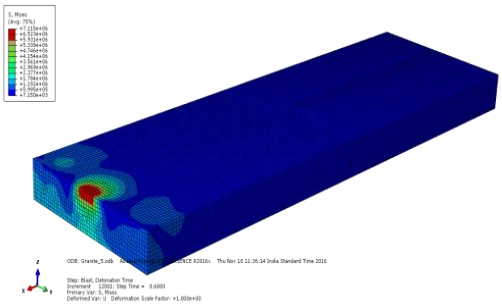

600ms

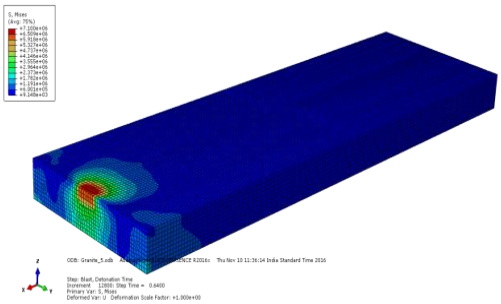

640ms

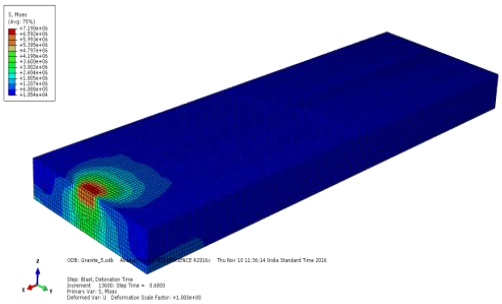

680ms

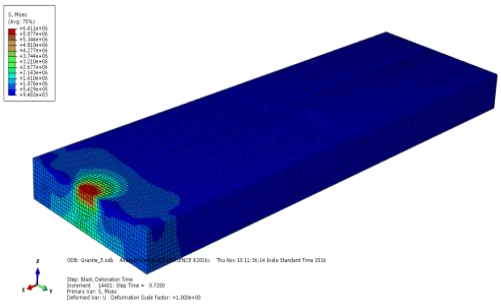

720ms

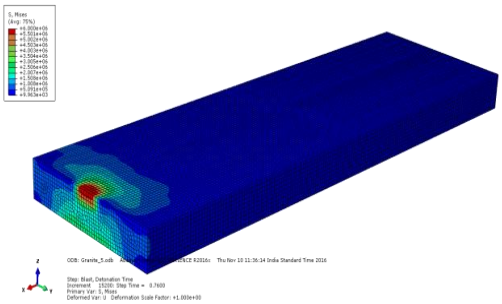

760ms

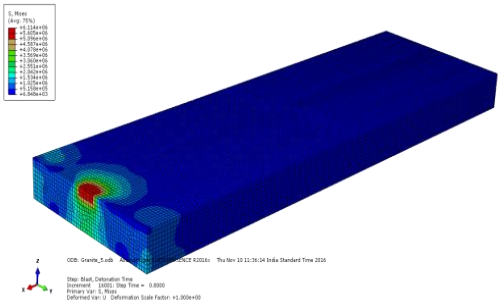

800ms

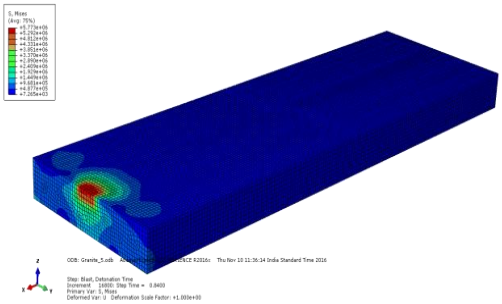

840ms

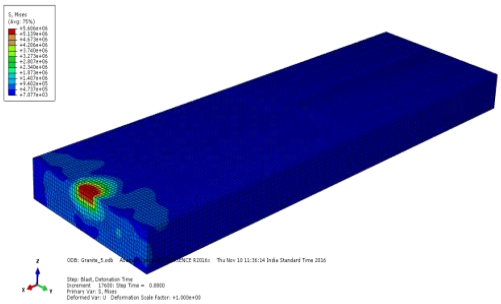

880ms

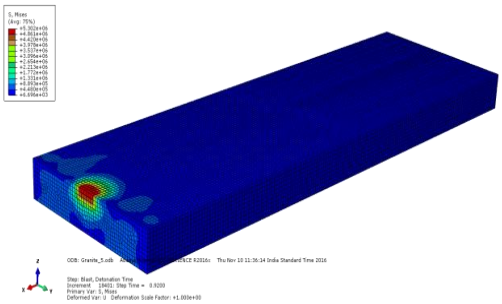

920ms

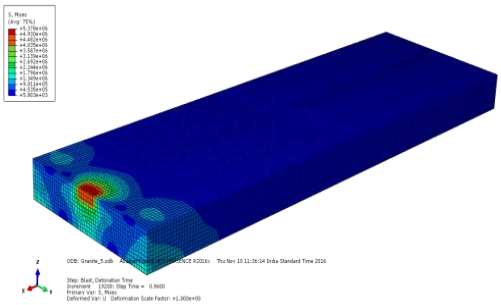

960ms

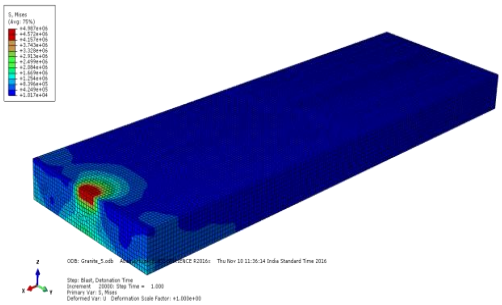

1000ms

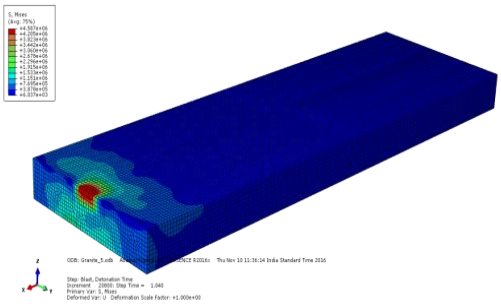

1040ms

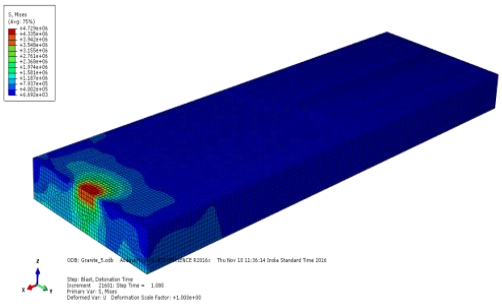

1080ms

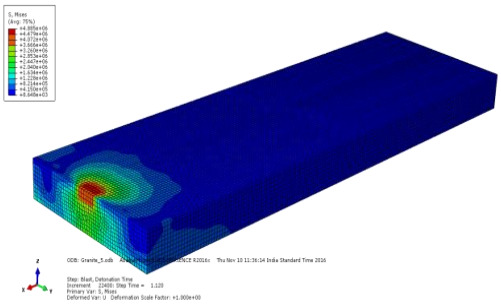

1120ms

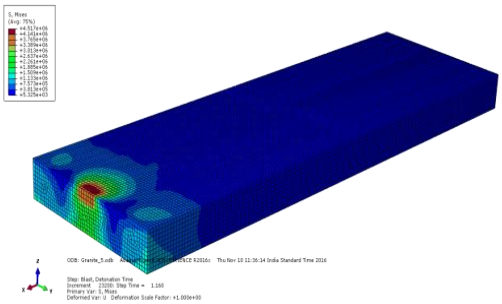

1160ms

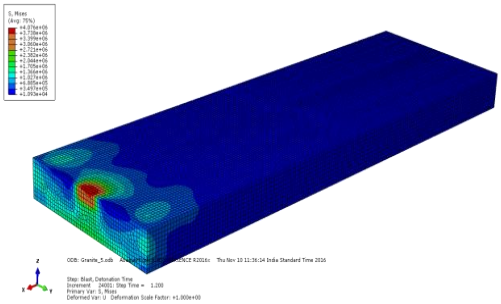

1200ms

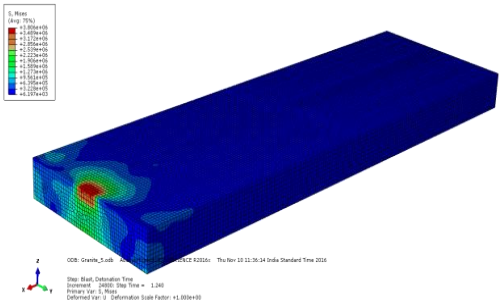

1240ms

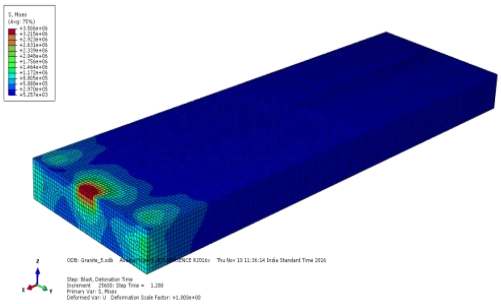

1280ms

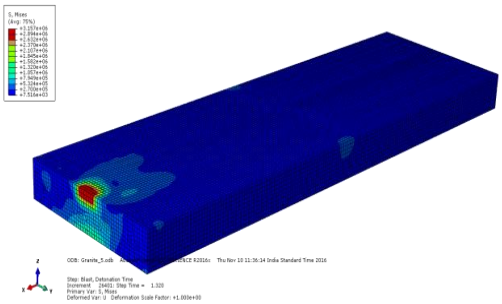

1320ms

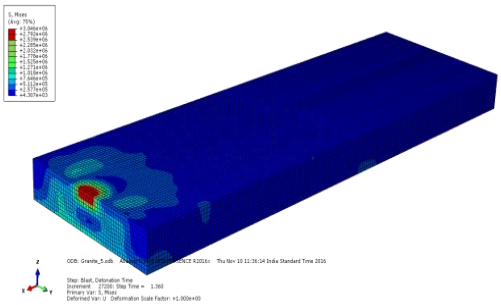

1360ms

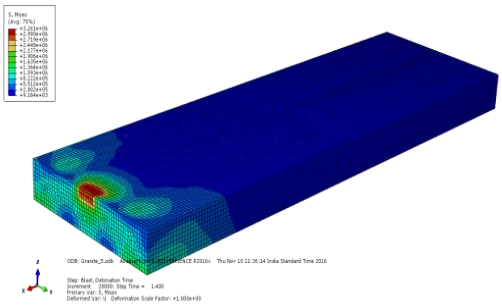

1400ms

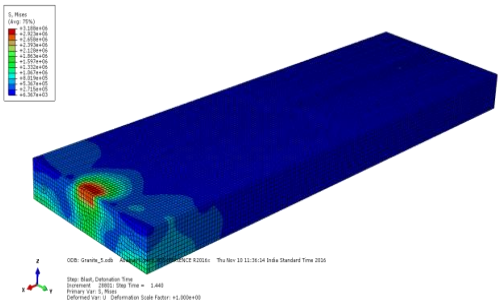

1440ms

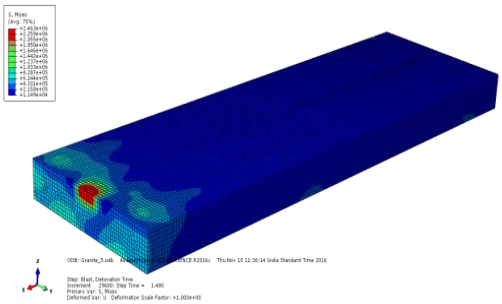

1480ms

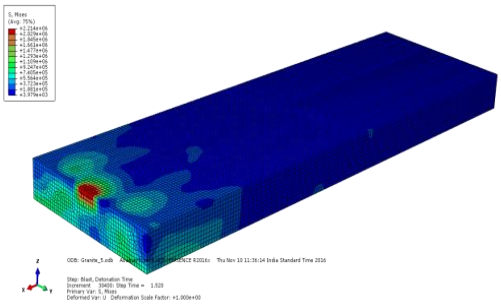

1520ms

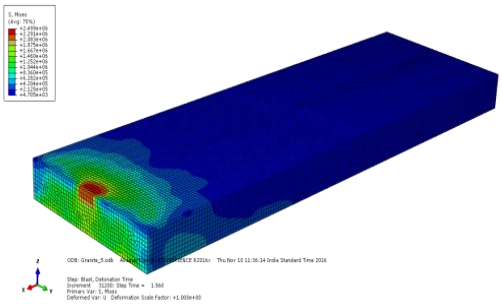

1560ms

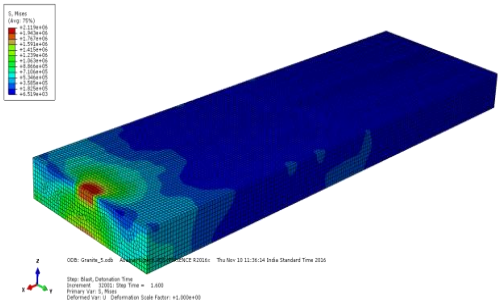

1600ms

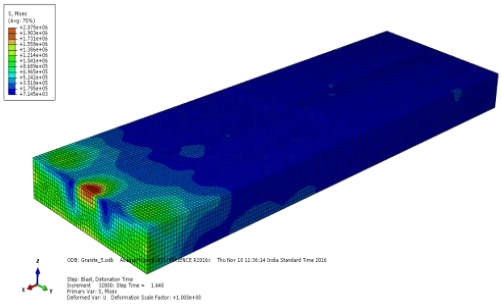

1640ms

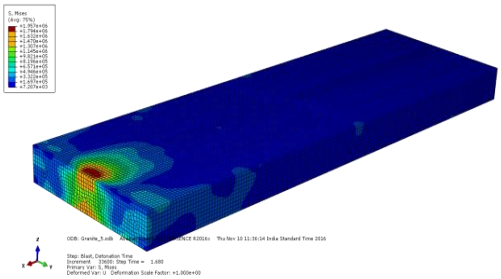

1680ms

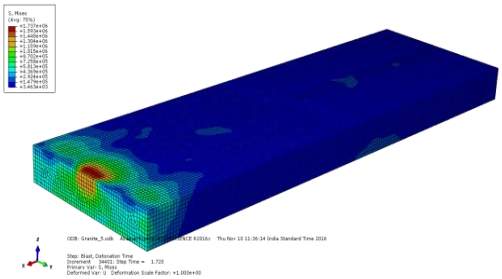

1720ms

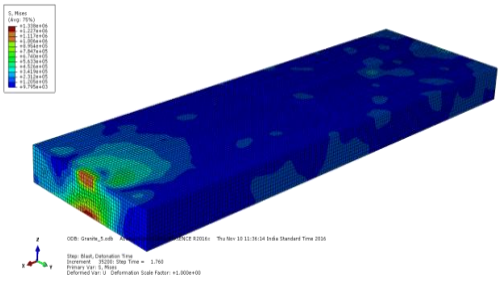

1760ms

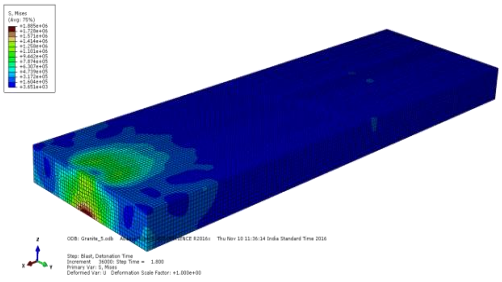

1800ms

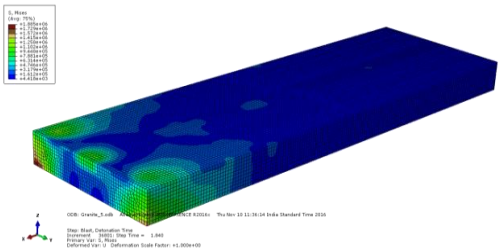

1840ms

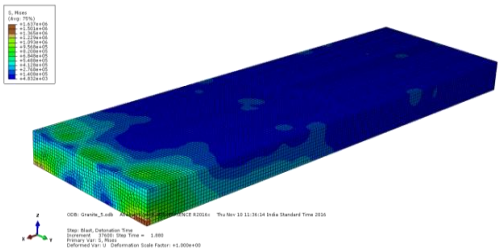

1880ms

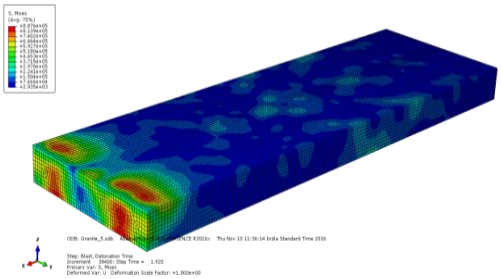

1920ms

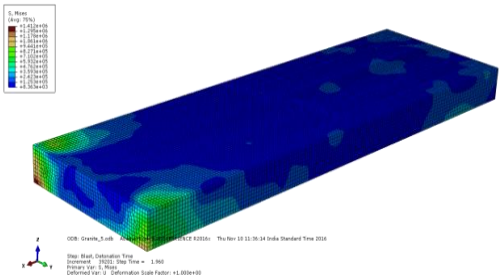

1960ms

Fig. A14.1 Stress components at integral points in a typical granite model

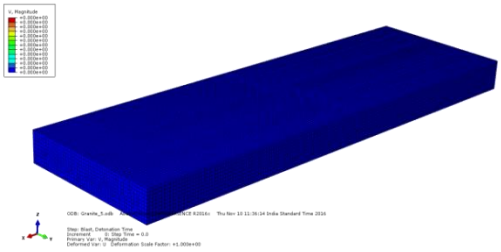

0ms

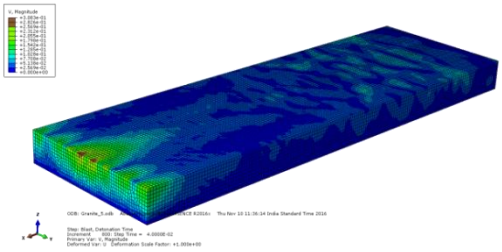

40ms

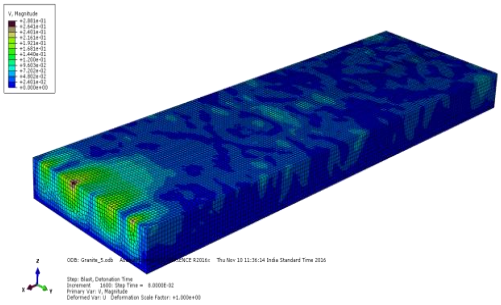

80ms

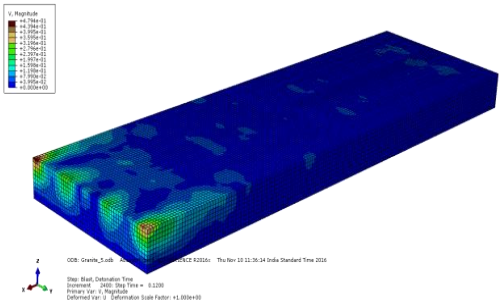

120ms

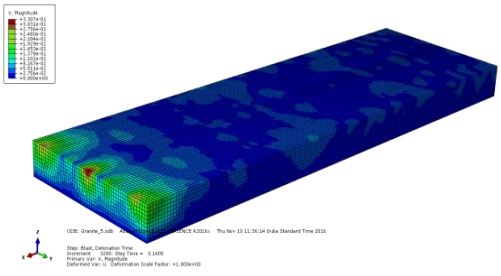

160ms

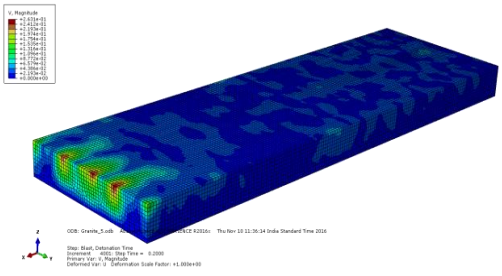

200ms

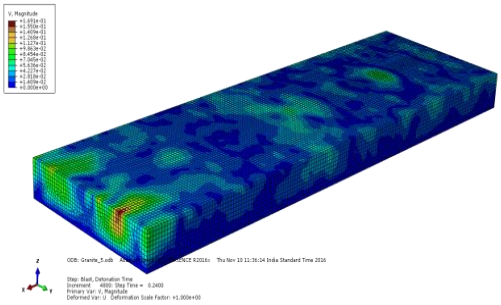

240ms

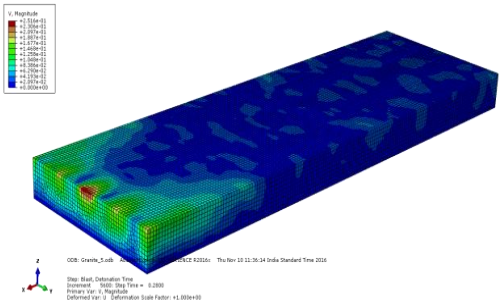

280ms

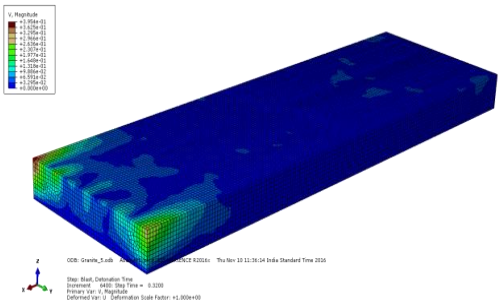

320ms

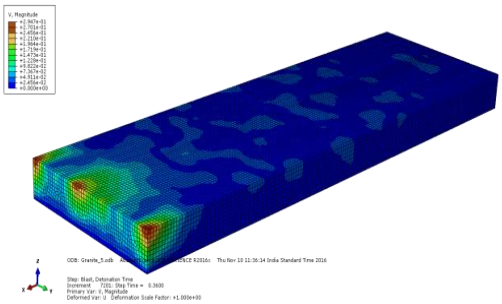

360ms

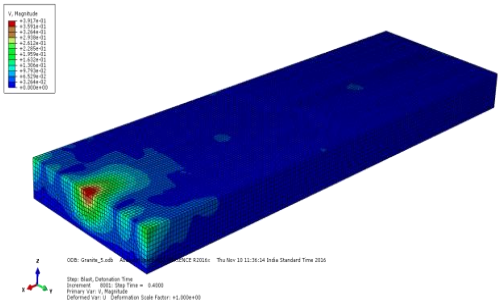

400ms

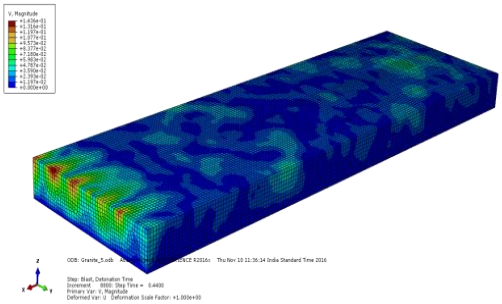

440ms

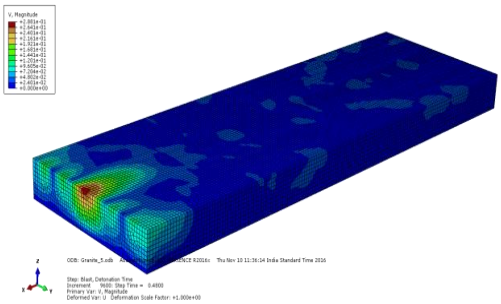

480ms

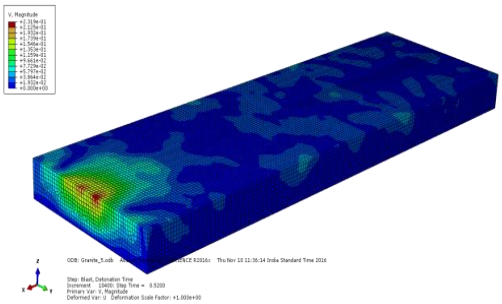

520ms

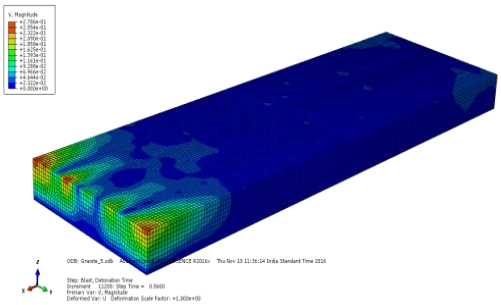

560ms

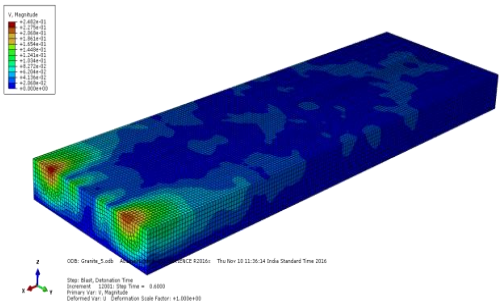

600ms

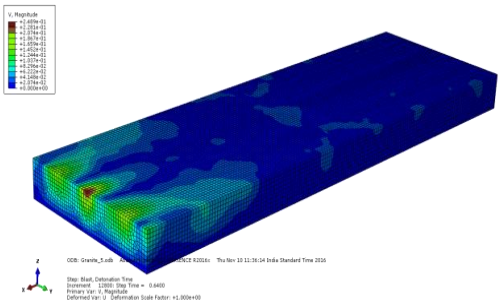

640ms

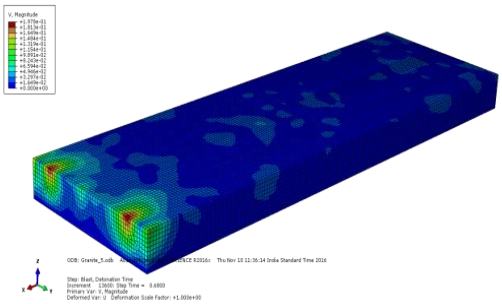

680ms

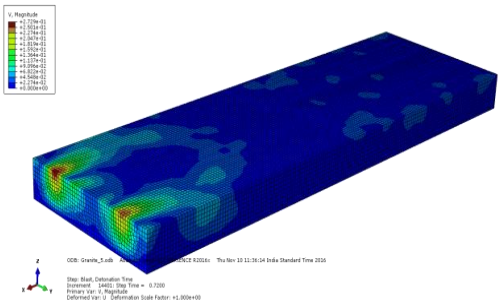

720ms

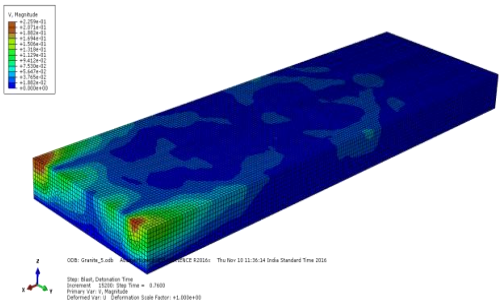

760ms

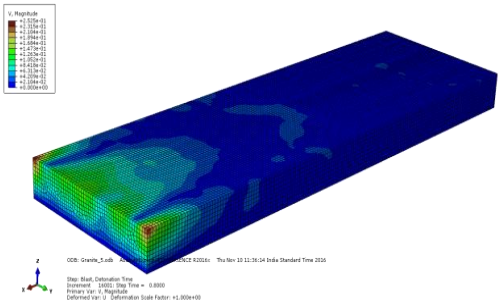

800ms

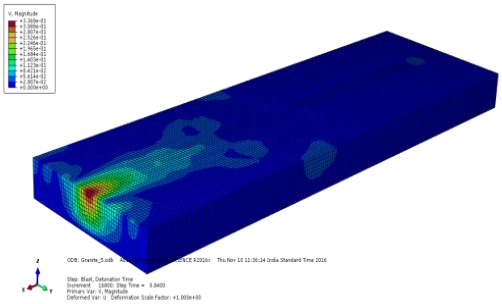

840ms

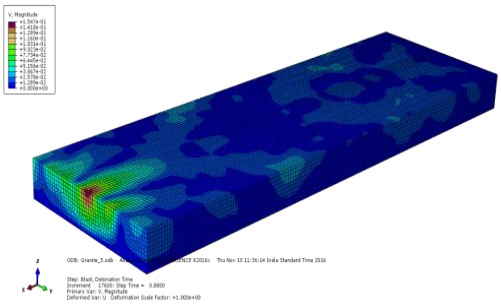

880ms

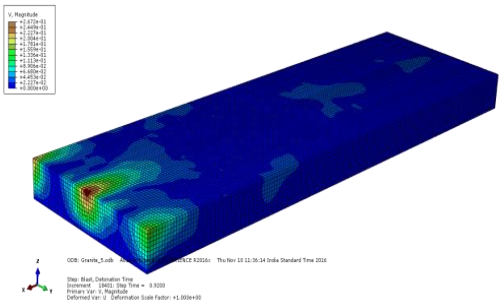

920ms

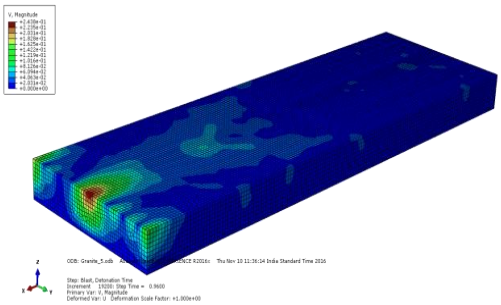

960ms

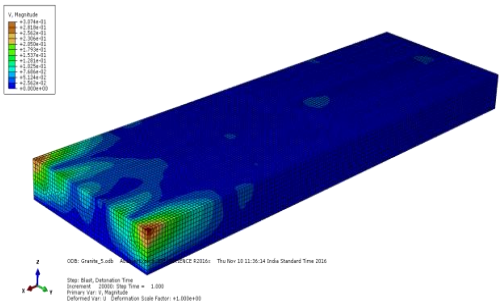

1000ms

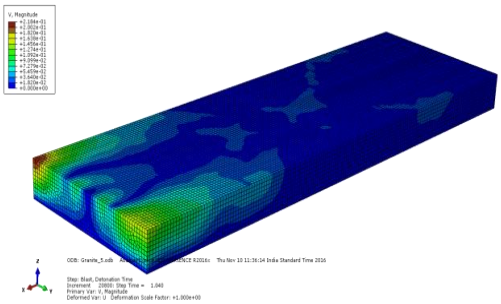

1040ms

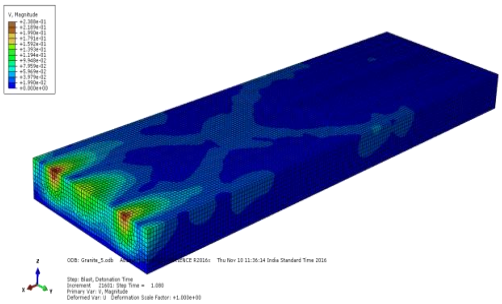

1080ms

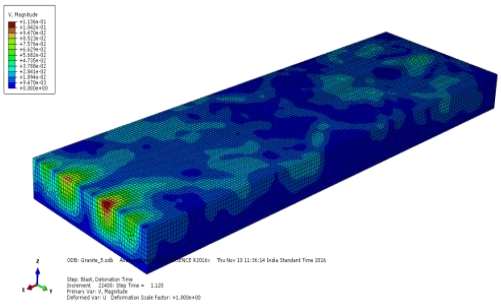

1120ms

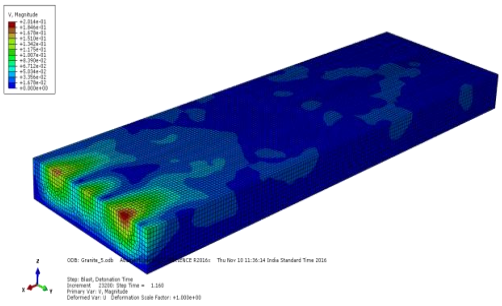

1160ms

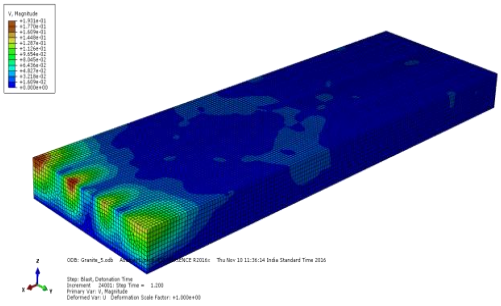

1200ms

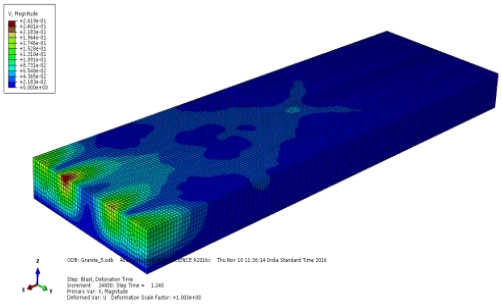

1240ms

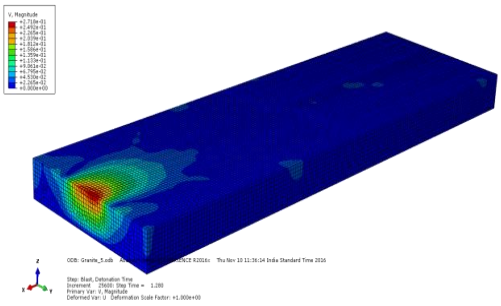

1280ms

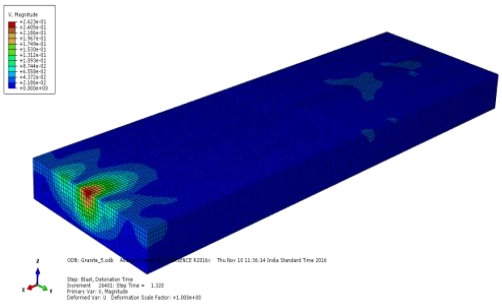

1320ms

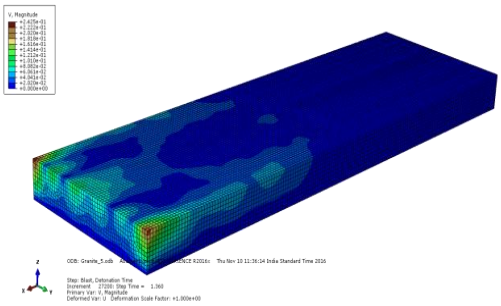

1360ms

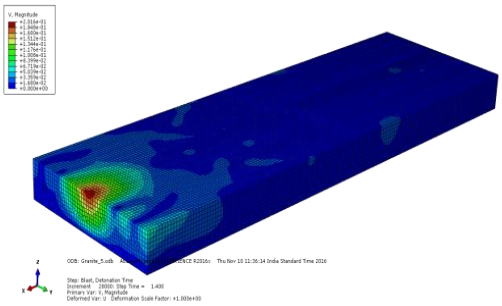

1400ms

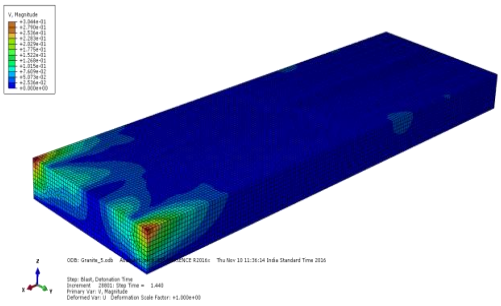

1440ms

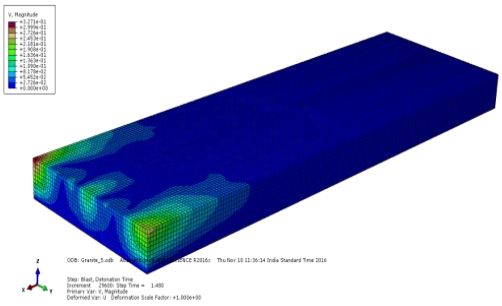

1480ms

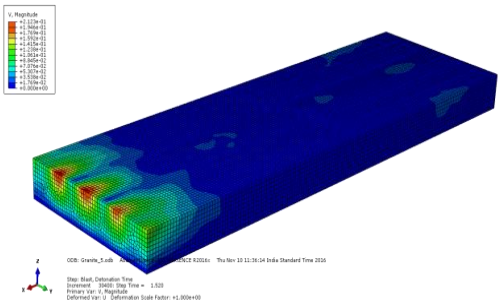

1520ms

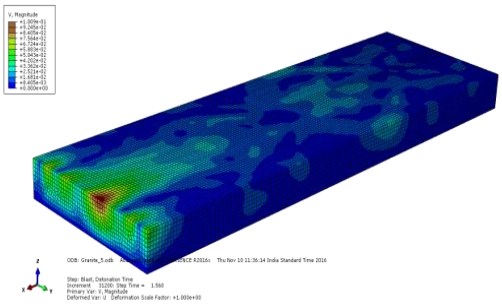

1560ms

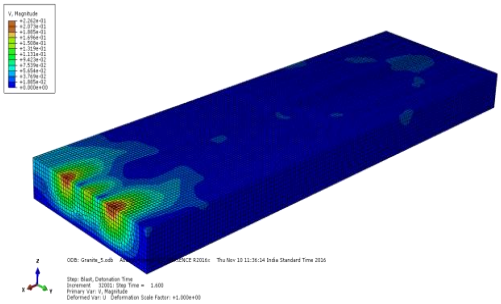

1600ms

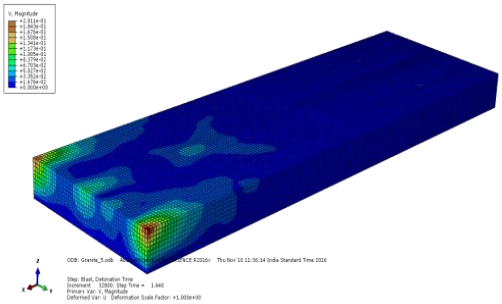

1640ms

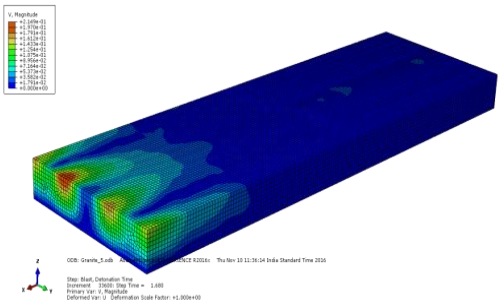

1680ms

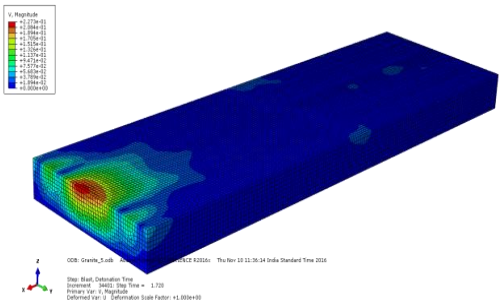

1720ms

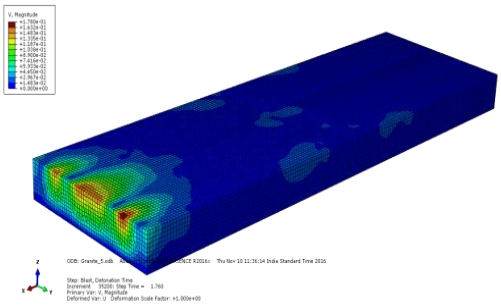

1760ms

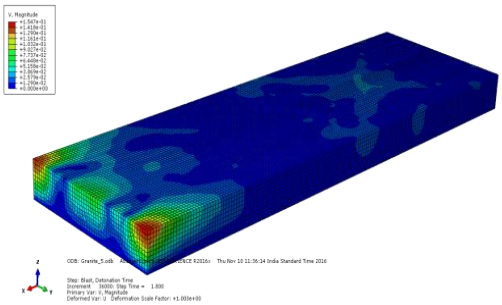

1800ms

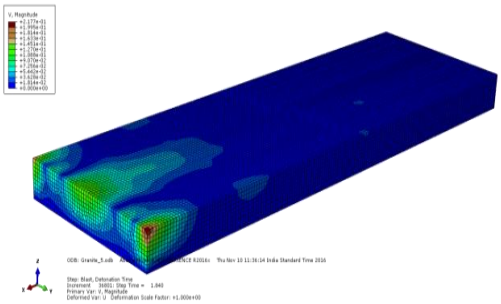

1840ms

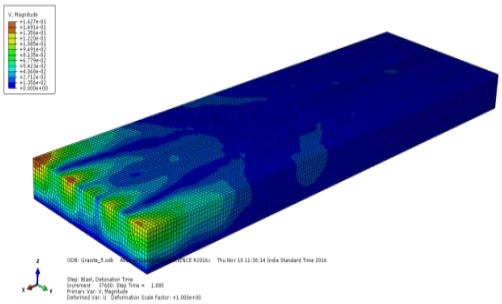

1880ms

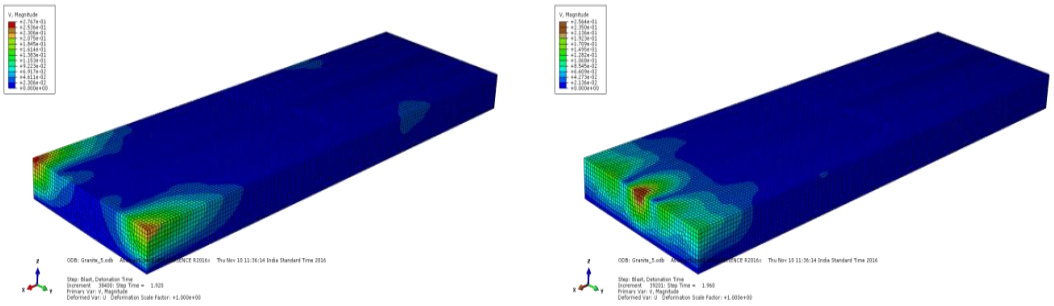

1920ms 1960ms

Fig. A14.2 Spatial velocity contours observed at nodes in a granite model

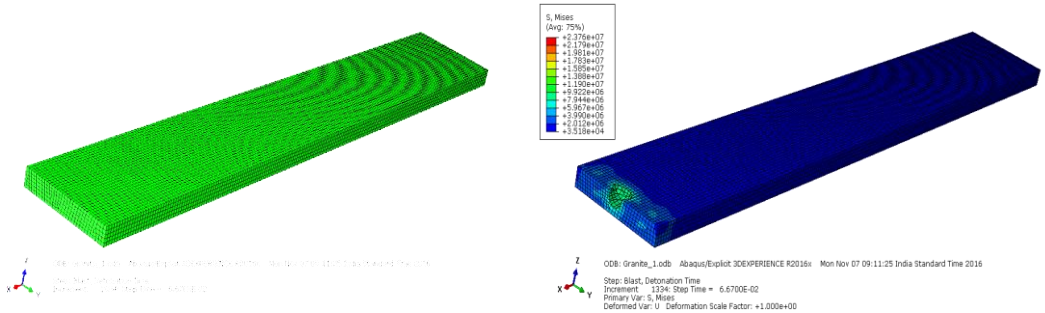

Granite model no. 1 with un-deformed (left) and deformed (right) shapes

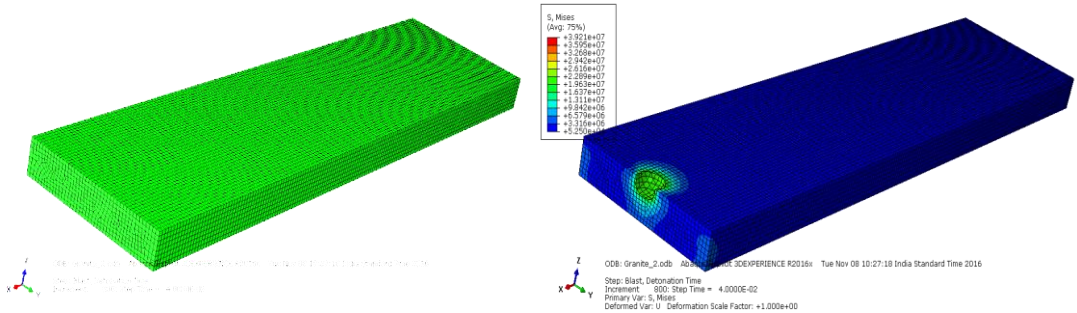

Granite model no. 2 with un-deformed (left) and deformed (right) shapes

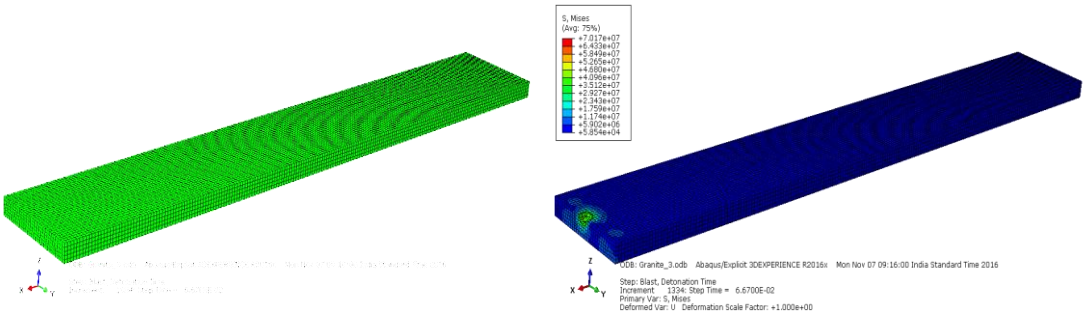

Granite model no. 3 with un-deformed (left) and deformed (right) shapes

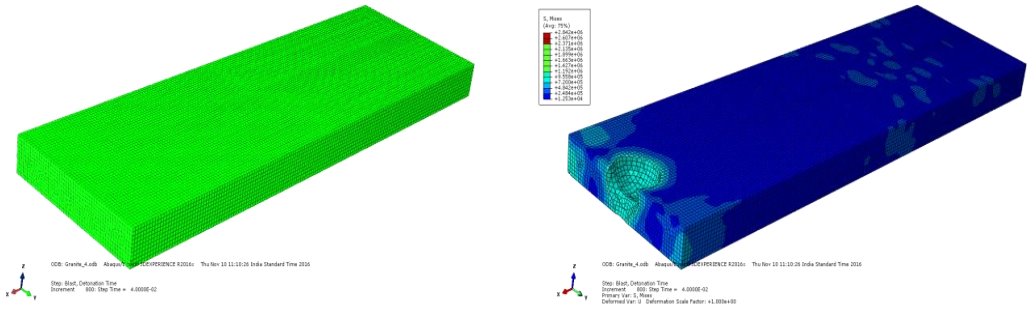

Granite model no. 4 with un-deformed (left) and deformed (right) shapes

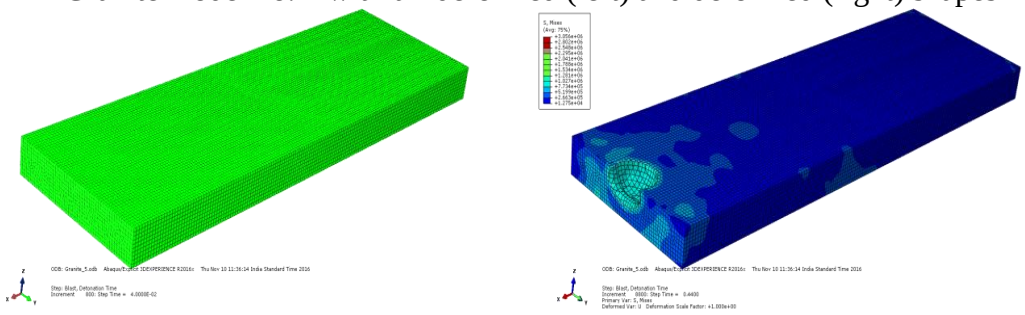

Granite model no. 5 with un-deformed (left) and deformed (right) shapes

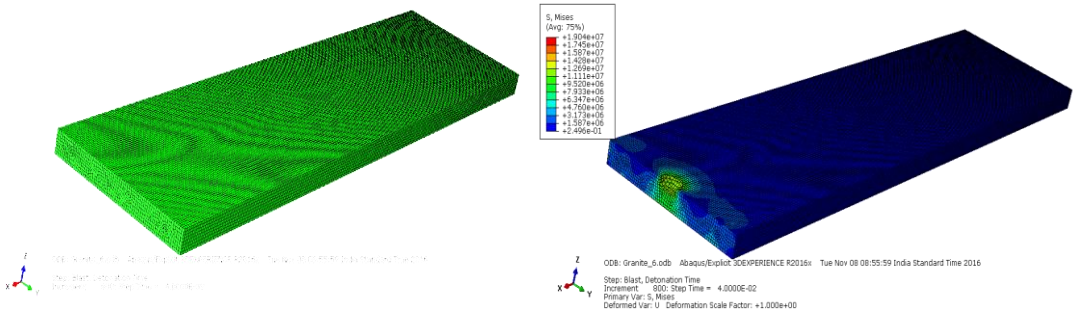

Granite model no. 6 with un-deformed (left) and deformed (right) shapes

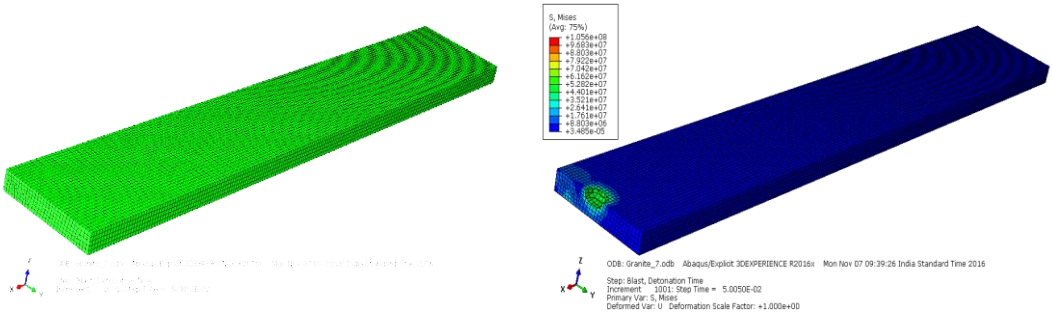

Granite model no. 7 with un-deformed (left) and deformed (right) shapes

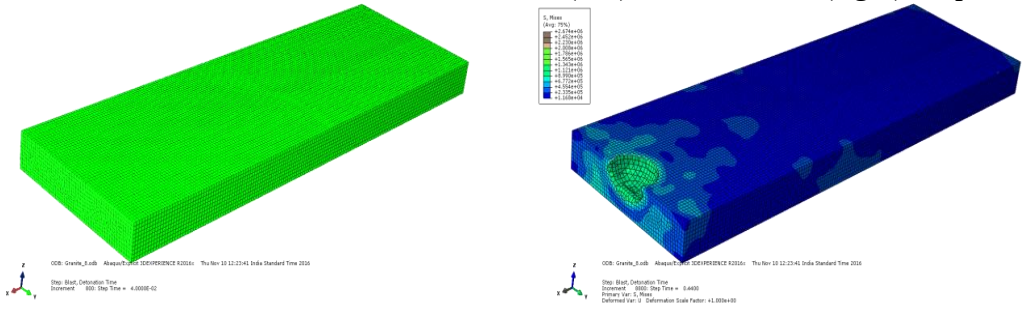

Granite model no. 8 with un-deformed (left) and deformed (right) shapes

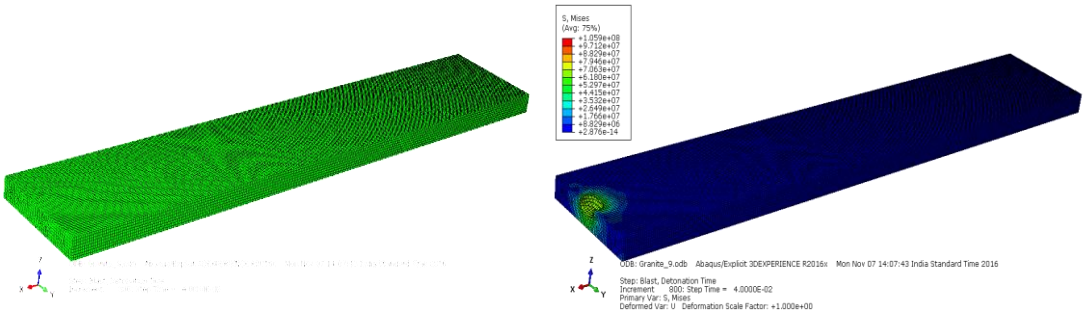

Granite model no. 9 with un-deformed (left) and deformed (right) shapes

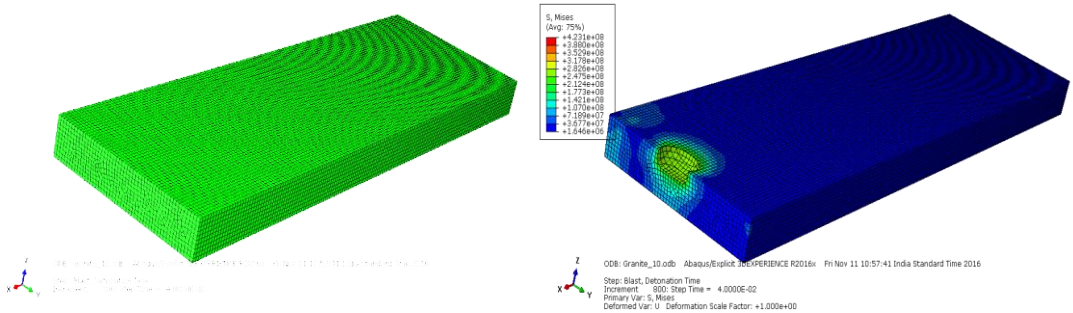

Granite model no. 10 with un-deformed (left) and deformed (right) shapes

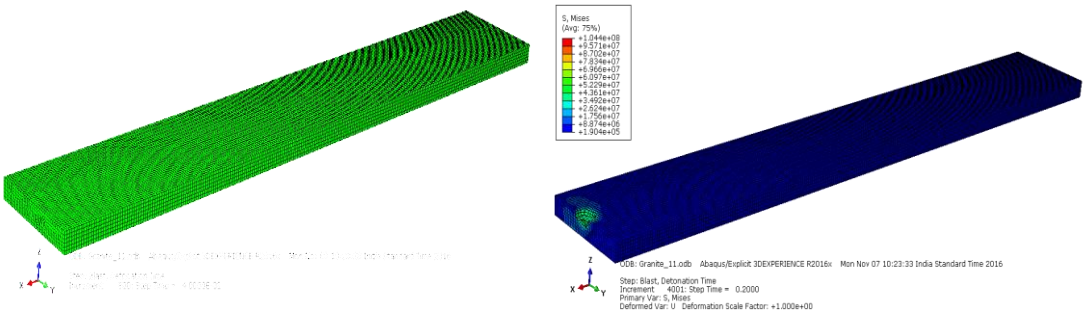

Granite model no. 11 with un-deformed (left) and deformed (right) shapes

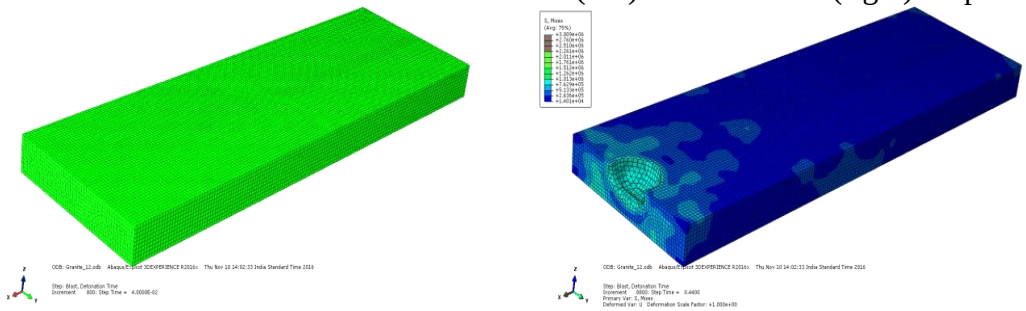

Granite model no. 12 with un-deformed (left) and deformed (right) shapes

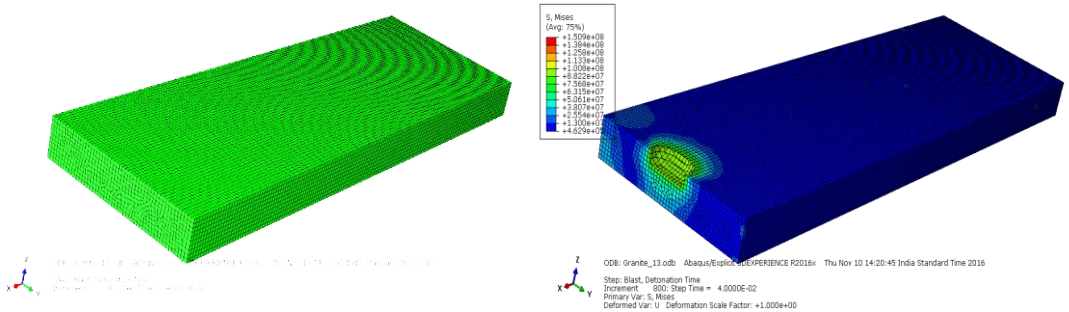

Granite model no. 13 with un-deformed (left) and deformed (right) shapes

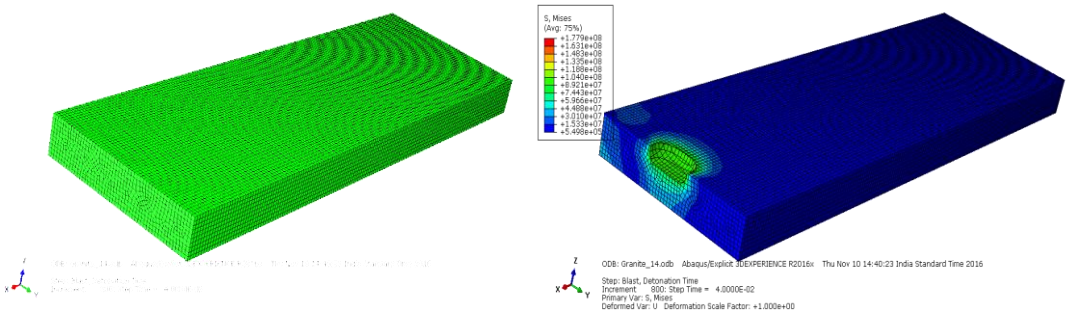

Granite model no. 14 with un-deformed (left) and deformed (right) shapes

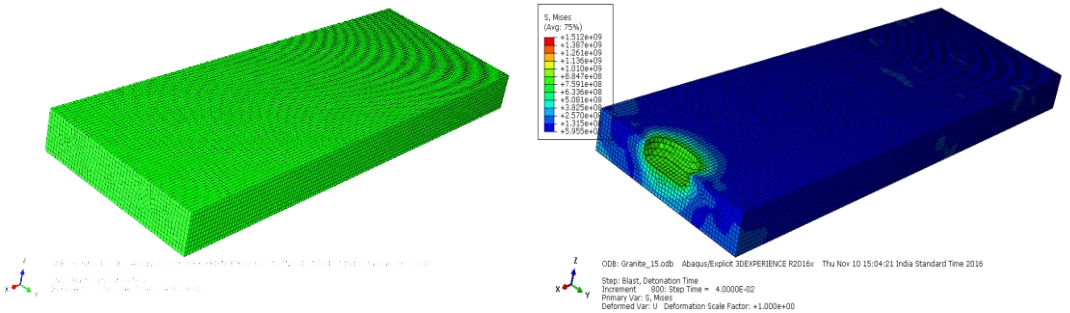

Granite model no. 15 with un-deformed (left) and deformed (right) shapes

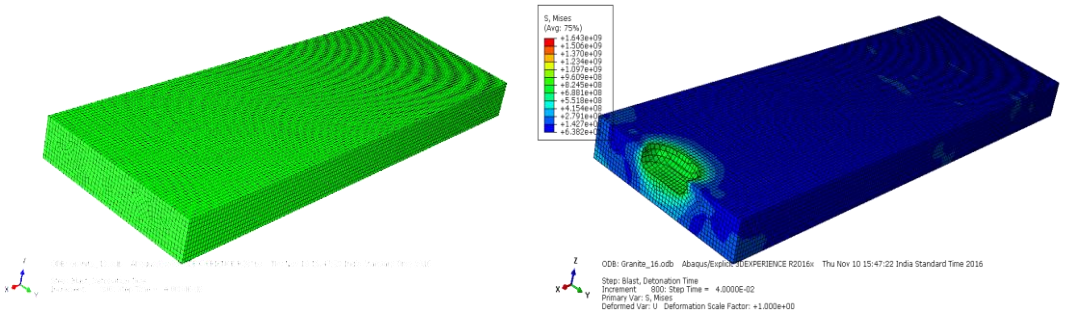

Granite model no. 16 with un-deformed (left) and deformed (right) shapes

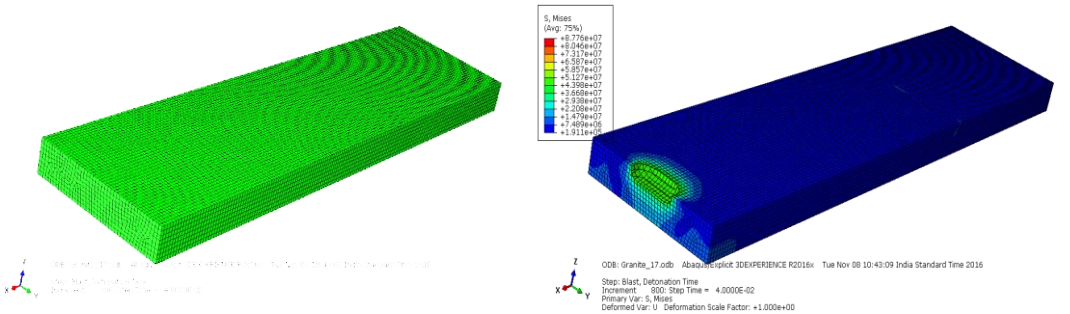

Granite model no. 17 with un-deformed (left) and deformed (right) shapes

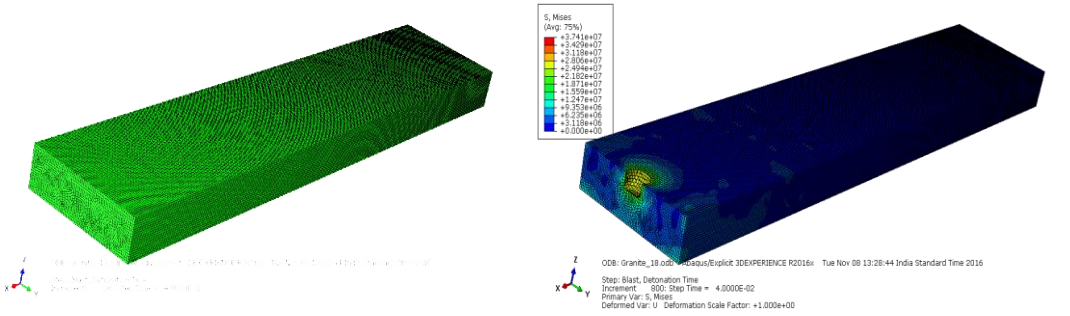

Granite model no. 18 with un-deformed (left) and deformed (right) shapes

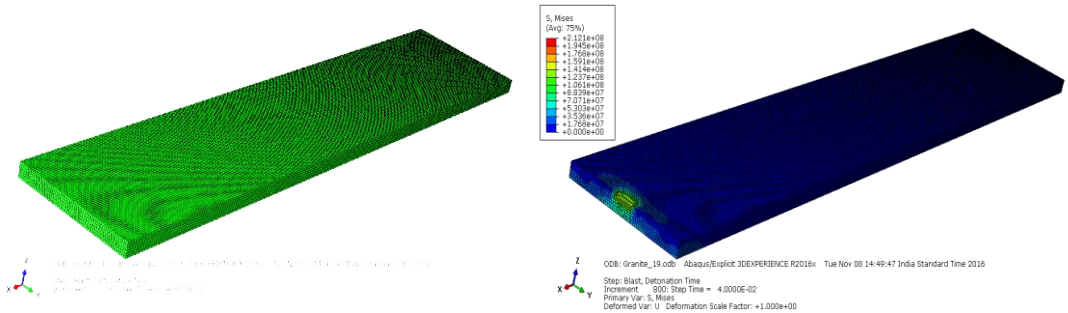

Granite model no. 19 with un-deformed (left) and deformed (right) shapes

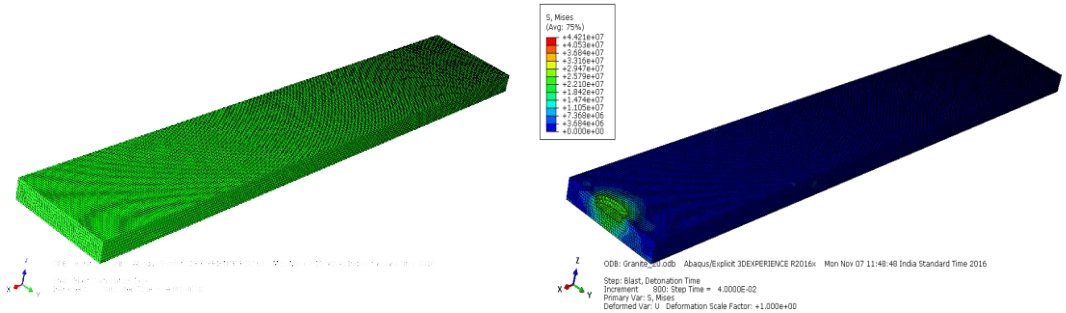

Granite model no. 20 with un-deformed (left) and deformed (right) shapes

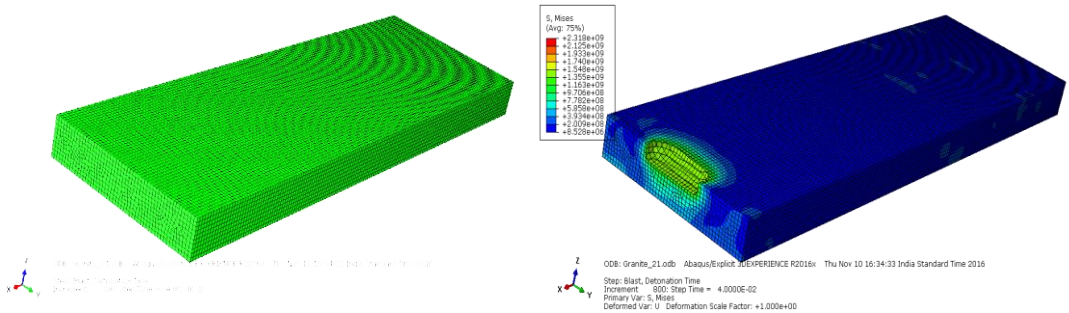

Granite model no. 21 with un-deformed (left) and deformed (right) shapes

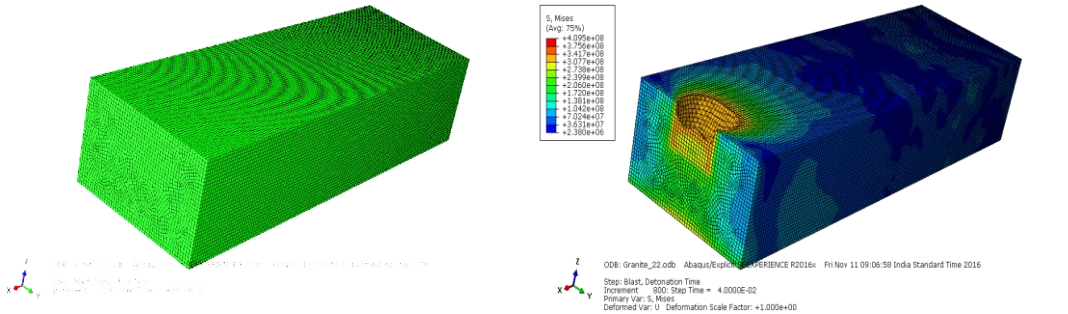

Granite model no. 22 with un-deformed (left) and deformed (right) shapes

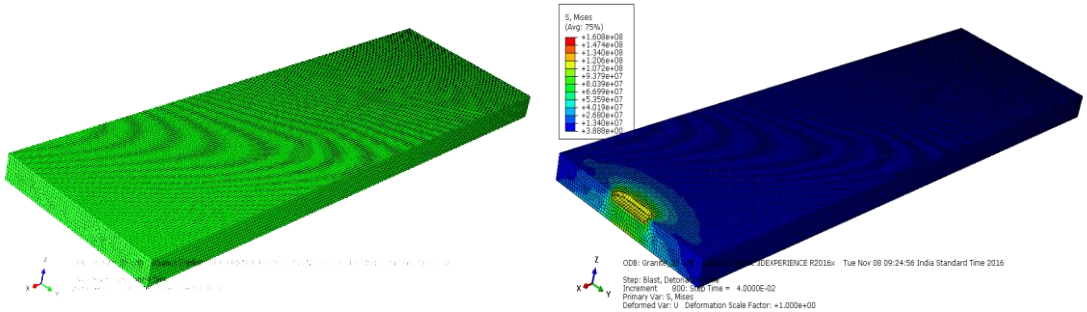

Granite model no. 23 with un-deformed (left) and deformed (right) shapes

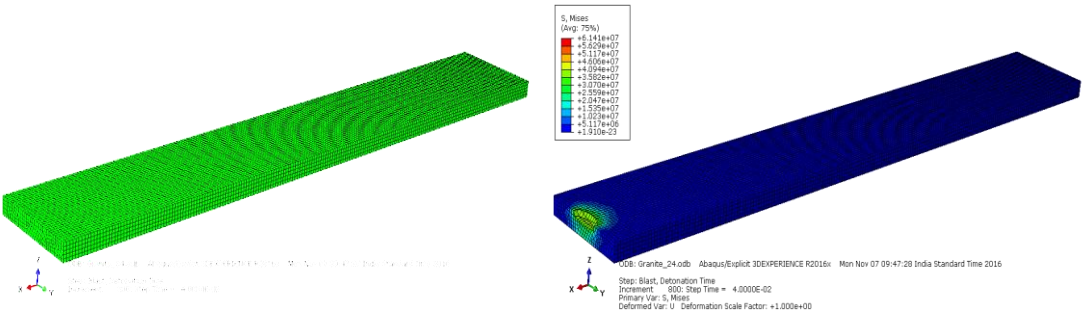

Granite model no. 24 with un-deformed (left) and deformed (right) shapes

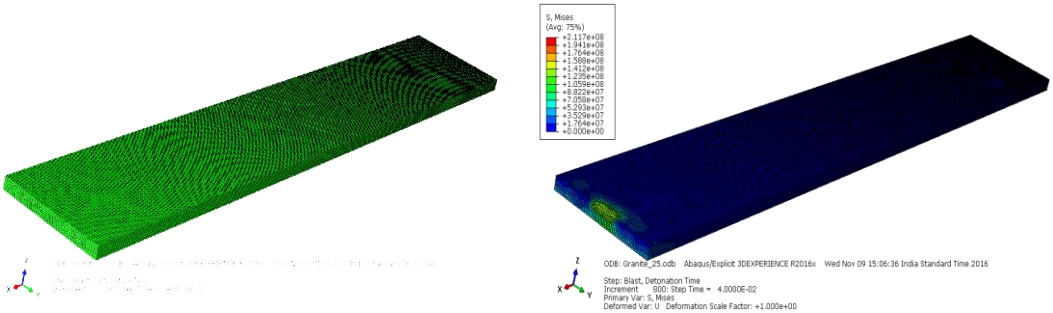

Granite model no. 25 with un-deformed (left) and deformed (right) shapes

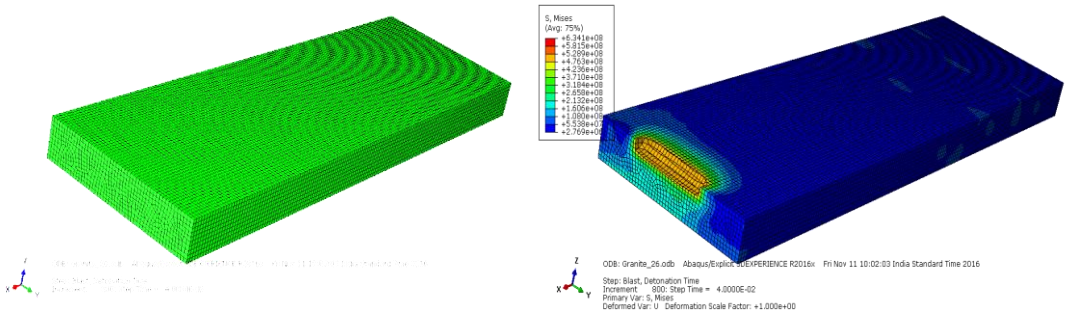

Granite model no. 26 with un-deformed (left) and deformed (right) shapes

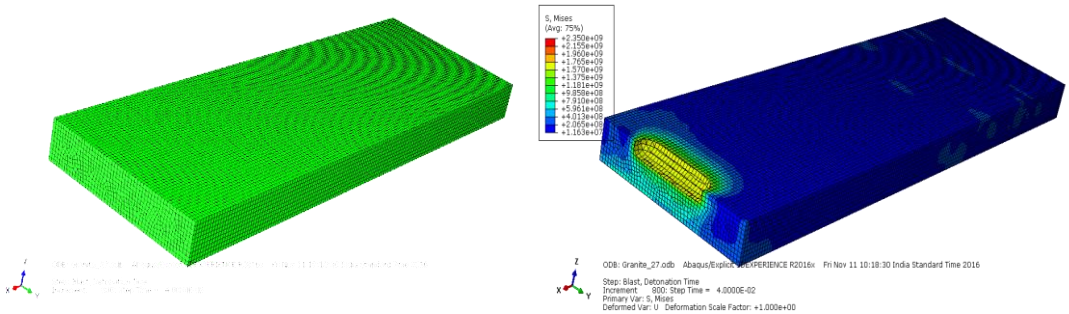

Granite model no. 27 with un-deformed (left) and deformed (right) shapes

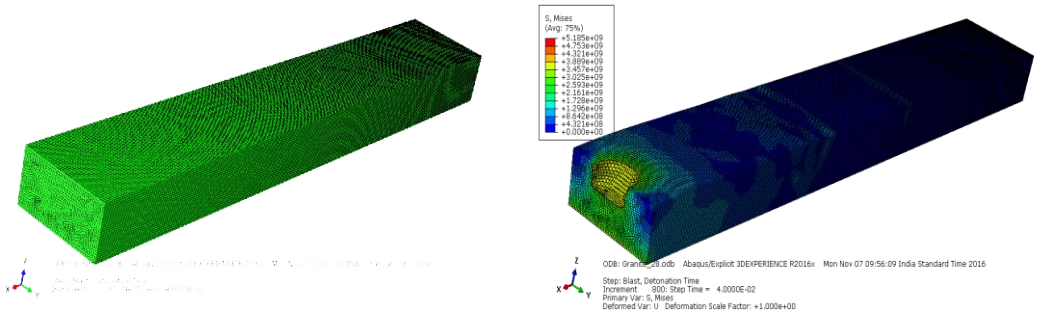

Granite model no. 28 with un-deformed (left) and deformed (right) shapes

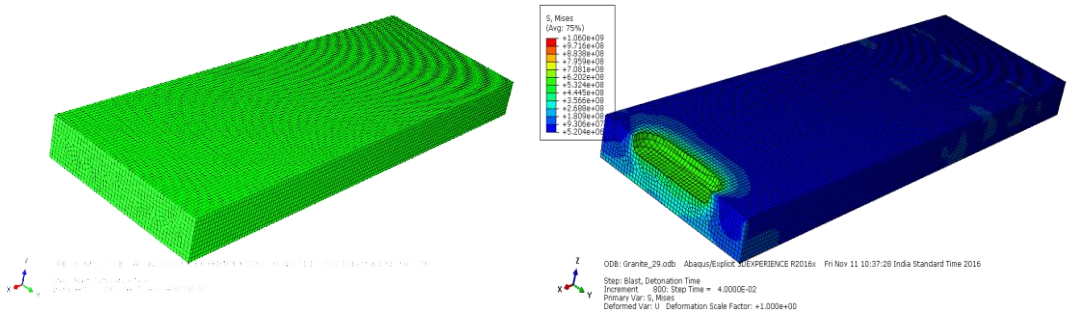

Granite model no. 29 with un-deformed (left) and deformed (right) shapes

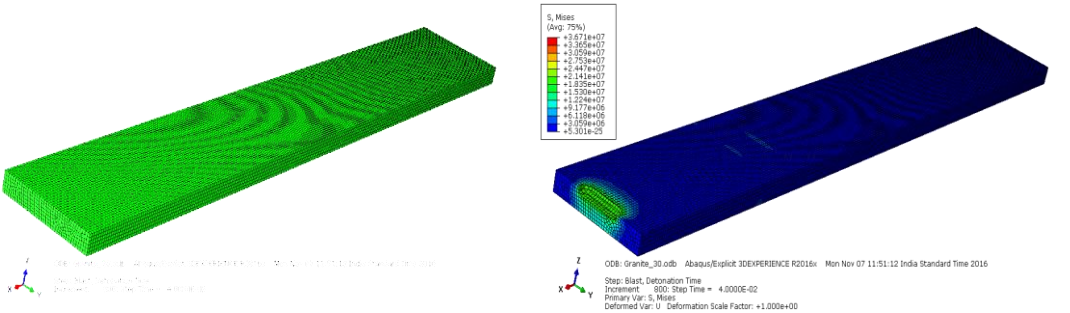

Granite model no. 30 with un-deformed (left) and deformed (right) shapes

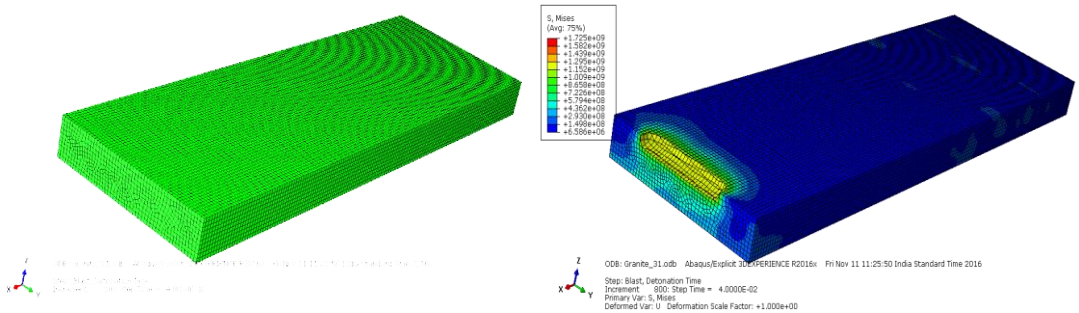

Granite model no. 31 with un-deformed (left) and deformed (right) shapes

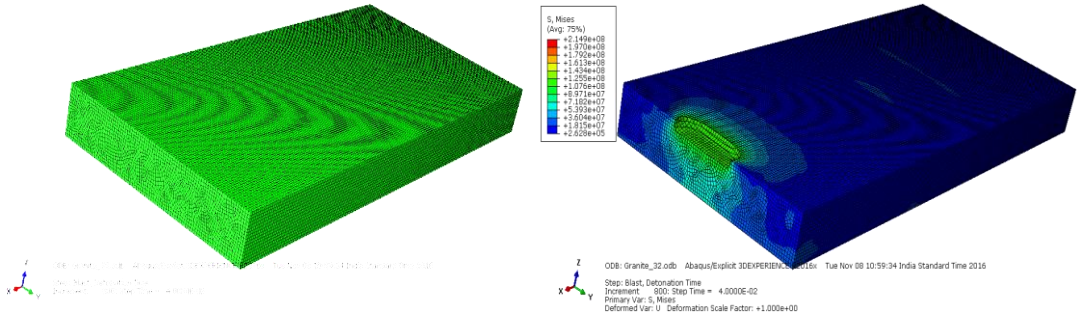

Granite model no. 32 with un-deformed (left) and deformed (right) shapes

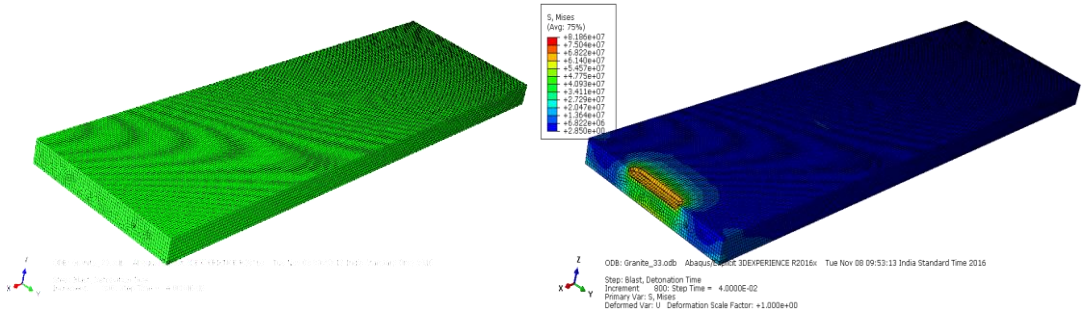

Granite model no. 33 with un-deformed (left) and deformed (right) shapes

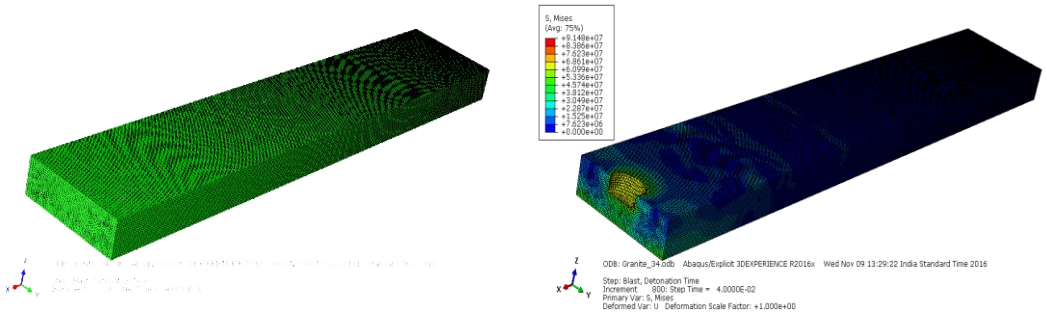

Granite model no. 34 with un-deformed (left) and deformed (right) shapes

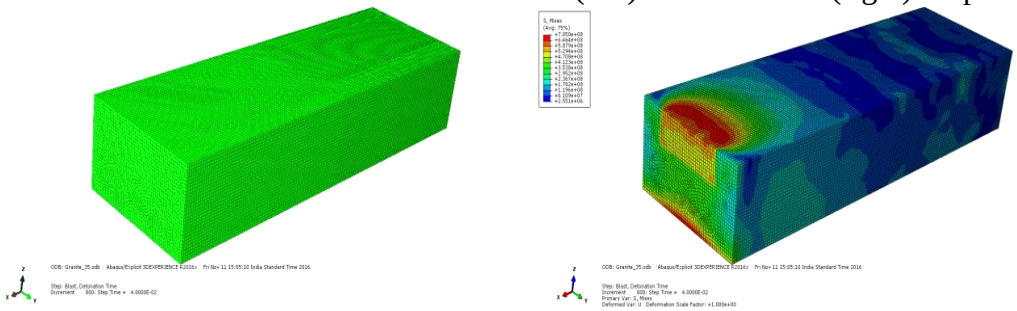

Granite model no. 35 with un-deformed (left) and deformed (right) shapes

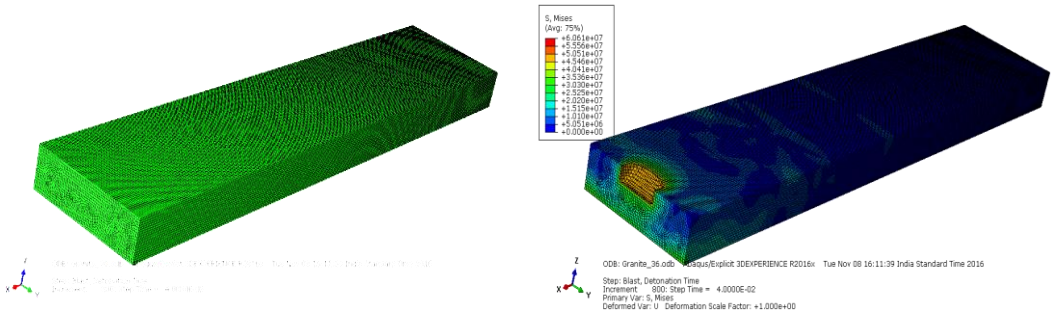

Granite model no. 36 with un-deformed (left) and deformed (right) shapes

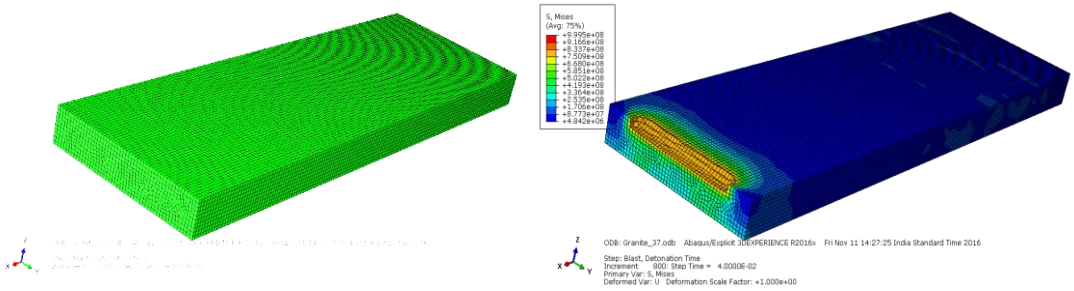

Granite model no. 37 with un-deformed (left) and deformed (right) shapes

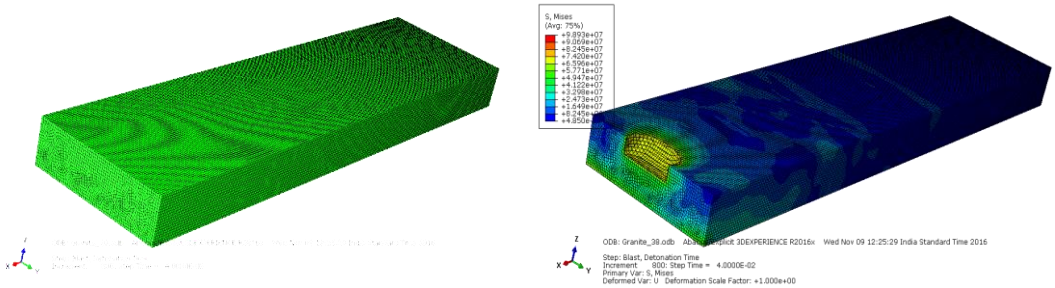

Granite model no. 38 with un-deformed (left) and deformed (right) shapes

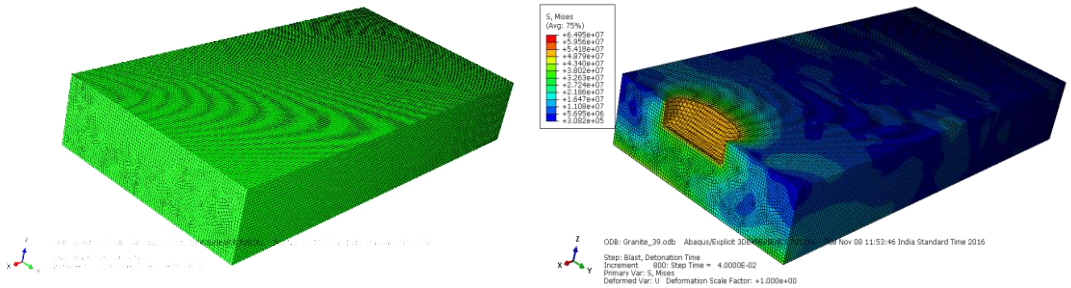

Granite model no. 39 with un-deformed (left) and deformed (right) shapes

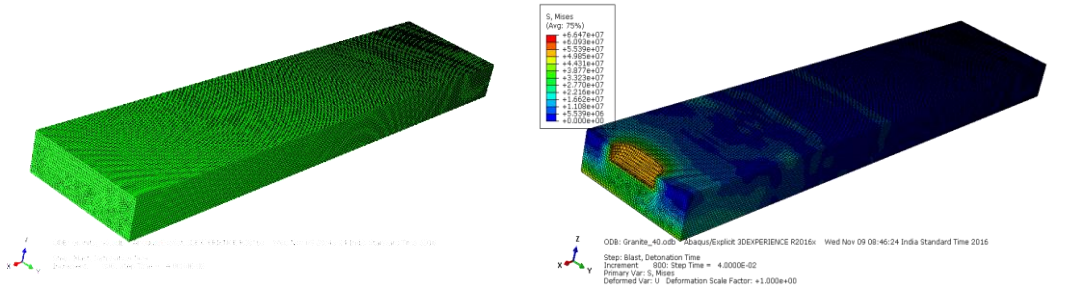

Granite model no. 40 with un-deformed (left) and deformed (right) shapes

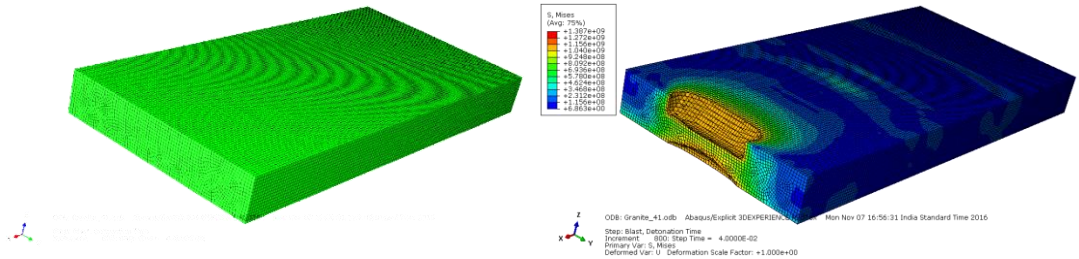

Granite model no. 41 with un-deformed (left) and deformed (right) shapes

Fig. A14.3 Un-deformed and deformed shapes of blast models in granite formation

LIST OF PUBLICATIONS BASED ON PH.D. RESEARCH WORK

Sl. No.	Title of the Paper	Authors	Name of the Journal / Conference / Symposium, Vol., No., Pages	Year of Publication	Category*
1	Piezo-Gen - An approach to generate electricity from vibrations	G. Raghu Chandra, V.R. Sastry, Mohiuddin M.S.	Procedia Earth and Planetary Science, **Elsevier**, 11, 464-465.	2015	1
2	Application of high-speed videography in assessing the performance of blasts	V.R. Sastry, G. Raghu Chandra, N. Adithya, S.A. Saiprasad	International Journal of Geological and Geotechnical Engineering, 1, 2, 19-22	2015	1
3	Assessing the explosive energy utilization in mine blasting – role of high speed videography	V.R. Sastry, B. Rajasekhar, G. Raghu Chandra	National Conference on Advanced Trends in Civil Engineering and Sustainable Development.	2016	3
4	Assessment of seismic energy obtained from blast induced ground vibrations using signal processing computation techniques	V.R. Sastry, G. Raghu Chandra	**IEEE** – International Conference on Recent Trends in Electronics Information and Communication Technology, Bangalore. (RTEICT-2016) **[SCOPUS INDEXED]**	2016	3
5	Signal processing computation based seismic energy estimation of blast induced ground vibration waves **[Bagged Best Paper Award]**	V.R. Sastry, G. Raghu Chandra	**IEEE** – International Conference on Distributed Computing, VLSI, Electrical Circuits and Robotics, Mangalore. (DISCOVER-2016) **[SCOPUS INDEXED]**	2016	3
6	Tapping of electrical energy from ground vibrations caused due to blasting – An innovation	V.R. Sastry, G. Raghu Chandra	International conference on Next Generation Technologies for Mini ng and Fuel Industries, CISR-CIMFR, Vigyan Bhawan, New Delhi. (NxGnMiFu 2017)	2017	3
7	Generation of electrical energy from blast induced vibrations	G. Raghu Chandra, V.R. Sastry	International Journal of Analysis of Electrical Machines.	2017	1

* Category: 1 : Journal paper, full paper reviewed; 2 : Journal paper, Abstract reviewed; 3 : Conference/Symposium paper, full paper reviewed;
4 : Conference/Symposium paper, abstract reviewed; 5 : others (including papers in Workshops, NITK Research Bulletins, Short notes, etc.)

BIO-DATA

NAME : RAGHU CHANDRA GARIMELLA

Contact No. : 9290796716

E-mail : raghuchandhra@india.com

Date of Birth : 08-08-1989

Permanent address : 4-138/D1, Bhupayya Agraharam,
Maha Aanandam Apartments, Amalapuram,
Andhra Pradesh – 533 201

ACADEMIC PROFILE

Course	Year of Passing	Name of University / Institution	Percentage/ CGPA
PH.D.	**--**	**National Institute of Technology Karnataka, Surathkal**	**10.00**
Electrical Engineering (Eight Week Course)	2017	The University of New Castle, Australia	93.00 %
MBA (Operations Management)	2014	Gandhi Institute of Technology and Management (GITAM), Visakhapatnam	6.44
M.TECH (Power Electronics)	2012	Jawaharlal Nehru Technological University Kakinada (JNTUK)	84.73 %
B.TECH (EEE)	2010	Jawaharlal Nehru Technological University Kakinada (JNTUK)	72.57 %

EXPERIENCE

- Working as an Associate Professor in Methodist College of Engineering and Technology, Affiliated to Osmania University from June 2018.
- Worked as an Assistant Professor (Grade-III) in Madanapalle Institute of Technology and Science, UGC-Autonomous during August 2017 to May 2018.
- Worked as an Assistant Professor in Rajahmahendri Institute of Engineering and Technology, Swarnandhra Group, Affiliated to JNTU Kakinada during May 2012 to April 2014.

MEMBERSHIPS OF PROFESSIONAL BODIES

- *Senior Member* Universal Association of Computers and Electronics Engineers (SMUACEE): ID Number – AM1005037.
- *Member* The Institute of Research Engineers and Doctors (MtheIRED): ID Number – SNM10100052733.
- *Life Member* International Association of Engineers (MIAENG): ID Number – 137627.
- *Former Member* The Institute of Doctors, Engineers and Scientists (MIDES): ID Number – 1389.
- *Former Member* The Association of Computer, Electronics and Electrical Engineers (MACEEE): ID Number – 1389.
- *Former Member* Society for Industrial and Applied Mathematics (MSIAM): ID Number – 020244865.

TOTAL PUBLICATIONS

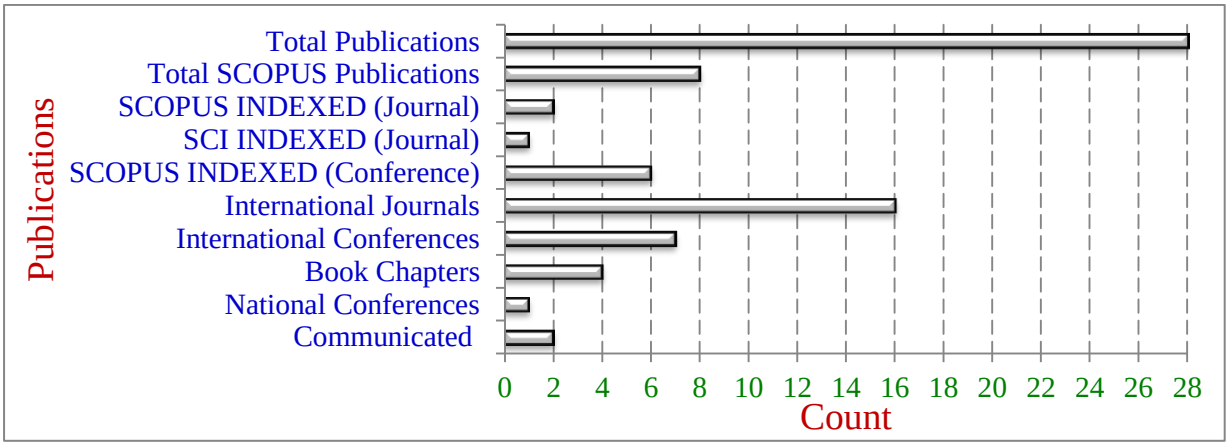

EDITORIAL BOARD MEMBERSHIPS

- **Editor-in-Chief** for Journal of **Modeling, Analysis and Simulation (SCOPUS Indexed),** *Clausius Scientific Press Inc.*, ISSN: 2516-3035 (weblink: https://www.clausiuspress.com/journal/JMAS/editorialBoard.html).
- **Editorial board member** for **American Journal of Electrical Power and Energy Systems (EPES)**, *Science Publishing Group*, ISSN Print: 2326-912X, ISSN Online: 2326-9200 (weblink: http://www.sciencepublishinggroup.com/journal/ditorialboard?journalid=165).
- **Editorial board member cum reviewer** for *Publons.*
- **Editorial board member** for Advances in Science, Technology and Engineering Systems Journal (ASTESJ) **(Thomson Reuters Indexed),** ISSN: 2415-6698.
- **Editorial board member** for *STM Journals*.
- **Editorial board member** for *JournalsPub*:
  - ☑ International Journal of Electrical Machines & Drives.
  - ☑ International Journals of Power Electronics Controllers and Converters.